Natural Resources Canada | Ressources naturelles Canada

GEOLOGICAL SURVEY OF CANADA
OPEN FILE 8536

Southern Ontario groundwater project 2014–2019: summary report

Edited by
H.A.J. Russell and B.A. Kjarsgaard

2020

Canada



GEOLOGICAL SURVEY OF CANADA
OPEN FILE 8536

Southern Ontario groundwater project 2014–2019: summary report

Edited by
H.A.J. Russell and B.A. Kjarsgaard

Geological Survey of Canada, 601 Booth Street, Ottawa, Ontario K1A 0E8

2020

© Her Majesty the Queen in Right of Canada, as represented by the Minister of Natural Resources, 2020

Information contained in this publication or product may be reproduced, in part or in whole, and by any means, for personal or public non-commercial purposes, without charge or further permission, unless otherwise specified.
You are asked to:
- exercise due diligence in ensuring the accuracy of the materials reproduced;
- indicate the complete title of the materials reproduced, and the name of the author organization; and
- indicate that the reproduction is a copy of an official work that is published by Natural Resources Canada (NRCan) and that the reproduction has not been produced in affiliation with, or with the endorsement of, NRCan.

Commercial reproduction and distribution is prohibited except with written permission from NRCan. For more information, contact NRCan at nrcan.copyrightdroitdauteur.rncan@canada.ca.

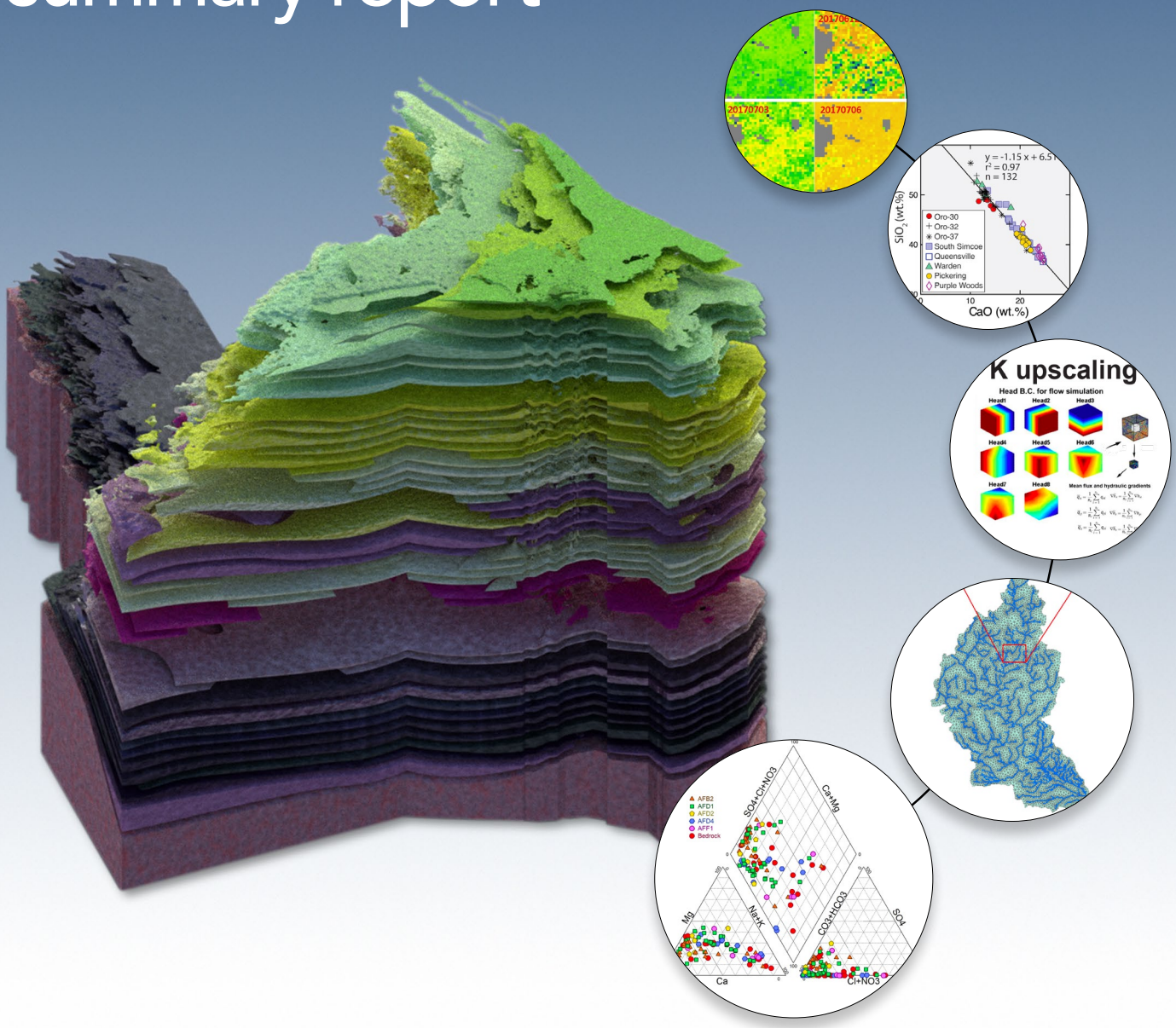
Permanent link: https://doi.org/10.4095/321078

This publication is available for free download through GEOSCAN (https://geoscan.nrcan.gc.ca/).

Recommended citation
Russell, H.A.J. and Kjarsgaard, B.A. (ed.), 2020. Southern Ontario groundwater project 2014–2019: summary report; Geological Survey of Canada, Open File 8536, 245 p. https://doi.org/10.4095/321078

Publications in this series have not been edited; they are released as submitted by the author.

Southern Ontario groundwater project 2014–2019: summary report



Edited by:

Hazen A.J. Russell and Bruce A. Kjarsgaard,
Geological Survey of Canada

Canada

Geological Survey of Canada, Open File 8536

CANADA 1842 GEOLOGICAL SURVEY - COMMISSION GÉOLOGIQUE

Cover Caption

Block diagram of modelled Paleozoic bedrock layers representing regional geological formations coloured by age from Precambrian to Devonian (top; see Carter et al.). View of diagram is from a perspective over the Michigan coast of Lake Huron looking east. Inset circular diagrams portray aspects of work presented in the summary volume from top to bottom: soil moisture mapping (Li et al.), geochemistry (Stepner et al.), upscaling of hydraulic conductivity (Benoit et al.), mesh with drainage for groundwater–surface-water modelling (Frey et al.), and Piper diagram for groundwater chemistry (Proteau-Bedard et al.). Block figure from Clark, J.K., Dupont, M.A., Logan, C.E., Russell, H.A.J., Carter, T.R., and Brunton, F.R. 2019. A first look at Ontario's geology in virtual reality. Geological Survey of Canada, Scientific Presentation 110, 2019; 8:56 min. https://doi.org/10.4095/321103

Table of Contents

Foreword iii
Michaud, Yves

Introduction to the southern Ontario groundwater project 2014–2019: summary report 1
Russell, H.A.J. and Kjarsgaard, B.A.

MODELLING

Three-dimensional geological modelling of the Paleozoic bedrock of southern Ontario: Status update 7
Carter, T.R., Brunton, F.R., Clark, J.K., Fortner, L., Logan, C.E., Russell, H.A.J., Somers, M., Sutherland, L., and Yeung, K.H.

Improving the 3-D geological data infrastructure of southern Ontario: Data capture, compilation, enhancement and QA/QC 23
Clark, J.K., Carter, T.R., Brunton, F.R., Logan, C.E., Somers, M., Sutherland, L., and Yeung, K.H.

Interface mapping of hydrochemical groundwater regimes in the Paleozoic bedrock of southwestern Ontario 37
Carter, T.R. and Sutherland, L.

A three-dimensional surficial geology model of southern Ontario: Progress report 49
Logan, C.E., Russell, H.A.J., Bajc, A.F., Burt, A., Mulligan, R.P.M., and Sharpe, D.R.

Machine learning applied to geoscience: Geo-referenced character recognition 65
Griffiths, M., Russell, H.A.J., and Logan, C.E.

Legacy seismic reflection data from the Great Lakes: Recovery and applications 75
Todd, B.J., Lewis, C.F.M., Russell, H.A.J., and Pyne, M.D.

GEOCHEMISTRY

Regional geochemical survey of surficial sediment in southern Ontario: A geochemical baseline for environmental and human health assessment 83
Sharpe, D.R., Kjarsgaard, B.A., Klassen, R.A., Knight, R.D., Logan, C.E., Russell, H.A.J., and Stepner, D.A.J.

An analytical protocol for determining the elemental chemistry of Quaternary sediments using a portable X-ray fluorescence spectrometer 95
Knight, R.D., Kjarsgaard, B.A., Stepner, D.A.J., and Russell, H.A.J.

A chemostratigraphic characterization of Newmarket Till in drill core from north of Lake Ontario 109
Stepner, D.A., Kjarsgaard, B.A., Knight, R.D., Russell, H.A.J., and Sharpe D.R.

Mineralogy, geochemistry, grain size and pebble componentry of the Newmarket Till and the Dummer Moraines in the Kaladar-Tweed-Belleville area of eastern Ontario 121
Kjarsgaard, B.A., Sharpe, D.R., Stepner, D.A.J., Knight, R.D., and Russell, H.A.J.

Table of Contents (continued)

GEOPHYSICS

Hydrogeophysics for the characterization of hydraulic properties of the Vars-Winchester esker, southeastern Ontario..... 131
Paradis, D., Pugin, A.J.-M., Crow, H.L., Oldenborger, G., Russell, H.A.J., and Melaney, M.

High-resolution seismic reflection profiles for groundwater studies of the Vars-Winchester esker, southeastern Ontario 139
Pugin, A. J.-M., Crow, H.L., Brewer, K., Cartwright, T., Dietiker, B., Griffiths M., and Paradis D.

Lithological and hydrogeological properties from a downhole geophysical dataset in the Vars-Winchester esker, Ontario 147
Crow, H.L., Pugin, A.J.-M., Dietiker, B., Paradis, D., Brewer, K., Cartwright, T., Griffiths, M., and Russell, H.A.J.

Improved analysis of Horizontal-to-Vertical Spectral Ratio measurements for groundwater investigations 159
Dietiker, B., Hunter, J.A., and Pugin, A.J.-M.

HYDROGEOLOGY

Downscaling SMAP soil moisture using Radarsat Constellation Mission (RCM) compact polarimetric SAR data: A case study in southern Ontario 171
Li, J., Wang, S., and Russell, H.A.J.

Progressing toward an understanding of groundwater geochemistry of Innisfil Creek watershed, southern Ontario 179
Proteau-Bedard, F., Benoit, N., Baudron, P., Post, R., and Mills, A.

Assessment of nearshore groundwater discharge to Lake Simcoe, Ontario and identification of regional hydrogeological controls 191
Wallace, H. and Robinson, C.E.

Constraining groundwater flow in Champlain Sea muds 203
Hinton M.J. and Alpay, S.

Stochastic hydrogeological modelling workflow in a glacial sedimentary basin, southern Ontario 217
Benoit, N., Marcotte, D., Molson, J.W., Bajc, A.F., and Russell, H.A.J.

A fully integrated groundwater–surface-water model for southern Ontario 231
Frey, S.K., Khader, O., Taylor, A., Erler, A.R., Lapen, D.R., Sudicky, E.A., Berg, S.J., and Russell, H.A.J.

Foreword

As program manager of the Groundwater Geoscience Program at the Geological Survey of Canada (GSC), Natural Resources Canada, it is my pleasure to introduce this summary report on the Southern Ontario Groundwater Project 2014–2019.

GSC Open File 8536 presents 20 contributions from researchers of the Geological Survey of Canada, the Ontario Geological Survey (OGS), academia, conservation authorities, and the private sector. The southern Ontario project was a key deliverable for the 2014–2019 Groundwater Geoscience Program cycle. The project marks a distinct change in program deliverables from individual aquifer studies to a large regional (>70,000 km^2) synthesis study. Contributions in this volume aim to fill knowledge gaps across various scales and geoscience subdisciplines identified in an OGS–GSC gap analysis at the start of the project. The project also completed a significant data compilation component of available geological and hydrogeological information in a rather large and complex geological setting, to facilitate current and future groundwater modelling.

This collection of public geoscience information provides new scientific knowledge and understanding of groundwater systems in southern Ontario, thus facilitating and enhancing improved groundwater resource management and protection.

I would like to thank all contributors involved in this publication, as well as our provincial, municipal, conservation authority, academic and private sector partners who made this project a success. I trust that readers will find the studies within this report of interest, and that they will assist in continued progress towards sustainable development of groundwater resources and water security for all users in southern Ontario.



Yves Michaud
Program Manager, Groundwater Geoscience Program
Geological Survey of Canada
Natural Resources Canada

2020-04-15

Introduction to the southern Ontario groundwater project 2014–2019: summary report

Hazen A.J. Russell* and Bruce A. Kjarsgaard

1. Introduction

The Groundwater Geoscience Program (GGP) of the Geological Survey of Canada (GSC), Natural Resources Canada (NRCan) conducts groundwater mapping and assessment activities with a focus on 30 key Canadian Aquifers (e.g., Jacob et al. 2015). These key aquifers are representative of different geological–hydrogeological contexts across Canada (e.g., Russell et al. 2011). Work had been completed by 2014 on 19 of the 30 key aquifers. Of the remaining eleven, three were located in southern Ontario: Upper Thames River, Grand River, and Credit River watersheds. After a decade of Source Protection work under the Clean Water Act (Ontario 2006); it was considered more appropriate and beneficial to approach southern Ontario groundwater geoscience from a regional perspective. This re-alignment at a regional scale followed recommendations in the 2013 GGP NRCan program review suggesting the need to re-evaluate approaches in light of new emerging issues (Evaluation 2013). Consequently, during the period 2014–2019 GGP undertook, in collaboration with the Ontario Geological Survey (OGS), a project with the objective of consolidating regional groundwater geoscience knowledge for southern Ontario. Specifically, by adapting a regional perspective, and aligning with multiple NRCan responsibilities, i.e. the USA and Canada International Joint Commission (IJC), the Great Lakes Water Quality Agreement (Annex 8 Groundwater) and the Ontario–Canada Agreement. Of particular significance and motivation were recommendations of Annex 8 (Grannemann and Van Stempvoort 2016) that identified the need to answer the question: What is the role and contribution of groundwater to the Great Lakes surface water. Development of the project scope and methods was also influence by a number of reviews on groundwater by the Council of Canadian Academies (2009, 2013). Notably the 2009 report which reviewed the question of sustainable management of Canada's groundwater resources. Finally, the collaborative OGS–GSC study was guided by the OGS gap analysis (Russell et al. 2015). The project thus set out to advance a number of issues of groundwater geoscience for the region, notably the development of a full three-dimensional (3-D) geological and hydrogeological numeric framework. Within that scope various local and regional studies were completed toward data consolidation, data management, data collection (geochemistry, geophysical) and analysis along with methods development. Much of the work completed within the project has been published as either data release Open Files, conference proceedings, or journal papers (e.g., Russell et al. 2018a; Conant et al. 2019; Li et al. 2019). Reference to much of this work has been documented at a project scale in Russell and Dyer (2016) and Russell (2018) along with the four annual workshops held collaboratively by the GSC, OGS, and Conservation Ontario (Russell and Priebe 2016; Russell et al. 2017a, 2018b, 2019).

The objective of this summary volume is to consolidate documentation of work in preparation, or published as data releases with limited interpretation provided. The document is organized by four key project themes: i) geological modelling, ii) geochemistry, iii) geophysics, and iv) hydrogeology. This introduction provides an overview context of the respective sections and work within each section will be previewed and placed in the context of the complete project work on that subject.

1.1 Collaborative Partners

To optimise resource allocation and project deliverables a formal collaboration was developed with the Ontario Geological Survey and their Groundwater Geoscience Initiative (e.g., Parker 2015; Russell and Dyer 2016; Schweyer 2016; Russell 2018; Simard 2017, 2018). Much of the OGS contribution continued to be focused on work of the OGS groundwater initiative and 3 specific activities: i) 3-D sediment mapping, ii) 3-D bedrock mapping, and iii) ambient groundwater chemistry. Three-dimensional sediment mapping was completed in Simcoe south (e.g., Bajc et al. 2019), Simcoe central (e.g., Mulligan 2018) and Niagara and Haldimand−Norfolk counties (e.g., Burt 2017). Three-dimensional bedrock mapping was advanced on the Silurian sequence stratigraphic framework

Geology Survey of Canada, Natural Resources Canada, 601 Booth Street, Ottawa, ON K1A 0E8

*corresponding author: hazen.russell@canada.ca

Recommended citation: Russell, H.A.J. and Kjarsgaard, B.A. 2020. Introduction to the southern Ontario groundwater project 2014–2019: summary report. In Russell, H.A.J. and Kjarsgaard, B.A. Eds. Southern Ontario groundwater project 2014–2019: summary report. Geological Survey of Canada, Open File 8536, 1-6. https://doi.org/10.4095/321079

(e.g., Sun et al. 2016). Additionally, progress advanced on the characterization of groundwater flow systems within Early Silurian rocks of the Niagara Escarpment cuesta (e.g., Priebe 2019). Work continued on a benchmark regional ambient groundwater chemistry study of southern Ontario (Hamilton 2015). The OGS also supported ongoing collection and development of shallow seismic reflection (e.g., Pugin et al. 2018) and downhole geophysics (e.g., Crow et al. 2017) data collection, and development of a regional chemostratigraphic framework (e.g., Russell et al. 2017b).

Formal partnerships were also developed for specific project components with Agriculture and Agrifoods Canada (AAFC), the Central Lake Ontario Conservation Authority (CLOCA), and the Moraine Coalition. The Oil Gas and Salt Resources Library was a key collaborator for development of the bedrock geological model. Informal collaborations with the Ministry of Environment Conservation and Parks (MECP) and the Ministry of Natural Resources and Forestry, particularly the Petroleum Resources Group were very beneficial. Collaboration was also exercised with individual academics at G360, and the universities of Guelph, Ottawa, Waterloo and Western. Most conservation authorities in southern Ontario contributed to the project in varying degrees, typically via sharing of Source Protection reports and supporting technical reports (e.g., Russell et al. 2017c).

2. Southern Ontario Context

The southern Ontario lowland region is defined as a sedimentary basin, covering 72,000 km^2 located within the Great Lakes watershed (e.g., Sharpe et al. 2014). It is bounded by Canadian Shield to the north and east, and three Great Lake (Ontario, Erie, and Huron), to the north, west and the south. The region is the economic heartland of Canada accounting for over 40% of the Canadian Gross Domestic Product. It contains one-third of the Canadian population and has the highest population density in the country. The Great Lakes cumulatively account for approximately 84% of North Americas available freshwater, forming the largest transboundary groundwater–surface-water resource between the USA and Canada (United States Environmental Protection Agency 2020). Ironically, given the availability of surface water there is highly significant reliance on groundwater for potable, commercial, and agricultural water uses. Approximately 3 million people use groundwater in Ontario, with the majority of these located in southern Ontario. Groundwater extraction by domestic systems support 1.3 million people, with an additional 1.9 million people utilizing municipal supplies (e.g., Waterloo, Cambridge, Guelph; Sharpe et al. 2014).

3. Summary Volume Overview

The content of this volume is structured under four principal subdisciplines with 4–6 contributions per section. The four sections are i) geological modelling, ii) geochemistry, iii) geophysics, and iv) hydrogeology.

3.1 Modelling

The six contributions in this section document the development of 3-D bedrock and surficial geology models, with four of the contributions on data capture and QA/QC. These regional 3-D models provide the first complete public domain models for the Phanerozoic geology (bedrock and surficial) of southern Ontario. The models provide the basis for reclassification of the geologic stratigraphy into a reduced hydrostratigraphic set of units, which were utilized for the numeric flow modelling presented in Frey et al. (2019; 2020, this vol.)

The 3-D Paleozoic bedrock geology model for southern Ontario is introduced by **Carter et al.** (2020, this vol.) and consists of 54 layers modelling 70 formations, plus Precambrian basement and overlying unconsolidated sediments. The model extends beneath the Great Lakes to the Canada–U.S.A. international border and covers 110,000 km^2. It captures the salient details of regional faults (e.g., the Electric fault), the Guelph pinnacle reefs, and minor bed offsets and geometry related to salt dissolution. Furthermore, it provides the first public domain and fully interactive geological model of the region (Russell et al. 2017d; Carter et al. 2019; Clark et al. 2019).

Extensive QA/QC was completed at the Ontario Oil and Gas Salt Resources Library (OGSRL) to correct uncertainties and errors identified in the data used for the modelling. **Clark et al.** (2020, this vol.) document this essential work, that improved data quality and provided consistency in the identification of many formation tops. The completion of the QA/QC at the OGSRL reinforces the value of robust data management and curation by the OGSR and the value this high-quality data has for future studies of subsurface geology.

To support a numeric groundwater flow model (Frey et al. 2019, 2020 this vol.) the depth of the interface/transition zone between the intermediate sulphur groundwater regime and the deep groundwater brine regime was mapped. **Carter and Sutherland** (2020, this vol.) use OGSRL records to document a regional depth transition at approximately 200 to 300 m below the top of bedrock. The interface boundary with deep brine approximates the base of groundwater interaction with surface water and this boundary can thus be used as a depth constraint for downward penetration of meteoric water.

In southern Ontario, thick surficial sediments typically overlie bedrock. **Logan et al.** (2020, this vol.) document a seven-layer surficial stratigraphic 3-D model for all of southern Ontario south of the Canadian Shield. This model, in contrast to the bedrock 3-D model, only extends to the shoreline of the Great Lakes (due to a paucity of data). The surficial 3-D model complements the work of Carter et al. (2019, 2020, this vol.) and supports the hydrostratigraphic classification

use for regional-scale groundwater flow modelling (Frey et al. 2019, 2020 this vol.)

To enhance the land surface digital elevation model and provide continuity beneath smaller navigable lakes bathymetric measurements were captured. **Griffiths et al.** (2020, this vol.) document the development of a machine learning application to capture geospatially registered hand written text for direct conversion into a vector GIS format. Using public domain Python script and Optical Character Recognition (OCR), a protocol was assembled for the capture of lake depth data from Canadian Hydrographic Service (CHS) field sheets.

The bathymetry of the Great Lakes is well defined, however, there is less certainty on the elevation of the bedrock surface beneath the Lakes, due to the unknown thickness of the overlying surficial sediments. **Todd et al.** (2020, this vol.) document the data rescue of legacy analogue (paper record) seismic reflection data from Lakes Ontario and Huron to support mapping sediment thickness and depth to bedrock. This data provides key constraints for the geological 3D modelling. This digital data set now allows for seismostratigraphic analysis, providing insight in to the deposition history of the lake sediments.

3.2 Geochemistry

The first of four contributions in this section documents a regional geochemistry dataset of soil horizon and till samples. The subsequent three papers sequentially address aspects of the subsurface geochemistry, analytical protocol development via portable XRF, and geochemistry of the Newmarket Till. Combined, these four papers provide both regional and detailed geochemical data sets that characterize the natural (background) geochemical state as well as regional variation both at the land surface and stratigraphically in the subsurface.

A regional low-density, reconnaissance scale sampling of paired soil A- and BC-horizons along with a proximally located C-horizon glacial till sample for multi-element geochemistry has been published by Sharpe et al. (2019). In this volume **Sharpe et al.** (2020) document the sample design and the baseline geochemistry across southern Ontario. Interpretation of these data reveal that regional-scale geochemical variation is largely derived from bedrock, with the impact of weathering and soil formation being less significant. This is the most comprehensive geochemical dataset for surficial sediments collected across southern Ontario that utilizes a standardized analytical protocol for each sample.

With a regional surface geochemical baseline complete, a significant question remained regarding subsurface stratigraphic geochemical variability. To develop a chemostratigraphic framework a cost effect analytical method was required to complete the number of necessary analyses. To address this challenge an analytical protocol for use of portable X-ray fluorescence (pXRF) was developed by **Knight et al.** (2020, this vol.) The use of pXRF resulted in the completion of approximately 4000 analysis from selected continuous cores, which documents the geochemical variability of these subsurface samples. To date, little subsequent interpretation has been completed on the chemostratigraphic dataset which have been published through numerous data releases.

Stepner et al. (2020, this vol.) document the spatial and stratigraphic variability in Newmarket Till geochemistry (laboratory ICP-MS) for series of boreholes located from Georgian Bay to Lake Ontario. A Provenance Indicator (P.I.) using the chemical ratio of Calcium plus Magnesium divided by Silica plus Aluminium ($CaO+MgO/SiO_2+ Al_2O_3$) indicates significant quantities of material from the Paleozoic carbonates occur in the till matrix. The sample analyses highlight geochemical variability due to source area, erosion potential, transport, and depositional processes that visual sedimentological core logging is unable to characterize.

A further study of Newmarket Till by **Kjarsgaard et al.** (2020, this vol.) investigated down-flow glacial dispersion along two detailed transects across the Canadian Shield–Paleozoic boundary north of Lake Ontario. Geochemistry and mineralogy analyses of the mud fraction, and pebble componentry provide the data required to elucidate the provenance of Newmarket Till and Dummer Moraines and their relationship to each other. This study highlights the rapid transition in till matrix and clast content when transitioning from Canadian Shield lithologies to Paleozoic carbonate rocks, and the geochemical complexities along different glacial flowlines.

3.3 Geophysics

Four papers in this section document geophysics studies and techniques, with three addressing aspects of a hydrogeophysics of the Vars–Winchester esker (near Ottawa) and one paper examining processing methods of passive Horizontal-to-Vertical Spectral Ratio seismic data.

Improved extrapolation methods of hydraulic properties are necessary to reduce uncertainty in modelling groundwater well-head protection and understanding of groundwater flow and solute transport. **Paradis et al.** (2020, this vol.) outline a general workflow to characterize hydraulic properties of unconsolidated aquifers from hydraulic and geophysical data using machine learning. It is challenging, however, to obtain adequate spatial coverage by conventional hydraulic characterization approaches. Within the context of this study, high-resolution seismic reflection, and resistivity data have been collected and are complemented by downhole geophysics and borehole hydraulic data.

Pugin et al. (2020, this vol.) document the collection and preliminary analysis of seismic profiles acquired using a novel GSC designed and fabricated microvibe seismic source and landstreamer two component (horizontal and vertical) geophone array. This has allowed for the acquisition of shear-wave signal and processing of high-resolution data

for surficial sediments and bedrock that can be integrated with borehole hydraulic data.

Crow et al. (2020, this vol.) document the downhole geophysical datasets for gamma, conductivity, magnetic susceptibility, density, and borehole magnetic resonance (BMR) logs from 4 boreholes. The BMR tool is a relatively new technique for small diameter groundwater wells that allows estimation of water content. These comprehensive downhole datasets are complemented by hydraulic testing within the same boreholes and are being integrated with adjacent geophysical transects and the hydraulic test data.

In groundwater studies data for estimation of depth to bedrock can be costly to obtain, or studies are reliant on archival datasets. **Dietiker et al.** (2020, this vol.) describe the use of ambient seismic noise and the Horizontal-to-Vertical Spectral Ratio (HVSR) analysis for estimation of depth to bedrock for two case studies in the Ottawa valley. The analysis highlights the complications introduced by variations in velocity, velocity inversions, and stratigraphic geometry, particularly as related to the peak frequency or period of a seismic resonator. This work provides a contextual understanding for interpretation and application of this technique.

3.4 Hydrogeology

The fourth and final section in the summary volume consists of six contributions related to soil moisture, water chemistry and hydrogeological modelling. It is organized from synoptic Remote Sensing methods, followed by two hydrogeochemical case studies and three groundwater modelling scenarios.

Soil moisture estimation is of critical interest for a range of water and land use practices that emerge during periods of drought. Existing remote sensing soil moisture datasets are limited by technology (passive vs active) and associated spatial resolution (~40 km vs ~1 km). **Li et al.** (2020, this vol.) provide a methodology to downscale coarse passive L-band radar signal of the Soil Moisture Active Passive (SMAP) data using multi-temporal C-band Radarsat Constellation Mission (RCM) compact polarimetric (CP) SAR data. The model is tested in southern Ontario to downscale 36 km resolution SMAP soil moisture to 1 km scale. This downscaled data is suitable for use at the scale of large agricultural tracts and able to exploit the high-frequency (<4 day) revisit time of the recently launched Radarsat Constellation Mission in 2019.

Groundwater represents an important source of water for agriculture in the Innisfil Creek watershed, and recent drought conditions have highlighted the vulnerability to periods of reduced precipitation. **Proteau-Bedard et al.** (2020, this vol.) report on a hydrogeochemical study designed to reduce the uncertainties regarding groundwater flow patterns. Improved understanding will support a more robust plan for sustainable groundwater use. This contribution documents survey design and early data classification to support a geochemistry and stable (oxygen) isotopic study.

Identifying the location of groundwater discharge to lakes and rivers is a challenge that is particularly critical in understanding recharge and discharge pathways. **Wallace and Robinson** (2020, this vol.) quantify the spatial variability and the volume of direct nearshore groundwater discharge in a study from Lake Simcoe. They evaluate linkages between the observed spatial distribution of groundwater discharge and regional hydrogeological features. Nearshore groundwater discharge was quantified using the naturally occurring radon isotope tracer ^{222}Rn collected from a small boat survey conducted along 80% of the Lake Simcoe shoreline. The spatial variability in direct nearshore groundwater discharge to Lake Simcoe was estimated.

In the first of three modelling papers **Hinton and Alpay** (2020, this vol.) use a one-dimensional groundwater transport model to match the distribution of chloride ion concentrations measured in pore water from Champlain Sea muds within a continuously sampled core from an ~80 m deep borehole. For the zone of measured peak chloride concentration, the model results suggest that pore water salinity remains at 98% of the modelled initial Champlain Sea water signature. Chloride concentrations decrease to fresh water values both above and below the position of the maximum concentration.

Most geological and hydrogeological modelling is deterministic, with limited stochastic modelling undertaken. **Benoit et al.** (2020, this vol.) explore and assess the uncertainty related to geological heterogeneity in regional groundwater flow models. A stochastic approach is adopted in which the hydrostratigraphic architecture and respective hydrofacies variability directly controls the three-dimensional hydraulic conductivity (K) field. The performance of the workflow is illustrated using a case study in Innisfil Creek watershed of southern Ontario. Results highlight the efficiency of the method in assessing model uncertainties and the impact on regional groundwater flow models.

A major question emerging from Annex 8 of the Great Lakes Water Quality Agreement (Grannemann and Van Stempvoort 2016) is the partitioning of groundwater flow to the Great Lakes, whether via stream baseflow or discharge along shorelines and within the Great Lakes. Following a feasibility review and data support survey (Frey et al. 2016) a prototype model for southern Ontario was developed. **Frey et al.** (2020, this vol.) document the three-dimensional, physics-based fully coupled groundwater–surface-water model solution. The model domain encompasses 109,565 km^2 of southern Ontario with extension into the Great Lakes. The model has been tested for its ability to reproduce average monthly surface-water flow rates and groundwater levels, and its sensitivity to spatial and temporal resolution. Results to-date demonstrate the utility of a regional scale, fully integrated hydrologic model for investigating water resources issues of southern Ontario.

4. Summary

This volume consolidates information on four core components of the southern Ontario groundwater geoscience project: geological modelling, geochemistry, geophysics, and hydrogeology. The summary volume is not a comprehensive review of the project or project publications. It is an attempt to capture aspects of work that may have otherwise been released as individual publications and lacked context and/or were difficult to specifically identify with the Southern Ontario Groundwater Project. This collaborative initiative with the Ontario Geological Survey has contributed to a number of regional groundwater geoscience datasets and initiatives (e.g., Pugin et al. 2018; Deitiker et al. 2019; Crow et al. 2019). A particularly noteworthy aspect of the project is the data support that can be framed within the regional numeric bedrock geology (Carter et al. 2020), surficial geology (Logan et al. 2020), and physically based groundwater–surface-water models (Frey et al. 2020).

5. Acknowledgements

Contributions from numerous individuals at conservation authorities, municipalities, universities and government ministries and departments is much appreciated. An internal review at the GSC by R. Knight helped clarify the text. Funding for this work was provided by the Ontario Geological Survey, Agriculture and Agrifoods Canada, the Central Lake Ontario Conservation Authority and at Natural Resources Canada the Climate Change Impacts and Adaptation Secretariat, Climate Change Geoscience Program and Groundwater Geoscience Program. This work is a contribution to the GSC–OGS southern Ontario project on groundwater 2014–2019.

6. References

Bajc, A.F., Mulligan, R.P.M. and Dodge, J.E.P. 2019. Three-dimensional mapping of surficial deposits in the southern part of the County of Simcoe, south-central Ontario. Ontario Geological Survey, Groundwater Resources Study 18.

Burt, A.K. 2017. 24. Project Unit 13-018. Digging Deep on the Niagara Peninsula: A Drilling Update. In Summary of Field Work and Other Activity 2017. Ontario Geological Survey Open File Report 6333, 24–1 to 24–16.

Carter, T.R., Brunton, F.R., Clark, J.K., Fortner, L., Freckelton, C., Logan, C.E., Russell, H.A.J., Somers, M., Sutherland, L., and Yeung, K.H. 2019. A three-dimensional geological model of the Paleozoic bedrock of southern Ontario. Geological Survey of Canada, Open File 8618. https://doi.org/https://doi.org/10.4095/315045

Clark, J.K., Dupont, M.A., Logan, C.E., Russell, H.A.J., Carter, T.R., and Brunton, F.R. 2019. A first look at Ontario's geology in virtual reality. Geological Survey of Canada, Scientific Presentation 110, 2019; 8:56 min. https://doi.org/10.4095/321103

Conant, B., Robinson, C.E., Hinton, M.J., and Russell, H.A.J. 2019. A framework for conceptualizing groundwater-surface water interactions and identifying potential impacts on water quality, water quantity, and ecosystems. Journal of Hydrology, 574: 609–627. https://doi.org/https://doi.org/10.1016/j.jhydrol.2019.04.050

Council of Canadian Academies. 2009. The Sustainable Management of Groundwater in Canada. Ottawa. The Expert Panel on Groundwater. https://cca-reports.ca/wp-content/uploads/2018/10/2009-05-11-gw-report.pdf

Council of Canadian Academies. 2013. Water and Agriculture in Canada: Towards Sustainable Management of Water Resources. The Expert Panel on Sustainable Management of Water in the Agricultural Landscapes of Canada. https://cca-reports.ca/wp-content/uploads/2018/10/wag_fullreporten.pdf

Crow, H.L., Olson, L.C., Mulligan, R.P.M., Cartwright, T.J., and Pugin, A.J.-M. 2017. Downhole geophysical logs in Quaternary sediments of central Simcoe County, southern Ontario. Geological Survey of Canada, Open File 8251. https://doi.org/10.4095/302783

Dietiker, B., Pugin, A.J.-M., Burt, A., Crow, H.L., Cartwright, T., and Brewer, K. 2019. High-resolution seismic reflection profiles for groundwater studies in the Niagara Peninsula region, Ontario. Geological Survey of Canada, Open File 8561. https://doi.org/10.4095/314730

Evaluation. 2013. Evaluation of the Groundwater Geoscience Program. Natural Resources Canada. https://www.nrcan.gc.ca/evaluation/reports/2013/11142 (accessed 2020-03-20)

Frey, S.K., Berg, S.J., and Sudicky, E.A. 2016. A Feasibility Study of Merits and Development Strategies for a Regional Water Resources Modelling Platform for Southern Ontario – Great Lakes Basin. Geological Survey of Canada, Open File 8021. https://doi.org/10.4095/298816

Frey, S.K., Khader, O., Taylor, A., Erler, A.R., Lapen, D.R., Sudicky, E.A., Berg, S.J., Russell, H.A.J. 2019. A fully integrated groundwater-surface-water model for southern Ontario: proof-of-concept and data release. Geological Survey of Canada, Open File 8639. https://doi.org/10.4095/321042

Grannemann, G. and Van Stempvoort, D. (Eds.) 2016. Groundwater science relevant to the Great Lakes Water Quality Agreement: A status report. Prepared by the Annex 8 Subcommittee for the Great Lakes Executive Committee, Final version, May, 2016. Published (online) by Environment and Climate Change Canada and U.S. Environmental Protection Agency. https://binational.net/wp-content/uploads/2016/09/PRP-160927-EN.pdf

Hamilton, S.M. 2015. Ambient groundwater geochemistry data for southern Ontario, 2007–2014. Ontario Geological Survey, Miscellaneous Release—Data 283–Revised.

Jacob, N., Michaud, Y., Russell, H.A.J., Rivera, A., and Brodaric, B. 2015. Natural Resources Canada 3rd National Workshop on Groundwater. Geological Survey of Canada, Open File 7857, 21 p. doi:10.4095/296668

Li, J., Wang, S., Michel, C., and Russell, H.A.J. 2020. Surface deformation observed by InSAR shows connections with water storage change in Southern Ontario. Journal of Hydrology Regional Studies, 27: 100661. https://doi.org/https://doi.org/10.1016/j.ejrh.2019.100661

Mulligan, R.P.M. 2018. 25. Project Unit 14-015. Last Phase of Subsurface Data Collection for Three Dimensional Mapping in the Central Part of the County of Simcoe, Southern Ontario. Summary of Field Work and Other Activity 2018, Ontario Geological Survey Open File Report 6350, 25–1 to 25–10.

Ontario. 2006. Clean Water Act, 2006, S.O. 2006, c. 22. https://www.ontario.ca/laws/statute/06c22

Parker, J.R. 2015. 2. Earth Resources and Geoscience Mapping Section: 2015 Program and Project Overview. Summary of Field Work and Other Activity 2015, Ontario Geological Survey Open File Report 6313, 1–1 to 1–10.

Priebe, E.H. 2019. Investigating new approaches for mapping groundwater systems in karstic carbonate bedrock: A case study in the Early Silurian formations of the Niagara Escarpment cuesta, southern Ontario, Canada. University of Waterloo, PhD., 154 p.

Pugin, A.J.-M., Dietiker, B., Mulligan, R.P.M., Crow, H.L., Brewer, K., Cartwright, T., Rainsford, D.R.B., Bajc, A.F., Sharpe, D.R., and Russell, H.A.J. 2018. High-resolution seismic reflection profiles for groundwater studies in Simcoe County, southern Ontario. Geological Survey of Canada, Open File 8383. https://doi.org/10.4095/308388

Russell, H.A.J. 2018. 27. Update on Geological Survey of Canada Activities in 2017–2018 Related to the Ontario Geological Survey Groundwater Collaboration in Southern Ontario. In Summary of Field Work and Other Activity, 2018. Ontario Geological Survey Open File Report 6350, p.27-1 to 27–12.

Russell, H.A.J. and Dyer, R.D. 2016a. 35. Ontario Geological Survey–Geological Survey of Canada Groundwater Geoscience Collaboration: Southern Ontario 2015–2019. Summary of Field Work and Other Activity, 2016. Ontario Geological Survey Open File Report 6323, p.35-1 to 35-15.

Russell, H.A.J. and Priebe, E.H. (comp.) 2016b. Regional-Scale Groundwater Geoscience in Southern Ontario: An Ontario Geological Survey and Geological Survey of Canada Groundwater Geoscience Open House. Geological Survey of Canada, Open File 8022, 34 p. https://doi.org/10.4095/297722

Russell, H.A.J., Sharpe, D.R., and Cummings, D.C. 2011. Sediment-aquifer play types in a list of 30 key Canadian aquifers. In: Geohydro 2011, Proceedings of the Joint Meeting of the CANQUA and International Association of Hydrogeologists. 1–8.

Russell, H.A.J., Priebe, E.H., and Parker, J.R. 2015. Workshop Summary and Gap Analysis Report: Unifying Groundwater Science in Southern Ontario. Ontario Geological Survey, Open File Report 6310, 64 p.

Russell, H.A.J., Ford, D., and Priebe, E.H. (comp.) 2017a. Regional-scale Groundwater Geoscience in Southern Ontario: an Ontario Geological Survey, Geological Survey of Canada, and Conservation Ontario Geoscientists open house. Geological Survey of Canada, Open File 8212, 56 p. https://doi.org/10.4095/299750

Russell, H.A.J., Bajc, A.F., Knight, R.D., and Stepner, D. 2017b. 30. A Surficial Sediment Chemostratigraphic Framework for Southern Ontario. In Summary of Field Work and Other Activity 2017. Ontario Geological Survey Open File Report 6333, 30-1 to 30-11.

Russell, H.A.J., Baranova, N., Crow, H.L., Cummings, D.I., Logan, C.E., McBride, A., Pugin, A.J-M. and Sharpe, D.R. 2017c. Building a geological framework to support regional groundwater management: Data capture, consolidation and reclassification in southern Ontario. In Summary of Field Work and Other Activities, 2017. Ontario Geological Survey, Open File Report 6333, 29-1 to 29-9.

Russell, H.A.J., Brodaric, B., Brunton, F.R., Carter, T., Clark, J., Logan, C.E., and Sutherland, L. 2017d. Communicating 3D geological models to a broader audience: a case study from southern Ontario. Geological Survey of Canada, Scientific Presentation 68: 3:36 min. https://doi.org/10.4095/305363

Russell, H.A.J., Arnaud, E., Bajc, A.F., and Sharpe, D.R. (eds.) 2018a. Quaternary geology of southern Ontario and applications to hydrogeology / Géologie quaternaire du sud de l'Ontario et applications à l'hydrogéologie, Canadian Journal of Earth Sciences. NRC Research Press. https://doi.org/10.1139/cjes-2017-0090

Russell, H.A.J., Ford, D., Priebe, E.H., and Holysh, S. (comp.) 2018b. Regional-scale groundwater geoscience in southern Ontario: an Ontario Geological Survey, Geological Survey of Canada, and Conservation Ontario Geoscientists open house. Geological Survey of Canada, Open File 8363, 62 p. https://doi.org/10.4095/306472

Russell, H.A.J., Ford, D., Holysh, S., and Priebe, E.H. 2019. Regional-scale groundwater geoscience in southern Ontario: an Ontario Geological Survey, Geological Survey of Canada and Conservation Ontario Geoscientists open house. Geological Survey of Canada, Open File 8528 (also Ontario Geological Survey, Open File Report 6349) 46 p. https://doi.org/10.4095/313529

Schweyer, J.E. 2016. 2. Earth Resources and Geoscience Mapping Section: 2016 Program and Project Overview. Summary of Field Work and Other Activity 2016. Ontario Geological Survey Open File Report 6323 2–1 to 2–21.

Sharpe, D.R., Piggott, A., Carter, T., Gerber, R.E., MacRitchie, S.M., de Loë, R.C., Strynatka, S., and Zwiers, G. 2014. Chapter 12 Southern Ontario hydrogeological region. In Rivera, A. Ed. Canada's Groundwater Resources. Fitzhenry & Whiteside, 443–499. https://doi.org/10.4095/296947

Sharpe, D.R., Klassen, R.A., Russell, H.A.J., Brennand, T.A., Dexter, K., Logan, C.E, and Stepner, D.A.J. 2019. Regional geochemical survey of earth materials in southern Ontario: a geochemical baseline for environmental and human health protection. Geological Survey of Canada, Open File 8452, 38 p. https://doi.org/10.4095/308373

Simard, R.-L. 2017. 4. Earth Resources and Geoscience Mapping Section: 2017–2018 Program and Projects Overview. Summary of Field Work and Other Activity 2017. Ontario Geological Survey Open File Report 6333, 4–1 to 4–29.

Simard, R.-L. 2018. 4. Earth Resources and Geoscience Mapping Section: 2018–2019 Program and Projects Overview. Summary of Field Work and Other Activity 2018. Ontario Geological Survey Open File Report 6350, 4-1 to 4-28.

Sun, S., Brunton, F.R., and Jin, J. 2016. 26. Project Unit 14-034. The Silurian–Devonian Unconformity in Subsurface and Outcrop of Southwestern Ontario. Summary of Field Work and Other Activity 2018. Ontario Geological Survey Open File Report 6323, 26–1 to 26–16.

United States Environmental Protection Agency. 2020. Facts and Figures about the Great Lakes. (accessed 2020-04-02). https://www.epa.gov/greatlakes/facts-and-figures-about-great-lakes

Three-dimensional geological modelling of the Paleozoic bedrock of southern Ontario: Status update

Terry R. Carter[1]*, Frank R. Brunton[2], Jordan K. Clark[3], Lee Fortner[4], Charles E.Logan[5], Hazen A.J. Russell[5], Maia Somers[4], Liz Sutherland[3,6], and Kei H. Yeung[2]

Abstract: A regional 3-D lithostratigraphic model of the Paleozoic bedrock of southern Ontario was completed in 2019. The model encompasses the entire Phanerozoic succession of southern Ontario (110,000 km^2), comprised of over 1,400 m of sedimentary strata straddling regional arches/forebulge zones separating the Appalachian Foreland Basin from the Michigan Structural Basin. This ambitious initiative provides an unprecedented regional 3-D perspective and digital framework and is amenable to numeric modelling of groundwater flow. Conversion to a 3-D hydrostratigraphic model is a future initiative.

Model construction is guided by an updated regional lithostratigraphic chart, and utilizes Leapfrog® Works – an implicit modelling application. There are 54 modelled Paleozoic bedrock layers representing 70 formations, plus the Precambrian basement, plus overlying unconsolidated sediments. Borehole records in Ontario's public petroleum well database (www.ogsrlibrary.com) are the principal data source, supplemented by Ontario Geological Survey (OGS) deep boreholes. A newly revised digital bedrock topography surface combined with revised subcrop geology and digitized 3-D surface polyline and point constraints are used to better align the modelled layers and their extrapolation to the subcrop surface. The modern topographic surface is integrated using Shuttle Radar Topography Mission (SRTM) DEM data, National Oceanic and Atmospheric Administration (NOAA) lake bathymetry and Canadian Hydrographic data for smaller lakes.

Model development is an iterative cycle of interim modelling, expert geological appraisal, and QA/QC editing of geological data using geophysical logs, drill cuttings, and core, supplemented by manual editing of model layers. From 2015 to 2018, project geologists and geological contract staff of the Oil, Gas and Salt Resources Library completed edits to 30,320 formation tops in a total of 7,490 wells, resulting in a revised dataset and improvements to the petroleum well database. The current and final model (iteration 7) provides a geologically robust representation of regional bedrock geology.

1. Introduction and objectives

Paleozoic bedrock underlies all of southwestern Ontario and the southern region of south-central Ontario. Bedrock heterogeneity constrains and controls penetration of meteoric water into the subsurface and the lateral movement of groundwater. Consequently, management of groundwater for agricultural, industrial, municipal, and domestic supply is enhanced by an improved understanding of the geology and hydrogeology, specifically the connectivity and continuity of bedrock strata, from subcrop into the deep subsurface. Improved geologic knowledge and mapping of these rocks also supports natural resource extraction (e.g., water, gypsum, salt, gas, oil, aggregate), site selection for nuclear waste disposal (Ontario Power Generation 2017), exploitation of geothermal energy, and sustainable waste disposal.

The Ontario Geological Survey (OGS) and the Geological Survey of Canada (GSC) are working under a collaborative initiative to advance knowledge of regional groundwater

[1] Consulting Geologist, Cartergeologic, London, ON N6K 3P4
[2] Earth Resources and Geoscience Mapping Section, Ontario Geological Survey, Sudbury, ON P3E 6B5
[3] Oil Gas and Salt Resources Library, London, ON N6E 1L3
[4] Ministry of Natural Resources and Forestry, London, ON N6E 1L3
[5] Geology Survey of Canada, Natural Resources Canada, 601 Booth Street, Ottawa, ON K1A 0E8
[6] University of Western Ontario, Western Libraries, Map & Data Centre, London, ON
*corresponding author: terry.carter@cartergeologic.com

Recommended citation: Carter, T.R., Brunton, F.R., Clark, J.K., Fortner, L., Logan, C.E., Russell, H.A.J., Somers, M., Sutherland, L., and Yeung, K.H. 2020. Three-dimensional geological modelling of the Paleozoic bedrock of southern Ontario: Status update. In Russell, H.A.J. and Kjarsgaard, B.A. Eds. Southern Ontario groundwater project 2014–2019: summary report. Geological Survey of Canada, Open File 8536, 7-21. https://doi.org/10.4095/321080

geoscience in Ontario. The present study is focussed on the development of a three-dimensional (3-D) bedrock geological and hydrogeological model of the region (Frey et al. 2019). This robust 3-D lithostratigraphic model is a new interpretation of previous work and all relevant geological data. Defining the fundamental physical and structural controls on occurrence and movement of water within the bedrock formations of southern Ontario is a necessary precursor for future development of a hydrostratigraphic model. This work is being completed in collaboration with the Ontario Ministry of Natural Resources and Forestry (MNRF) and the Oil, Gas and Salt Resources Library, London, Ontario (OGSRL). A parallel project to model the geology and hydrogeology of the overlying unconsolidated surficial sediment is also underway (Russell et al. 2016). Conversion of the lithostratigraphic model to a hydrostratigraphic model as described by Seaber (1988) and Maxey (1964) is a future initiative.

This report documents iterative geological model development, data sources, quality assurance and control (QA/QC), and plans for model delivery and applications. Information in previous reports and presentations (Russell et al. 2015; Russell and Dyer 2016; Carter et al. 2016, 2017; Russell et al. 2017) are superseded by this document. It is supported by and complementary to, reports on QA/QC (Davis 2017), data capture (Clark et al. 2020), and hydrochemical groundwater regimes (Carter and Sutherland 2018, 2020)

1.1 Project coordination

Project direction and coordination was provided by Terry Carter and Hazen Russell. Team meetings were held by teleconference every two months with discussion of project tasks, priorities, achievements and milestones, review of new model versions, and assignment of action items. These meetings included written agendas and recorded minutes. Informal telephone liaison took place between meetings. Annual one to two-day groundwater workshops were hosted by the OGS, GSC, and Conservation Ontario at the Delta Hotel in Guelph at which team members made presentations on progress of the project. Written progress reports were prepared and published by the OGS and GSC (Russell et al. 2016; Russell and Dyer 2016; Carter et al. 2016, 2017; Russell et al. 2017)

1.2 Project area

The project area encompasses all the contiguous Paleozoic sedimentary rocks underlying southern Ontario west of the Frontenac Arch and south of the exposed Precambrian Canadian Shield, an area of approximately 110,000 km^2. The area extends beneath the waters of the Great Lakes (Huron, Erie, Ontario, St. Clair) to the international boundary with the United States, and to the subcrop edge of these strata beneath the waters of Georgian Bay (Figure 1). Manitoulin Island is not included in the study area. Stratigraphically, the project encompasses the complete Paleozoic sedimentary succession and includes the interface with the Precambrian crystalline basement rocks of the Canadian Shield (Figure 2). Above the bedrock erosional surface, the unconsolidated surficial sediments are included in the model as a single layer.

The maximum elevation of the model is 546 m above sea level (asl) along the Niagara Escarpment. The maximum thickness from drift to top of Precambrian is 1,639 m near the U.S. border in Lake Huron, including over 1,500 m of Paleozoic bedrock. The model depth extends to an arbitrary elevation of -2,000 masl within the Precambrian.

1.3 Previous work

In the deeper Paleozoic geological formations, a conceptual model of a regional study area centred on the Bruce nuclear generating station at Tiverton has been developed (Nuclear Waste Management Organization 2011; Hobbs et al. 2011; Itasca and AECOM 2011) and used as the basis for a numerical groundwater model for the same area (Sykes et al. 2011). Two-dimensional geological and hydrogeological models for the Paleozoic strata of southern Ontario have also been developed (Brunton and Dodge 2008; Brunton 2009a; Carter 2012; Carter and Fortner 2012; Carter et al. 2014; Sharpe et al. 2014).

2. Geological and hydrogeological setting southern Ontario

South of the exposed Canadian Shield, southern Ontario bedrock comprises marine sedimentary rocks of the northern Appalachian foreland basin and eastern Michigan structural basin (Brunton et al. 2012), which straddle a broad northeast-oriented basement structural high, the Algonquin Arch and its southwestern extension, the Findlay Arch. These sedimentary strata unconformably overlie the crystalline metamorphic, igneous, and metasedimentary rocks of the Canadian Shield, all of which are often covered by a veneer of unconsolidated surficial sediments of variable thickness. Bedrock strata consist of an interlayered succession of sandstones, carbonates, evaporites, shales, and siltstones. The bedrock formations dip to the southwest at 3 to 6 m/km along the crest of the Algonquin and Findlay arches into a structural low, the Chatham Sag, and at 3 to 12 m/km down the flanks of the arches westward into the Michigan structural basin and southward into the Appalachian foreland basin (Armstrong and Carter 2010) (see Figure 1).

The Niagara Escarpment is a natural hydrological and hydrogeological divide that separates the study area into two sections (Figures 3A, 3B), east and west of the escarpment. The Paleozoic section is much thicker to the west of the Escarpment, ranging from 540 m to nearly 1,400 m in the Chatham Sag, and range in age from late Cambrian to late Devonian and possibly early Mississippian (Armstrong and Carter 2010; Carter et al. 2017) (Figure 2). To the east of the Escarpment, strata range in age from late Cambrian to late Ordovician in age, due to erosional removal of all younger

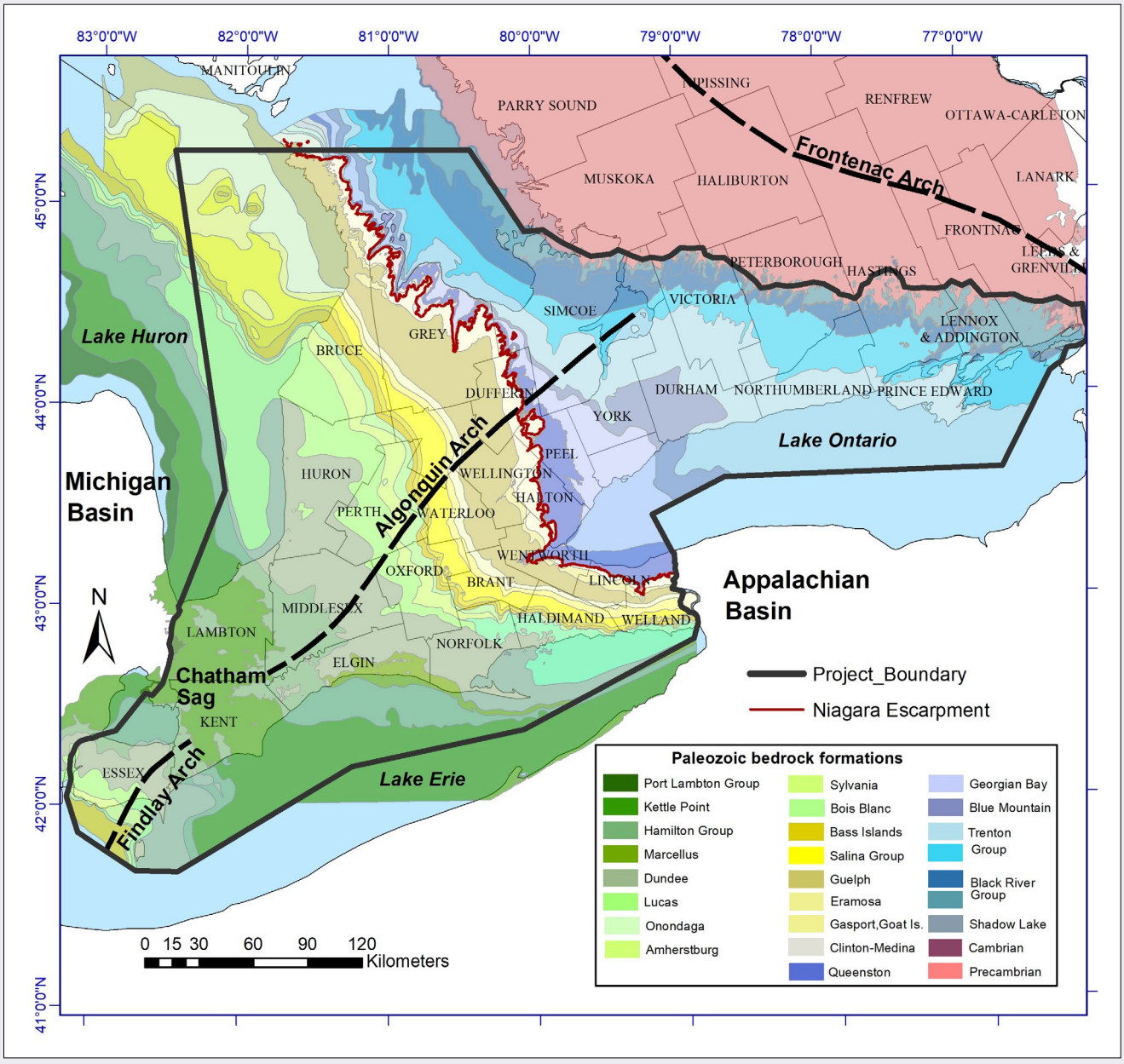


Figure 1. Bedrock geology and project boundary of model area. The Niagara Escarpment forms a hydrogeologic boundary between the east and west portions of the study area.

formations. Maximum thickness of Paleozoic strata to the north and east of the Escarpment is 650 m at the Niagara River and 250 m on the south shore of Georgian Bay, thinning northeasterly to zero at the erosional edge in eastern Ontario (Armstrong and Carter 2010).

The bedrock surface is a low-relief angular unconformity resulting from subaerial exposure and erosion of the slightly inclined Paleozoic strata over an extended period of geologic time. This surface is an important hydrogeological feature, forming the recharge area where dipping bedrock is exposed at surface, as well as the interface between the fresh water-dominated unconsolidated surficial sediments and the relatively less permeable and less porous sedimentary bedrock in the subsurface. This contact, or interface aquifer zone, is the most widespread potable water aquifer in southern Ontario (Husain et al. 2004; Brunton 2009a, b; Carter 2012), and occurs at this variably karstic boundary beneath large parts of southern Ontario (Carter and Clark 2018).

Extensive modern karstic dissolution has occurred in areas of thin surficial sediments where carbonate rocks form the

uppermost bedrock layer (Brunton and Dodge 2008; Brunton et al. 2016). These karstic strata form a complex shallow system of potable water down to 250 m below the surface that is the subject of ongoing investigations by the OGS (Brunton et al. 2016).

In areas of thicker surficial sediment and areas underlain by shale, wells that penetrate the bedrock more than a few metres encounter groundwater that is brackish to saline and locally sulphurous. Conceptual modelling based on petroleum well data and geochemical and isotopic analyses has documented an intermediate to deep system of thick regional aquitards and thin confined aquifers containing brackish to highly saline water within the bedrock (Nuclear Waste Management Organization 2011; Hobbs et al. 2011; Carter 2012; Carter and Fortner 2012; Carter et al. 2014; Sharpe et al. 2014; Skuce 2015; Skuce et al. 2015a, b; Carter et al. 2016). The brackish to saline water containing dissolved H_2S occurs at intermediate depths, from 30 to 350 m, overlapping with a deep brine regime that contains no dissolved H_2S and begins at depths greater than 200 m (Carter and Sutherland 2018).

3. Conceptual model development

Development of a 3-D model that reliably represents geology requires a multidisciplinary team of expert and experienced professionals.

In the initial stages of the project, the project geologists visualized the 3-D geology by combining the geological knowledge gathered from publications and reports on conventional geological outcrop mapping, subsurface geological maps and cross-sections based on data from wells and boreholes, and their own knowledge and experience. This expert conceptual knowledge is essential in identifying shortcomings and inaccuracies while building and editing iterative versions of the model that incorporate this knowledge.

3.1 Lithostratigraphic chart

A fundamental requirement for geologic modelling is definition of the model bedrock layers. For the 3-D bedrock modelling project the primary model layers are the Paleozoic bedrock formations of southern Ontario, and the unsubdivided surficial sediments. Lithostratigraphic subdivisions were initially based on Armstrong and Carter (2010). All stratigraphic units are colour-coded by lithology, including salt, shale, sandstone, argillaceous limestone, limestone, organic-rich carbonate, and dolostone.

Revisions and updates to the lithostratigraphic chart by project geologists (Frank Brunton, Terry Carter, Lee Fortner) were based largely on recent work by the OGS (Brunton 2009b; Brunton and Brintnell 2011; Cramer et al. 2011; Brunton et al. 2012; Bancroft et al. 2016; Sun et al. 2017; Brunton et al. 2017; Armstrong 2017, 2018). Revisions and updates to terminology included reassignment of the Amabel Formation to the Irondequoit and Lions Head formations of the Clinton Group and the Gasport Formation and Niagara Falls member of Goat Island Formation of the Lockport Group. The Eramosa Member was elevated to formation status within the Lockport Group (Brunton 2009b; Cramer et al. 2011; Brunton et al. 2012). Strata previously referred to as the Reynales Formation actually constitute the younger Fossil Hill/Merriton formations and the Rockway Formation. The true Reynales Formation is present at the Niagara Gorge in Ontario but is generally not present to the west and northwest of Thorold area. The Merritton Formation is equivalent to the upper (informal) member of the Fossil Hill Formation (Brunton et al. 2009), inferring significant tectonic cut-down of almost 100 m of strata from Manitoulin Island to Niagara Falls (Brintnell et al. 2009). In the Niagara Peninsula improved mapping and interpretation of stratigraphic relationships of the Middle Devonian Onondaga Formation and Detroit River Group has been completed by Sun (2018) and Sun et al. (2017).

Of particular importance for future hydrostratigraphic modelling are improved detail and accuracy in identification and representation of depositional and erosional disconformities and unconformities (Brunton et al. 2017). Enhanced porosity and permeability in paleokarst in carbonate rocks at these surfaces (Smith et al. 1988; Carter et al. 1994; Brunton and Dodge 2008; Brunton 2008; Carter 2012; Carter et al. 2014) are spatially associated with sequence stratigraphic breaks, which are amongst the most significant controls on the occurrence of regional bedrock hydrological flow zones in the subsurface bedrock formations of southern Ontario (Brunton et al. 2007; Brunton 2008, 2009a, b; Brunton et al. 2012; Carter et al. 2014; Banks and Brunton 2017).

Orientation of the Paleozoic stratigraphic chart (Figure 2) from southwest (left) to northeast (right) was chosen to display regional dip, and lateral changes in facies, depth, and thickness from southwest to northeast, with five columns representing different geographic areas in southern Ontario (Brunton et al. 2017). Cumulative strata thickness ranges from over 1,400 m to zero from left to right, southwest to northeast. Importantly, it illustrates the erosional profile of the Paleozoic strata and regional nature of the carbonate-capped cuestas and associated escarpment cliffs that form the subcrop edges of the stratigraphy (see Hewitt 1971; Brunton 2009a; Brunton et al. 2017). The erosional edges of the strata, especially the Silurian Lockport Group stacked dolostones that form the Niagara Escarpment, are hydrogeologically significant because the ground elevations and current position of the erosional scarp influence the regional hydrology resulting in significant precipitation occurring in the uplands and the establishment of regional potable groundwater flow systems (<200 m deep) in karstic carbonates (Brunton et al. 2007; Brunton 2009a, b; Brunton and Brintnell 2011; Brunton et al. 2012; Brunton et al. 2017; Carter and Clark 2018). The updip subcrop/outcrop edges of the strata are also sites for

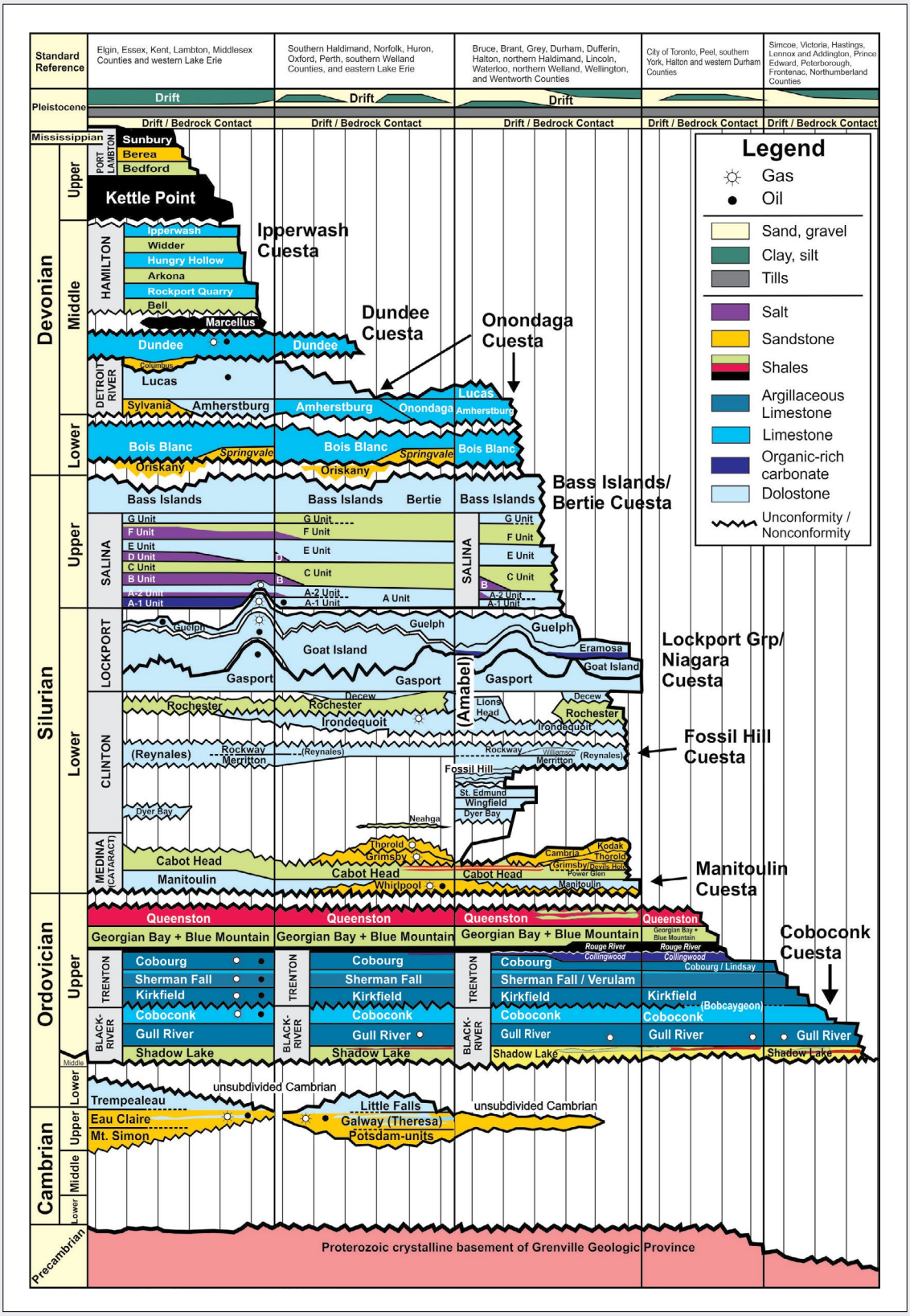


Figure 2. Revised lithostratigraphic chart of the Paleozoic bedrock strata of southern Ontario, from Brunton et al. (2017).

downdip infiltration of meteoric water into the subsurface where it accentuates pre-glacial and glacially-enhanced horizontal paleokarst flow zones.

4. Data sources

A number of datasets relevant to, and necessary for, model generation were identified (Table 1) and compiled, incorporating the most relevant and up-to-date data. Details on data capture and compilation, enhancements, and QA/QC activities completed at the Oil Gas and Salt Resources Library are provided in an accompanying paper in this volume (Clark et al. 2020).

4.1 Petroleum well records

Petroleum well records of the Ontario Petroleum Data System (OPDS) are the primary data set used for modelling formation layers in the subsurface of southern Ontario. OPDS is a custom Oracle database designed and maintained by MNRF for managing data collected from the drilling and operation of petroleum wells in the province of Ontario (e.g., Carter and Castillo 2006). The digital data is sourced from hard copy well files collected and maintained by the MNRF. OPDS contains records associated with approximately 26,950 wells, with top depth and elevation values for nearly 300,000 unique formation picks (Figures 2, 3A). Geographic co-ordinates are available for all wells, although at varying levels of accuracy. Additional data includes collection and submission records of drill core and cuttings, drill core analyses, formation water analyses, geophysical logs, and oil/gas/water interval data recorded while drilling.

3-D modelling of formation layers would not have been feasible without the OPDS data. The initial task of data compilation and database construction for the 3-D model was greatly

Table 1. Primary data sources for lithostratigraphic modelling.

Data Set	Description	Application
OPDS database	26,952 petroleum well records with 300,000 formation tops, MNRF/Library	Primary data for model layer interpolation
Library	Drill cuttings 11,000 wells, well files, drill core 1,014 wells, geophysical logs >20,000	QA/QC
Bedrock geology maps	Armstrong and Dodge (2007), GSC 1335A (Sanford and Baer 1971), GSC 1263a (Sanford 1969), Sun (2018), Armstrong (2017, 2018)	Constrain extrapolation from subsurface to subcrop
Digital bedrock geology map	Revision of Armstrong and Dodge (2007)	Constrain extrapolation of bedrock layers to bedrock surface
Measured sections	Bolton (1957)	Constrain extrapolation to Escarpment edge
Control points	Prognostic wells	Constrain interpolation in data-poor areas
OGS strat tests	300+ diamond-drill holes	Constrain interpolation in data-poor areas
Digital Elevation Model	https://www.ontario.ca/data/provincial-digital-elevation-model-version-30	Surface topography
Bedrock topography	Gao et al. (2006), revisions by GSC (Logan) and OGS (Yeung, Brunton, Armstrong)	Top of bedrock surface
Structure+isopach maps	Hand-interpreted formation layers (OGS 2011)	Constrain interpolation in data-poor areas
Michigan petroleum wells	Lilienthal (1978)	Constrain extrapolation beneath L. Huron
MECP water wells	Correct/verification of 5,500 well records	Bedrock topography revisions
Great Lakes seismic	Shallow reflection seismic of top of bedrock	Bedrock topography Great Lakes

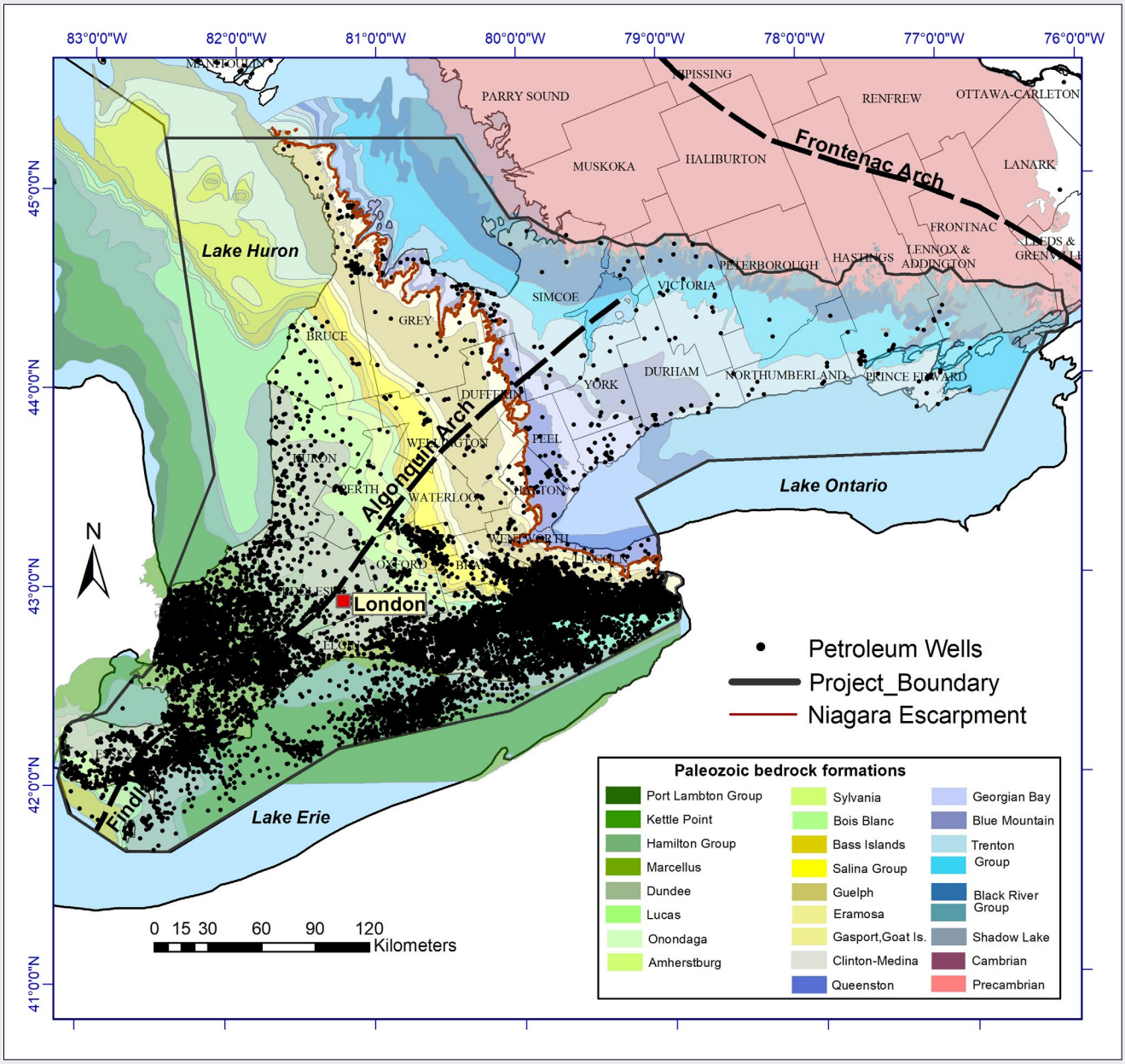


Figure 3. A) Distribution of petroleum wells in southern Ontario, N = 26,952. There are 357 wells east of the Niagara Escarpment. West of the Niagara Escarpment, only 639 wells occur north of the southern boundary of Huron Waterloo, Perth, Halton and Wellington counties.

facilitated by utilization of the existing OPDS data tables. This data was complemented by the addition of stratigraphic borehole data from the OGS, measured sections from field work, and control points at which the formation contact depths have been interpolated based on neighbouring wells. Control points are chosen at locations where there is insufficient data to guide generation of model layers.

Well/data density is highly variable (Figure 3A, 3B). Only 357 wells occur in the East, an area of 44,000 km^2, for a density of 0.008 wells/km^2. In the West there are 639 wells north of the southern boundaries of Huron, Perth, Waterloo, Wellington and Halton counties, an area of 31,500 km^2, for a density of 0.02 wells/km^2. Within the remaining area of approximately 35,000 km^2 there are nearly 26,000 wells, with a density of 0.74 wells/km^2. Availability of formation top data also declines with depth and decreases the accuracy of deeper model formation layers. For southern Ontario only 916 (<0.4%) wells penetrate the full thickness of Paleozoic strata and intersect the Precambrian basement (Figure 3B).

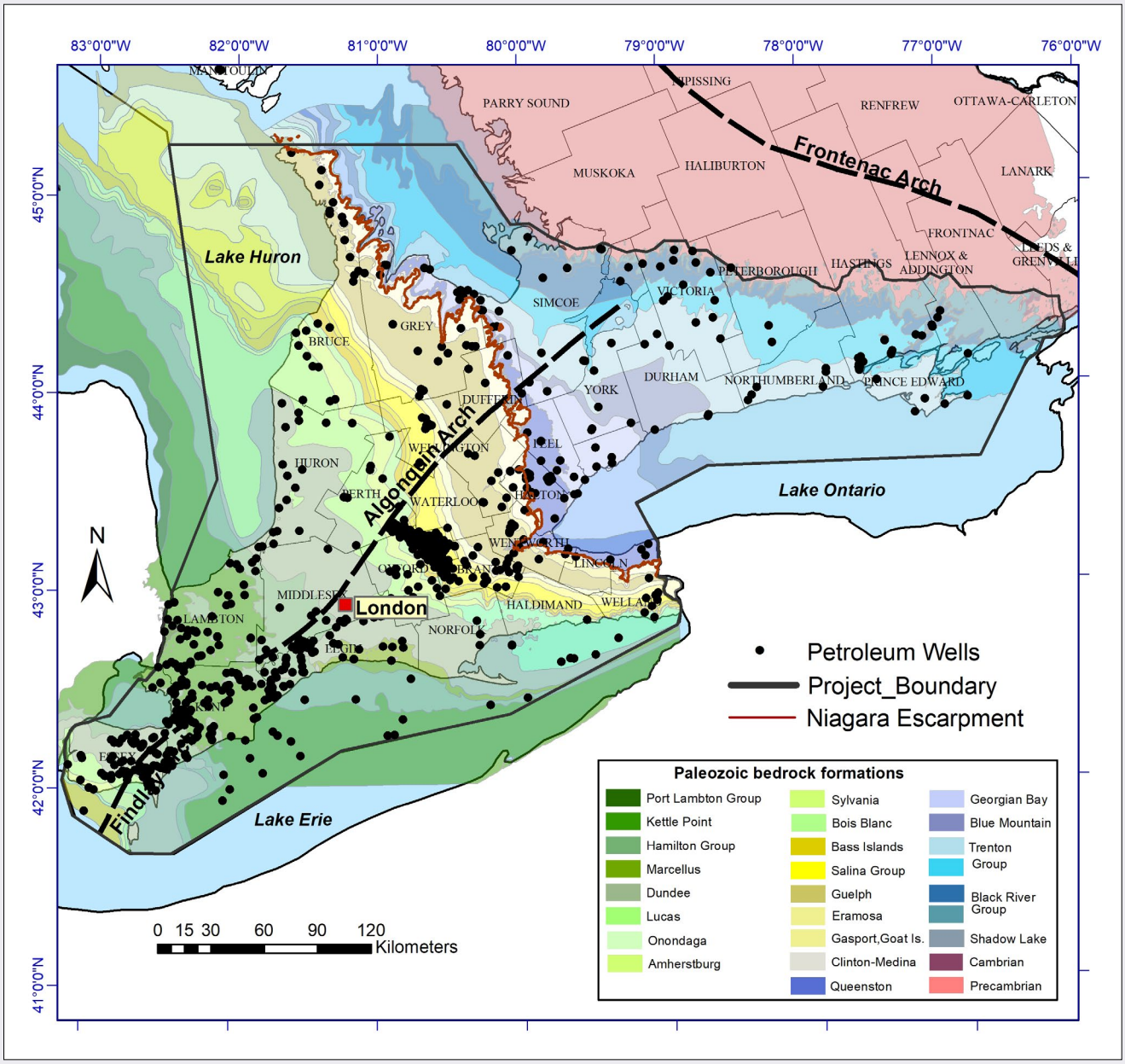


Figure 3. B) Distribution of petroleum wells penetrating the full thickness of Paleozoic strata in southern Ontario. There are 774 wells west of the Niagara Escarpment and 142 east of the Niagara Escarpment.

4.2 Quality assurance–quality control process

The formation-top picks recorded in OPDS are the primary control on interpolation of modelled layers in the 3-D model. Errors, inconsistencies, and missing data create inaccuracies in the model. Considerable project resources have been focussed on identifying and correcting these data issues and are the main focus of data QA/QC in this project. Most of this work was completed at the OGSRL. From 2015 to 2018, project geologists and geological contract staff of the OGSRL completed edits to 30,320 formation tops in a total of 7,490 wells. Well revision edits include formation top additions, deletions, and pick depth changes. Full details are provided in Clark et al. (2020).

Four distinct quartzose sandstone units occur within the Middle to Lower Devonian stratigraphy: the Columbus sand lithofacies in the uppermost Lucas Formation (Anderdon Member) (Birchard et al. 2004), the Sylvania Formation, the Springvale Member of the Bois Blanc Formation, and the Oriskany Formation. Numerous inconsistencies in identification of these sandstones were observed by project staff, and a separate project was initiated to correct these issues (Davis 2017).

4.3 Digital bedrock geology map

For this model, digital bedrock topography (i.e., a Digital Elevation Model, DEM) and 2-D digital bedrock geology mapping are combined to assemble grids of 3-D points for each mapped formation to control extrapolation to the subcrop surface. Initial versions of the model utilized the existing OGS digital bedrock geology map (Armstrong and Dodge 2007). Shortcomings with the existing map were identified that required manual intervention by the modeller. This necessitated preparation of an updated version of the map by MNRF to resolve issues with geographic extent, stratigraphic terminology, and bedrock unit polygon boundaries and subdivisions, and to incorporate new mapping (Armstrong 2017; Sun et al. 2017; Sun 2018).

Initial map revisions edited a base map that had been created by merging OGS and GSC maps by Armstrong and Dodge (2007), Sanford (1969) and Sanford and Baer (1971). The majority of edits of mapped geologic boundaries in this synthesis map were completed using the formation top picks for top of bedrock in OPDS. The tops of bedrock were confirmed or revised by examining drill cuttings and geophysical logs from corresponding petroleum wells. This is an ongoing project. This revised bedrock map information is incorporated into the 3-D model and has greatly expedited generation of revised model iterations via improvement of bedrock layer extrapolation to the bedrock surface.

4.4 Surface DEM and bedrock topography

A DEM defines the upper surface boundary for the 3-D model. Because the model includes large areas covered by the Great Lakes and other large lakes in Ontario, the topographic boundary required the addition of accurate lake bottom elevation. The topographic surface used for modelling was a composite of Shuttle Radar Topography Mission (SRTM) 90m DEM data, Great Lake bathymetry from the National Oceanic and Atmospheric Administration (NOAA) and Canadian Hydrographic Survey (CHS). For other significant lakes (e.g., Lake Simcoe) within Ontario, interpolated lake bathymetry measurements extracted from archival, hand-drawn CHS bathymetric charts were also incorporated (Griffiths et al. 2020). As a model boundary surface, the topographic DEM acts as an erosional surface that truncates interpolated contact surfaces to form realistic model geometry. The OGS digital bedrock topography map (Gao et al. 2006) was used in early versions of the 3-D model to constrain the bedrock surface. The bedrock surface in the current model is a refined version, with updates on the Devonian Onondaga Escarpment and the Niagara Escarpment, which was prepared and updated by GSC.

From a companion model of the Pleistocene glacial sediments being concurrently developed by the GSC and OGS, a revised version of the bedrock topography has been produced. To make the models spatially compatible, the revised topography represents the contact between lithified bedrock and unlithified surficial sediment in both models. The revised bedrock topography is supported by surficial mapping, archival borehole logs, and geophysical data (Logan et al. 2020). As the surficial sediment model includes only the onshore portion of the bedrock model area, the bedrock topography surface was extended by using Great Lakes bedrock elevation surfaces derived from seismic sediment thickness maps of Lake Huron and Ontario (Todd and McNamara 2018; McNamara and Todd 2018; Todd et al 2020) and 'top of bedrock' picks from the OPDS database for Lake Erie. Ministry of Environment, Conservation and Parks (MECP) water well logs from the Water Well Information System (WWIS) database are the most extensive data source that was used for delineating bedrock topography. This data, collected over many decades, contains location errors and inconsistent lithologic descriptions (Russell et al. 1998). The identification of incorrect locations and bedrock terminology were subjected to vetting and revisions, as supplied by OGS staff currently working towards the new bedrock topography map of southern Ontario (Clark et al. 2020).

4.5 3-D vector data

In some cases, areas with a low density of data support for layer surface interpolation required additional control to maintain proper layer thickness integrity. Following resource exploration efforts in Ontario, most borehole data is concentrated to the west of the Niagara Escarpment and south into Lake Erie. East of the Niagara Escarpment and within Lake Huron, Lake Ontario and Georgian Bay, little to no borehole data exists. There is also a general data reduction with depth. Gradual undulations of strata over large distances may result in layers that are rendered too thick, too thin or potentially removed completely if data control points are too sparse. When these layer inconsistencies were identified on interim models, 3-D control polylines were constructed in context of other layers to extrapolate layer geometry between widely separated data points.

5. Modelling

5.1 Model layers

The project objective was to create model layers for all mapped bedrock strata in the subsurface of southern Ontario. There are presently 70 identified bedrock strata in southern Ontario, principally at formation rank (Figure 2). In the 3-D model there are 54 modelled Paleozoic bedrock layers, plus the Precambrian basement, plus overlying unconsolidated surficial sediments (Figure 4). It has not been possible to individually represent all the geologic formations in the modelled formation layers due to data constraints in the petroleum well database maintained by MNRF and also due to software constraints, e.g., in modeling of thin formations (Table 2). All Cambrian formations are represented as unsubdivided Cambrian. The Upper Devonian Sunbury, Berea and Bedford formations of the Port Lambton Group are represented at the group

Table 2. Table of modeled bedrock and sediment layers

Group	Formation(s)	#	Model Layer	Group	Formation(s)	#	Model Layer
		1	Overburden		Guelph	31	Guelph
Port Lambton	(un-subdivided)	2	Port Lambton Group	Lockport	Eramosa	32	Eramosa
	Kettle Point	3	Kettle Point		Goat Island	33	Goat Island
Hamilton	(un-subdivided)	4	Hamilton Group		Gasport	34	Gasport
	Marcellus	5	Marcellus	Clinton	DeCew	35	DeCew
	Dundee	6	Dundee		Rochester, Lion's Head	36	Rochester (Lion's Hd)
Detroit River	Columbus	7	Columbus		Irondequoit, Fossil Hill, Rockway, Merritton, Reynales	37	Irond-FH-Reynales
	Lucas	8	Lucas		St Edmund	38	St Edmund
	Amherstburg, Onondaga	9	Amherstburg		Wingfield	39	Wingfield
	Sylvania	10	Sylvania		Dyer Bay	40	Dyer Bay
	Bois Blanc	11	Bois Blanc		Neahga	41	Neahga
	Springvale	12	Springvale	Medina	Thorold	42	Thorold
	Oriskany	13	Oriskany		Grimsby	43	Grimsby
	Bass Islands, Bertie	14	Bass Islands/ Bertie		Cabot Head	44	Cabot Head
Salina	G Unit	15	G Unit		Manitoulin	45	Manitoulin
	F Unit	16	F Unit		Whirlpool	46	Whirlpool
		17	F Salt		Queenston	47	Queenston
	E Unit	18	E Unit		Georgian Bay, Blue Mountain	48	Georgian Bay-Blue Mtn.
	D Unit	19	D Unit	Trenton	Cobourg	49	Cobourg
	C Unit	20	C Unit		Sherman Fall	50	Sherman Fall
	B Unit	21	B Unit		Kirkfield	51	Kirkfield
		22	B Equivalent	Black River	Coboconk	52	Coboconk
		23	B Salt		Gull River	53	Gull River
		24	B Anhydrite		Shadow Lake	54	Shadow Lake
	A-2 Unit	25	A-2 Carbonate		Cambrian (un-subdivided)	55	Cambrian
		26	A-2 Shale		Precambrian	56	Precambrian
		27	A-2 Salt				
		28	A-2 Anhydrite				
	A-1 Unit	29	A-1 Carbonate				
		30	A-1 Evaporite				

Notes: Onondaga members can be correlated with members of Amherstburg and Lucas, however Onondaga is combined with Amherstburg due to modelling constraints.

Lion's Head is age equivalent to lower Member of Rochester Formation and so combined to simplify model.

Irondequoit, Fossil Hill, Merritton, Rockway and Reynales are not consistently identified in the wells database and so combined due to data constraints.

Age relationship between Dyer Bay and Neahga remains uncertain currently.

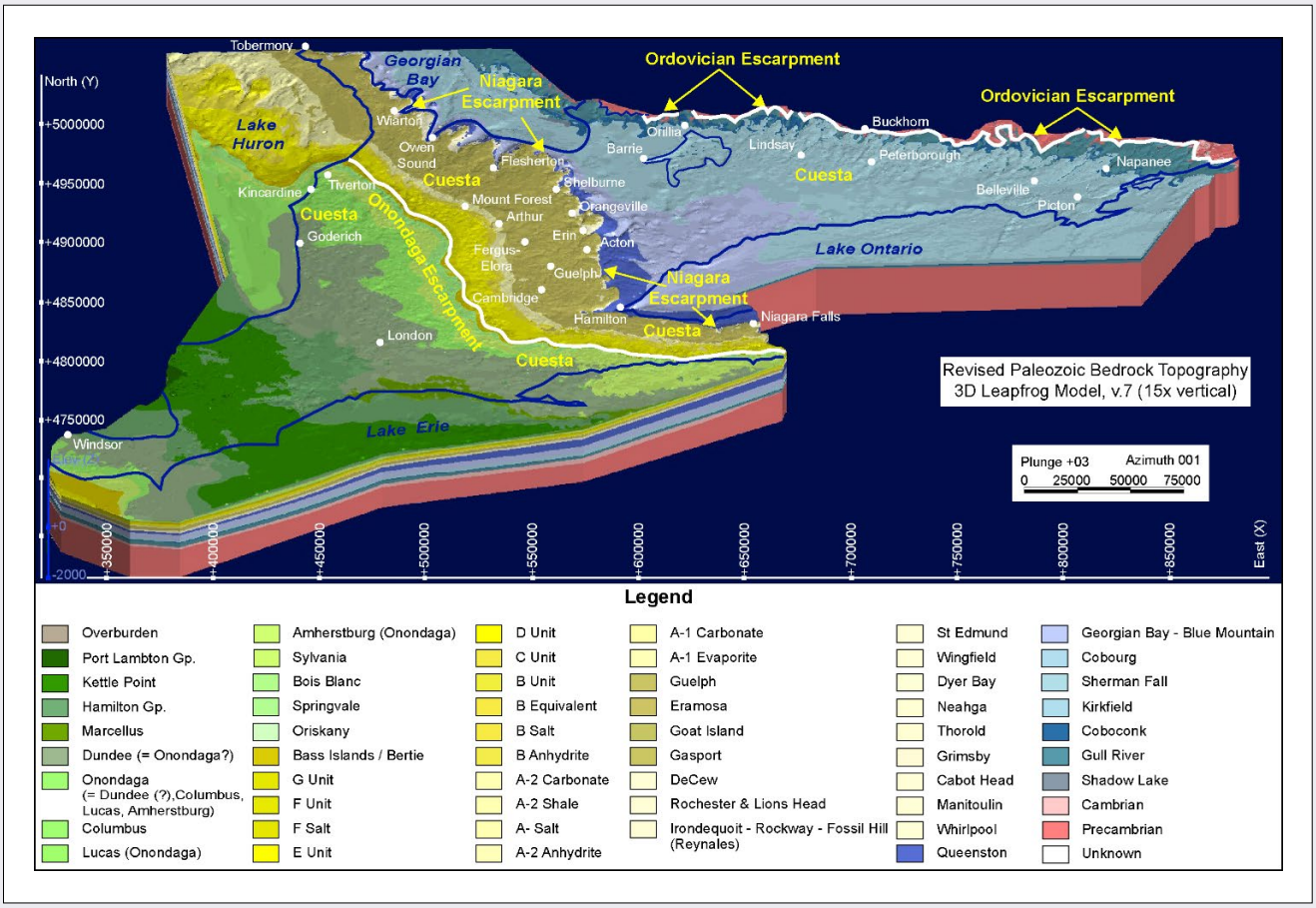


Figure 4. Interim 3-D lithostratigraphic model of the Paleozoic geology of southern Ontario. The model is displayed at 15x vertical exaggeration, tilted towards the viewer, with the tilted horizontal plane showing the bedrock surface with the overlying layer of unconsolidated overburden removed.

level, as are the Ipperwash, Widder, Hungry Hollow, Arkona, Rockport Quarry and Bell formations of the Hamilton Group. Lateral facies changes with complex stratigraphic relationships create interpolation issues for the modelling software and are represented as combined layers in the model. The Onondaga Formation has been grouped with the Amherstburg Formation, the Rockway, Merriton, Fossil Hill and Reynales formations are grouped together, the Power Glen Formation is grouped with the Cabot Head Formation, the Lions Head Formation is grouped with the Rochester Formation, and the Blue Mountain and Georgian Bay formations are combined. There is insufficient data to accurately represent the Collingwood Member of the Cobourg (Lindsay) Formation and the Rouge River Member of the Blue Mountain Formation. There are no formation picks in OPDS for the Cambria, Kodak or Devils Hole formations, which have a very localized distribution in the Niagara area.

5.2 Software

From 2015 to 2018, LeapFrog© Hydro, an implicit 3-D modelling application developed by ARANZ Geo Limited, was used for modelling. Leapfrog© Works was utilized for the final model version. LeapFrog© is implicit modelling software within which contact surfaces are implied by math functions whose parameters are assigned by depths in borehole log tables. Subjective interpretations are kept separate from measured data to allow easier model revisions based on new or updated data. In contrast to an explicit model whose surfaces are manually manipulated, the implicit model can be easily re-rendered by simply re-loading the updated lithology depths table. This lends itself well to the iterative model-building, assessment, or data-revision cycle needed for this scale of model development.

5.3 Modelling process and workflow

After initial data compilation, QA/QC, and addition of enhanced and updated data is complete, all of the datasets are loaded into the modelling software. Model construction is an iterative process of:

- interim model construction incorporating all loaded data,
- critical geological appraisal of the interim model,

- identification of errors and inconsistencies and priorities for editing,
- QA/QC data review and editing of errors and inconsistencies, followed by
- remodelling using the edited and updated data set

The process is repeated as necessary to achieve incremental improvements in the modelled result.

Borehole log "Depth From – To" data is the primary data source as the modelling software utilizes the formation depth intervals to enforce model layer chronology. However, surfaces can also be augmented by 3-D vector objects. For this model, digital bedrock topography and 2-D geological subcrop mapping are combined to assemble grids of 3-D points for the subcrop edge of each mapped formation. These point grids are added to corresponding model formations to better align them to mapped geology in areas of little or no borehole data, particularly east of the Niagara Escarpment and beneath water bodies. The bedrock topography was also used as a secondary model boundary / erosional surface to constrain the geometry of bedrock layers by acting as a boundary between bedrock and unconsolidated surficial sediments. This boundary effectively truncates upward-trending bedrock layers and enforces the structural discontinuity between bedrock and unconsolidated surficial sediments layers. To accurately render layer geometry based on expert feedback, manually digitized guidelines were applied in data-poor and/or topographically complex areas. Although the model automatically re-renders with these guidelines in effect, these edits were kept to a minimum as a reassessment was needed after each model iteration to ensure borehole data revisions did not cause conflicts. Revisions to the digital bedrock geology map, the utilization of the bedrock topography as an erosional surface and the addition of mapped geology point grids greatly reduced the need for manually digitized guidelines.

5.4 Project progression

To date, the modelling project has generated 7 iterative versions of the model to advance QA/QC of the input data (Table 1). An initial 3-layer model of the unconsolidated surficial sediments, the Paleozoic bedrock, and the Precambrian basement has evolved to the latest model version that contains 56 layers representing 70 Paleozoic bedrock formations, the Precambrian basement, and overlying unconsolidated sediments (Figure 4). The model was published as a copublication by the GSC and the OGS (Carter et al. 2019).

6. Discussion and summary

The project has produced the first 3-D geological model to include all of the Western St. Lawrence Lowlands region of south-central and southwestern Ontario. Three-dimensional modelling of the subsurface bedrock geology of southern Ontario is a fundamental improvement to, and the logical next step in, the evolution of geological mapping. It illustrates the geological connections and continuity between the surface and subsurface; a necessary precursor for understanding hydrogeological links between surface water systems and groundwater in unconsolidated surficial sediments and bedrock.

Practical applications of the model will include:

- Public outreach and education
- Studies related to deep geological disposal of nuclear wastes
- Exploration for and development of hydrocarbon and mineral resources
- Regional context for local-scale studies
- Identification of gaps in knowledge and data
- Identification of shortcomings in modelling algorithms
- Modelling of hydrochemical zonation in groundwater
- Numeric modelling of groundwater flow
- Provides framewok to test/predict and illustrate the regional karstic potable water flow systems in upper parts of main cuesta-forming carbonate units

As with all models, users must be cautious to recognize that the model is a data-driven algorithmic representation and interpretation of the actual bedrock geology. It is the first version and will necessarily always be a work-in-progress as more data becomes available and improvements are made to existing data and software processing capabilities, leading to future refinements and revisions.

The primary project deliverable is a 3-D lithostratigraphic model of the Paleozoic bedrock of southern Ontario (Carter et al. 2019). Publication will occur as simultaneous releases of Open File reports by the GSC and OGS, with subsequent posting on the website of the OGSRL.

The availability of a properly designed system for reporting and collection of well data, coupled with a detailed digital geology map, construction and management of digital databases of well data, spatially enabled by linkage to a GIS application, are critical components in the successful development of a 3-D model. The iterative development of a 3-D model has, in turn, improved the quality of the OPDS borehole database and related databases by the process of QA/QC, for the benefit of future users.

This project has generated a robust lithostratigraphic model that provides a physical basis for future development of a full hydrostratigraphic model. Note that fault block modelling was beyond the capability of the software utilized in all except the last version of the model and should be included in future revisions.

7. Acknowledgements

This project could not be completed without the extensive archive of physical and digital petroleum well data collected,

managed, and maintained by the Petroleum Operations Section of the MNRF and the Oil, Gas and Salt Resources Library. Data query and display tools in PetroGIS, an ArcGIS application designed and built by MNRF, greatly expedited the data QA/QC process and creation of raster surfaces, in particular the digital bedrock geology map, which were utilized in the modelling process. The Ontario Petroleum Institute is thanked for providing administrative and management support to the Library in its role as Trustee of the Oil, Gas and Salt Resources Trust. Contributions to data enhancement and QA/QC were made by a number of staff at the Oil, Gas and Salt Resources Library, with particular thanks to Candace Freckelton. An internal review at the GSC by R. Knight is much appreciated. This work is a contribution to the GSC–OGS southern Ontario project on groundwater 2014–2019.

8. References

Armstrong, D.K. 2017. Paleozoic geology of the Welland-Fort Erie area, southern Ontario. Ontario Geological Survey, Preliminary Map P.3811, scale 1:50,000

Armstrong, D.K. 2018. Paleozoic geology of the Dunnville area, southern Ontario. Ontario Geological Survey, Preliminary Map P.3810, scale 1:50,000

Armstrong, D.K. and Carter, T.R. 2010. The subsurface Paleozoic stratigraphy of southern Ontario. Ontario Geological Survey, Special Volume 7, 301p.

Armstrong, D.K. and Dodge, J.E.P. 2007. Paleozoic geology of southern Ontario. Ontario Geological Survey, Miscellaneous Release—Data 219.

Bancroft, A.M., Kleffner, M.A., and Brunton, F.R. 2016. Biochemostratigraphy of the Eramosa Formation in southwestern Ontario, Canada. Canadian Journal of Earth Sciences, 53: 749-762.

Banks, W.D. and Brunton, F.R. 2017 Collaboration between Ontario Geological Survey, Consultants and Municipal staff results in discovery and development of a safe and sustainable bedrock groundwater supply for the Town of Shelburne, southern Ontario. In IAH Canada; GeoOttawa 2017 – 70 years of Canadian Geotechnics and Geosciences, p.1-6.

Birchard, M.C., Rutka, M.A., and Brunton, F.R. 2004. Lithofacies and geochemistry of the Lucas Formation in the subsurface of southwestern Ontario: A high-purity limestone and potential high-purity dolostone resource. Ontario Geological Survey, Open File Report 6137, 180p.

Bolton, T.E. 1957. Silurian stratigraphy and palaeontology of the Niagara Escarpment in Ontario. Geological Survey of Canada, Memoir 289, 145p.

Brintnell, C., Brunton, F.R., Brett, C.E., and Jin, J. 2009. Characterization of the Fossil Hill-Cabot Head formational disconformity between Tobermory and Guelph, Niagara Escarpment region, southern Ontario. In Summary of Field Work and Other Activities 2009, Ontario Geological Survey, Open File Report 6240, 26-1 to 26-1

Brunton, F.R. 2008. Preliminary revisions to the Early Silurian stratigraphy of Niagara Escarpment: Integration of sequence stratigraphy, sedimentology and hydrogeology to delineate hydrogeologic units. In Summary of Field Work and Other Activities 2008, Ontario Geological Survey, Open File Report 6226, 3-1 to 31-18.

Brunton, F.R. 2009a. Karst mapping and groundwater of southern Ontario. in Groundwater and Geology – Foundation for Watershed Planning, Latornell Conference, pre-meeting core workshop, November 17, 2009, 1-15.

Brunton, F.R. 2009b. Update of revisions to the Early Silurian stratigraphy of the Niagara Escarpment: Integration of sequence stratigraphy, sedimentology and hydrogeology to delineate hydrogeologic units. In Summary of Field Work and Other Activities 2009, Ontario Geological Survey, Open File Report 6240, 25-1 to 25-20.

Brunton, F.R. and Brintnell, C. 2011. Final update of Early Silurian stratigraphy of the Niagara Escarpment and correlation with subsurface units across southwestern Ontario and the Great Lakes Basin. In Summary of Field Work and Other Activities 2011, Ontario Geological Survey, Open File Report 6270, 30-1 to 30-11.

Brunton, F.R. and Dodge, J.E.P. 2008. Karst of southern Ontario and Manitoulin Island. Ontario Geological Survey, Groundwater Resources Study 5.

Brunton, F.R., Belanger, D., DiBiase, S., Yungwirth, G., and Boonstra, G. 2007. Caprock carbonate stratigraphy and bedrock aquifer character of the Niagara Escarpment – City of Guelph region, southern Ontario. In Diamond Jubilee Canadian Geotechnical Conference and the 8th Joint CGS/IAH-CNC Groundwater Conference, Ottawa, Ontario, Oct. 21-24th, 2007, 371-377.Brunton, F.R., Brintnell, C., Jin, J., and Bancroft, A.M. 2012. Stratigraphic architecture of the Lockport Group in Ontario and Michigan – A new interpretation of Early Silurian "basin geometries" and "Guelph Pinnacle Reefs". In 51st Annual Conference – Ontario – New York, Oil & Gas Conference, Oct. 23-25, 2012, Niagara Falls, Ontario, 1-37.

Brunton, F.R., Priebe, E.H., and Yeung, K.H. 2016. Relating sequence stratigraphic and karstic controls of regional groundwater flow zones and hydrochemistry within the Early Silurian Lockport Group of the Niagara Escarpment, southern Ontario. In Regional-scale Groundwater Geoscience in Southern Ontario: An Ontario Geological Survey and Geological Survey of Canada groundwater geoscience open house, Geological Survey of Canada, Open File 8022, 4. https://doi.org/10.4095/297722

Brunton, Frank R., Carter, T.R., Logan, C., Clark, J., Yeung, K., Fortner, L., Freckelton, C., Sutherland, L., and Russell, H.A.J. 2017. Lithostratigraphic compilation of Phanerozoic bedrock units and 3D geological model of southern Ontario. In Russell, H.A.J., Ford, D., and Priebe, E.H. Compilers. Regional-scale Groundwater Geoscience in Southern Ontario: an Ontario Geological Survey, Geological Survey of Canada, and Conservation Ontario open house. Geological Survey of Canada, Open File 8212, 3. https://doi.org/10.4095/299759

Carter, T.R. 2012. All is well – Regional groundwater systems in southern Ontario. Ontario Oil & Gas 2012, Ontario Petroleum Institute, 44-48.

Carter, T.R. and Castillo, A.C. 2006. Three-dimensional mapping of Paleozoic bedrock formations in the subsurface of southwestern Ontario: A GIS application of the Ontario Petroleum Well Database. In Harris, J. Ed. GIS Applications in the Earth Sciences, Geological Association of Canada, Special Paper 44: 439-454.

Carter, T.R. and Clark, J. 2018. Base of Fresh Water, Inferred Bedrock Karst, and the Contact Aquifer in Southern Ontario, as Interpreted from Water Well Records. Oil, Gas and Salt Resources Library, Open File Data Release 2018-1, 16 p.

Carter, T.R. and Fortner, L. 2012. Regional bedrock aquifers and a geological groundwater model for southern Ontario. International Association of Hydrogeologists, 39th International Congress, Session TH1-G, Abstract 369, 238.

Carter, T.R., and Sutherland, L. 2018. Mapping the interface between the intermediate sulphur water regime and deep brine in the Paleozoic bedrock of southwestern Ontario. Oil, Gas and Salt Resources Library, Open File Data Release 2018-2, 22 p.

Carter, T.R. and Sutherland, L. 2020. Interface mapping of hydrochemical groundwater regimes in the Paleozoic bedrock of southwestern Ontario. In Russell, H.A.J. and Kjarsgaard, B.A. Eds. Southern Ontario groundwater project 2014–2019: summary report. Geological Survey of Canada, Open File 8536, 37-48. https://doi.org/10.4095/321083

Carter, T.R., Trevail, R.A. and Smith, L. 1994. Core workshop: Niagaran reef and inter-reef relationships in the subsurface of southwestern Ontario. Geological Association of Canada–Mineralogical Association of Canada, Annual Meeting, Waterloo 1994, Field Trip A5 Guidebook, 38p.

Carter, T.R., Fortner, L., Skuce, M.E. and Longstaffe, F.J. 2014. Aquifer systems in southern Ontario: Hydrogeological considerations for well drilling and plugging. abstract, Canadian Society of Petroleum Geologists, Geoconvention 2014.

Carter, T.R., Brunton, F.R., Clark, J., Fortner, L., Hamblin, A., Logan, C. and Russell, H.A.J. 2016. 3D hydrostratigraphic modelling of the Paleozoic bedrock of southern Ontario. In Regional-scale Groundwater Geoscience in Southern Ontario: An Ontario Geological Survey and Geological Survey of Canada groundwater geoscience open house, Geological Survey of Canada, Open File 8022, p.5. https://doi.org/10.4095/297727

Carter, T.R., Brunton, F.R., Clark, J., Fortner, L., Freckelton, C.N., Logan, C.E., Russell, H.A.J., Somers, M., Sutherland L. and Yeung, K.H. 2017. Status report on three-dimensional geological and hydrogeological modelling of the Paleozoic bedrock of southern Ontario. In Summary of Field Work and Other Activities, 2017, Ontario Geological Survey, Open File Report 6333, 28-1 to 28-15.

Carter, T.R., Brunton, F.R., Clark, J.K., Fortner, L., Freckelton, C., Logan, C.E., Russell, H.A.J., Somers, M., Sutherland, L., and Yeung, K.H., 2019. A three-dimensional geological model of the Paleozoic bedrock of southern Ontario; Geological Survey of Canada, Open File 8618; Ontario Geological Survey, Groundwater Resources Study 19, 1 .zip file. https://doi.org/10.4095/315045

Clark, J.K., Carter, T.R., Brunton, F.R., Fortner, L., Freckelton, C.N., Logan, C.E., Russell, H.A.J., Somers, M., Sutherland L. and Yeung, K.H. 2020. Improving the 3-D geological data infrastructure of southern Ontario: Data capture, compilation, enhancement and QA/QC. In Russell, H.A.J. and Kjarsgaard, B.A. Eds. Southern Ontario groundwater project 2014–2019: summary report. Geological Survey of Canada, Open File 8536, 23-36. https://doi.org/10.4095/321081

Cramer, B.D., Brett, C.E., Melchin, M.J., Männik, P., Kleffner, M.A., McLaughlin, P.I., Loydell, D.K., Munnecke, A., Jeppsson, L., Corradini, C., Brunton, F.R. and Saltzman, M.R. 2011. Revised correlation of Silurian Provincial Series of North America with global and regional chronostratigraphic units and δ13Ccarb chemostratigraphy. Lethaia, 44: 185-202. https://doi.org/10.1111/j.1502-3931.2010.00234.x

Davis, C.L. 2017. Quartzose sands in the Lower to Middle Devonian strata of southwestern Ontario: Geographic distribution and characterization in drill cuttings and geophysical logs. Geological Survey of Canada, Open File Report 8286, 37p. https://doi.org/10.4095/305359

Frey, S.K., Khader, O., Taylor, A., Erler, A.R., Lapen, D.R., Sudicky, E.A., Berg, S.J., and Russell, H.A.J. 2019. A fully integrated groundwater–surface-water model for southern Ontario: proof of concept and data release. Geological Survey of Canada, Open File 8639, 1 .zip file. https://doi.org/10.4095/321042

Gao, C., Shirota, J., Kelly, R.I., Brunton, F.R. and Van Haaften, S. 2006. Bedrock topography and overburden thickness mapping, southern Ontario. Ontario Geological Survey, Miscellaneous Release—Data 207.

Griffiths, M., Russell, H.A.J., and Logan, C.E. 2020. Machine learning applied to geoscience: Geo-referenced character recognition. In Russell, H.A.J., and Kjarsgaard, B.A. Eds. Southern Ontario groundwater project 2014–2019: summary report. Geological Survey of Canada, Open File 8536, 65-74. https://doi.org/10.4095/321092

Hewitt, D.F. 1971 The Niagara Escarpment. Ontario Geological Survey Industrial Minerals Report No.35, 71p.

Hobbs, M.Y., Frape, S.K., Shouakar-Stash, O. and Kennell, L.R. 2011. Regional hydrogeochemistry—Southern Ontario. Nuclear Waste Management Report NWMO DGR-TR-2011-12, Toronto, Canada.

Husain, M.M., Cherry, J.A. and Frape, S.K. 2004. The persistence of a large stagnation zone in a developed regional aquifer, southwestern Ontario. Canadian Geotechnical Journal, 41: 943-958. https://doi.org/10.1139/t04-040

Itasca Consulting Canada Inc. and AECOM Canada Ltd. 2011. Three-dimensional geological framework model. Nuclear Waste Management Organization, Report DGR-TR-2011-42, 16p. PDF document, accessed at: http://www.opg.com/generating-power/nuclear/nuclear-waste-management/Deep-Geologic-Repository/Pages/Project-Development.aspx, under "Geoscience Reports".

Lilienthal, R.T. 1978. Stratigraphic cross-sections of the Michigan Basin. Michigan Department of Natural Resources, Geological Survey Division, Report of Investigation 19, 36p.

Logan, C.E., Russell, H.A.J., Bajc, A.F., Burt, A., Mulligan, R.P.M. and Sharpe, D.R. 2020. A three-dimensional surficial geology model of southern Ontario: Progress report. In Russell, H.A.J. and Kjarsgaard, B.A. Eds. Southern Ontario groundwater project 2014–2019: summary report. Geological Survey of Canada, Open File 8536, 49-64. https://doi.org/10.4095/321084

Maxey, G.B. 1964. Hydrostratigraphic units. Journal of Hydrology v.2, p.124-129.

McNamara, G.D. and Todd, B.J. 2018. Processing of seismic reflection data from expedition 69-2-01 of the CSS Limnos, Lake Huron, Ontario, Canada, and Michigan USA. Geological Survey of Canada, Open File 8429, 7p., https://doi.org/10.4095.308377

Nuclear Waste Management Organization, 2011. Geosynthesis. Nuclear Waste Management Report NWMO DGR-TR-2011-11, PDF document, accessed at: http://www.opg.com/generating-power/nuclear/nuclear-waste-management/Deep-Geologic-Repository/Pages/Project-Development.aspx, under "Geoscience Reports", accessed on June 30, 2014.

Ontario Geological Survey, 2011. Regional structure and isopach maps of potential hydrocarbon-bearing strata for southern Ontario. Ontario Geological Survey, Miscellaneous Release—Data 276.

Ontario Power Generation, 2017. The Deep Geologic Repository, accessed at: www.opgdgr.com.

Russell, H.A.J., Bajc, A.F., Brunton, F.R., Carter, T.R. and Logan, C.E. 2015. Toward a 3D hydrostratigraphic framework for southern Ontario. In Abstracts with Programs, Geological Society of America Annual Meeting in Baltimore, Maryland, USA (1–4 November 2015), 47: 7, 407.

Russell, H.A.J., Brennand, T. A., Logan, C., and Sharpe, D. R. 1998, Standardization and assessment of geological descriptions from water well records: Greater Toronto and Oak Ridges Moraine areas, southern Ontario, Current Research 1998-E: Geological Survey of Canada, 89-102. https://doi.org/10.4095/209956

Russell, H.A.J., Bajc, A.F., Burt, A.K., Logan, C.L., Mulligan, R.P.M., and Sharpe, D.R. 2016. A three-dimensional surficial stratigraphic model for southern Ontario. In Regional-scale Groundwater Geoscience in Southern Ontario: An Ontario Geological Survey and Geological Survey of Canada groundwater geoscience open house, Geological Survey of Canada, Open File 8022, 16. https://doi.org/10.4095/297739

Russell, H.A.J., Brodaric, B., Brunton, F.R., Carter, T.R., Clark, J., Logan, C.E. and Sutherland, L. 2017. Communicating 3D geological models to a broader audience: A case study from southern Ontario. Geological Survey of Canada, Scientific Presentation 68, https://doi.org/10.4095/305363

Russell, H.A.J. and Dyer, R.D. 2016. Ontario Geological Survey–Geological Survey of Canada Groundwater Geoscience Collaboration: Southern Ontario 2015–2019. In Summary of Field Work and Other Activities 2016, Ontario Geological Survey, Open File Report 6323, 35-1 to 35-15.

Sanford, B.V. 1969. Geology, Toronto–Windsor area, Ontario. Geological Survey of Canada, Map 1263A, scale 1:250 000. https://doi.org/10.4095/109120

Sanford, B.V. and Baer, A.J. 1971. Southern Ontario, sheet 30S. Geological Survey of Canada, Map 1335A, scale 1 000 000.

Seaber, P.R. 1988. Hydrostratigraphic units. In The Geology of North America, Hydrogeology; Decade of North American Geology series, v.O-2, Geological Society of America, 9-14.

Sharpe, D.R., Piggott, A., Carter, T., Gerber, R.E., MacRitchie, S.M., de Loë, R.C., Strynatka, S. and Zwiers, G. 2014. Southern Ontario hydrogeological region. In Canada's Groundwater Resources, Fitzhenry & Whiteside, 443-499. https://doi.org/10.4095/296947

Skuce, M.E. 2015. Isotopic fingerprinting of shallow and deep groundwaters in southwestern Ontario and its applications to abandoned well remediation. unpublished MSc thesis, University of Western Ontario, Electronic thesis and dissertation repository, article 1926, 276 p.

Skuce, M., Longstaffe, F.J., Carter, T.R. and Potter, J. 2015a. Isotopic fingerprinting of groundwaters in southwestern Ontario: Applications to abandoned well remediation. Applied Geochemistry, 58: 1-13. https://doi.org/10.1016/j.apgeochem.2015.02.016

Skuce, M, Potter, J. and Longstaffe, F.J. 2015b. The isotopic characterization of water in Paleozoic bedrock formations in southwestern Ontario. Ontario Oil, Gas and Salt Resources Library, Open File Data Release 2015-3.

Smith, L., Grimes, D.J. and Charbonneau, S.L. 1988. Karst episodes and permeability development, Silurian reef reservoirs, Ontario. In Geoscience Research Grant Program, Summary of Research 1987–1988, Ontario Geological Survey, Miscellaneous Paper 140, 124-132.

Somers, M.R., Fortner, L., Carter, T.R., and Clark, J. in preparation. A Revised Digital Map of the Paleozoic Bedrock Geology of Southern Ontario. Oil, Gas and Salt Resources Library, Open File Data Release

Sykes, J.F., Normani, S.D. and Yin, Y. 2011. Hydrogeologic Modelling, 2011. OPG's Deep Geologic Repository for low & intermediate level waste, NWMO DGR-TR-2011-16, 428p. accessed at: http://www.opg.com/generating-power/nuclear/nuclear-waste-management/Deep-Geologic-Repository/Pages/Project-Development.aspx, under "Geoscience Reports", accessed on June 30, 2014.

Sun, S. 2018. Stratigraphy of the Upper Silurian to Middle Devonian, southwestern Ontario. University of Western Ontario, Electronic Thesis and Dissertation Repository, article 5230.

Sun. S., Brunton, F.R., and Jin, J. 2017. Lithofacies and stratigraphy of the Devonian Onondaga Formation, southwestern Ontario. Ontario Geological Survey, Summary of Field Work and Other Activities, Open File Report 6333, 23-1 to 23-23.

Todd, B.J. and McNamara, G.D. 2018. Processing of seismic reflection data from expedition 91800 of the RV Laurentian, Lake Huron and Georgian Bay, Ontario and Michigan USA. Geological Survey of Canada, Open File 8428, 7. https://doi.org/10.4095.308328

Todd, B.J., Lewis, C.F.M., Russell, H.A.J., and Pyne, M.D. 2020. Legacy seismic reflection data from the Great Lakes: Recovery and applications. In Russell, H.A.J. and Kjarsgaard, B.A. Eds. Southern Ontario groundwater project 2014–2019: summary report. Geological Survey of Canada, Open File 8536, 75-82. https://doi.org/10.4095/321093

Improving the 3-D geological data infrastructure of southern Ontario: Data capture, compilation, enhancement, and QA/QC

Jordan K. Clark[1]*, Terry R. Carter[2], Frank R. Brunton[3], Charles Logan[4], Maia Somers[5], Liz Sutherland[1,6], and Kei H. Yeung[3]

Abstract: Well records of the Oil Gas and Salt Resources Library (OGSRL) are maintained in the Ontario Petroleum Data System (OPDS) and are the principal source of data on the subsurface geology of southern Ontario. In this project significant improvements have been made to data quality in OPDS through a process of capture and compilation of existing data, QA/QC edits to the existing data, and creation and addition of new data. Edits were completed to 30,320 formation top picks in 7,812 wells. These improvements were completed as part of the development of a 3-D lithostratigraphic model of the Paleozoic bedrock of southern Ontario. The completion of this QA/QC at the OGSRL has the permanent benefit that any future users of the library data will have access to these corrections. OPDS data supports resource industries involved in exploration for and development of salt, oil, natural gas, groundwater, compressed air energy storage, disposal of oil field fluids, geological storage of hydrocarbons, and permanent geological storage of nuclear wastes. It also supports public education and the training of new geoscientists and geological engineers. The southern Ontario 3-D model is data-driven. OPDS is the key source of data for the model and illustrates the value of a properly constructed and actively maintained wells database. Without OPDS the 3-D modelling project would not have been possible.

1. Introduction and objectives

In 2015, the Ontario Geological Survey (OGS) and the Geological Survey of Canada (GSC) initiated a project to develop a three-dimensional (3-D) geological and hydrogeological model of the Paleozoic bedrock geology of southern Ontario (Russell et al. 2015; Russell and Dyer 2016; Carter et al. 2016, 2017). This work is being completed in collaboration with the Ontario Ministry of Natural Resources and Forestry (MNRF) and the Oil, Gas and Salt Resources Library (OGSRL), London, Ontario. A parallel project to model the geology and hydrogeology of the overlying unconsolidated surficial sediments is also underway (Russell et al. 2016; Logan et al. 2020).

The southern Ontario 3-D geological model is a data-driven initiative. Consequently, project resources have been heavily focussed on compilation of existing data, identification of data gaps and data anomalies, quality assurance / quality control (QA/QC) review and edits to existing data, and addition of data enhancements and new data created by project contributors. Geological formation picks in the petroleum wells database (Figure 1) for the province of Ontario (OPDS) are the primary data source for the 3-D model (Carter and Castillo 2006; Carter 2017). Additional data is available for modelling the lithostratigraphy and hydrostratigraphy of the Paleozoic bedrock formations in southern Ontario (Tables 1, 2), including measured sections of outcrop data, e.g., from the Niagara Escarpment.

A properly constructed well database and its supporting information is an essential requirement for construction of a 3-D model at a reasonable cost. Nonetheless, data errors, inconsistencies, data gaps, well location errors, etc. can compromise the reliability of the model. This paper highlights the need for QA and QC of well data and in particular formation top picks and summarizes the data improvements made in support of the 3-D model.

[1] Oil Gas and Salt Resources Library, London, ON N6E 1L3
[2] Consulting Geologist, London, ON N6K 3P4
[3] Ontario Geological Survey, Sudbury, ON P3E 6B5
[4] Geology Survey of Canada, Natural Resources Canada, 601 Booth Street, Ottawa, ON K1A 0E8
[5] Ministry of Natural Resources and Forestry, London, ON N6E 1L3
[6] University of Western Ontario, Western Libraries, Map & Data Centre, London, ON N6A 3K7
*corresponding author: jordan@ogsrlibrary.com

Recommended citation: Clark, J.K., Carter, T.R., Brunton, F.R., Logan, C.E., Somers, M., Sutherland, L., and Yeung, K.H. 2020. Improving the 3-D geological data infrastructure of southern Ontario: Data capture, compilation, enhancement and QA/QC. In Russell, H.A.J. and Kjarsgaard, B.A. Eds. Southern Ontario groundwater project 2014–2019: summary report. Geological Survey of Canada, Open File 8536, 23-36. https://doi.org/10.4095/321081

Table 1. Primary data sources for lithostratigraphic modelling.

Data Set	Description	Application
OPDS database	26,952 petroleum well records with 300,000 formation tops, MNRF/Library	Primary data for model layer interpolation
Library	Drill cuttings 11,000 wells, well files, drill core 1,014 wells, geophysical logs >20 000	QA/QC
Bedrock geology maps	Armstrong and Dodge (2007), GSC 1335A (Sanford and Baer 1971), GSC 1263a (Sanford 1969), Sun (2018), Armstrong (2017, 2018)	Constrain extrapolation from subsurface to subcrop
Digital bedrock geology map	Revision of Armstrong and Dodge (2007)	Constrain extrapolation of bedrock layers to bedrock surface
Measured sections	Bolton (1957)	Constrain extrapolation to Escarpment edge
Control points	Prognostic wells (Carter)	Constrain interpolation in data-poor areas
OGS strat tests	300+ diamond-drill holes (Brunton)	Constrain interpolation in data-poor areas
Digital Elevation Model	https://www.ontario.ca/data/provincial-digital-elevation-model-version-30	Surface topography
Bedrock topography	Gao et al. (2006), revisions by GSC (Logan) and OGS (Yeung, Brunton, Armstrong)	Top of bedrock surface
Structure+isopach maps	Hand-interpreted formation layers (OGS 2011)	Constrain interpolation in data-poor areas
Michigan petroleum wells	Lilienthal (1978)	Constrain extrapolation beneath L. Huron
MECP water wells	Correct/verification of 5,500 well records	Bedrock topography revisions
Great Lakes seismic	Shallow reflection seismic of top of bedrock	Bedrock topography Great Lakes

2. Oil, gas and salt resources well data

Oil, gas and salt resources (petroleum) well records of the Ontario Petroleum Data System (OPDS) are the primary data set for modelling formation layers in the subsurface of southern Ontario. 3-D modelling of formation layers would not have been feasible without the OPDS data. Consequently, most of the data QA/QC efforts were focussed on the review and editing of this data.

OPDS is a custom Oracle database designed and maintained by MNRF and OGSRL for managing data collected from the drilling and operation of petroleum wells in the province of Ontario (Carter and Castillo 2006). The digital data is sourced from hard copy well files collected and maintained by the MNRF. OPDS has records for approximately 27,000 wells with well collar geographic co-ordinates and collar elevation values and includes nearly 300,000 unique formation top picks recorded in metres below the well collar/rig floor (Figure 1).

A well location accuracy code is recorded in OPDS for each well in the database. Geographic co-ordinates for the wells have estimated accuracies varying from 1 metre to over 1,000 metres. Over 95% of the wells have coordinates with accuracies within 200 metres of true locations. Additional data includes collection and submission records of drill core and cuttings, drill core analyses; formation water analyses; oil and natural gas analyses; drill core; drill cuttings; geophysical logs; and oil, gas, and water interval data recorded while drilling. The unique identifier for each well is a well licence number issued by the MNRF.

A library of 27,000 hard copy well drilling and completion records, rock chip samples from 13,000 wells, 1,100 rock cores from 1,000 unique wells and over 20,000 geophysical logs are the original source of information for the digital well records. This same data is the principal reference for QA/QC review, edit and enhancement of the OPDS well data, particularly the formation top picks.

Table 2. Secondary data sources that help define and constrain lithostratigraphic and hydrostratigraphic modelling.

Data Set	Description	Application
Oil interval data	OPDS – 6,000 records	Fluid zonation, porous strata
Gas interval data	OPDS – 26,000 records	Fluid zonation, porous strata
Water interval data	OPDS – 35,000 records	Bedrock aquifers
Isotopic/geochemical analyses	130 analyses, Skuce et al. (2015), Skuce, Potter and Longstaffe (2015), Skuce (2015)	Hydrochemical zonation, groundwater flow, isotopic fingerprinting,
Petroleum industry water analyses	1,024 standard water analyses	Hydrochemical zonation, salinity gradients, numeric modelling
Water type maps	89 maps of bedrock saline aquifers, Carter et al. (2015a)	Hydrochemical zonation, groundwater flow
Static level maps	17 maps of bedrock saline aquifers, Carter et al. (2015b)	Groundwater flow
NWMO 3-D model	1/3 southern Ontario, Itasca and AECOM (2011)	Comparative analysis
Base fresh water map	GIS interpretation from water well records, Carter and Clark (2018)	Base of fresh water, hydrochemical zonation, contact aquifer, inferred karst, numeric modelling
Base of sulphur water map	Carter and Sutherland (2018)	Hydrochemical zonation, numeric modelling, hydrostratigraphic modelling
OGS groundwater mapping	In progress	Water well drilling, Modelling of potable water aquifers
Petroleum industry core analyses	Data digitized late 2018.	Hydrogeology, groundwater flow, hydrostratigraphic modelling

Two sets of formation tops are recorded in OPDS for each well. One set comprises picks submitted by industry well operators to the MNRF on drilling completion records (Form 7, Form 107), with a second set picked by geological staff of MNRF or OGSR Library. Picks are made by examination and interpretation of drill cuttings samples, geophysical logs, and drill core if available. The industry picks have been completed by dozens of different geologists and non-geologists, with widely varying knowledge, skills and experience, and sometimes using differing standards. These picks can be inconsistent, especially for formations with similar lithologies and gradational contacts. Picks by MNRF and OGSRL are much more reliable as they have been made by fewer individuals using published standards of either Armstrong and Carter (2010) or Beards (1967). Repicking of formation tops by MNRF and OGSRL is incomplete, consequently, a rigorous QA/QC process was required to improve data quality and consistency of formation top picks for use in the 3-D model. Additional common data quality issues include data entry errors, inaccurate well locations, missing picks, etc.

Formation tops reviewed by MNRF and OGSRL carry additional metadata in OPDS recording the reviewing geologists' confidence in the accuracy of the top picks. The metadata levels and QA Codes (Table 3), are used to prevent data from being reviewed multiple times and to explicitly include or exclude picks based on the quality of review data available and the confidence the reviewer has in the pick.

In this study formation top edits were made using methodology and standards established by Armstrong and Carter (2010) and a revised stratigraphic chart prepared for this study (Figure 2) (Brunton et al. 2017; Carter et al. 2017).

3. QA-QC process

The first rounds of reviews and edits focussed on anomalies, principally structural highs and lows, produced by single wells or small groups of wells. These are the easiest errors to detect, although it should be noted that not all anomalies are in fact errors, as is verified by examination of the source records and supporting data. Anomalies were identified visually from the 3-D model formation layers and from ESRI® ArcScene® formation-top surfaces generated using the natural neighbour interpolator. Isopach layers were also generated for salt formations of the Salina Group using the natural neighbour interpolator in ArcGIS®, which identified 20 wells with negative thickness values. Correction of these data errors usually result in removal of structural highs and lows and a smoother formation surface with a more consistent formation thickness.

Subsequently wells and formation picks requiring QA/QC

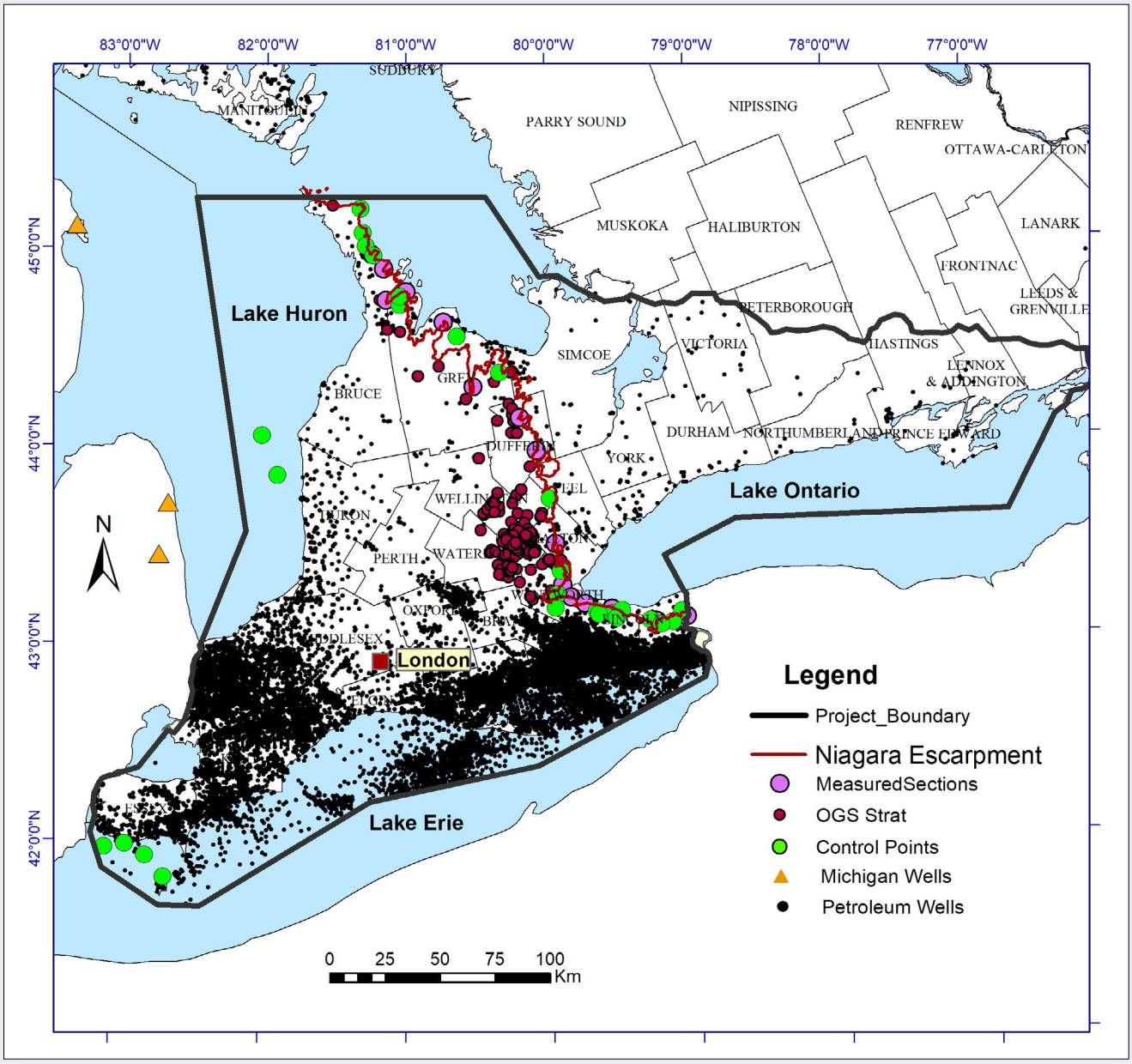


Figure 1. Location of well data points used as input to 3-D modelling of the bedrock geology of southern Ontario.

were identified in a quality scoring analysis undertaken by data technicians at the OGSRL under the guidance of the project geologists. Scores were calculated by identifying gaps in data records for individual wells caused by missing formation picks, while also assessing the availability of geophysical logs and/or drill cuttings needed for geologic QA/QC. Wells with neither logs nor cuttings were not considered for geologic QA/QC.

It was not practical to investigate and correct all wells with questionable data in the project time frame. Some efficiencies were gained by having OGSRL clerical staff cross-reference database entries with original documents submitted by the well drillers and correcting data entry errors, saving time for the project geologist. Further QA/QC of the remaining wells may be needed for other applications of the well data, or in any future efforts to refine the 3-D model.

QA/QC of formation tops is a labour-intensive process involving repicking of questionable formation tops by project geologists using geophysical logs, drill cuttings, and/or drill core in this order of preference and where available. From 2015 to 2018, project geologists and geological contract staff of the OGSRL completed edits to 30,320 formation tops in a total of 7,812 wells (Table 4). Well revision edits include formation top additions, deletions, and pick depth changes.

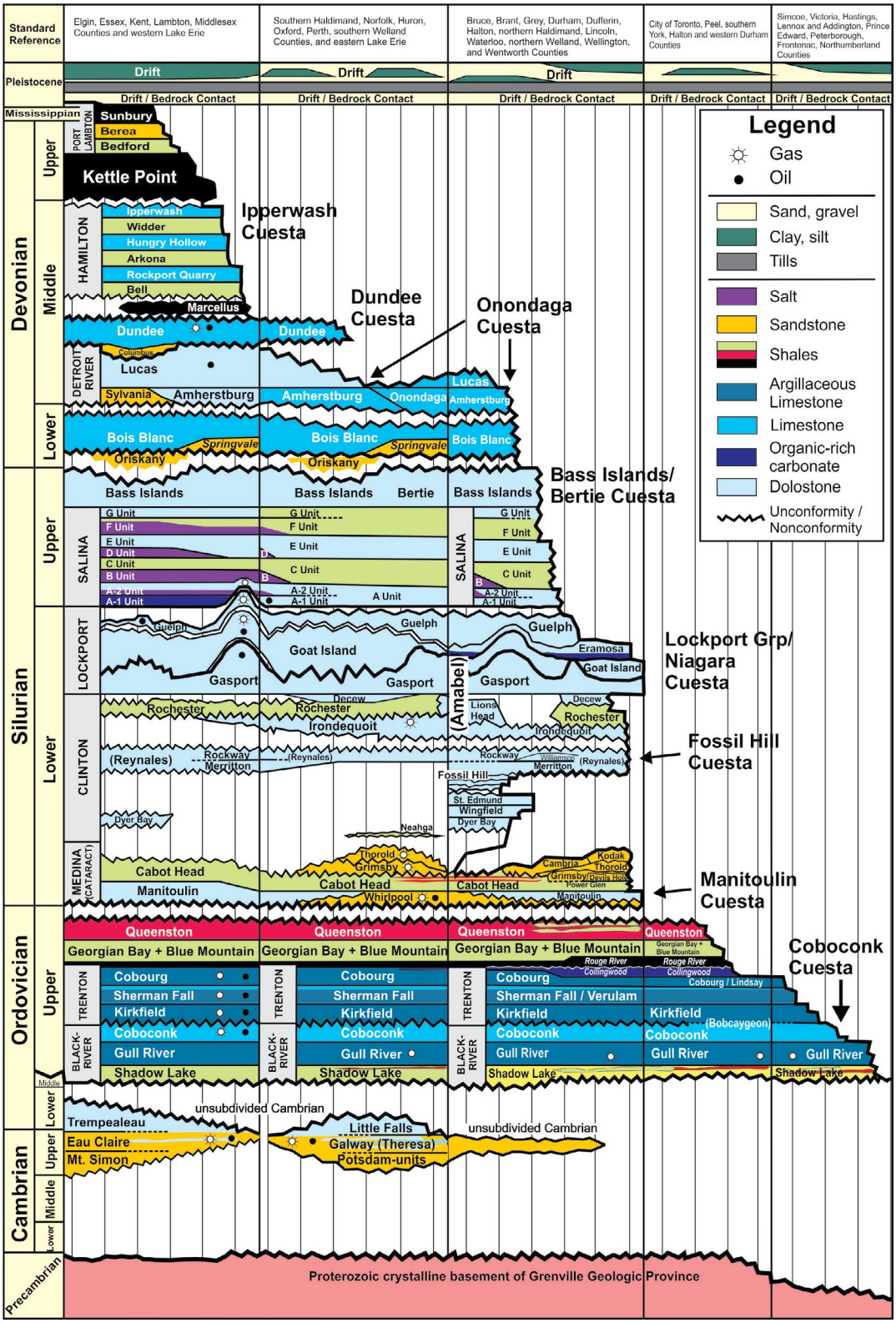


Figure 2. Lithostratigraphic chart of the Paleozoic bedrock of southern Ontario (Brunton et al. 2017; Carter et al. 2017).

Table 3. Geological quality assurance (QA) codes used in OPDS.

Code	Pick Confidence	Reviewer Type	Description
2.0	Confirmed	MNRF P.Geo	The reviewer had good data; rock cuttings, geophysical logs, or rock cores; and is confident in confirming the pick.
1.9		OGSRL P.Geo	
1.8		OGSRL GIT or Graduate	
1.7		OGSRL Geology Student	
1.5	Reviewed	MNRF P.Geo	The reviewer made the best possible pick based on the data available; rock cuttings, geophysical logs, or rock cores; however, more data or review should be considered.
1.4		OGSRL P.Geo	
1.3		OGSRL GIT or Graduate	
1.2		OGSRL Geology Student	
1.0	Not Anomalous	Any	Not reviewed but based on 3-D mapping does not cause local anomalies.
Null	Not Evaluated	MNRF Well Records	No geological review but does not cause anomalies in 3-D model
-1.0	Anomaly, requires review	Any	Causing local anomalies when used in 3-D mapping and requires review.
-2.0	Anomaly, unresolvable	Any	Causing local anomalies when used in 3-D mapping but could not be confirmed or corrected due to absence of data (rock cuttings, geophysical logs, or rock cores).

Table 4. Geological QA/QC edits of the OPDS database.

Date	Project	Number of Wells Reviewed	Formation Top Picks Reviewed/Edited
2015	Chatham Sag	3,638	All picks reviewed and verified not necessarily resulting in edits
2016	Devonian sands (Davis 2017)	1,319	198 picks removed, 818 revised
2016–2017	Regional hydrogeology	1,107	All formations top to bottom of each well not necessarily resulting in edits
2016–2017	Top of bedrock/subcrop formations	616	One per well – 616
2016–2018	Anomaly edits	322	771 picks edited or removed
2018	MNRF edits	810	4,572 Lockport/Salina/Rochester picks reviewed/500 edits; 6,096 other formation tops/1,000 edits
2015–2018	Total	7,812	30,320 formation top picks reviewed and verified or edited

3.1 Lockport Group

The scoring analysis identified the Lockport Group as a priority for review and edit of formation top picks. The Lockport Group, in particular the Guelph Formation and locally the Gasport Formation and Goat Island Formation, are important regional aquifers (Brunton 2009; Brunton et al. 2012; Brunton and Brintnell 2011; Carter et al. 2014). The top of Lockport Group is penetrated by 15,585 wells and 13,153 penetrate the full thickness of the Lockport Group, but at the beginning of the project most of these wells recorded a formation top only for the Guelph Formation with no picks for the stacked dolostones that comprise the three underlying formations of the Lockport Group (Eramosa, Goat Island and Gasport Formations) (Brunton 2009; Brunton and Brintnell 2011; Cramer et al. 2011; Brunton et al. 2012). In 59 wells the Lockport Group was referenced as Amabel Formation, an outdated term (Brunton and Brintnell 2011; Cramer et al. 2011; Brunton et al. 2012).

Without edits to provide picks for the Eramosa, Goat Island and Gasport, the formations could not be modelled separately.

Since it was not practical to edit all the wells, geological QA/QC was prioritized to provide good geographic coverage of the project area. Geological picks for these formations have been added to nearly 3,000 wells in support of the 3-D modelling project.

3.2 Devonian sandstones

Devonian sands were also identified as a priority in the scoring analysis due to their importance as intervals of enhanced porosity and permeability, and inconsistent identification of these sands in the OPDS well records (Davis 2017). Four distinct quartzose sandstone units occur within the Middle to Lower Devonian succession: the Columbus sand lithofacies which has been correlated with the uppermost member of the Lucas Formation (Birchard et al. 2004), the Sylvania Formation, the Springvale Member of the Bois Blanc Formation, and the Oriskany Formation. Enhanced porosity and permeability in these sandstones make them significant from a hydrogeological and petroleum reservoir perspective. Numerous inconsistencies in identification of these sandstones were identified by contract geological staff at the OGSRL, and a separate project was initiated to re-examine and re-interpret the distribution and characterization of these sands (Davis 2017).

Over 1,300 wells containing Devonian-aged strata were examined using binocular microscopy of drill cuttings, interpretation of geophysical well logs, and Geographic Information System (GIS) queries of OPDS database well records. These included wells drilled since the last time that these sands were mapped (Bailey and Cochrane 1985). The geographic extent of all four sands were updated, with sands identified in areas not previously documented. In other cases, stratigraphic assignments were corrected. Petrographic characteristics of the sands, based upon examination of samples of drill cuttings, are now documented. Formation or member top picks have been added or edited for 818 wells, and 198 picks determined to be erroneous have been deleted from OPDS. The revised data has been incorporated into the 3-D model.

3.3 Data filtering, processing and export

The edited and enhanced formation top data is exported from the OPDS Oracle database and provided to the modelling group in a text-based (csv) format suitable for importing to Leapfrog. Prior to creation of the csv file the data is processed through a series of filters as a final data quality routine.

Data is extracted from OPDS by the OGSRL using a direct connection to the database available at the OGSRL. The data extraction process is run on a weekly basis and used by the OGSRL to update petroleum well data on the OGSRL website and to provide data access to library clients and partners, including those involved in modeling. OGSRL and MNRF have security measures in place that ensure only non-confidential geological data is exported. Under Ontario petroleum permit regulations new petroleum development well results remain confidential for thirty days after reaching total depth and exploration well results remain confidential for a year. Regardless of suitability for modeling, geological data from confidential wells are not included.

OGSRL petroleum well data is a weekly snapshot of OPDS stored in a MySQL database. All further data editing and screening is done on the snapshot data in MySQL. MySQL is widely available in webserver environments and is used by the OGSRL in its main duty of providing access to data.

OPDS geology data is stored as formation top picks with each row being one pick. LeapFrog modeling software requires formation tops and bottoms to create 3-D formation volumes. The first major processing step is to add a new field to the database and assign formation bottoms to all formation top picks that will be used in the model. Although not explicitly recorded in OPDS as bottoms, the bottom of any formation is the top of the next formation below it. Problems arise when the top of the next formation has not been picked, has not been picked correctly, and when the next expected formation changes due to the geographic constraints on some formations. These problems are resolved by OGSRL staff filling in and correcting formation pick data as part of the QA process and by assigning the uppermost in a range of formations (Table 5) as the formation bottom. Some formations from the total stratigraphic sections (Figure 2) have too few picks to model. By not including formations with a small number of picks in the top-bottom lookup table (Table 5) they are automatically dissolved into the overlying modeled formation in the modeling data. For example, the Reynales Formation was dissolved into the Irondequoit Formation. Early models exhibited poor characteristics for these formations when modeled separately and combining the two formations produced superior results. Any wells with only a Reynales Formation pick became Irondequoit Formation picks and in all wells the bottom of Irondequoit Formation was pushed to the bottom of the Reynales Formation. For the Precambrian an arbitrary maximum thickness of 500 m was added for modeling purposes.

A final filter was applied using the QA codes (Table 3) that had been added during the geological QA – QC process. Geologic formation picks with a QA code of -1 or -2 were removed from the modeling data. A total of 1,352 picks were removed from the model by this filter. These picks had been observed to cause anomalies but could not be corrected in the project timeframe (QA code = -1) or could not be corrected or verified in the absence of geologic data (QA code = -2).

Geological data were exported for modeling in two text-based csv files. A primary table containing approximately 194,000 geologic picks with formation tops and formation bottoms was exported to create the main volumes. A secondary table containing approximately 52,000 geologic picks with only formation tops was exported to assist the modeler in filling gaps in the model surfaces. The secondary geologic table

Table 5. Formations to include in model and the deepest formation to be used for assignment of a bottom depth.

Formation Name	Deepest Formation Bottom
Port Lambton Group	Kettle Point
Kettle Point	Hamilton Group
Hamilton Group	Dundee
Marcellus	Dundee
Dundee	Amherstburg
Columbus	Lucas
Lucas	Sylvania
Amherstburg, Onondaga	Bois Blanc
Sylvania	Bois Blanc
Bois Blanc	Bass Islands/Bertie
Springvale	Bass Islands/Bertie
Oriskany	Bass Islands/Bertie
Bass Islands/Bertie	G Unit
G Unit	F Salt
F Unit	C Unit
F Salt	C Unit
E Unit	C Unit
D Unit	C Unit
C Unit	A-2 Carbonate
B Unit	A-2 Carbonate
B Equivalent	A-2 Carbonate
B Salt	A-2 Carbonate
B Anhydrite	A-2 Carbonate
A-2 Carbonate	Guelph
A-2 Shale	Guelph
A-2 Salt	Guelph
A-2 Anhydrite	Guelph
A-1 Carbonate	Guelph
A-1 Evaporite	Guelph
Guelph	Gasport
Eramosa	Gasport
Goat Island	Gasport
Gasport	Irondequoit
Decew	Irondequoit
Rochester, Lion's Head	Irondequoit
Irondequoit, Reynales, Fossil Hill, Rockway, Merriton	Cabot Head
St Edmund	Wingfield
Wingfield	Dyer Bay
Dyer Bay	Cabot Head
Neahga	Cabot Head
Thorold	Cabot Head
Grimsby	Cabot Head
Cabot Head	Whirlpool
Manitoulin	Queenston
Whirlpool	Queenston
Queenston	Georgian Bay-Blue Mountain
Georgian Bay-Blue Mountain	Cobourg
Cobourg	Sherman Fall
Sherman Fall	Kirkfield
Kirkfield	Coboconk
Coboconk	Gull River
Gull River	Shadow Lake
Shadow Lake	Precambrian
Cambrian	Precambrian
Precambrian	Precambrian Top + ~500m

does not have overlapping formation picks with the primary table and data exists in this table only when a corresponding bottom pick could not be found for a formation. Approximately 46,000 formation top picks in OPDS belong to formations or groups that were not modeled or were modeled as part of another formation.

Well collars located with latitude, longitude, and elevation are provided in a separate csv table. During the QA process erroneous well surface locations and/or elevations were found to be the cause of some geologic anomalies. Any anomalies caused by bad location data were corrected in OPDS. All corrections to geologic data and well collars in OPDS automatically become available to all OGSRL clients and partners on a weekly basis with each refreshed database snapshot.

4. Measured sections, stratigraphic control points and Michigan wells

After several modelling iterations there remained areas where the modeled formation layers did not agree with existing mapping or exhibited unrealistic changes in thickness or structure. In particular, model layers of many Silurian

formations that outcrop on the face of the Niagara Escarpment displayed gaps or did not extend to the escarpment edge. In many cases this is due to sparse data coverage due to lack of petroleum wells drilled near the escarpment. The sparse data density does not provide sufficient guidance to the modeling algorithm to control interpolation/extrapolation of layers. This was resolved by addition of a limited number of control points and measured sections to control formation layer extrapolation to more closely match the published geological maps of the Paleozoic geology of southern Ontario, especially near the Niagara Escarpment.

Formation top picks for 15 locations at the escarpment edge have been added using measured outcrop sections adapted from Bolton (1957), in addition to unpublished data from shallow OGS boreholes provided by Yeung and Brunton. Geologic data from 3 Michigan petroleum wells (Lilienthal 1978) were added to the project database to resolve an extrapolation issue beneath Lake Huron caused by lack of data (Figure 1).

To minimize interpolative artifacts due to sparse data, "prognostic" or synthetic boreholes were created in areas with gaps in the modelled formation layers. A prognostic well is a location for which the geological formation contacts have been interpreted based on the data available from the nearest petroleum wells and/or measured sections, at distances varying from 2 to nearly 15 km. A total of 23 prognostic wells were added to the database as control points (Figure 1). Ground elevation for these wells is derived from the MNRF Digital Elevation Model, depth to top of bedrock is derived from Gao et al. (2006), and the latitude and longitude coordinates and the lot/concession/township is derived from the MNRF digital base maps of Ontario. Control points and measured sections in the project database have unique codes as the borehole identifier so that these values can be removed in the future as new well data becomes available.

5. Bedrock topography data enhancements

For early model iterations, a published bedrock surface (Gao et al. 2006) was used as part of a 3-D reference framework to aid borehole log interpretation and to constrain the extrapolation of the modelled layers to the subcrop surface. An updated bedrock surface was developed using revised well log vetting. The identification of incorrect bedrock terms and location vetting for modelling was enhanced by identified data issues and location revisions along the Niagara Escarpment supplied by OGS staff (Yeung and Brunton) and by OGSRL staff (Somers, Sun) for the southern Niagara Peninsula. An additional 16,304 top of bedrock values were supplied from the OPDS database by OGSRL staff. This updated and vetted data was developed through collaborative bedrock modelling efforts (Carter et al. 2020).

6. Digital subcrop map

OPDS formation top data is the primary data source for 3-D modelling. The modelling software utilizes the formation depth intervals to enforce model layer chronology. The surfaces of model layers are also augmented by 3-D vector objects. For this model, digital bedrock topography and 2-D geological subcrop mapping are combined to assemble grids of 3-D points for each mapped formation. These point grids are added to corresponding model formations to better align them to mapped geology in areas of little or no borehole data. Initial versions of the model utilized digital mapping by Armstrong and Dodge (2007).

MNRF (Lee Fortner, Maia Somers) initiated an independent project in 2016 to edit and update the digital subcrop map previously published by OGS (Armstrong and Dodge 2007) GSC Map 1263A (Sanford 1969). The initial focus of this project was a review of the subcrop formation identifications recorded in OPDS, by comparison to the digital bedrock geology map. Any inconsistencies between the formations identified as Top of Bedrock within petroleum well records in OPDS and the subcropping formations named in the corresponding locations on the digital map were identified. Subsequent corrections were made to bring OPDS and the mapped layer boundaries into geospatial continuity by either changing the formation designated as Top of Bedrock in OPDS or adjusting the boundaries of a formation's mapped area in the digital map, or both. Corrections are based, in part, on examination of drill cuttings and geophysical logs for 616 wells in OPDS. Other corrections, including some associated with legacy data entry errors, were identified after examination of original petroleum well drilling records. In particular, detailed documentation of 68 revised formation-top picks have been made for the problematic subcropping Onondaga, Amherstburg, Bois Blanc, and Bass Islands formations, and formations of the Salina Group in the Niagara Peninsula and neighbouring parts of Lake Erie.

Later stages of the MNRF project were synchronised with the 3-D project to improve accuracy, precision and extent of 3-D point grids to control interpolation and extrapolation of modelled formation layers. Extrapolation of the bedrock geology beneath the Lake Huron and Lake Erie is based in part on GSC Map 1335A (Sanford and Baer 1971) and GSC Map 1263A (Sanford 1969), with new interpretations for Lake Huron and Georgian Bay based on recently interpreted bedrock topography (Todd et al. 2020; Todd and McNamara 2018; McNamara and Todd 2018). The Salina Group polygon has been subdivided into formations based on Sanford (1969) and the Clinton-Medina Group polygon has been subdivided into the Clinton Group and the Medina (Cataract) groups and their constituent formations based on mapping by Armstrong and Dodge (2007). Formation contacts in the Niagara Peninsula were updated for consistency with new mapping (Armstrong 2017; Sun 2018; Sun et al. 2017). Detailed notes contain

formation top depth and thickness, descriptions of drill cuttings, drill cutting photographs, as well as quality assurance codes and the geological reasoning for the revisions. Stratigraphic terminology and subdivisions are consistent with the revised stratigraphic chart (Figure 2) (Brunton et al. 2017; Carter et al. 2017). Further improvements are ongoing as the digital subcrop map is intended to be a live electronic document open to regular review and updates.

7. Petroleum well drill core analyses

Operators of petroleum wells in southern Ontario have acquired approximately 1,100 drill cores from selected depth intervals and geological formations, using standard petroleum industry drilling and coring techniques. Core analysis data includes: well licence number, date analysed, depth interval, geological formation, porosity, vertical permeability, horizontal permeability, oil saturation, water saturation, bulk density and grain density. This information is available for viewing by Library members at www.ogsrlibrary.com. A subset of these drill cores have been analyzed at commercial laboratories for the well operator (Figure 3). The analyzed interval is usually within an oil or gas reservoir or interval and may include both the reservoir rock and the surrounding rocks comprising the reservoir seal(s). The core analyses in the possession of the OGSRL have been completed by a small number of commercial laboratories from 1954 to 2003, using methods and standards in use at the time of analysis. These analyses provide valuable hydrogeologic data reflecting geographic and stratigraphic variations in porosity and permeability within the bedrock formations of southern Ontario. Comparison and normalization of analytical methods and results of the different laboratories has not yet been completed.

The core analysis source data are hard-copy reports archived in individual well files at the OGSRL. The reports were scanned during a previous data digitization project. For the present project the data in the core analysis reports were manually entered into an Excel spreadsheet. For quality assurance purposes formations represented by each core analysis interval were identified by an algorithm matching the depth interval in the core analysis report to the formation contact depths recorded for the corresponding well in OPDS and appended to the spreadsheet. A quality assurance review indicated that the algorithm worked well with the exception of a small number of mismatches caused principally by unit of measure errors in the core depth interval (metres vs feet) in the database. This caused a match to the wrong depth intervals in the OPDS database and have been corrected. Geographic coordinates for each core analysis were also appended to the spreadsheet.

A total of 28,839 core interval analyses are available from 491 different wells, representing a cumulative cored interval of nearly 13,850 metres. Analyses are available for 43 of the 54 bedrock formations within the current 3-D model with the number of wells with analysis per formation ranging from 1 to 228. The formations with analyses from the greatest number of wells includes: Grimsby Formation (228 wells); Thorold Formation (182 wells); Lockport Group (157 wells); Cabot Head Formation (142 wells); Irondequoit-Fossil Hill-Reynales Formation (84 wells); A-1 Carbonate Unit (77 wells); and Cambrian (53).

8. Hydrochemical regime interface mapping

Over 35,000 records of water-bearing intervals have been entered into OPDS (Carter et al. 2015a) from the hard-copy petroleum well records. These records include a subjective description of the type of water encountered (black, brackish, fresh, mineral, salt, sulphur), including loss of circulation zones, and the top of the depth interval at which it occurs. The geological formation(s) in which water occurs has been interpreted by MNRF geologists, by comparison of the water interval depths to the formation top depths recorded for the wells and recorded in OPDS. This data has been used to interpret depth-related hydrochemical zonation of water in the bedrock of southern Ontario: shallow fresh water in the surficial sediments and shallow bedrock; brackish to saline sulphur water at intermediate depths; and dense brines in the deepest bedrock (Figure 4; Carter et al. 2014, 2015a, 2015b; Clark et al 2010, 2013; Hobbs et al. 2011; Nuclear Waste Management Organization 2011; Sharpe et al. 2014).

There are approximately 9,000 records where water type was recorded as sulphur water by the driller. This was the principal source of data used to generate a map interpreting geographic variations in the depth to the base of the deepest recorded intervals of sulphur water relative to the top of bedrock. The resulting map approximates the minimum depth of the interface between the intermediate regime of brackish to saline sulphur water and the deep brines at approximately 200 to 300 metres below the top of bedrock and locally to 350 metres (Carter and Sutherland 2018, 2020). Map QA/QC review and interpretation was supplemented with mapping of salinity gradients in the Lockport Group using water analyses from Skuce (2014) and petroleum industry water analyses compiled from MNRF petroleum well records.

9. Field mapping of bedrock groundwater flow systems of the Lockport Group

The OGS is involved in a program of regional-scale mapping of bedrock groundwater flow systems within the Early Silurian Lockport Group of the Niagara Escarpment (e.g., Priebe et al. 2017, 2018). The program has three main components: Geologic mapping and sampling of key outcrops, quarry sections and cores, hydrogeological investigations of selected deep bedrock wells, and instrumentation of selected deep bedrock wells. Phase 1 involved the mapping of key outcrops within select quarry, roadside, railway and cliff sections.

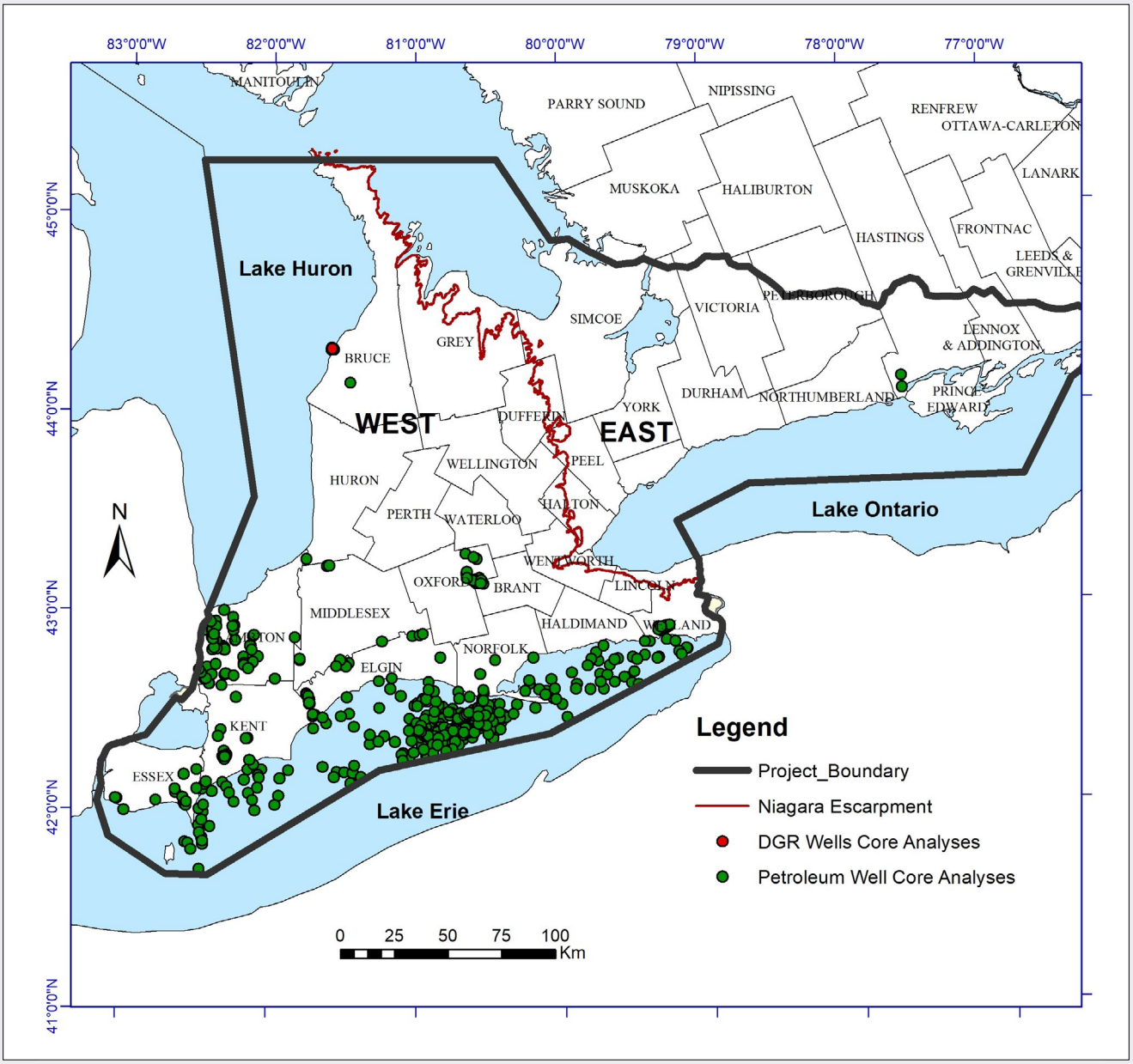


Figure 3. Location of wells with drill core analysis.

Stratigraphic sections were measured and used to establish and/or update reference and type sections for the various formations of the Lockport Group (e.g., Brunton 2009; Brunton et al. 2009; Brunton and Brintnell 2011; Cramer et al. 2011; Brunton et al. 2012; Bancroft, Kleffner and Brunton 2016). Phase 2 involved hydrogeological investigations of select OGS and municipal partner bedrock boreholes, and phase 3 involved instrumentation of select holes (see Priebe et al. 2017, 2018).

Insights gained from these ongoing studies and stratigraphic data from shallow boreholes were utilized in this project to improve reliability of OPDS formation top picks for the Lockport Group and were the principal basis for development of the revised stratigraphic chart utilized for the project (Figure 2).

10. Summary and discussion

Significant improvements have been made to the geological data infrastructure of southern Ontario through a process of capture and compilation of existing data, QA/QC edits to the existing data and creation and addition of new data with edits completed to 30,320 formation top picks in 7,812 wells. These improvements are incremental to ongoing programs of data collection and improvement at the OGS, MNRF and OGSRL,

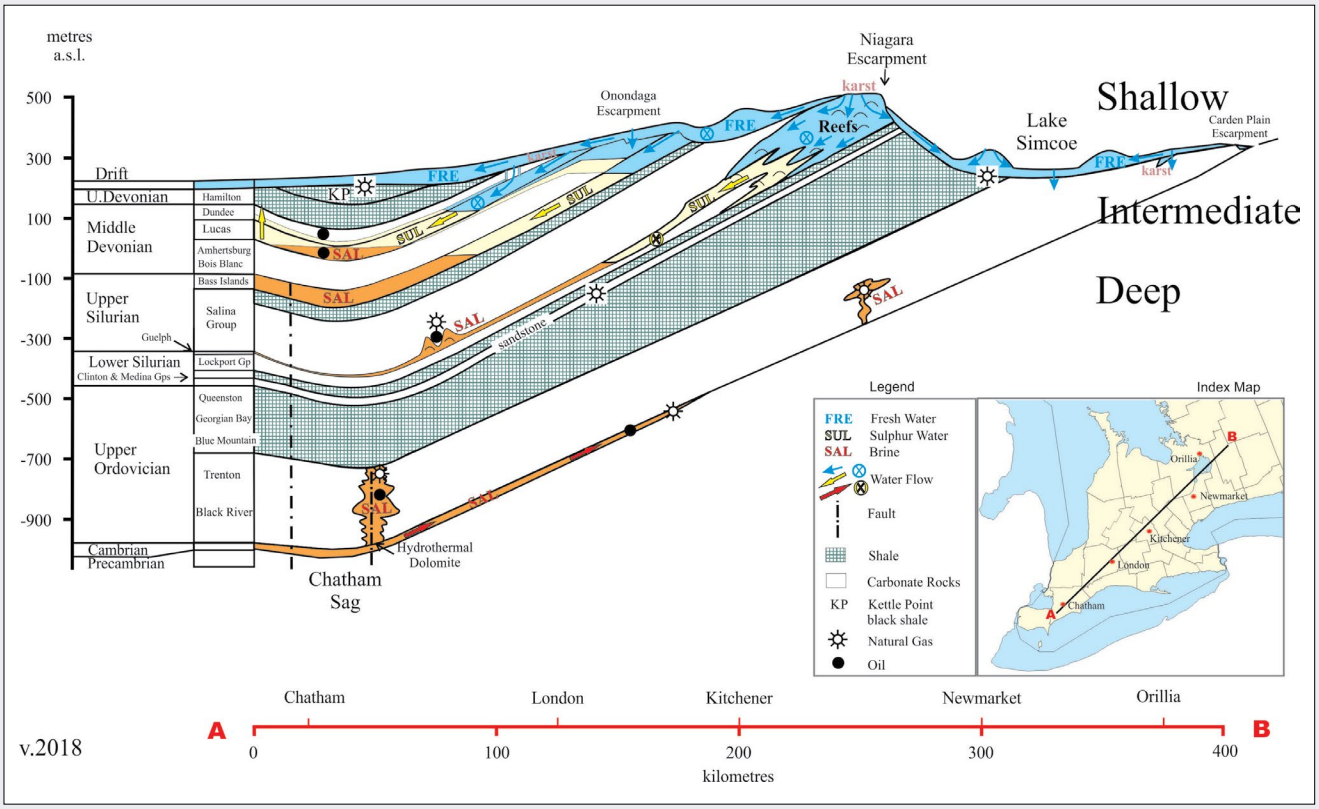


Figure 4. Hydrochemical depth zonation of bedrock aquifers in southern Ontario, showing location of sulphur water relative to the bedrock surface. Modified from Carter et al. (2014).

and were specifically directed at supporting generation of a 3-D lithostratigraphic model of the Paleozoic bedrock of southern Ontario (Carter et al. 2020).

The OPDS and its supporting information was a key source of data and illustrates the value of a properly constructed and actively maintained wells database. Mapping and modelling of the subsurface bedrock geology of southern Ontario is only possible thanks to a long history of petroleum well data collection and data management efforts by many individuals and organizations, initiated by the GSC in the late 1800's and continued by the MNRF since 1971. The first petroleum well database was created in 1964 and has undergone a long history of updates, enhancements, and replacements since that time, without which this project would not have been possible.

Further improvements to formation top picks in OPDS are still needed, which would in turn result in improvements in 3-D modelling of the bedrock geology. The database is known to have incomplete/inaccurate picks for: Collingwood Member of Cobourg/Lindsay Formation, Rouge River Member of Blue Mountain Formation, and the Decew Formation. There are still approximately 9,000 wells for which the Guelph Formation is the only formation within the Lockport Group with a formation top pick. Picks have not been made for the constituent formations of the Hamilton Group (Ipperwash, Widder, Hungry Hollow, Arkona, Rockport Quarry, Bell formations) or for the unsubdivided Cambrian. The Georgian Bay and Blue Mountain formations are modelled as one layer as formation top picks have not been made for the Blue Mountain Formation. Subdivision of the Irondequoit-Rockway-Merriton-Fossil Hill-Reynales interval into its constituent formations is inconsistent and inaccurate. There are also a miscellaneous assortment of minor inconsistencies in the 3-D model caused by scattered data anomalies.

11. Acknowledgements

We thank all the early and modern data visionaries at GSC and MNRF for their recognition of the value of collection and management of subsurface geological data from the drilling of petroleum wells in Ontario. Since 1998, funds for the continued management of this data and for public access at the Oil, Gas and Salt Resources Library have been provided by the petroleum industries of Ontario through the Oil, Gas and Salt Resources Trust. The Ontario Petroleum Institute is thanked for providing administrative and management support to the Library in its role as Trustee of the Oil, Gas and Salt Resources Trust. An internal review at the GSC was completed by H. Russell. This work is a contribution of the GSC–OGS Southern Ontario project on groundwater 2014–2019.

12. References

Armstrong, D.K. 2017. Paleozoic geology of the Welland-Fort Erie area, southern Ontario. Ontario Geological Survey, Preliminary Map P.3811, scale 1:50,000.

Armstrong, D.K. 2018. Paleozoic geology of the Dunnville area, southern Ontario. Ontario Geological Survey, Preliminary Map P.3810, scale 1:50,000.

Armstrong, D.K. and Carter, T.R. 2010. The subsurface Paleozoic stratigraphy of southern Ontario. Ontario Geological Survey, Special Volume 7, 301 p.

Armstrong, D.K. and Dodge, J.E.P. 2007. Paleozoic geology of southern Ontario. Ontario Geological Survey, Miscellaneous Release—Data 219.

Bailey Geological Services Ltd. and Cochrane, R.O. 1985. Evaluation of the conventional and potential oil and gas reserves of the Devonian of Ontario (Volume 1). Ontario Geological Survey, Open File Report 5555, 178 p.

Bajc, A.F. and Dodge, J.E.P. 2011. Three-dimensional mapping of surficial deposits in the Brantford–Woodstock area, southwestern Ontario. Ontario Geological Survey, Groundwater Resources Study 10.

Bajc, A.F. and Shirota, J. 2007. Three-dimensional mapping of surficial deposits within the Regional Municipality of Waterloo, southwestern Ontario. Ontario Geological Survey, Groundwater Resources Study 3, 41p. ISBN 978-1-4249-4393-7

Bancroft, A.M., Kleffner, M.A., and Brunton, F.R. 2016. Biochemostratigraphy of the Eramosa Formation in southwestern Ontario, Canada. Canadian Journal of Earth Sciences, 53: 749-762. https://doi.org/10.1139/cjes-2015-0223

Beards, R.J. 1967. Guide to the subsurface Paleozoic stratigraphy of southern Ontario. Ontario Department of Energy Resources Management, Paper 67-2, 19 p.

Birchard, M.C., Rutka, M.A., and Brunton, F.R. 2004. Lithofacies and geochemistry of the Lucas Formation in the subsurface of southwestern Ontario: A high-purity limestone and potential high-purity dolostone resource. Ontario Geological Survey, Open File Report 6137, 180 p.

Bolton, T.E. 1957. Silurian stratigraphy and palaeontology of the Niagara Escarpment in Ontario. Geological Survey of Canada, Memoir 289, 145 p.

Brunton, F.R. 2009. Update of revisions to Early Silurian stratigraphy of Niagara Escarpment: integration of sequence stratigraphy/sedimentology/hydrogeology to delineate hydrogeologic units (HGUs). In Summary of Field Work and Other Activities 2009, Ontario Geological Survey, Open File Report 6240, 25-1 to 25-20.

Brunton, F.R. and Brintnell, C. 2011. Final update of Early Silurian stratigraphy of the Niagara Escarpment and correlation with subsurface units across southwestern Ontario and the Great Lakes Basin. In Summary of Field Work and Other Activities 2011, Ontario Geological Survey, Open File Report 6270, 30-1 to 30-11.

Brunton, F.R., Brintnell, C., Jin, J., and Bancroft, A.M. 2012. Stratigraphic architecture of the Lockport Group in Ontario and Michigan – A new interpretation of Early Silurian "basin geometries" and "Guelph Pinnacle Reefs". In 51st Annual Conference – Ontario – New York, Oil & Gas Conference, Oct. 23-25, 2012, Niagara Falls, Ontario, 1-37.

Brunton, F.R., Turner, E., and Armstrong, D. 2009. A guide to the Paleozoic geology and fossils of Manitoulin Island and northern Bruce Peninsula, Ontario, Canada. Geological Association of Canada, Canadian Paleontological Conference, Field Trip Guidebook 14, www.researchgate.net/publication/304540057.

Brunton, F.R., Carter, T.R., Logan, C., Clark, J., Yeung, K., Fortner, L., Freckelton, C., Sutherland, L., and Russell, H.A.J. 2017. Lithostratigraphic compilation of Phanerozoic bedrock units and 3D geological model of southern Ontario. In Russell, H.A.J., Ford, D., and Priebe, E.H. compilers. Regional-scale Groundwater Geoscience in Southern Ontario: an Ontario Geological Survey, Geological Survey of Canada, and Conservation Ontario open house, Geological Survey of Canada, Open File 8212, p.3.

Burt, A.K. and Dodge, J.E.P. 2011. Three-dimensional modelling of surficial deposits in the Barrie–Oro moraine area of southern Ontario. Ontario Geological Survey, Groundwater Resources Study 11, 125 p.

Burt, A.K. and Dodge, J.E.P. 2016. Three-dimensional modelling of surficial deposits in the Orangeville–Fergus area of southern Ontario. Ontario Geological Survey, Groundwater Resources Study 15, 155 p.

Carter, T.R. 2001. Digital well data for Ontario – a progress report. Ontario Petroleum Institute, v. 40, technical paper 4, 8 p.

Carter, T.R. 2017. Ontario Oil, Gas and Salt Resources Library: A model for groundwater data sharing in Ontario? Geological Survey of Canada, Open File 8213, 25 p.

Carter, T.R. and Castillo A.C. 2006. Three-Dimensional Mapping of Paleozoic Bedrock Formations in the Subsurface of Southwestern Ontario: A GIS Application of the Ontario Petroleum Well Database. In Harris, J. Ed. GIS for the Earth Sciences, Geological Association of Canada, 435-450.

Carter, T.R. and Clark, J. 2018. Base of fresh water, bedrock karst, and the contact aquifer in southern Ontario, as interpreted from water well records. Oil, Gas and Salt Resources Library, Open File Data Release 2018-1, 16 p.

Carter, T.R. and Sutherland, L. 2018. Mapping the interface between the intermediate sulphur water regime and deep brine in the Paleozoic bedrock of southwestern Ontario. Oil, Gas and Salt Resources Library, Open File Data Release 2018-2, 22 p.

Carter, T.R. and Sutherland, L. 2020. Interface mapping of hydrochemical groundwater regimes in the Paleozoic bedrock of southwestern Ontario. In Russell, H.A.J. and Kjarsgaard, B.A. Eds. Southern Ontario groundwater project 2014–2019: summary report. Geological Survey of Canada, Open File 8536, 37-48. https://doi.org/10.4095/321083

Carter, T.R., Fortner, L., Skuce, M.E., and Longstaffe, F.J. 2014. Aquifer systems in southern Ontario: Hydrogeological considerations for well drilling and plugging. abstract, Canadian Society of Petroleum Geologists, Geoconvention 2014.

Carter, T.R., Wang, D., Castillo, A.C., and Fortner, L. 2015a. Water type maps of deep groundwater from petroleum well records, southern Ontario. Open File Data Release 2015-1, 10 p.

Carter, T.R., Wang, D., Castillo, A.C., and Fortner, L. 2015b. Static level maps of deep groundwater from petroleum well records, southern Ontario. Oil, Gas and Salt Resources Library, Open File Data Release 2015-2, 11 p.

Carter, T.R., Brunton, F.R., Clark, J., Fortner, L., Hamblin, A., Logan, C., and Russell, H.A.J. 2016. 3D hydrostratigraphic modelling of the Paleozoic bedrock of southern Ontario; In Russell, H.A.J. and Priebe, E. Compilers. Regional-scale Groundwater Geoscience in Southern Ontario: An Ontario Geological Survey and Geological Survey of Canada groundwater geoscience open house, Geological Survey of Canada, Open File 8022, p.5.

Carter, T.R., Brunton, F.R., Clark, J., Fortner, L., Freckelton, C.N., Logan, C.E., Russell, H.A.J., Somers, M., Sutherland L., and Yeung, K.H. 2017. Status report on three-dimensional geological and hydrogeological modelling of the Paleozoic bedrock of southern Ontario. In Summary of Field Work and Other Activities, 2017, Ontario Geological Survey, Open File Report 6333, 28-1 to 28-15.

Carter, T.R., Brunton, F.R., Clark, J.K., Fortner, L., Logan, C.E., Russell, H.A.J., Somers, M., Sutherland, L., and Yeung, K. 2020. Three-dimensional geological modelling of the Paleozoic bedrock of southern Ontario: Status update. In Russell, H.A.J. and Kjarsgaard, B.A. Eds. Southern Ontario groundwater project 2014–2019: summary report. Geological Survey of Canada, Open File 8536, 7-21. https://doi.org/10.4095/321080

Clark, I.D., Al, T., Jensen, M., Kennell, L., Mazurek, M., Mohapatra, R., and Raven, K.G. 2013. Paleozoic-aged brine and authigenic helium preserved in an Ordovician shale aquiclude. Geology, 41: 9, 951-954. https://doi.org/10.1130/G34372.1

Clark, I., Mohapatra, R., Mohammadzadeh, H., and Kotzer, T. 2010. Porewater and gas analysis in DGR-1 and DGR-2 core. Nuclear Waste Management Organization, Technical Report TR—07-21, 25 p.

Cramer, B.D., Brett, C.E., Melchin, M.J., Männik, P., Kleffner, M.A., McLaughlin, P.I., Loydell, D.K., Munnecke, A., Jeppsson, L., Corradini, C., Brunton, F.R., and Saltzman, M.R. 2011. Revised correlation of Silurian Provincial Series of North America with global and regional chronostratigraphic units and $\delta^{13}C_{carb}$ chemostratigraphy. Lethaia, 44: 185-202. https://doi.org/10.1111/j.1502-3931.2010.00234.x

Davis, C.L. 2017. Quartzose sands in the Lower to Middle Devonian strata of southwestern Ontario: Geographic distribution and characterization in drill cuttings and geophysical logs. Geological Survey of Canada, Open File Report 8286, 37 p.

Gao, C., Shirota, J., Kelly, R.I., Brunton, F.R., and Van Haaften, S. 2006. Bedrock topography and overburden thickness mapping, southern Ontario. Ontario Geological Survey, Miscellaneous Release—Data 207.

Griffiths, M., Russell, H.A.J., and Logan, C.E. 2020. Machine learning applied to geoscience: Geo-referenced character recognition. In Russell, H.A.J. and Kjarsgaard, B.A. Eds. Southern Ontario groundwater project 2014–2019: summary report. Geological Survey of Canada, Open File 8536, 65-74. https://doi.org/10.4095/321092

Hobbs, M.Y., Frape, S.K., Shouakar-Stash, O., and Kennell, L.R. 2011. Regional hydrogeochemistry—Southern Ontario. Nuclear Waste Management Report NWMO DGR-TR-2011-12, Toronto, Canada.

Intera Engineering Ltd, 2011. Descriptive geosphere site model. Nuclear Waste Management Organization, Technical Report DGR-TR-2011-24.

Liberty, B.A. and Bolton, T.E. 1971. Paleozoic geology of the Bruce Peninsula area, Ontario. Geological Survey of Canada, Memoir 360, 163 p. https://doi.org/10.4095/102382

Lilienthal, R.T. 1978. Stratigraphic cross-sections of the Michigan Basin. Michigan Department of Natural Resources, Geological Survey Division, Report of Investigation 19, 36 p.

Logan, C.E., Russell, H.A.J., Bajc, A.F., Burt, A., Mulligan, R.P.M. and Sharpe, D.R. 2020. A three-dimensional surficial geology model of southern Ontario: Progress report. In Russell, H.A.J. and Kjarsgaard, B.A. Eds. Southern Ontario groundwater project 2014–2019: summary report. Geological Survey of Canada, Open File 8536, 49-64. https://doi.org/10.4095/321084

McNamara, G.D. and Todd, B.J. 2018. Processing of interpreted seismic-reflection data from expedition 69-2-01 of the CSS Limnos, Lake Huron, Ontario, Canada and Michigan, U.S.A. Geological Survey of Canada, Open File 8429, 1 .zip file. https://doi.org/10.4095/308377

Nuclear Waste Management Organization 2011. Geosynthesis. Nuclear Waste Management Report NWMO DGR-TR-2011-11, PDF document, accessed at: http://www.opg.com/generating-power/nuclear/nuclear-waste-management/Deep-Geologic-Repository/Pages/Project-Development.aspx, under "Geoscience Reports", accessed on June 30, 2014.

Priebe, E.H., Neville, C.J., and Brunton, F.R. 2017. Discrete, high-quality, hydraulic conductivity estimates for the early Silurian carbonates of the Guelph region. Ontario Geological Survey, Groundwater Resources Study 16, 45 p.

Priebe, E.H., Brunton, F.R., Rudolph, D.L., and Neville, C.J. 2018. Geologic controls on hydraulic conductivity in a karst-influenced carbonate bedrock groundwater system in southern Ontario, Canada. Hydrogeology Journal, https://doi.org/10.1007/s10040-018-1911-2

Russell, H.A.J., Bajc, A.F., Brunton, F.R., Carter, T.R., and Logan, C.E. 2015. Toward a 3D hydrostratigraphic framework for southern Ontario. In Abstracts with Programs, Geological Society of America Annual Meeting in Baltimore, Maryland, USA (1–4 November 2015), 47: 7, 407.

Russell, H.A.J., Bajc, A.F., Burt, A.K., Logan, C.L., Mulligan, R.P.M., and Sharpe, D.R. 2016. A three-dimensional surficial stratigraphic model for southern Ontario. In Russell, H.A.J. and Priebe, E.H. Compilers. Regional-scale Groundwater Geoscience in Southern Ontario: An Ontario Geological Survey and Geological Survey of Canada groundwater geoscience open house, Geological Survey of Canada, Open File 8022, p.16.

Russell, H.A.J. and Dyer, R.D. 2016. Ontario Geological Survey–Geological Survey of Canada Groundwater Geoscience Collaboration: Southern Ontario 2015–2019. In Summary of Field Work and Other Activities 2016, Ontario Geological Survey, Open File Report 6323, p.35-1 to 35-15.

Sanford, B.V. 1969. Geology, Toronto–Windsor area, Ontario. Geological Survey of Canada, Map 1263A, scale 1:250 000. https://doi.org/10.4095/109120

Sanford, B.V. and Baer, A.J. 1971. Southern Ontario, sheet 30S. Geological Survey of Canada, Map 1335A, scale 1 000 000.

Sharpe, D.R., Piggott, A., Carter, T., Gerber, R.E., MacRitchie, S.M., de Loë, R.C., Strynatka, S., and Zwiers, G. 2014. Southern Ontario hydrogeological region. In Rivera, A. Ed. Canada's Groundwater Resources, Fitzhenry & Whiteside, p.443-499. https://doi.org/10.4095/296947

Sun, S. 2018. Stratigraphy of the Upper Silurian to Middle Devonian, southwestern Ontario. University of Western Ontario, Electronic Thesis and Dissertation Repository, article 5230.

Sun. S., Brunton, F.R., and Jin, J. 2017. Lithofacies and stratigraphy of the Devonian Onondaga Formation, southwestern Ontario. Ontario Geological Survey, Summary of Field Work and Other Activities 2017, Open File Report 6333, 23-1 to 23-23.

Todd, B.J. and McNamara, G.D. 2018. Processing of seismic-reflection data from expedition 91800 of the RV Laurentian, Lake Huron and Georgian Bay, Ontario, Canada and Michigan, U.S.A. Geological Survey of Canada, Open File 8428, 1 .zip file. https://doi.org/10.4095/308328

Todd, B.J., Lewis, C.F.M., Russell, H.A.J., and Pyne, M.D. 2020. Legacy seismic reflection data from the Great Lakes: Recovery and applications. In Russell, H.A.J. and Kjarsgaard, B.A. Eds. Southern Ontario groundwater project 2014–2019: summary report. Geological Survey of Canada, Open File 8536, 75-82. https://doi.org/10.4095/321093

Interface mapping of hydrochemical groundwater regimes in the Paleozoic bedrock of southwestern Ontario

Terry R. Carter[1]* and Liz Sutherland[2]

Abstract: Groundwater in southern Ontario exhibits a crude hydrochemical zonation, by increasing depth, of shallow fresh water, brackish to saline sulphur water at intermediate depths, and deep brine, within a system of thin aquifers separated by thick aquitards. Aquifers are recharged by meteoric water at their outcrop and subcrop edges.

The present study has mapped geographic variations in the interpreted depth of the interface/transition zone between the intermediate sulphur water regime and deep brine. Available data indicates a regional depth transition from brackish-to-saline sulphur water to deep brine at approximately 200 to 300 m below the top of bedrock and locally to 350 m, with local variation largely related to down-dip distance from subcrop/outcrop edges.

The intermediate regime is interpreted to be formed by penetration of both modern meteoric water and glacial meltwater into subcropping/outcropping porous and permeable bedrock strata, with downdip flow over a distance of 25 to 65 km, and partial to complete displacement and dilution of original pore fluids. Stratigraphically, the water of the shallow and intermediate regimes is generally confined above the Salina Group. The interface boundary with deep brine approximates the base of interaction of groundwater with surface water and can be used as a depth constraint for downward penetration of meteoric water in numeric modelling. Accurate knowledge of interface boundary depths is also needed in design of petroleum well drilling, casing and cement programs to mitigate drilling hazards posed by corrosive sulphur water and potential release of H_2S gas at surface. The maps can be used as a constraint on the drilling depth of new water wells, as at deeper depths progressively more saline waters will likely be encountered.

1. Introduction and purpose

Groundwater in Paleozoic bedrock formations and the overlying unconsolidated sediments in southern Ontario has depth-related hydrochemical zonation. Fresh water occurs at or near the surface in the surficial sediment and shallow bedrock; brackish to saline sulphur water occurs at intermediate depths (30 to 350 m); and dense brines occur in the deepest bedrock (Carter et al. 2015a, 2015b; Carter et al. 2014; Clark et al. 2010a, 2010b, 2011, 2013; Hobbs et al. 2011; Nuclear Waste Management Organization 2011; Sharpe et al. 2014) (Figure 1). The base of the fresh water regime, i.e. the depth at which the water is no longer potable, has been mapped by Carter and Clark (2018) in a cooperative project of the MNRF and the Oil, Gas and Salt Resources Library. The term sulphur water is used by drillers of water wells and petroleum wells to describe any water with a distinctive rotten egg smell which indicates the presence of dissolved H_2S. In this report sulphur water is used in a slightly more restricted sense to refer to brackish to saline water containing dissolved H_2S at intermediate depths and does not include brines associated with deep sour gas reservoirs in southwestern Ontario.

In this report, description of water salinity uses the terminology of Carpenter (1978) and Freeze and Cherry (1979) as adopted by Hiscock and Bense (2014).

Water type	mg/l TDS
Fresh	0–1,000
Brackish	1,000–10,000
Saline	10,000–100,000
Brine	>100,000

[1] Consulting Geologist, London, ON
[2] Western Libraries, University of Western Ontario, London, ON N6A 3K7
*corresponding author: terry.carter@cartergeologic.com

Recommended citation: Carter, T.R. and Sutherland, L. 2020. Interface mapping of hydrochemical groundwater regimes in the Paleozoic bedrock of southwestern Ontario. In Russell, H.A.J. and Kjarsgaard, B.A. Eds. Southern Ontario groundwater project 2014–2019: summary report. Geological Survey of Canada, Open File 8536, 37-48. https://doi.org/10.4095/321083

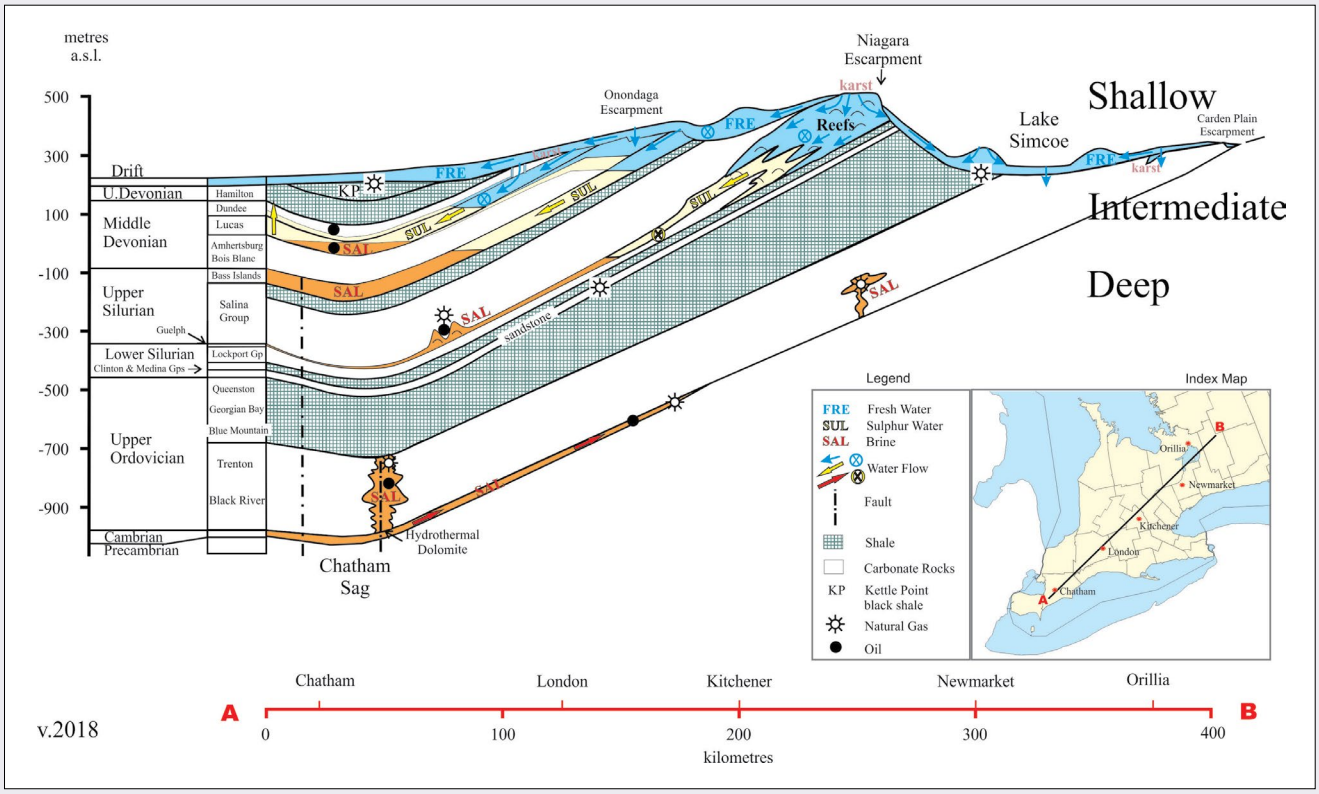


Figure 1. Conceptual model showing hydrochemical groundwater regimes in the subsurface of southern Ontario: shallow fresh water regime, intermediate brackish to saline sulphur water regime, and deep brine regime (Carter and Sutherland 2018).

Depth to the subsurface interface between these regimes varies geographically. A better understanding of geographic and stratigraphic variations in the depths at which these hydrochemical transitions occur provide practical guidance for:

- Depth constraints for drilling of water wells;
- Design constraints for drilling, casing and cementing of petroleum wells and other deep wells;
- Depth constraints on numeric modelling of penetration and lateral movement of meteoric water in the subsurface.

This paper provides details on the mapping method of the interface between the intermediate sulphur water regime and the deep brine regime mapped by Carter and Sutherland (2018). The mapping results are reviewed and highlight regional and geological variation in the interface depth.

The study area comprises that portion of the province of Ontario, underlain by Paleozoic sedimentary rocks, occurring south and west of the Niagara Escarpment (Figure 2).

2. Geological and hydrogeological setting

Southern Ontario is underlain by marine sedimentary rocks of the Appalachian Basin and Michigan Basin (Figure 2). These Paleozoic sedimentary strata unconformably overlie crystalline metamorphic and igneous rocks of the Canadian Shield and are covered by a thin veneer of unconsolidated Quaternary and Recent sediments in most of the area. Paleozoic bedrock strata consist of an interlayered succession of sandstones, carbonates, evaporites, mudstones, and siltstones (Figure 3). The bedrock formations dip shallowly to the southwest at 3 to 6 m/km along the crest of the Algonquin Arch, and at 3.5 to 12 m/km down the flanks of the arch westward into the Michigan Basin and southward into the Appalachian Basin (Armstrong and Dodge 2007; Armstrong and Carter 2010).

The unconsolidated sediments have variable porosity and permeability and are utilized as a source of potable water by most of the water wells drilled in southwestern Ontario (Sharpe et al. 2014). Aquifers in these sediments are complex and discontinuous. The contact with the underlying bedrock is a low-relief angular unconformity resulting from subaerial exposure and erosion of the slightly inclined Paleozoic strata over an extended period of geologic time. The interface between the fresh water-dominated surficial sediment and the relatively less permeable and less porous sedimentary bedrock forms a regional water-bearing interval. This contact aquifer is the most widespread potable water aquifer in southern Ontario (Husain et al. 2004; Brunton 2009a, 2009b; Carter 2012; Carter and Clark 2018). In areas of thicker surficial

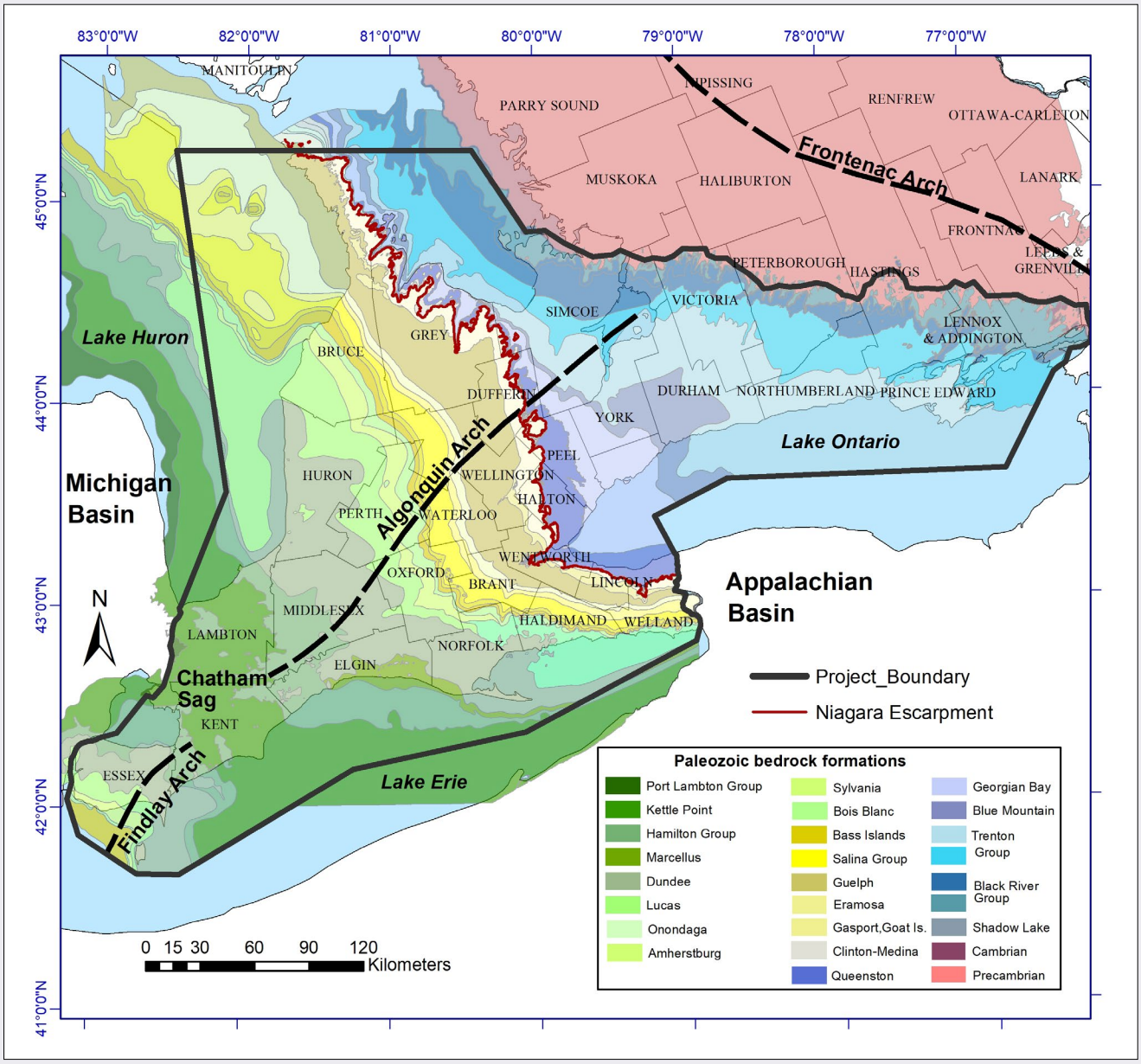


Figure 2. Bedrock geology of southern Ontario, from Somers and Fortner (2017).

sediment in southwestern Ontario, where karst is not well-developed (Golder Associates and OGS 2008), and in areas underlain by shaly bedrock formations, wells that penetrate the bedrock more than a few metres encounter groundwater that is increasingly saline and contains dissolved H_2S (with local exceptions).

In areas of thin surficial sediment, where carbonate rocks form the uppermost bedrock layer, extensive karstic dissolution has occurred (Brunton et al. 2016; Brunton and Dodge 2008; Golder Associates and Ontario Geological Survey 2008), resulting in greatly enhanced porosity and permeability. These karstic strata form a system of potable water that extends below the surficial sediment/bedrock contact. Fresh water occurs up to 130 m below the top of the bedrock within areas of inferred karst (Figure 4; Carter et al. 2018). The potable water regime in the shallow bedrock is the subject of ongoing investigations by the Ontario Geological Survey (OGS) as part of its groundwater mapping program (Brunton 2009a, 2009b; Brunton et al. 2016; Priebe and Brunton 2016; Priebe et al. 2017).

A system of thick regional aquitards and thin confined aquifers have been identified within the bedrock of southwestern Ontario (Carter et al. 2014; Sharpe et al. 2014). Regional confined aquifers occur within the Middle Devonian Lucas

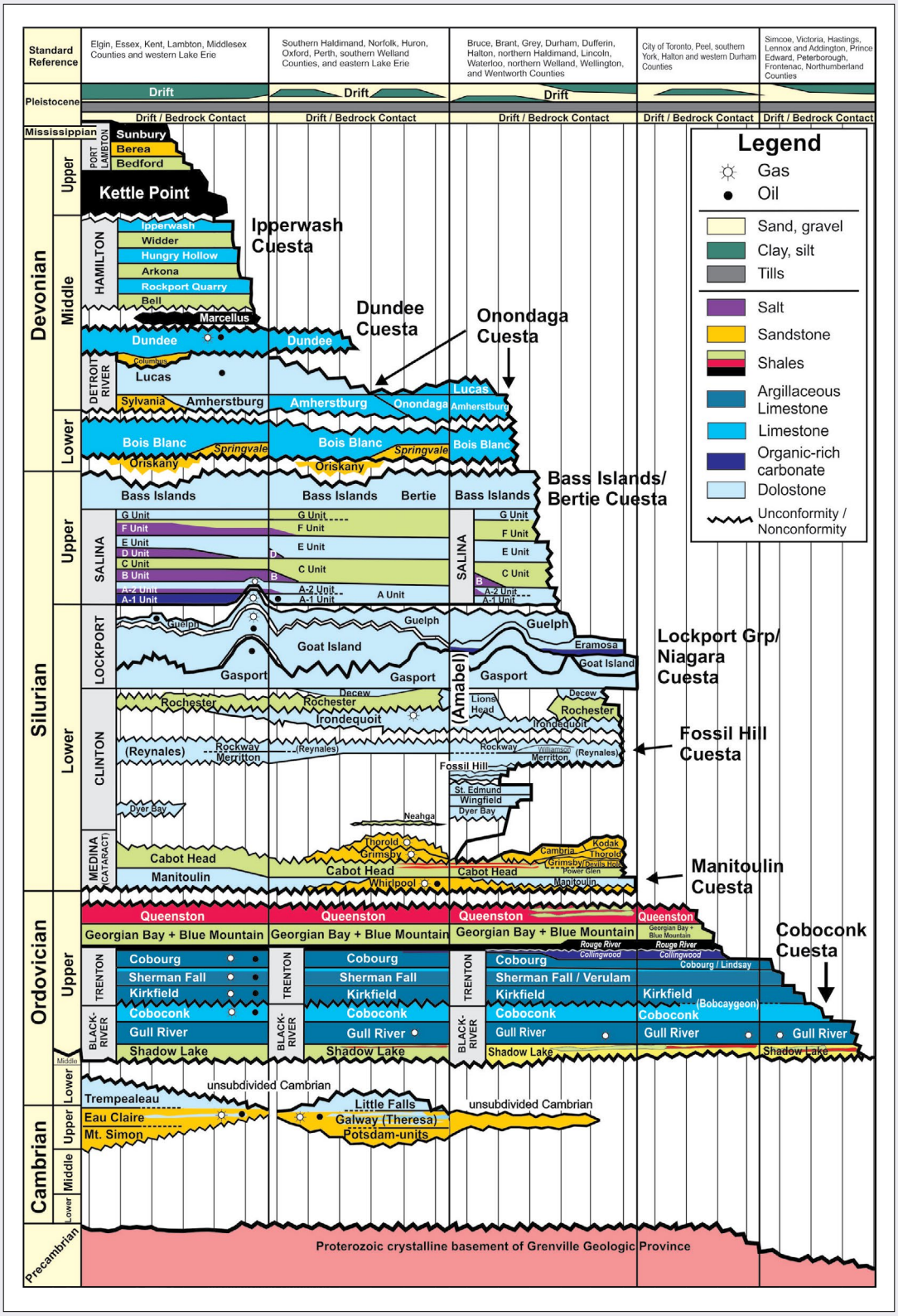


Figure 3. Lithostratigraphy of southern Ontario, from Brunton et al. (2017), showing regional unconformities representing past periods of exposure, erosion, and/or karstification. Karst/paleokarst intervals in the carbonate strata greatly enhance porosity and permeability and are the main geological control on regional aquifers in the bedrock strata of southwestern Ontario.

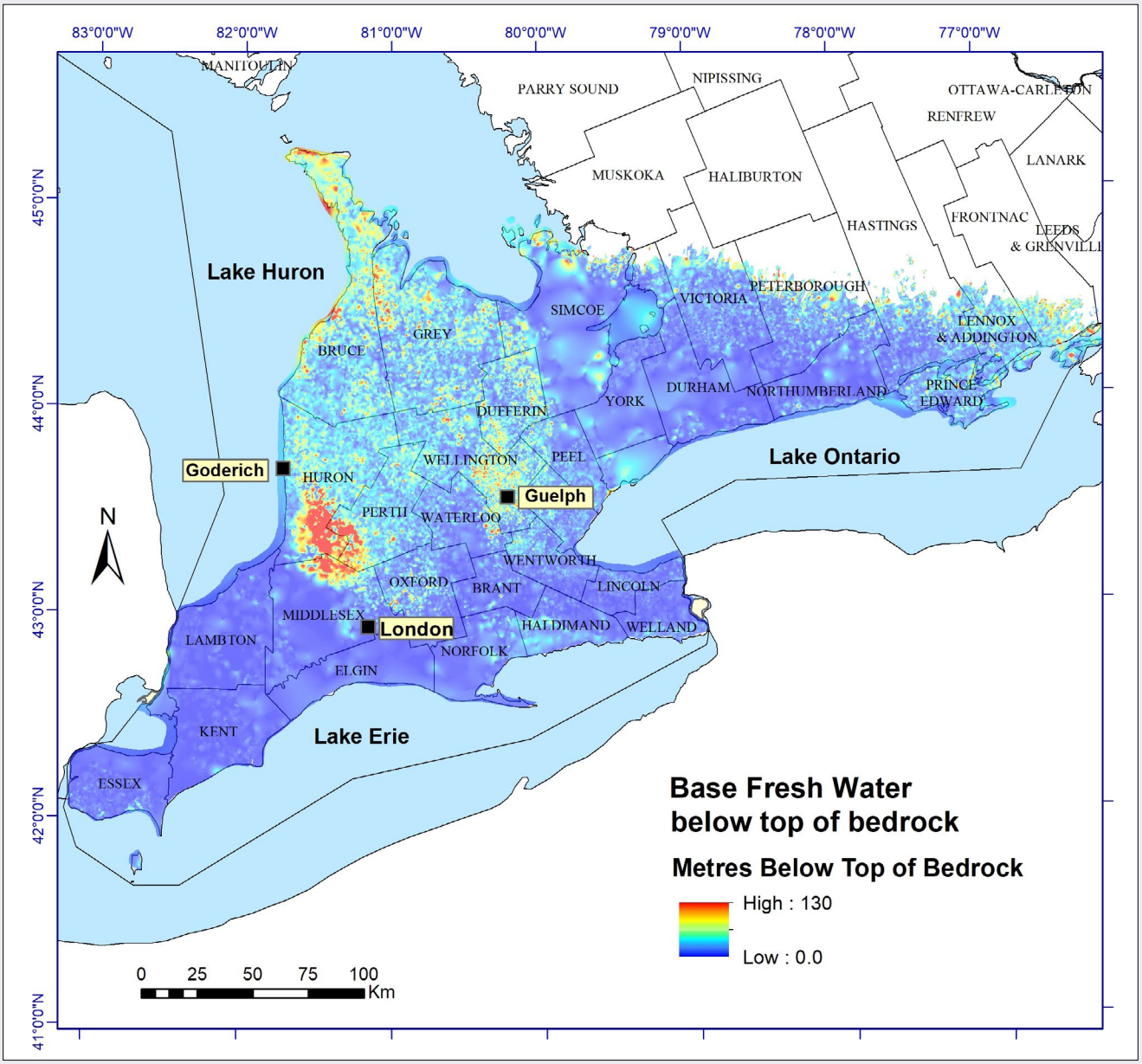


Figure 4. Base of fresh water, metres below top of bedrock, based on water well data maintained by the MECP (Carter and Clark 2018). Areas in blue identify the extent of the contact aquifer. Areas in green, yellow and red indicate deep occurrences of fresh water in areas of inferred karst. The large red feature between Goderich and London corresponds to the breathing well aquifer identified by Freckelton (2013).

and lower Dundee formations, the Upper Silurian Bass Islands Formation, the Upper Silurian Guelph Formation, within fault-related hydrothermal dolomite zones in the Upper Ordovician limestones of the Trenton and Black River groups and in Cambrian sandstones (Carter and Fortner 2012), with important shallow fresh water aquifers within the Goat Island and Gasport formations (Priebe and Brunton 2016; Brunton 2009b; Brunton et al. 2016) . The aquifers are separated by thick aquitards formed by shale strata, most notably the Upper Ordovician Queenston, Georgian Bay and Blue Mountain formations which exceed 300 m in combined thickness, and by thick evaporites of the Salina Group. Carbonate rocks also generally form aquitards except where they have been fractured or exposed to near-surface karstic dissolution. Additional constraints on water movement are: the low topographic gradients in the region; the density contrast between the brine and the shallow to intermediate waters; natural gas saturation in Silurian sandstones of the Medina Group; and a general lack of discharge pathways for the deep brine (Hobbs et al. 2011; Sharpe et al. 2014; Clark et al. 2013).

Paleokarst occurs at subsurface unconformities in the Paleozoic sedimentary strata where carbonate rock has been exposed to prolonged periods of weathering in the geologic past (Figure 3) (Brunton and Dodge 2008; Brunton 2008; Smith et al. 1988; Carter et al. 1994; Carter 2012). The porous and permeable rock associated with these paleokarst horizons form the principal regional aquifers in the subsurface bedrock formations. Each of these aquifers are recharged by fresh meteoric water at their outcrop and subcrop edges. This water then flows down-dip and is interpreted to have previously flushed out or diluted the original pore water at shallow to intermediate depths. The depth of penetration depends on the permeability of the formation, past and present hydraulic gradients, and the counteracting buoyancy effects caused by elevated salinity of the intermediate and deep groundwaters. Each subcropping aquifer exhibits a downdip transition from fresh water at shallow depths, to brackish to saline sulphur water at intermediate depths, to highly saline deep brines (Carter et al. 2015a). Sulphur water is also locally reported by water well drillers within the surficial sediment (Singer et al. 2003). Cambrian formations do not subcrop in southwestern Ontario and only contain brine.

The sulphur water regime overlaps in depth with a deep brine regime that contains brine with no dissolved H_2S. Depth of this transition is documented by Carter and Sutherland (2018) and in this report. The brines contain extremely high concentrations of total dissolved solids (140–390 g/l or more) dominated by sodium and calcium chlorides (Carter and Fortner 2012). In deep continental bedrock aquifer systems similar to southern Ontario it is a common phenomenon that the concentration of dissolved salts increases with depth, with dense brines occupying the deep bedrock. There is likely little or no movement in these deep brine systems, even on a geologic time scale (Hiscock and Bense 2014).

Isotopic fingerprinting ($\delta^{18}O$ and $\delta^{2}H$) indicates that shallow fresh water has a modern meteoric signature while available samples from the intermediate sulphur water regime exhibit modern meteoric to cold-climate isotopic ratios, indicating at least some of the water originated as glacial meltwater (Skuce 2014; Skuce et al. 2015a). The deep brine is interpreted to be modified remnants of highly evaporated seawater (Dollar et al. 1991; Hobbs et al. 2011, Skuce 2014; Skuce et al. 2015b) and is inferred to have formed under evaporitic conditions prevailing during deposition of the Salina Group (Clark et al. 2013) and possibly also the Lucas Formation.

The sulphur water in the intermediate regime contains elevated concentrations of dissolved sulphate. Isotopic ratios of sulphur ($\delta^{34}S_{SO4}$) and oxygen ($\delta^{18}O_{SO4}$) indicate that this sulphate is largely derived from dissolution of marine sulphates (Skuce 2014), principally anhydrite, which is abundant in many of the Devonian and Silurian strata of southwestern Ontario, in particular in the evaporitic Lucas Formation and the Salina Group.

The H_2S in the sulphur water is interpreted to be the result of bacterial sulphate reduction under anaerobic conditions in the subsurface. The presence of an active bacterial community is confirmed by the odour of hydrogen sulphide and the presence of yellowish-white filamentous bacteria at sulphur water seeps in quarries and springs in southern Ontario, as observed by the first author. This is a common field indicator of the presence of sulphate-reducing bacteria (Dyer 2003). Unusually high (>35‰) $\delta^{34}S_{SO4}$ values for several samples from Skuce (2014), McIntosh and Walter (2006) and Matheson (2012), are best explained by bacterial sulphate reduction of marine sulphate.

3. Sources of information

3.1 Petroleum well records

The Ministry of Natural Resources and Forestry (MNRF) regulates the drilling, operation and eventual decommissioning of petroleum wells in the province of Ontario and collects and manages data from petroleum wells. Source records for petroleum wells drilled in Ontario are maintained at the Petroleum Operations Section of the MNRF in London, Ontario, with public access via the Oil, Gas and Salt Resources Library (OGSRL). Source records for this information are paper reports stored in conventional hard-copy well files. There is a separate well file for each unique petroleum well.

3.2 Petroleum well database

Digital petroleum well records are maintained by the MNRF on the Ontario Petroleum Data System (OPDS). Data management and quality assurance is a shared responsibility of MNRF and the OGSRL. Public access to petroleum well data is managed by the OGSRL.

OPDS contains information for approximately 27,000 petroleum and related wells drilled under the authority of the Oil, Gas and Salt Resources Act and Ontario Regulation 245/97. Stored data includes well location, status, depths, geological formation tops, well construction, oil/gas/water intervals, logged and cored intervals, and storage location of drill cuttings from bedrock formations penetrated by the well (Carter and Castillo 2006; Carter 2017). Water interval data includes depth, static level, water type and host geological formation. Petroleum well records contain very little information about unconsolidated sediments that overlie the bedrock. Basic data for petroleum wells in southern Ontario are available for public viewing at www.ogsrlibrary.com. Oil, gas and water interval data and formation top depths are value-added data available only to registered OGSRL members.

3.3 OPDS water interval records

OPDS contains over 35,000 records of water-bearing intervals encountered during the drilling of petroleum wells in Ontario (Carter et al. 2015a). Most of these records are obtained

from wells drilled by the cable tool method. Drillers record a subjective description of the water type/quality from each of the water-bearing intervals they encounter using terminology similar to that used by water well drillers (Table 1).

Table 1. Water types recorded in OPDS water interval records.

BLK – Black
BRA – Brackish
FRE – Fresh
LOS – Loss of circulation
MIN – Mineral
SAL – Salt (saline water and/or brine)
SUL – Sulphur (dissolved H_2S, identified by rotten egg smell)

The geological formation within which the water occurs has been interpreted by MNRF or OGSRL staff by comparison of the water interval depths to the formation top depths recorded for the wells. The terminology used to identify formations in the database is consistent with Armstrong and Carter (2010) (Figure 3). The coding of the geological formation in the data record makes it possible to map the occurrence of water, by type, in each geological formation (Carter et al. 2015a).

The water interval data has a number of quality issues which required a QA/QC review. Corrective edits were applied to several hundred records. If a corrective edit could not be identified, the unreliable records were omitted from the mapping process.

3.4 Water analyses

Chemical analyses of 109 water samples from selected subsurface bedrock formations of southern Ontario were acquired by the MNRF in 2011–2013 in partnership with the University of Western Ontario. Formations sampled include the Dundee, Columbus, Lucas, Amherstburg, Salina E Unit, Salina A-2 Carbonate, Salina A-1 Carbonate, Guelph, Irondequoit, Grimsby, Thorold, Cobourg, Sherman Fall, Coboconk, and Cambrian, as well as several samples from surface springs of sulphur water. The complete set of data, description of sampling methods, and data quality issues are available in Skuce (2014).

Standard petroleum industry chemical analyses are also available for 1024 water samples collected by the operators of licensed petroleum wells and analyzed at commercial laboratories. A copy of the analytical results is required to be submitted to the MNRF and becomes part of the public record after a 1-year confidentiality period. The water analyses are measurements of the concentration of a limited suite of dissolved elements and compounds, including Na, Ca, Mg, Cl, SO_4, HCO_3, and total dissolved solids, as well as pH, density, and resistivity. The water analysis data from these reports has been compiled in an Excel data file by the OGSRL.

The industry water samples were collected by a wide variety of well operators from a variety of sources or collectors, including drill stem test chamber, wellhead valve, flow line, swab, bailer, production tank, and separator, each of which may create issues with data quality. Samples collected during drilling operations may be susceptible to contamination by drilling fluids. Dilution of the very saline deep brines typical of southern Ontario is a possibility. The laboratory analyses were completed by several different commercial laboratories between 1948 and 2001 with one sample collected and analyzed in 1907. These issues create uncertainty about the consistency and precision of individual results. Nonetheless, taken as a group of data, the water analyses provide quantitative values for water salinity which are inherently more precise than the qualitative judgements of well drillers for the water interval data, and provide valuable insights into regional variations in salinity in bedrock groundwaters.

Brine can be reliably identified in chemical analyses. The database of industry water analyses was filtered to select analyses where the total dissolved solids exceeds 100,000 mg/l. Other quality constraints resulting in exclusion were: no recorded depth, and duplicate analyses of the same water sample. Out of the 1,024 records in the water analysis database, only 312 analyses were suitable for mapping after QA/QC filtering. The analytical data shows that most brine occurs at depths greater than 200 m below the top of bedrock. Only 9 of 312 available records show brine at depths shallower than 200 m below the bedrock top. These shallow brine occurrences are scattered and isolated, and with one exception (Bass Islands Formation), are within bedrock formations of Devonian age.

4. Mapping methods and results

Creating geologically meaningful maps from the available data is dependent on the design of GIS data filters and selection methods to derive a subset of wells with the required attributes, and quality assurance editing of this new dataset. For this mapping exercise, the data filtering procedure was designed to select the deepest reported occurrences of sulphur water at each well location.

An interim map was prepared for the data set after the initial data filtering exercises. Anomalous data were identified by visually reviewing the maps and editing or deleting individual records contributing to contouring anomalies. This process was repeated at least four times before a geologically acceptable result was obtained.

Three data interpolation algorithms are supplied with the Spatial Analyst extension of ArcMap 10.1; inverse distance weighted, kriging and natural neighbours. After trial and error, it was determined that the natural neighbours algorithm produced the most geologically meaningful results and was therefore used to create interpolated surface and contour maps of the edited data.

4.1 Total dissolved solids – Lockport Group + Salina A-1 and A-2 units

Bedrock formations of the Lockport Group, in particular the Guelph Formation and locally the Gasport Formation and Goat Island formations, form important regional aquifers in southwestern Ontario (Figures 1, 5, 6; Brunton 2009b; Brunton et al. 2012; Brunton and Brintnell 2011; Carter et al. 2014). The Lockport Group has the most geographically and stratigraphically extensive set of available hydrochemical data, with 4,163 water interval records in OPDS (Carter et al. 2015a) and was mapped in detail to identify regional variations and trends. In southern Ontario a large number of oil and natural gas reservoirs, with associated water, in the Guelph Formation, are in reservoir communication with the lowermost formations of the overlying Salina Group — the Salina A-1 and A-2 units. For the purposes of this study, analyses of water from all these formations has been compiled and grouped to map regional variations in total dissolved solids.

The Lockport Group and the lower Salina Group forms a northwest-southeast subcrop–outcrop belt in southwestern Ontario, dipping shallowly southwest into the Chatham Sag (Figure 2). In the deepest part of the Chatham Sag the top

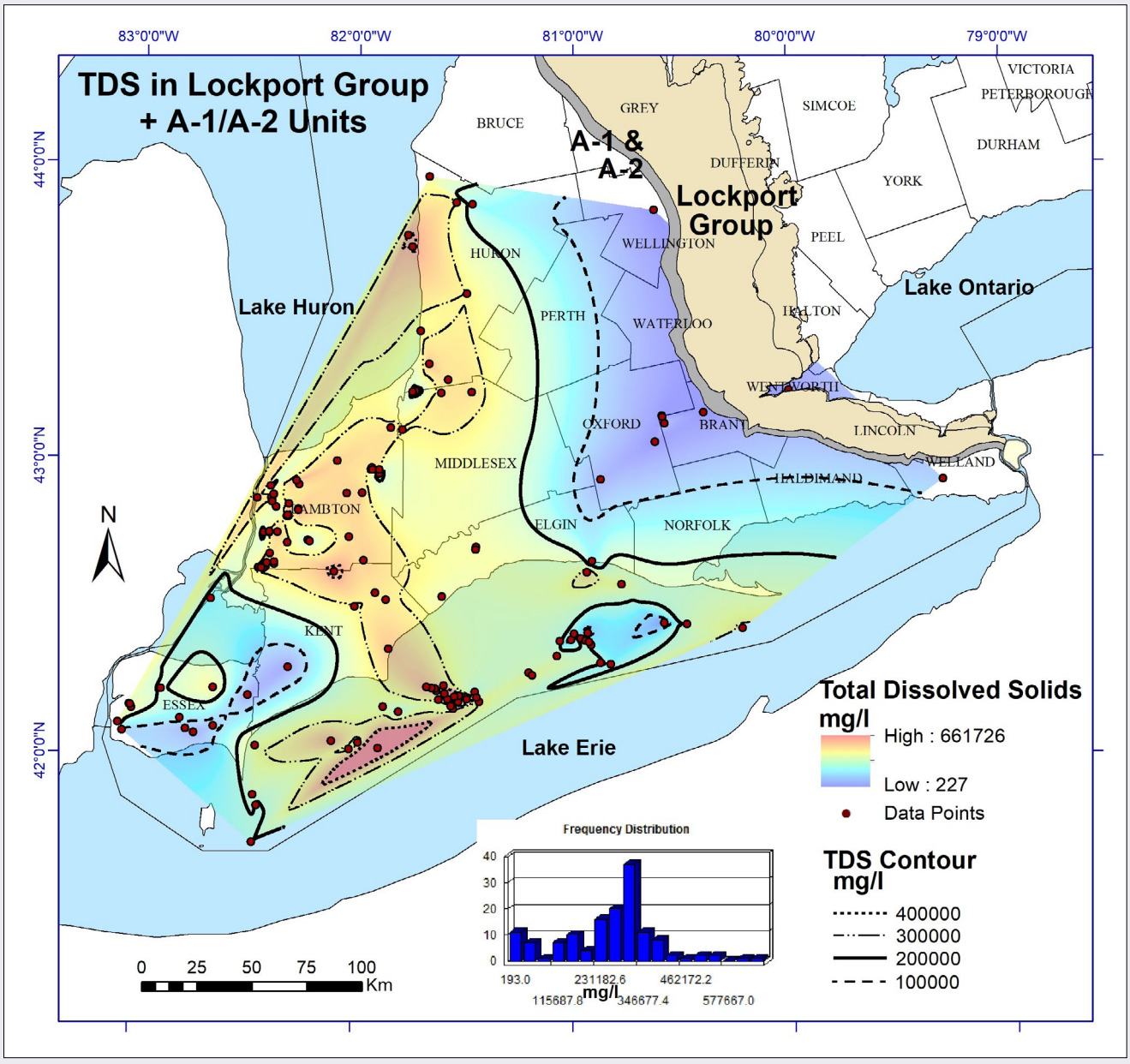


Figure 5. Raster surface and contour map of total dissolved solids in the Lockport Group + Salina A-1 Unit and Salina A-2 Unit in the subsurface of southern Ontario downdip from the subcrop belt of these formations.

of the Lockport Group is over 750 m below the surface and is overlain by thick halite beds of the Salina Group (Figure 3). These halite beds are impermeable barriers to vertical movement of water and their preservation is a testament to the lack of water movement in the deep subsurface.

After QA/QC filtering, water analysis results were available for 139 Lockport samples of the 312 samples. Of these, 2 are classified as fresh water, 21 as brackish to saline water, and 116 as brine. Eighty percent of the brine samples have values ranging from 230,00 to 410,000 mg/l with a median value of 314,000 mg/l total dissolved solids. The overwhelmingly large proportion of brine vs fresh water samples is a direct result of the greater depth of most petroleum wells relative to the depth of water wells, and preferential sampling of deep formation water from oil and gas reservoirs.

The data was plotted and contoured to highlight regional variation in total dissolved solids (Figure 5). Salinity increases downdip from approximately 200 mg/l total dissolved solids in the outcrop belt to a maximum reported value of over 600,000 mg/l in the deep subsurface. The interface between brackish and saline water of the intermediate sulphur water regime and deep brine occurs approximately 35 to 65 km downdip from the subcrop exposure of these formations. This correlates to a depth of approximately 250 to 300 m below the top of bedrock.

4.2 Base of sulphur water

Approximately 9,000 depth values from the water interval data set, where water type was recorded as sulphur water by the driller, were used to generate a map of the deepest recorded intervals of sulphur water relative to the top of bedrock (Figure 6). No water analysis data was incorporated. It should be noted that there is an inherent inaccuracy in these maps as only the top of the water interval is recorded in the data set. The raster map values should be interpreted as minimum depths due to lack of data for the base of the water intervals in the petroleum well records.

Comparison to the base of fresh water mapping of Carter and Clark (2018) identified isolated areas where the interpolated sulphur water raster surface extended above the fresh water raster surface, which is inconsistent with the observed regional hydrochemical zonation. Within these areas a raster calculation was used to reassign the base-of-sulphur-water pixels to equal the value from the base-of-fresh-water raster.

QA/QC review of the initial mapping results identified a large number of wells where the driller identification of sulphur water, based on a rotten egg odour of the water, coincided with areas in western and central Lake Erie, between Norfolk County and Essex County, where the analytical data documents the presence of dense brines with total dissolved solids content ranging from 250,000 to over 400,000 mg/l (Figure 5). Within this area all data points identified as sulphur water by the driller were reclassified as brine. Outside this area, at scattered locations, there are a number of wells with sulphur water reported in these formations (Lockport+ A-1–A-2) which cannot be verified, consequently this data has been retained in the data set.

The final map documents sulphur water at depths ranging from the top of bedrock to approximately 200 m below the top of bedrock (Figure 6). This depth range is largely confined to the Dundee, Lucas, Amherstburg and Onondaga formations, and to a lesser extent in the Bois Blanc and other formations stratigraphically above the Salina Group. Sulphur water is also widely reported in the overlying unconsolidated sediments within the water well records maintained by MECP (Singer et al. 2003). There are a number of widely scattered, isolated, anomalously deeper occurrences of sulphur water within the Lockport Group, principally within the Guelph Formation.

There are two distinctive areas of deeper occurrence of sulphur water. In Huron and southern Bruce counties there is a distinctive NNW-SSE trending zone confined to the A-1 Carbonate Unit, at depths of 300 to 350 m below the bedrock surface (Figure 6). This "Huron-Bruce Anomaly" occurs 25 to 50 km southwest and downdip from the A-1 Carbonate subcrop belt. The second is a large zone beneath west-central Lake Erie where sulphur water occurs at depths from 200 to 285 m below the top of bedrock. Petroleum well records indicate this water is largely confined to the Bass Islands/ Bertie Formation.

4.3 Top of "salt water"

The OPDS water interval records include a subjective water type identified as "salt water". This water type includes both saline water and brine, with no odour of dissolved H_2S. This data could not be uniquely assigned to either the intermediate sulphur water regime or to the deep brine regime, consequently was not useful in mapping the interface between these two water regimes.

5. Discussion and interpretation

This study documents considerable geographic variations in the reported depth of occurrence of brackish-to-saline sulphur water in the bedrock of southwestern Ontario, with a strong spatial relation to down-dip distance from subcrop/ outcrop edges. The base of the sulphur water regime cannot be precisely defined, but interpretation of the available data indicates a regional depth transition from brackish-to-saline sulphur water to deep brine at approximately 200 to 300 m below the top of bedrock and locally to 350 m (Figure 6). These depths should be considered as minimum depths due to lack of data for the base of the water intervals in the petroleum well records. These depths are consistent with the much more precisely-measured findings of Hobbs et al. (2011) and Nuclear Waste Management Organization (2011) at the proposed Deep Geological Repository for low-to-intermediate level nuclear wastes at the Bruce Generating

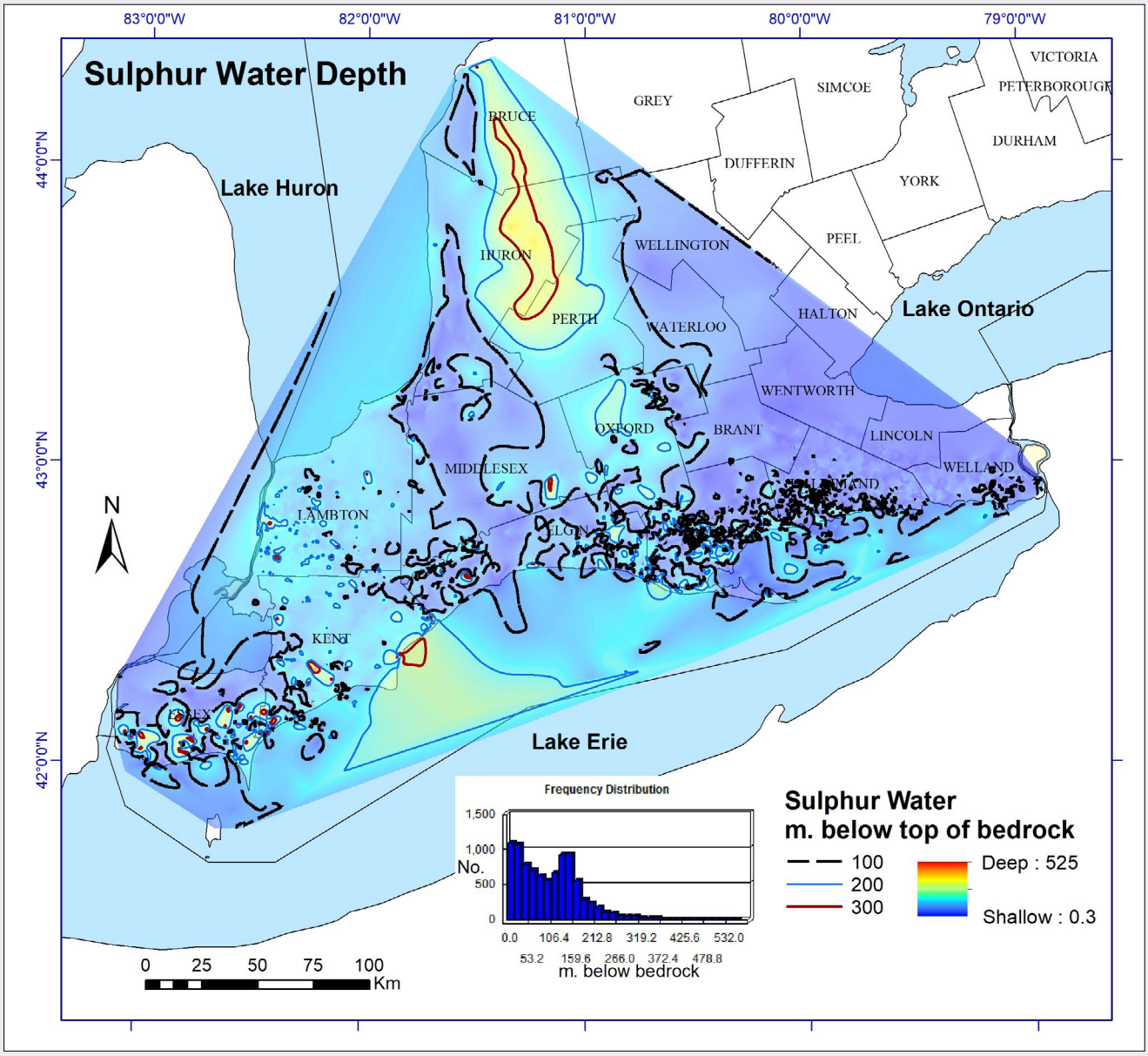


Figure 6. Deepest occurrence of sulphur water recorded in petroleum well records, measured in metres below top of bedrock. The map indicates widespread occurrence of sulphur water at shallow to intermediate depths in bedrock formations stratigraphically above the top of the Salina Group. Geographic depth variation shows a strong spatial relationship to downdip distance from outcrop/subcrop belts of the bedrock. Depth values should be interpreted as minimum depths due to lack of data for the base of the water intervals in the petroleum well records.

Station on Lake Huron.

The intermediate regime is interpreted to represent penetration of both modern meteoric water and glacial meltwater into subcropping/outcropping porous and permeable bedrock strata, and downdip flow, with partial to complete displacement and dilution of original pore fluids. Stratigraphically, the water of the shallow to intermediate regimes is generally confined above the Salina Group. The principal exception is penetration of meteoric water beneath the subcrop/outcrop edges of the Salina evaporites through subcropping/outcropping porous and permeable strata of the Lockport Group, proximal to and immediately west of the Niagara Escarpment, with a downdip penetration distance of approximately 25 to 65 km.

The interface boundary represents the deepest penetration of meteoric water into the bedrock formations of southern Ontario. Numeric modelling of groundwater movement in the bedrock can use the maps of the geographic variations

in depth of this interface as an approximation of the base of interaction of groundwater with surface water. The maps can be used as a constraint in the search for potable water, as at depths below this interface only progressively more saline waters will likely be encountered. Accurate knowledge of interface boundary depths is also needed in design of petroleum well drilling, casing and cement programs and mitigation of drilling hazards posed by corrosive qualities of sulphur water and potential release of H_2S gas at surface.

6. Acknowledgements

This research was not possible without the collection and active QA/QC management of petroleum well records and the related petroleum well database (OPDS) by staff of the MNRF and the Oil, Gas and Salt Resources Library. The first author thanks F. Brunton of the Ontario Geological Survey for numerous informative discussions on the subject of bedrock stratigraphy, karst and groundwater in southern Ontario over the past several years. An internal review at the GSC was completed by H.A.J. Russell and B.A. Kjarsgaard. Funding for this work was by the Geological Survey of Canada Groundwater Geoscience Program. Mapping of the interface between the intermediate sulphur water regime and the deep brines is a contribution to the OGS–GSC southern Ontario project on groundwater 2014–2019.

7. References

Armstrong, D.K. and Carter, T.R. 2010. The subsurface Paleozoic stratigraphy of southern Ontario. Ontario Geological Survey, Special Volume 7, 301 p.

Armstrong, D.K. and Dodge, J.E.P. 2007. Paleozoic geology of southern Ontario. Ontario Geological Survey, Miscellaneous Release—Data 219.

Brunton, F.R. 2008. Preliminary revision to the early Silurian stratigraphy of Niagara Escarpment: integration of sequence stratigraphy, sedimentology, and hydrogeology to delineate hydrogeologic units. Ontario Geological Survey, Summary of field work and other activities, Open File Report 6226, p. 31-1 to 31-18.

Brunton, F.R. 2009a. Karst mapping and groundwater of southern Ontario; in Groundwater and Geology – Foundation for Watershed Planning, Latornell Conference, pre-meeting core workshop, November 17, 2009, 1-15.

Brunton, F.R. 2009b. Update of revisions to the Early Silurian stratigraphy of the Niagara Escarpment: Integration of sequence stratigraphy, sedimentology and hydrogeology to delineate hydrogeologic units. In Summary of Field Work and Other Activities 2009, Ontario Geological Survey, Open File Report 6240, 25-1 to 25-20.

Brunton, F.R. and Brintnell, C. 2011. Final update of Early Silurian stratigraphy of the Niagara Escarpment and correlation with subsurface units across southwestern Ontario and the Great Lakes Basin. In Summary of Field Work and Other Activities 2011, Ontario Geological Survey, Open File Report 6270, 30-1 to 30-11.

Brunton, F.R., Brintnell, C., Jin, J., and Bancroft, A.M. 2012. Stratigraphic architecture of the Lockport Group in Ontario and Michigan – A new interpretation of Early Silurian "basin geometries" and "Guelph Pinnacle Reefs". In 51st Annual Conference – Ontario – New York, Oil & Gas Conference, Oct. 23-25, 2012, Niagara Falls, Ontario, 1-37.

Brunton, F.R. and Dodge, J.E.P. 2008. Karst of southern Ontario and Manitoulin Island. Ontario Geological Survey, Groundwater Resources Study 5.

Brunton, F.R., Priebe, E.H., and Yeung, K.H. 2016. Relating sequence stratigraphic and karstic controls of regional groundwater flow zones and hydrochemistry within the Early Silurian Lockport Group of the Niagara Escarpment, southern Ontario. In Regional-scale Groundwater Geoscience in Southern Ontario: An Ontario Geological Survey and Geological Survey of Canada groundwater geoscience open house, Geological Survey of Canada, Open File 8022, p.4. https://doi.org/10.4095/297722

Brunton, Frank R., Carter, T.R., Logan, C., Clark, J., Yeung, K., Fortner, L., Freckelton, C., Sutherland, L., and Russell, H.A.J., 2017. Lithostratigraphic compilation of Phanerozoic bedrock units and 3D geological model of southern Ontario; in Regional-scale Groundwater Geoscience in Southern Ontario: an Ontario Geological Survey, Geological Survey of Canada, and Conservation Ontario open house, compiled by H.A.J Russell, D. Ford and E.H. Priebe, Geological Survey of Canada, Open File 8212, p.3.

Carpenter, A.B. 1978. Origin and chemical evolution of brines in sedimentary basins. In Thirteenth annual forum on the geology of industrial minerals. In Johnson, K.A. and Russell, J.A. Eds. Oklahoma Geological Survey, Circular 79, p.60-77.

Carter, T.R. 2012. All is well – Regional groundwater systems in southern Ontario. In Ontario Oil & Gas 2012, Ontario Petroleum Institute, p.44-48.

Carter, T.R. 2017. Ontario Oil, Gas and Salt Resources Library: A model for groundwater data sharing in Ontario? Geological Survey of Canada, Open File 8213, 25 p. https://doi.org/10.4095/305611

Carter, T.R. and Clark, J. 2018. Base of fresh water, bedrock karst, and the contact aquifer in southern Ontario, as interpreted from water well records. Oil, Gas and Salt Resources Library, unpublished report.

Carter T.R. and Castillo A.C. 2006. Three-Dimensional Mapping of Paleozoic Bedrock Formations in the Subsurface of Southwestern Ontario. In Harris, J. Ed. A GIS Application of the Ontario Petroleum Well Database. GIS for Earth Sciences; Geological Association of Canada, 435–450.

Carter, T.R. and Fortner, L. 2012. Regional bedrock aquifers and a geological groundwater model for southern Ontario. International Association of Hydrogeologists, 2012 Congress Niagara Falls, abstract.

Carter, T.R., Trevail, R.A., and Smith, L. 1994. Niagaran reef and inter-reef relationships in the subsurface of southwestern Ontario. Geological Association of Canada – Mineralogical Association of Canada, Annual Meeting Waterloo 1994, core workshop, 38 p.

Carter, T.R., Fortner, L., Skuce, M.E., and Longstaffe, F.J. 2014. Aquifer systems in southern Ontario: hydrogeological considerations for well drilling and plugging. Canadian Society of Petroleum Geologists, Geoconvention 2014, abstract, accessed at: http://www.geoconvention.org/archives/2014abstracts/298_GC2014_Aquifer_Systems_in_Southern_Ontario.pdf

Carter, T.R., Wang, D., Castillo, A.C., and Fortner, L. 2015a. Water Type Maps of Deep Groundwater from Petroleum Well Records, Southern Ontario. Oil, Gas and Salt Resources Library, Open File Data Release 2015-1.

Carter, T.R., Wang, D., Castillo, A.C., and Fortner, L. 2015b. Static level maps of deep groundwater from petroleum well records, Southern Ontario. Oil, Gas and Salt Resources Library, Open File Data Release 2015-2.

Clark, I., Mohapatra, R., Mohammadzadeh, H., and Kotzer, T. 2010a. Porewater and Gas Analyses in DGR-1 and DGR-2 Core. Technical Report TR-07-21, Intera Engineering Ltd., Ottawa.

Clark, I., Liu, I., Mohammadzadeh, H., Mohapatra, R., Zhang, P., and Wilk, M. 2010b. Porewater and Gas Analyses in DGR-3 and DGR-4 Core. Technical Report TR-08-19, Intera Engineering Ltd., Ottawa.

Clark, I., Scharf, V., Zuliani, J., and Herod, M. 2011. Porewater and Gas Analyses in DGR-3 and DGR-4 Core. Technical Report TR-09-04, Intera Engineering Ltd., Ottawa.

Clark, I.D., Al, T., Jensen, M., Kennell, L., Mazurek, M., Mohapatra, R., and Raven, K.G. 2013. Paleozoic-aged brine and authigenic helium preserved in an Ordovician shale aquiclude. Geology, 41: 9, 951-954.

Dyer, B.D. 2003. A field guide to bacteria. Cornell University Press, Ithaca, New York, 355 p.

Freckelton, C.N. 2013. A Physical and Geochemical Characterization of Southwestern Ontario's Breathing Well Region. University of Western Ontario, Electronic Thesis and Dissertation Repository. 1105, 242 p. https://ir.lib.uwo.ca/etd/1105Freckelton

Freeze, R.A. and Cherry, J.A. 1979. Groundwater. Prentice-Hall Inc, Englewood Cliffs, New Jersey, USA, 603 p.

Golder Associates Ltd, and Ontario Geological Survey. 2008. 3-D field investigation of Paleozoic bedrock and boreholes in thin-drift limestone-dolostone plains of southern Ontario; Ontario Geological Survey, Supplementary Report to Groundwater Resources Study 5, 53 p.

Hiscock, K.M. and Bense, V.F. 2014. Hydrogeology: Principles and practice, Wiley Blackwell, Oxford, U.K., 518 p.

Hobbs, M.Y., Frape, S.K., Shouakar-Stash, O., and Kennell, L.R. 2011. Regional hydrogeochemistry-southern Ontario. Nuclear Waste Management Organization, Report NWMO DGR-TR-2011-12, Toronto, Canada, http://www.nwmo.ca/uploads/DGR%20PDF/Geo/Regional-Hydrogeochemistry---Southern-Ontario.pdf, accessed on June 11, 2013.

Husain, M.M., Cherry, J.A., and Frape, S.K. 2004. The persistence of a large stagnation zone in a developed regional aquifer, southwestern Ontario. Canadian Geotechnical Journal, 41, 943-958. https://doi.org/10.1139/t04-040

Matheson, E. 2012. Analysis of the anomalous groundwater geochemistry of the Niagara Peninsula, Ontario, Canada. B.Sc. thesis, Queen's University, Kingston, Ontario, Canada.

McIntosh J. C. and Walter L. M. 2006. Paleowaters in Silurian-Devonian carbonate aquifers: Geochemical evolution of groundwater in the Great Lakes region since the late Pleistocene. Geochimica et Cosmochimica Acta, 70: 2454-2479. https://doi.org/10.1016/j.gca.2006.02.002

Nuclear Waste Management Organization, 2011b. Geosynthesis; Nuclear Waste Management Report NWMO DGR-TR-2011-11, Toronto, Canada. Accessed June 11, 2013 at: http://www.nwmo.ca/uploads/DGR%20PDF/Geo/Geosynthesis.pdf

Priebe, E.H. and Brunton, F.R. 2016. Regional-scale groundwater mapping in the early Silurian carbonates of the Niagara Escarpment: Final update. In Summary of Field Work and Other Activities, 2016, Ontario Geological Survey, Open File Report 6323, p.29-1 to 29-10.

Priebe, E.H., Neville, C.J., and Brunton, F.R. 2017. Discrete, high-quality hydraulic conductivity estimates for the Early Silurian carbonates of the Guelph region. Ontario Geological Survey, Groundwater Resources Study 16, 45 p.

Sharpe, D.R., Piggott, A., Carter, T.R., Gerber, R.E., MacRitchie, S.M., de Loe, R., Strynatka, S., and Zwiers, G. 2014. Southern Ontario hydrogeological region. In Rivera, A. ed. Canada's Groundwater Resources, Fitzhenry and Whiteside, Canada, 444-499. https://doi.org/10.4095/296947

Singer, S.N., Cheng, C.K., and Scafe, M.G. 2003. The hydrogeology of southern Ontario. Ontario Ministry of Environment, Environmental Monitoring and Reporting Branch, 395 p.

Skuce, M. 2014. Isotopic fingerprinting of shallow and deep groundwaters in southwestern Ontario and its applications to abandoned well remediation. University of Western Ontario, MSc thesis, Electronic thesis and dissertation repository, Paper 1926, 267 p. http://ir.lib.uwo.ca/do/search/?q=skuce&start=0&context=686929

Skuce, M., Longstaffe, F.J., Carter, T.R., and Potter, J. 2015a. Isotopic fingerprinting of groundwaters in southwestern Ontario: application to abandoned well remediation. Applied Geochemistry, 58: 1-13. https://doi.org/10.1016/j.apgeochem.2015.02.016

Skuce, M., Longstaffe, F.J., and Potter, J. 2015b. The isotopic characterization of water in Paleozoic bedrock formations of southwestern Ontario. Oil, Gas and Salt Resources Library, Open File Data Release 2015-3.

Smith, L., Grimes, D.J., and Charbonneau, S.L. 1988. Karst episodes and permeability development, Silurian reef reservoirs, Ontario. Ontario Geological Survey, Miscellaneous Paper 140, Geoscience Research Grant Program Summary of Research 1987-1988, 124-132.

Somers, M. and Fortner, L. 2017. Paleozoic bedrock geology of southern Ontario. Oil, Gas and Salt Resources Library, Open File Data Release 2017-2.

A three-dimensional surficial geology model of southern Ontario: Progress report

Charles E. Logan[1], Hazen A.J. Russell[1], Andy F. Bajc[2], Abigail Burt[2], Riley P.M. Mulligan[2], and David R. Sharpe[1]

Abstract: A 3-D model consisting of 7 surficial geology layers overlying bedrock for 66,870 km^2 of southern Ontario has been constructed. Model development involved the assembly of a comprehensive subsurface database that includes archival water well and geotechnical material logs, cored boreholes, and stratigraphically interpreted geophysical data. Other geospatial constraints are derived from topographic Digital Elevation Models (DEM), bathymetric DEMs and depth soundings, a bedrock surface DEM, and seamless surficial geology mapping. Existing sub-regional (<10,000 km^2) higher resolution 3-D models were used to support the model development. The surficial geological legend provided the basis for a simplified stratigraphic layer structure (from oldest to youngest): 1–Bedrock, 2–Lower Sediment, 3–Regional Till, 4–Glaciofluvial Sediment, 5–Upper Till, 6–Glaciolacustrine Mud, 7–Glaciolacustrine Sand, and 8–Recent/Organic Sediment. A preliminary model based on high-quality interpreted data was used along with surficial geological mapping and expert knowledge in a rules-based algorithm to help assign stratigraphic coding to the widespread, archival material log data. An iterative cycle of automated coding, manual coding, periodic interim model inspection and revision has led to this 3-D surficial geological model. This model supports regional-scale groundwater flow modelling and, along with a companion model of bedrock geology, will comprise the first complete 3-D model coverage of southern Ontario from the Precambrian basement to post-glacial sediment.

1. Introduction

Southern Ontario has been the focus of extensive groundwater studies since the release of the O'Connor report (2002a, b) following the Walkerton tragedy in 2000. To support Ontario's Clean Water Act (S.O. 2006, c.22), the provincial Source Water Protection Program (SWP) completed numerous studies as part of a three-tiered approach focusing on municipal water supply (e.g., Frind et al. 2014). In parallel and coordinated with SWP, the Ontario Geological Survey (OGS) has completed investigations of both bedrock and surficial geology to support groundwater understanding (e.g., Brunton et al. 2007), as well as studies of ambient groundwater geochemistry (e.g., Hamilton 2015). Surficial studies have involved new Quaternary mapping, extensive drilling, geophysical surveying and development of three-dimensional (3-D) geological models for areas up to 10,000 km^2 within and around the Greater Toronto Area. A recently released 3-D bedrock model covers 109,800 km^2 from the Precambrian Shield margin in the northeast to the US border including the Great Lakes (Carter et al. 2019; 2020, this vol.).

The current sediment model covers 66,870 km^2 of the on-shore portion of the same region (Figure 1). For interregional Great Lakes study, there is a need to consolidate existing knowledge gained through previous geological studies and extend the coverage to include all of southern Ontario. This level of 3-D model coverage would support regional issues such as cumulative impacts, gap analysis, and regional groundwater modelling for climate change scenarios. The Geological Survey of Canada (GSC) and the OGS began a collaborative effort in 2015 to produce 3-D geological models covering southern Ontario for both the Paleozoic bedrock stratigraphy (Carter et al. 2017, 2019; 2020, this vol.) and surficial sediment (Russell et al. 2016). Both models were developed independently but are spatially compatible. Combined, they have provided a hydrostratigraphic framework for a proof-of-concept, physically based, coupled groundwater–surface-water numeric flow model (Frey et al. 2020, this vol.).

[1] Geology Survey of Canada, Natural Resources Canada, 601 Booth Street, Ottawa, ON K1A 0E8
[3] Ontario Geological Survey, Sudbury, ON P3E 6B5
*corresponding author: charles.logan@canada.ca

Recommended citation: Logan, C.E., Russell, H.A.J., Bajc, A.F., Burt, A., Mulligan, R.P.M. and Sharpe, D.R. 2020. A three-dimensional surficial geology model of southern Ontario: Progress report. In Russell, H.A.J. and Kjarsgaard, B.A. Eds. Southern Ontario groundwater project 2014–2019: summary report. Geological Survey of Canada, Open File 8536, 49-64. https://doi.org/10.4095/321084

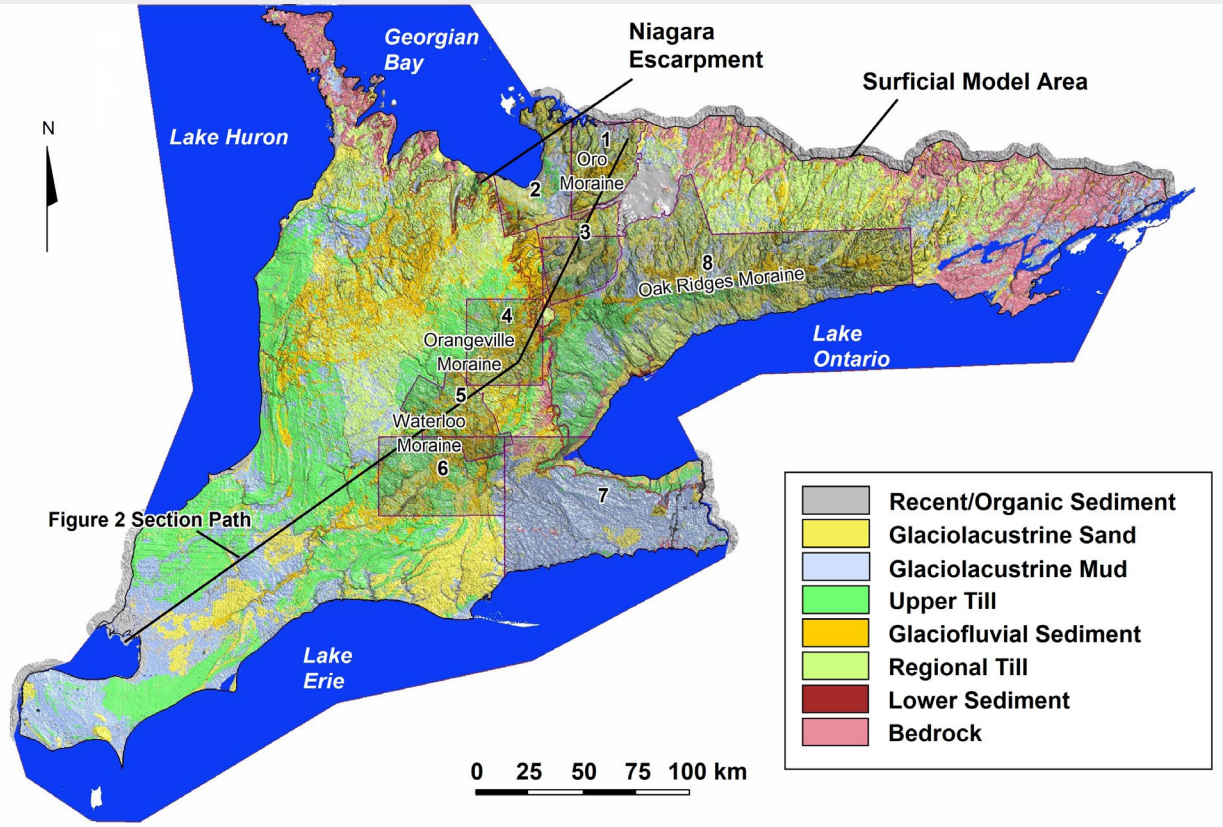


Figure 1. Simplified 8-unit surficial sediment geology draped on a hill-shaded Digital Elevation Model (DEM). Geology is simplified from Ontario Geological Survey (2010) and the DEM is modified 30 arc-second Shuttle Radar Topography Mission (STRM) data (NASA JPL, 2013). Existing OGS and GSC 3-D model study areas are shown as shaded regions: 1. Barrie-Oro Moraine (Burt and Dodge 2011); 2. Central Simcoe (Mulligan 2019); 3. South Simcoe (Bajc et al. 2019); 4. Orangeville-Fergus (Burt and Dodge 2016); 5. Waterloo (Bajc and Shirota 2007); 6. Brantford-Woodstock (Bajc and Dodge 2011); 7. Niagara (Burt 2017b); 8. Oak Ridges Moraine (Sharpe et al. 2005). The approximate path of the generalized section in Figure 2 is shown.

2. Objectives

This paper describes the construction of a 3-D surficial geology model of southern Ontario. The development of a simplified geological unit (layer) assignment and the conceptual stratigraphic architecture supporting the model layers are presented. The data support for the model is documented, the data processing workflow is described and model results are shown. The paper concludes with a discussion of model limitations due to data support and the influence of conceptual geological models.

3. Geological context

Across the southern Ontario model area, the landscape varies from bedrock-dominated terrain (e.g., Niagara Escarpment; northeastern margin along Canadian Shield) to sediment successions over 200 m thick (e.g., Oak Ridges Moraine, Dundas valley; Gao et al. 2006). The region is characterized by two distinct domains east and west of the Niagara Escarpment. The Niagara Escarpment is the most prominent and completely exposed of a series of escarpments controlled by bedrock lithology and differential erosion. The terrain is further characterized by broad troughs (e.g., Laurentian trough) and re-entrant valleys (e.g., Dundas valley). In southern Ontario, glacial sediments were deposited during at least two glaciations, each including numerous ice margin oscillations (e.g., Barnett 1992). The resulting sediment consists of tills, glaciolacustrine, glaciofluvial, fluvial, and lacustrine sediments (e.g., Barnett 1992; Sharpe et al. 2002; Burt 2018; Bajc et al. 2019). Older glacial features can be fully or partially buried by younger tills and stratified deposits.

4. Stratigraphic model layers

More than 100 years of surficial mapping and subsurface investigation by the OGS, GSC and academia has established a landform and till stratigraphic framework for southern Ontario (e.g., Chapman and Putnam 1984; Karrow 1974; Barnett 1992). This knowledge, compiled as a seamless 1:50,000 surficial

geological map coverage (OGS 2010), provides the cornerstone dataset for the surficial geological model. Subsurface studies, supported predominantly by continuous core and lakeshore and river bluff outcrops, provided the necessary subsurface sedimentological and stratigraphic context (e.g., Morris and Kelly 1997; Sharpe et al. 2003; Bajc et al. 2014; Burt 2018) for regional 3-D modelling. Integration of subsurface and 1:50,000 scale mapping has provided a rationalized stratigraphic framework of up to 20 units for regional modelling (e.g. Bajc and Shirota 2007). For a regional subsurface model using disparate datasets, the stratigraphic groupings required simplification to the minimum number of units (Table 1) that could be correlated across the broader region and recognized in all datasets. These datasets are derived from archival Water Well Information System (WWIS) data, published geological data, reflection seismic and borehole geophysical data, geotechnical drilling and sedimentologically-logged core. Subsurface datasets have varying levels of accuracy, geological detail, vertical resolution and thus variable ability to resolve specific stratigraphic units. Additionally, surficial map units may be diachronous and of local extent which, when considered regionally, can be correlated within a simplified stratigraphic structure of 8 units (Table 1). Model units (layers), from oldest to youngest are: 1–Bedrock, 2–Lower Sediment, 3–Regional Till, 4–Glaciofluvial Sediment, 5–Upper Till, 6–Glaciolacustrine Mud, 7–Glaciolacustrine Sand, and 8–Recent/Organic Sediment (see Table 1; Figure 2).

1. *Bedrock* unit: The base layer of the model is a generic unit that represents all sedimentary bedrock strata and crystalline basement rock.
2. *Lower Sediment* unit: A range of Illinoian to Middle Wisconsin stratigraphic units identified in lakeshore bluffs (e.g., Karrow 1967; Barnett and Karrow 2018), river valley sections, excavations (e.g., Karrow 1989; Bajc et al. 2015; Mulligan et al. 2018a), cored/geophysically-logged boreholes (e.g., Eyles et al. 1985; Mulligan and Bajc 2018; Sharpe et al. 2018; Burt and Webb 2013), and seismic reflection profiles (e.g., Sharpe et al. 2018; Gerber et al. 2018). Lower Sediment unconformably overlies bedrock and consists of a variety of geological materials including diamicton, gravel, sand, mud and organics. It is difficult to uniquely assign the Lower Sediment stratigraphically in WWIS material logs without knowledge of their position relative to other stratigraphic markers and 3-D geospatial context.
3. *Regional Till* unit: A group of commonly dense, over-consolidated sandy silt till units that are generally <30 m thick; however, locally they can be up to 70 m thick (Boyce and Eyles 2000; Knight et al. 2016). East of the Niagara Escarpment, Regional Till is predominantly the Newmarket Till (or Northern Till) and to the west it is comprised of Catfish Creek Till and Elma Till and also locally Wentworth and Port Stanley tills (Table 1). In WWIS records, Catfish Creek Till and Newmarket Till are sometimes described as hardpan (e.g., Karrow 1977). This description aligns with geophysical properties that commonly identify these units with a high seismic velocity, approaching velocity ranges of local bedrock (Pugin et al. 1999; Pullan et al. 2000; Crow et al. 2018).

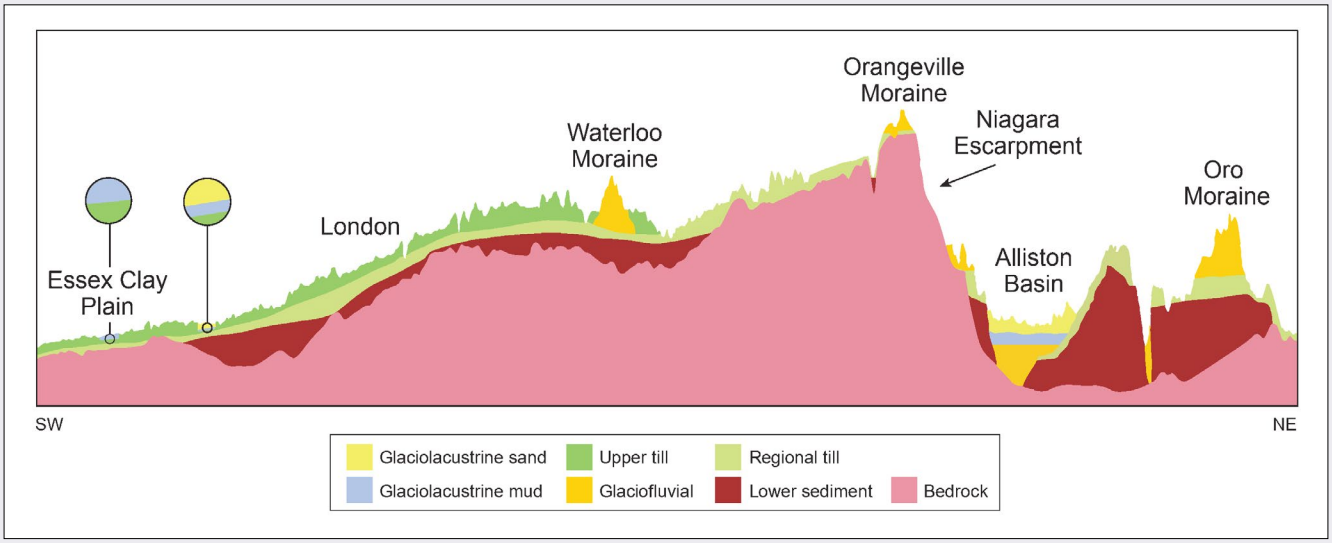


Figure 2. Conceptual representation of stratigraphic architecture for southern Ontario along a southwest-northeast cross-section from Essex Clay Plain to the Oro Moraine. See Figure 1 for approximate section path. This section is a composite of stratigraphic relationships described in various regions of southern Ontario to illustrate the conceptual basis used for this 3-D model. Geometry, relationships and fill characteristics of tunnel valleys may be drawn from areas beyond the cross-section path.

Table 1. Surficial model layers providing correlation between simplified 8 unit 3-D model layers and geological map units of seamless surficial map coverage (Ontario Geological Survey 2010). Thickness values are typical, local thicknesses may be greater.

Age	3-D Model Layer	Material(s) / Stratigraphic Formation(s)	Properties
Holocene	8–Recent/Organic Sediment	organics, colluvium, alluvium, eolian, lacustrine sediment	Thin, discontinuous. Fine to coarse grained sediment and organics
Late Wisconsin	7–Glaciolacustrine Sand	glaciolacustrine sediment – sand	Generally thin (10–15 m), discontinuous. Medium to coarse grained sediment
	6–Glaciolacustrine Mud	glaciolacustrine sediment – mud	Generally thin (10–15 m), discontinuous. Fine grained sediment
	5–Upper Till	Dunkeld Till	Up to 30 m thick, discontinuous massive to laminated mud till (clayey silt to silt)
		Halton Till	
		Kettleby Till	
		Mornington Till	
		Maryhill Till	
		Neustadt Till	
		Port Stanley Till	
		Rannoch Till	
		Stratford Till	
		St Joseph Till	
		Southern Till	
		Stirton Till	
		Tavistock Till	
		Wartburg Till	
		Wentworth Till	
	4–Glaciofluvial Sediment	Galt Moraine	Up to 150 m thick, silt, sand and gravel with minor clay beds
		Oro Moraine	
		Oak Ridges Moraine	
		Paris Moraine	
		Orangeville Moraine	
		Waterloo Moraine	
	3–Regional Till	Catfish Creek Till	10–30 m thick (locally up to 70 m), dense, compact, massive sandy silt and sand till Local equivalents Northern and Bowmanville tills (Boyce et al. 1996; Martini and Brookfield 1995)
		Elma Till	
		Leaside Till	
		Newmarket Till	
Middle Wisconsin to Illinoian	2–Lower Sediment	Thorncliffe Formation	Wide range of textures and physical properties
		Canning Till	
		Lower Stony Till	
		Meadowcliffe Till	
		Port Hope Till	
		Sunnybrook Till	
		Scarborough Formation	
		Don formation	
		York Formation	
		Basal aquifer	
Paleozoic – Precambrian	1–Bedrock	Bedrock	Undifferentiated Precambrian and Paleozoic bedrock strata

4. *Glaciofluvial Sediment* unit: A collection of primarily coarse-grained, stratified kame, esker and subaqueous fan deposits comprising stratified moraines (e.g., Sharpe et al. 2002; Russell et al. 2004; Bajc et al. 2014; Burt 2018). Some of the tunnel valleys, that are locally eroded into the Regional Till and Lower Sediment and potentially extending to bedrock, are partially infilled with sediment that is included in this layer (e.g., Sharpe et al. 2002; Russell et al. 2003a, b; Brennand et al. 2006; Sharpe et al. 2018; Mulligan et al. 2018a). This unit includes the Oak Ridges, Oro, Waterloo and Orangeville moraines which host significant aquifers (e.g., Frind et al. 2014).
5. *Upper Till* unit: A collection of laminated clay and silt to massive silty clay to silty sand till units that cover smaller, discontinuous areas within the model area and are up to 30 m thick (e.g., Karrow 1967, 1974; Sharpe and Russell 2016). Upper Till may directly overlie either the Regional Till or Glaciofluvial Sediment layers. This unit includes interbedded glaciolacustrine sediment and local beds of sand and gravel (e.g., Sharpe and Russell 2016). It includes notable till units such as Halton, Tavistock and St. Joseph.
6. *Glaciolacustrine Mud* unit: Commonly consists of varved silt and clay with minor fine sand and is typically <15 m thick, although thicknesses up to 100 m have been identified locally (e.g., Bajc et al. 2019). It was deposited in low-energy, distal deep-water parts of ice supported glacial lakes (Chapman and Putnam 1984; Barnett and Karrow 2018). This layer includes notable mud units deposited in Peel Ponds, Lake Schomberg, and ancestral Great Lakes within the Erie-Ontario and Huron basins (e.g., Burt 2016; Mulligan et al. 2018a).
7. *Glaciolacustrine Sand* unit: Composed of fine to medium sand deposited in deltas, littoral environments and shallow water areas of former glacial lakes (e.g., Norfolk sand plain, Lake Algonquin sand, beaches).
8. *Recent/Organic Sediment*: A collection of all non-glacial sediment and organic material that has accumulated in the Holocene. These sediments are thin, localized, commonly occur along river valleys, and range from fine-grained (eolian, lacustrine) to coarse-grained (alluvial, lacustrine and colluvial) material plus organics (loam, peat).

4.1 Stratigraphic architecture

A basin analysis approach of high-quality data collection was used to support interpretation of sedimentological, depositional and paleogeographic conceptual models (e.g., Eyles et al. 1985; Sharpe and Barnett 1985; Sharpe et al. 2002). Such models provide a predictive framework to support interpretation of disparate low-quality archival datasets (i.e. WWIS). The current modelling initiative is supported by the integration of stratigraphic relationships from key subsurface studies: i) ORM (Sharpe et al. 2002); ii) Waterloo Moraine (Bajc and Shirota 2007); iii) Oro Moraine (Burt and Dodge 2011); iv) Orangeville Moraine (Burt 2018); v) Simcoe County (Bajc et al. 2019; Mulligan et al. 2018a, b; Pugin et al. 2018; Sharpe et al. 2018); vi) Paris Moraine (Arnaud et al. 2018); vii) Brantford–Woodstock area (Bajc and Dodge 2011); viii) Ingersoll area (Bajc et al. 2015); ix) Essex and Oxford county (Morris and Kelly 1997); and x) the Niagara region (Burt 2016; Burt 2017a). A generalized southwest-to-northeast transect from the Essex Clay Plain through the Waterloo Moraine to the Oro Moraine illustrates the simplified stratigraphy used for this regional 3-D model (Figure 2).

The Regional Till unit, with distinct physical properties and widespread distribution, forms a stratigraphic marker bed across the model domain (Karrow 1974; Boyce and Eyles 2000; Gerber et al. 2001; Sharpe et al. 2002, 2018; Pullan et al. 2002; Logan et al. 2006; Bajc and Shirota 2007; Bajc and Dodge 2011; Burt and Dodge 2016; Mulligan et al. 2018a, b). A primary constituent, the Newmarket Till, has a distribution that is relatively well constrained (e.g., Boyce et al. 1995; Boyce and Eyles 2002; Sharpe and Russell 2016) with some significant regional variations. The Newmarket Till is thick south of the Oak Ridges Moraine (Boyce et al. 1995; Knight et al. 2016) and considerably thinner north of the ORM (Sharpe et al. 2005; Mulligan et al. 2018b; Bajc et al. 2019). It is drumlinized and eroded to varying degrees and locally completely truncated by subglacial erosional processes involving meltwater and ice (e.g., Sharpe et al. 2004; Mulligan et al. 2018b).

A major element of the model is a network of valleys that truncate the Regional Till and Lower Sediment. The valleys are locally buried beneath the ORM (e.g. Sharpe et al. 2004) and elsewhere are exposed and only partially infilled (e.g., Mulligan et al. 2018b; Sharpe et al. 2018). The depth and truncation of deposits is variable with some valleys floored by Newmarket Till, others by Lower Sediment and some extending to bedrock (e.g., Pugin et al. 1999, Pugin et al. 2011; Pugin et al. 2017; Russell et al. 2003a; Sharpe et al. 2002; Sharpe et al. 2018; Mulligan and Bajc 2018, Mulligan et al. 2018b; Bajc et al. 2019). The valleys are interpreted to be tunnel valleys although the formative mechanism continues to be debated (e.g. Sharpe et al. 2003; Mulligan et al. 2018b).

The overlying Glaciofluvial unit is well described from a range of moraine studies and locally includes the basal parts of tunnel valley fill (e.g., Barnett et al. 1998; Russell et al. 2003a, b; Bajc et al. 2014). The Upper Till unit is mapped extensively across the surface of southern Ontario (OGS 2010) and thickness estimates supported by a number of subsurface studies (e.g., Bajc and Dodge 2011, Russell et al. 2003; Sharpe and Russell 2016). The extents and thicknesses of Glaciolacustrine Mud and Sand units and the Recent unit are constrained by conceptual models of deglaciation, proglacial and post glacial landscape evolution (e.g., Bajc et al. 2019, Arnaud et al. 2018; Barnett and Karrow 2018; Mulligan et al. 2018a).

5. Data support

5.1 Subsurface data

Subsurface data support for the 3-D surficial geological model comes from multiple sources with variable coverage, detail and reliability. Subsurface data sources are treated differently in the model-building process based on their quality and detail. They are classified as Level 1, 2 or 3 (Table 2). Level 1 data consists solely of water well records from the Water Well Information System (WWIS) managed by the Ministry of Environment, Conservation and Parks (MECP). It

Table 2. Data inputs for modelling grouped according to data class.

Data Quality Class	Agency	Data Source	Data Type	No. of Boreholes	Avg. Units per Borehole	Avg. Depth (m)	% to Bedrock
Level 1	MECP	WWIS	borehole log	287977	4.2	27.7	45.6
Level 2	Conservation Ontario	publication	borehole log	2	32.5	60.5	100
	OGS	various	borehole/meas. section	2173	6.1	13.7	9.8
	OGS	various	shallow hole/field mapping	8899	1.6	1.4	0.9
	MTO	hardcopy	borehole log	408	3.8	11.6	27.7
	MECP	PMN	borehole log	134	6.7	37.4	20.1
	GSC	UGAIS	borehole log	3135	4.1	5.3	1.8
	GSC	WAGAIS	borehole log	3841	3.6	7.9	3.7
	Regional Municipality	digital database	borehole log	165	6.8	39	46.7
	GSC	digital database	shallow hole/field mapping	329	1.5	2	0.3
	University of Waterloo	digital database	borehole log	3	6.7	14.2	66.7
Level 3	GSC	digital database	cored borehole (simplified)	33	53.5	107.4	48.5
	GSC	digital database	shallow hole/field mapping	2513	1.5	1.67	0.5
	GSC	digital database	geophysical observation	3297	NA	NA	5
	OGS	various	cored borehole/meas. section	2186	6.8	18.6	21.4
	OGS	various	shallow hole/field mapping	3584	1.1	1	10.5
	OGSR	OPDS	bedrock top pick	366	NA	NA	100
	Consultant	various	borehole log	328	4	14.4	2.4
	MTO	hardcopy	borehole log	1053	3.3	15.3	25.7
	IWA	digital database	borehole log	255	9.8	37.9	14.5
	Consumers Gas	digital database	borehole log	76	3.5	5.3	40.8
	EC	digital database	borehole log	1	9	46.3	100
	Eldorado Nuclear Ltd.	digital database	borehole log	127	5.2	20.4	4.7
	LLRWMO	digital database	borehole log	89	3.4	7.7	12.4
	MECP	digital database	borehole log	86	8.7	101.9	38.4
	Regional Municipality	digital database	borehole log	192	9	64.3	29.2
	Siting Task Force	digital database	borehole log	66	6.4	19	6.1
	TTC	digital database	borehole log	22	7.4	28.6	0
	GSC	UGAIS	borehole log	500	5	11.3	6
	University of Guelph	digital database	borehole log	3	4	18	0

Organizations: EC – Environment Canada; GSC – Geological Survey of Canada; IWA – Interim Water Authority; LLRWMO – Low-Level Radioactive Waste Mgt. Office; MECP – Ministry of Environment, Conservation and Parks; OGSRL – Oil, Salt, Gas Repository Library; OGS – Ontario Geological Survey; MTO – Ontario Ministry of Transportation; TTC – Toronto Transit Commission.

Data management systems: OPDS – Ontario Petroleum Data System; PGMN – Provincial Groundwater Monitoring Network; UGAIS – Urban Geology Automated Info. System; WWIS – Water Well Info. System; WAGAIS – Waterloo Area Geology Automated Info. System.

is the most abundant dataset and, in many areas, the only source for subsurface information. Level 1 data have potential location, depth and material reporting issues and contain no stratigraphic unit information (e.g., Russell et al. 1998). It is not possible to discriminate many of the stratigraphic units in WWIS data without additional context due to the lack of attribute information and issues of generic material descriptions.

Level 2 data include borehole logs from geotechnical and hydrogeological site investigations. These boreholes are accurately located and contain detailed material depth logs. These data are often site-specific and collected to assess material properties for engineering purposes and hydrogeological investigations. The overall coverage and abundance of this data is much lower than Level 1 data and it tends to be clustered, particularly in the areas of infrastructure development (e.g., gas lines, bridges, etc.). Another constraint is that geotechnical data collected for structural engineering purposes tends to be shallow (i.e., less than 30 m). Sediment descriptions are commonly based on the Unified Soil Classification System (ASTM 1986) and lack sedimentological detail.

Level 3 data have a similar or better level of location accuracy as Level 2 data and the materials are predominantly logged in greater sedimentological detail. Most importantly for modelling, Level 3 data are separated from Level 2 based on the presence of interpreted stratigraphic unit information. Level 3 data includes cored borehole logs that were obtained from GSC and OGS projects (e.g., Bajc and Shirota 2007) where the primary objectives were to gain sedimentological and stratigraphic insight (e.g., Sharpe et al. 2002). Over 300 cored boreholes and measured sections collected in the Barrie-Oro Moraine, Orangeville and Waterloo moraines, Simcoe County, Niagara Peninsula, Dundas Valley and Brantford–Woodstock areas form the largest component of the Level 3 data (Burt and Dodge 2011; Burt and Dodge 2016; Bajc and Shirota 2007; Bajc and Dodge 2011; Bajc et al. 2015; Mulligan, unpublished data; Burt 2015, 2016, 2017a, b; Burt et al. 2016). This data class also includes former Level 2 geotechnical data that have been assessed and manually classified by geologists with assignment of stratigraphic units, interpreted geophysical data and 'top of bedrock' picks from the Ontario Petroleum Data System (OPDS) database. Level 3 data has sparse coverage at the scale of southern Ontario modelling.

A number of geophysical datasets were utilized for modelling. Digital images of 37 seismic profiles were imported and registered in the 3-D model environment. Interpreted contact lines were digitized and added to model layer inputs to provide additional subsurface control. Pseudo-boreholes created from depth picks along 15 seismic profiles that were assembled for an older model of the Oak Ridges Moraine area (Logan et al. 2005) were also utilized. These profiles have been collected during the past 2 decades using a 3-component landstreamer system (Pugin et al. 1999, Pugin 2016). Profiles were mostly collected on stratified moraines (Oak Ridges, Waterloo, Oro) with secondary data collection on buried valleys (e.g., Laurentian trough, Erigan valley) (Pugin et al. 2018; Dietiker et al. 2019). Data quality is variable depending upon the nature of the processed wave form, p-wave and/or s-wave, surface conditions (sand, mud, road bed) and stratigraphic succession and thickness. A number of gravity surveys have been completed in areas of buried valleys and thick sediment cover to better resolve bedrock topography (e.g., Annecchione et al. 2001; OGS 2014).

5.2 Bedrock and topographic DEM

The bedrock/surficial sediment contact surface forms the base of the surficial geological model and an upper erosional surface boundary for the bedrock model. An updated bedrock surface from Gao et al., (2006) was developed using revised well log vetting and integration of additional data. Vetting of the WWIS data for incorrect bedrock terms and location errors was completed by OGS staff (e.g., Carter et al. 2020, this vol.). Additionally, 16,304 "top of bedrock" / "sediment thickness" values were supplied from the Ministry of Natural Resources and Forestry (MNRF) OPDS database and drilling results from over 300 Level 3 OGS boreholes were also integrated. This newly updated and vetted dataset was developed through collaborative bedrock modelling efforts (Clarke et al. 2020, this vol.; Carter et al. 2020, this vol.). Additional lake-based seismic data (Todd et al. 2003) was integrated to complete the bedrock surface below water bodies within the terrestrial model domain.

A topographic DEM provides the upper boundary surface of the surficial model. This DEM is a composite model surface composed of Shuttle Radar Topography Mission (SRTM) 30 arc second DEM data (NASA JPL 2013) and bathymetric information. For the Great Lakes, bathymetry from the National Oceanic and Atmospheric Administration (NOAA) and Canadian Hydrographic Survey (CHS) was used (National Geophysical Data Center, 1999a, b, c). For other waterbodies in southern Ontario (e.g., Lake Simcoe, Kawartha lakes), depth soundings were extracted from CHS bathymetric field charts. To automate the digital capture of the hand-written depth points, a Python™ application was developed using a machine-learning optical character recognition algorithm (Griffiths et al. 2020, this vol.). Geo-referenced bathymetry data sets were then interpolated and merged with the SRTM DEM to provide a seamless topographic DEM.

5.3 Surficial geology mapping

The most extensive set of observations and data collection supports 1:50,000 surficial geological mapping (OGS 2010). Hence, 2-D surficial mapping provides the most extensive and consistent source of data control for regional 3-D modelling. The 1:50,000 scale map legend was reclassified to the 8 units

of the subsurface modelling study to harmonize with other data inputs. To allow the surficial geology to control the surface expression of the 3-D model, the map polygons were used to isolate and trim portions of the topographic DEM. The trimmed DEM sections were then converted into regular grids of elevation points and added to the data support for corresponding model layers. The 3-D modelling software uses these points along with borehole contacts to support 3-D interpolation of layer contact surfaces thereby smoothly blending subsurface data with surficial mapping.

6. 3-D Modelling workflow

6.1 QA/QC

The shortcomings of WWIS water well records in terms of location accuracy, depth accuracy and geological rigour are well known and studies that use them invariably apply some level of data vetting to reduce errors (Kenny et al. 1997; Bajc and Shirota 2007; Bajc and Dodge 2011; Burt and Dodge 2011, 2016). For the surficial sediment model, well location errors are screened by comparing coordinates with water bodies, municipality boundaries and lot/concession maps (e.g., Kenny et al. 1997; Logan et al. 2006). In addition, vetting and well location corrections from OGS bedrock elevation investigations were applied (Carter et al. 2020, this vol.).

6.2 Standardizing material descriptions

After location error vetting, material descriptions were standardized to a common system of material codes (i.e., silt, sand, etc.) to facilitate stratigraphic interpretation. Where materials were described with free-form text in Level 2 data, material terms were extracted and parsed into a structured set of adjective/noun material terms. Discreet material terms reported in the remainder of Level 2 and all Level 1 data were similarly restructured and then reclassified to a single geologically meaningful description following the methodology used in Russell et al., (1998) and Logan et al., (2006).

6.3 Semi-automated stratigraphic assignment

The primary task towards producing a viable 3-D model is correctly interpreting subsurface material depth logs and determining what portion of the model stratigraphy is represented therein. With the potential for multiple sequences of similarly-textured tills and coarse-grained units in large areas of the model, stratigraphic benchmarks and depth frameworks based on surficial mapping, expert knowledge and nearby Level 3 data are utilized. Level 3 data have pre-existing stratigraphic assignments and are usually reclassified to the simplified model stratigraphy (see Table 1). A multistep, iterative approach was employed to assign model stratigraphy to Level 1 and 2 data. A preliminary set of layer surfaces was developed with Level 3 data along with digitized surficial mapping and used to provide a rough estimate of the depth range and thickness of the model layers. The intersection of these preliminary surfaces with Level 1 and 2 data was used to attach layer depth estimates to each borehole. The distance to Level 3 control data was also attached and the surficial geological map unit covering the borehole location was assigned to the uppermost corresponding borehole unit to serve as a stratigraphic 'maximum'. A rules-based algorithm was then applied to each Level 1 and 2 borehole log using preliminary layer depths, surficial geological unit assignment, and expert rules (Table 3) to automatically assess log material depths and assign partial model stratigraphy.

The rule-based interpretation algorithm is applied downward from the surface using the surficial geology unit assignment for the first depth interval if its material description is in agreement (e.g., if the borehole lies within mapped Glaciolacustrine Mud and the uppermost material is fine-grained, then it is

Table 3. Model layer guidelines used for limited automated interpretation of material logs. Values and terms used are based on typical thicknesses and are conservative generalities selected to avoid excessive over-estimation of model layers. Additional interbedded materials can exist and thicknesses can be greater in some cases.

Model Layer	Acceptable Materials	Max Thickness (m)	Max Interbed (m)
8–Recent/Organic Sediment	sand, silt, organic	10	0
7–Glaciolacustrine Sand	sand, silt	20	1
6–Glaciolacustrine Mud	silt, clay	20	1
5–Upper Till	diamicton, silt, clay	30	1
4–Glaciofluvial Sediment	gravel, sand, silt	60	2
3–Regional Till	diamicton, clay	40	2
2–Lower Sediment	(all non-bedrock terms)	30	1
1–Bedrock	bedrock	NA	0

coded as Glaciolacustrine Mud if all other expert rules are met). The second depth interval may be assigned based on surficial geology if the first material interval is a thin veneer (i.e., <2 m). Material intervals at the surface that are 'organic' are included in the Recent/Organic layer regardless of the mapped geology, and the second interval is then evaluated against the surface geology. In some cases, older mapped geology polygons that surround younger, disconnected Glaciolacustrine or Recent/Organic polygons are used to assign a model layer to the second material interval. Bedrock intervals are assigned directly from bedrock material codes when available. Additional Level 1 and 2 borehole intervals are assigned a model layer only if the depth range of a suitable material overlaps the preliminary model depths within +/- 5 m. Finally, the algorithm assigned a model layer to fill gaps in the stratigraphy if material type and geospatial constraints are in agreement. Well logs with top-most depth intervals described as 'previously drilled' are discarded since the thickness of material at the top of the log is unknown and therefore a stratigraphic starting position can not be determined based on surface mapping.

Intervals were assigned only if they conformed to expert rules, conformed to the geospatial context of the preliminary surfaces, maintained the correct stratigraphic relationships, and were located within 2,000 m of a control data point. These constraints restricted the algorithm in an attempt to limit the amount of "false-positives" and reduce layer over-estimation. Material intervals that do not fit with expert rules and the geospatial constraints of the preliminary model are left as an undefined generic material type for subsequent manual inspection in the 3-D modelling software.

The 3-D model and borehole model layer assignments gradually evolved over an iterative development process with the first of several intermediate models produced by combining the partially assigned Level 1 and 2 data with Level 3 data. Unassigned material intervals in each iteration are systematically filtered based on similar materials, rendered in 3-D space and visually compared to relevant contextual data (i.e., surficial mapping, the topographic DEM, assigned borehole intervals and intermediate model layers). Likely populations of unassigned intervals that aligned texturally and spatially with the intermediate model were captured in bulk and assigned to the appropriate model layer. These visual inspections were also used to manually check and correct previous assignments of Level 1 and 2 data. After this phase of new assignments and corrections, the next intermediate model was processed and visually inspected. The borehole lithology table was then exported, checked for stratigraphic integrity (i.e., younger units are above older units), an automated layer assignment was re-applied and the updated lithology was re-imported to begin the next model iteration. Two interim models were examined by project geologists to gain insight and feedback to help correct layer assignments and improve the geometry of model layers. This cycle concluded as the model stabilized and appeared reasonable based on expert geological insight and given the level of data support. Approximately 62% of over 1.2 million Level 1 and 2 material depth intervals were automatically assigned an initial stratigraphic code. Through numerous iterative model refinements, an additional 208,770 intervals were coded for a total of ~80% of depth intervals. The remaining 20% un-coded intervals either contradicted other nearby data, contravened expert rules / knowledge or both and were disregarded.

6.4 3-D software / model setup

Leapfrog® Works implicit 3-D modelling software was used to develop the geological models. The speed and flexibility of implicit modelling lends itself well to the large size, large datasets and multiple iteration cycles involved in the development of the southern Ontario geological models. The software requires the model extents to be defined in 3-D space by a base elevation or surface, X/Y lateral extents or a polygon boundary and an upper surface — usually a topographic Digital Elevation Model (DEM). These boundaries truncate contact surfaces and layer volumes when the model is rendered for visualization. In an implicit model, a layer contact surface is defined as the zero set of a Radial Basis Function fitted to the layer contact data (Carr et al. 2001). For the southern Ontario surficial geology 3-D model, a 2-layer primary model was developed to render a generic bedrock and sediment volume. A refined model was then developed using the sediment volume as a container to constrain and truncate all surficial layers below at the bedrock contact surface and above at the topographic DEM.

In the modelling software, a number of options exist to control how support data (e.g., interpreted borehole contacts) are rendered into model layers. In the configuration used for surficial modelling, an upper contact surface for each model layer is developed that both honours contact data and avoids all younger borehole lithology intervals. Aside from avoiding younger borehole formations, the contact surfaces are estimated in 3-D space independently from one another. Upper, lower and lateral layer boundaries are defined by contact surfaces in chronological succession along with overall model boundaries. Using the 'deposit' surface rendering option in the modelling software, older layers supersede younger ones. This results in the removal of the younger layer where interpolated surfaces overlap. The 'deposit'-type was used for all model layers except Regional Till. The upper surface contact of Regional Till is an unconformity / erosional surface (Sharpe et al. 2004) and therefore is more suitably modelled as an 'erosion'. When modelled as an erosion, however, a younger surface can remove older volumes where contact surfaces overlap. The unrealistic removal of bedrock was prevented by confining sediment layers within the generic sediment container defined by the refined model.

6.5 Model editing

The modelling software workflow expects that borehole log contacts will act as the primary data input for the model. Surfaces and 3-D vector objects can augment borehole contacts. Implicit model surfaces are directly estimated from borehole contacts and other measured contact data (e.g., seismic profiles, geological mapping and field observations), however trend surfaces and manual editing can be applied independently in areas of low data support. Within tunnel valleys, for example, the truncation of Regional Till and some or all Lower Sediment is evident in some boreholes and seismic profiles. However, the long, narrow geometry of tunnel valleys (i.e., a few kms wide, by 10s of kms long) compared to the regional layered architecture requires a substantially higher concentration of subsurface data to fully resolve the valley geometry than is available. Although seismic profiles are directly used to digitize 3-D surface control polylines, their coverage is not adequate to fully render all buried valleys. Where one or more profiles transected a buried tunnel valley, manual polyline edits were used to enforce continuity, and/or extrapolate a small distance (~5 km) beyond the plane of profiles. For partially filled valleys visible at ground surface, Regional Till occurrences mapped at a higher elevation outside of channel valleys tend to connect across narrow valleys and fill them unrealistically compared to interpreted relationships on seismic profiles. Since data coverage is generally sparse within recognized valley areas, mapped valleys (Brennand et al. 2006) were used to guide manual point editing to remove Regional Till and Lower Sediment where needed to align better with seismic data and field observations.

7. Model results

The surficial 3-D model depicts the stratigraphic unit distribution and geometry of 8 surficial units at a regional-scale. In order to fully establish the geometry and continuity of buried structures like tunnel valleys, a substantially larger set of high-quality data is required. Other prominent features such as bedrock valleys, glaciofluvial moraines and tills and glaciolacustrine sediment, are generally represented within the constraints of the data support (Figures 3 and 4). Figure 4, A–A′ is an east–west cross-section along the crest of the ORM transverse to roughly north–south trending tunnel

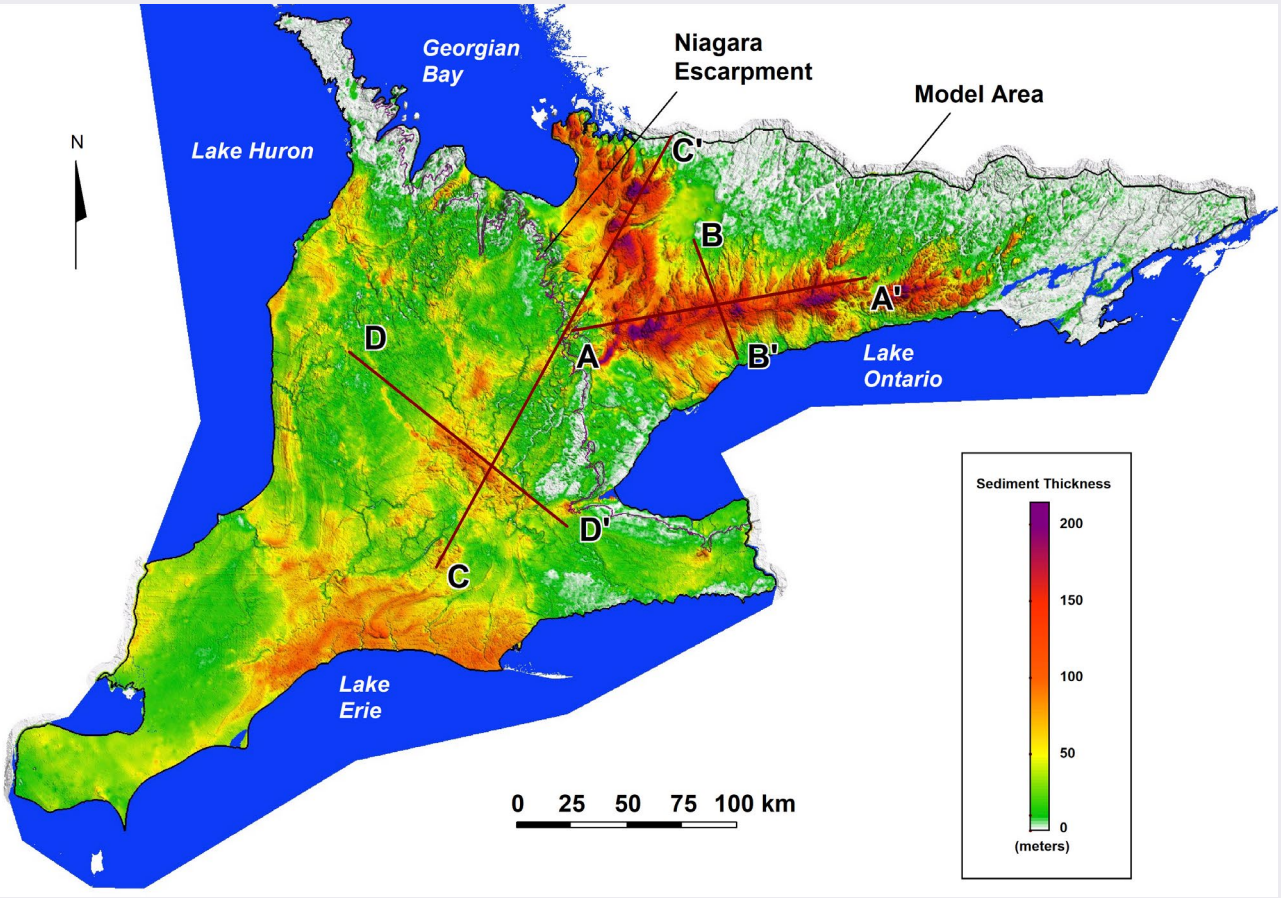


Figure 3. 3-D model sediment thickness. Cross-section locations for Figure 4 are shown. Model does not extend beneath the Great Lakes.

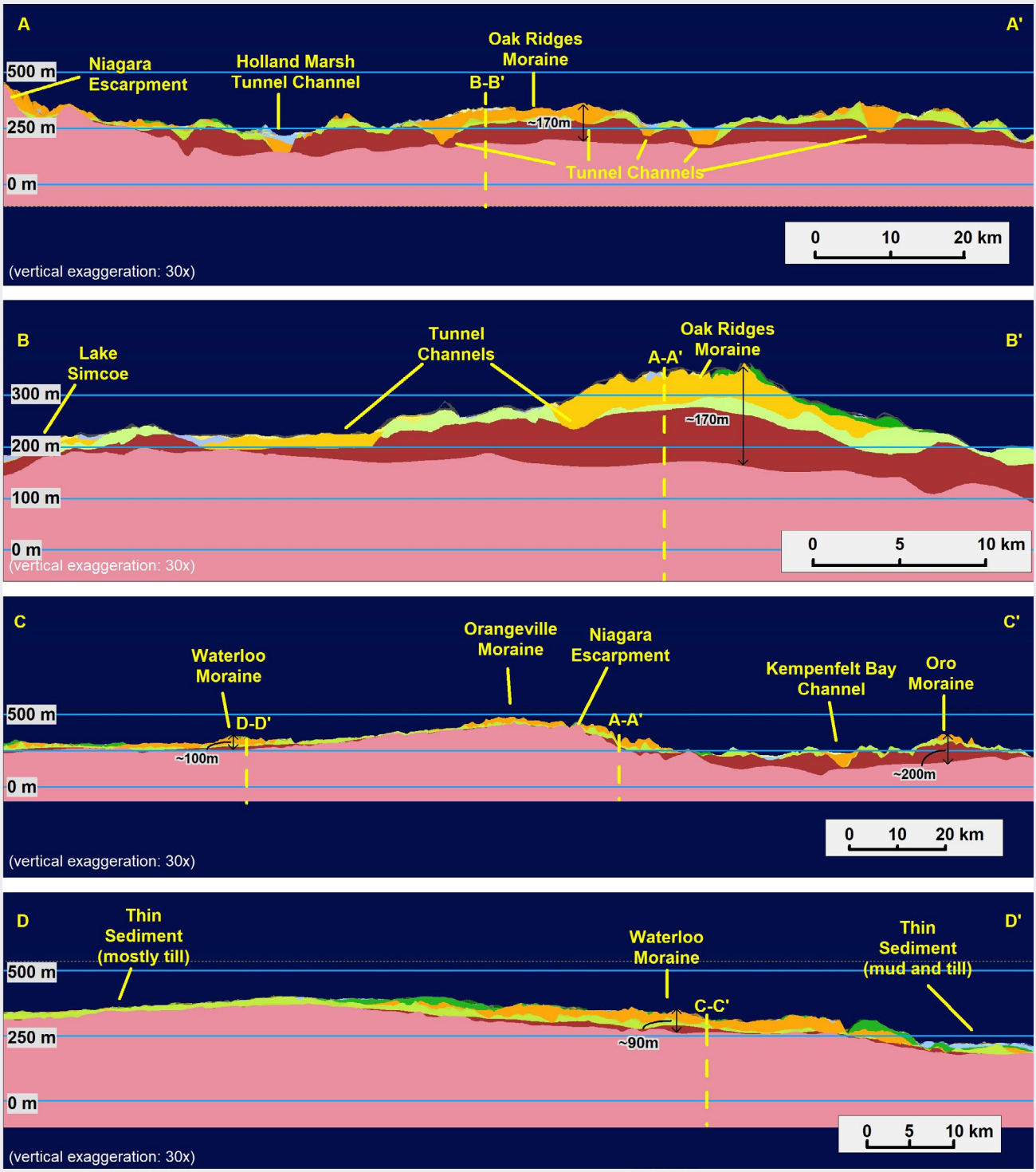


Figure 4. Preliminary model cross-sections (refer to Fig. 1 for colour legend). Section A–A': Along the crest of Oak Ridges Moraine (ORM) Glaciofluvial Sediment. Tunnel channels in Regional Till and Lower Sediment layers are visible. Section B–B': N-S section from Lake Simcoe to Lake Ontario crossing the Glaciofluvial Sediment (ORM) above irregular, Regional Till (Newmarket Till). Upper Till (e.g., Halton Till) drapes the south flank of ORM. Section C–C': SW to NE section from near Woodstock to Oro Moraine with thinner sediment west of the Niagara Escarpment and thicker sediment of the Laurentian Trough and Oro Moraine. Section D–D': NW-SE section from near Lake Huron to near Paris across the Waterloo Moraine. Mostly thin (10–20 m) Regional Till over bedrock to the north and Glaciolacustrine Mud with till to the south of the moraine.

valleys. This subsurface view of the area shows both partially and fully incised Regional Till (Newmarket Till). Upper Till (Halton Till) can be seen to the west at the surface overlying the ORM sediment. To the east, the ORM is exposed at the ground surface. Figure 4, B–B′ is a north–south cross-section from Lake Simcoe to Lake Ontario and highlights the general slope of the bedrock toward Lake Ontario. It also highlights the increasing surficial sediment thickness southward to a maximum along the axis of the ORM. The ORM overlies a slight Lower Sediment high that may be a modelling artifact caused by the overall lack of data at depth below the ORM. Figure 4, C–C′ is a southwest to northeast cross-section from Brantford to north of Lake Simcoe / Oro Moraine. It highlights the Niagara Escarpment and southwest slope of the Paleozoic bedrock. Sediment is thickest beneath the Waterloo and Orangeville moraines and thins to the southwest. Figure 4, D–D′ is a northwest to southeast section across the Waterloo Moraine. The northwest region typically shows thin Regional Till directly overlying bedrock, while mainly thin Glaciolacustrine Mud and tills overlie bedrock to the southeast of the thicker (~100 m) moraine.

8. Discussion

8.1 Data support limitations

The combination of a topographic DEM with lake bathymetry and surficial mapping controls the near-surface portion of the 3-D model; however, the deeper subsurface geometry of the model relies mainly on interpolated contacts from 321,843 subsurface data records (Table 2). Although there are on average 4.8 records per km^2, the data are generally clustered around populated areas and close to 90% are water wells (Level 1 data) which have low-quality descriptions and variable depth coverage. Water well drilling stops when productive aquifers are encountered, often well above older sequences, resulting in poor representation of Middle Wisconsin sediments in areas of thick glacial sediment (up to approximately 250 m thick). For example, less than half (45.6%) of the archival water well logs used in this model were deep enough to encounter bedrock. Of these, only 5.3% occur in areas of total sediment thickness >50 m based on sediment thickness estimates (Gao et al. 2006). The average depth for boreholes located in areas of >50 m thick sediment is 30.1 m. For the surficial sediment model, 25% of the area is covered by sediment over 50 m thick with an estimated 60% of the total sediment volume (Figure 3).

8.2 Impact of geological conceptualization

New data, revised interpretations or new evidence to support mapping changes, borehole log corrections and revision of the knowledge of the geological history and setting will affect the 3-D model. The complexity of southern Ontario glacial sediments has led to multiple geological interpretations in portions of the model area that may require additional data to resolve. The current model utilizes a conceptual model involving widespread truncation of the Regional Till and Lower Sediment within tunnel valleys across south-central Ontario (e.g. Sharpe et al. 2002, 2004, 2018; Sharpe and Russell 2016; Russell et al. 2003, 2004). Data collected by contributing geologists in parts of the tunnel valley network suggests the drumlinized Regional Till is more continuous and may be encountered along the floors of tunnel valleys (Mulligan and Bajc 2012, 2018; Bajc et al. 2015; Bajc et al. 2019; Mulligan et al. 2018a,b; 2019). The southern Ontario surficial geological model, like all such models, is a prediction based on the conceptualization (e.g., Sharpe et al. 2002) and should be evaluated against new high-quality subsurface data and/or revised geological insights.

9. Summary

A 66,870 km^2 regional 3-D geological model has been constructed to represent the surficial sediments of southern Ontario. The model integrates the surficial geological mapping units of the seamless southern Ontario 1:50,000 mapping (OGS 2010) to a simplified 8 units (layers) for model construction. A framework of manually interpreted high-quality subsurface data (Level 3) is used to guide a semi-automated, iterative process to interpret archival borehole logs (Level 1 and 2) and develop intermediate 3-D models for expert review. In the current model workflow, surfaces are augmented with additional 3-D vector polyline and point control derived from seismic profiles and expert guidance to better depict detailed features beyond the resolution of the borehole distribution (e.g., tunnel valleys). Improved model versions will be possible using new high-quality data that improves knowledge of spatial variations of the glacial geology in southern Ontario. The model along with a companion model of bedrock geology (Carter et al. 2019; 2020, this vol.) provides the first complete 3-D model coverage of southern Ontario from the Precambrian basement to post-glacial sediment and hence regional hydrostratigraphic framework for regional numeric groundwater modelling (e.g., Frey et al. 2019; 2020, this vol.)

10. Acknowledgements

The authors are grateful for the assistance of Katie MacDonald and Matt Griffiths in processing CHS bathymetry data. Work by Matt Pyne in preparing seismic data for Lake Ontario and Lake Huron and providing an interpolated Lake Huron bedrock DEM is also greatly appreciated. Barbara Dietiker and André Pugin prepared and provided interpreted digital seismic profiles. An internal GSC critical review by Ross Knight is appreciated. This work was funded through the Groundwater Program of the GSC. This work is a contribution to the GSC–OGS southern Ontario project on groundwater 2014–2019.

11. References

Annecchione, M.A., Chouteau, M., and Keating, P. 2001. Gravity interpretation of bedrock topography: the case of the Oak Ridges Moraine, southern Ontario, Canada. Journal of Applied Geophysics, 47: 1, 63-81. https://doi.org/10.1016/S0926-9851(01)00047-7

Armstrong, D.K. and Dodge, J.E.P. 2007. Paleozoic geology of southern Ontario. Ontario Geological Survey, Miscellaneous Release—Data 219.

Arnaud, E., McGill, M., Trapp, A., and Smith, J.E. 2018. Subsurface heterogeneity in the geological and hydraulic properties of the hummocky Paris Moraine, Guelph, Ontario. Canadian Journal of Earth Sciences, 55: 768-785. https://doi.org/10.1139/cjes-2016-0161

American Society of Testing Methods Annual Book of Standards (ASTM), 1986. Standard recommended practice for particle size analysis for soils. ASTMD, pp 422–463.

Bajc, A.F. and Shirota, J. 2007. Three-dimensional mapping of surficial deposits within the Regional Municipality of Waterloo, southwestern Ontario. Ontario Geological Survey, Groundwater Resources Study 3, 41p.

Bajc, A.F. and Dodge, J.E.P. 2011. Three-dimensional mapping of surficial deposits in the Brantford–Woodstock area, southwestern Ontario; Ontario Geological Survey, Groundwater Resources Study 10.

Bajc, A.F., Burt, A.K., Priebe, E.H., Mulligan, R.P.M. 2019. Regional Groundwater Systems Mapping in the County of Simcoe, Southern Ontario: Second Phase of Field Work, Ontario Geological Survey, Open File Report 6360.22

Bajc, A.F., Mulligan, R.P.M., Pugin, A.J.-M., Rainsford, D.R.B. 2014. An Update on the Final Phase of Subsurface Data Collection in the Southern Part of the County of Simcoe, Southern Ontario, Ontario Geological Survey, Open File Report 6300.33

Bajc, A.F., Karrow, P.F., Yansa, C.H., Curry, B.B., Nekola, J.C., Seymour, K.L., and Mackie, G.L. 2015. Geology and paleoecology of a Middle Wisconsin fossil occurrence in Zorra Township, southwestern Ontario, Canada. Canadian Journal of Earth Sciences, 52: 386–404. https://doi.org/10.1139/cjes-2015-0005

Barnett, P.J. 1992. Quaternary geology of Ontario. In Geology of Ontario. Ontario Geological Survey, Special Volume 4, Part 2, 1011-1090.

Barnett, P.J. and Karrow, P.F. 2018. Ice-marginal sedimentation and processes of diamicton deposition in large proglacial lakes, Lake Erie, Ontario, Canada. Canadian Journal of Earth Sciences, 55: 846-862. https://doi.org/10.1139/cjes-2017-0006

Barnett, P.J., Cowan, W.R., and Henry, A.P. 1991. Quaternary geology of Ontario, southern sheet. Ontario Geological Survey, Map 2556. scale 1:1,000,000.

Barnett, P.J., Sharpe, D.R., Russell, H.A.J., Brennand, T.A., Gorrell, G., Kenny, F.M., Pugin, A. 1998. On the origin of the Oak Ridges Moraine. Canadian Journal of Earth Sciences, 35: 1152–1167. https://doi.org/10.1139/cjes-35-10-1152

Boyce, J.I. and Eyles, N. 2000. Architectural element analysis applied to glacial deposits: internal geometry of a late Pleistocene till sheet, Ontario, Canada. Geological Society America Bulletin 112: 98–118. https://doi.org/10.1130/0016-7606(2000)112<98:AEAATG>2.0.CO;2

Boyce, J.I., Eyles, N., Pugin, A. 1995. Seismic reflection, borehole and outcrop geometry of Late Wisconsin tills at a proposed landfill near Toronto, Ontario. Canadian Journal of Earth Sciences, 32: 1331–1349. https://doi.org/10.1139/e95-108

Brennand, T.A., Russell, H.A.J., and Sharpe, D.R. 2006. chp. 6 Tunnel channel character and evolution in central southern Ontario. In Knight, P. Ed. Glacier Science and Environmental Change. Blackwell Publishing, Malden, MA. https://doi.org/10.1002/9780470750636.ch6

Brunton, F.R., Belanger, D., DiBiase, S., Yungwirth, G. and Boonstra, G. 2007. Caprock carbonate stratigraphy and bedrock aquifer character of the Niagara Escarpment – City of Guelph Region, southern Ontario. In Proceedings of the 60th Canadian Geotechnical Conference and the 8th joint Canadian Geotechnical Society–International Association of Hydrogeologists conference, Canadian Geotechnical Society, Ottawa, Ontario, 371-377.

Burt, A.K. 2012. Conceptual geologic model for the Orangeville Moraine three dimensional project. In Summary of field work and other activities 2012. Ontario Geological Survey, Open File Report 6280, 32-1–32-6.

Burt, A.K. 2015. Quaternary stratigraphy of the Niagara Peninsula revealed with three-dimensional mapping; in Summary of Field Work and Other Activities, 2015, Ontario Geological Survey, Open File Report 6313, 35-1–35-17.

Burt, A.K. 2016. The Niagara Peninsula in three dimensions: a drilling update; in Summary of Field Work and Other Activities 2016, Ontario Geological Survey, Open File Report 6323, p. 30-1 to 30-13.

Burt, A.K. 2017a Graphic logs with analytical and geochronological data from hand auger, probe and section sites in the Niagara Peninsula; Ontario Geological Survey, Miscellaneous Release—Data 353.

Burt, A.K. 2017b. Digging deep on the Niagara Peninsula: a drilling update. In Summary of Field Work and Other Activities 2017, Ontario Geological Survey, Open File Report 6333, p. 24-1 to 24-16.

Burt, A.K. 2018. Three-dimensional hydrostratigraphy of the Orangeville Moraine area, southwestern Ontario, Canada. Canadian Journal of Earth Sciences, 55, 802-828. https://doi.org/10.1139/cjes-2017-0077

Burt, A.K. and Dodge, J.E.P. 2011. Three-dimensional modelling of surficial deposits in the Barrie–Oro moraine area of southern Ontario. Ontario Geological Survey, Groundwater Resources Study 11, 125 p.

Burt, A.K. and Dodge, J.E.P. 2016. Three-dimensional modelling of surficial deposits in the Orangeville–Fergus area of southern Ontario. Ontario Geological Survey, Groundwater Resources Study 15, 155 p.

Burt, A.K. and Webb, J.L. 2013. Results of the 2008, 2009 and 2010 Drilling Programs in the Orangeville-Fergus Area of Southwestern Ontario, Ontario Geological Survey, Miscellaneous Release – Data 303

Burt, A.K., Rainsford, D.R.B., Pugin, A., Dietiker, B., Crow, H. and Campbell, J.D. 2016. The Niagara Peninsula project: An integrated approach to 3-D mapping for groundwater characterization; abstract in Geological Society of America, Abstracts with Programs, v.48, no.5, doi: 10.1130/abs/2016NC-275152.

Calkin, P.E. and Feenstra, B.H. 1985. Evolution of the Erie basin Great Lakes. In Quaternary Evolution of the Great Lakes. In Karrow P.F. and Calkin, P.E. Eds. Geological Association of Canada, Special Paper 30, 149–170.

Carr J.C., Beatson R.K., Cherrie J.B., Mitchell T.J., Fright W.R., McCallum B.C., and Evans T.R. 2001. Reconstruction and representation of 3-D objects with radial basis functions. In: Siggraph A.C.M. Computer graphics proceedings. ACM Press, New York, 67–76.

Carter, T.R., Brunton, F.R., Clark, J., Fortner, L., Freckelton, C.N., Logan, C.E., Russell, H.A.J., Somers, M., Sutherland L. and Yeung, K.H. 2017. Status report on three-dimensional geological and hydrogeological modelling of the Paleozoic bedrock of southern Ontario. In Summary of Field Work and Other Activities, 2017, Ontario Geological Survey, Open File Report 6333, p.28-1 to 28-15.

Carter, T.R., Brunton, F.R., Clark, J.K., Fortner, L., Freckelton, C., Logan, C.E., Russell, H.A.J., Somers, M., Sutherland, L., and Yeung, K.H. 2019. A three-dimensional geological model of the Paleozoic bedrock of southern Ontario; Geological Survey of Canada, Open File 8618; Ontario Geological Survey, Groundwater Resources Study 19, 1 .zip file. https://doi.org/10.4095/315045

Carter, T.R., Brunton, F.R., Clark, J.K., Fortner, L., Logan, C.E., Russell, H.A.J., Somers, M., Sutherland, L., and Yeung, K.H. 2020. Three-dimensional geological modelling of the Paleozoic bedrock of southern Ontario: Status update. In Russell, H.A.J. and Kjarsgaard, B.A. Eds. Southern Ontario groundwater project 2014–2019: summary report. Geological Survey of Canada, Open File 8536, 7-21. https://doi.org/10.4095/321080

Chapman, L.J. and Putnam, D.F. 1984. The Physiography of Southern Ontario, third edition Ministry of Energy, Northern Development and Mines, Special Volume 02

Clark, J.K., Carter, T.R., Brunton, F.R., Logan, C.E., Somers, M., Sutherland, L., and Yeung, K.H. 2020. Improving the 3-D geological data infrastructure of southern Ontario: Data capture, compilation, enhancement and QA/QC. In Russell, H.A.J. and Kjarsgaard, B.A. Eds. Southern Ontario groundwater project 2014–2019: summary report. Geological Survey of Canada, Open File 8536, 23-36. https://doi.org/10.4095/321081

Crow, H., Brewer, K., Cartwright, T., Dietiker, B., Pugin, A. J. –M., Russell, H. A. J. 2018. The Bells Corner borehole geophysical calibration facility of the Geological Survey of Canada, Regional-scale groundwater geoscience in southern Ontario: an Ontario Geological Survey, Geological Survey of Canada, and Conservation Ontario geoscientists open house; by Russell, H A J; Ford, D; Priebe, E H; Holysh, S; Geological Survey of Canada, Open File 8363, 2018 p. 11, https://doi.org/10.4095/306493 (Open Access)

Dietiker, B., Pugin, A.J.-M., Burt, A., Crow, H., Cartwright, T., and Brewer, K. 2019. High-resolution Shallow Seismic Reflection Profiles for Groundwater Studies in the Niagara Peninsula region, Ontario. Geological Survey of Canada, Open File 8561, 49p. https://doi.org/10.4095/314730

Eyles, N., Clark, B.M., Kaye, B.G., Howard, K.W.F., and Eyles, C. 1985. The application of basin analysis techniques to glaciated terrains: an example from the Lake Ontario basin, Canada. Geoscience Canada 12: 22-32.

Frind, E.O., Russell, H.A.J., Rudolph, D.L., and Sharpe, D.R. 2014. The Waterloo Moraine: Water, science and policy, Canadian Water Resources Journal, 39:2, 85-87. https://doi.org/10.1080/07011784.2014. 1914793

Frey, S.K., Khader, O., Taylor, A., Erler, A.R., Lapen, D.R., Sudicky, E.A., Berg, S.J., and Russell, H.A.J. 2019. A fully integrated groundwater-surface-water model for southern Ontario: proof-of-concept and data release Geological Survey of Canada, Open File 8639, 23 p. https://doi.org/10.4095/321042

Frey, S.K., Khader, O., Taylor, A., Erler, A.R., Lapen, D.R., Sudicky, E.A., Berg, S.J., and Russell, H.A.J. 2020. A fully integrated groundwater–surface-water model for southern Ontario. In Russell, H.A.J. and Kjarsgaard, B.A. Eds. Southern Ontario groundwater project 2014–2019: summary report. Geological Survey of Canada, Open File 8536, 231-245. https://doi.org/10.4095/321108

Gao, C., Shirota, J., Kelly, R.I., Brunton, F.R., and Van Haaften, S. 2006. Bedrock Topography and Overburden Thickness Mapping, Southern Ontario. Ontario Geological Survey Miscellaneous Release—Data 207.

Gao C. 2011. Buried bedrock valleys and glacial and subglacial meltwater erosion in southern Ontario, Canada. Canadian Journal of Earth Sciences 48: 801-818. https://doi.org/10.1139/e10-104

Gerber, R.E., Boyce, J.I., and Howard, K.W. 2001. Evaluation of heterogeneity and field-scale groundwater flow regime in a leaky till aquitard. Hydrogeology Journal, 9: 60–78. doi:10.1007/s100400000115

Gerber, R.E., Sharpe, D.R., Russell, H.A.J., Holysh, S., and Khazaei, I. 2018. Conceptual hydrogeological model of the Yonge Street aquifer, south-central Ontario: A glaciofluvial channel–fan setting. Canadian Journal of Earth Sciences, 55: 730-767. https://doi.org/10.1139/cjes-2017-0172

Griffiths, M., Russell, H.A.J., and Logan, C.E. 2020. Machine learning applied to geoscience: Geo-referenced character recognition. In Russell, H.A.J. and Kjarsgaard, B.A. Eds. Southern Ontario groundwater project 2014–2019: summary report. Geological Survey of Canada, Open File 8536, 65-74. https://doi.org/10.4095/321092

Hamilton, S.M. 2015. Ambient groundwater geochemistry data for southern Ontario, 2007–2014; Ontario Geological Survey, Miscellaneous Release—Data 283–Revised.

Karrow, P.F. 1967. Pleistocene Geology of the Scarborough Area; Ontario Ministry Natural Resources. Toronto, Rep. 46 108 p.

Karrow, P.F. 1974. Till Stratigraphy in Parts of Southwestern Ontario. Geological Society of America Bulletin 85: 761–768. https://doi.org/10.1130/0016-7606(1974)85<761:TSIPOS>2.0.CO;2

Karrow, P.F. 1977. Quaternary geology of the St. Marys area, southern Ontario; Ontario Division of Mines, Geological Report 1 48, 59p.

Karrow, P.F. 1989. Last interglacial sediments of the Don Valley Brickyard, Toronto, Canada, and their paleoenvironmental significance: Discussion; Canadian Journal of Earth Sciences, 26: 1078–1082. https://doi.org/10.1139/e89-091

Kenny, F. M., Hunter, G. and Chan, P. 1997. Georeferencing quality control of Ontario's water well data base for the greater Toronto and Oak Ridges Moraine areas of southern Ontario, Proceedings of the 1997 Canadian Geomatics Conference, GER '97; 1997, https://doi.org/10.4095/216738 (Open Access)

Knight, R.D., Landon-Browne, A.R.R., and Russell, H.A.J. 2016. Portable XRF spectrometry of glacial-derived sediment from the Purple Woods borehole, southern Ontario. In Geological Survey of Canada, Open File. Natural Resources Canada. doi:10.4095/297890

Logan, C., Russell, H.A.J. and Sharpe, D.R. 2005. Regional 3-D structural model of the Oak Ridges Moraine and Greater Toronto area, southern Ontario: version 2.1, Geological Survey of Canada, Open File 5062, 2005, 27 pages; 1 CD-ROM, https://doi.org/10.4095/221490 (Open Access)

Logan, C., Russell, H.A.J., Sharpe, D.R., and Kenny, F.M. 2006. The Role of GIS and Expert Knowledge in 3-D Modelling, Oak Ridges Moraine, Southern Ontario. In: Harris, J. (Ed.), GIS for the Earth Sciences. Geological Association of Canada, Special Paper 44, 519-541. https://doi.org/10.4095/214575

Maclachlan, J.C. and Eyles, C.H. 2011. Subglacial deforming bed conditions recorded by late Quaternary sediments exposed in Vineland Quarry, Ontario, Canada. Sedimentary Geology, 238: 277–287. https://doi.org/10.1016/j.sedgeo.2011.04.016

Martini, I.P., Brookfield, M.E. 1995. Sequence Analysis of Upper Pleistocene (Wisconsinan) Glaciolacustrine Deposits of the North-shore Bluffs of Lake Ontario, Canada. Journal of Sedimentary Research, 65: 3B, 388–400. https://doi.org/10.1306/D426825C-2B26-11D7-8648000102C1865D

Morris T.F. and Kelly R.I. 1997. Origin and physical and chemical characteristics of glacial overburden in Essex and Kent counties, southwestern Ontario. Canadian Journal of Earth Science, 34: 2 33–246. doi: 10.1139/e17-022

Mulligan, R.P.M. 2018. Last Phase of Subsurface Data Collection for Three-Dimensional Mapping in the Central Part of the County of Simcoe, Southern Ontario; in Summary of Field Work and Other Activities, 2018, Ontario Geological Survey, Open File Report 6350, p.25-1 to 25-10.

Mulligan, R.P.M. and Bajc, A.F. 2018. The pre-Late Wisconsin stratigraphy of southern Simcoe County, Ontario: Implications for ice sheet buildup, decay, and Great Lakes drainage evolution. Canadian Journal of Earth Sciences, 55: 709-729. https://doi.org/10.1139/cjes-2016-0160

Mulligan, R.P.M., Eyles, C.H., and Bajc, A.F. 2018a. Stratigraphic analysis of Late Wisconsin and Holocene glaciolacustrine deposits exposed along the Nottawasaga River, southern Ontario, Canada. Canadian Journal of Earth Sciences, 55: 863-885. https://doi.org/10.1139/cjes-2017-0081

Mulligan, R.P.M., Bajc, A.F., and Eyles, C.H. 2018b. Drumlinized tunnel valleys in south-central Ontario. Quaternary Science Reviews, 197: 49–74. https://doi.org/10.1016/j.quascirev.2018.07.026

Mulligan, R.P., Eyles, C.H., & Marich, A.S. 2019. Subglacial and ice-marginal landforms in south-central Ontario: implications for ice-sheet reconfiguration during deglaciation. Boreas, 48(3), 635-657.

McNamara, G.D. and Todd, B.J. 2018. Processing of interpreted seismic-reflection data from expedition 69-2-01 of the CSS Limnos, Lake Huron, Ontario, Canada and Michigan, U.S.A.; Geological Survey of Canada, Open File 8429, 1 .zip file. https://doi.org/10.4095/308377

NASA JPL. NASA Shuttle Radar Topography Mission Global 30 arc second. 2013, distributed by NASA EOSDIS Land Processes DAAC, https://doi.org/10.5067/MEaSUREs/SRTM/SRTMGL30.002.

National Geophysical Data Center, 1999a. Bathymetry of Lake Erie and Lake Saint Clair. National Geophysical Data Center, NOAA. doi:10.7289/V5KS6PHK

National Geophysical Data Center, 1999b. Bathymetry of Lake Huron. National Geophysical Data Center, NOAA. doi:10.7289/V5G15XS5 [accessed October 10, 2015]

National Geophysical Data Center, 1999c. Bathymetry of Lake Ontario. National Geophysical Data Center, NOAA. doi:10.7289/V56H4FBH [accessed October 10, 2015]

O'Connor, D.R. 2002a. Report of the Walkerton Inquiry, part one. The events of May 2000 and related issues; Ministry of the Attorney General, Toronto, Ontario, 539p. + appendixes.

O'Connor, D.R. 2002b. Report of the Walkerton Inquiry, part two. A strategy for safe drinking water; Ministry of the Attorney General, Toronto, Ontario, 588p.

Ontario Geological Survey, 2010. Surficial geology of southern Ontario. Ontario Geological Survey, Miscellaneous Release—Data 128 – Revised. Ontario Government 2006. Clean Water Act (S.O. 2006, Chapter 22)

Ontario Geological Survey. 2014. Ontario geophysical surveys, ground gravity data, grid and point data (ASCII and Geosoft® formats) and vector data, Niagara area; Ontario Geological Survey, Geophysical Data Set 1073

Pugin A.J.-M., Pullan S.E., and Sharpe D.R. 1999. Seismic facies and regional architecture of the Oak Ridges Moraine area, southern Ontario. Canadian Journal of Earth Sciences 36: 409-432. https://doi.org/10.1139/e98-104

Pugin A.J.-M., Pullan S.E., and Sharpe D.R. 2011. Seismic reflection data and hydro-stratigraphic implications for Ballantrae-Aurora area buried valley aquifers. Geological Survey of Canada, Open File 6685, 21p. https://doi.org/10.4095/288542

Pugin, A.J.-M. 2016. Geophysical data acquisition for hydro-stratigraphic mapping in Southern Ontario [Abstract]. In Russell, H.A.J. and Priebe, E.H. Compilers. Regional-scale groundwater geoscience in southern Ontario: an Ontario Geological Survey and Geological Survey of Canada groundwater geoscience open house; Geological Survey of Canada, Open File 8022, p.14. https://doi.org/10.4095/297737

Pugin, A.J.-M., Crow, H., Dietiker, B., Rainsford, D., Mulligan, R.P.M. and Burt, A., Russell, H.A.J. 2017. Near surface hydro-geophysics in southern Ontario, Regional-scale groundwater geoscience in southern Ontario: an Ontario Geological Survey, Geological Survey of Canada, and Conservation Ontario open house; by Russell, H A J; Ford, D; Priebe, E H; Geological Survey of Canada, Open File 8212, 2017 p. 30, https://doi.org/10.4095/299797 (Open Access)

Pugin, A.J.-M., Dietiker, B., Mulligan, R.P.M., Crow, H.L., Brewer, K., Cartwright, T., Rainsford, D.R.B., Bajc, A.F., Sharpe, D.R., and Russell, H.A.J. 2018. High-resolution seismic reflection profiles for groundwater studies in Simcoe County, southern Ontario. Geological Survey of Canada, Open File 8383, 23p. https://doi.org/10.4095/308388

Pullan, S.E., Hunter, J.A., Good, R.L. 2002. Using downhole geophysical logs to provide detailed lithology and stratigraphic assignment, Oak Ridges Moraine, southern Ontario, Geological Survey of Canada, Current Research (Online) no. 2002-E8, 2002, 12 pages, https://doi.org/10.4095/213689 (Open Access)

Pullan, S.E., Hunter, J.A., Pugin, A., Burns, R.A., Hinton, M.J. 2000. Downhole seismic logging techniques in a regional hydrogeology study, Oak Ridges Moraine, Southern Ontario, Proceedings of the symposium of the application of geophysics to engineering and environmental problems; by Powers, M H (ed.); Ibrahim, A -B (ed.); Cramer, L (ed.) ; Environmental and Engineering Geophysical Society; 2000 p. 643-652, https://doi.org/10.4095/216698 (Open Access)

Russell, H.A.J., Brennand, T.A., Logan, C., and Sharpe, D.R. 1998. Standardization and assessment of geological descriptions from water well records: Greater Toronto and Oak Ridges Moraine areas, southern Ontario. In Current Research 1998-E: Geological Survey of Canada, 89-102. https://doi.org/10.4095/209956

Russell, H.A.J., Arnott, R.W.C., and Sharpe, D.R. 2003a. Evidence for rapid sedimentation in a tunnel channel, Oak Ridges Moraine, southern Ontario, Canada. Sedimentary Geology, 160: 33-55. https://doi.org/10.1016/S0037-0738(02)00335-4

Russell, H.A.J., Sharpe, D.R., Brennand, T.A., Barnett, P.J., and Logan, C. 2003b. Tunnel channels of the Greater Toronto and Oak Ridges Moraine areas, southern Ontario. Geological Survey of Canada, Open File 4485. https://doi.org/10.4095/214777

Russell, H.A.J., Arnott, R.W.C., and Sharpe, D.R. 2004. Stratigraphic architecture and sediment facies of the western Oak Ridges Moraine, Humber River watershed, southern Ontario. Geographique physique Quaternaire. 58: 241–267. https://doi.org/10.7202/013141ar

Russell, H.A.J., Bajc, A.F., Burt, A., Logan, C., Mulligan, R., and Sharpe, D.R. 2016. A three dimensional surficial stratigraphic model for southern Ontario. In Russell, H.A.J., and Priebe, E.H. Compilers. Regional-scale groundwater geoscience in southern Ontario: an Ontario Geological Survey and Geological Survey of Canada groundwater geoscience open house; Geological Survey of Canada, Open File 8022, p. 16. https://doi.org/10.4095/297739

Sharpe, D.R.; Barnett, P.J. 1985, Significance of sedimentological studies on the Wisconsinan stratigraphy of southern Ontario (Canada), Géographie physique et Quaternaire vol. 39, no. 3, 1985 p. 255-273, https://doi.org/10.7202/032607ar (Open Access)

Sharpe, D.R. and Russell, H.A.J. 2016. A revised depositional setting for Halton sediments in the Oak Ridges Moraine area, Ontario. Canadian Journal of Earth Sciences, 53: 281–303. https://doi.org/10.1139/cjes-2015-0150

Sharpe, D.R., Hinton, M.J., Russell, H.A.J., and Desbarats, A.J. 2002. The need for basin analysis in regional hydrogeological studies: Oak Ridges Moraine, Southern Ontario. Geoscience Canada, 29: 3–20.

Sharpe D.R., Dyke L.D., Good R.L., Gorrell, G., Hinton, M.J., Hunter, J.A., and Russell, H.A.J. 2003. GSC high-quality borehole, "Golden Spike", data - Oak Ridges Moraine, southern Ontario. Geological Survey of Canada, Open File 1670. https://doi.org/10.4095/214289

Sharpe, D.R., Pugin, A., Pullan, S.E., and Gorrell, G. 2003. Application of seismic stratigraphy and sedimentology to regional hydrogeological investigations: an example from Oak Ridges Moraine, southern Ontario, Canada. Canadian Geotechnical Journal, 40: 4, 711-730. https://doi.org/10.1139/T03-020

Sharpe, D.R., Pugin, A., Pullan, S.E., and Shaw, J. 2004. Regional unconformities and the sedimentary architecture of the Oak Ridges Moraine Area, southern Ontario. Canadian Journal of Earth Sciences, 41: 183–198. https://doi.org/10.1139/e04-001

Sharpe, D.R., Russell, H.A.J, and Logan, C. 2005. Stratigraphic architecture of a regional till sheet/aquitard: Newmarket Till, Oak Ridges Moraine area, southern Ontario, Canada, International Conference on Glacial Sedimentary Processes and Products: abstracts; 2005 p. 127

Sharpe, D.R., Russell, H.A.J, and Logan, C. 2007. A three-dimensional geological model of the Oak Ridges Moraine area, Ontario, Canada. Journal of Maps, 3: 239-253. https://doi.org/10.1080/jom.2007. 19710842

Sharpe, D.R., Pugin, A.J.-M., and Russell, H.A.J. 2018. Geological framework of the Laurentian trough aquifer system, southern Ontario. Canadian Journal of Earth Sciences, 55: 677-708. https://doi.org/10.1139/cjes-2017-0113

Todd, B.J., Hunter, J.A.M., Good, R.L., Burns, R.A., Douma, M., Pullan, S.E. and S.E. Lewis, C.F.M. 2003. Seismostratigraphy of Quaternary sediments beneath Lake Simcoe, Ontario: results of 1992 and 1993 expeditions of the MV J. Ross Mackay. Geological Survey of Canada, Open File 3037. 1 CD-ROM, https://doi.org/10.4095/214292

Todd, B.J., Lewis, C.F.M., Russell, H.A.J., and Pyne, M.D. 2020. Legacy seismic reflection data from the Great Lakes: Recovery and applications. In Russell, H.A.J. and Kjarsgaard, B.A. Eds. Southern Ontario groundwater project 2014–2019: summary report. Geological Survey of Canada, Open File 8536, 75-82. https://doi.org/ 10.4095/321093

Machine learning applied to geoscience: Geo-referenced character recognition

Matt Griffiths[1,2]*, Hazen A.J. Russell[2], and Charles Logan[2]

Abstract: Significant quantities of non-digital geoscience data exists on maps. In many cases this information has been scanned and is available in a raster format, but remains irretrievable for digital operations. This information may be in both a text and symbol format and it is also necessary to capture the georeferenced location. In many cases this data may also consist of handwritten characters, which have much greater variability than typed characters. An example of such a dataset is handwritten depth soundings that are a common aspect of Canadian Hydrographic Service (CHS) field sheets. CHS maintains a collection of scanned and geo-referenced digital image files with handwritten depth soundings recorded directly on lake maps. To make use of this data for digital 3-D modelling, it needed to be converted to geo-referenced vector data. To avoid the time-consuming process of entering thousands of data points, a machine-learning algorithm was applied to automate the digitization process using open-source software. Robust machine-learning libraries available in Python were integrated within a custom work environment for this application. This is an example of how analogue geoscience datasets can be captured in a cost effective, timely and reliable manner.

1. Introduction

Geoscience activities often require the digital capture of archival data that is available only in analogue or hardcopy format. Prior to the common use of computers, remote data collection devices and Global Positioning Systems (GPS), field survey information was recorded in notebooks and/or directly on maps or aerial photographs. Points, symbols, lines, and areas drawn on maps were often coupled with handwritten text (e.g., geophysical measurement, station ID, strike, dip, photo ID). To utilize this information in GIS applications, the data has to be converted into a vector format. Although scanning and geo-referencing hardcopy data is a straight-forward process in converting to a digital raster format, traditonal vector digitization and data entry steps are time consuming. To identify and capture text from scans of typed text, Optical Character Recognition (OCR) is now commonly employed in e.g. Adobe Acrobat™ and other programs, and typically integrated with scanning hardware. The accurate recognition of handwritten text is more difficult, however, due to irregularities in the characters and handwriting variability from one person to another. Machine learning based on training datasets of the specific handwriting is needed to identify written characters at an acceptable level that approaches human recognition ability. Converting cartographic features (e.g. text, symbols) to vector formats requires capture of additional attritube information, such as geographic coordinates, orientation, etc., and must make use of the maps Cartesian grid and geo-referencing of the scanned raster image.

For the construction of three-dimensional geological models of southern Ontario, it is necessary to have as continuous a topographic surface as possible to improve constraints on the interpolation of subsurface layers and minimize voids in the model. This includes the bathymetry of lakes within the region. Digital bathymetry is available for the Great Lakes (Schwab and Sellers 1996), however, only scanned, handwritten charts could be obtained for other large lakes in Ontario (Figure 1). At present, Digital Elevation Models (DEM) of the land surface rarely includes bathymetric information on lakes. This commonly reflects the origin of DEM production and applications from topographic map data via aerial photographic sources. The Geological Survey of Canada (GSC) 3-D modelling initiative for southern Ontario (Logan et al. 2020; Carter et al. 2020) utilizes National Oceanic and Atmospheric Administration (NOAA) and CHS bathymetric maps for the Great Lakes in combination with a 90 meter Shuttle Radar Topography Mission (SRTM) topographic DEM.

[1] Department of Earth Sciences, Carleton University, 1125 Colonel By Drive, Ottawa, ON K1S 5B6
[2] Geology Survey of Canada, Natural Resources Canada, 601 Booth Street, Ottawa, ON K1A 0E8

*corresponding author: matt.griffiths@earthphysics.ca

Recommended citation: Griffiths, M., Russell, H.A.J., and Logan, C.E. 2020. Machine learning applied to geoscience: Geo-referenced character recognition. In Russell, H.A.J. and Kjarsgaard, B.A. Eds. Southern Ontario groundwater project 2014–2019: summary report. Geological Survey of Canada, Open File 8536, 65-74. https://doi.org/10.4095/321092

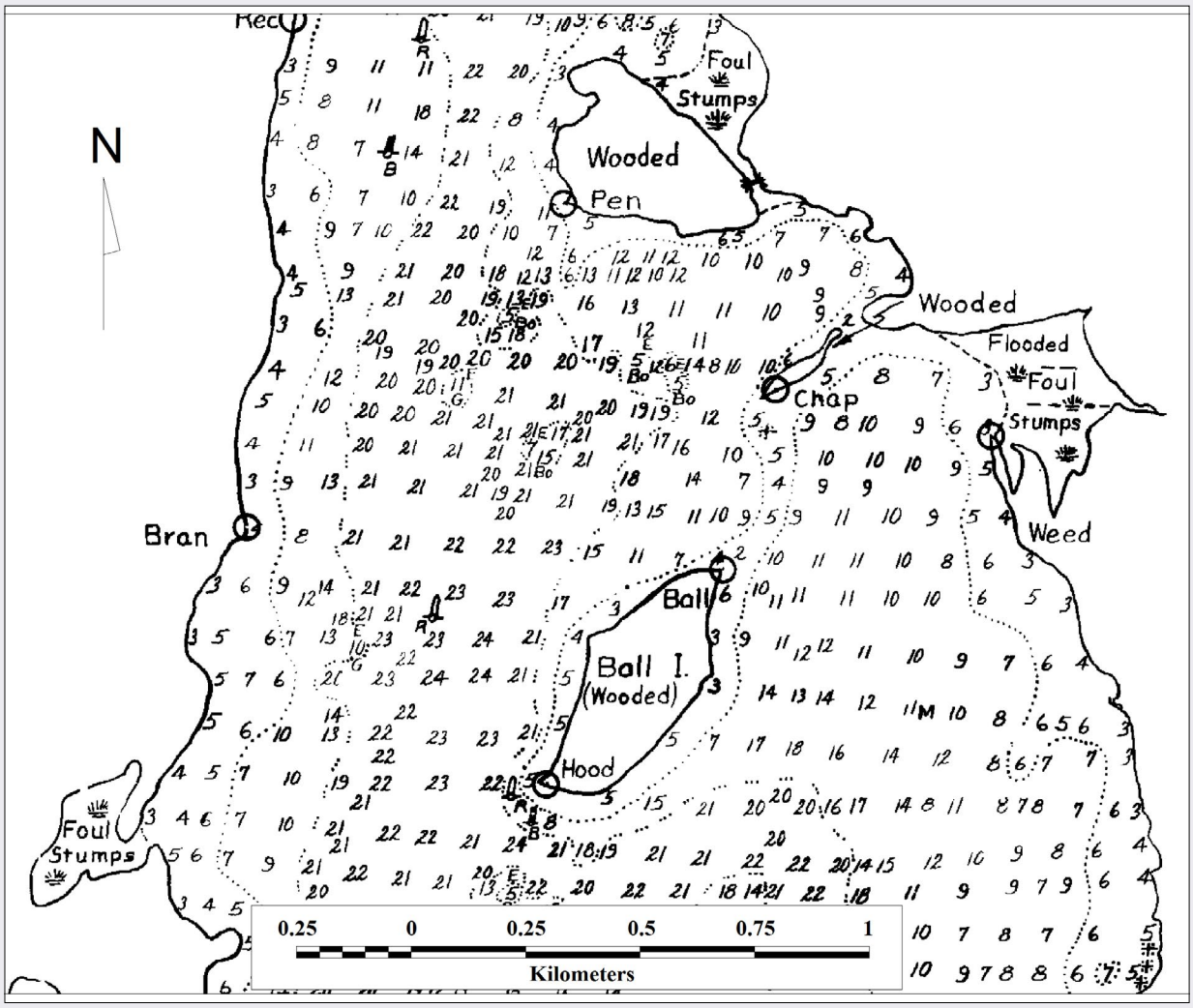


Figure 1. Example of a CHS scanned bathymetric chart with hand-written depth soundings.

Within southern Ontario, the Canadian Hydrographic Survey (CHS) has collected bathymetry measurements for the lakes in the Trent Severn waterway, a system of navigable lakes, rivers, and canals constructed in the 1800's. Much of the most recent data was collected in the 1960's based on depth soundings recorded manually (handwritten) on spatially referenced field sheets. The sheets have been scanned and stored as spatially referenced images and subsequently archived by CHS. The GSC utilizes the CHS data to further develop a topographic DEM with lake bottom coverage to support the 3-D modelling initiative. To increase the efficiency and reliability of digitizing bathymetric points, an automated approach based on machine-learning was initiated. A Python™ based application was developed to build point datasets from scanned fieldsheets with depth and geographic location attributes. OCR of handwritten digits is accomplished by using training samples of character images to support a machine-learning algorithm.

This paper documents the development and workflow of the approach. Some background is provided as to why off-the-shelf solution could not fully address the problem. The method adopted in this study is then described detailing an overview/flow chart of the developed protocol along with information on the open-source libraries that the protocol depends on. Next, compilation of the training dataset is described detailing the development of algorithms used to accomplish this task. Based on this training dataset several machine-learning algorithms were tested for prediction accuracy, and the two best performing methods were selected. Lastly the program is evaluated by comparing the bathymetric surface derived using the machine-learning approach against the same surface digitized manually.

2. Background

Bathymetry data from the original handwritten field-data charts was scanned and stored as black and white, geo-referenced

TIF images (GeoTIFF; Figure 2). For each sounding, the location and depth had to be interpreted and extracted from the images, then tabulated. Each number (digit) has a basic pattern easily recognized by eye; however, their digitized (i.e. scanned) representation must be reformatted in order for the computer to recognize it. This problem of character-recognition is a classic example of a supervised machine-learning problem.

OCR functionality is commercially available in a range of software. Commerical off-the-self solutions; however, were inadequate for two reasons. Depth sounding values were not typed, but handwritten. Prediction accuracy is typically low for handwritten characters as most software is optimized for typed fonts. Secondly, the spatial location of each character is an important data parameter. In most OCR applications the absolute position of words or characters is not relevant, so long as they are interpreted accurately. However, interpretation of spatial geo-referencing of handwritten characters is not a commonly implemented function within either commercial GIS software (e.g., ArcInfo™) or open source packages (Q-GIS, SAGA, etc.).

The problem of character classification is simplified for this application because only 10 classes are relevant, corresponding to numerical characters 0–9, additionally there was no need to consider decimal or angular measurements. The consistency of the handwritten digits also simplifies the classification process, allowing for less cumbersome pre-processing as compared to algorithms that classify hand printed numbers (or words) written by different people (e.g., Chiang 1997). With an increasing number of machine-learning resources freely available online, it was possible to create a geo-referenced character recognition program specifically for bathymetric charts using open-source machine learning implementations. After evaluating several methods, two classification algorithms were used; the K-nearest neighbours and the Support Vector Machine (SVM) algorithms.

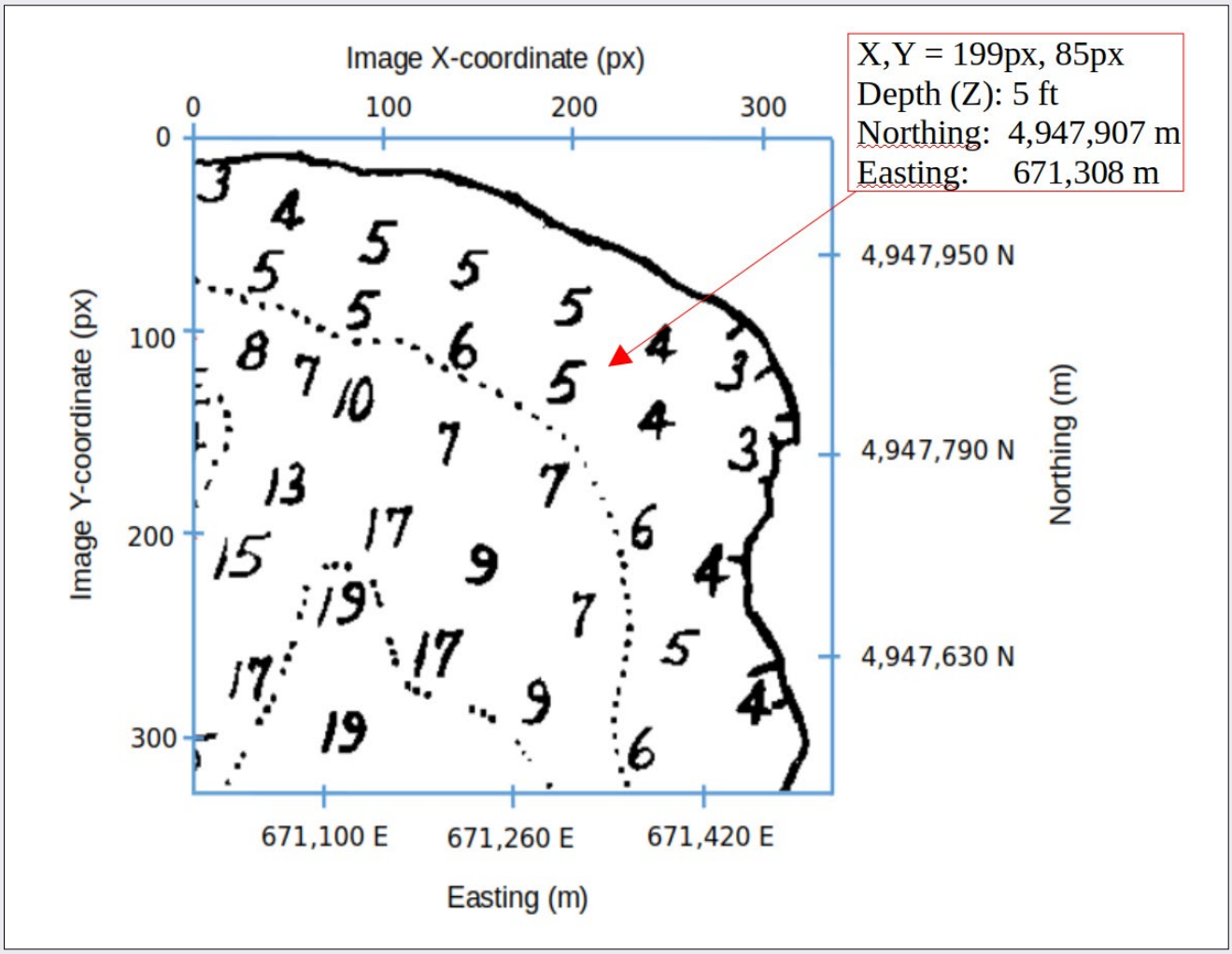


Figure 2. Dataset sample showing original data format and associated image and UTM coordinate systems. The bathymetry measurements are hand-written on the chart. The location and value of each measurement in vector form is necessary to use this data quantitatively.

3. Methods

This project was implemented in Python™ as there are many relevant open-source libraries, a large user base, and strong peer-support via online forums. Instrumental to this project was Scikit-Learn, an open-source machine-learning library. The goal of this package is "to bridge the gap between machine-learning research and application" (Varoquaux et al. 2015). Scikit Learn includes a number of classification algorithms, including K-Nearest Neighbours and SVM.

A flowchart of the program is presented in Figure 3. The program is divided into 3 modules:

1. digitize.py – accepts the digital image file, and creates output folders.
2. mapdigitizer.py – hosts the bulk of the program and serves as a function library.
3. gather.py – takes the output from digitize.py, combines the 2-digit depth sounding numbers, and then transforms pixel location coordinates to the GIS projection coordinates.

As a first step within the digitize.py module, the images are loaded and converted to a binary matrix. This simplifies the image manipulations. Instead of having 3 values (Red-Blue-

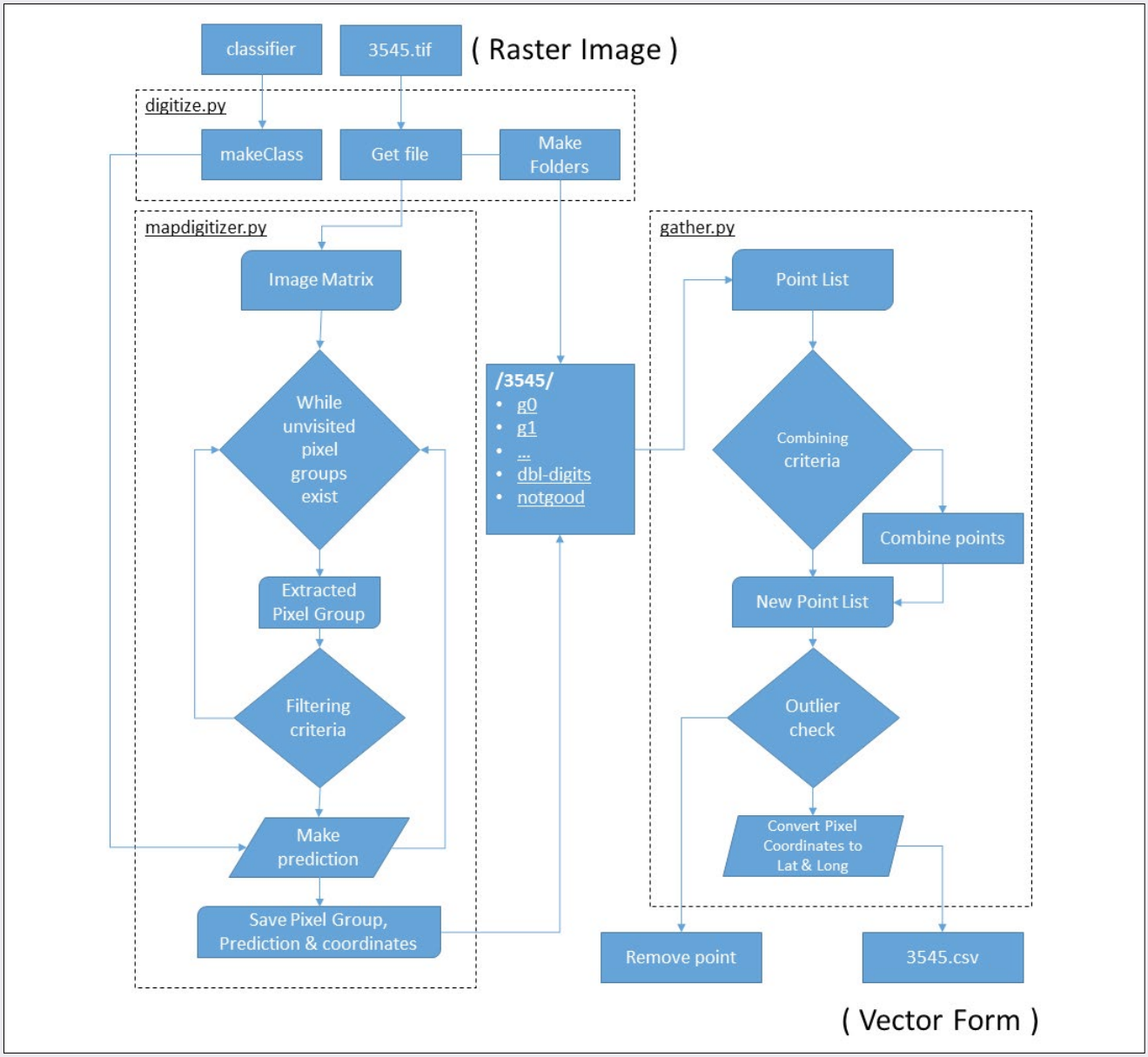


Figure 3. High-level flow chart of digitization program. The program is separated into 3 modules. 1) Digitize.py calls the functions and makes output folders. 2) Mapdigitizer.py hosts the functions. 3) Gather.py gathers the output images, and transforms between the pixel coordinates and projection coordinates.

Green), each pixel is represented by one value; 1 representing black, and 0 representing white. This also reduces the amount of system memory required. Functions are called from the mapdigitizer.py where the matrix manipulation tools (traversal, extraction, filtering, etc.) are stored.

In supervised classification problems a set of known samples are required to build a training dataset. The training dataset consists of known samples (digits in this case of 0–9) that are used as a comparative dataset. The larger the dataset, generally the better performance the classification will have. New samples can be classified based on the population in the training dataset. To start compiling a database of known samples, the first step was to extract the numbers and format them consistently. In this case, the characters written on the charts were no larger than 30x30 pixels. This is a study specific size based on analysis of the size of the hand written depth soundings. With a 30x30 window, the classifiers operates in a 900-dimensional space. A small Python program was written to extract samples. Essentially a 30x30 pixel moving window traverses the image, and extracts the sub-image when it meets the following criteria: i) there are more than 25 black pixels in the window and ii) all the border pixels are white (Figure 4).

With this simple extraction technique a small database was compiled, with about 200 samples for each digit 0–9, which were subsequently classified manually to construct the initial training dataset. Using this limited training set a larger training set was developed using the linear SVM machine-learning classifier in Scikit-Learn. This allowed for rapid sample extraction, prediction, and review for accuracy by the operator, followed by integration into a larger training database. Using this process a final training dataset of ~23,000 classified samples was compiled.

Eight supervised classification algorithms implemented in Scikit Learn were tested to find the optimal classifiers for this application. These eight algorithms are well documented, and the prediction output is uniform making the tests and comparison simple to conduct. The test consisted of training each classifier on 500 known samples of each digit 0–9 (ie., a 5000 sample subset of the training samples) from the 23,000 classified samples, then testing the predictions of the remaining classified samples (~18,000). Results of the tests are summarized in Table 1. K-Nearest Neighbours, and SVM with a linear kernel function yielded the best results, with an overall prediction accuracy of 98.1 and 97.3%, respectively. Using two classifiers together was found to improve the robustness of the classification, which will be described in greater detail in a following section. Other algorithms such as Random Forest, and Linear Discriminant Analysis also had a high-prediction accuracy, but were not used in the final program.

3.1 Revised character extraction

The initial method of extraction performed well for acquiring a small database of numbers; however; the results were not satisfactory for large-scale classifications on cluttered charts because extracted samples were often contaminated with small line segments from contour lines (e.g., the extracted '6' in the middle of Fig 4a). As a result, extracted numbers would be displaced from the bottom right corner of the image. For this implementation the machine learning algorithm is sensitive to this relative position for example, a '9' in the top right corner will have a different signature than a '9' in the bottom left corner. For this reason, an alternative sample extraction algorithm was sought; one that could extract a single cluster of black pixels from the images, independent of their proximity to neighbouring clusters (such as contour lines). The solution was to establish pixel groups by traversing connected components instead of using extraction criteria for the sliding window previously mentioned. When a black pixel is found, all the adjacent black pixels are recursively searched out and extracted. The algorithm for determining

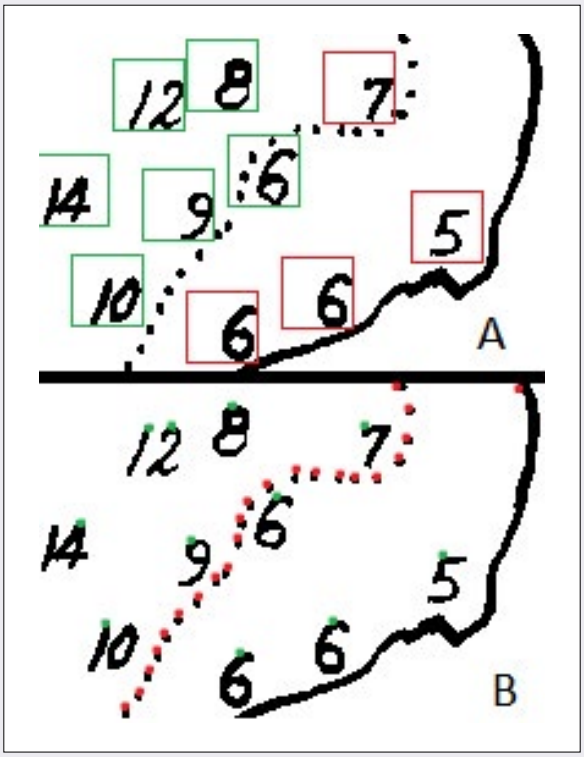


Figure 4. Character Segmentation and Extraction comparison. A: Numbers within the green boxes meet the criteria for extraction, while numbers in red box are too close to borders or contours and are therefore overlooked with the initial algorithm. Some digits can be contaminated by line segments, i.e. the extracted '6' in the center of the panel. B: Pixel groups are marked with a dot that indicates the initial coordinate from which the pixel group is traversed. Green dots indicate that they met the criteria and were extracted, while red dots indicate that they were either too small or too large. The extraction algorithm used for B performs much more effectively.

Table 1. Classifier Evaluation Summary.

Classifier	Prediction Accuracy (%)										
	0	1	2	3	4	5	6	7	8	9	overall
K Nearest Neighbors	99.7	99.9	98.5	97.3	98.8	97.3	96.5	96.7	96.5	97.6	98.1
Support Vector Machine (Linear)	98.3	99.8	97.7	95.8	97.7	96.4	95.2	98.3	94.3	96.2	97.3
Decision Tree (e.g., CART)	93.9	97.1	88.2	85.3	87.5	90.1	88.7	90.1	81.3	89.9	89.9
Random Forest	98.9	99.7	97.5	94.9	96.9	95.7	94.8	97.0	93.3	95.9	96.8
AdaBoost	36.4	83.5	55.5	19.7	8.3	7.5	11.2	45.3	0.9	93.6	40.7
Gaussian Naive Bayes	7.1	98.6	89.9	0.9	13.1	36.3	8.6	16.7	10.8	11.0	39.9
Linear Discriminant Analysis	95.9	97.4	93.0	92.0	93.7	90.2	93.8	89.3	89.7	93.3	93.3
Quadratic Discriminant Analysis	93.2	95.7	72.2	50.2	38.6	58.5	37.3	72.0	43.7	47.7	63.9

the connected components is described in Hopcroft and Tarjan (1973), which uses a depth-first search and an auxiliary Boolean matrix to keep track of which pixels have been visited. In addition to finding the connected components, determining their distribution is also significant. Figure 4 illustrates the difference between the two extraction algorithms, and the advantages of the traversing connected components, rather than the purely row-by-row based search method, particularly for extracting samples near lake edges. With connected pixel groups extracted independently of other groups, they could then be filtered by size. Pixel groups with a pixel count of less than 20 or greater than 400 are filtered out. This filter was applied pre-extraction; other criteria were implemented such as coordinate spacing and classifier comparison. As the algorithm traverses a pixel group, it logs the coordinates of pixels so that the image can be reconstructed without contamination from surrounding groups. This can also be used to screen extractions; for example, if the range in y coordinates of the group is <10 pixels, it is not likely a number in this dataset (Figure 5). If the group meets all the criteria, the extracted group can be input into the classifier and a prediction is made.

K-Nearest Neighbours and the linear SVM both performed well for this classification problem. Comparing predictions from both classifiers provided another filtering criterion, specifically for flagging falsely extracted characters. The charts contain many other characters other than the target numerals 0–9. In some cases these other characters (letters or symbols) meet the extraction criteria, and are subsequently classified as one of the digits, resulting in a false point. By comparing the predictions from K-Nearest Neighbours and the SVM these false extractions/prediction could be filtered out. For numeric characters the two classifiers agree, but for letters or symbols, the predictions were often inconsistent with each other. When the predictions differed, the pixel group was flagged as a potential false bathymetry point value and added to a special folder for manual review.

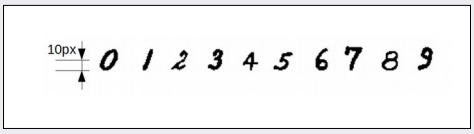


Figure 5. Sample digits 0–9. Minimum 10 pixel vertical spread was used as a threshold for filtering false extractions.

The classifiers were trained on single digits, so in the case that a point has a double-digit value, each digit is classified independently, and combined at a later stage. When the pixel groups of a 2-digit number intersect each other; however, the numbers have to be segmented before they can be classified. Since digits range in size, an '8' typically has more pixels than a '1' for instances, the digits could not be isolated from each other by cutting the image in half down the middle. Instead 15 test slices were made and the results were evaluated using the distance function in Nearest-Neighbour classifier. This process is illustrated for two examples in Figure 6. The combined distance (dissimilarity) between potential characters and their nearest-neighbour in the training dataset is used to rank the effectiveness of the slice. The minimum combined distance value is used to select the optimal slice pattern. The separated characters from the optimal slice are then stored as single digit values.

Predictions extracted as the program traverses the scanned chart are stored with their 30x30 pixel sub-image in a folder where all of the classified numbers can be observed with their associated prediction. The predicted depth value, along with the pixel coordinates are stored in a file with the format 'z value – y value – x value'. In this way the user can check the predictions efficiently in any file explorer program (Windows Explorer, MacOS Finder) that provides thumbnails of the extracted image files. Because the extracted characters are sorted by depth first, incorrect predictions are obvious from the thumbnail. Corrections are easily applied by editing the

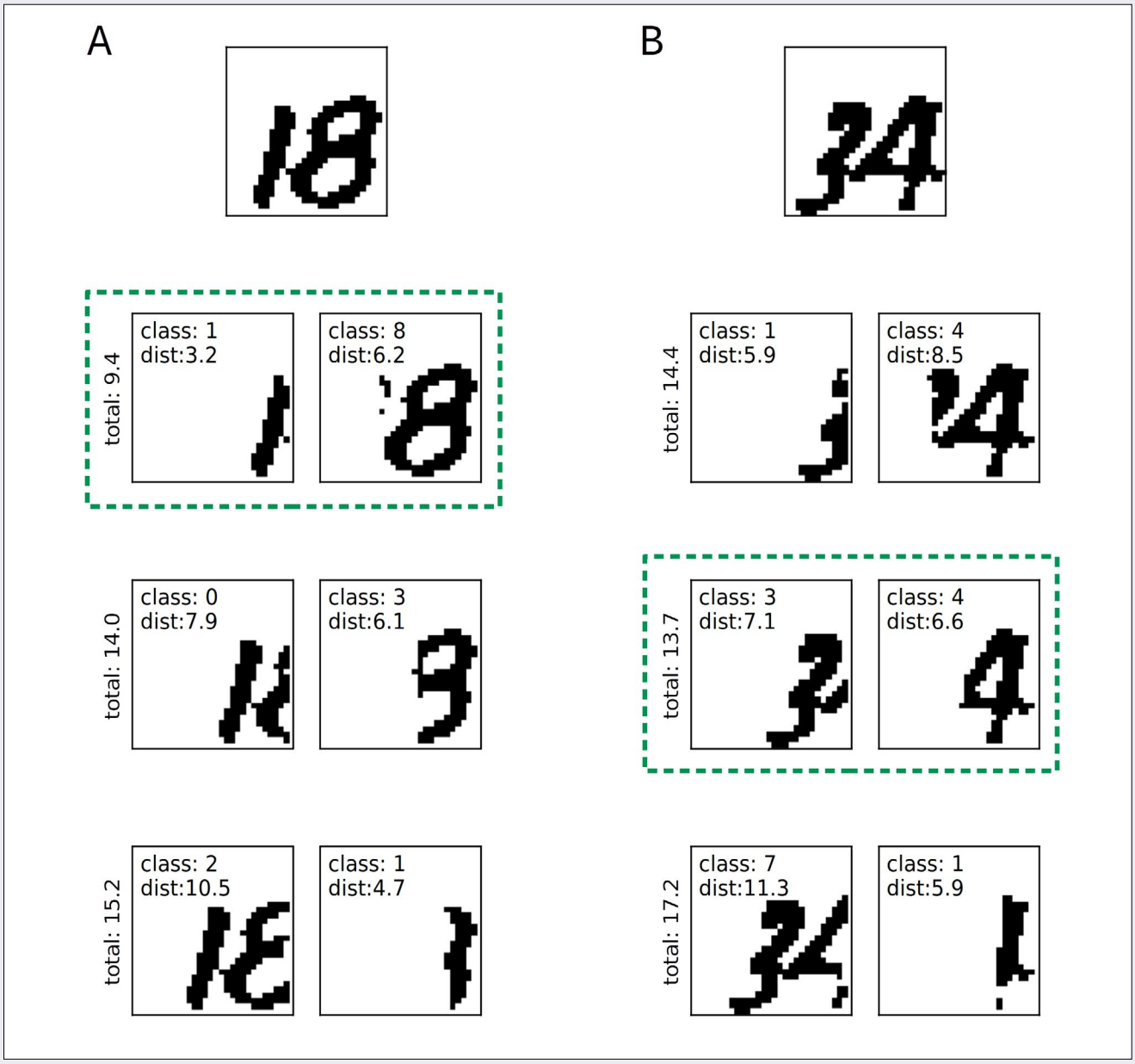


Figure 6. Segmentation of intersecting characters. Two digit numbers that intersect each other will be extracted as a whole and must be isolated from each other in order to classify them. Several slices are tested and the slice yielding the smallest combined Nearest-Neighbours distance is chosen. A: intersecting digits of 18 ft depth point. In this case the optimal slice is not exactly in the middle of the pixel group, but off center. B: The optimal slice for the 34 ft depth point is through the middle of the pixel group.

z value in the filename of the sub-image. This is an advisable quality control step.

The last module, gather.py, tabulates the extracted and classified digits from the output folders. During this process, two-digit numbers are combined to get the correct values. (multiply the left digit by 10 and add the right digit). To handle two-digit numbers, the program reads all the file names of the storage folders, then sorts the extracted numbers by their x and y coordinates. It then iterates through each point to check if another digit is within 20 pixels in the x-direction and within a y-coordinate tolerance of +/- 5 pixels. When two points are combined, the average x and y value is saved with the combined z value.

The program then iterates through the list of points and determines the mean of the 5 nearest points. If the difference between the z value and this average is greater than 9, the

point is discarded. This step suppresses instances where 2-digit numbers are left uncombined because they are too far apart. Consider the case when a number between 10–20 is left uncombined. A '12' left uncombined leaves 1ft and 2ft points that are 10–11ft less than the actual value. Figure 7 illustrates one of these instances. The digits are left uncombined because at a spacing of 22 pixels, they fail the combination criterion of being within 20 pixels (in the x-direction) of each other. Instances like these cause spikes in the bathymetric surface when left unattended. By discarding the points, the interpolated surface is much closer to the actual value. A drawback to this approach is that real anomalies in the bathymetric surface may be filtered out. This situation is rare; however, based on the fact that it was not observed during the manual digitization process. In this study most of the lakes are relatively shallow with few abrupt lake bottom escarpments. Therefore in this study using this filtering criterion yields a more reliable bathymetric surface than without it.

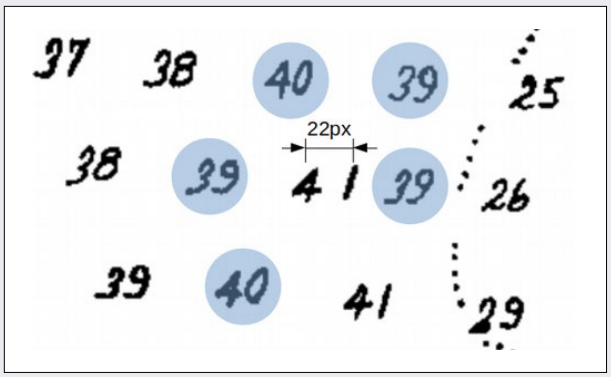


Figure 7. Two digits left uncombined resulting in falsely shallow points. Comparison with the average of 5 nearest points serves a quality check for this case.

The program then transforms the x and y image coordinates to the projection of the spatially referenced image file using the Python library osGeo. The points are saved in a CSV file that can be imported into GIS software in a format suitable for quantitative analysis.

4. Results

To validate the methodology, complementary datasets were captured from a single scanned chart, Balsam Lake (Figure 8). For this lake, data captured using the machine-learning approach outlined above was compared to manually captured data. The number of extracted points was similar;

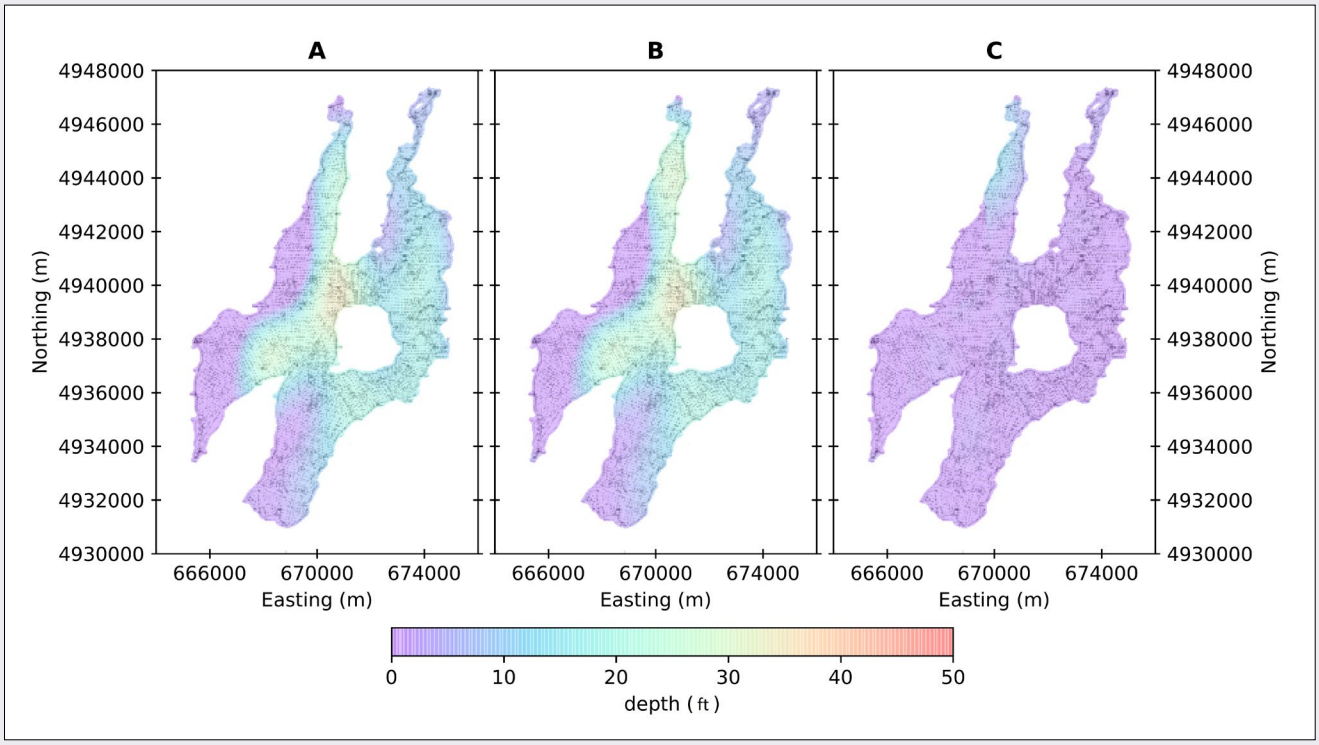


Figure 8. Balsam Lake manual vs automated interpolated bathymetric surface comparison. A) Manually digitized bathymetric surface. B) Automatically digitized bathymetric surface. C) Absolute difference between automatically and manually digitized surfaces. Bathymetric surfaces were interpolated on to a uniform grid using the Kriging method.

5,769 and 5,295 points for the manual and automatic methods respectively, leaving a minimum of 474 points (~8%) uncaptured by the automatic method. The spatial uncertainty in the position from each method (due to size of the handwriting, where the user clicked in the manual digitization, and the extraction in the automatic method) makes direct comparison of the points non-trivial. Considering the 5,295 points captured automatically, we look at the nearest complementary point from the manually captured dataset within a given cutoff radius. Figure 9 plots the percentage of points that have a complement in the manually captured data within the specified radius (measured in m), along with the percentage agreement between such points. As the cutoff radius increases, more points in the automatically captured dataset have complements in manually captured set. With a cutoff radius of 30 m, which roughly corresponds to the size of the handwriting on the charts, the overall accuracy plateaus. By expanding the cutoff radius, no additional points are consistent with each other between the datasets, so the overall accuracy is unchanged. It is thus unlikely that beyond this range points in the manually and automatically captured sets are true complements. Using 30 m as the distance cutoff, 88.7% of points had complementary points in the manually captured dataset, of which the agreement rate was 97.3%. This implies the manual method did not perfectly capture the chart. Another consistency metric is plotted using the percentage of points where the nearest complementary point is within a 2 foot depth tolerance. This second accuracy measure is to accommodate cases where the exact point isn't captured in both datasets, and the bathymetric surface is not perfectly flat, so the nearest complementary point is within a couple feet. Assuming the data entry for the manual digitization was perfect the automated approach has an overall accuracy of 86%. The impact of the difference in accuracy was also tested by interpolating the point values to create bathymetric surfaces (Figure 8). Surfaces were interpolated using the Kriging method (Gaussian process regression in Scikit-learn version 0.17.1). The interpolated surface was overlain on the original raster chart image, and the point data captured manually and automatically. A difference surface between interpolated surfaces using the manually captured and automated captured values was also created. The range in depths captured by each algorithm is consistent. Although the difference map highlights discrepancies of up to 20ft, the average absolute difference between the interpolated surfaces is 1ft, which is acceptable for the necessary accuracy of the project. These larger differences occur in the near shore region of the lake.

5. Discussion

In the comparison for Balsam Lake, the automatically digitized dataset had a lower point density than the manually digitized dataset, a reduction of 8% was present in the number of points captured. Two factors have been identified that may contribute to this: i) digit intersection with other lines, ii) double digits separated by too much space. Where digits intersect boundaries and contour lines they will be filtered out due to the size of the pixel group. This also implies that measurements on the edges of lakes are more likely to be

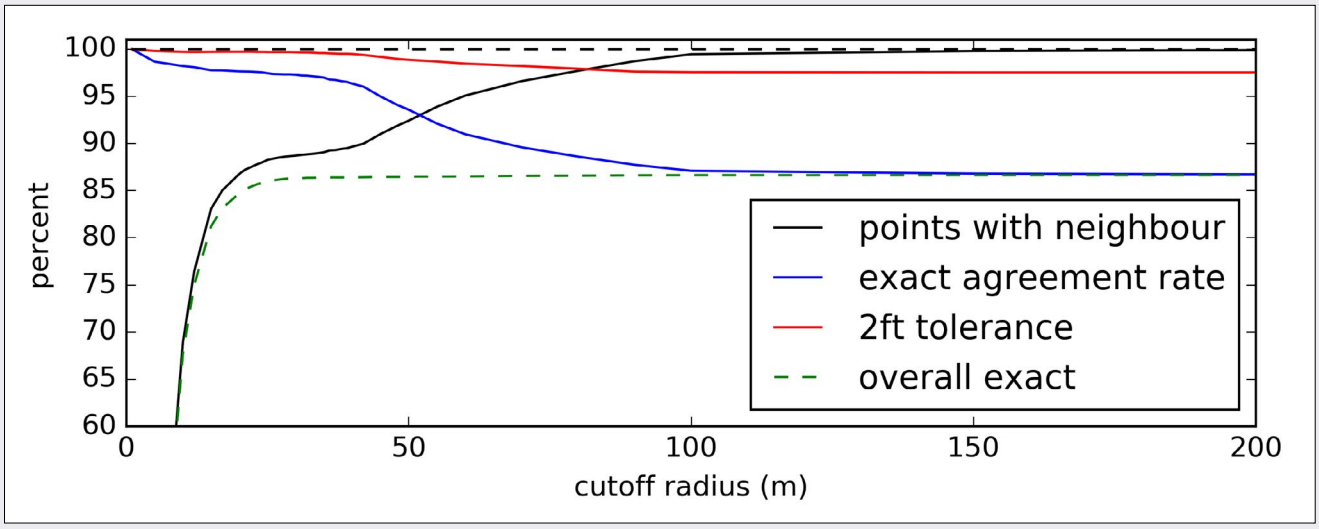


Figure 9. Balsam Lake manual vs automated data capture comparison. The solid black curve shows the percentage of points in the automatically captured dataset that have a complementary point in the manually captured dataset within the cutoff radius. The blue line is the percentage of these complementary points that are in exact agreement. The red line shows the percentage of points that agree within a 2ft depth tolerance. The dashed green line is the overall performance (number of points in exact agreement/number of point captured automatically).

missed than those in the center. The second possibility is that widely spaced double digits are not correctly combined and may be discarded if they are not within the depth range of their nearest neighbours (Figure 7). The discrepancy between the two methods is mainly located at lake boundaries and involved single digits, which suggest the first mechanism plays a larger role in the lower point density. The Balsam Lake example had an agreement rate of 97.3% for points that could be directly compared. This number is dependent on the accuracy of both data capture methods, and serves as a lower limit of accuracy for both manual and automatic methods. In light of the classifier test accuracy (Table 1), it seems likely that the automatic method is the limiting factor in agreement rate between the two methods, though further analysis is needed to verify this. The 97.3% agreement between the methods, demonstrates the automated data capture method developed here is successful in creating a first order vector representation of the bathymetric surface.

There are many potential avenues through which to improve this method of digitization. One way is to add number-specific screening criteria. For example, if the classifier predicts a '8', a secondary criterion might be to check that there are 2 enclosed loops. Number specific criteria could greatly reduce the amount of time the user spends in the quality control step. The algorithm for segmenting double-digit pixel groups into their respective digits could also be improved, and expanded to other multi-digit numbers. Alternatively, a new classifier could be made that includes 2 digit numbers, with an expanded window. This would increase the number of classes from 10 to 100. Compiling an initial training database for such a classifier would require some time, as a large number of samples would be needed to distinguish 100 classes reliably. By extending the classifier in this manner, the training dataset must be updated for every additional digit required.

The current program does not operate for numbers with more than 2 digits. This could be accommodated by including a second iteration through the list of points to combine a third digit. This was not done, because there were few cases with more than 2 digits, and having the second iteration increases the chances of undesired combinations. Other OCR implementations make use of pixel distribution statistics (such as variance from center) as attributes rather than using each pixel as an attribute. This may provide an improved approach to classification, especially for making the training stages more efficient.

6. Conclusions

The program automates the vectorization of handwritten charts, producing a first order vector representation of the lake bathymetry. The user can supplement the automated digitization with manual digitization if greater point density is necessary. The Balsam Lake test example had a classification agreement rate of 97.3% with manually captured points, though the automated method had a notably lower point density than the manually captured data (5,295 vs. 5,769). This yields an estimated 86% overall accuracy for the automated approach. This is a good example of the application of machine learning to geoscience and demonstrates the accessibility of using such methods.

7. Acknowledgements

An internal review at the GSC was completed by M. Hillier. Manual digitization was completed by K. Macdonald. This work was funded through the Groundwater Geoscience Program of the GSC. This work is a contribution to the GSC–OGS southern Ontario project on groundwater 2014–2019.

8. References

Carter, T.R., Brunton, F.R., Clark, J.K., Fortner, L., Logan, C., Russell, H.A.J., Somers, M., Sutherland, L., and Yeung, K. 2020. Three-dimensional geological modelling of the Paleozoic bedrock of southern Ontario: Status update. In Russell, H.A.J. and Kjarsgaard, B.A. Eds. Southern Ontario groundwater project 2014–2019: summary report. Geological Survey of Canada, Open File 8536, 7-21. https://doi.org/10.4095/321080

Chiang, J. H. and Gader, P. D. 1997. Recognition of handprinted numerals in VISA® card application forms. Machine Vision and Applications, 10: 3, 144-149. https://doi.org/10.1007/s001380050067

Hopcroft, J. and Tarjan, R. 1973. Agorithm 447: efficient algorithms for graph manipulation. Communications of the ACM, 16: 6, 372-378. https://doi.org/10.1145/362248.362272

Hunter, J.D. 2007. Matplotlib: A 2D Graphics Environment. Computing in Science & Engineering, 9: 90-95. https://doi.org/10.1109/MCSE.2007.55

Logan, C.E., Russell, H.A.J., Bajc, A.F., Burt, A., Mulligan, R.P.M. and Sharpe, D.R. 2020. A three-dimensional surficial geology model of southern Ontario: Progress report. In Russell, H.A.J. and Kjarsgaard, B.A. Eds. Southern Ontario groundwater project 2014–2019: summary report. Geological Survey of Canada, Open File 8536, 49-64. https://doi.org/10.4095/321084

Schwab. D.J. and Sellers, D.L. 1996. Computerized Bathymetry and Shorelines of the Great Lakes. NOAA Data Report ERL GLERL-16.

Jones, E., Oliphant, T.E., and Peterson, P. 2001. SciPy: Open Source Scientific Tools for Python. http://www.scipy.org/ DOI:10.1109/MCSE.2007.55 [Online; accessed 2018-08-03].

Oliphant, T.E. 2007. Python for Scientific Computing. Computing in Science & Engineering, 9: 10-20. https://doi.org/10.1109/MCSE.2007.58

Oliphant, T.E. 2006. Guide to NumPy. Trelgol Publishing. cy References.

Pedregosa, F., Varoquaux, G., Gramfort, A., Michel, V., Thirion, B., Grisel, O., Blondel, M., Prettenhofer, P., Weiss, R., Dubourg, V., Vanderplas, J., Passos, A., Cournapeau, D., Brucher, M., Perrot, M., and Duchesnay E. 2011. Scikit-learn: Machine Learning in Python. Journal of Machine Learning Research, 12: 2825-2830.

Sharpe D.R., Russell, H.A.J., and Logan, C. 2007. A 3-dimensional geological model of the Oak Ridges Moraine area, Ontario, Canada. Journal of Maps, 3: 1, 239-253. https://doi.org/10.1080/jom.2007.9710842

Varoquaux, G., Buitinck, L., Louppe, G., Grisel, O., Pedregosa, F., and Mueller, A. 2015. Scikit-learn: Machine Learning Without Learning the Machinery. GetMobile, 19: 29-33. https://doi.org/10.1145/2786984.2786995

Legacy seismic reflection data from the Great Lakes: Recovery and applications

Brian J. Todd[1]*, C.F. Michael Lewis[1], Hazen A.J. Russell[2], and Matt D. Pyne[2]

Abstract: Great Lakes legacy geoscience data have been recovered and processed for inclusion in the Geological Survey of Canada's Expedition Database. Interpretation of seismic reflection data from Lakes Ontario and Huron reveals sediment thickness and depth to bedrock; these measurements contribute to the surficial framework geology within the Canada-3D project and southern Ontario 3-D geological modelling. In addition, seismostratigraphic analysis of the legacy data reveals the sediment deposition history and contributes to understanding the evolution of these two Great Lakes.

1. Introduction

The Expedition Database (ED) contains information (metadata) and data related to marine and lacustrine field surveys conducted by, or on behalf of, the Atlantic and Pacific offices of the Geological Survey of Canada (GSC). ED is the source of track line navigation for seismic reflection profiles collected by the GSC (http://ed.gdr.nrcan.gc.ca/index_e.php). Corresponding to the navigation information in ED, scanned seismic reflection profiles are available in the Seismic Data Archive (SDA; http://ftp.maps.canada.ca/pub/nrcan_rncan/raster/marine_geoscience/Seismic_Reflection_Scanned). These two sources are the points of contact for researchers seeking marine and lacustrine seismic geoscience data. It is important for users to recognize that these are evergreen databases, meaning that the databases are updated when new data are acquired, or when previously collected data are discovered, which is the subject of this report.

Great Lakes geoscience data previously not identified in ED or SDA, including seismic reflection profiles and interpretive maps on paper and film, have been recovered, repaired, scanned, and digitally processed. Future work will result in the eventual inclusion of these in ED and SDA. These data are identified as "legacy". The scientific significance and inherited financial value of the legacy data are considerable. In the Great Lakes, the seismostratigraphy revealed by these legacy high-resolution seismic reflection profiles provides insight to sediment thickness, depth to bedrock (or acoustic basement), and sediment stratigraphy. This information aids in the interpretation of the history of sediment deposition and lake evolution and possible pathways for movement of groundwater or contaminants. In particular, digital analysis of the Great Lakes legacy seismic data is a cost-effective method to generate the offshore broad scale 3-D surfaces pertinent to the surficial framework geology layer required by the Canada-3D project (Brodaric et al. 2015).

2. Legacy data

2.1 Lake Ontario

Sixteen geoscience expeditions in Lake Ontario were processed (Table 1, Figure 1). Half a century ago, metadata were not always given the priority that it is assigned today, thus the geophysical survey parameters on Table 1 are incomplete judged by modern standards. However, the data themselves remain valid. The total line kilometres is 18,827, consisting of both boomer and Kelvin Hughes (KH) 26B records. Because the boomer records are of lower frequency (1–10 kHz) than those collected using the KH 26B echo sounder (14.25 kHz), penetration into the lakebed sediments is greater (up to many tens of metres) with the former. The total number of ship days was approximately 160. Using a conservative cost estimate of $20,000 a day for ship time, to collect a similar quantity of data as captured from the legacy seismic data in Lake Ontario would cost $3.2 million.

2.2 Lake Huron

The *Laurentian* 91800 and 95800 expeditions surveyed the northern part of Lake Huron and Georgian Bay, and collected about 3500 km of data (Table 2, Figure 2; Rea 1991, Rea et al. 2018). The seismic surveys were carried out using an IKB

[1] Geological Survey of Canada-Atlantic, Natural Resources Canada, P.O. Box 1006, Dartmouth, NS B2Y 4A2
[2] Geology Survey of Canada, Natural Resources Canada, 601 Booth Street, Ottawa, ON K1A 0E8

*corresponding author: brian.todd@canada.ca

Recommended citation: Todd, B.J., Lewis, C.F.M., Russell, H.A.J., and Pyne, M.D. 2020. Legacy seismic reflection data from the Great Lakes: Recovery and applications. In Russell, H.A.J. and Kjarsgaard, B.A. Eds. Southern Ontario groundwater project 2014–2019: summary report. Geological Survey of Canada, Open File 8536, 75-82. https://doi.org/10.4095/321093

Table 1. Lake Ontario legacy seismic reflection expeditions.

Year	Expedition	Vessel	Line kilometres	Instrument	Energy or source	Source depth (feet)	Hydrophone depth (feet)	Source–hydrophone distance (feet)
1966	–	*Brandal*	952	Boomer	–	–	–	–
1966	–	*Mandarin*	2007	Boomer	–	–	–	–
1967	–	*Explorer*	455	Boomer	–	–	–	–
1967	67-0-06	*Theron*	1015	KH26B	–	–	–	–
1967	67-0-08	*Theron*	417	Boomer	500 W	6	3	100
1967	67-0-14	*Theron*	1093	Boomer	400 J	6	3	150
1967	67-0-18	*Theron*	1417	KH26B	–	–	–	–
1968	68-0-13	*Limnos*	1663	KH26B	–	–	–	–
1968	68-0-17	*Theron*	1101	KH26B	–	–	–	–
1968	68-0-18	*Limnos*	1365	KH26B	–	–	–	–
1969	69-0-13	*Martin Karlsen*	911	KH26B	–	–	–	–
1969	69-0-16	*Martin Karlsen*	2305	KH26B	–	–	–	–
1970	70-0-29	*Limnos*	1344	KH26B	–	–	–	–
1970	70-0-34	*Limnos*	102	KH26B	–	–	–	–
1972	72-00-012	*Limnos*	749	Boomer	–	–	–	–
1972	72-00-012	*Limnos*	749	Airgun	5 and 10 inch^3	–	–	–
1974	74-00-102	*Martin Karlsen*	1931	KH26B	–	–	–	–

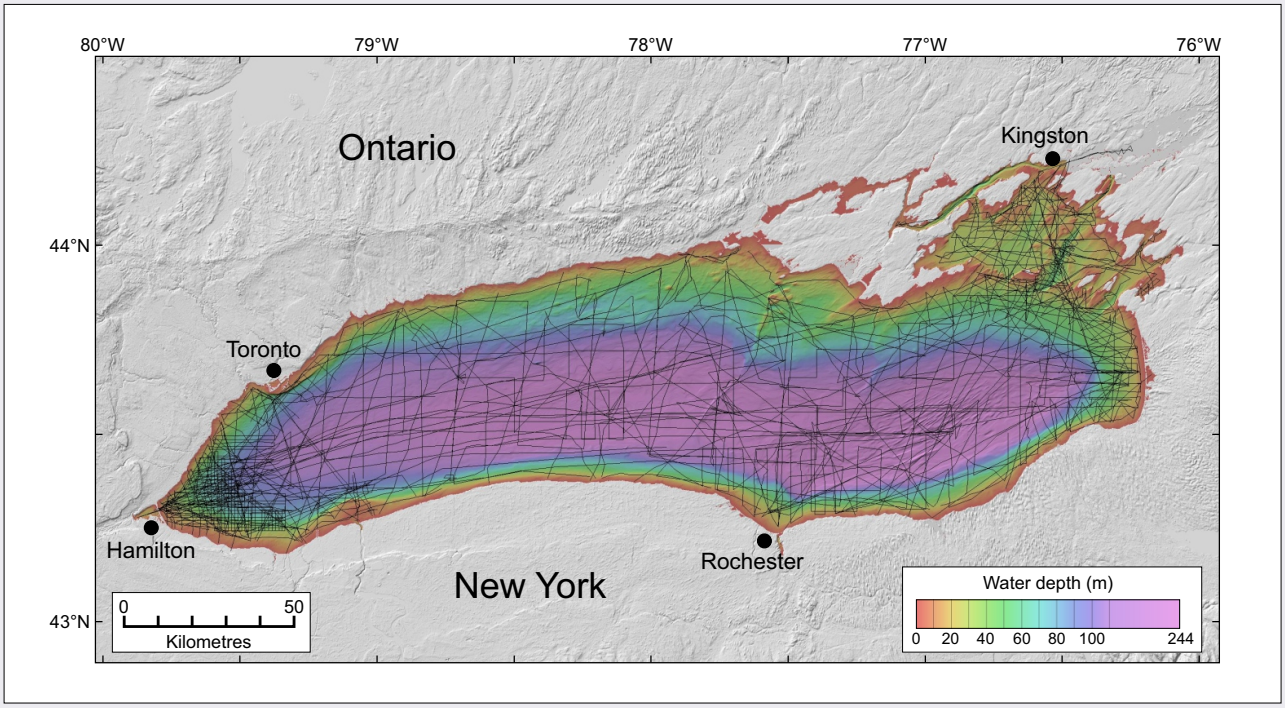


Figure 1. Map of Lake Ontario illustrating the distribution of legacy seismic reflection survey lines listed in Table 1. The total line kilometres is 18078. Bathymetric data from Virden et al. (1999).

Table 2. Lake Huron legacy seismic reflection expeditions.

Year	Expedition	Vessel	Line kilometres	Instrument
1969	69-2-01	*Limnos*	3680	Airgun (interpreted)
1991	91800	*Laurentian*	2813	Seistec, chirp
1995	95800	*Laurentian*	652	Seistec

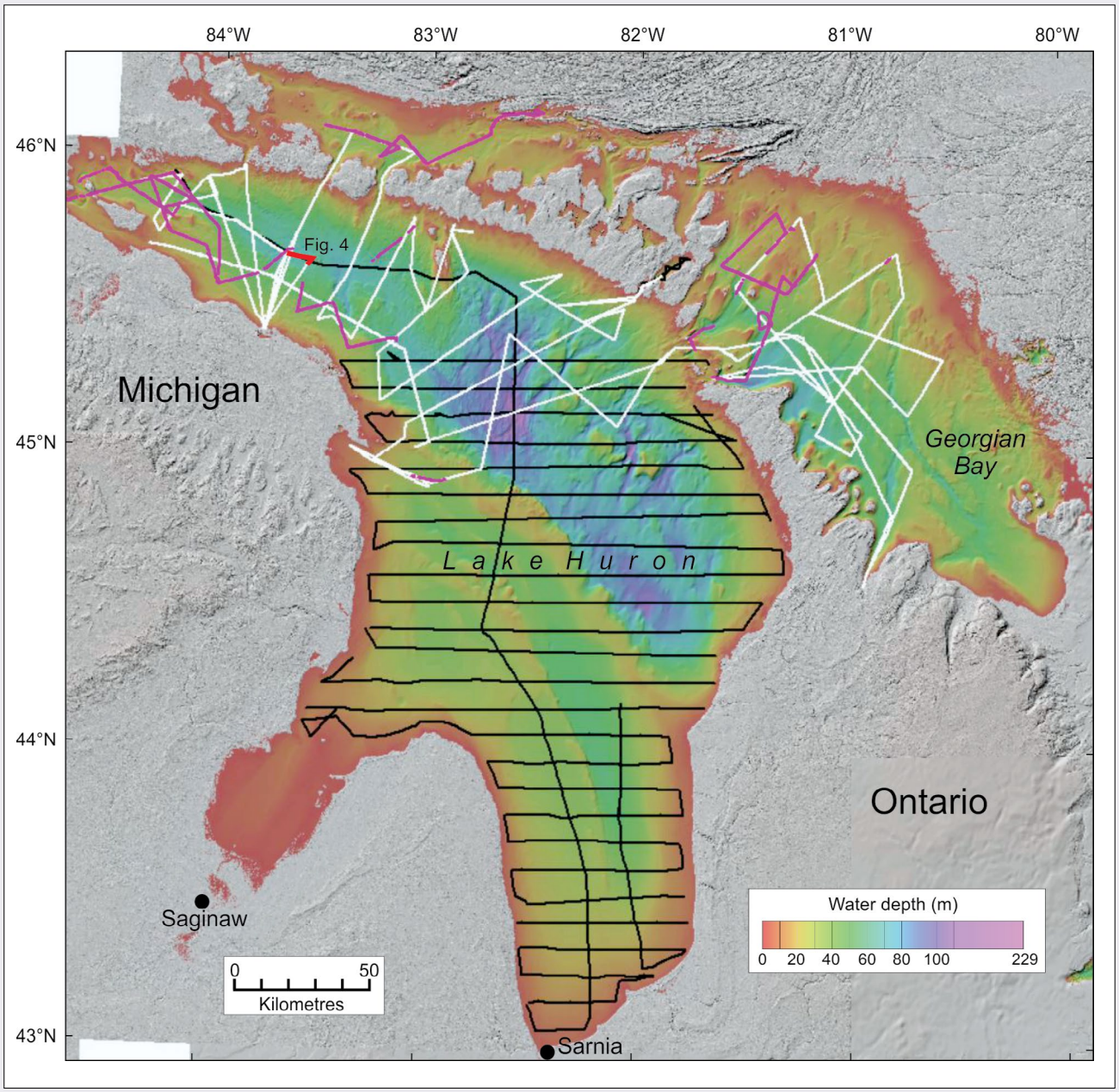


Figure 2. Map of Lake Huron and Georgian Bay illustrating the distribution of legacy seismic reflection survey lines listed in Table 2. White denotes *Laurentian* 91800; Pink lines denote *Laurentian* 95800; black denotes *Limnos* 69-2-01. The total line kilometres is 7145. Red line in northwestern Lake Huron shows extent of *Laurentian* 91800 seismic reflection profile in Figure 4. Bathymetric data from Vincent et al. (1999).

Seistec high-resolution seismic profiler, towed at 4 knots (7.4 km/hr) from the RV *Laurentian*. The data were recorded digitally and on an EPC dry paper recorder (Figure 3). The seismostratigraphic framework was established by Moore et al. (1994) and Rea et al. (1994). In the present analysis only the paper records from *Laurentian* 91800 were used (Todd and McNamara 2018). Thirty-eight rolls were processed (rolls 1 to 39; roll 38 is missing). The whereabouts of the digital data are unknown.

The Seistec system uses a broadband (2–10 kHz) boomer source with three in-line hydrophone receivers protected from noise sources by housing in a downward-facing cone (Simpkin and Davis 1993). The Seistec boomer sound source was located in a surface-towed sled. For part of the Laurentian 91800 survey, a Datasonics high-resolution Chirp seismic profiler was also used. This instrument uses an array of transducers that are swept between 2 and 10 kHz and pulse compression techniques to achieve the theoretical resolution prescribed by the system bandwidth (Mayer and LeBlanc 1983). The Chirp sound source was in a fiberglass fish towed 1–2 m beneath the water surface.

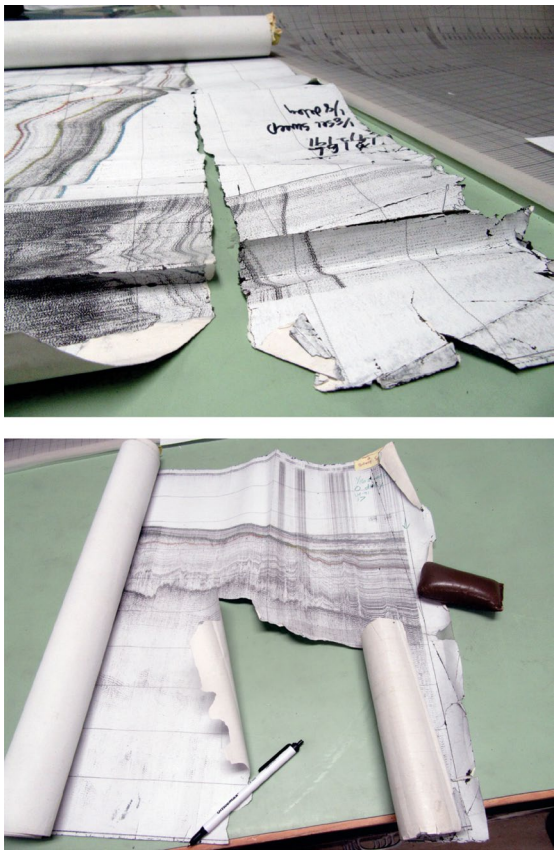


Figure 3. Damaged legacy seismic data paper rolls prior to restoration.

Both instruments provided depth penetration up to 60 m through lake floor sediments. Beneath these sediments, glacial till or bedrock forms the acoustic basement (Figure 4).

The CSS *Limnos* expedition 69-2-01 surveyed all of Lake Huron using a 5 cubic inch (0.08 l) airgun source at an average speed of 8 knots (14.8 km/hr) (Lewis et al. 1969). Southern and central Lake Huron was surveyed using an east–west line pattern with a north–south tie line through the centre of the lake (Table 2, Figure 2).

The original paper plot of the survey tracks was scanned and georegistered and the fix locations were digitized to create navigation data to be used in subsequent data processing (McNamara and Todd 2018). Thirty-three plastic film rolls of interpreted seismic data constitute the information available; the whereabouts of the analogue paper records from the original survey are unknown. Given this limitation of access to the original data, the interpretation of the lake bottom and bedrock (perhaps more accurately considered acoustic basement) performed by Huntec Limited (Figure 5), is considered useful in the future compilation of an isopach map of sediment thickness and a depth to acoustic basement map for Lake Huron.

3. Methods

3.1 Record repair

The paper and film records and maps were in poor physical condition and required the application of acid-free archival tape to enable them to be handled safely (Figure 3). The records and maps were scanned in greyscale at 300 dots per inch in tagged image file (TIF) format. Colour scans were made when warranted by the use of colour in the source material. The greyscale scans were used as input into the seismic data processing software described below.

3.2 Navigation

Seismic data without associated navigation cannot be used for any analysis. The expeditions reported here are only those for which written positions and/or track plots exist. Many thousands of navigation positions were entered into spreadsheets and many thousands of positions were digitized from georegistered track plots. In ED and SDA, and in the software described below, all times are standardized to Coordinated Universal Time (UTC). The majority of the legacy expeditions recorded local time when noting positions, thus the UTC times for all written and mapped positions had to be determined.

3.3 Maps

All maps were georeferenced using Esri ArcGIS software.

3.4 Seismic processing

The following description outlines the steps used in processing from scanned records of seismic data to digital

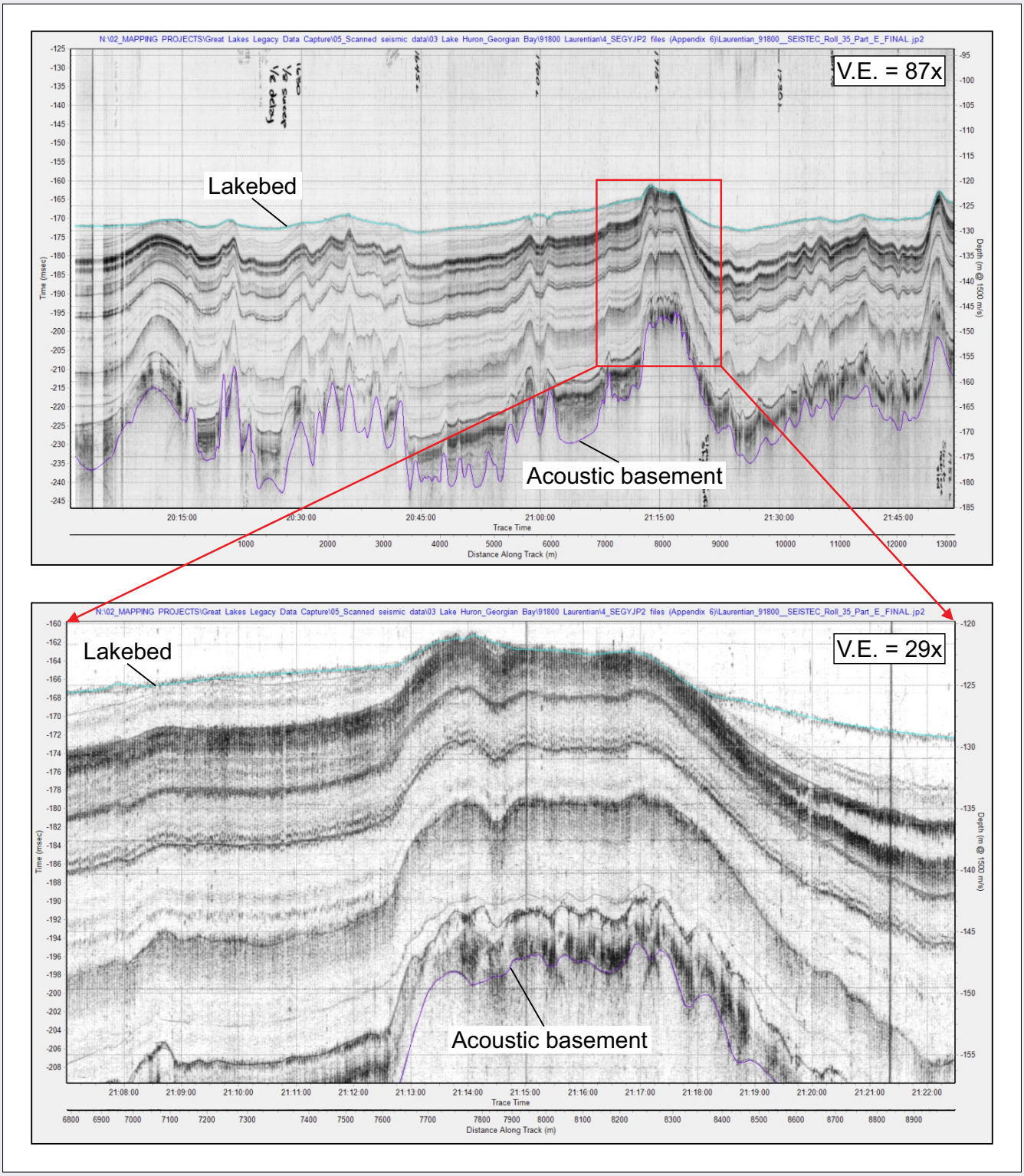


Figure 4. Example of digitally processed legacy Lake Huron seismic data illustrating the capability of the software in examining the seismostratigraphy at different scales and vertical exaggerations. The blue line is lakebed and the purple line is acoustic basement (*Laurentian* 91800, Roll 35E, day 249). Upper: Small scale display of the total line from 2001–2152 (11.3 km). Lower: Large scale display from 2107–2122 (2.2 km). See Figure 2 for location of profile.

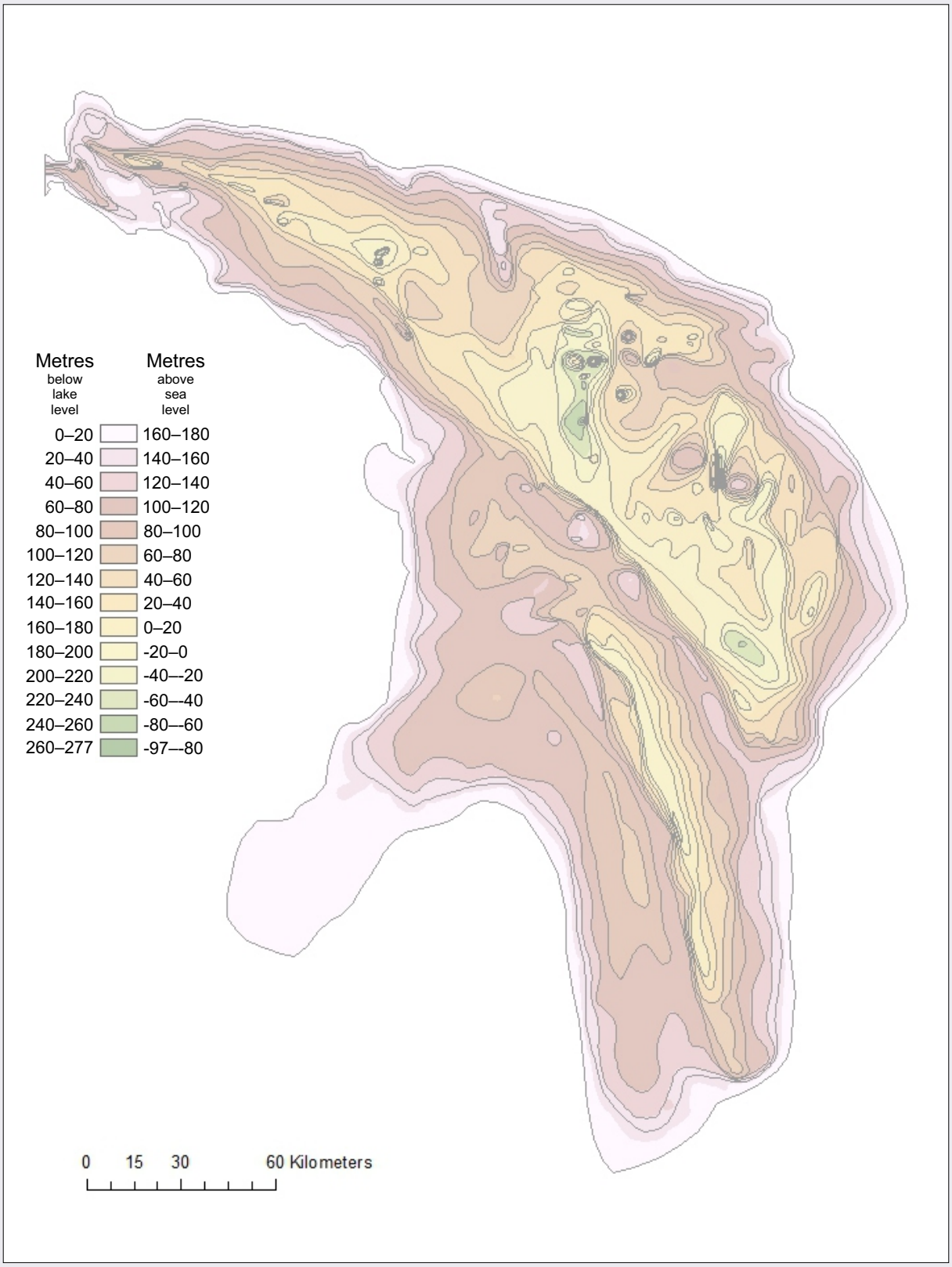


Figure 5. Map of Lake Huron acoustic basement elevation in metres below lake level and above sea level (Cooper and Blasco 1969). Note that the elevation of Lake Huron water surface is 176 m above sea level.

images that can be interpreted, placed in the SDA, located on a GIS, and shared on the worldwide web. All the software is available for free download at:

http://ftp.maps.canada.ca/pub/nrcan_rncan/raster/marine_geoscience/Seismic_Reflection_Scanned/tools.

This software was created by Dr. Robert C. Courtney of the Geological Survey of Canada–Atlantic (Courtney 2012) and is the intellectual property of the Government of Canada. All rights to modify and distribute this software are retained by the Government of Canada.

Step 1.

Using program SectionJP2, the greyscale TIF files were image compressed to JPEG 2000 (or JP2) format.

Step 2.

Program RegJP2000 was used to register the scanned seismic sections in JP2 format and project them into SEG-Y format for subsequent processing. Horizontal and vertical scales were applied. Vertical time shifts and/or changes in sweep rate were accounted for.

Step 3.

Program SegyJP2 was used to convert from SEGY format to JP2 format once again.

Step 4.

Program JP2Viewer was used to view and manipulate the output files from step 3. This software enables the insertion of navigation data and the interpretation of seismostratigraphy (Figure 4).

4. Future work

Completion of the processing of the legacy seismic data is the necessary basic step to enable a modern and thorough seismostratigraphic analysis of Lake Ontario and Lake Huron. The digital lines in Step 4 (above) now need to be digitally interpreted using program JP2Viewer and applying the seismostratigraphic scheme of Hutchinson et al. (1993). Once the interpreted lines are compared through their many tie points, the Hutchinson et al. (1993) scheme can be evaluated and modified if required. Isopach and structural contour maps can then be constructed from the interpreted suite of seismic profiles.

The legacy maps of Lake Huron depth to basement (Figure 5; Cooper and Blasco 1969) and Lake Ontario sediment thickness (Figure 6; Hobson 1967) are half a century old. Within a GIS environment, these maps could be updated using seismic data tied to the Lake Ontario 74 m a.s.l. and Lake Huron 176 m a.s.l. lake levels (Environment Canada

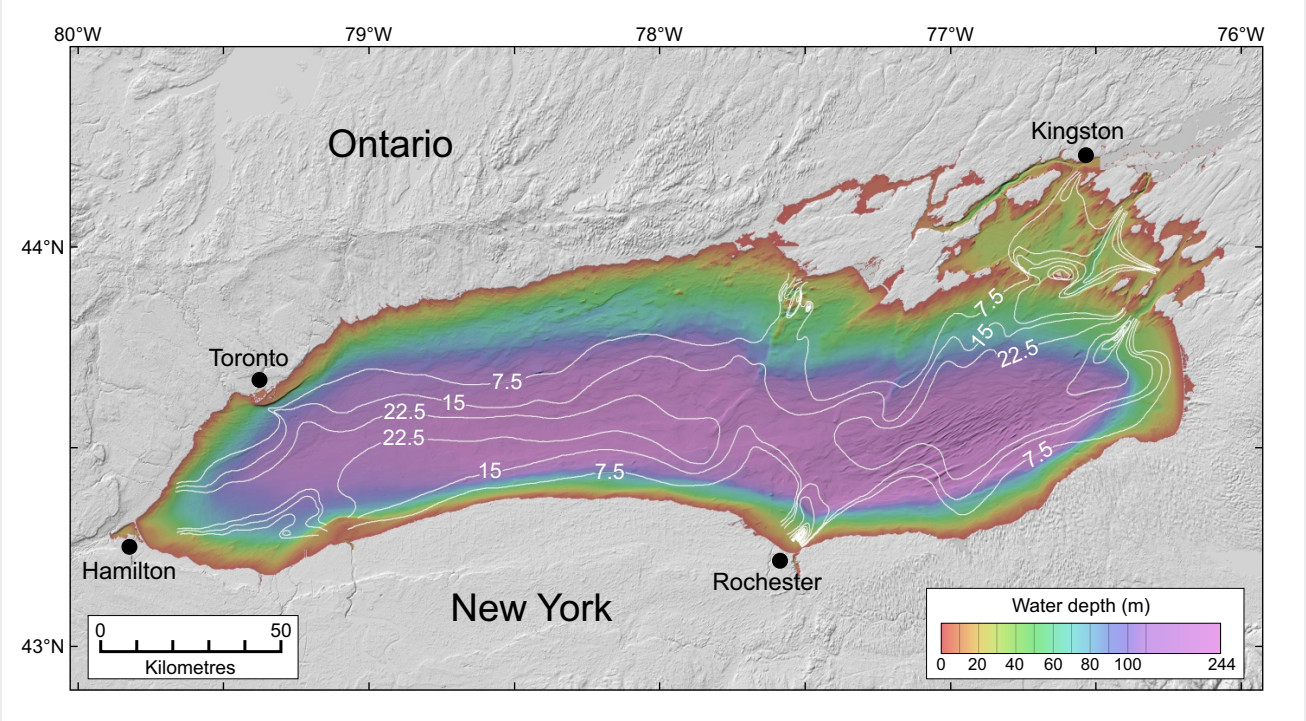


Figure 6. Isopach map of sediment thickness in metres in Lake Ontario adapted from Hobson (1967). Sediment thickness was determined using a sound speed of 1500 m/s in lakebed sediments.

and United States Environmental Protection Agency 1995). A new compilation for Lake Ontario would also take into consideration the quarter century old syntheses of Hutchinson et al. (1993) and Lewis et al. (1995a, b).

The scanned legacy seismic profiles need to be migrated to the Seismic Data Archive. As processing (outlined above) of the scanned profiles progresses, the completed profiles also need to be migrated to the SDA. The legacy paper and film records, along with Information extracted from the legacy data (navigation spreadsheets) need to be migrated to the Expedition Database with the required associated metadata.

Legacy seismic data have also been discovered for Lake Erie, although not to the same degree of spatial coverage as lakes Ontario and Huron. With this limited coverage, lake-wide mapping of depth to acoustic basement is not possible for Lake Erie. However, maps of glacial sediment topography and postglacial sediment thickness in Lake Erie are provided by Lewis et al. (2012).

5. Acknowledgements

We thank Professor Theodore C. Moore Jr. (Department of Geological Sciences and Center for Great Lakes and Aquatic Research, University of Michigan) for making the 91800 *Laurentian* seismic data rolls and the associated navigation data available for digital processing. Dr. Robert C. Courtney (GSCA) provided valuable software edits during the Great Lakes legacy data recovery. Gordon Cameron and Dr. Edward King (GSCA) provided practical suggestions for using the Courtney software. Data processing assistance was provided by Elliot McLauchlan and Gavin McNamara. Funding for this work was provided by Canada 3D and the Open Geoscience Program, and the Groundwater Geoscience Program, Geological Survey of Canada. This work is a contribution to the GSC–OGS southern Ontario project on groundwater 2014–2019.

6. References

Brodaric, B., Pilkington, M., Snyder, D.B., St-Onge, M.R., Russell, H.A.J. 2015. Canada in 3D - toward a sustainable 3D model for Canadian geology from diverse data sources. American Geophysical Union, Fall Meeting 2015, San Francisco, abstract IN13A-1816.

Cooper, H.W. and Blasco, S. 1969. Lake Huron bedrock elevation based on Huntec seismic data from expedition *Limnos* 69-2-01. Geological Survey of Canada, unpublished map, scale 1:400,000.

Courtney, R.C. 2012. RegJP2000 Version 2.0. Geological Survey of Canada, internal report, 50 p.

Environment Canada and United States Environmental Protection Agency, 1995. The Great Lakes: An Environmental Atlas and Resource Book. https://nepis.epa.gov/Exe/ZyPDF.cgi/P1004ICU.PDF?Dockey=P1004ICU.PDF

Hobson, G.D. 1967. Lake Ontario, thickness of sediments. Geological Survey of Canada, unpublished map, scale 1:400,000.

Hutchinson, D.R., Lewis, C.F.M., and Hund, G.E. 1993. Regional stratigraphic framework of surficial sediments and bedrock beneath Lake Ontario. Géographie physique et Quaternaire, 47: 3, 337–352. doi:10.7202/032962a

Lewis, C.F.M., Goodacre, A., and Holler, A. 1969. Cruise report, limnology, Lake Huron, cruise number 69-2-01. Canada Centre for Inland Waters, Burlington, Ontario, 34 p.

Lewis, C.F.M., Cameron, G.D.M., King, E.L., Todd, B.J., and Blasco, S.M. 1995a. Structural contour, isopach and feature maps of Quaternary sediments in western Lake Ontario. Atomic Energy Control Board of Canada, Project No. 2.243.1, Ottawa, Ontario, 115 p., Map 4, https://inis.iaea.org/collection/NCLCollectionStore/_Public/27/031/27031091.pdf

Lewis, C.F.M., Cameron, G.D.M., King, E.L., Todd, B.J., and Blasco, S.M. 1995b. Structural contour, isopach and feature maps of Quaternary sediments in western Lake Ontario. Atomic Energy Control Board of Canada, Project No. 2.243.1, Ottawa, Ontario, 115 p., Map 9, https://inis.iaea.org/collection/NCLCollectionStore/_Public/27/031/27031091.pdf

Lewis, C.F.M., Cameron, G.D.M., Anderson, T.W., Heil Jr., C.W., Gareau, P.L. 2012. Lake levels in the Erie Basin of the Laurentian Great Lakes. Journal of Paleolimnology, 47: 493–511. https://doi.org/10.1007/s10933-012-9578-5

Mayer, L.A., and LeBlanc, L.R. 1983. The Chirp sonar: A new quantitative high-resolution profiling system. In Acoustics and the Sea-Bed. Edited by N.G. Pace, Bath University Press, Bath, United Kingdom.

McNamara, G.D., and Todd, B.J. 2018. Processing of interpreted seismic reflection data from expedition 69-2-01 of the CSS *Limnos*, Lake Huron, Ontario, Canada and Michigan, U.S.A. Geological Survey of Canada, Open File 8429, 1 .zip file. https://doi.org/10.4095/308377

Moore, T.C., Jr., Rea, D.K., Mayer, L.A., Lewis, C.F.M., and Dobson, D.M. 1994. Seismic stratigraphy of Lake Huron–Georgian Bay and postglacial lake level history. Canadian Journal of Earth Sciences, 31: 1606–1617.

Rea, D.K. 1991. Preliminary cruise report, USDS Cruise No. 91-050, R/V *Laurentian*. LH-91, 37 p.

Rea, D.K., Todd, B.J., and Lewis, C.F.M. 2018. *Laurentian* 95800 expedition report, Lake Huron, Georgian Bay, and Lake Michigan, Ontario, Canada and Michigan, U.S.A. Geological Survey of Canada, Open File 8431, 12 p. https://doi.org/10.4095/308482

Rea, D.K., Moore, T.C., Jr., Lewis, C.F.M., Mayer, L.A., Dettman, D.L., Smith, A.J., and Dobson, D.M. 1994. Stratigraphy and paleolimnologic record of lower Holocene sediments in northern Lake Huron and Georgian Bay. Canadian Journal of Earth Sciences, 31: 1586–1605.

Simpkin, P.G. and Davis, M. 1993. For seismic profiling in very shallow water, a novel receiver. Sea Technology, 34: 5 p.

Todd, B.J. and McNamara, G.D. 2018. Processing of seismic reflection data from expedition 91800 of the RV *Laurentian*, Lake Huron and Georgian Bay, Ontario, Canada and Michigan, U.S.A.; Geological Survey of Canada, Open File 8428, 1 .zip file. https://doi.org:10.4095/308328

Virden, W.T., Warren, J.S., Holcombe, T.L., Reid, D.F., and Berggren, T.L. 1999. Bathymetry of Lake Ontario. National Geophysical Data Center, World Data Center for Marine Geology and Geophysics, Boulder, Colorado, Report MGG-15.

Vincent, P., Warren, J.S., Holcombe, T.L., Reid, D.F., Divins, D., Virden, W.T. 1999. Bathymetry of Lake Huron. National Geophysical Data Center, National Oceanic and Atmospheric Administration. doi:10.7289/V5G15XS5

Regional geochemical survey of surficial sediment in southern Ontario: A geochemical baseline for environmental and human health assessment

David R. Sharpe[1]*, Bruce A. Kjarsgaard[1], Rod A. Klassen[2], Ross A. Knight[1], Charles Logan[1], Hazen A.J. Russell[1], and Daniel A.J. Stepner[1,3]

Abstract: Low-density sampling and analysis of soil A- and BC-horizons and glacial till, establish a baseline to characterize geochemical background variation in glacial sediments across southern Ontario. Interpretation of these data reveal that regional-scale geochemical variation of earth materials is largely derived from bedrock, with the impact of weathering and soil formation being less significant. For example, geochemical provenance indicators (e.g., Paleozoic carbonate terrane with elevated CaO+MgO, versus Precambrian Shield terrane with elevated SiO_2+Al_2O_3) distinguishes the influence of these source lithologies. Thus, interpretations of geochemical sediment surveys as a basis for geochemical modeling are best approached in terms of geological provenance, process, and weathering. Furthermore, because chemical concentration levels in surficial sediment is also directly related to analytical protocol, knowledge of both mineralogy and strength of chemical digestion is required to understand geochemical processes. This approach, of assessing all chemical variation, contributes greater certainty to risk assessment and decision-making in geochemical models related to environmental and human health protection.

1. Introduction

This report presents geochemical data for earth materials collected from a regional, low-density geochemical survey of southern Ontario (Figure 1) in 1994 and 1995. The survey provides empirical evidence for natural geochemical background levels and geochemical variation in unconsolidated sediment. Data in this report support environmental and human health protection by showing geographic variation in relative geochemical presence, and by providing a baseline for estimating levels of potential contaminants. The sampled media represent soil A- and BC-horizons, and shallow (weathered) glacial till parent material (i.e., the soil C-horizon).

This report interprets the origins of geochemical variation in unconsolidated deposits in terms of bedrock provenance and mineralogy, surficial geology, weathering, and soil formation, with the aid of chemical digestion. The report demonstrates how geoscience contributes to the geochemical models that support environmental and human health risk assessment. We do not assess the geochemistry of sediment and rock with respect to the significant effects on the geochemistry of groundwater that flows through the subsurface (e.g., McIntosh and Walter 2006).

1.1 Setting

Southern Ontario includes both urban and rural environments characterized by wide variations in population density, and in diversity of human activities, for example, agriculture, forestry, mineral resource development, and manufacturing. The study area is underlain by the Canadian Shield (Ontario Geological Survey 1991a, b) in the north and by a younger Paleozoic platform sequence of sedimentary bedrock in the south (Figure 1). The two geological terranes have marked contrasts in lithology, mineralogy, and geochemistry. Shield terrane comprises variably metamorphosed volcanic, intrusive and sedimentary rock types, of quite variable geochemical composition. An earlier till geochemical survey of the Shield-region between Ottawa and Georgian Bay characterizes this area (Kettles and Shilts 1994). The Paleozoic sedimentary bedrock terrain comprises little-altered marine carbonate,

[1] Geology Survey of Canada, Natural Resources Canada, 601 Booth Street, Ottawa, ON K1A 0E8
[2] Retired
[3] 1-5 Ossington Ave, Ottawa, ON K1S 3B3
*corresponding author: david.sharpe@canada.ca

Recommended citation: Sharpe, D.R., Kjarsgaard, B.A., Klassen, R.A., Knight, R.D., Logan, C.E., Russell, H.A.J., and Stepner, D.A.J. 2020. Regional geochemical survey of surficial sediment in southern Ontario: A geochemical baseline for environmental and human health assessment. In Russell, H.A.J. and Kjarsgaard, B.A. Eds. Southern Ontario groundwater project 2014–2019: summary report. Geological Survey of Canada, Open File 8536, 83-94. https://doi.org/10.4095/321094

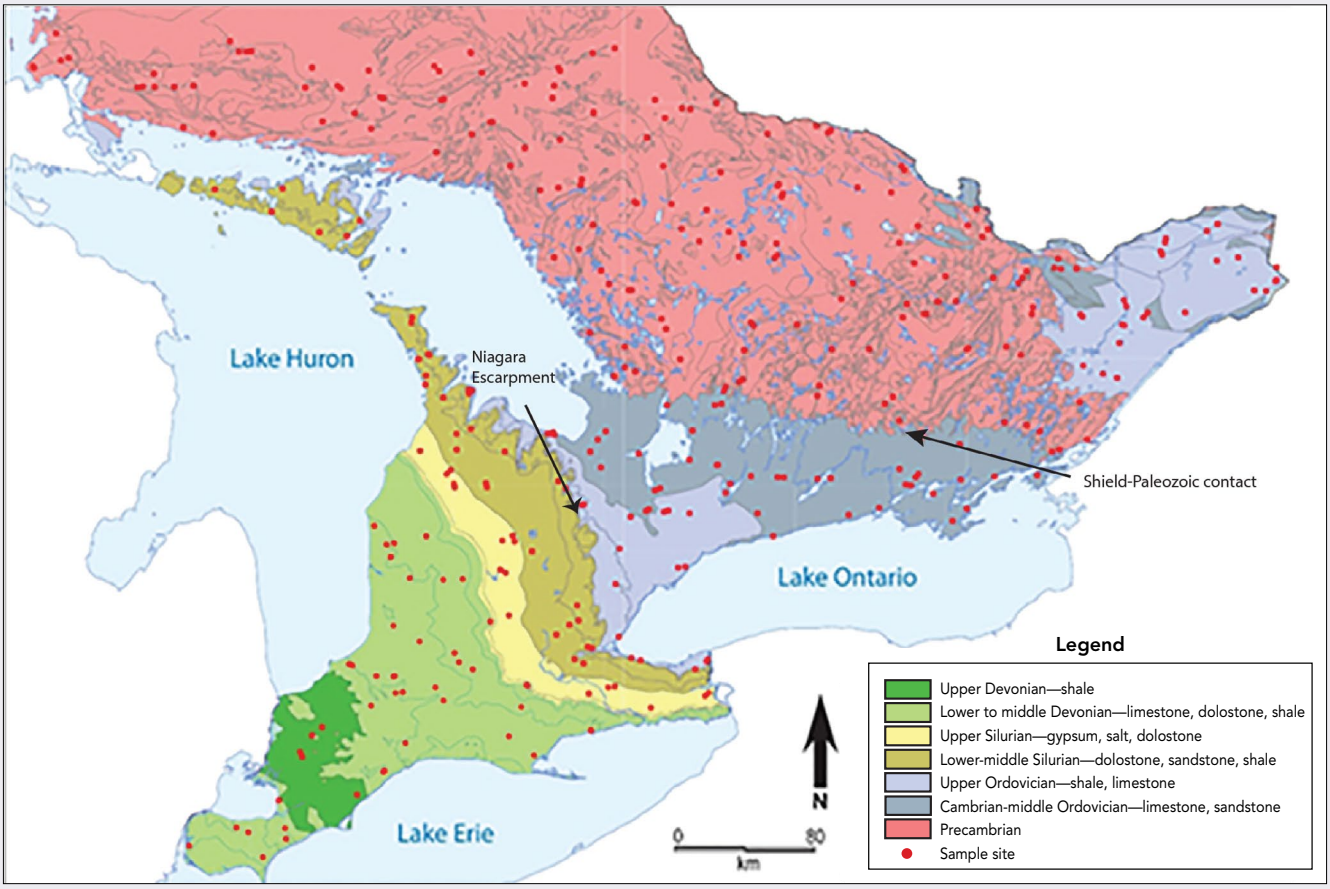


Figure 1. Sampling locations for regional geochemical survey of Southern Ontario superimposed on bedrock geology. Geology of southern Ontario bedrock from Ontario Geological Survey, 1991a, b.

sandstone, and shale of Cambrian to Silurian ages (Figure 1; Sanford and Baer 1971), areas preferentially associated with agriculture, industry, and urbanization.

Surficial geological processes such as glaciation affected texture, mineralogy, and sediment thickness, as well as geochemical variation in surficial sediment. Ontario had multiple glaciations, the last of which left a complex of glacial and postglacial deposits mantling bedrock. Surficial sediment cover over Shield terrane is in general thin (<5 m). In contrast, surficial sediment overlying Paleozoic sedimentary rocks is much thicker (10s–100s m). Surficial sediment can occur as thick successions, ~100–200 m in stratified moraines and former glacial lake basins. Till, a glacial sediment deposited directly by ice, is most extensive in Shield areas, where it is thin (<1 m) and in topographic lows glaciofluvial and glaciolacustrine deposits are common (Barnett et al. 1991). Till derived from Shield terrain is typically stony and discontinuous, with minimal agricultural value, whereas, thicker, fine-grained, tills and glaciolacutrine sediments associated with sedimentary rocks is well-suited for cultivation and agriculture.

2. Methods

2.1 Regional survey

The survey had a mean sampling density of 1 site per 1,600 km^2, with a total sample collection of 296 paired soil samples (A- and BC-horizons) and 300 complementary till samples from the same location (Figure 1). Location of sampling sites was based on a framework, with a randomly chosen origin, and a grid of 80 x 80 km cells. Sample design was based on protocols of the 1992 Prairie soil sampling project (Garrett and Thorleifson 1993, 1995) and is similar to those used for the Soil Geochemical Landscapes Project for North America (Grunsky et al. 2018).

A sampling site was chosen within a 1 x 1 km target-cell within a quadrant of the 80x 80 km domain. The site represents the dominant landscape attributes of the target-cell, including topography and vegetation, soil type, and soil parent material type (Sharpe et al. 2019). Paired 2 kg samples were collected from pits in the organic-rich part of the soil (e.g., soil A-horizon; 1 to 15 cm depth), and the underlying inorganic soil (e.g., soil BC-horizon within a 10 cm interval

at ~30 to 50 cm depth). Till samples were collected at ~0.6 to 2 m below ground surface in partially weathered parent material (soil C-horizon). Soil and till samples analyses were undertaken on the <2 mm and <0.063 mm size fractions, respectively.

Sampling sites were organized according to a hierarchical sample design (Garrett and Thorleifson 1995). To assess geochemical variability within the nested design, a number ranging from 1 to 7 was assigned to the samples to represent the primary sampling site (1); or other-wise as a quality control, including site duplicate (2); target-cell duplicate (3); field duplicate (5); laboratory duplicate (6); and, analytical reference standard (7). To assess geochemical variability at individual sites, two additional sites were sampled within the regional grid.

At each site, sample location data (UTM coordinates; Lat-Long) and field observations including landscape morphology, Munsell soil colours (determined moist), sample reactivity to dilute HCl, sampling depth, and sample texture were recorded (see Sharpe et al. 2019). Bedrock and surficial geological attributes of sampling sites are based on reference to 1: 1,000,000 scale geological maps (Ontario Geological Survey 1991a, b), and soil classifications on southern Ontario soil maps (CANSIS database - Agriculture Canada; 1: 63,000 scale). Sample preparation was done by Bondar-Clegg & Co., Gloucester, Ontario, and additional sample details are reported in Sharpe et al. (2019).

2.2 Analytical methods

Geochemical analyses of soil and till samples were completed using: instrumental neutron activation analysis (INAA); atomic absorption spectrometry (AAS); inductively coupled plasma mass spectrometry (ICP—MS); and, X-ray fluorescence (XRF) under commercial contracts. For AAS and ICP—MS analyses two digestion techniques were used: i) a 3-Acid (HF-$HClO_4$-HNO_3) digestion; and ii) aqua regia) digestion. Major elements were determined by fused disc XRF, and trace elements determined by AAS, INAA, and ICP—MS. For each method, element mean, standard deviations and standard errors are summarized in Sharpe et al. (2019; see Tables 1, 2, and 3). In addition to samples collected in the field, sample suites submitted for analyses comprise approximately 2% reference standards and 5% duplicate sample splits as analytical quality controls, with their order randomized prior to analysis.

3. Results

Descriptive data for sampling site and sample media, location, including colour, field moisture, reactivity to dilute HCl, and their geological and soil associations are presented in Sharpe et al. (2019, Appendix I; geochemical data, Appendix III, and regional maps in Appendices IV, V, VI and VII).

3.1 Quality control – quality assurance (QA/QC)

Quality of both analytical and field duplicates was demonstrated (Sharpe et al. 2019) and presented graphically in log-log scaled Youden plots (e.g., Figure 2). Both the 1:1 and orthogonal re-gression lines were plotted, with a statistical test to indicate if the orthogonal regression line was effectively 1:1, i.e. intercept zero and slope 1, and through analyses of variance.

For the soil data, the stratified-random survey sample design (Garrett and Thorleifson 1993) permitted 'triples' of survey samples, field duplicates and analytical duplicates of the field duplicates, to be assessed. Where the analysis of variances are equivalent, the results of the 'triples' test can be extrapolated to the whole survey because variation in sample geochemical values relate to natural landscape variation. This nested duplicate design determined that the data were 'fit-for-purpose' in preparing maps of spatial variability; rarely was significant variability present at-site or due to analytical variability, which would reduce the reliability of regional maps.

Precision and accuracy of each analytical method was evaluated using the inclusion of blind Certified Reference Materials (Bowman et al. 1979; see Sharpe et al. 2019, Appendix II). Field and analytical duplicates were used to evaluate summary statistics for the regional survey, and for the construction of summary graphics (e.g., histogram, Tukey boxplot and probability plots, Sharpe et al. 2019).

All statistical estimates and graphical displays were prepared

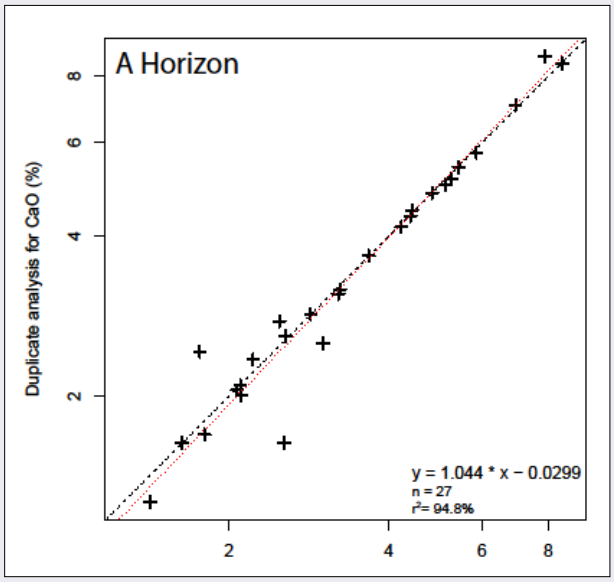


Figure 2. Quality control of analytical duplicates demonstrated graphically in a log-log scaled (Youden) plot where the regression line (red) is plotted for CaO; the statistical test indicates that the regression line of duplicates is effectively 1:1 (black dashed line).

using the 'rgr' package in the R programing environment (Garrett 2013a, b) as presented in Sharpe et al. (2019, Appendix II).

3.2 Geochemical analyses results

Sharpe et al. (2019, Appendix III) provides the soil and till geochemical compiled datasets. Geochemical charts and maps for soil and till are presented here as highlights (e.g., Figures 3, 4, 5, 6, 7), whereas all maps are provided in Sharpe et al. (2019, Appendices IV, V, VI and VII) for XRF, AAS, INAA, and ICP—MS analyses. Contours were interpolated through inverse distance weighting (IDW, MapInfo; cell radius 50 km, cell size 1 km); thus, the maps are generalized at the regional

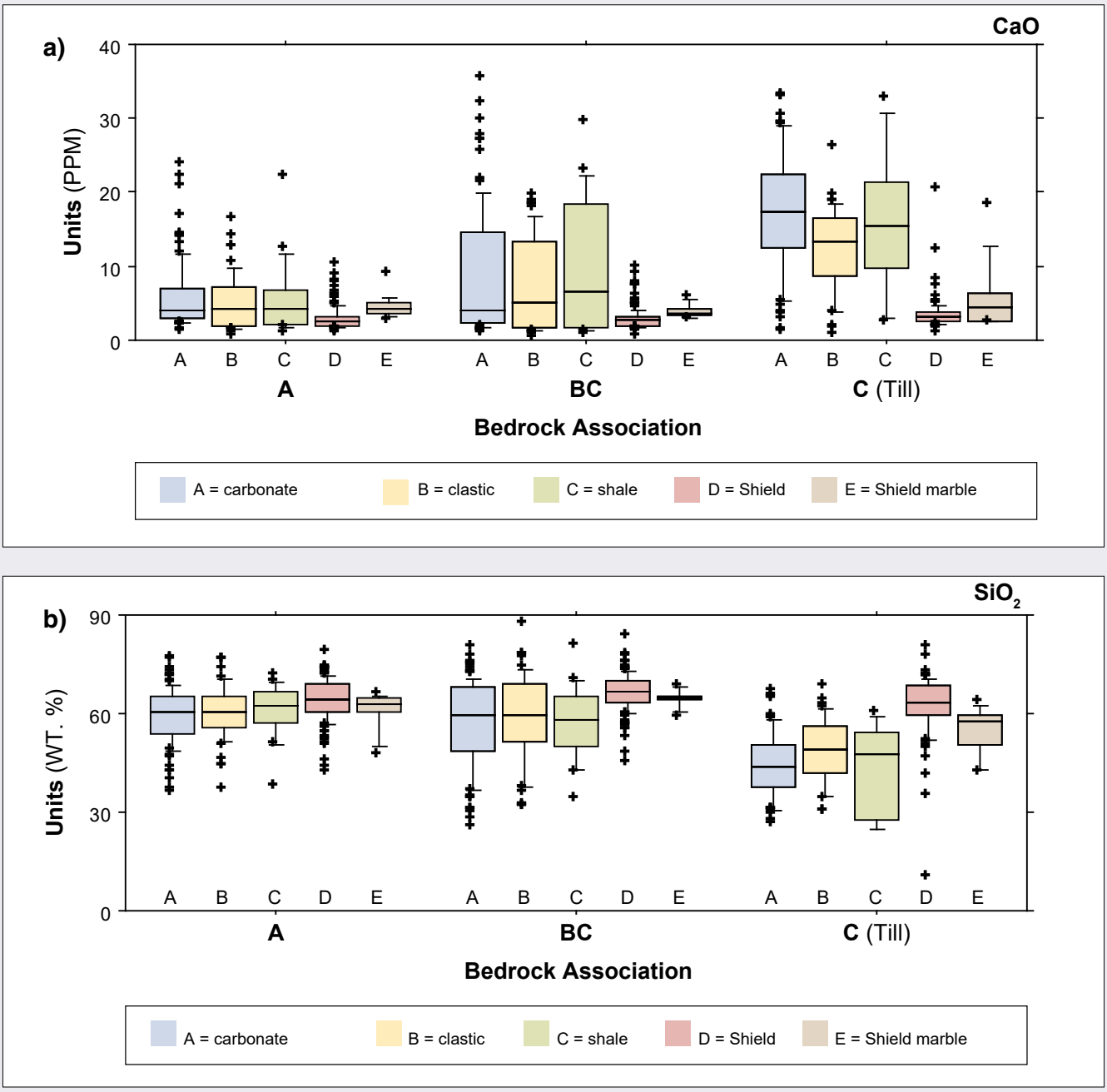


Figure 3. Box plot for: a) CaO (wt %) content as determined by fused disc XRF. The plots indicate that there are significant geochemical differences between bedrock terranes. b) SiO_2 (wt %) content as determined by fused disc XRF. The range of values is smaller in A- and BC-horizon soil samples as compared to parent material (till). Additional element plots can be found in Sharpe et al. 2019 (Appendix VIII).

scale (10s to 100s of km); they may not reflect repeatable levels at more localized scales (e.g., 1–10s of km).

4. Interpretation and discussion

4.1 Origins of natural geochemical background variation in earth materials

Fundamental geological concepts govern our understandings of the natural geochemical variation in near-surface (<1 m depth) earth materials (bedrock and overlying sediment) identified in this study (e.g., Figure 3). In glaciated terrain, minerals are eroded from bedrock and redistributed through geological processes, primarily related to the actions of ice, and to a lesser extent to water, wind and gravity. The eroded and transported minerals exist in the current geological environment with geochemically different ranges as a response to weathering and to soil formation.

Parent material variation originates via bedrock provenance (e.g., mineralogy) and geological processes (e.g., glacial, glaciofluvial), and is reflected in both mineralogy and mineral partitioning among grain sizes (e.g., <2 mm vs. <0.063 mm in soil and till size fractions). Variability in soil reflects environment (e.g., moisture, topography, organic matter), in addition to parent material. Consequently, geochemical variability in soil is inherently greater than in its underlying parent material (compare A, BC samples versus till samples, Figure 3a). The deepest sediment sampled in this study was till and these samples are the least affected by weathering and soil formation, and thus best portrays the geological controls, bedrock and surficial, on geochemial background variation.

The key elements of the common rock-forming minerals, silica (Si), alumina (Al), magnesium (Mg), calcium (Ca), sodium (Na) and potassium (K), occur in both soil and till. Aluminum and silica are most abundant in surficial materials overlying the Precambrian Shield terrane because of the predominance of alumino-silicate minerals. In contrast, Ca and Mg are most abundant in carbonate-dominated Paleozoic sedimentary bedrock (Figure 4). Box plots (e.g., CaO, Figure 3) indicate that there can be significant geochemical differences between bedrock terranes (Figure 1). Paleozoic carbonates, clastic sedimentary rocks, and shale, versus Shield igneous, volcanic, carbonate rocks and their metamorphic equivalents, for different sample types (soil A, soil BC, till).

Contoured geochemical maps also illustrate regional-scale geochemical variation (10s–100s of km, e.g., Shilts 1978, 1984) for southern Ontario (Sharpe et al. 2019, Appendices IV – VII). Many elements that vary in concentration across the study area can be linked to major geological domains such as the Superior and Grenville provinces of the Canadian Shield, and Paleozoic rocks in eastern and southwestern Ontario. For example, CaO analyses from till samples (Figure 4c) has a strong variation in concentration south of the Shield and east of Niagara Escarpment in correspondence with areas of Paleozoic limestone. A complementary pattern for MgO

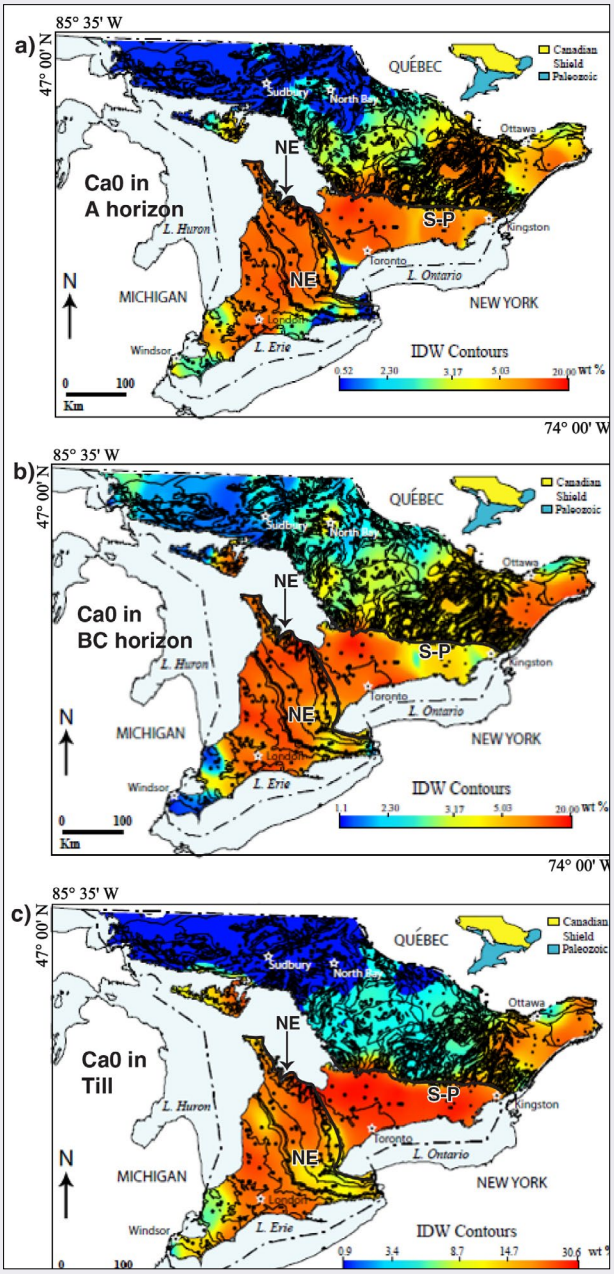


Figure 4. A direct link between surficial sediment chemistry and Paleozoic bedrock is shown by higher CaO values in Paleozoic as compared to Shield terrane, across all sample types. a) CaO in A-horizon; b) CaO in BC-horizon, and, c) CaO in till; NE=Niagara Escarpment and S-P= Shield-Paleozoic boundary.

shows high concentrations west of the Niagara Escarpment where Paleozoic dolomitic carbonate rocks are prominent. CaO and MgO may also be locally enriched in the Shield terrane of eastern Ontario in association with Precambrian marble-bearing lithologies.

Till samples are the product of glacial erosion, transport, and deposition of bedrock and pre-glacial deposits lying

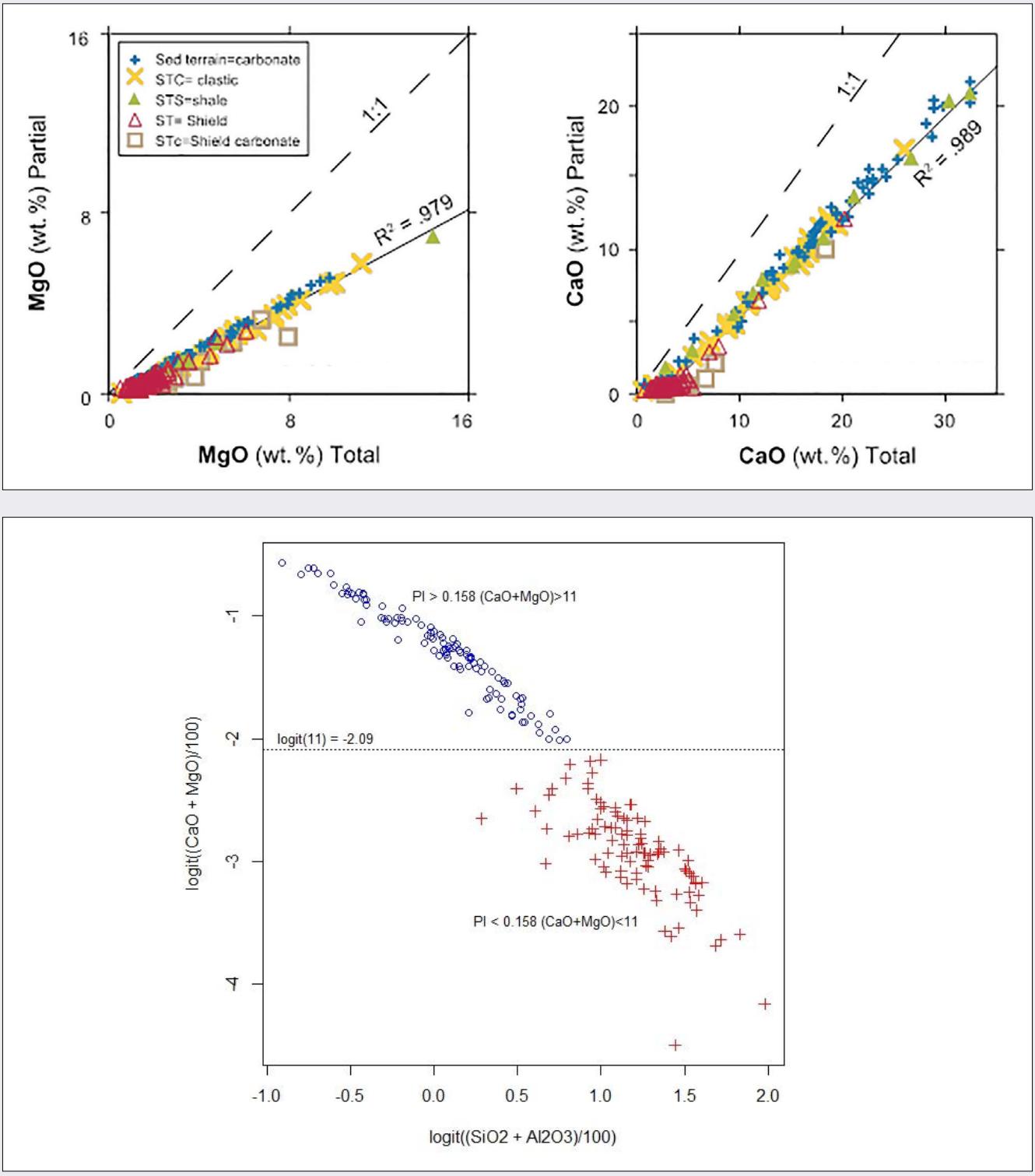


Figure 5. a) Binary plots (e.g., CaO-CaO) for elemental concentrations as determined by XRF analysis (total) and Aqua Regia (partial) dissolution, ICP—MS. There are under-reported concentrations by partial dissolutions (e.g., Mg, Ca) as both regression lines plot below the 1:1 line; this likely indicates the presence of resistate minerals (i.e. feldspars and pyroxenes) in sediments derived from Shield rocks. Note that Shield samples are clustered close to the 0-0 axis in binary plots. The provenance signal from Shield–Paleozoic samples is bettered illustrated with log type plots, see 5b). b) A log-log plot of (MgO+CaO)/100 versus (SiO_2+Al_2O_3/100) illustrates the Provenance Indicator (PI) index as it separates Shield samples (red; PI<0.158) from carbonate basin samples (PI>0.158).

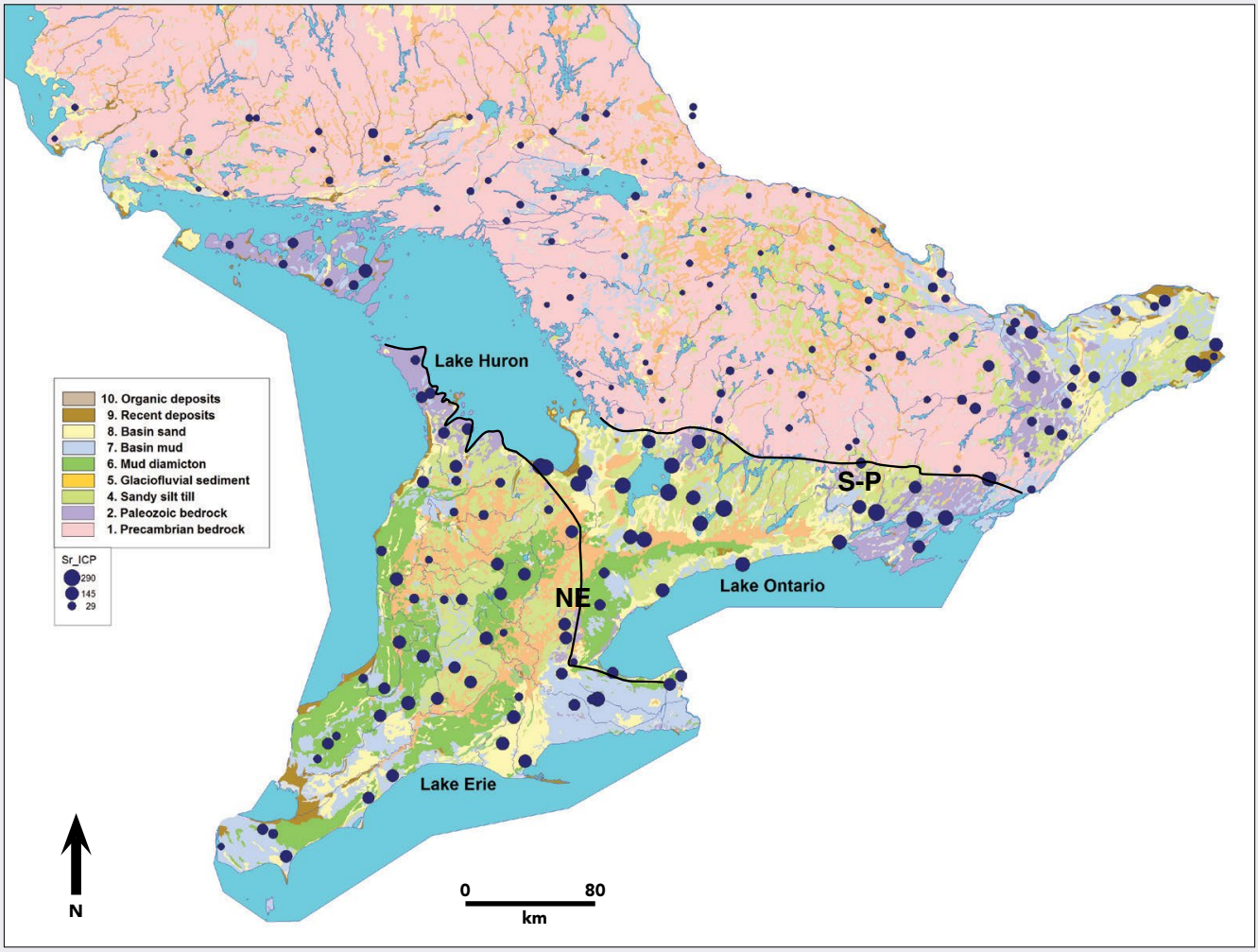


Figure 6. Strontium occurs in minerals of both Shield and Paleozoic basin lithologies. However, the similarity of Sr to Ca in terms of atomic properties means that Sr is very common in surficial sediments overlying Paleozoic basin carbonate rocks. NE=Niagara Escarpment and S-P= Shield-Paleozoic boundary.

along the path of ice flow. Some elements e.g., arsenic (As), appear to have a dispersal pattern to the south from Grenville volcanic terrane, for example northwest of Kingston (Sharpe et al. 2019). However, some potential dispersal patterns (e.g., Ca and Mg) are not resolved by the 'low-density' survey design. Glacial transport studies however, show that carbonate composition increased over short distances (<0.5 km; Kjarsgaard et al. 2017), where ice flowed from north to south across the Shield-Paleozoic contact (Figure 4c). In addition, other geological process models for wind and water may also help to interpret geochemical background variation in other surficial sediment samples.

Soil horizon samples for CaO have different patterns than those in the underlying, little-altered (C-horizon) till. Soil A- and BC-horizon samples have 10–25 wt % less CaO content compared to till samples (compare Figure 4 with Figure 3a) on Paleozoic carbonate bedrock terrane east of the Niagara Escarpment. Variations in soil chemistry reflect the soil-forming factors of time, temperature, moisture, organic material and biological interaction (e.g., Hazlett et al. 1984), that created conditions leading to dissolution of Ca-rich carbonate minerals, which explains the lower CaO concentrations in soil A- and BC-horizon samples as compared to the corresponding till samples.

Other processes are apparent in the geochemical patterns. Note that CaO values in soil A- and BC-horizon are higher on Precambrian Grenville province terrane from Kingston-Renfrew towards Georgian Bay compared with those in till (C-horizon) (Figure 4a-c). It is not likely that weathering of the most reactive of mineral species or soil-forming processes could explain these soil horizon CaO values. More likely, wind blowing from the SW carried carbonate dust from the agricultural fields that are common on limestone bedrock terrane found on the north side of Lake Ontario Figure 4c). It is also possible that Ca in Grenville marble is less reactive

and hence more resistant to weathering and leaching. Soil (shallow, <0.5 m earth material) in general, can be strongly influenced by human activities, affected by atmospheric deposition resulting from industrial and agricultural practices.

4.2 Mineralogy, analytical protocol and geochemical data

For earth materials, geochemical availability is closely tied to chemical form and the residence site of an element within its mineral host. As minerals vary widely in grain size, structure, chemical composition, and reactivity, the determination of elemental availability is closely tied to analytical protocol (e.g., Figure 5a), as well as to the mineral species present and their grain size distributions (e.g., Eriksson 1973). The type and strength of acid digestion determines the degree to which elements may be released from their mineral residence sites and made available for analytical determination (e.g., Koljonen and Malisa 1991). For most rock-forming minerals, analyses are based on "total methods", i.e. 3-Acid (HF-$HClO_4$-HNO_3) digestion, or INAA, or fused disc XRF. The data reported for samples in this study may be considered as either near-total or total. Nevertheless the 3-Acid mixture may not completely dissolve resistate minerals such as zircon (e.g., zirconium, Zr) and chromium-rich spinels (e.g., Cr_2O_3).

In contrast, aqua regia is a 'partial digestion" and many of the common rock-forming minerals like carbonates, phosphates, sulphides, and Mg-bearing phyllosilicates (e.g., biotite) dissolve, other common minerals such as quartz, feldspar, and garnet, are essentially undigested (Snäll and Liljefors 2000). Aqua regia also decomposes a wide range of the organic and inorganic compounds (e.g., Fe-Mn oxides and oxyhydroxides) observed in soil A- and BC-horizons. Non-resistate minerals and compounds have greater potential for transformation in weathering and soil formation. As a consequence, aqua regia based-analyses data may better characterize environmental hazard potential than those based on total digestions.

Analytical differences between total/near-total and partial (i.e., aqua regia) digestions reflect the mineral composition of the sample and the partitioning of elements between resistate and non-resistate minerals. For till, statistically significant Pearson correlation coefficients between results based on total and on partial (aqua regia) digestions indicate those elements that occur either predominantly or entirely in non-resistate mineral hosts. This is the case for CaO (Figure 5a), and, similar patterns occur for major elements like phosphorus (P), Mg, manganese (Mn), iron (Fe), and trace elements such as copper (Cu), nickel (Ni), zinc (Zn), As, manganese (Mn), lead (Pb), and uranium (U). The low concentration levels reported by partial dissolutions of Ca (and Mg) indicates the presence of resistate minerals (e.g., feldspars and pyroxenes) likely in minerals derived from Shield rocks. This Shield signal is partly 'hidden' as Shield samples are clustered close to the 0-0 axis in binary plots. However, because CaO and MgO do not fall on 1:1 lines (Figure 5a), this indicates that all samples must contain Ca- and Mg-bearing resistate minerals (e.g., plagioclase, hornblende) that is, Shield-derived minerals. Samples derived solely from Shield terrane are dominated by alumino-silicate mineral assemblages and hence the correlation of partial and total digestions is poor (Figure 5a). The strength of correlation for Ca and for Mg (Figure 5a) reflects the high concentrations of carbonate minerals in samples derived from Paleozoic carbonate bedrock, but also a consistent alumino-silicate 'dilution' by Shield minerals.

To better distinguish mineralogical input to surficial sediment samples i.e. from Paleozoic carbonate or from Shield terrane, a log transform is applied using geochemical provenance indicators. Here, the Paleozoic carbonate terrane indicator is $CaO + MgO$, and Shield indicator is $SiO_2 + Al_2O_3$), which separate surficial sediment samples from these two terranes (Figure 5b). This plot has an inverse relationship because as Ca and Mg increases, Al and Si are proportionately lower. Calcium may also occur in alumino-silicate minerals (e.g., feldspar, hornblende, phyllosilicates), but in those forms it is a minor component (<15 wt. %) compared to carbonate minerals (29 to 55 wt. %). Also, sedimentary bedrock of southern Ontario are predominantly calcite- and dolomite- bearing carbonate rocks, nevertheless all surficial sediments on Paleozoic terrane (including soil samples) have signs of silicate minerals, as these soils contain between ~30–50 wt % SiO_2 (Figure 3b). Hence, most till geochemistry south of the Shield margin is compositionally bi-partite, comprising alumino-silicate minerals derived dominantly from the Precambrian Shield terrane (and some component from Paleozoic shale), and carbonate minerals dominantly derived from sedimentary bedrock (Figures 3, 5).

The well-defined contrasts between alumino-silicate and carbonate mineral dominated terranes, along the southern Shield margin extending from Parry Sound to Kingston (Figure 4a), is instructive in terms of process. It indicates that carbonate sedimentary rock occur as a significant component of till within a few kilometers of the Shield margin due to rapid glacial erosion and deposition (Figure 4c; Kjarsgaard et al. 2017); ice flow was from the Shield roughly southward toward sedimentary bedrock terrane. The Shield bedrock is typically much harder (silicate minerals typically 3 orders of magnitude harder) and structurally more competent than sedimentary bedrock, thus it is more difficult to erode. Consequently, Shield-derived till tends to be thinner (<1 to 2 m) and is more coarsely textured (sand-rich) than sedimentary bedrock-derived till (typically more silt-rich).

4.3 Trace elements

Trace elements may be associated with an array of mineral species originating in diverse geological and weathering environments (e.g., Shilts and Kettles 1990; DiLabio 1995). Reflecting their preferential associations with a variety of minerals e.g. silicate, alumino-silicate and phosphate minerals, the elements cerium (Ce), cobalt (Co), Fe, lanthanum

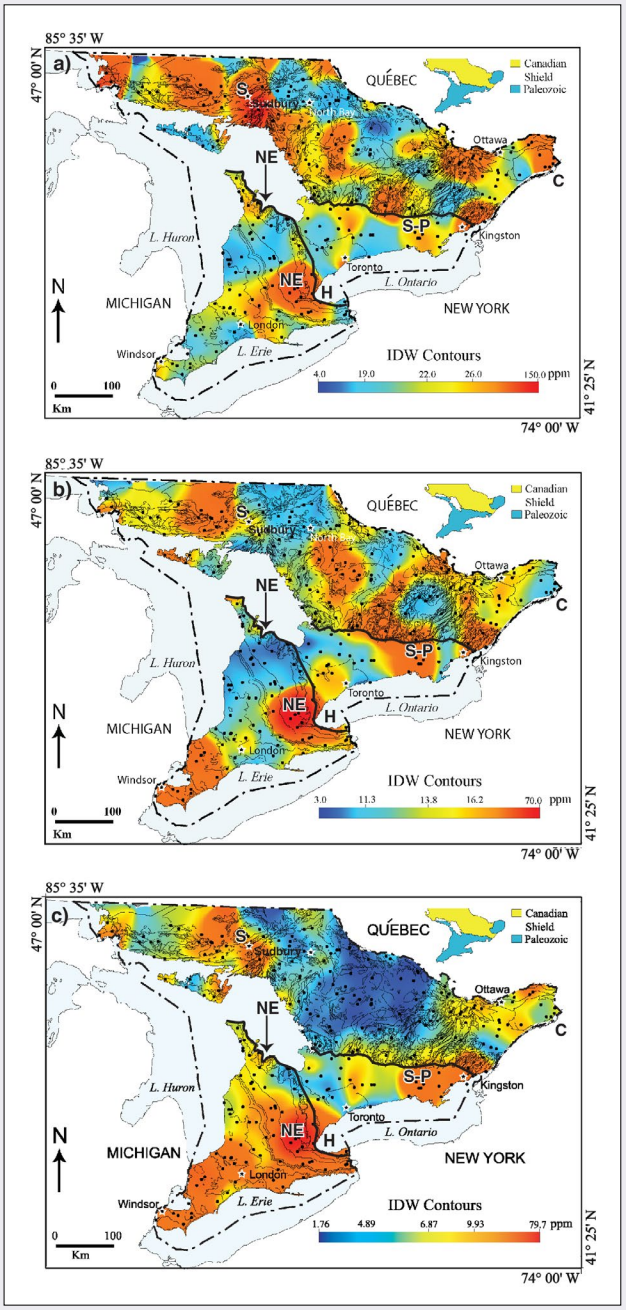


Figure 7. Pb concentration levels in a) Soil A-horizon, b) Soil BC-horizon, and c) till samples across southern Ontario as determined by partial dissolution ICP—MS. NE=Niagara Escarpment, S-P= Shield-Paleozoic boundary, C=Cornwall, H=Hamilton and S=Sudbury.

(La), scandium (Sc) and thorium (Th) are more enriched in Shield-derived till than in sedimentary bedrock-derived till. For elements such as barium (Ba) that are more uniformly distributed between alumino-silicate and carbonate minerals, geochemical contrasts between bedrock terranes may be more poorly defined. In contrast, because Sr is similar in atomic properties (atomic radius and electronegativity) to Ca, Sr is prominent in Paleozoic terrane of southern Ontario (Figure 6).

Within Shield terrane, differences in bedrock composition are reflected by geochemical differences in till. For example, southwest of Ottawa, till is generally enriched in As, cesium (Cs), Cu, fluorine (F), mercury (Hg), Zn, and U, and depleted in K. The U concentrations are greatest near felsic igneous intrusive bedrock of the Bancroft area, an historic U-mining region. Although best defined by major elements, the southern Shield margin is also well defined by trace element contrasts (e.g., cerium (Ce), Co, Fe, La, Na, Th, and Zr); for these elements, till overlying Shield terrain is relatively enriched.

Along the Niagara Escarpment, till is characterized by localized enrichments in Ce, Co, Cu, F, Fe, La, Ni, Pb, rubidium (Rb), Sc, samarium (Sm), Th, U, vanadium (V), Ytterbium (Yb) and Zn. Pb values (Figure 7b) likely relate to lead-zinc mineralization. In areas underlain by black shale near Sarnia-Windsor and the Ottawa Valley east of Ottawa (Figure 1), till is relatively enriched in As, Mn, molybdenum (Mo), Na, Ni, U, antimony (Sb), and Sr. Further, in the Sarnia area, there is relative enrichment in Mn, P, Rb, Yb, Zn and Zr, and, depletion of Ca and Mg compared to the Windsor area; this indicates geochemical differences between the shale bedrock of those two areas. There are two distinct and unrelated areas of anomalous As values controlled by local bedrock. The Windsor black shale has high As values whereas Grenville metavolcanic terrane, NW of Kingston has lower, yet still, anomalous As (Sharpe et al. 2019).

4.4 Soil formation, weathering and anthropogenic effects

Decreases in total Ca in the soil A-horizon as compared to the BC-horizon is interpreted to reflect net leaching of carbonate minerals (calcite, dolomite) (Figure 4). Such geochemical differences among and between soil horizons indicate that geochemical background variation is controlled by soil formation and weathering processes related to sample depth and soil horizon development, and in geological factors, including provenance, mineralogy, mineral partitioning, combined with analytical protocol.

Enrichments in soil A-horizon not reflected in the underlying BC-horizon (e.g., As, Cu, Ni, Cr) may originate from natural soil formation processes, or from surface contamination, or both. Pb enrichment in soil A-horizon occurs across all terranes; higher Pb values occur near Hamilton, Cornwall and Sudbury as compared to values in the BC-horizon or in till (Figure 7a). Some sites are distant from industrial activity and such patterns may reflect natural Pb accumulation in near-surface organic material. Soils (A- and BC-horizons) in the Sudbury region appear generally enriched for As, Ni, Cu and Cr. Atmospheric dispersal of metal-rich dust and smelter particulates controlled by the prevailing wind patterns has been documented (e.g., Henderson and McMartin 1995; Knight et al. 2006). Some enrichment, however, likely originates from mineralized bedrock and resultant till.

In defining natural geochemical background variation, data originating from regional geochemical surveys support both mineral resource exploration and also hazard/ risk assessment for environmental and human health protection (Reimann et al. 2005). Only recently have geochemical baselines and hazard potential been used to estimate environmental liabilities and linked to industrial contamination (e.g., Tarvainen and Paukola 1998). Health hazards may originate in either excess or deficiency of elements that may be either toxic (e.g., As, cadmium (Cd) Hg, Pb) or essential to human health (e.g., Cu, Mn, Zn). Some elements (e.g., F, Mn, selenium (Se), Zn) may be both toxic and essential, depending on concentration, whereas hazard potential for others may reflect element associations (e.g., Cu–Mo; Hg–Se). Further, elements that serve as nutrients have the potential to affect health through release by environmental transformations due to weathering.

In southern Ontario, health hazards originating in earth materials are known related to radon in dwellings of the Bancroft region (McCallum 1992), and in natural F concentrations exceeding Health Canada drinking water standards in groundwater near London (Lucas, Dundee Formations; Gingerich 2006). Potential hazards may occur in areas of black shale near Windsor-Sarnia (Chen et al. 2008), formations outcropping along the Niagara Escarpment (e.g., Lockport Formation, Pb-Zn), and bedrock of the Grenville Province (As; see also Kettles and Shilts 1994). This report illustrates how and why geochemical data for southern Ontario is presented in terms of parent material type, provenance and mineralogy, weathering and soil formation, and analytical protocol, represented by grain size and strength of wet chemical digestion. In doing so, it illustrates how geoscience may contribute to hazard potential modeling, risk assessment and decision-making for environmental and human health protection.

5. Summary and conclusions

Empirical data of this report establish a basis to characterize geochemical background variation in sediment of southern Ontario. Samples of soil A- and BC-horizons reflect a potential range of parent material types, whereas the C-horizon samples consist of weathered till. Geochemical maps of soil A- and BC-horizons are broadly similar to the soil parent material (C-horizon, i.e. till). This indicates that regional-scale geochemical variation based on low-density surveys of earth materials largely originates in bedrock, with net impacts of weathering and soil formation being less significant. As such, geochemistry for soils overlying glacial sediments may be simplified and interpreted in geological terms of provenance, process, and weathering as a basis for geochemical modeling. In this way, geoscience contributes greater certainty to risk assessment and decision-making in geochemical hazard models.

For environmental protection, estimates of natural background are used to gauge the extent and degree of contamination originating from human activities, to assess environmental liabilities, and to guide risk assessment. Typical mean and range values (e.g., Ontario Ministry of Environment and Energy 1993) are defined only by land use (e.g., residential, urban, parkland, and industrial) or political boundary (e.g., county, province) and are unrelated to the geological origins of earth materials and hence, to their mineralogy. This report demonstrates why and how a primary subdivision of geochemical data by geological criteria supports geochemical background definitions. In using such approaches, empirical data for one area are made relevant to similar geological terranes elsewhere. In compiling and presenting geochemical data collected as part of a systematic survey of earth materials, this report supports the definition of natural geochemical background variation in southern Ontario. By illustrating how geoscience supports greater understanding of geochemical variation in earth materials, it may be used to establish better approaches to environmental and human health protection. The impact of this survey would be enhanced by integrating both groundwater (e.g., Hamilton 2015) and sediment geochemistry in southern Ontario.

6. Acknowledgements

Fieldwork was carried out with support of summer students, 1993, 1994. Data compilation and editing were assisted by R. Laframboise, K. Dexter, and W. Spirito. We apologize for forgotten or omitted credits. Laboratory preparation was by P. Lindsay, I. Girard, and M. Wygergangs. Dr. R. Garrett provided figures 5b and 6 and helpful comments on the manuscript by carrying out an internal review. This work was originally completed as part of the ORM NATMAP project and was co-funded by the Ontario Geological Survey and the Low-Level Radioactive Waste Management Office (laboratory analyses). This work is a contribution to the GSC–OGS southern Ontario project on groundwater 2014–2019.

7. References

Barnett, P.J., Cowan, W.R., and Henry, A.P. 1991. Geological map of southern Ontario. Ontario Geological Survey, Map 256, scale 1:1,000,000.

Bowman, W.S., Faye, G.H., Sutarno, R., McKeague, and Kodama, H. 1979. Soil samples SO-1, SO-2, SO-3, SO-4-certified reference materials. CANMET, Report 79-3, 10 p.

Chen, J., Ly, J., Bergman, L., Weirdsma, J., and Klassen, R.A. 2008. Variation of soil radon concentrations in southern Ontario. Radiation Protection Dosimetry 131: 3, 385-389. https://doi.org/10.1093/rpd/ncn192

DiLabio, R.N.W. 1995. Residence sites of trace elements in oxidized till. In Bobrowsky P.T. and Sibbick, S.J. Eds. Drift Exploration in Glaciated and Mountainous Terrain, British Columbia Ministry of Energy, Mines and Petroleum Resources Paper.

Eriksson, K. 1973. The distribution of some metals in different till fractions. Bulletin of the Geological Institutions of the University of Uppsala 5: 157-164.

Garrett, R.G. and Thorleifson, L.H. 1993. Prairie kimberlite study-soil and till geochemistry and mineralogy, low density orientation survey traverses, Winnipeg-Calgary-Edmonton-Winnipeg. Geological Survey

of Canada, Open File 2685. https://doi.org/10.4095/184150

Garrett, R.G. and Thorleifson, L.H. 1995. Kimberlite Indicator Mineral and Till Geochemical Reconnaissance, Southern Saskatchewan. In Richardson, D.G. Ed. Investigations Completed by the Saskatchewan Geological Survey and the Geological Survey of Canada under the Geoscience program of the Canada-Saskatchewan Partnership Agreement on Mineral Development (1990-1995), Geological Survey of Canada, Open File 3119, pp.227-253. https://doi.org/10.4095/205426

Garrett, R.G. 2013a. Assessment of local spatial and analytical variability in regional geochemical surveys with a simple sampling scheme. Geochemistry: Exploration, Environment, Analysis, 13: 4, 349-354. http://dx.doi.org/10.1144/geochem2011-085

Garrett, R.G. 2013b. The 'rgr' package for the R Open Source statistical computing and graphics environment - a tool to support geochemical data interpretation. Geochemistry: Exploration, Environment, Analysis, 13: 4, 355-378. http://dx.doi.org/10.1144/geochem2011-106

Gingerich, H.D. 2006. The occurrence and distribution of flouride in the groundwater environment of Oxford County, Ontario, Canada. Earth Science, University of Waterloo, Waterloo: 184 p.

Grunsky, E.C., Drew, L.J., and Smith, D.B. 2018. Analysis of the United States portion of the North American soil geochemical landscapes project-a compositional framework approach. In: Daya Sagar B., Cheng Q., Agterberg F. Eds. Handbook of Mathematical Geosciences. Springer, 313-346. http://dx.doi.org/10.1007/978-3-319-78999-6_17

Hamilton, S.M. 2015. Ambient groundwater geochemistry data for southern Ontario, 2007–2014. Ontario Geological Survey, Miscellaneous Release—Data 283–Revised.

Hazlett, P. W., Rutherford, G. K. and Van Loon, G. W. 1984. Characteristics of soil profiles affected by smelting of nickel and copper at Coniston, Ontario, Canada. Geoderma, 32: 273-285. https://doi.org/10.1016/0016-7061(84)90007-7

Henderson, P.J. and McMartin, I. 1995. Mercury distribution in humus and surficial sediments, Flin Flon, Manitoba, Canada. Water, Air, and Soil Pollution, 80: 1043-1046. https://doi.org/10.1007/BF01189763

Kettles, I.M. and Shilts, W.W. 1994. Composition of glacial sediments in Canadian Shield terrane, southeastern Ontario and southwestern Quebec. Geological Survey of Canada, Bulletin 463, 58 p. https://doi.org/10.4095/194485

Kettles, I.M., Rencz, A.N. and Friske, P.B.F. 2008. The North American Soil Geochemical Landscapes Project - A Canadian Perspective. Explore: Newsletter of the Association of Exploration Geochemists 141: 12-22.

Kettles, I.M., Shilts, W.W. and Coker, W.B. 1991. Surficial geochemistry, south-central Canadian Shield: implications for environmental assessment. In Rose A.W. and Taufen, P.M. Eds. Geochemical Exploration 1989, Journal of Geochemical Exploration, 41: 29-57. https://doi.org/10.1016/0375-6742(91)90073-4

Knight, R.D. and Henderson, P.J. 2006. Smelter dust in humus around Rouyn-Noranda, Québec. Geochemistry: Exploration, Environment, Analysis, 6: 203-214, https://doi.org/10.1144/1467-7873/05-087

Kjarsgaard, B.A., Sharpe, D.R., Knight, R.D., Stepner, D., and Russell, H.A.J. 2017. Newmarket Till Aquitard: Optimum grain packing with a pore-filling Calcite-rich cement. In Russell, H.A.J., Ford, D., Priebe, E.H., and Holysh, S. compilers. Regional-scale groundwater geoscience in southern Ontario: an Ontario Geological Survey, Geological Survey of Canada, and Conservation Ontario Geoscientists open house; Geological Survey of Canada, Open File 8363, 62 p. https://doi.org/10.4095/306472

Koljonen, T. and Malisa, E. 1991. Solubility in aqua regia of selected chemical elements occurring in the fine fraction of till. Environmental Geochemistry in Northern Europe, Geological Survey of Finland, 49-52.

McCallum, B.A. 1992. A gamma spectroscopy analysis of the distribution of 226Ra in Ontario Soils-a preliminary study. Low-Level Radioactive Waste Management Office, AECL Research, 26 p.

McIntosh, J.C. and Walter, L.M. 2006. Paleowaters in Silurian-Devonian carbonate aquifers: geochemical evolution of groundwater in the Great Lakes region since the Late Pleistocene. Geochimica et Cosmochimica Acta, 70: 2454–2479. https://doi.org/10.1016/j.gca.2006.02.002

Ontario Geological Survey. 1991a. Bedrock geology of southern Ontario. Ontario Geological Survey, Map 2544, scale: 1:1,000,000.

Ontario Geological Survey, 1991b. Quaternary Geology of southern Ontario. Ontario Geological Survey, Map 2556, scale: 1:1,000,000.

Ontario Ministry of Environment and Energy. 1993. Ontario typical range of chemical parameters in soil, vegetation moss bags and snow (version 1.0a, April 1994). Phytotoxicology section, Standards Development Branch, 212 p.

R. 2017. The R Project for Statistical Computing. https://www.r-project.org/ (accessed July 12, 2017).

Reimann, C. and Garrett, R.G. 2005. Geochemical background - Concept and reality. Science of the Total Environment, 350: 1-3, 12-27. https://doi.org/10.1016/j.scitotenv.2005.01.047

Reimann, C., Filzmoser, P. and Garrett, R.G. 2005. Background and threshold: critical comparison of methods of determination. Science of the Total Environment, 346: 1-3, 1-16. https://doi.org/10.1016/j.scitotenv.2004.11.023

Sanford, B.V. and Baer, H.J. 1971. Bedrock geology of southern Ontario. Geological Survey of Canada, Map 1335A.

Sharpe, D.R., Klassen, R.A., Russell, H.A.J., Brennand, T.A., Dexter, K., Logan, C., and Stepner, D.A.J. 2019. Regional Geochemical Survey of Earth Materials in Southern Ontario: A Geochemical Baseline for Environmental and Human Health Protection; Geological Survey of Canada, Open File 8257, 1 zip file. https://doi.org/10.4095/308373

Shilts, W.W. 1978. Nature and genesis of mudboils, central Keewatin, Canada. Canadian Journal of Earth Sciences, 15: 7, 1053-1068. https://doi.org/10.1139/e78-113

Shilts, W.W. 1984. Till geochemistry in Finland and Canada. Journal of Geochemical Exploration, 21: 95-117. https://doi.org/10.1016/0375-6742(84)90037-2

Shilts, W.W. and Kettles, I.M. 1990. Geochemical-mineralogical profiles through fresh and weathered till. In Kujansuu, R. and Saarnisto, M. Eds. Glacial Indicator Tracing, Rotterdam, A. A. Balkema, 187-216.

Snäll, S. and Liljefors, T. 2000. Leachability of major elements from minerals in strong acids. Journal of Geochemical Exploration, 71: 1, 1-12. https://doi.org/10.1016/S0375-6742(00)00139-4

Tarvainen, T. and Paukola, T. 1998. Use of geochemical database to delineate risk areas. Journal of Geochemical Exploration, 64: 1-3, 177-184. https://doi.org/10.1016/S0375-6742(98)00031-4

An analytical protocol for determining the elemental chemistry of Quaternary sediments using a portable X-ray fluorescence spectrometer

Ross D. Knight*, Bruce A. Kjarsgaard, Daniel A.J. Stepner, and Hazen A.J. Russell

Abstract: Advances in portable X-ray fluorescence (pXRF) technology have resulted in the ability to collect high-quality geochemical data for sediments at a fraction of the cost of traditional laboratory methods. The analytical quality of pXRF derived geochemical data is dependent on numerous factors including sample heterogeneity, grain size, moisture content, sample thickness, and instrument specifications such as power parameters, X-ray tube type, and dwell time. In order to ensure precise and accurate results using a pXRF spectrometer an analytical protocol has been developed using reference materials and prepared Quaternary sediments. This protocol considers 1) Sample preparation, 2) Analysis, and 3) Data compilation/presentation.

Although the pXRF spectrometer provides concentrations for 41 elements it has been determined that only a subset of these elements meet the criteria for near definitive, quantitative, and qualitative data. Although the analytical protocol is robust, sample collection and preparation is still the key to a successful geochemical study. A significant advantage of pXRF technology is the opportunity to refine sampling strategies in near real time and the ability to add additional samples to a project with little budget increase.

1. Introduction

Geochemistry is an established branch of geoscience and has become a common tool in mineral and hydrocarbon exploration, and environmental remediation. Geochemical data provides critical information to the understanding of geology and the environment. As the cost of traditional laboratory geochemical analysis can be beyond the scope of many regional surficial geology projects (i.e., comprehensive aqua regia, plus multi acid, plus fusion digestions followed by ICP—MS/ES, at ~90–100$/sample), alternative methods of analysis where cost is not a barrier are required.

Advances over the past 20 years in portable X-ray fluorescence (pXRF) technology have resulted in the ability to collect geochemical data for a suite of elements ranging in atomic masses from magnesium (Mg) to uranium (U). Although there have been over 200 peer-reviewed journal papers published on the use of pXRF technology in the geosciences, few provide details on methods and techniques used for precise and accurate data acquisition (see Fisher et al. 2014; Gazley et al. 2014). As the analytical quality of pXRF derived geochemical data is dependent on numerous factors including sample heterogeneity, grain size, moisture content, sample thickness, and instrument specifications such as power parameters and X-ray tube type the development of a robust analytical protocol is vital to any successful application.

Utilizing pXRF technology complemented by analyses using traditional laboratory geochemical methods, the Groundwater Program at the Geological Survey of Canada (GSC), in a collaborative effort with Ontario Geological Survey, Conservation Authorities, and universities have undertaken the analyses of 3815 unconsolidated surficial sediment samples collected from 53 boreholes across southern Ontario (Table 1). To date, this is the largest, and possibly first, comprehensive subsurface study to examine the geochemistry of unconsolidated surficial sediments within the southern Ontario Quaternary basin. In order to assure compatibility of these data with future studies, both a sample collection protocol and an analytical protocol were developed, tested, and modified between 2010–2018, building upon previous research on precision, accuracy, instrument drift, dwell time optimization, and calibration (Knight et al. 2013).

This paper summarises results obtained from the analyses of a series of Certified Reference Materials (CRMs) and Standard Reference Materials (SRMs) to define the pXRF

Geology Survey of Canada, Natural Resources Canada, 601 Booth Street, Ottawa, ON K1A 0E8

*corresponding author: ross.knight@canada.ca

Recommended citation: Knight, R.D., Kjarsgaard, B.A., Stepner, D.A.J., and Russell, H.A.J. 2020. An analytical protocol for determining the elemental chemistry of Quaternary sediments using a portable X-ray fluorescence spectrometer. In Russell, H.A.J. and Kjarsgaard, B.A. Eds. Southern Ontario groundwater project 2014–2019: summary report. Geological Survey of Canada, Open File 8536, 95-107. https://doi.org/10.4095/321095

Table 1. Summary of southern Ontario boreholes and associated open file reports with geochemical analysis completed as part of a regional geochemical framework. Geochemical data from boreholes by pXRF methods are referenced in the right hand column. The following short form names under Source agency refer to GSC – Geological Survey of Canada, OGS – Ontario Geological Survey, CAMC – Conservation Authorities Moraine Coalition, UTRCA – Upper Thames River Conservation Authority, CLOCA – Central Lake Ontario Conservation Authority, U of Guelph – University of Guelph, U of Ottawa – University of Ottawa.

Borehole Name	Borehole ID	Easting	Northing	Depth (m)	Source Agency	Number of samples	pXRF	Laboratory Chemistry	Reference
Aurora	GSC-BH-AUR-01	626120	4871860	141	GSC	120	120	32	Knight et al., 2015a
Brantford-Woodstock	BW-07-05	504440	4784065	67.2	OGS	44	44	42	Knight et al., 2018c
	BW-07-06	516750	4766800	79.7	OGS	53	53		
	BW-07-07	527089	4764908	61.6	OGS	42	42		
	BW-07-09	510649	4761686	55.1	OGS	40	40		
	BW-07-15	542576	4773875	38.4	OGS	35	35		
	BW-07-17	537484	4783222	61.2	OGS	43	43		
	BW-07-20	559256	4789517	65.8	OGS	34	34		
	BW-08-06	500814	4762673	36.2	OGS	29	29		
Clarington	GSC-BH-CLA	672905	4872453	127	U of Guelph	96	96		Knight et al., 2016d
Dundas Valley	DV-05	541105	4800483	103.1	OGS	60	60	94	Stepner et al. 2018
	DV-06	518276	4814982	78.2	OGS	94	94		
	DV-08	520975	4812880	75.7	OGS	81	80		
Gads Hill	GH-10-01	509313	4812153	56.9	OGS	40	40		Knight et al., 2018b
GTA – Grasshopper	GSC-BH-GHP-01	679505	4879974	139.8	CAMC / GSC	185	185		Knight et al., 2018a
GTA – Kleinburg	GSC-BH-KLN-01	608497	4859678	104.9	CAMC / GSC	162	162		
GTA – Mount Albert	GSC-BH-MTA-01	635892	4886251	98.9	CAMC / GSC	92	92		
GTA – Pontypool	GSC-BH-PON-01	689068	4886446	171.1	CAMC / GSC	150	150		
GTA – Rice Lake	GSC-BH-RLK-01	735964	4887130	181.6	CAMC / GSC	170	170		
High Park	GSC-BH-HPK-01	624104	4834313	43.8	CAMC / GSC	58	58		Knight et al., 2015b
Strathroy	GSC-BH-SRY	448621	4751759	68.7	UTRCA / GSC	118	118		
London, Westminster	GSC-BH-WMR	484324	4754562	70.5	UTRCA / GSC	108	108		
Niagara Peninsula	BH13-NP-2014	628215	4749786	45.7	OGS	47		47	
	BH14-NP-2014	640187	4756676	42.1	OGS	38		38	
	BH27-NP-2014	633076	4758904	51.1	OGS	52		52	
	BH32-NP-2014	619599	4746591	46.4	OGS	41		41	
	BH33-NP-2014	638538	4777117	53.1	OGS	48	48		
	BH59-NP-2015	591658	4776011	42.2	OGS	39	39	22	
	BH77-NP-2015	562792	4762132	33.25	OGS	27	27		

Table 1. *continued.*

Borehole Name	Borehole ID	Easting	Northing	Depth (m)	Source Agency	Number of samples	pXRF	Laboratory Chemistry	Reference
Orangeville	BH09-OF-2008	553171	4852413	52.8	OGS	46		46	
	BH20-OF-2009	561002	4863630	22.5	OGS	25		25	
	BH23-OF-2009	568074	4864148	74.4	OGS	66		66	
	BH25-OF-2009	553103	4832245	31.7	OGS	29		29	
	BH27-OF-2009	561045	4834791	46.7	OGS	38		38	
	BH43-OF-2010	549394	4829200	36.7	OGS	43		43	
Oro	BH-30-AKB-2006	612147	4943667	54.9	OGS	66		66	
	BH-32-AKB-2006	609032	4928931	70.5	OGS	61		61	
	BH-37-AKB-2006	610966	4927024	102.1	OGS	94		94	
Pickering	GSC-BH-PIK1	657068	4867918	71.6	GSC/CAMC/ U of Ottawa	97	97	97	
	GSC-BH-PIK2	657061	4867916	11.4	GSC/CAMC/ U of Ottawa	14	14	14	
Purple Woods	GSC-BH-PWD	666973	4878158	151.8	CLOCA / GSC	135	135		Knight et al., 2016a
Queensville	GSC-BH-QUE	626499	4889266	96.2	CAMC / GSC	87	87	32	Knight et al., 2016b
South Simcoe	SS-12-02	602163	4902748	161.2	OGS	98	98	98	Knight et al., 2018d
	SS-11-04	586055	4878237	124.4	OGS	86	86		
	SS-11-08	590082	4894188	145.6	OGS	91	91		
	SS-12-03	593299	4906003	91.1	OGS	48	48		
	SS-12-04	610758	4905514	153.9	OGS	85	85		
	SS-12-07	612194	4877514	95.2	OGS	60	60	60	
	SS-12-08	604560	4890531	68.7	OGS	40	40		
	SS-13-06	612674	4896493	174.4	OGS	138	138		
Warden	2010-WAR	638868	4840084	80.5	CAMC / GSC	119	119	37	Knight et al., 2016c
Waterloo	OGS-03-04	526733	4809858	292	OGS	57		57	
	OGS-03-05	515170	4816991	244	OGS	46		46	

analytical protocol for surficial sediments that includes 1) Sample preparation, 2) Analysis, and 3) Data compilation and presentation (Figure 1). Prior to discussion of the protocol a brief overview of pXRF instrument characteristics including analytical parameters, optimal dwell time, and potential instrument drift is presented to provide background information on key aspects of the protocol.

2. Portable XRF instrument characteristics

Glazman and Closs (2007) and Lemiere (2018) summarize the development of early instruments and their transition to a mainstream geochemical analytical tool. Portable XRF spectrometry analyses a sample via an X-ray beam (emitted by interaction of an electron beam with an anode), a Silicon Drifted Detector (SDD), and an amplifier combined with a multi-beam analyser. The ability of the detector to separate different energy levels and to minimize spectral interferences defines the resolution of the collected data. All pXRF instruments use filter settings to help differentiate elements and associated peak overlaps. Filter settings utilize a combination of voltage, current, and a series of stacked metal foil plates placed between the X-ray tube and the sample to isolate specific regions of the energy spectra. Each

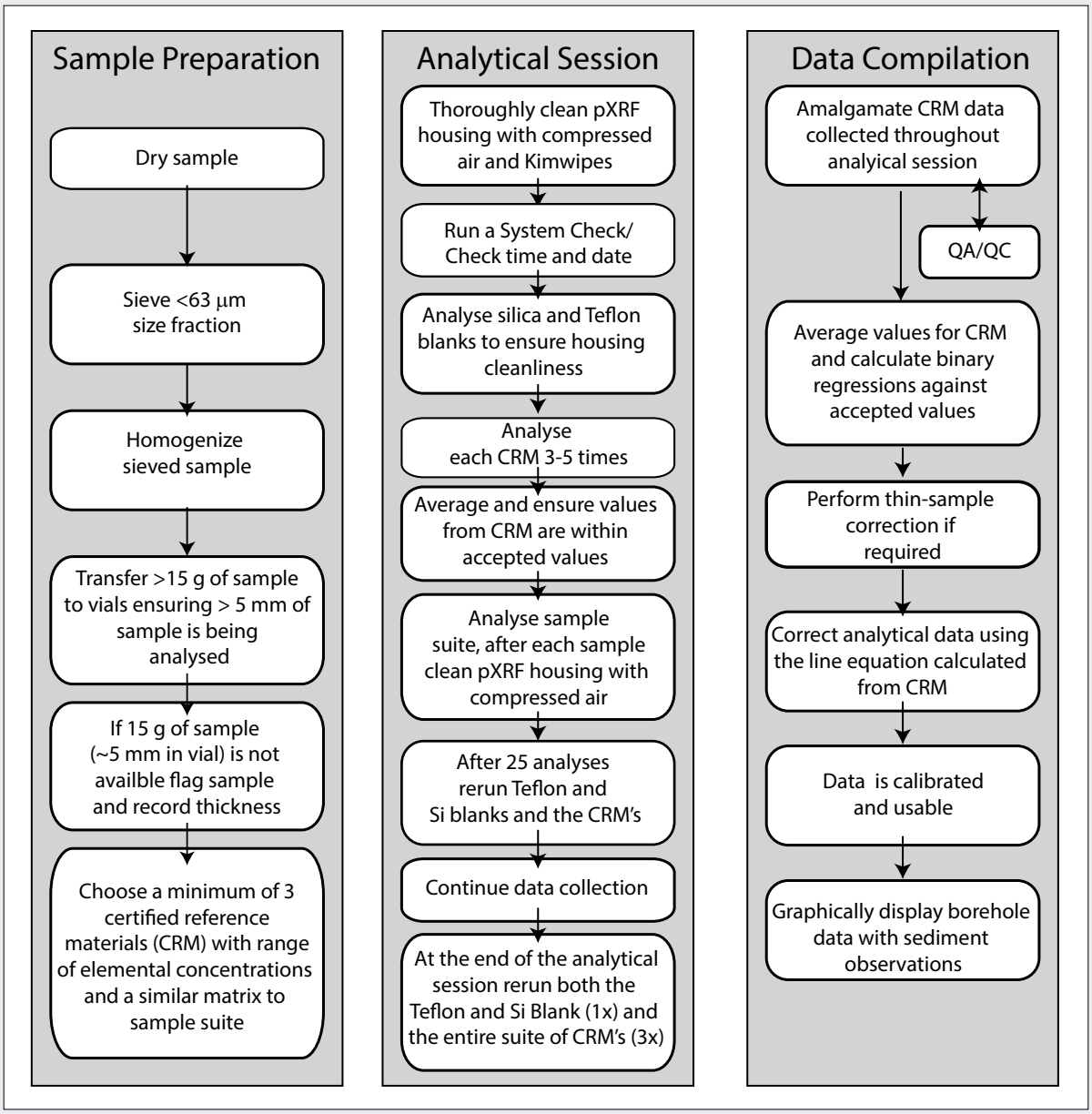


Figure 1. Protocol flow chart to ensure precise and accurate data collection using pXRF methods.

filter eliminates X-rays outside a specific region of the energy spectra and contributing to background noise at the detector. To increase accuracy and precision while maximizing the efficiency of elemental detection, a combination of variable X-ray kV intensities and filters are used. Most instruments have two factory calibrated analytical modes, termed 'Soil Mode' and 'Mining Mode'. Soil Mode uses Compton normalization, an algorithm based on a certified standards measured results versus the Compton peak produced from incoherent backscatter radiation; Soil Mode is used for elements expected to occur with <1% concentration (trace elements). Potts and Webb (1992) show that normalization to the Compton peak is less effective when measuring elements occurring above 2–3%. According to Conrey et al. (2014), Compton normalization is ideal for heavy elements with simple matrices, but is difficult to apply to light elements. To detect elements expected to exceed 1% concentration (major elements) Mining Mode and Fundamental Parameters, which measures the internal detector's response to pure elements, is used. Fundamental parameters utilizes X-ray physics and applies corrections for overlapping peaks and matrix differences (Figura 1987; Murphy et al. 2010).

In this study, a NITON XL3t GOLDD spectrometer manufactured by Thermo Scientific, was mounted in a manufacturer-designed test stand for analyses carried out as part of the southern Ontario

groundwater program. Table 2 lists the physical parameters of the instrument. The NITON instrument is equipped with 4 filters; High and Main (50kv/40μA max) differentiated by filter material composition and thickness, Low (20kv/100μA max), and Light (8kv/200μA max). Data were collected in 2 factory pre-set modes; Soil Mode, with data collected with a 60 second dwell (total count) time per filter (Main, Low, High), and Mining Mode Cu/Zn with data collected with a 45 second dwell time per filter using 4 filters (Main, Low, High, Light). Data collection utilized an un-collimated 8 mm window width with NITON pre-set factory specification calibrated to convert counts to concentration.

3. Analytical parameters

Limitations of pXRF include difficulty in the analysis of elements lighter than sodium (Na), due to adsorption of their X-rays by air. In order to increase the detection efficiency for lighter elements such as Al and Mg, a vacuum or helium purge reduces the density of the medium between the spectrometer window (Kapton tape) and the detector, thereby minimizing adsorption by air. Choosing an appropriate electron voltage for the elements of interest will partially address problematic peak overlaps. An example of this is shown in Table 3, where As and Pb overlap Kα and Lα peaks, and Ba and Ti overlap Lα and Kα peaks. In general, the energy required to move an electron from a K or L shell is twice the energy of the desired spectral line. Choosing an instrument with a 50 kV tube voltage compared to a 40 kV tube voltage allows for enhanced differentiation of Ba from Ti using the Ba Kα peak at 32 keV, and provides a lower limit of detection for Ba compared with a 40 kV instrument (Knight et al. 2013; and Hughes and Barker 2017). For some elements (e.g., Ca and Sc, Table 3), peak overlap cannot be differentiated and these data have to be examined for accuracy. Stanley (2009), Conery et al. (2014), and Gallhofer and Lottermoser (2018) discuss in detail the effects of peak overlaps on accuracy.

Table 2. Specifications of the pXRF spectrometer used in this study.

Manufacturer	Thermo Scientific
Model	NITON XL3t GOLDD
Design year	2008
Excitation source	2W Ag tube
Voltage and current	6-50kV 0-200 uA
Detector	25 mm^2 SDD
Throughput	180,000 cps
Pressure/Temp compensation	Yes
Spot size	8 mm
Filters	4
Beam Path	Air
Elemental range	Mg - U
Internal Camera	Yes
PC operating system	Windows 7
Data entry	Touch screen
Data storage	128 MB
Internal memory	10,000 readings with spectra
Data transfer	USB

4. Dwell time

Quantification and effective elimination of instrument-generated background noise from the sample signal is a limiting factor in all analytical methods. Varying analytical dwell time addresses the assessment of precision for element detection versus background effects. NITON defines dwell time for their pXRF spectrometers as the duration of time for which the sample is analysed by the pXRF under a single filter in a single mode. Data collection below a "minimum" dwell time results in a reduction of precision, whereas collection of data above this "minimum" dwell time should increase precision (Berger et al. 2009; Knight et al. 2013). For studies incorporating hundreds or thousands of analyses, an optimum dwell time becomes important for a timely and cost effective procedure. In order to assess an optimal dwell time, a suite of 4 CRMs and SRMs was analysed for between 5 and 80 seconds per filter in Soil Mode (Knight et al. 2013).

Table 4 lists an example of increased precision with increased dwell time for CRM Till-1 lead (Pb) concentrations. At a dwell time of 5 seconds, Pb is 432 ppm with a RSD of 12% and a

Table 3. Examples of peak overlaps for a selection of elements.

Element	Line	Energy (keV)	Line	Energy (keV)
As	K_α	10.54	K_β	11.73
Pb	L_α	10.55	L_β	12.61
Ba	L_α	4.47	K_α	32.19
Ti	K_α	4.51	K_β	4.93
Ca	L_α	0.34	K_α	3.69
Sc	L_α	0.39	K_α	4.09

Table 4. Variable dwell times with mean Pb concentration, mean error of ±2σ and %RSD for CRM-NIST 610 in Soil mode. Recommended Pb concentration is 426 ppm with a limit of detection of 8 ppm.

Reference material	Dwell time/filter seconds	# of analyses	Pb average concentration ppm	Pb average uncertainty ±2σ ppm	%RSD
NIST 610	5	171	432	99	12.02
NIST 610	10	115	429	41	4.87
NIST 610	20	116	425	24	3.31
NIST 610	30	112	424	19	2.6
NIST 610	40	104	426	16	2.11
NIST 610	50	176	424	15	2.52
NIST 610	60	111	426	13	1.72
NIST 610	70	105	426	12	1.7
NIST 610	80	117	417	12	4.39

corresponding uncertainty (±2σ) of 99 ppm. With an increase in dwell time from 10 to 70 seconds at ten second intervals, the RSD decreases from 4.87 to 1.7% with uncertainty decreasing from ±41 to ±12 ppm (±2σ). The effect of different pXRF dwell times for Zr concentrations (Figure 2) are consistently higher than the recommended value (dashed line). Fisher et al. (2014) summarises that precision increases as a function of the square root of the dwell time. However, increasing dwell time beyond a certain point for some elements may result in erroneous data, as shown in Figure 3 for Ca, determined on CRM NIST610. The optimum dwell time for unconsolidated silicate-matrix CRMs and SRMs as determined by Knight et al. (2013) corresponds to 30–40 seconds per filter. This dwell time optimizes sample throughput without compromising precision. For many elements, increasing dwell time does not increase accuracy. This demonstrates the need to assess the optimal dwell time that warrants fit for purpose results for any given study prior to initiating analyses.

5. Instrument drift

In analytical geochemistry, data collection instruments can experience 'drift' (defined by a continuous or incremental change in results over time periods that may be as short as a few hours or as great as a year (e.g., Ryan et al. 2017; Young et al. 2016). This drift can be associated with many variable factors such as a change in analytical conditions including temperature, humidity, and air pressure. A study was carried out to assess the NITON pXRF instrument drift over a daily, weekly, monthly and yearly time periods by analyzing and interpreting a suite of CRMs and SRMs data (Knight et al. 2013; Landon-Browne et al. 2017). Collected data demonstrate that over time most elements have some variation in concentration. However, most of these variations are within the uncertainty of the data collected within a typical multi week project (Figure 4). This study also demonstrated that for some elements, such as for U (Figure 5) drift in measured data can be significant even over a few hours. Examination of instrument drift obtained from data collected in isolation over periods of up to several months demonstrated that some elements have no drift, some minor drift, and others significant drift (Table 5; Landon-Browne et al. 2017).

As part of the pXRF protocol development for the chemical characterization of samples collected between 2010 and 2018, approximately 8600 analyses of CRM/SRMs associated with eleven different projects were analysed using the same NITON instrument. For these analyses, the X-ray tube was replaced twice, resulting in three X-ray tubes being employed during the study. Figure 6 shows results for Ca and Zr obtained from CRM Till-4 plotted as box and whisker diagrams. Between December 2009 and January 2011, Ca and Zr determined on the same samples using two different X-ray tubes varied considerably. In late 2011 the second X-ray tube failed and was replaced with a new third tube that returned similar results to the second X-ray tube (Figure 6). Examination of the data indicates that there can be significant instrument drift over time, and between different X-ray source tubes placed in the same instrument. However, there is only minor drift within a narrow analytical time period (i.e., a single project, analysed in <1 month), suggesting that samples from a given project should be analysed in as short a time period as possible (Landon-Browne et al. 2017). Analysing 30–40 samples in one day should produce more precise results than analyzing 10 samples/week until all analyses are completed. Our studies also indicate the importance of analysing an identical suite of CRMs and SRMs for any project, as well as reference materials (CRMs and SRMs) specific to an individual project. This ensures that data

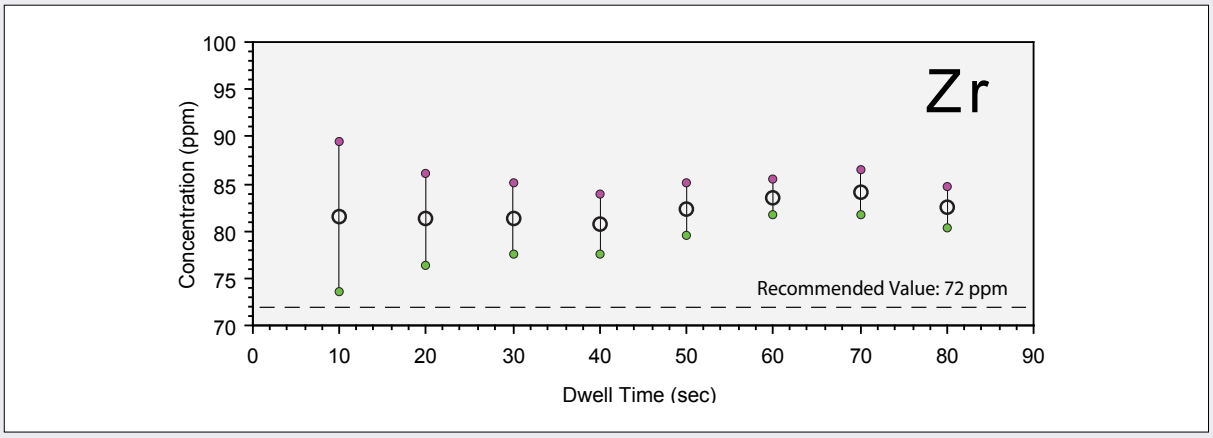


Figure 2. Variable dwell times with mean Zr concentration for SRM-DLH 7. Open circles represent the mean of ~110 analyses. Solid red and green dots represent the mean uncertainty of ±2σ. The recommended value for Zr is shown by the dashed horizontal line.

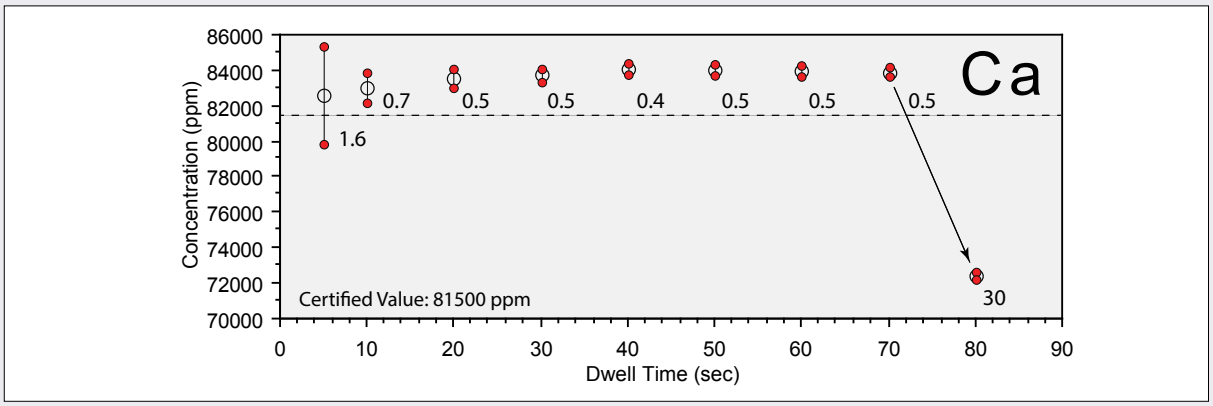


Figure 3. Variable dwell times with mean Ca concentration for CRM-NIST 610. Open circles represent the mean of ~110 analyses. Solid red dots represent the mean uncertainty of ±2σ. %RSD value is (number) is presented next to each set of data. The recommended value for Ca is shown by the dashed horizontal line.

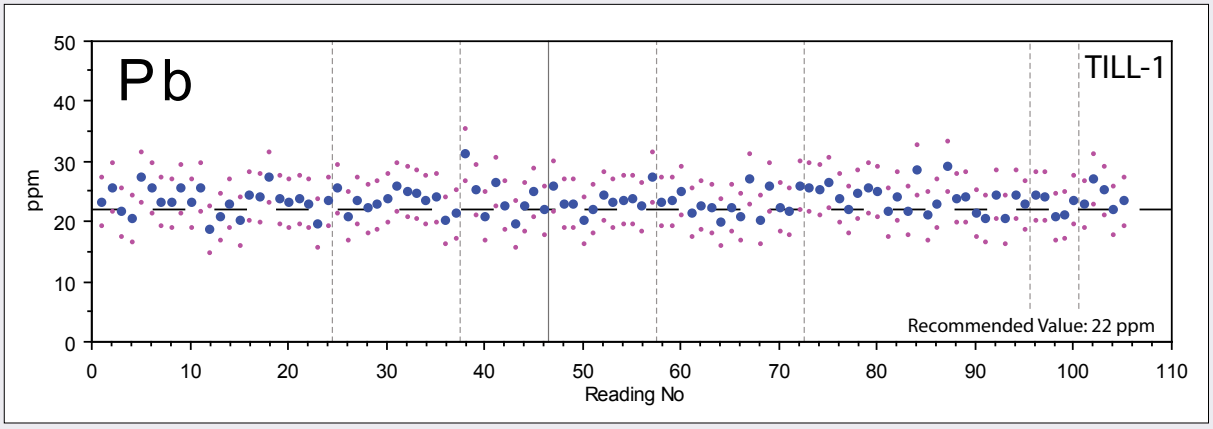


Figure 4. Lead analyses for Till-1 in Soil mode with a dwell time of 60 seconds per filter. Blue dots are the analyses with red dots representing the uncertainty of ±2σ. The recommended value of 22 ppm for Pb is shown by the dashed horizontal line. The solid vertical line at reading 46 indicated the spectrometer was turned off for a period greater than 24 hours. The vertical dashed lines indicated that the spectrometer was turned off for several hours.

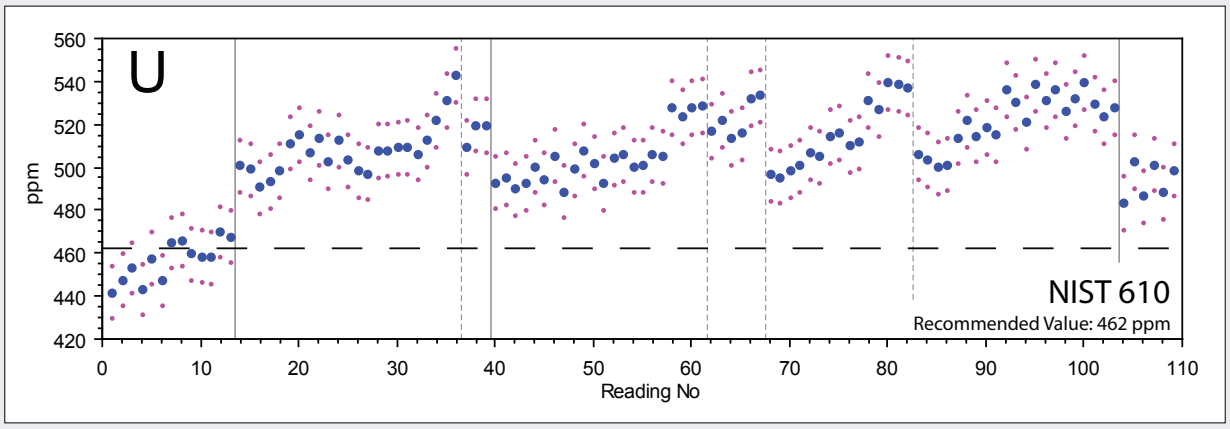


Figure 5. Uranium analyses for NIST 610 in Soil mode with a dwell time of 60 seconds per filter. Blue dots are the analyses with red dots representing ±2σ. The recommended value of 462 ppm for U is shown by the dashed horizontal line. The solid vertical lines at reading 14, 40, and 104 indicated the spectrometer was turned off for a period greater than 24 hours. The vertical dashed lines indicated that the spectrometer was turned off for several hours.

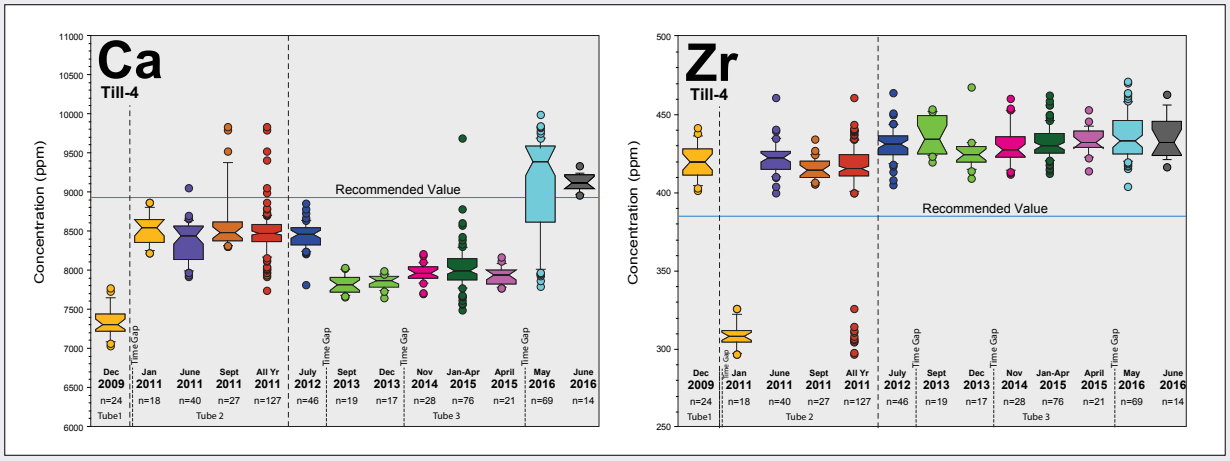


Figure 6. Box and whisker diagrams for Ca and Zr values obtained from CRM Till-4. The recommended value is shown by the solid horizontal line. The vertical dashed lines indicated analyses carried out using 3 different X-ray tubes. Short vertical dashed lines indicate significant time gaps when the spectrometer was not in operation.

from each project can be cross-calibrated for analytical drift between projects using a common suite of reference materials.

6. A pXRF analytical protocol for surficial sediments

The following analytical protocol as outlined in Figure 1 has been refined since 2010 to ensure precise and accurate results using a pXRF spectrometer.

6.1 Sample preparation

Portable XRF studies carried out on surficial sediments by Plourde et al. (2012, 2013) demonstrate that direct (e.g., outcrop, drillcore) analysis does not provide viable results due to a high degree of variability in grain size (e.g., clay–silt–sand and gravel content). Consequently unconsolidated sediment samples should first be air-dried to reduce X-ray attenuation from moisture content and subsequently, gently disaggregated with an agate mortar and pestle and sieved to <63 µm (silt and clay size fraction). The sediment is placed in a 2 cm in diameter by 5 cm in height plastic vial and covered with 4 µm thick Chemplex® Prolene®film held in place by an elastic band. A study carried out by Knight et al. (2012) concluded that Prolene®film surpassed Mylar for both accuracy and precision. Wilson et al. (1999) suggests that the decreased density of Prolene®film allows the same thickness of material to have less absorption, resulting in better detection of elements in the low keV range. Portable XRF spectrometry is a surface to near-surface analytical technique where primary X-ray radiation penetrates the sample to a depth known as the depth of excitation, or penetration depth (PD). Further to the PD there is an escape depth or critical penetration depth

Table 5. List of elements that display significant, minor, or no drift in concentration over time.

Elements that may exhibit significant drift	Elements that exhibit minor drift	Elements that exhibit little to no drift
Ca	Ba	As
Fe	Co	Cs
K	Cr	Ni
Ti	Cu	Pb
U	Mn	Rb
	Mo	Sr
	Zr	Th
		V
		W
		Zn

(CPD) that is defined by the thickness of the sample that will account for 99% of the returned fluorescence. Samples prepared for pXRF analysis must have sufficient thickness to be infinite in terms of X-ray penetration. This infinite thickness corresponds to the thickness of a sample where the analyzer returns a result that will not change if a thicker sample is analysed. Compacting the sediment sample provides an increase in density at the sample surface, i.e. the interface with the X-ray beam, and hence more X-ray beam interaction with the sample. The denser the sample, the less thickness of material required for infinite thickness. Temporary storage of samples once prepared for analyses will undergo granular convection partially differentiating silt from clay. Since pXRF is a near surface technique, homogenization of the sample prior to analyses is crucial to the characterization of the bulk composition, especially for light elements (Huntley 2012).

Landon-Browne et al. (2017) demonstrated that a minimum thickness of ≥5 mm of <63 µm sediment in a 2cm diameter vial is sufficient to obtain reproducible data for unconsolidated surficial sediments. This study verifies the earlier research carried out by Kalnicky and Singhvi (2001), who concluded that to be infinitely thick 5 mm of soil was required. There are instances when very little <63 µm size sample material is recovered from surficial sediments that are predominantly coarse sand or gravel. Results for some elements obtained from samples of insufficient thickness will be inaccurate as demonstrated by Landon-Browne et al. (2017).

6.2 Analysis

Prior to any analytical session a system check and time check should be carried out followed by cleaning the pXRF analytical environment is a key component for accurate results thus, the pXRF equipment should be cleaned with compressed air and KimWipes, with care being taken not to damage the Kapton tape sealing the analytical window of the pXRF. In order to test the cleanliness of the test stand window and safety housing a Teflon disk and silicon (Si) blank are analysed at the start and finish of each day and after every ~20 samples. The Teflon disk is a solid material does not contain any elements detected by the pXRF and is not covered by any film interface between the sample and the instrument. However, the Teflon blank often returns values in the 10's of ppm for Ti and trace amounts of Mo. The Si blank, CRMs, SRMs, and the plastic vials used to hold these samples are covered with 4 µm thick Chemplex® Prolene®film. Often the SiO_2 blank returns values for Ca and Fe slightly above the limits of detection and occasionally returns values below the recommended limit of detection for Cd, Hg, K, Pd, Sr, and V in Soil Mode and Al in Mining Mode. To avoid any progressive contamination it is recommended that the Prolene®Film be replaced on a regular basis. If analysis of the Si or Teflon blanks return concentration levels of any element (especially at or near the detection limit for that element), thoroughly and carefully clean the test stand housing with compressed air and methanol and clean or replace the spectrometer window (Kapton tape) and rerun the blank samples.

To provide information on precision, accuracy, and for post data-collection corrected results, a suite (minimum of three) of CRMs, SRMs should be analysed routinely. Numerous studies have incorporated standards into their analytical protocol, but only a few studies have assessed pXRF precision and accuracy by carefully examining suites of reference materials (e.g., Morris 2009; Knight et al. 2013; Fisher et al. 2014; Piercey and Devine 2014; Simandl et al. 2014; Hughes and Barker 2017; Gallhofer and Lottermoser 2018). It is important to note that the CRMs, SRMs should have the same size fraction, matrix, and range of elemental concentrations as the samples being analysed during a specific project to minimize uncertainty. Each of the reference samples selected is analysed 3 times (reference samples A, B, C; repeat, A, B, C; repeat, A, B, C)

at both the beginning and end of each analytical session, and interspersed with the project samples being analysed (for larger sample suites). (Note the analysis of the reference samples is not A, A, A, then B, B, B, then C, C, C). If the data falls outside the acceptable values, replace the Chemplex® Prolene®film cover of the reference material and reanalyze the sample. Prolene covers are very susceptible to static charge and can attract fine particles when in storage or during sample preparation resulting in contamination. Analyses of project specific samples should only be initiated when the analyses of reference materials are within the published acceptable limits. After 20 analyses, the Teflon and Silica blanks, along with reference materials are analysed again, and verified to be within acceptable parameters before continuing with further data collection. At the end of the analytical session, the Teflon and Silica blanks are analysed once each and the reference materials analysed 3 times each. Table 6 lists values for Ca, Fe, Sr, Ti, and Zr in Soil and Mining Mode for Till-1, Till-4 and GSC standard TCA 8010 obtained during research projects using the NITON pXRF. If values are significantly different that those listed in Table 6 the pXRF should be cleaned and restarted to retest blanks and standards.

6.3 Data compilation and presentation

Save raw data from the pXRF as a primary reference file. Use copies of the raw data file for any subsequent post-analysis data correction, manipulation, plotting and interpretation. The pXRF can return values for elements that are less than the Limit of Detection (<LOD). For our chemostratigraphic plotting purposes, the value of the concentration reported as <LOD is entered as ½ the known LOD value (e.g., Grunsky 2009). When an element returns a value of <LOD, the uncertainty associated with that element is also reported and this uncertainty value should be deleted from the data set. Verify the run time of each analysis in the data file, as there are occasions when the pXRF will stop recording analyses after a few seconds. Examine the data for geochemical outliers, as occasionally reported data are considerably higher or lower than data acquired from similar samples in spatial proximity. These outliers should be checked and verified (i.e. re-analysed), and possibly deleted if there is no corroborating evidence for their validity. The NITON pXRF returns 2 decimal places for all elements even if detection limits are listed as integers. Adjust data decimal places to record the appropriate number of significant digits.

Table 6. Expected results in ppm from analysis of Till-1, Till-4, and TCA 8010 using a NITON Xl3t pXRF spectrometer.

Soil Mode

	Till-1	Till-4	TCA-8010
Ca	~18000	~7900	~13000
Fe	~41000	~34000	~14000
Sr	~425	~106	~265
Ti	~5600	~4900	~2375
Zr	~565	~425	~295

Mining Mode

	Till-1	Till-4	TCA-8010
Ca	~18300	~8700	~13600
Fe	~48600	~41600	~19500
Sr	~220	~85	~215
Ti	~5250	~4550	~2325
Zr	~440	~340	~230

Calibrations of pXRF data to known standards is typically carried out by entering a calibration slope and intercept (y=mx+b) into the pXRF spectrometer after running a suite of matrix-matched CRMs, SRMs prior to data-collection, or post data-collection by using software outside of the pXRF. If necessary, apply thin-sample correction factors prior to accuracy calibration. Accuracy can be further improved by collecting a subset of samples (~10%) with elemental abundances ranging from low to high concentrations for analyses using laboratory methods (multi acid and fusion). Comparing the laboratory data to the pXRF data produces a least-squares regression equation (y=mx+b) that can be used to calibrate the pXRF data for accuracy under the assumption that the laboratory methods are accurate.

During this study all data were calibrated post collection. In general, calibration adjustment is not necessary for all elements, and is often only necessary for those elements present at very high concentrations, e.g., well above 1% when measured in Soil Mode, or, low concentrations near the limit of detection. For many elements (e.g., Ba, Cr, Cu, K, Pb, Sr, and Zn) no calibration is required as the mean uncertainty of ± 2σ of the pXRF result corresponds to the recommended value of the CRM or SRM. Elemental concentrations of some elements (e.g., Fe) benefit from post-data collection calibration. Iron concentrations obtained from multiple measurements of Tills 1–4 during a study by Knight et al. (2013) determined that Fe exhibits a very high r^2 of 0.9999 and high precision (RSD = 0.6%), but was not accurate (m = 1.11). To post-correct Fe for accuracy, a least-squares regression and the correction equation: y = 0.90x + 6730 were utilized (where x is the measured concentration and y is the calibrated concentration). Ideally, linear equations should be valid for all concentrations, but, for very high concentrations, this may not be the case (i.e. the equations may be limited to concentrations near the analytical range). It should be noted that the Till 1–4 series of CRMs comprises sediments with a siliciclastic matrix, and thus the equations will not apply to sediments with a high carbonate or iron-oxide matrix.

Rowe et al. (2012) demonstrate that most CRMs are not adequate to capture the diversity of elements collected in geological materials. For this reason, prior to an extensive pXRF study of shales in north–central Texas, they produced a series of mudrock standards with a matrix and range of elemental concentrations similar to those expected in the samples to be analysed. Furthermore, Conrey et al. (2014) suggest that existing standard manufacturer-provided calibrations fail to take full advantage of the pXRF methodology and that further advances in the technology will be accomplished by utilizing specific calibrations for matrix-matched geological material. The process of post data collection calibration to a suite of CRMs/SRMs reduces the difference between individual standard analyses and the accepted values by an order of magnitude; i.e. 10's of percent difference prior to corrections reduced to <5% post calibration.

Numerous methods of evaluating data robustness are available in the geochemical literature for traditional laboratory wet chemical analyses. For environmental studies, the United States Environmental Protection Agency (US EPA) provides a method specific for pXRF spectrometry to evaluate data robustness utilizing a combination of the coefficient of determination (r^2), percent relative standard deviation (%RSD), and the slope of the regression line as outlined in US EPA method 6200 (US EPS 1998 2007). The method outlines parameters for the following data definitions:

1) definitive: $r^2 \geq 0.85$, RSD $\leq 10\%$, and y=x,
2) quantitative: $r^2 \geq 0.7$, RSD $< 20\%$, and y=mx+b,
3) qualitative: $r^2 < 0.7$, RSD $> 20\%$, and y=x has no relationship

For this study definitive with y=x is modified to near definitive with y=mx+b, qualitative is modified to r^2 <0.7–0.6, and a fourth classification is added to address elements that are detected but do not fall into any of the EPA classifications.

4) inconclusive: $r^2 \leq 0.6$ RSD >20%, and y=x has no relationship

In Soil Mode using a 60 second dwell time for each of three filters (total analytical time of 180 seconds per sample), 3126 analyses were carried out on a suite of 11 CRM/SRMs. In Mining Mode (Cu/Zn) using 45 seconds dwell time for each of four filters (total analytical time of 180 seconds per sample), 1834 analyses were carried out on the same suite of 11 CRMs/SRMs. Results of applying these analyses to the above-modified US EPA parameters for each element determined by pXRF spectrometry are summarized in Table 7. Elements listed as near definitive will most likely not benefit from post data collection correction for improved accuracy, whereas elements listed as quantitative and qualitative will benefit from this type of data processing. Elements classified as inconclusive either display a broad range of results and thus are difficult or impossible to calibrate, or returned a result below the limit of detection (<LOD). Depending on the concentration of an element in the sample (which is matrix dependent), the location of that element in Table 7 will vary.

7. Discussion

An analytical protocol for determining the elemental chemistry of Quaternary sediments using a portable X-ray fluorescence spectrometer has been developed using a suit of CRM/SRM,s. The protocol (Figure 1) outlines how to collect high-quality data using the pXRF at a fraction of the cost of traditional laboratory methods (using a combination of multi acid and fusion digestion methods with ICP—MS/ES analyses). The pXRF provides elemental concentrations for 33 elements in Soil Mode and 41 elements in Mining Mode. By applying modified criteria for data quality as outlined in US EPA method 6200, it has been determined that only a subset of these elements meet the criteria for near definitive, quantitative, and qualitative data (Table 6). Build on comments by others (e.g., Rowe et al. 2012), Rouillon and Taylor (2016) state for the first time in the published literature that "Individual recoveries of soil reference materials by both ICP—AES and pXRF showed that pXRF was equivalent to or better than ICP—AES for all but two elements, nickel (Ni) and arsenic (As)".

Table 7. Modified classification scheme for data precision and accuracy.

Mode	Near Definitive $r^2 \geq 0.85$, RSD $\leq 10\%$, y = mx + b	Quantitative $r^2 \geq 0.7$, RSD $< 20\%$, y = mx + b	Qualitative $0.6 < r^2 < 0.7$, RSD $> 20\%$, y = mx + b	Inconclusive $r^2 \leq 0.6$, RSD $> 20\%$, $y \neq x$
Soil	Ca, Fe, Rb, Sr, Ti, Zn, Zr	As, Ba, Cu, K, Mn, Pb, V	Cr, Mo, S, Se, Th, U	Ag, Au, Cd, Co, Cs, Hg, Ni, Pd, Sb,(Sc) Sn, Te, W
Mining Cu/Zn	K, Ba, Ca, Fe, Rb, Sr, Ti, Y, Zn, Zr	As, La, Mn, Pb, S, U, W	Cu, Mo, Th	Ag, Al, Au, Bi, Cd, Ce, Cl, Co, Cr, Mg, Nb, Nd, Ni, P, Pr, Sb, Se, Si, Sn, V

This technology opens up new frontiers in geochemical studies by providing elemental analyses of unconsolidated surficial sediments that are rarely if ever used in groundwater studies. Although the analytical protocol is robust, sample collection and preparation is still the key to a successful geochemical study. According to Craigie (2018), the primary failure of many geochemical studies is inadequate sampling and preparation techniques. Improper sampling will lead to poor results and erroneous interpretation of data. For unconsolidated surficial sediment boreholes (e.g., glacial till, glaciofluvial sands, lacustrine silt and clay etc.) two samples per drill run (1.53 m or 5 feet) provides robust results, even if the sediment being sampled is the same composition as the runs below or above (see references in Table 2). Collection of the first sample occurs at 20–30 cm, from the base of the run with the second sample at 110–130 cm, from the base of the run. Significant lithological units between these depths are also collected. A major advantage of pXRF technology is the opportunity to refine sampling strategies in near real time and the ability to add additional samples to a project with little budget increase.

In summary, pXRF allows for rapid, cost effective and reliable geochemical characterization of unconsolidated surficial sediment samples. The application of this technology is most useful in conjunction with traditional geological observations and other geological tools such as geophysical surveys and mineralogy studies.

8. Acknowledgements

The following students carried out various aspects of the data analyses: A. Landon-Browne, E. Holdsworth, M. Macquistan, M. Moroz, A. Plourde, A. Reynen, and L. Valiquette. The authors appreciate the comments toward improving the manuscript provided by internal GSC reviewers S. Jackson and P. Pelchat. The analytical work occurred at GSC-Ottawa under the Aquifer Assessments and Support to Mapping, Groundwater Inventory Project of the Groundwater Geoscience Programme. This work is a contribution of the GSC–OGS Southern Ontario project on groundwater 2014–2019.

9. References

Berger, M., Zou, L., and Schleicher, R. 2009. Analysis of sulphur in the Copper Basin and Muddy River sites. International Journal of Soil, Sediment and Water, 12: 3, 1-17. https://scholarworks.umass.edu/intljssw/vol2/iss3/1

Conrey, R.M., Goodman-Elgar, M., Bettencourt, N., Seyfarth, A., Van Hoose, A., and Wolff, J.A. 2014. Calibration of a portable X-ray fluorescence spectrometer in the analysis of archaeological samples using influence coefficients. Geochemistry: Exploration, Environment, Analysis, 14: 291-301. http://dx.doi.org/10.1144/geochem2013-198

Craigie, N. 2018. Principles of elemental chemostratigraphy: A practical user guide. Springer International Publishing. https://doi org/10.1007/978-3-319-71216-1

Figura, P.M. 1987. Standardless quantitative X-ray fluorescence analysis using stored calibration constants. American Laboratory, v. 19, p. 156-164.

Fisher, L., Gazley, M.F., Baensch, A., Barnes, S.J., Cleverley, J., and Duclaux, G. 2014. Resolution of geochemical and lithostratigraphic complexity: a workflow for application of portable X-ray fluorescence to mineral exploration; Geochemistry: Exploration, Environment, Analysis, v. 14, p. 149–159.

Gallhofer, D. and Lottermoser, B.G. 2018. The influence of spectral interferences on critical elemental determination with portable X-ray fluorescence (pXRF). Minerals, 8: 320. https://doi.org/10.3390/min8080320

Gazley, M.F., Tutt, C.M., Fisher, L.A., Latham, A.R., Duclaux, G., Taylor, M.D., and de Beer, S.J. 2014. Objective geological logging using portable XRF geochemical multi-element data at Plutonic Gold Mine, Marymia Inlier, Western Australia. Journal of Geochemical Exploration, 143: 74–83. https://doi.org/10.1016/j.gexplo.2014.03.019

Glanzman, R.K. and Closs, L.G. 2007. Field portable x-ray fluorescence geochemical analysis – its contribution to onsite real-time project evaluation. in Proceedings of Exploration 07: Fifth Decennial International Conference on Mineral Exploration, 291–301.

Grunsky, E.C. 2009. Statistical analysis in the geosciences. in Geoinformatics, Volume II, Encyclopedia of Life Support Systems, ed. Peter M Atkinson. 1-64.

Hughes, R. and Barker, S. 2017. Using portable XRF to infer halos within the Waihi Au-Ag system, New Zealand. Geochemistry: Exploration, Environment, Analysis, 18: 97–108. https://doi.org/10.1144/geochem2016-006

Huntley, J.A. 2012. Taphonomy or paint recipe: in situ portable X-ray fluorescence analysis of two anthropogenic motifs from the Woronora Plateau, New South Wales. Australian Archeology, 75: 78-94. https://doi.org/10.1080/03122417.2012.11681952

Kalnicky, D.J. and Singhvi, R. 2001. Field portable XRF analysis of environmental samples; Journal of Hazardous Material, 83: 93–122.

Knight, R.D., Moroz, M., and Russell, H.A.J. 2012. Geochemistry of a Champlain Sea aquitard, Kinburn, Ontario: portable XRF analysis and fusion chemistry. Geological Survey of Canada, Open File 7085, 28 p. https://doi.org/10.4095/290969

Knight, R.D., Kjarsgaard, B.A., Plourde, A.P., and Moroz, M. 2013. Portable XRF spectrometry of standard reference materials with respect to precision, accuracy, instrument drift, dwell time optimization, and calibration. Geological Survey of Canada, Open File 7358, 45 p. https://doi.org/10.4095/292677

Knight, R.D., Sharpe, D.R., and Valiquette, L.J. 2015a. Portable XRF spectrometry, fusion, multi acid, and aqua regia results from the Aurora borehole, Yonge Street Aquifer, southern Ontario. Geological Survey of Canada, Open File 7919, 21 p. https://doi.org/10.4095/297418

Knight, R.D., Valiquette, L.J., and Russell, H.A.J. 2015b. Portable XRF spectrometry results from the High Park borehole, southern Ontario. Geological Survey of Canada, Open File 7918, 24 p. https://doi.org/10.4095/297627

Knight, R.D., Landon-Browne, A.R.R., and Russell, H.A.J. 2016a. Portable XRF spectrometry of glacial-derived sediment from the Purple Woods borehole, southern Ontario. Geological Survey of Canada, Open File 7921, 26 p. https://doi.org/10.4095/297890

Knight, R.D., Valiquette, L.J., and Russell, H.A.J. 2016b. Portable XRF spectrometry, fusion, multi acid, and aqua regia results from the Queensville borehole, Young Street Aquifer, southern Ontario. Geological Survey of Canada, Open File 7855, 23 p. https://doi.org/10.4095/297721

Knight, R.D., Coffin, L.M., Valiquette, L.J., and Russell, H.A.J. 2016c. Portable XRF spectrometry, fusion, multi acid, and aqua regia results from the Warden borehole, southern Ontario. Geological Survey of Canada, Open File 7922, 21 p. https://doi.org/10.4095/297841

Knight, R.D., Landon-Browne, A.R.R., Arnaud, E., and Russell, H.A.J. 2016d. Portable XRF spectrometry results from the Clarington borehole, southern Ontario. Geological Survey of Canada, Open File 7920, 18 p. https://doi.org/10.4095/298819

Knight, R.D., Stepner, D.A.J., Gerber, R.E., Holysh, S., and Russell, H.A.J. 2018a. Geochemistry of surficial sediment cores, Greater Toronto Area, southern Ontario. Geological Survey of Canada, Open File 8298, 16 p. https://doi.org/10.4095/311222

Knight, R.D., Bajc, A.F., Moroz, M.J., and Russell, H.A.J. 2018b. Geochemistry of glacially derived sediment from the Gads Hill Moraine area, southwestern Ontario. Geological Survey of Canada, Open File 8299, 8 p. https://doi.org/10.4095/308207

Knight, R.D., Stepner, D.A.J., Bajc, A.F., and Russell, H.A.J. 2018c. Geochemistry of surficial sediment cores, Brantford-Woodstock area, southern Ontario. Geological Survey of Canada, Open File 8336, 12 p. https://doi.org/10.4095/313110

Knight, R.D., Bajc, A.F., Mulligan, R.P.M., Moroz, M.J., and Russell, H.A.J. 2018d. Geochemistry of surficial sediment cores, southern Simcoe County, southern Ontario. Geological Survey of Canada, Open File 8257. https://doi.org/10.4095/308450

Lemiere, B. 2018. A review of pXRF (field portable X-ray fluorescence) applications for applied geochemistry. Journal of Geochemical Exploration, 188: 350–360. https://doi.org/10.1016/j.gexplo.2018.02.006

Landon-Browne, A.R.R., Knight, R.D., Kjarsgaard, B.A., and Russell, H.A.J. 2017. Quality control of pXRF spectrometry. Geological Survey of Canada, Scientific Presentation 53, 1 sheet. https://doi.org/10.4095/299726

Morris, P.A. 2009. Field-portable X-ray fluorescence analysis and its application in GSWA. Geological Survey of Western Australia, Record 2009/7, 23p.

Murphy, R.V., Maharaj, H., Lachapelle, J., and Yuen, P.K. 2010. Operator of portable X-ray fluorescence analysers, certification information and examination preparation booklet. Natural Resources Canada, Government of Canada.

Piercey, S.J. and Devine, M.C. 2014. Analysis of powdered reference materials and known samples with a benchtop, field portable x-ray fluorescence (pXRF) spectrometer: evaluation of performance and potential applications for exploration lithogeochemistry. Geochemistry: Exploration, Environment, Analysis, doi: 10.1144/geochem2013-199.

Plourde, A.P., Knight, R.D., and Russell, H.A.J. 2012. Portable XRF spectrometry of insitu and processed glacial sediment from a borehole within the Spiritwood buried valley, southwest Manitoba. Geological Survey of Canada, Open File 7262, 30 p. https://doi.org/10.4095/291922

Plourde, A.P., Knight, R.D., Kjarsgaard, B.A., Sharpe, D.R., and Lesemann, J–E. 2013. Portable XRF spectrometry of surficial sediments, NTS 75-I, 75-J, 75-O, 75-P (Mary Frances Lake - Whitefish Lake - Thelon River area), Northwest Territories. Geological Survey of Canada, Open File 7408, 25 p. https://doi.org/10.4095/292714

Potts, P.J. and Webb, P.C. 1992. X-ray fluorescence spectrometry; Journal of Geochemical Exploration, 44: 251-296. https://doi.org/10.1016/0375-6742(92)90052-A

Rouillon, M. and Taylor, M. 2016. Can field portable X-ray fluorescence (pXRF) produce high quality data for application in environmental contamination research? Environmental Pollution, 214: 225-264. https://doi.org/10.1016/j.envpol.2016.03.055

Rowe, H., Hughes, N., and Robinson, K. 2012. The quantification and application of handheld energy-dispersive fluorescence (ED-XRF) in mudrock chemostratigraphy and geochemistry. Chemical Geology, 324-325: 122-131. https://doi.org/10.1016/j.chemgeo.2011.12.023

Ryan, J.G., Shervais, J.W., Li, Y., Reagan, M.K., Li, H.Y., Heaton, D., Godard, M., Kirchenbaur, M., Whattam, S.A., Pearce, J.A., Chapman, T., Nelson, W., Prytulak, J., Shimizu, K., and Petronotis, K. 2017. Application of a handheld X-ray fluorescence spectrometer for real-time, high-density quantitative analysis of drilled igneous rocks and sediments during IODP Expedition 352. Chemical Geology, 451: 55–66. https://doi.org/10.1016/j.chemgeo.2017.01.007

Stepner, D.A.J., Knight, R.D., Bajc, A.F., and Russell, H.A.J. 2018. Geochemistry of surficial sediment cores, Dundas buried bedrock area, southwestern Ontario. Geological Survey of Canada, Open File 8300, 11 p. https://doi.org/10.4095/311182

Simandl, G.J., Stone, R.S., Paradis, S., Fajber, R., Reid, H.M., and Grattan, K. 2014. An assessment of a handheld X-ray fluorescence instrument for use in exploration and development with an emphasis on REEs and related specialty metals. Mineralium Deposita, 49: 999–1012. https://doi.org/10.1007/s00126-013-0493-0

Stanley, G., Gallagher, V., Ní Mhairtín F., Brogan, J., Lally, P., Doyle, E., and Farrell, L. 2009. Historic mines site - inventory and risk classification. Geochemical characterization and environmental matters - Appendix 4-XRF analyser, Assessment of analytical performance of NITON XLt 792Y field-portable analyser. Geological Survey of Ireland, 1: 40 p.

US-EPA, 1998. Test methods for evaluating solid waste, physical/chemical methods. In: SW-846, Method 6200, Revision 0. Vol IA. https://www.epa.gov/sites/production/files/2015-12/documents/6200.pdf

US-EPA, 2007. Method 6200. In: Field Portable X-ray Fluorescence Spectrometry for the Determination of Elemental Concentrations in Soil and Sediment, (Accessed on 2014/12/02 from). www.epa.gov/osw/hazard/testmethods/sw846/pdfs/6200.pdf

Wilson, A.W., Turner, D.C., and Robbins, A.A. 1999. Evlauation of some sample support films for microsample X-ray analysis. Advances in X-ray Analysis, 41: 301-307.

Young, K.E., Evans, C.A., Hodges, K.V., Bleacher, J.E., and Graff, T.G. 2016. A review of the handheld X-ray fluorescence spectrometer as a tool for field geologic investigations on earth and in planetary surface exploration. Applied Geochemistry, 72: 77–87. https://doi.org/10.1016/j.apgeochem.2016.07.003

A chemostratigraphic characterization of Newmarket Till in drill core from north of Lake Ontario

Daniel A.J. Stepner[1,2], Bruce A. Kjarsgaard[1], Ross D. Knight[1]*, Hazen A.J. Russell[1], and David R. Sharpe[1]

Abstract: The Newmarket Till (NT) covers much of the south-central Ontario forming a regional stratigraphic marker. Geochemical analysis was performed using aqua regia, four-acid, and flux-fusion digestion on 137 samples of NT collected from 8 boreholes across two regional transects to quantify potential geochemical variations through the till. The geochemistry of the <63 µm size fraction exhibits strong elemental correlations between major and trace element contents and CaO. All major elements exhibit negative correlations with CaO contents indicative of the incorporation of Paleozoic carbonates flooring the southern Ontario Basin. A chemical ratio of $CaO+MgO/SiO_2+Al_2O_3$ (Provenance Indicator) suggest significant quantities of material from the Paleozoic carbonates were incorporated into the till matrix as ice moved south of the Canadian Shield. High precision sampling using portable XRF methods for a continuous sediment core located near Pickering Ontario, allowed for the identification of 4 geochemical subfacies unidentifiable on the macro scale along with 3 interbeds. These geochemical subunits in the NT cannot be traced to nearby boreholes and hence do not have regional extent.

1. Introduction

In the last 20 years, the application of chemostratigraphy in sedimentary basins (Craigie 2018) has increased with the advent of high-speed, high-precision and accuracy, and relatively low-cost geochemical analyses. In Canada, geochemical analysis has been applied extensively across the surficial geological landscape with particular emphasis on reconnaissance-scale mineral exploration by governments (Shilts 1993; Klassen, 2001; Kjarsgaard et al. 2013a, b) and less commonly for environmental applications (e.g., Bonham-Carter 2005; Sharpe et al. 2019), though few, if any, glaciated basins have subsurface chemostratigraphic frameworks.

Continuous surficial sediment cores were collected in southern Ontario by the Geological Survey of Canada and the Ontario Geological Survey for stratigraphic (e.g., Sharpe et al. 2011; Russell et al. 2017; Burt and Dodge 2011) and hydrogeologic studies. These cores provide an ideal opportunity to establish a baseline chemostratigraphic framework (Russell et al. 2017), to complement soil A- and B-horizons and soil C-horizon (i.e. till protolith) sampling (Sharpe et al. 2019) and ambient groundwater chemistry studies (Hamilton 2018). The southern Ontario chemostratigraphic study has completed analyses of 3815 samples of surficial sediments from 53 boreholes by portable X-ray fluorescence spectrometry (pXRF). A subset of these samples were also analysed by traditional laboratory geochemical methods to verify accuracy of the pXRF data.

The objective of this paper is to provide a detailed analysis of the geochemistry of Newmarket Till, observed in the area north of Lake Ontario and east of the Niagara Escarpment. Data presented here represent the analysis for 137 samples from eight boreholes collected by both pXRF and traditional laboratory geochemical methods (Figures 1, 2), running in a roughly north-south transect, provides a regional geochemical overview study of the Newmarket Till. Laboratory data were used primarily, as pXRF data were limited for Mg content, a key element for determining a provenance indicator. The analysis of elemental laboratory chemistry is used to assess i) vertical trends in geochemistry, ii) changes in geochemical signature across major unit contacts and intra-formational contacts, and iii) the relationship between the till matrix composition and the Shield–Paleozoic terrain boundary (i.e. the source rocks).

2. Geological setting/framework

2.1 Bedrock

Southern Ontario is underlain by two distinct bedrock domains. The northern area comprises the Central Metasedimentary

[1] Geology Survey of Canada, Natural Resources Canada, 601 Booth Street, Ottawa, ON K1A 0E8
[2] 1-5 Ossington Ave, Ottawa, ON K1S 3B3

*corresponding author: ross.knight@canada.ca

Recommended citation: Stepner, D.A., Kjarsgaard, B.A., Knight, R.D., Russell, H.A.J., and Sharpe D.R. 2020. A chemostratigraphic characterization of Newmarket Till in drill core from north of Lake Ontario. In Russell, H.A.J. and Kjarsgaard, B.A. Eds. Southern Ontario groundwater project 2014–2019: summary report. Geological Survey of Canada, Open File 8536, 109-119. https://doi.org/10.4095/321097

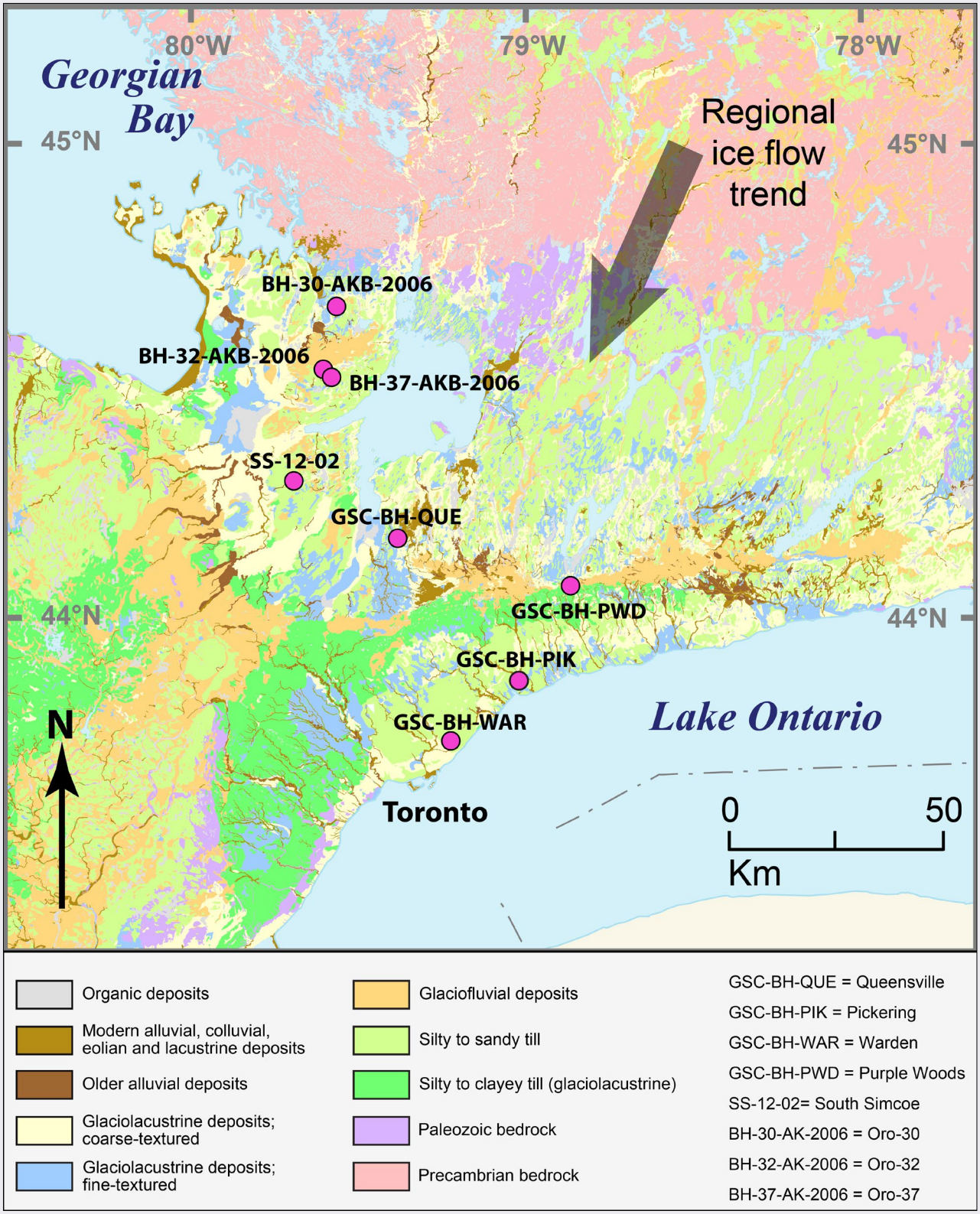


Figure 1. Southern Ontario study area highlighting borehole locations overlain on the surficial geology (modified Barnett et al., 1991) Geochemistry for Oro (Stepner et al. 2018), South Simcoe (Knight et al. 2018), Queensville (Knight et al. 2016b), Purple Woods (Knight et al. 2016a), Pickering (Knight et al. 2020), and Warden (Knight et al. 2016c).

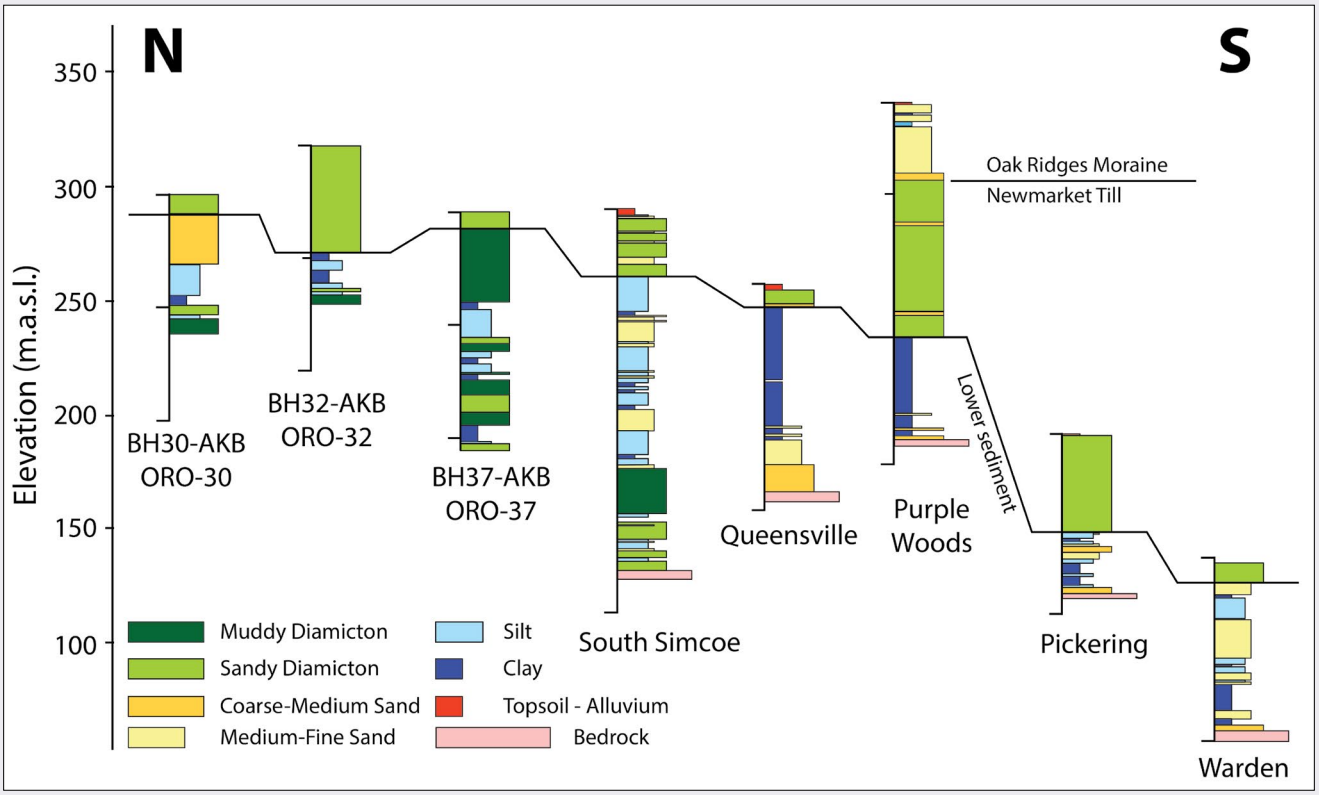


Figure 2. Simplified stratigraphic columns for the studied southern Ontario boreholes, hung on a common datum. The thin black line demarcates the base of Newmarket Till unit.

Belt of the Precambrian Grenville province of the Canadian Shield (Easton and Thurston 1992; Johnson et al. 1992). It is composed of metamorphosed igneous and sedimentary rocks (marble, gneiss) along with numerous igneous intrusions (alkalic, felsic, and mafic). To the south, Phanerozoic sedimentary rocks (predominantly carbonates with subordinate amounts of shale and sandstone), overlie the Shield rocks of the Grenville Province (Armstrong and Dodge 2007).

2.2 Quaternary

Up to 200 m of surficial sediment deposited during several glaciations overlies the bedrock of southern Ontario (Barnett et al. 1991). Based on various scales of mapping and generalization, the glacial geology represents 21 to 35 genetic units of gravel, sand, silt, and diamicton (e.g., Barnett et al. 1991). To facilitate subsurface mapping and integration of borehole and geophysical data, the surficial stratigraphy of southeastern Ontario is generalized into eight units overlying bedrock: (1) Lower Sediment, (2) Newmarket Till, (3) glaciofluvial deposits, (4) muddy diamicton, (5) glaciolacustrine mud, (6) glaciolacustrine sand (7) alluvial sediment and organics (e.g., Logan et al. 2020).

The Newmarket Till has a poorly sorted, stoney, dense silty sand composition which commonly has a streamlined surface in the landscape (Gwyn and Dilabio 1973; Sharpe et al. 2002a, Kjarsgaard et al. 2017). It is also termed the "Northern till" (Karrow 1974; Boyce et al. 1995). Due to distinct textural properties and high-seismic velocity, the Newmarket Till forms a regional stratigraphic marker (Boyce et al. 1995; Pugin et al. 1999; Sharpe et al. 2002b). It extends from the Canadian Shield southward to Lake Ontario and westward from the Lanark Highlands to the Niagara Escarpment. West of the Niagara Escarpment, the Catfish Creek Till is interpreted to be correlative with the Newmarket Till (Bajc et al. 2014). The massive diamicton facies (with local interbeds of clay, silt, sand and gravel) of the Newmarket Till can be up to 68 m thick (Knight et al. 2016a); however, thickness is highly variable across the region (Boyce and Eyles 2000; Sharpe et al. 2007; Crow et al. 2017).

Newmarket Till appears consistently brown to grey, with color changing as a response to weathering. Grain size measurements from multiple locations demonstrate a predominantly sand (51%) silt till (36% silt, 13% clay) (n=442, Sharpe and Russell 2016; Gerber 1999; Golder and Associates 1999). Clasts are composed of rounded and angular fragments of igneous and metamorphic rocks (commonly granite and schist) along with rounded and angular clasts of limestone and shale.

The Newmarket Till was deposited by ice flowing from approximately NE to SW (Gwyn and Dilabio 1973). Field and drill-core studies of Newmarket Till have recognized multiple

subfacies (or beds) within thicker sediment sequences (Boyce et al. 1995; Boyce and Eyles 2000; Sharpe et al. 2002b). Boyce and Eyles (2000) identify 3 architectural elements i) diamict elements, ii) intebeds, and iii) deformed zones. They recognized that a number of macro bounding conditions permitted subdivision of Newmarket Till (near Pickering, Ontario) into 5 distinct diamict elements separated by identifiable bounding discontinuities.

3. Methods

Samples from the Newmarket Till (119 till samples and 18 from sand and silt interbeds) were collected from eight boreholes north of Lake Ontario (Figure 1) and analyzed for geochemical composition; borehole locations and brief descriptions are summarized in Table 1. Sediment core samples were disaggregated by mortar and pestle and screened using stainless steel sieves to isolate the silt and clay (<63 µm) size fraction. Approximately 30 g of material in total was sent to Bureau Veritas Commodities Ltd. in Vancouver, Canada for analysis. Samples were digested by i) aqua regia, ii) four-acid, iii) flux-fusion and nitric acid following the methodology of Kjarsgaard et al. (2013a, b). The aqua regia and multi-acid digestions were analysed by inductively coupled plasma mass spectrometry (ICP—MS), while the fusion samples were analysed using inductively coupled plasma emission spectrometry (ICP—ES) for major element as well as ICP—MS for trace element determinations. Analytical accuracy was monitored by the blind inclusion of certified reference materials, and analytical precision was evaluated by the duplicate analysis of selected samples; results of QA/QC are reported in individual Open File publications (Table 1). Grain size analysis of all samples was undertaken at the GSC sedimentology laboratory using a combination of wet sieving with a CAMSIZER Particle Size Analysis System (grain sizes >0.063 mm) and a Beckman Coulter LS 13-320 laser diffraction particle size analyser (grain sizes <0.063 mm).

4. Results & analysis

The thickness of the Newmarket Till varies considerably across the study area, ranging from 7.5 m to 68 m at the eight boreholes sites (Figure 2). At three of the locations (boreholes BH30-AKB, BH37-AKB, Queensville) Newmarket Till is <8 m thick.

4.1 Granulometry

Grain size data for the Newmarket Till samples varies across the study area; consisting of 25.9 to 83.9% sand (mean = 57.7%), 14.2 to 66.7% silt (mean = 34.4%) and 1.54 to 17.17% clay (mean = 7.8%). Sand interbed samples yielded up to 98.7% sand with no clay content. A single silt interbed sample yielded 82% silt, 18% sand and no clay. Grain size has a general association with borehole location relative to the shield-margin; Newmarket Till intersected in the South Simcoe and Oro area is generally sandier (an exception being BH-37-AKB) with less clay than samples taken further east and south.

Table 1. Summary borehole information for boreholes intersecting Newmarket Till. Easting and Northing measurement are reported in NAD83. Distance to the Canadian Shield-margin was estimated using Google Earth, assuming an ice flow direction of 45 degrees NE to SW.

Referenced Borehole Name	Borehole ID	Easting	Northing	Depth (m)	Collar Elevation (m a.s.l.)	Depth to Top Newmarktet Till (m a.b.s.)	Thickness of Newmarket Till (m)	Number of Newmarket Samples	Approx. Distance from Shield-margin (km)
Oro	BH-30-AKB-2006	612147	4943667	54.9	298	298	8	6	15
Oro	BH-32-AKB-2006	609032	4928931	70.5	320	320	48	33	40
Oro	BH-37-AKB-2006	610966	4927024	102.1	290	290	8	7	45
South Simcoe	SS-12-02	602163	4902748	161.2	292	288	26	19	60
Queensville	GSC-BH-QUE	626499	4889266	96.2	262	259.5	7.5	4	75
Warden	2010-WAR	638868	4840084	80.5	141	138.5	8.5	7	125
Pickering	GSC-BH-PIK	657052	4687962	70.5	188	184	38.5	47	95
Purple Woods	GSC-BH-PWD	666973	4878158	151.8	336	301	69	8	85

4.2 Chemistry of Newmarket Till

Fifty-four (54) elements were analyzed; 11 major element oxides and 43 trace elements; four elements occur below detection limits (beryllium, Be; molybdenum, Mo; tin, Sn; tungsten, W). Newmarket Till is geochemically heterogeneous from a major element oxide perspective, with SiO_2 values in the range of 36.53–52.61 wt. %, TiO_2 (0.40–0.97 wt. %), Al_2O_3 (7.28–11.76 wt. %), MgO (2.18–4.41 wt. %) and CaO (10.73–24.68 wt. %). Although major and trace element contents are variable in Newmarket Till, all elements analyzed have strong correlations with CaO contents (Figure 3), and also sample distance to the shield-margin. With the exception of Sr, all elements have a negative correlation with CaO content (Figure 3). SiO_2 content decrease from a maximum of ~55 wt. % near the shield margin in the Oro and South Simcoe areas to ~35 wt. % further south at the Queensville and Warden boreholes. Calcium content increases from ~10 wt. % adjacent to the shield to ~25% near Lake Ontario. Over the same distance, Al_2O_3 content decreases from ~12 wt. % to 6 wt. % and MgO values decrease from ~4.5 wt. % to ~2 wt. %. Similarly, K_2O, Na_2O and TiO_2 all decrease in concentration

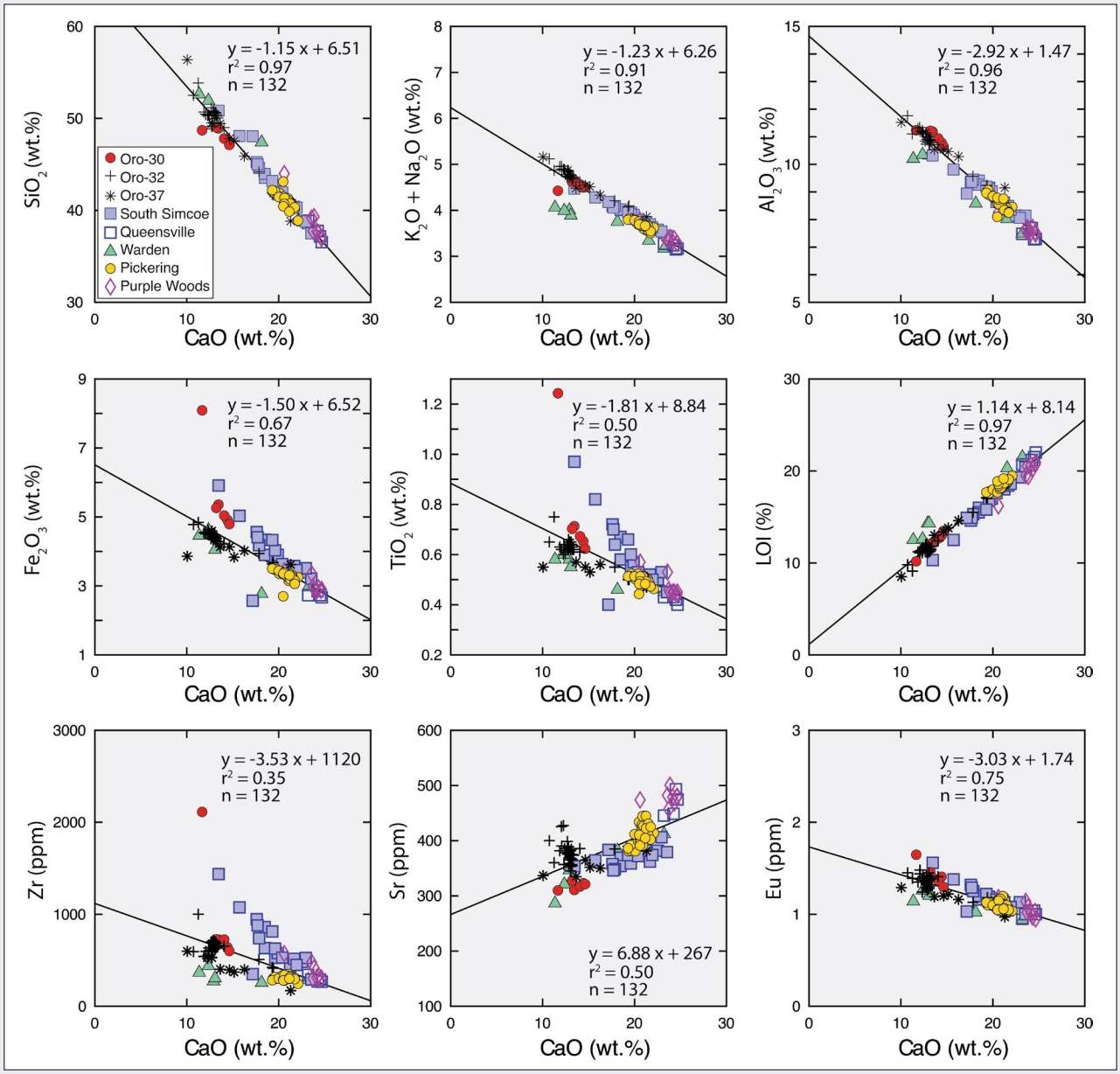


Figure 3. Select bivariate element plots showing element concentrations plotted against CaO contents. Note the high degree of association (r^2 >0.9) and strong negative correlations. Excursions from the regression line (e.g. Fe_2O_3, TiO_2, Zr) are all associated with heavy mineral contents and represent an overprinting of grain-size dependent geochemistry over the regional signal.

with distance from the shield margin. Chromium (as Cr_2O_3) oxide and phosphorus (as P_2O_5), while correlated with CaO content have no obvious correlation between distance from the shield and concentration. Rare-earth elements (REE) have similar patterns to major element geochemical patterns across Newmarket Till reflecting general dilution of shield-derived components southward. Chondrite-normalized rare-earth element diagrams (Figure 4) have a similar pattern for Newmarket Till with enriched light REEs (LREE) and nearly-flat heavy REEs (HREE). This suggests the types of minerals hosting REE (i.e. heavy minerals) are relatively consistent regionally throughout the till, only changing in modal amount.

4.3 Newmarket Till geochemical provenance indicator (P.I.)

The Quaternary sedimentary basin of southern Ontario is dominated by input from two main sources: the igneous and metamorphic rocks of Canadian Shield to the north, and the Paleozoic carbonates to the south. A chemical ratio (Provenance Indicator, P.I.) can reflect the relative chemical input from these two sources (Figure 5). Utilizing major element oxide data (total digestion), the ratio of (CaO+MgO) / (SiO_2+Al_2O_3) in wt. % is used to assess the approximate proportion of carbonate input relative to shield derived minerals; a higher P.I. value reflects greater input of material derived from sedimentary rocks. Calcium and magnesium do occur in shield derived material, although in significantly lower concentrations than in the limestones and dolomites.

4.4 Geochemical identification of Newmarket Till subfacies

Newmarket Till stratigraphy can be subdivided into discrete geochemical subfacies in three of the eight boreholes sampled (Warden, Pickering, Purple Woods). The Newmarket Till stratigraphic unit intersected at the Warden borehole is comprised of two subfacies; a lower subunit enriched in SiO_2, Al_2O3_3, Fe_2O_3, Rb, Zr, V, Co, Pb and REE , and a higher second subfacies enriched in CaO and Sr. At the Pickering borehole, the 42 m thick Newmarket Till sequence can be subdivided into four distinct geochemical subfacies (Figures 6, 7). Each Newmarket Till subfacies becomes progressively enriched in CaO and Sr relative to the underlying subfacies, with proportional decreases in other major and trace element concentrations. Subfacies 1–3 are relatively similar in terms of geochemical characterization, with minor variation across geochemical boundaries. The uppermost subfacies (subunit 4) is the most geochemically distinct; this subunit is the most enriched in CaO and Sr of all the samples of Newmarket Till analysed, excepting the top sample which appears to be leached of CaO and trace elements. The wet chemistry dataset provided insufficient resolution in the Purple Woods borehole to resolve chemostratigraphic units however the discrimination of two discrete subunits using a pXRF with higher resolution sampling was described in detail in Knight et al. (2016a).

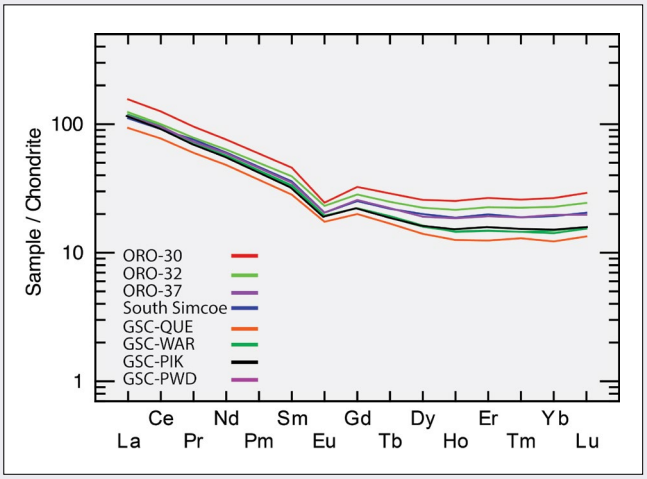


Figure 4. Rare earth element (REE) concentration diagram for the Newmarket Till normalized using chondrite values from Sun and McDonough (1989). Borehole data is plotted as average elemental concentrations. Trace elements are more compatible (higher concentrations) in accessory mineral phases sourced from metamorphic and igneous rocks, a consistent pattern for these elements in all regional holes suggests the proportions of these accessory phases remains relatively unchanged. Lower concentrations of these elements occur in boreholes with higher P.I. values, indicating the variation of concentrations is caused by dilution with the addition of more carbonate-derived elements.

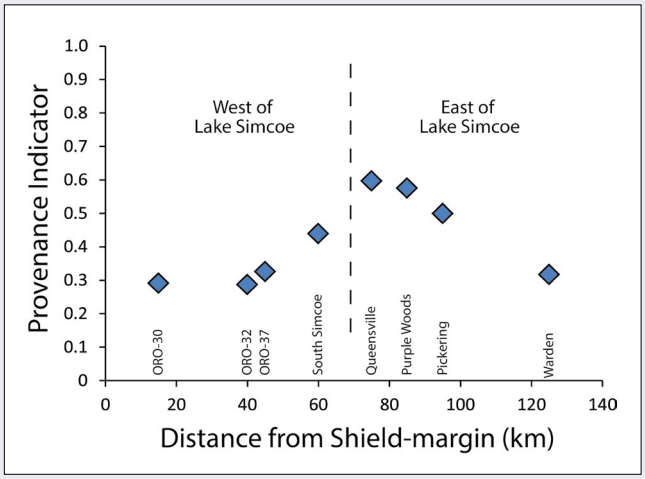


Figure 5. Provenance indicator (P.I.) versus distance from the shield-margin. P.I. = (CaO+MgO) / (SiO_2+Al_2O_3) and is used as a simple metric to determine elemental components contributed from carbonate source material compared to elemental components contributed from shield-type sources (i.e. igneous and metamorphic rocks). Note the bell-shaped distribution indicating the deposition of more carbonate-rich sediments approximately 80–100 km from the shield-margin.

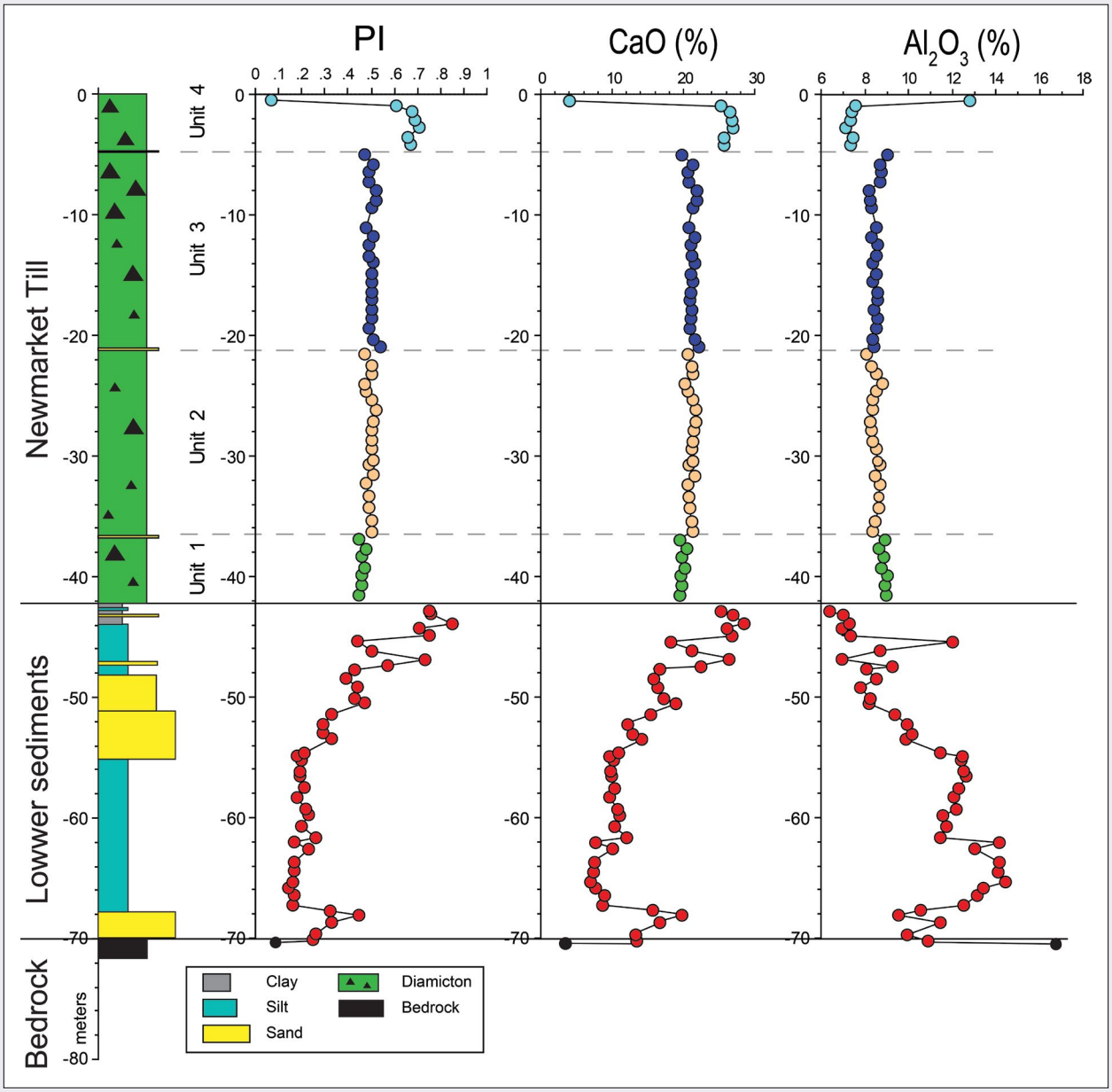


Figure 6. Chemostratigraphic profile of the Pickering borehole. Note the internal stratigraphy evident in the Newmarket Till sequence distinguished by four distinct geochemical subunits, separated by three interbeds.

4.5 Geochemical identification of interbeds

Interbeds within the Newmarket Till can be identified in seven of the eight boreholes (Figures 2, 7). Predominately these interbeds are sandy, however there are clay-rich, silty, and coarse-grained sand-gravel interbeds. In the Oro area, a sand interbed occurs in all three of the boreholes (Figures 2, 7); the interbeds have a minor enrichment in SiO_2, a minor depletion in CaO, and a significant increase in Zr contents. These sand interbeds are also marked to a lesser degree by enrichments in Al_2O_3, Fe_2O_3, Na_2O_3, Hf, Lu and depletions in MgO, Rb, Nb, Co, Ni, Cu, Zn, Th, REE, relative to Newmarket Till both above and below. In the South Simcoe borehole, the topmost interbed appears geochemically similar to those identified in the Oro area boreholes, with enrichment in SiO_2 and Zr along with depletion in CaO contents. The other two sand interbeds are geochemically similar to the Till, while the silt interbed intersected in the South Simcoe borehole can be identified by enrichments of REE relative to the diamicton. The single clay interbed sampled in the Warden borehole appears to cap a fining upwards sequence with decreasing SiO_2, Al_2O_3 and Zr contents through the lower subunit, which then transitions into a predominantly carbonate-rich till matrix

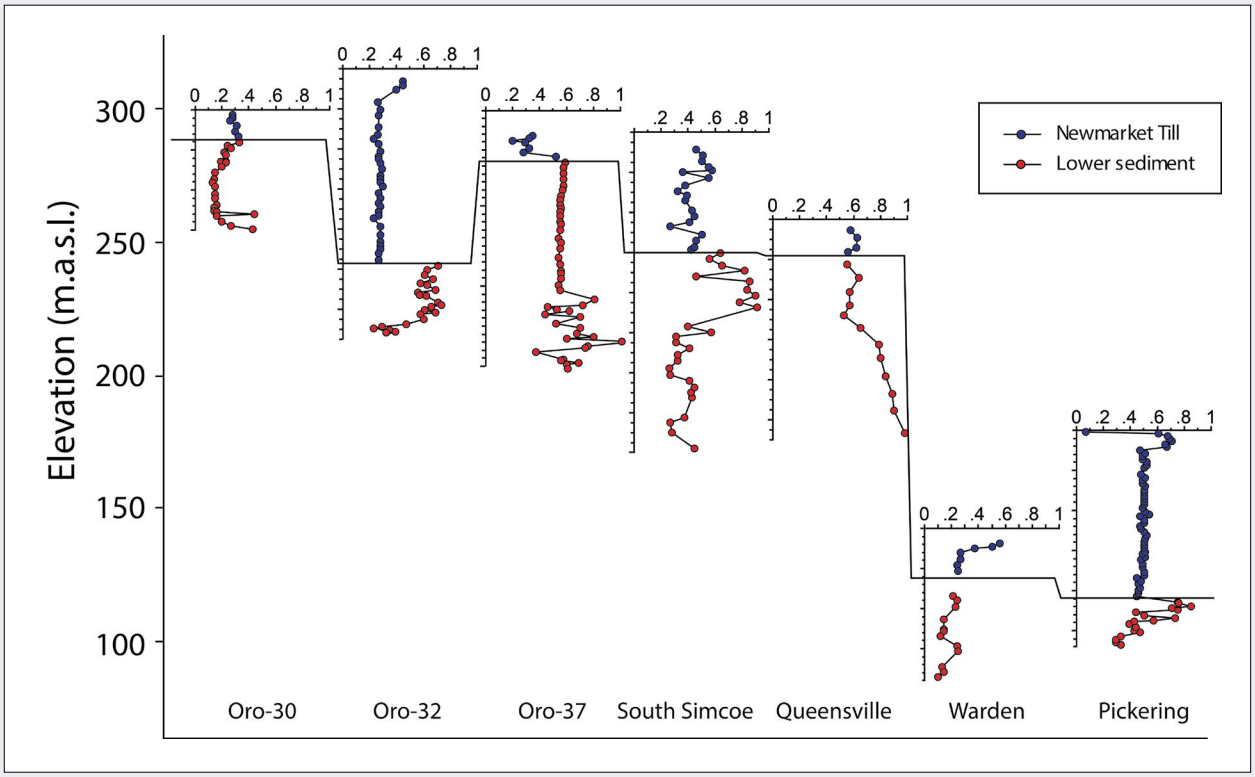


Figure 7. Chemostratigraphy plots showing Provenance Indicator (PI) normalized to a common datum. Black bounding line indicates base of Newmarket Till unit.

of the upper subunit. This change in matrix composition represents an increase of nearly 50% carbonate-derived material-elemental components. The interbed itself is not resolvable on chemostratigraphic plots. The two sand interbeds and a thin gravel-cobble horizon in the Pickering borehole (Figure 6) separate out the four chemostratigraphic subunits of the Newmarket Till sequence.

4.6 Contact with underlying sediments

Newmarket Till overlies Thorncliffe Formation sediments (a unit within the Lower Sediments) in seven of the eight boreholes. Thorncliffe Formation sediments vary in grainsize from clay (boreholes: Purple Woods, Pickering, Queensville, South Simcoe) to sand (borehole: Warden). The contact with the underlying Thorncliffe sediments is generally a sharp geochemical boundary (based on pXRF data) when the underlying sediments are clay or silt rich (Boreholes: Oro-32, Oro-37, South Simcoe, Purple Woods, Pickering) and more transitional or similar geochemistry boundary where the underlying sediments are more sand-rich (boreholes: Oro-30 and Warden) or clay rich (borehole Queensville) (Figures 6, 7). For the Queensville borehole only Ba and Ni contents vary at the boundary and decrease upward in concentration into the Newmarket Till matrix. In South Simcoe and Warden boreholes, the Newmarket Till has less CaO and Sr than the underlying Lower Sediments; however, there is a proportional enrichment in all other elements. An opposite relationship occurs at the Pickering borehole (Figure 6). Here Newmarket Till is less siliceous and more enriched in Ca than the Thorncliffe sediments and shows a depletion of all elements excepting Sr. The matrix of Newmarket Till appears enriched in carbonate-derived material relative to underlying sediments when the underlying sediments are coarse grained. While the grain sizes may change across the Thorncliffe–Newmarket Till contact, the geochemical signatures can be varied, providing unique information about the provenance of the sediments and the depositional conditions. In boreholes where the underlying sediments are of a finer grain size, such as Queensville (silt and clay), the chemostratigraphic profile has no observable geochemical boundary across the contact.

5. Discussion

5.1 Regional and stratigraphic geochemical variation of the Newmarket Till

Geochemical trends in the Newmarket Till can be linked to carbonate-derived bedrock material in the till-matrix. Bivariate plots of all elements compared to CaO contents have strong linear correlations (Figure 3); all major element oxides and trace elements analyzed (excepting Sr which is compatible in

calcite) have negative correlations with CaO contents. Strong linear relationships between elements and CaO contents indicate the presence of large amounts of carbonate in the till matrix having a diluting effect, thus potentially masking minor geochemical variations.

Geochemical data indicate a correlation between the amount of carbonate-derived material in the till-matrix and the sample distance relative to the shield margin (Figure 5). This suggests that significant quantities of material from the Paleozoic carbonates were incorporated once ice advanced south from the Shield margin. Closest to the shield margin P.I. values ~0.3 are found in the Oro region ~0–40 km from the margin, PI increases marginally at the South Simcoe borehole (~60 km) to ~0.4 and increase further to 0.5–0.6 in borehole, Queensville (~75 km), Purple Woods (~85 km) and Pickering (~95). At further distances, i.e. the Warden borehole (~125 km), P.I. values have dropped by almost 30% relative to the peak and have an average value of 0.3. Although application of P.I. as a depositional proxy is overly simplified and assumes material was eroded and transported evenly across the glacial front, it appears there is measureable variation in matrix-composition regionally throughout the diamicton. The data indicate that glacial ice rapidly eroded and incorporated material from the Paleozoic bedrock; within a few tens of km's from the shield-margin, as till matrix is dominated by carbonate materials at that distance (Kjarsgaard et al. 2020).

5.2 Chemo-architectural analysis of the Newmarket Till

Geochemical identification and classification of sub-units, facies and interbeds supports the observations of Boyce and Eyles (2000) that the Newmarket Till has subfacies (diamict elements) in the Pickering area. Geochemical data from the Pickering borehole indicate four stratigraphic Newmarket Till subfacies having a systematic increase of the carbonate fraction of the till matrix (evidenced by P.I., Figure 6) upward from the base of the Newmarket Till. These geochemical subunits cannot be traced to nearby boreholes and hence do not have regional extent. At the Warden site, Newmarket Till chemostratigraphy is sharply divided into two distinct units separated by a clay interbed; at the macro scale, till matrix above and below this horizon is not recognizably different; however geochemical characterization shows a difference. The recognition and characterization of geochemical subdivisions support the concept that large till sequences are not deposited as single events, but rather during repeated, incremental depositional events. The progressive increase in P.I. upwards suggests the glacier did not source additional materials from the Shield during younger periods of sedimentation (likely dilution effect), but rather continued to erode and recycle underlying carbonate material. Carbonate debris was rapidly incorporated at the Shield-basin margin and was persistently available southward from the margin (<100 km of glacial transport). Rare earth elements (REE's) that occur at much higher concentrations in accessory phases common to many Shield-type rocks have consistently decreasing concentration trends upwards through the stratigraphic sequence corresponding to mineral (and elemental) dilution with increasing carbonate contents. This further supports the idea that Shield-material was a limited resource during deposition of the Newmarket Till and glacial erosion was sourcing a significant fraction of material from Paleozoic bedrock.

6. Summary

This study highlights that within a basin stratigraphic context, the addition of high precision and accurate geochemical data can provide significant information that is not apparent on the outcrop- or macro-scale. The primary variation in the signature of till matrix geochemistry in the Newmarket Till is inherently linked to glacial advance–erosion over the Paleozoic carbonates of southern Ontario.

Thicker Newmarket Till was not deposited by a single continuous depositional event. Rather, thick Newmarket Till is an amalgamation of multiple episodes of deposition with limited variation in sediment provenance. Successive episodes of Newmarket Till deposition are suggested to be a result of glacial processes that are not fully understood at this time, and that likely have implications for glacial dynamics within the Laurentide Ice Sheet in southern Ontario. With the presence of interbeds and the lack of incorporation of underlying sediment, we can speculate that periodic lifting/floating of ice from the sub-glacier bed may be a factor in depositing Newmarket Till subfacies. The decrease in P.I. for the most distal data from the Shield margin in the concentration of carbonate-linked elements suggests the erosion and deposition of Paleozoic carbonate bedrock was rapid and significant within short (<100 km) distances of glacial transport (Kjarsgaard et al. 2020).

Geochemical "finger-printing", when added to other methods of observation (e.g. core and outcrop analyses), and analytical techniques (e.g. surficial and borehole geophysics), provides a more complete understanding of regional till units.

7. Acknowledgements

Sediment cores and samples for the Oro moraine and Simcoe county were provided by the Ontario Geological Survey (OGS) and particularly A. Burt and A. Bajc. Core and information for Pickering borehole was provided by the Oak Ridges Groundwater Program and the University of Ottawa, by R. Gerber and T. Al, respectively. H. L. Crow completed an internal review at the GSC. Analytical work was completed under the Aquifer Assessments and Support to Mapping, Groundwater Inventory Project of the Groundwater Geoscience Programme. This work is a contribution of the GSC–OGS Southern Ontario project on groundwater 2014–2019.

8. References

Armstrong, D.K. and Dodge, J.E.P. 2007. Paleozoic geology of southern Ontario. Ontario Geological Survey, Miscellaneous Release—Data, 219.

Bajc A.F., Russell H.A.J., and Sharpe D.R. 2014. A three-dimensional hydrostratigraphic model of the Waterloo Moraine area, southern Ontario, Canada, Canadian Water Resources Journal. http://dx.doi.org/10.1080/07011784.2014.914794

Barnett, P.J., Cowan, W.R., and Henry, A.P. 1991. Quaternary geology of Ontario, southern sheet; Ontario Geological Survey, Map 2556, scale 1:1 000 000.

Bonham-Carter, G.F. 2005. Introduction to the GSC MITE Point Sources project; in Metals in the environment around smelters at Rouyn-Noranda, Quebec, and Belledune, New Brunswick: In. Bonham-Carter, G. Ed. Results and conclusions of the GSC MITE Point Sources Project. Geological Survey of Canada, Bulletin no. 584, 14; 1 CD-ROM. https://doi.org/10.4095/221130

Boyce, J.I., Eyles, N., and Pugin, A. 1995. Seismic reflection, borehole and outcrop geometry of late Wisconsin tills at a proposed landfill near Toronto, Ontario. Canadian Journal of Earth Sciences, 32: 1331–1349. https://doi.org/10.1139/e95-108

Boyce, J.I. and Eyles, N. 2000. Architectural element analysis applied to glacial deposits: internal geometry of a late Pleistocene till sheet, Ontario, Canada. Geological Society of America Bulletin, 112: 98–118. https://doi.org/10.1130/0016-7606(2000)112<98:AEAATG>2.0.CO;2

Burt, A.K. and Dodge, J.E.P. 2011. Three-dimensional modelling of surficial deposits in the Barrie–Oro Moraine area of southern Ontario; Ontario Geological Survey, Groundwater Resources Study 11.

Craigie, N. 2018. Principles of elemental chemostratigraphy. Springer.

Crow H.L., Hunter J.A.H., Olson L., Pugin A.J.M., Russell H.A.J. 2017. Borehole geophysical log signatures and stratigraphic assessment in a glacial basin, southern Ontario; Canadian Journal of Earth Sciences, doi 10.1139/cjes-2017-0016

Easton, R.M. and Thurston, P.C. 1992. The Grenville Province and the Proterozoic history of central and southern Ontario. Geology of Ontario. Special, 4 (Part 2), pp.714-904.

Gerber, R. 1999. Hydrogeologic behaviour of the Northern till aquitard near Toronto, Ontario PhD. University Toronto, National Library of Canada.

Golder and Associates. 1999. Foundation investigation and design proposed Highway 407 easterly, West Duffins Creek and tributary overpass bridges, fills, cuts and culverts. Pickering Ontario, 47 p.

Gwyn, Q.H.J. and DiLabio, R.N.W. 1973. Quaternary geology of the Newmarket area, southern Ontario. Ontario Division of Mines, Preliminary map P.836, scale 1 : 50 000.

Hamilton, S.M. 2018. The Use of Wide Spectrum Groundwater Geochemistry in Regional Groundwater Mapping in Ontario. Regional-scale groundwater geoscience in southern Ontario: an Ontario Geological Survey, Geological Survey of Canada, and Conservation Ontario geoscientists open house. Geological Survey of Canada, Open File 8363, 18. https://doi.org/10.4095/306532.

Johnson, M.D., Armstrong, D.K., Sanford, B.V., Telford, P.G., and Rutka, M.A. 1992. Paleozoic and Mesozoic geology of Ontario. In Thurston, P.C., Williams, H., Sutcliffe, R.H., and Stott, G.M. Eds. Geology of Ontario; Ontario Geological Survey, Special Volume 4, part 2, 907–1010.

Karrow, P.F. 1974. Till stratigraphy in parts of southwestern Ontario. Geological Society of America Bulletin, 85: 5, 761-768. https://doi.org/10.1130/0016-7606(1974)85<761:TSIPOS>2.0.CO;2

Kjarsgaard, B.A., Knight, R.D., Sharpe, D.R., Kerr, D.E., Cummings, D.I., Russell, H.A.J., and Lemkow, D. 2013a. Till Geochemistry Studies of the Thaidene Nene MERA Study area. In Wright, D F., Ambrose, E.J., Lemkow, D., and Bonham-Carter, G. Eds. Mineral and Energy Resource Assessment of the proposed Thaidene Nene National Park Reserve in the area of the east arm of Great Slave Lake, Northwest Territories. Geological Survey of Canada, Open File 7196, 279-312. https://doi.org/10.4095/292458

Kjarsgaard, B.A., Plourde, A.P. Knight, R.D., and. Sharpe, D.R. 2013b. Geochemistry of regional surficial sediment samples from the Thelon River to the East Arm of Great Slave Lake, Northwest Territories, Canada. Geological Survey of Canada, Open File 7649, 17 p. https://doi.org/10.4095/295195

Kjarsgaard, B.A., Knight, R.D., Russell, H.A.J., Sharpe, D.R., Crow, H., and Olson, L. 2017. Newmarket Till aquitard: optimum grain packing with a pore-filling calcite-rich cement. In Regional-scale groundwater geoscience in southern Ontario. An Ontario Geological Survey, Geological Survey of Canada, and Conservation Ontario open house. Geological Survey of Canada, Open File 8212, p. 22. https://doi.org/10.4095/299778

Kjarsgaard, B.A., Sharpe, D.R., Stepner, D.A.J., Knight, R.D., and Russell, H.A.J. 2020. Mineralogy, geochemistry, grain size and pebble componentry of the Newmarket Till and the Dummer Moraines in the Kaladar-Tweed-Belleville area of eastern Ontario. In Russell, H.A.J. and Kjarsgaard, B.A. Eds. Southern Ontario groundwater project 2014–2019: summary report. Geological Survey of Canada, Open File 8536, 121-129. https://doi.org/10.4095/321096

Klassen R.A., 2001. A Quaternary geological perspective on geochemical exploration in glaciated terrain. In Drift Exploration in Glaciated Terrain; edited by M.B. McClenaghan, P.T. Bobrowsky, G.E.M. Hall, and S.J. Cook, Geological Society Special Publication 185, p. 1-17.

Knight, R.D., Landon-Browne, A.R.R., and Russell, H.A.J. 2016a. Portable XRF spectrometry of glacial-derived sediment from the Purple Woods borehole, southern Ontario. Geological Survey of Canada, Open File 7921, 1 .zip file. https://doi.org/10.4095/297890

Knight, R.D., Valiquette, L.J., and Russell, H.A.J. 2016b. Portable XRF spectrometry, fusion, multi acid, and aqua regia results from the Queensville borehole, Young Street Aquifer, southern Ontario. Geological Survey of Canada, Open File 7855. https://doi.org/10.4095/297721

Knight, R.D., Coffin, L.M., Valiquette, L.J., and Russell, H.A.J. 2016c. Portable XRF spectrometry, fusion, multi acid and aqua regia results from the Warden borehole, southern Ontario. Geological Survey of Canada, Open File 7922. https://doi.org/10.4095/297841

Knight, R.D., Bajc, A.F., Mulligan, R.P.M., Moroz, M.J., and Russell, H.A.J., 2018. Geochemistry of surficial sediment cores, southern Simcoe County, southern Ontario; Geological Survey of Canada, Open File 8257, 1 .zip file. https://doi.org/10.4095/308450

Knight, R.D., Stepner, D.A.J., Kjarsgaard, B.A., Sharpe, D.R., Crow, H., and Gerber, R. 2020. Lithology and geochemistry of a sediment core, Pickering area, Southern Ontario. Geological Survey of Canada, Open File 8511.

Logan, C.E., Russell, H.A.J., Bajc, A.F., Burt, A., Mulligan, R.P.M. and Sharpe, D.R. 2020. A three-dimensional surficial geology model of southern Ontario: Progress report. In Russell, H.A.J. and Kjarsgaard, B.A. Eds. Southern Ontario groundwater project 2014–2019: summary report. Geological Survey of Canada, Open File 8536, 49-64. https://doi.org/10.4095/321084

Pugin, A., Pullan, S.E., and Sharpe, D.R. 1999. Seismic facies and regional architecture of the Oak Ridges Moraine area, southern Ontario. Canadian Journal of Earth Sciences, 36: 3, 409–432. https://doi.org/10.1139/e98-104

Russell, H.A.J., Bajc, A.F., Knight, R.D., and Stepner, D. 2017. A Surficial Sediment Chemostratigraphic Framework for Southern Ontario. Summary of Field Work and Other Activity 2017, Ontario Geological Survey, Open File Report 6333, 30-1 to 30-11.

Sharpe, D.R. and Russell, H.A.J. 2016. A revised depositional setting for Halton sediments in the Oak Ridges Moraine area, Ontario. Canadian Journal of Earth Sciences, 53: 3, 281-303. https://doi.org/10.1139/cjes-2015-0150

Sharpe, D.R., Hinton, M.J., Russell, H.A.J., and Desbarats, A.J. 2002a. The need for basin analysis in regional hydrogeological studies, Oak Ridges Moraine, Southern Ontario. Geoscience Canada, 29: 3–20.

Sharpe, D.R., Russell H.A.J., and Logan, C.E. 2002b. Geological Characterization of a Regional Aquitard: Newmarket Till, Oak Ridges Moraine Area, Southern Ontario. Proceedings of the 55th Canadian Geotechnical and 3rd Joint IAH-CNC and CGS Groundwater Specialty Conferences, Niagara Falls, Ontario, October 20-23, 2002.

Sharpe, D.R., Russell H.A.J., and Logan, C.E., 2007. A 3-dimensional geological model of the Oak Ridges Moraine area, Ontario, Canada, Journal of Maps, 3:1, 239-253, DOI: 10.1080/jom.2007.9710842

Sharpe, D. R., Pullan, S. E., and Gorrell, G., 2011. Geology of the Aurora high-quality stratigraphic reference site and significance to the Yonge Street buried valley aquifer, Ontario; Geological Survey of Canada, Current Research no. 2011-1, 24 pages, doi:10.4095/286269

Sharpe, D.R., Kjarsgaard, B.A., Klassen, R.A., Knight, R.D., Logan, C.E., Russell, H.A.J., and Stepner, D.A.J. 2020. Regional geochemical survey of surficial sediment in southern Ontario: A geochemical baseline for environmental and human health assessment. In Russell H.A.J. and Kjarsgaard, B.A. Eds. Southern Ontario Groundwater Project 2014-2019 Summary. Geological Survey of Canada, Open File 8536, 83-94. https://doi.org/10.4095/321094

Shilts, W.W. 1993. Geological Survey of Canada's contributions to understanding the composition of glacial sediments. Canadian Journal of Earth Sciences, 30: 2, 333-353.

Stepner, D. A. J., Bajc, A.F., Burt, A. K., Knight, R.D., Russell, H. A. J. 2018. Geochemistry of surficial sediment cores, southern Ontario: data release; Geological Survey of Canada, Open File 8467, 10p. https://doi.org/10.4095/311224

Sun, S.-s. and McDonough, W.F. 1989. Chemical and Isotopic systematics of ocean basalts: Implications for mantle composition and processes. Geological Society, London, Special publications, v.42, p. 313-345, https://doi.org/10.1144/GSL.SP.1989.042.01.19

Mineralogy, geochemistry, grain size and pebble componentry of the Newmarket Till and the Dummer Moraines in the Kaladar-Tweed-Belleville area of eastern Ontario

Bruce A. Kjarsgaard*, David R. Sharpe, Daniel A.J. Stepner, Ross D. Knight, and Hazen A.J. Russell

Abstract: Downflow glacial dispersal was investigated across the southern Ontario Canadian Shield–Paleozoic boundary along two detailed transects with surficial sediment sampling, sub-parallel to the dominant NNE–SSW transport direction. The transects started on the Shield, transited the Shield–Paleozoic boundary and extended into the Paleozoic basin, with the target sediments being the Newmarket Till and the Dummer Moraines. Geochemistry and mineralogy analyses of the clay + silt (<0.063 mm) size fraction, and pebble componentry provide the data required to elucidate the provenance of these two glaciogenic sediment formations, and their potential relationship to each other. Till thickness increases from <2 m (on the Shield) to ≥10 m (on the Paleozoic basin) within 1 km south of the Shield–Paleozoic boundary. The Newmarket Till and Dummer Moraines both consist of carbonate-rich glaciogenic sediments, resultant from source material input dominated by limestone, shaly limestone and dolostone of the Paleozoic Gull River, Bobcaygeon and Verulam formations. Based on data from this study (matrix mineralogy and geochemistry, pebble componentry), we conclude that the Dummer Moraines are best termed as pebble-, cobble-, boulder-rich facies equivalents of the Newmarket Till. This study highlights the rapid transition in till matrix and clast content when transitioning from hard Canadian Shield lithologies to Paleozoic carbonate rocks and complexities along different glacial flowlines.

1. Introduction

A widespread region of southeastern Ontario is covered by surficial sediment deposits of Newmarket Till (Figure 1). The northern (and eastern) extent of Newmarket Till is the Precambrian Shield–Paleozoic terrain boundary, and to the west the Niagara escarpment (Figure 1). Newmarket Till is a silty sand-rich and clay-poor diamicton with high but quite variable stone content. It has unusually high densities (2.2–2.4 g/cm^3) and elevated seismic velocities (Vp ~2600 m/s) as determined by downhole geophysical studies, which can be traced across the region as a seismo-stratigraphic marker (Pugin et al. 1996, 1999; Sharpe et al. 2002). As Newmarket Till has low permeability, it forms a regional aquitard (Gerber 1999) that confines underlying aquifers, and is also a basal aquitard for overlying aquifers (e.g., the Oak Ridges Moraine; see Figure 1). Given the high sand content of this diamicton, the low permeability and overconsolidated nature is highly unusual. A number of basic questions exist with respect to better understanding the Newmarket Till, including:

1) What is the provenance of the Newmarket Till?
2) What is the relationship between the Newmarket Till and the Dummer Moraines?

We address these questions by undertaking two detailed sampling transects that start on the Canadian Shield and cross the Precambrian Shield–Paleozoic boundary southward into the Paleozoic basin. These transects are sub-parallel to the dominant NNE-SSW ice flow (Gadd 1980). A third transect, transverse to paleo-flow direction connects the two main transects in the vicinity of Shield–Paleozoic terrain and provides additional till sample sites in the region of the terrain boundary.

2. Previous work

A variety of quite similar tills in the Greater Toronto Area (GTA) have been described as: (1) dense, stony sand-silt till; (2) stony sand-silt till, and; (3) dense, stony sand till. Local names were used to describe these tills e.g. Wentworth Till (Karrow 1959), Leaside till (Karrow 1967), Humber till (Karrow 2005 and references therein), Newmarket Till (Gwyn and Dilabio 1973),

Geology Survey of Canada, Natural Resources Canada, 601 Booth Street, Ottawa, ON K1A 0E8

*corresponding author: bruce.kjarsgaard@canada.ca

Recommended citation: Kjarsgaard, B.A., Sharpe, D.R., Stepner, D.A.J., Knight, R.D., and Russell, H.A.J. 2020. Mineralogy, geochemistry, grain size and pebble componentry of the Newmarket Till and the Dummer Moraines in the Kaladar-Tweed-Belleville area of eastern Ontario. In Russell, H.A.J. and Kjarsgaard, B.A. Eds. Southern Ontario groundwater project 2014–2019: summary report. Geological Survey of Canada, Open File 8536, 121-129. https://doi.org/10.4095/321096

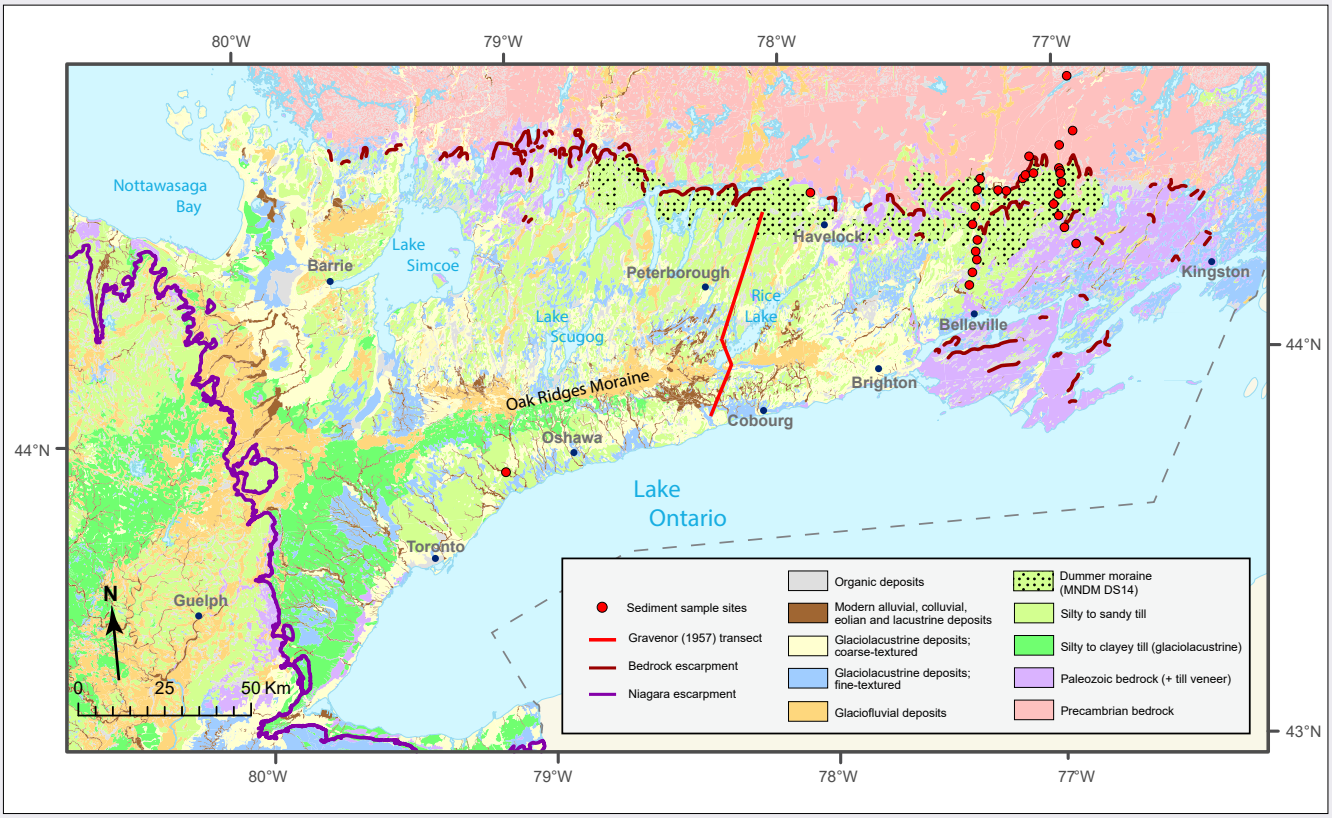


Figure 1. Simplified surficial geology map of southern Ontario, north of Lake Ontario (modified after Barnett et al. 1991), illustrating the sample sites of this study (filled red circles) with respect to mapped areas of the Dummer Moraines, and silty sand till (i.e. Newmarket Till). Thick red line demarcates the transect of Gravenor (1957).

Bowmanville till (Brookfield et al. 1982), and Northern till (Boyce et al. 1995; Boyce and Eyles 2000). Sharpe and Russell (2016), examined and integrated previous work on these tills (e.g., matrix grain size), and correlated all these dense stony sand-rich tills to be equivalents of Newmarket Till. An important aspect of the Newmarket Till is that the upper surface is often drumlinized (e.g., Peterborough drumlin field; Gravenor 1957; Boyce and Eyles 2000), and that, while till thickness is quite variable (~1–69 m), it typically ranges from 10–35 m in thickness (Sharpe et al. 2005; Knight et al. 2016a).

To the north of the drumlinized Newmarket Till and south of the Shield–Paleozoic boundary lies an area termed the Dummer Moraines (Chapman and Putnam 1984; Gravenor 1957; Barnett et al. 1991; Gadd 1980; Shulmeister 1989; Figure 1). The Dummer Moraines are described by Chapman and Putnam (1951) as rough, stony land bordering the Canadian Shield (to the north), with an irregular boundary that merges almost imperceptibly with the drumlinized (Newmarket) till plain to the south (Gravenor 1957; Shulmeister 1989). The Dummer Moraines are of low topographic relief (6–8 m; Gravenor 1957; Gadd 1980), contain abundant cobbles and boulders of Paleozoic and Shield rocks, but include areas of bare limestone and shallow till, and also a few areas of thicker, drumlinized till (Chapman and Putnam 1984; Gravenor 1957).

3. Sampling and methods

3.1 Sampling

Twenty-five till samples, two esker samples, and three Paleozoic bedrock samples were collected over two days in October 2016 (Figure 1). Samples of till were collected at depths of 0.1–0.5 m and weighed 7.3–15.2 kg. Two additional Newmarket Till samples were collected in 2017, one from the Duffins Creek area (Boyce et al. 1995), and one from the Dummer Moraines north-northwest of Havelock (Figure 1). Till samples are herein denoted by 'T' and esker samples by 'E' (numbered in Figure 2).

3.2 Methods

Samples were processed at Overburden Drilling Management, Nepean, Ontario. Two 500 g splits were taken before processing (excepting the esker and bedrock samples); one for archival purposes, and the other for grain size analysis, and mineralogy and geochemistry studies. Samples were disaggregated and wet sieved to <2 mm, 2–4 mm, 4–8 mm,

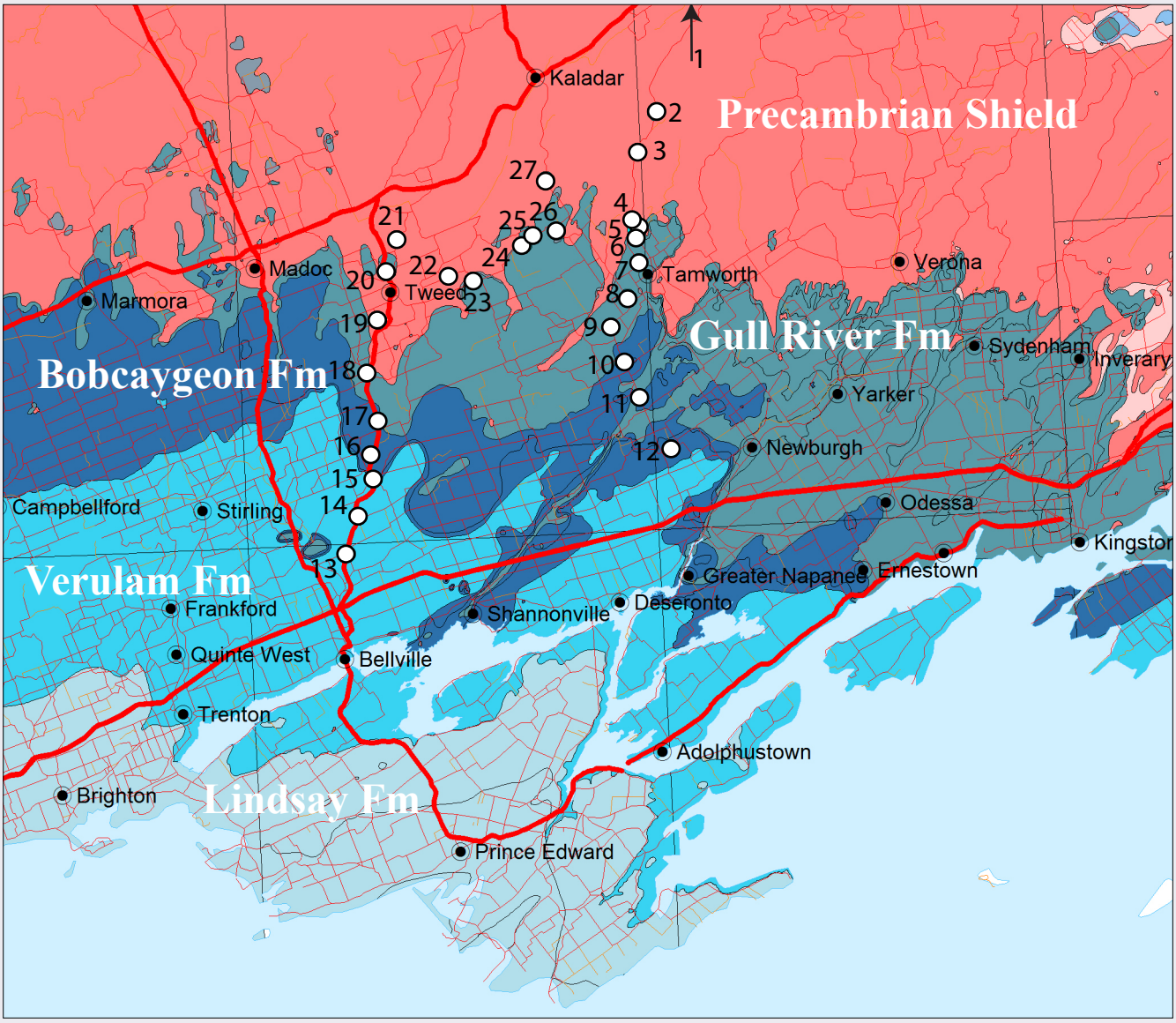


Figure 2. Location of samples from the two transects and cross-transect in the Kaladar – Tweed – Belleville region overlain on a bedrock geology backdrop, with the Precambrian geology simplified to one unit. Note the numerous Paleozoic Gull River Fm outliers north of the Precambrian Shield–Paleozoic terrain boundary.

8–16 mm and >16 mm size fractions. Pebbles (>2 mm size fractions) where cleaned in an oxalic acid wash, with each size fraction weighed. Pebble lithology counts were undertaken on the 8–16 mm and >16 mm size fractions.

Grain size analysis of the <2 mm size fraction for all samples was undertaken at the GSC sedimentology laboratory using wet sieving to produce a sand size fraction, and a clay + silt size fraction. A CAMSIZER Particle Size Analysis System was used for sand size (0.063–2 mm) particles, and a Beckman Coulter LS 13-320 laser diffraction particle size analyser for grain sizes <0.063 mm, i.e. clay plus silt size particles.

The mineralogy of the samples was determined by X-ray powder diffraction analysis (XRD). The clay + silt (<0.063 mm) size fraction of the samples where micronized using a McCrone mill in distilled water until a grain size of about 5–10 µm was obtained. The samples where dried and then back pressed into an aluminum holder to produce a randomly oriented specimen. Analysis was performed on a Bruker XRD, with quantitative interpretation carried out using TOPAS (Bruker AXS Inc.), a PC-based program that performs Rietveld refinement of the XRD spectra to identify mineral phases with a whole pattern fitting algorithm for determining abundances (in modal %) of the identified minerals.

A ~30 g split of the silt and clay (<0.063 mm) size fraction was sent to Bureau Veritas Commodities Ltd. in Vancouver, Canada for analysis. Sample analysis followed the methodology

detailed in Kjarsgaard et al. (2013a, b). Three sample digestion techniques where utilized i) aqua regia, ii) four-acid, iii) flux-fusion followed by nitric acid. Major element analysis of the fusion samples was undertaken by using inductively coupled plasma emission spectrometry (ICP—ES). The aqua regia and multi-acid digestions were analysed by inductively coupled plasma mass spectrometry (ICP—MS), which was also utilized for trace element determinations for the fusion samples. Analytical accuracy was monitored by the blind inclusion of certified and standard reference materials. A synthetic calcite-rich till standard based on CANMET Till-2 plus calcite was included as a reference monitor, given the bedrock underlying the Newmarket Till is carbonate-rich (predominantly limestone and dolostone). Analytical precision was evaluated by the duplicate analysis of selected samples.

4. Results

4.1 Surficial landscape observations

The most northerly 8 samples (#1T, 2E, 3E, 4T, 19T, 21T, 22T, 27T) are underlain by Shield terrain, all remaining till samples are underlain by Paleozoic bedrock terrain (Figure 2), as indicated on available geology maps. However, a number of Paleozoic inliers and Precambrian outliers are known in the study area (Figure 2), thus defining the bedrock underlying the till sample sites is in part problematic. The occurrence of Paleozoic outliers north of the Shield–Paleozoic terrain boundary (Figure 2) suggests that during the Quaternary, this boundary was likely even further to the north. A prominent set of topographic features in the study area are multiple, north facing Paleozoic cuestas, at the contact or just south of, the Shield–Paleozoic terrain boundary (Figures 1, 2).

Shield till samples are typically of limited thickness (10s cm to ~2 m) and red-brown in colour. Till samples 5T through 10T, and 17T, 18T, 20T and 23T through 26T where sampled from areas mapped as the Dummer Moraines (Barnett et al. 1991), whereas samples 11T through 16T are from areas mapped as silty-sandy till (i.e. the Newmarket Till). Samples from the Newmarket Till are typically olive drab to grey-green, depending on weathering; the matrix of samples from the Dummer Moraines is similar in colour. The Newmarket Till thickens from ~1 m to ~10 m thick over a down-flow distance of 1–2 km from the Shield–Paleozoic terrain boundary; further down-flow Newmarket Till is drumlinized and is suggested here to be of similar (or greater) thickness.

4.2 Grain size data

The <2 mm (sand + silt + clay) size fraction for the transect samples is compared with existing data (Singer et al. 1974; Sibul 1977; Gerber 1999; Golder and Associates 1999; Knight et al. 2020). for the Newmarket Till in Figure 3a. There is an overlap in the grain size distribution of transect samples that are from the Dummer Moraines, and those from Newmarket Till sampled immediately to the south of the Dummer Moraines (Figure 3a). The sand–silt–clay size distribution for Dummer Moraines samples lies within the range of this studies Newmarket Till sample data (Figure 3a). Based on this study, the matrix of both the Dummer Moraines and the Newmarket Till is best termed silty-sandy and clay-poor, with a subset of slightly more silt-rich samples being sandy-silty and clay poor. The clay size fraction of the Dummer Moraine and Newmarket Till samples from this study constitutes less than 10% of the <2 mm (clay + silt + sand) size fraction (Figure 3a).

The granulometry of the pebble (4 size fractions) + sand + silt + clay for nine samples from the East transect is illustrated in Figure 3b, plotted against distance from the Shield–Paleozoic terrain boundary. A number of basic observations can be made based on the data plotted. (1) There is an increase in all four pebble size fractions immediately down-flow of the terrain boundary (2 km distance), followed by a decrease in pebble content, for all four pebble size fractions with increasing transport distance. (2) There is a complementary initial decrease in the sand and silt content (2 km distance), followed by a steady increase in the sand and silt content. (3) Clay-sized particle abundance is variable, but low, typically in the range 0.4–1.5% (Figure 3b).

The decrease in % pebbles with distance, and complementary increase in the % sand- and % silt-size fractions is interpreted to be resultant from comminution of pebble-sized particles to sand- and silt-sized particles. The total pebble (stone; >2 mm) content of fifteen Dummer Moraines samples ranges from 24–64 weight %, average = 41.6%. The total pebble content of six Newmarket Till samples ranges from 9–50 weight %, average = 24.8%. The observation that pebble contents are higher in Dummer Moraines samples as compared to down-ice Newmarket Till samples supports the notion that pebble size particles are comminuted with increased transport distance. Of further interest is that the Newmarket Till pebble contents of this study are significantly higher than the estimated 5–15% stone content often quoted for Newmarket Till (Golder and Associates 1999); note that a single sample from Duffins Creek (this study) contained 22.4% pebbles.

4.3 Pebble lithology counts

The 8–16 mm and >16 mm pebble size fractions where examined for provenance studies. In detail, a wide variety of Precambrian Shield, and multiple Paleozoic lithologies were recognized and distinguished. For both pebble size classes, for each sample, the number of each lithology type was counted, and then weighed. All individual Shield and Paleozoic pebble types weights where then added to determine the total weight for each of these two main pebble groups (Shield and Paleozoic). The data is plotted as total % Paleozoic and total % Precambrian Shield, for the 8–16 mm and >16 mm size fractions for the East and West transects in Figure 4 (samples 4–12). For the East

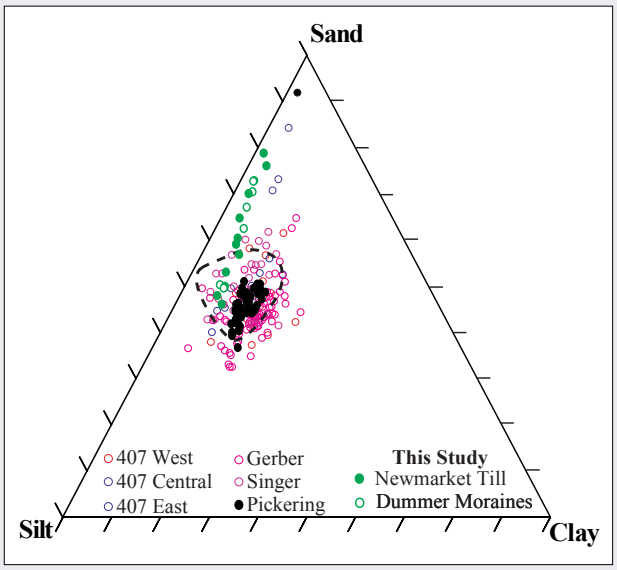


Figure 3a. Sand–Silt–Clay ternary diagram, comparing the granulometry of <2 mm fraction of samples from the Newmarket Till and Dummer Moraines (this study), with existing data for Newmarket Till from Singer et al. (1974), Sibul (1977), Gerber (1999), Golder and Associates (1999), and the Pickering borehole (Knight et al. 2020).

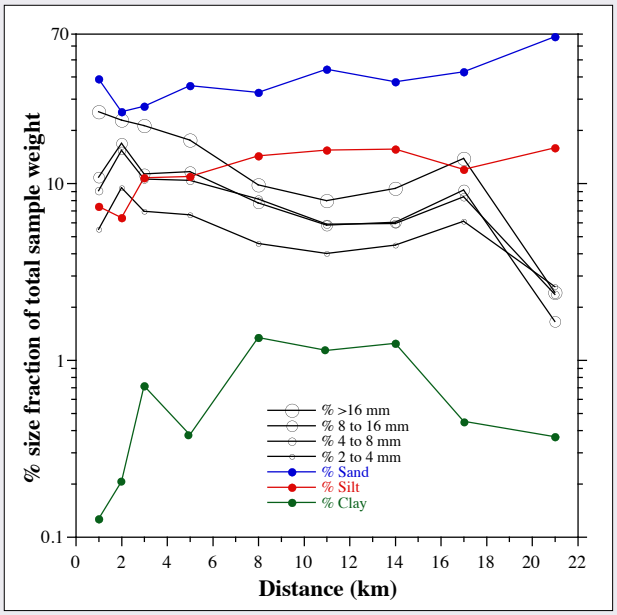


Figure 3b. Grain size variation with transport distance from the Shield–Paleozoic terrain boundary for till samples from the East transect.

transect there is a significant increase (from 0 to ~75%) in the amount of Paleozoic pebbles in both the 8–16 mm and >16 mm size fractions immediately down-flow of the terrain boundary (1 and 2 km distance), followed by fluctuating but high % Paleozoic pebbles to 11 km transport distance, followed by a decrease in % Paleozoic pebbles in till samples

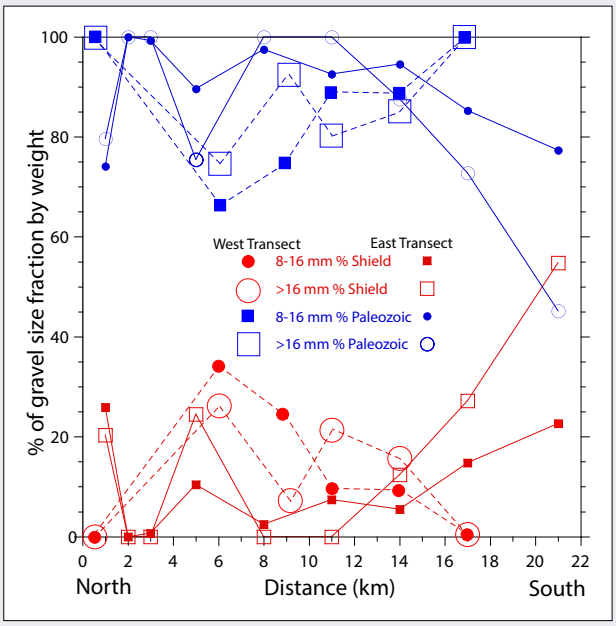


Figure 4. Provenance of pebbles in the 8–16 mm and >16 mm size fractions for the East, plotted as weight % Shield clasts and weight % Paleozoic clasts versus transport distance from the Shield–Paleozoic terrain boundary.

>12 km from the terrain boundary. At distances greater than 12 km from the terrain boundary, the percentage decrease for the >16 mm Paleozoic pebbles is more pronounced as compared to the percentage of 8–16 mm Paleozoic pebbles. The opposite results are observed in the Precambrian Shield derived pebbles. There is a sharp decrease (from 100 to ~25%) in the amount of Shield pebbles in both the 8–16 mm and >16 mm size fractions immediately down-flow of the terrain boundary (1 and 2 km distance), followed by fluctuating but low % Shield pebbles to 11 km transport distance, followed by an increase in % Shield pebbles from samples >12 km from the terrain boundary. The % increase is greater for the >16 mm Shield pebbles as compared to the 8–16 mm Shield pebbles (Figure 4). These results suggest that there is more effective comminution of Paleozoic pebbles as compared to Shield pebbles with greater transport distance from the Shield–Paleozoic terrain boundary. The West transect, in contrast, shows variable results for the two pebble size fractions and pebble types. For the West transect (samples 13–18), Paleozoic pebble counts are 100% 1 km down-flow of the terrain boundary, oscillate at lower Paleozoic pebble contents (65–90%) from 6 to 14 km down-flow, and then increase back to 100% 17 km down-flow. It is unclear if the differences between the East and West transects is related to transport differences, or a sub-optimum understanding of the underlying bedrock lithologies i.e. non-recognized bedrock inliers or outliers.

4.4 Mineralogy

The modal mineralogy of the clay + silt fraction, as determined by XRD analysis provide insight to the provenance source materials of the Dummer Moraines and the Newmarket Till. In Figure 5a, the modal % dolomite is plotted versus transport distance from the Shield–Paleozoic terrain boundary. Precambrian Shield source rocks are low in dolomite (and calcite). In contrast, the Lower Gull River Fm, which outcrops at the terrain boundary is a dolostone, while the Upper Gull River Fm is a lime mudstone (marlstone). There is a significant increase in modal % dolomite content of the clay + silt fraction of the sampled tills, from <1% in Shield till samples, to 8–48% at distances of 1–2 km down-ice from the Shield–Paleozoic terrain boundary (Figure 5a). These results indicate a significant uptake and incorporation of Lower Gull River Fm dolostone into till samples south of the terrain boundary, followed by decreasing dolomite contents with increasing distance from the terrain boundary i.e. a dilution effect. Notably, the East, West and Cross transects differ in terms of maximum dolomite content 1–2 km down-flow from the terrain boundary. This suggests fundamental differences with respect to the spatial distribution of Lower Gull River dolostone, and/or incorporation of this dolostone into the Dummer Moraines and Newmarket Till samples.

The clay + silt fraction modal mineralogy data is also instructive to examine from the perspective of Precambrian Shield derived minerals (quartz, plagioclase feldspar, K-feldspar, amphibole, clinopyroxene and phlogopite/biotite), versus Paleozoic bedrock derived minerals (calcite, dolomite, clay minerals). Total modal % Shield minerals and total modal % Paleozoic minerals are plotted versus transport distance from the terrain boundary (Figure 5b). Both transects show a sharp increase in calcite + dolomite immediately down-flow of the terrain boundary, with a complementary decrease in Shield-derived minerals. However, at greater transport distances, data for the East and West transects diverge and show completely opposite trends. The East transect has decreasing calcite + dolomite and increasing Shield mineral contents (Figure 5b). In contrast the West transect, from 1 km to 5 km transport distance has lower modal calcite + dolomite content that subsequently increases with transport distance, whereas Shield mineral content increases at 5 km followed by decreasing modal abundance at greater transport distance. These results are consistent with the variations in modal dolomite (+ calcite) content for the East and West transects (Figure 5a) suggesting fundamental differences in the spatial distribution and/or incorporation of Gull River Fm dolostone (and marlstone) source rocks into the till.

The parallel to ice-flow 50 km long transect data of Gravenor (1957) from Center Dummer to just northeast of Port Hope (Figure 1), starting in the Dummer Moraines and transiting through the Newmarket Till, is also plotted on Figure 5b, along with the mineralogy data (this study) from the Purple Woods borehole (Knight et al. 2016a). For the Centre Dummer to Port Hope transect, Gravenor (1957) determined the amount of Shield material (minerals) in the till by utilizing a geochemical approach with respect to soluble (Paleozoic dominated) and insoluble (Shield dominated) residues. The results are similar to that of the East transect, with a notable increase in Shield material (mineral) content at 18 km down-flow from the Shield–Paleozoic terrain boundary (Figure 5b). Gravenor (1957) also denoted variable, but high Shield material (mineral) contents of 45–50% at ~25–55 km down-flow (Figure 5b). This Shield-derived content in the Newmarket Till samples of Gravenor (1957) is quite similar to the 48–52% Shield mineral content of six Newmarket Till samples from the Purple Woods borehole (Figure 5b), which is 100 km down-flow from the Shield–Paleozoic terrain boundary (Knight et al. 2016a).

A final note with respect to the mineralogy of the silt + clay fraction of the Newmarket Till from transect samples in this study is the very low abundance of clay minerals (i.e. bonafide sheet silicate clay minerals). In the silt + clay size fraction, total clay mineral content is <6 modal % (from samples 1–2 km down-ice from the Shield–Paleozoic terrain boundary), but typically ranges from trace amounts to 4 modal % (avg. = 1.8 modal %). The higher clay content just south of the terrain boundary is interpreted to be related to uptake of clay minerals from the Upper Gull River lime mudstone (marlstone).

4.5 Geochemistry

Geochemistry data on the clay + silt fraction for the Newmarket Till transect samples (n = 6; this study) is combined with additional samples (n = 89) from boreholes in the Greater Toronto area (South Simcoe, Queensville, Warden, Aurora, Pickering, Purple Woods) plus one Duffins Creek sample, and compared to samples from the Dummer Moraines in the transect area (n = 12) plus one sample from north of Havelock (Figure 6). Basic observations of the geochemical data (Figure 6) are as follows: (1) The overall range of concentration levels for all oxides/elements for the Newmarket Till and Dummer Moraines samples are similar; (2) The box (representing 50% of the data) and the whiskers, for all oxides/elements, show much less dispersion for the Newmarket Till samples as compared to the Dummer Moraines samples, but there are outliers in the Newmarket data set; (3) The median for the Newmarket Till samples falls within the upper or lower quartile of the Dummer Moraines samples, and; (4) High Cr and Zr contents in the Dummer Moraines samples is consistent with their proximity to Precambrian Shield source-rocks, and their high MgO (and CO_2) contents consistent with their proximity to Paleozoic Lower Gull River Fm dolostone source rocks.

5. Discussion

New information characterizing the geochemistry and mineralogy of the clay + silt fraction, and pebble lithology

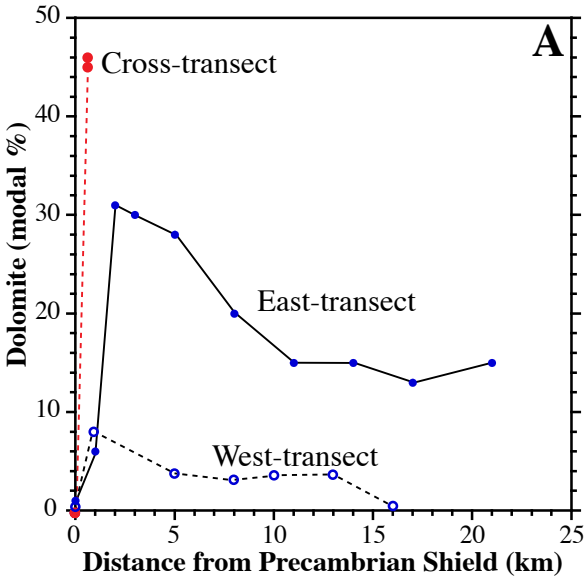


Figure 5a. Modal % dolomite in the silt + clay fraction (as determined by XRD), versus transport distance from the Shield–Paleozoic terrain boundary, for the East-, West- and cross-transects.

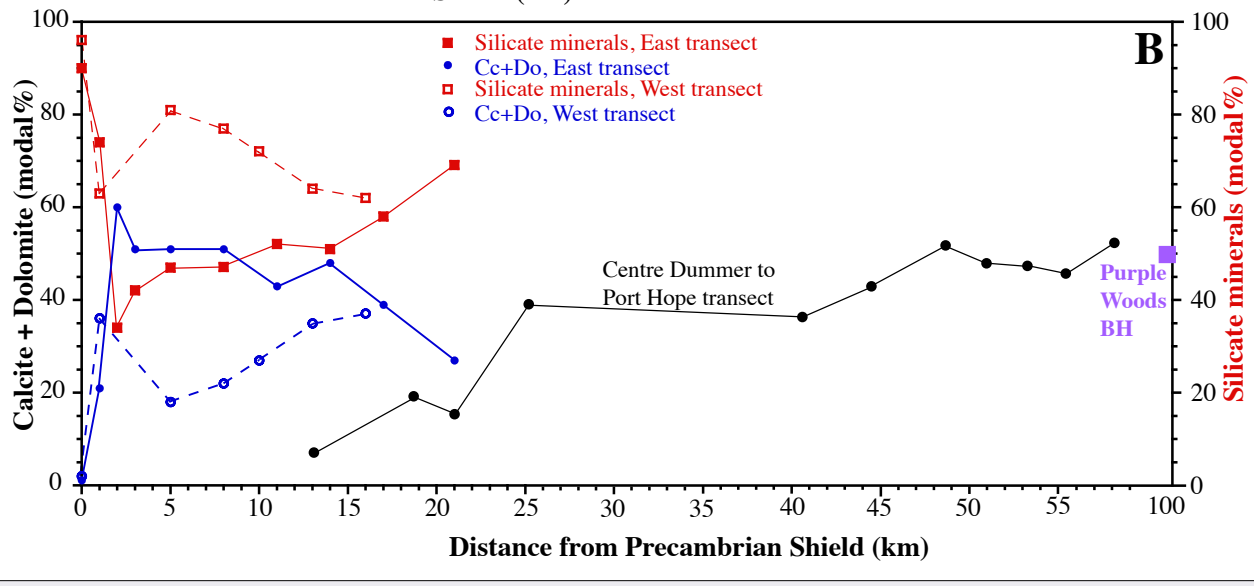


Figure 5b. Modal % calcite + dolomite (Cc + Do), for the silt + clay fraction (as determined by XRD, left axis) and modal % silicate minerals (quartz + plagioclase + K-feldspar + amphibole + clinopyroxene + phlogopite/biotite) for the silt + clay fraction (as determined by XRD, right axis), versus transport distance from the Shield–Paleozoic terrain boundary. Centre Dummer to Port Hope transect data is from Gravenor (1957); see text for details.

abundances of the Newmarket Till and Dummer Moraines fills an important knowledge gap. The provenance of the Newmarket Till consists of two sources: the Precambrian Shield, and; the Paleozoic limestones, dolostones, and shaly limestones of the Gull River, Bobcaygeon and Verulam formations (Figure 2). A comparison of geochemistry and mineralogy data for the clay + silt matrices of the Newmarket Till and Dummer Moraines samples indicates they are very similar, with limited variability. The minor variations observed in the mineralogy (and hence geochemistry) of Newmarket Till and Dummer Moraines can be directly attributed to the incorporation of specific bedrock lithology types (e.g. Lower Gull River dolostone) into the till. An important qualifier with respect to the terminology (and understanding) of Newmarket Till is that it is a carbonate-rich till, with 18–50 modal % calcite + dolomite. Dummer Moraines samples are similar (but extending to higher carbonate contents), with 35–60 modal % calcite + dolomite. Newmarket Till and Dummer Moraines samples are also very poor in clay minerals with <6 modal % of the clay + silt fraction consisting of bonafide clay-sized sheet silicates (average = 1.8%).

Pebble (stone) contents of Newmarket Till samples are quite high (9–50 weight %, average this study = 25%), and it is suggested that previous visual estimates of 5–15% stone

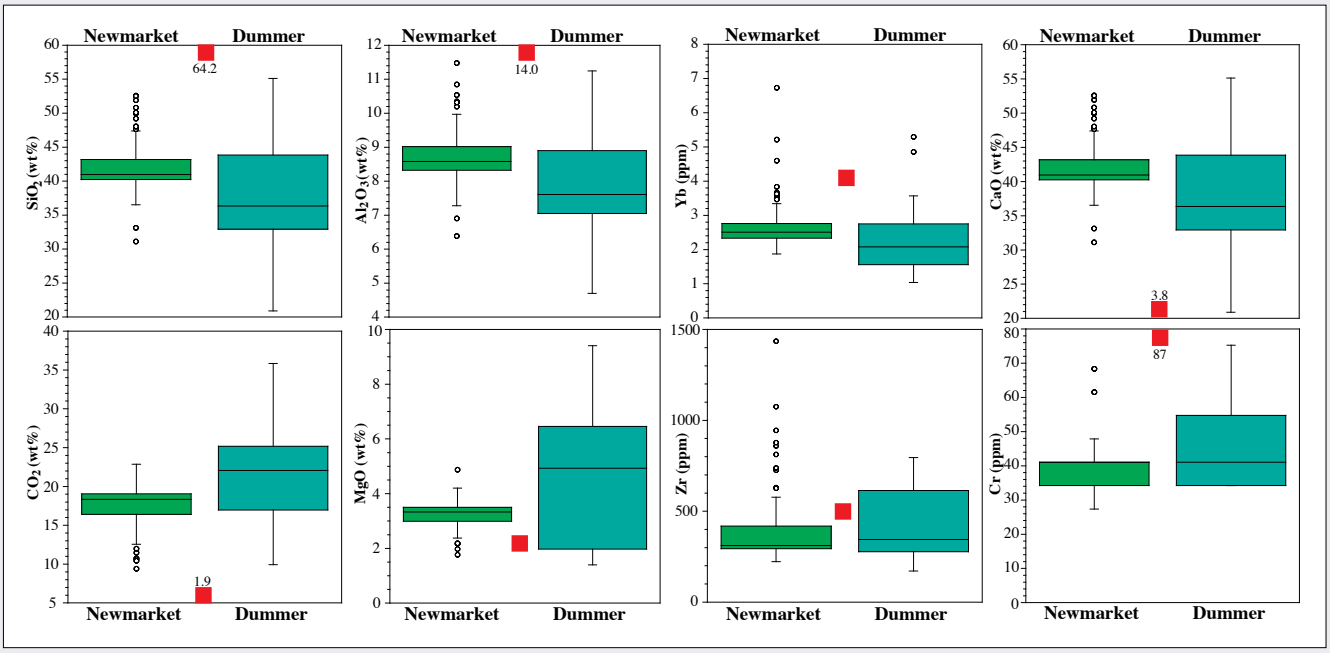


Figure 6. Box and Whisker plots for selected oxides/elements for the clay + silt fraction of the Newmarket Till (n = 95), Dummer Moraines (n = 13), and an average Shield till composition (red squares, n = 5). All sample data are from fusion total digestion ICP—ES/MS analyses. Data sources: Aurora borehole (n = 5; Knight et al. 2015); Warden borehole (n = 7; Knight et al. 2016c); Queensville borehole (n = 4; Knight et al. 2016b); South Simcoe borehole (n = 19; Knight et al. 2018); Pickering borehole (n = 47; Knight et al. 2020); Purple Woods borehole (n = 6; this study); Duffins Creek (n = 1; this study); Kaladar – Tweed – Belleville transects (n = 6; this study); Dummer Moraines (n = 13; this study); Shield till (n = 5; this study). The upper and lower limits of the box are the upper and lower quartiles, and the thin line within the box is the median. The upper and lower whiskers are 1.5x the interquartile range plus the upper quartile, and lower quartile, respectively. Open circles represent outliers beyond the whiskers. Average Shield till compositions that lie outside the range for Newmarket and Dummer samples have their average concentration level beside the red square i.e. SiO_2 64.2 wt %. See text for discussion.

contents should be re-evaluated. In contrast, the Dummer Moraines samples have higher pebble contents of 21–64% (average = 42%) as compared to Newmarket Till samples. We therefore conclude, given the similarity of the matrix mineralogy and geochemistry and the pebble lithology data, that the Dummer Moraines and Newmarket Till are facies equivalents, with the Dummer Moraines being the extremely pebble-, cobble- and boulder-rich variant. Similar conclusions were previously reached by Gadd (1980) and Schulmeister (1989). The field observations that the low relief and variably drumlinized Dummer Moraines transitions imperceptibly into drumlinized Newmarket Till (Gravenor 1957, Schulmeister 1989) is consistent with our observations (i.e. the clay + silt matrices and the pebble lithology types of Newmarket Till and Dummer Moraines have the same provenance). The higher pebble (stone) and boulder contents of the Dummer Moraines in comparison to Newmarket Till was interpreted by Gadd (1980) and Schulmeister (1989) to be from enhanced incorporation of karstic Paleozoic bedrock from north-facing (perpendicular to ice-flow) cuestas.

Current results allow a preliminary assessment of sediment dispersion. Sampled sediment lithology, mineralogy and grain size all indicate rapid incorporation of Paleozoic rocks at or within ~1–2 km of the Shield–Paleozoic boundary. The sediment load increase is reflected by <1 m to ~10 m of till deposition across this zone. Deposition is high in this short transport zone, and maintains a ~10 m sediment thickness for many 10s of km down flow. The East transect data for this study corroborates the work of Gravenor (1957), with resistate Shield material (both >2 mm pebbles and <63 µm minerals) less susceptible to comminution, and thus increasing in concentration with increasing distance down-flow as compared to Paleozoic sourced dolostone and limestone pebbles, and calcite and dolomite. However, the East and West transects have contrasting pebble lithologies and mineralogy, as well as comminution characteristics, indicating differential erosion and transport of source region Shield material and limestones, dolostones, and shaly limestones of the Gull River, Bobcaygeon and Verulam formations. This study highlights the spatial heterogeneity (i.e. East and West transects) and hence potential significance for aquitard characteristics of the Newmarket Till depending upon upflow source provenance. The presence of readily erodible carbonate or mud-rich carbonate units can certainly influence the matrix grain size and geochemistry.

6. Future work

Additional and longer NNE–SSW transects, from the Precambrian Shield to Lake Ontario, and to the west of the current study area to the east side of Lake Simcoe would be extremely beneficial to further understand Newmarket Till / Dummer Moraines provenance, and particle comminution with transport distance. Given the facies equivalency of Newmarket Till / Dummer Moraines, what is the origin of the low relief (i.e. areas of very thin till and/or exposed bedrock) and high relief (i.e. variably drumlinized) regions of the Dummer Moraines, which imperceptibly transition into drumlinized Newmarket Till (Gravenor 1957; Shulmeister 1989; this study).

7. Acknowledgements

An internal review at the Geological Survey of Canada was completed by J. Bednarski. This work was funded through the Groundwater Geoscience Program of the GSC. This work is a contribution to the GSC–OGS southern Ontario project on groundwater 2014–2019.

8. References

Barnett, P.J., Henry, A.P., and Cowan, W.R. 1991. Quaternary geology of Ontario, southern sheet. Ontario Geological Survey, Map 2556, scale 1:1 000 000.

Boyce, J.I. and Eyles, N. 2000. Architectural element analysis applied to glacial deposits: internal geometry of a late Pleistocene till sheet, Ontario, Canada. Geological Society of America Bulletin, 112: 98–118.

Boyce, J.I., Eyles, N., and Pugin, A. 1995. Seismic reflection, borehole and outcrop geometry of Late Wisconsin tills at a proposed landfill near Toronto, Ontario. Canadian Journal of Earth Sciences, 32: 1331–1349.

Brookfield, M.E., Gwyn, Q.H.J., and Martini, I.P. 1982. Quaternary sequences along the north shore of Lake Ontario: Oshawa – Port Hope. Canadian Journal of Earth Sciences, 19: 1836–1850.

Chapman, L.J. and Putnam, D.F. 1984. The Physiography of southern Ontario (3rd edition). Ontario Geological Survey, Special Volume 2, 270 pp.

Gadd, N.R. 1980. Late-stage regional ice-flow patterns in eastern Ontario. Canadian Journal Earth Sciences, 17: 1439–1453.

Gerber R.E. 1999. Hydrogeologic behaviour of the Northern till aquitard near Toronto, Ontario. PhD thesis, University of Toronto.

Golder and Associates, 1999. Foundation investigation and design proposed Highway 407 easterly, West Duffins Creek and tributary overpass bridges, fills, cuts and culverts. Pickering Ontario, 47 pp.

Gravenor, C.P. 1957. Surficial geology of the Lindsay-Peterborough area, Ontario, Victoria, Durham and Northumberland Counties. Geological Survey of Canada, Memoir 288, 60 p.

Gwyn, Q.H.J. and DiLabio, R.N.W. 1973. Quaternary geology of the Newmarket area; southern Ontario. Ontario Division of Mines, Preliminary Map P836, scale 1:50 000.

Karrow, P.F. 1959. Pleistocene geology of the Hamilton area. Ontario Department of Mines, Geological Circular No. 8, 16 pp.

Karrow, P.F. 1967. Pleistocene geology of the Scarborough area. Ontario Department of Mines, Maps 2076, 2077, scale 1:50 000.

Karrow, P.F. 2005. Quaternary geology of the Brampton area. Ontario Geological Survey, Report 257, 59 pp.

Kjarsgaard, B.A., Knight, R., Plourde, A.P., Sharpe, D. R. and Lesemann, J.-E. 2013a. Geochemistry of till samples, NTS 75-I, 75-J, 75-O, 75-P (Mary Frances Lake – Whitefish Lake – Thelon River area), Northwest Territories. Geological Survey of Canada, Open File 7351, 28 p. and 3 digital appendices.

Kjarsgaard, B.A., Knight, R.D., Grunsky, E.C., Kerr, D.E., Sharpe, D.R., Cummings, D.I., Russell, H.A.J., Kerswill, J.A. and Wright, D.F. 2013b. till geochemistry studies of the Thaidene Nene MERA study area. Geological Survey of Canada, Open File 7196, p. 313–337.

Knight, R.D., Sharpe, D.R., and Valiquette, L.J. 2015. Portable XRF spectrometry, fusion, multi acid, and aqua regia results from the Aurora borehole, Yonge Street Aquifer, southern Ontario. Geological Survey of Canada, Open File 7919, 21 p.

Knight, R.D., Landon-Browne, A.R.R., and Russell, H.A.J. 2016a. Portable XRF spectrometry of glacial-derived sediment from the Purple Woods borehole, southern Ontario. Geological Survey of Canada, Open File 7921, 26 p.

Knight, R.D., Valiquette, L.J., and Russell, H.A.J. 2016b. Portable XRF spectrometry, fusion, multi acid, and aqua regia results from the Queensville borehole, Young Street Aquifer, southern Ontario. Geological Survey of Canada, Open File 7855, 23 p.

Knight, R.D., Coffin, L.M., Valiquette, L.J., and Russell, H.A.J. 2016c. Portable XRF spectrometry, fusion, multi acid, and aqua regia results from the Warden borehole, southern Ontario. Geological Survey of Canada, Open File 7922, 21 p.

Knight, R.D., Bajc, A.F., Mulligan, R.P.M., Moroz, M.J., and Russell, H.A.J. 2018. Geochemistry of surficial sediment cores, southern Simcoe County, southern Ontario. Geological Survey of Canada, Open File 8257.

Knight, R.D., Stepner, D.A.J., Kjarsgaard, B.A., Sharpe, D.R., Crow, H., and Gerber, R. 2020. Lithology and geochemistry of surficial sediment cores, Pickering area, southern Ontario. Geological Survey of Canada, Open File 8511, 45 p.

Pugin, A., Pullan, S.E., and Sharpe, D.R. 1996. Observations of tunnel channels in glacial sediments with shallow land-based seismic reflection. Annals of Glaciology, 22: 176–180.

Pugin, A.J.-M., Pullan, S.E., and Sharpe, D.R. 1999. Seismic facies and regional architecture of the Oak Ridges Moraine area, southern Ontario. Canadian Journal of Earth Sciences, 36: 3, 409–432.

Shulmeister, J. 1989. A conceptual model for the deposition of the Dummer Moraine, Southern Ontario. Geomorphology, 2: 385–392. https://doi.org/10.1016/0169-555X(89)90022-6

Sharpe, D.R., Hinton, M.J., Russell, H.A.J., and Desbarats, A.J. 2002. The need for basin analysis in regional hydrogeological studies, Oak Ridges Moraine, Southern Ontario. Geoscience Canada, 29: 3–20.

Sharpe, D.R., Russell, H.A.J., and Logan, C. 2005. Structural model of the Greater Toronto and Oak Ridges Moraine areas, southern Ontario: Newmarket Till. Geological Survey of Canada, Open File 5066, 1 poster.

Sharpe, D.R. and Russell, H.A.J. 2016. The depositional setting of Halton Formation sediments in the Oak Ridges Moraine Area, Ontario. Canadian Journal Earth Sciences. 53: 281–303.

Sibul, U., Wang, K.T., and Vallery, D. 1977. Ground-water resources of the Duffins Creek-Rouge River drainage basins. Ministry of the Environment, Water Resources Branch, Water Resources Report 8, Toronto, Ontario, 65 pp.

Singer, S. 1974. A hydrological study along the north shore of Lake Ontario in the Bowmanville-Newcastle area. Ontario Ministry of Environment, Water Resources Report 5d, 72 pp.

Hydrogeophysics data acquisition for the characterization of hydraulic properties of the Vars-Winchester esker, southeastern Ontario

Daniel Paradis[1]*, André J.-M. Pugin[2], Heather L. Crow[2], Greg A. Oldenborger[2], Hazen A.J. Russell[2], and Michael Melaney[3]

Abstract: A general workflow is proposed to characterize hydraulic properties of unconsolidated aquifers from geophysical data. Three-dimensional hydraulic property models are essential for groundwater flow and solute transport studies aimed at assessing water resources sustainability. Spatial coverage offered by conventional hydraulic characterization approaches based on hydraulic tests in wells are; however, often limited due to the time required to perform hydraulic tests, especially when high-resolution and/or large complex areas need to be characterized. On the other hand, geophysical surveys can reveal important architectural features of an aquifer system; however, the quantification of geophysical attributes into hydraulic properties is difficult to achieve under field conditions. To overcome those limitations, a hydrogeophysical approach based on the definition of site-specific relationships between collocated geophysical and hydraulic data is proposed to allow the translation of geophysical attributes into hydraulic properties. The development and application of this approach that is currently underway for the Vars-Winchester esker system in south-east Ontario is reported here.

Résumé: Un cadre général de caractérisation des propriétés hydrauliques des aquifères granulaires à partir des données géophysiques est proposé. La définition de modèles tridimensionnels de propriétés hydrauliques est essentielle pour l'étude de l'écoulement de l'eau souterraine et du transport de masse dans les systèmes aquifères. La couverture spatiale pouvant être achevé par les approches de caractérisation hydraulique conventionnelles basées sur des essais hydrauliques en puits est souvent très limitée à cause du temps requit pour la réalisation des essais. Ceci est d'ailleurs exacerbé lorsque qu'une caractérisation fine et/ou la couverture de grandes régions complexes géologiquement sont nécessaires. Toutefois, même si la géophysique permet d'imager l'architecture complexe des systèmes aquifère, la quantification des attributs géophysiques en valeurs de propriétés hydrauliques est souvent difficile à réaliser in-situ. Pour pallier ces limitations, une approche hydrogéophysique basée sur la définition de relations in-situ entre des mesures géophysiques et hydrauliques co-localisées est proposée afin de permettre la conversion des attributs géophysiques en propriétés hydrauliques. Les avancées récentes dans le développement et l'application de cette approche pour l'esker Vars-Winchester dans le sud-est de l'Ontario sont ici rapportées.

1. Introduction

A complete characterization of an aquifer system would ideally yield a site-specific three-dimensional model of hydraulic properties (e.g., hydraulic conductivity-*K*) delineating hydrogeological heterogeneities such as barrier to flow (low-*K*) and preferential pathways (high-*K*). Hydraulic properties are mostly estimated using hydraulic tests carried out in wells (e.g., slug and pumping tests). Although such tests are generally reliable sources of data about hydraulic properties, they are costly and time consuming to complete. Consequently, hydraulic property estimates are usually available only from a few wells and at such a low-spatial resolution that it prevents adequate definition of hydrogeological heterogeneities (Butler 2005).

Given the limitations of conventional hydraulic characterization, hydrogeophysics is increasingly recognized as an effective alternative to compensate for the scarcity of

[1] Geological Survey of Canada, 490 rue de la Couronne, Quebec City, QC G1K 9A9
[2] Geology Survey of Canada, Natural Resources Canada, 601 Booth Street, Ottawa, ON K1A 0E8
[3] South Nation Conservation Authority, 38 Victoria Street, Finch, ON K0C 1K0
*corresponding author: daniel.paradis@canada.ca

Recommended citation: Paradis, D., Pugin, A.J.-M., Crow, H.L., Oldenborger, G., Russell, H.A.J., and Melaney, M. 2020. Hydrogeophysics for the characterization of hydraulic properties of the Vars-Winchester esker, southeastern Ontario. In Russell, H.A.J. and Kjarsgaard, B.A. Eds. Southern Ontario groundwater project 2014–2019: summary report. Geological Survey of Canada, Open File 8536, 131-138. https://doi.org/10.4095/321098

hydrogeological data by using geophysical data to estimate hydraulic properties (Rubin and Hubbard 2005). The value of using geophysical data for hydrogeological characterization lies in the extensive spatial coverage generally offered by geophysical methods, which could yield invaluable information about aquifer system architecture and on trends in hydraulic properties within those structures. Reliable estimates of hydraulic properties from geophysical data should be based on sound relations between hydraulic and geophysical data (Chen et al. 2001; Paradis et al. 2015).

The concept of translating geophysical data into hydraulic properties is not new in the scientific literature; however, very few field studies have been published to demonstrate the robustness of such approaches for hydrogeological studies. Existing studies generally are applied to relatively homogeneous media and/or over very small sites (e.g., Binley et al. 2005; Dubreuil-Boisclair 2006; Paasche et al. 2006; Dafflon et al. 2009; Ruggeri et al. 2013), which in practice are of limited scope. The large degree of uncertainties associated with hydrogeophysical relationships under field conditions may explain the restricted popularity of the approach among practitioners. Typically, disparity in scales between hydraulic and geophysical data, as well as the insensitivity of certain geophysical parameter to hydraulic property variations for different geological materials are the more important problems which can limit the quantification of hydraulic properties from geophysical data.

The aim of this study is to extend hydrogeophysical methodologies previously developed by the Geological Survey of Canada (GSC) in other projects (Pugin et al. 2009a; Oldenborger et al. 2014; 2016; Paradis et al. 2014; 2015) at a scale relevant for groundwater resource investigations (e.g., few square kilometers). For this purpose, the Vars-Winchester esker near Ottawa (Ontario) was chosen as a pilot site to develop the methodology. This site was chosen for its simple geological architecture, quality of existing data, ability to collaborate with Conservation Authority, ease of land access, and potential interest in the esker as a groundwater supply for the local community.

As the current research is still underway, the remainder of this paper is devoted to the general description of the workflow proposed for hydrogeophysical data acquisition and integration. Then, a description of the study area and the hydraulic and geophysical methods selected for the study. We conclude with some perspectives on the work to be completed to achieve the project goals.

2. General workflow for data acquisition and integration

The general workflow for data acquisition and integration followed in this study to characterize heterogeneity of hydraulic properties is outlined in Figure 1. This sequential workflow is centred on the acquisition of a training dataset to establish

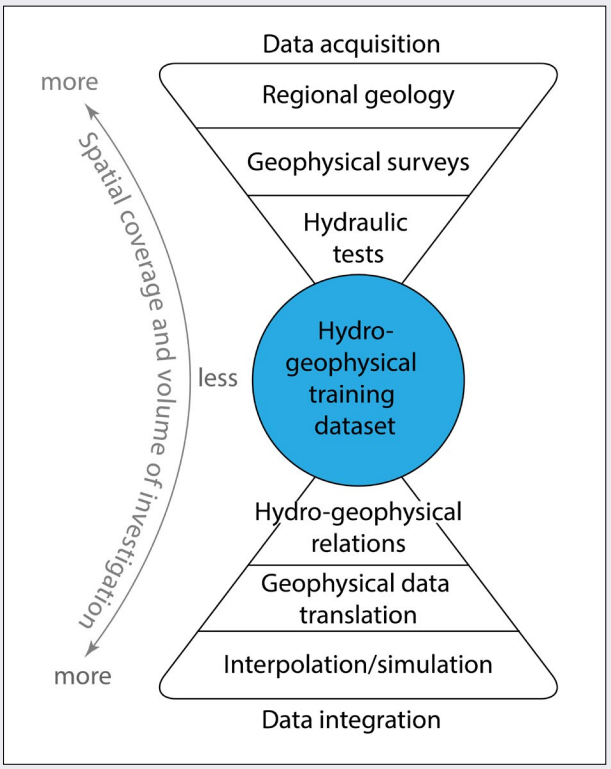


Figure 1. General workflow for the acquisition and integration of hydro-geophysical data leading to the production a site-specific three-dimensional model of hydraulic properties of an aquifer system.

hydrogeophysical relations specific for the study area, which are thereafter used to translate geophysical data into hydraulic properties. While this approach leads to site-specific relations, the overall approach is general and can be adapted to different hydrogeological contexts. This workflow was successfully applied in hydrogeology to solve issues related to transport of contaminants (Paradis et al. 2014), and is commonly used in the oil industry for hydrocarbon exploration (e.g., Bradford and Babcock 2013).

First, data acquisition sequence follows a zoom-in approach initially using general methods with greater spatial coverage and less resolution (e.g., regional geology), followed by more targeted methods with higher resolution and smaller volume of investigation (e.g., hydraulic tests in wells). Methods with smaller volume of investigation are applied only at strategic locations according to changes in stratigraphic and/or geophysical responses deduced from the more general methods. This allows for the inclusion of the range of material types (geological and/or geophysical) present over the study area. This sequence is intended to rationalize data collection by minimizing the amount of information collected and maximizing their significance by providing the general context of each measurement. For instance, because high-resolution hydraulic tests are expensive to collect for a large region,

the proposed approach allows for the selection of only the hydraulic test locations (e.g., specific intervals within a well) that are representative of the study area (according to the geology and the geophysics) and in a number sufficient to establish meaningful hydrogeophysical relations. As estimates of hydraulic properties provided by hydraulic tests are generally more laborious to acquire than geophysical data, the size of the training dataset will be limited by the number of hydraulic tests available. Thus, the selection of the testing intervals to build the training dataset is critical to make sure that all lithological and/or geophysical facies have been tested. Also, an effort is made to acquire a colocated dataset (e.g., wells along or very close to the geophysical surveys) to properly compare data of various sources.

Once the training dataset is acquired, hydrogeophysical data are integrated to establish site-specific relations. In this study, different approaches will be compared, such as theoretical petrophysical expressions (e.g., Archie's law) and statistical techniques (e.g., learning machine). The relations defined with the different integration approaches will also be verified through internal and external verification processes. Internal verification involves cross-validation techniques where different subsets of the training datasets are used sequentially as predictors and predictands. For external validation, the hydraulic data for one of the wells will be hidden (not used to establish relations) and used only at the end of the process to compare with converted geophysical data. Once the hydrogeophysical relations are properly defined, the prediction of hydraulic properties from unseen geophysical data (without associated hydraulic data) is carried out. Interpolation of translated geophysical data can also be conducted over the study area to complete a three-dimensional model of hydraulic properties.

3. Study area

The study area is located near Embrun (Ontario) approximately 45 km south-east of Ottawa in the South Nation River watershed (Figure 2). The area was part of a previous GSC groundwater study in collaboration with the South Nation Conservation Area (e.g., Cummings and Russell 2007; Cummings et al. 2011). This region is characterized by the presence of extensive Champlain Sea mud deposits which bury and encase the Vars-Winchester esker (Cummings et al. 2011). The esker has a north-south orientation and its approximate length is 80 km, extending from near the Ottawa River at the north to Chesterville in the south. The overall width of the esker is generally a few hundred meters. The local bedrock geology is dominated by Paleozoic carbonate. Three main stratigraphic units compose the esker system: (i) a till sheet over carbonate bedrock; (ii) the Vars-Winchester esker; and (iii) overlying Champlain Sea mud (Figure 3). As described by Cummings et al. (2011), the till is massive, mud dominated carbonate rich, and drumlinized. The esker is also dominated by carbonate lithologies and overlies erosively either bedrock or till. It consists of two elements, a narrow gravelly central ridge and a broad sandy carapace. Three units comprise the overlying mud package: gray carbonate-rich rhythmites, massive bioturbated mud, and carbonate-poor, red-and-gray rhythmites.

4. Data acquisition methods

The ordering of the next sub-sections follows the sequence used in the field for the characterization of the Vars-Winchester esker (Figure 1). Data for the study has been collected along three transects of the esker using public roads, route 300, route 200 and St Pierre rd. Seismic data was collected along several kilometer profiles. Boreholes were drilled to intercept and permit hydraulic characterization of specific sedimentary facies. No coring was completed during this study; however, cuttings were recovered, and sedimentological characterization relies on the earlier core collection (Cummings et al. 2011). Borehole geophysics was collected within the respective hydraulic test wells and complements earlier collected data (Cummings et al. 2011). Resistivity profiles were collected in the vicinity of the hydraulic test wells. Drilling for the wells was completed using a dual air-rotary rig. Wells were screened over the entire saturated thickness.

4.1 Seismic surveys

Multi-component high-resolution reflection seismic data were acquired for this study using a MicroVibe seismic source developed by the GSC (Pugin et al. 2020 this volume; Pugin et al. 2013). 240 source kg vibrates in either vertical or horizontal directions. The receivers array consists of 48 thee-component geophones as a landstreamer (Pugin et al. 2009b) towed behind a vehicle to record shear- (s) and compressional- (p) wave data. According to the anticipated near-surface velocities and depths of the formations, the 48 geophones were spaced at 0.75 m. Each of the 30 Hz omni-directional geophones can record in three orthogonal directions: one vertical (V) and two horizontals (in-line/H1 and cross-line/H2). Thus, for each shot point spaced at 2.25 m, six components were recorded: three receiver directions (V, H1 and H2) for each vibration direction of the source (H1 and H2). The MicroVibe/landstreamer system allowed collection of approximately 1 km of data per day, and a total of 5 km of survey data were acquired (Figure 2b).

Seismic data were processed and converted into depth using information gained from sediments collected during observation well installation and borehole geophysics logging carried out in the wells (Pugin et al. 2020 in this vol.). Four seismic facies can be recognized using continuity and amplitudes of wave reflections (Figure 3): (1) the diamicton seismic facies with a sharper and continuous top reflector; (2) the gravel with complex and discontinuous reflectors; (3) the sand with discontinuous and weaker reflectors; and (4) the marine clay with strong continuous and parallel reflectors. The vertical resolution of the esker units is estimated at 1 m and 3 m for shear-wave

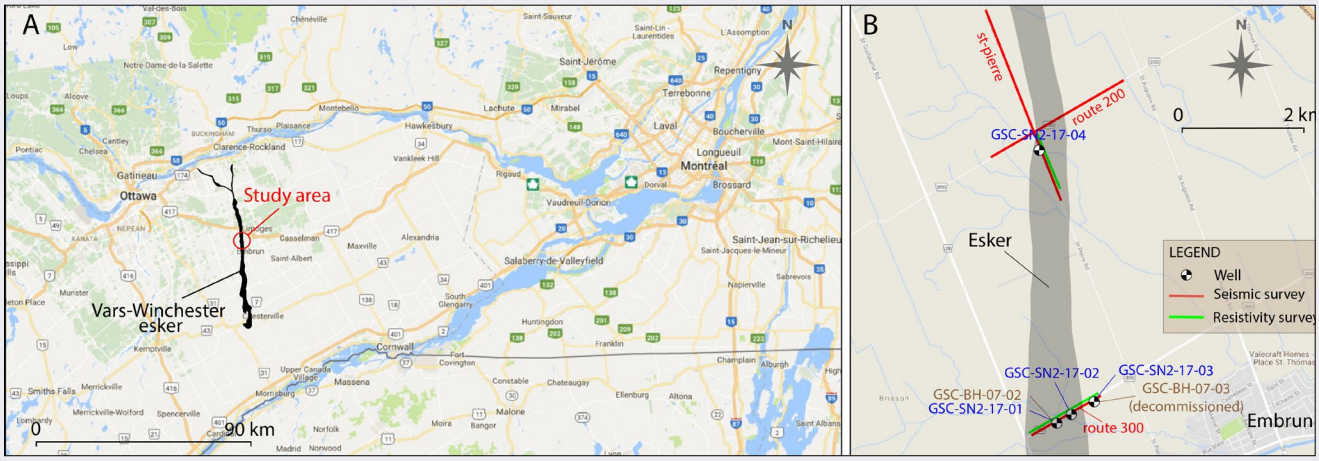


Figure 2. (a) General locations of the study area near the town of Embrun (Ontario) between Ottawa and Montreal, and the Vars-Winchester esker (after Cummings et al. 2011). (b) Close-up on the study area with locations of the wells and geophysical surveys used for this study.

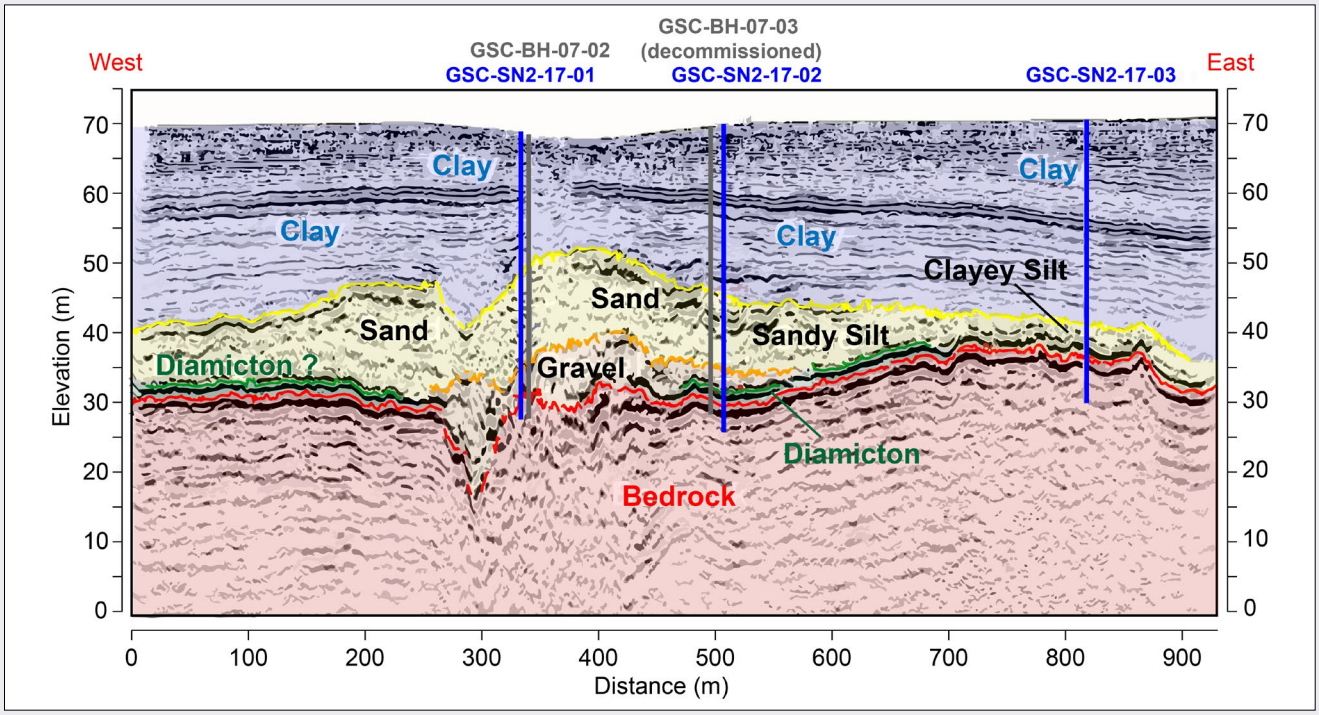


Figure 3. Seismic reflexion survey and wells along Route 300 (see Figure 2b for location) showing the different components of the buried Vars-Winchester esker system. Sand and gravel compose the esker.

and compressional-wave, respectively.

4.2 Well installation

For this study, four observation wells were installed based on seismic surveys (Figure 2b). Three were installed along a transverse cross-section of the esker, one in the core of the esker, one in the flank, and a third off the esker in basin muds. The fourth well was installed 4 km away from the first three within the esker. Each well is located as close as possible to seismic reflection survey (within a distance <20 m) to reduces the uncertainty related to the colocation of hydraulic and geophysical measurements.

The installation of the wells followed the protected screen procedure proposed by ASTM (2004). This procedure does not require the use of sand-pack, which is more suitable for hydraulic tests carried out over small intervals (1 m vertical resolution) because it reduces the risk of developing hydraulic short-circuits along the well screen during testing.

The installation procedure involved the drilling of a 142 mm diameter hole (corresponding to the outside diameter of the metal casing in Figure 4) over the entire thickness of the sediment sequence using a dual-rotary drill (Comacchio 900 GT). This drilling procedure involves a drilling bit inserted within a metal casing to retain sediments. Then, once at the desired depth, the drilling bit was removed, and a PVC screen with a 115 mm outside diameter was inserted inside the casing. The metal casing was then withdrawn to the surface to expose the PVC screen to the sediments. To ensure a complete collapse of the sediments on the well after withdrawing the casing, the outside diameter of the PVC was chosen as large as possible to reduce the space between the drilled hole and the screen (13.5 mm for the actual wells).

For this study, fully screened wells across the whole saturated zone were installed to provide continuous profiling of hydraulic properties with hydraulic tests. Screen length for all wells varied between 30.50 to 33.50 m. Wells were also thoroughly developed after their installation to unclog screens and surrounding sediments related to well installation operations. Each well was then developed by a pumping-surging operation at 0.3 m intervals using an inertial pump (Waterra) with development rings until turbidity was no longer observed in the discharged water.

4.3 Borehole geophysics

Borehole geophysical surveys were conducted in spring and summer 2018 to interpret depths of lithological contacts, measure physical and chemical properties of the sediments and groundwater, and assess the collapse of the sediments around the casing for hydraulic testing (Crow et al. 2020 in this vol.). A suite of geophysical tools, including natural gamma, induction (bulk conductivity and magnetic susceptibility), gamma-gamma density, fluid temperature/conductivity, and velocity (compressional-V_p and share-V_s wave velocities) were run in the four wells. Borehole nuclear magnetic resonance (NMR) logs were also collected in wells GSC-SN2-17-01, -02, and -04 to estimate sediment porosity (n) and estimate hydraulic conductivities (K) in the sands.

The natural gamma, induction, and density logs together refined the depths of lithological contacts interpreted from drill cuttings between the muds, esker, till, and bedrock units. Gamma counts are elevated in the carbonates, defining the lower contact at the bedrock surface. A slight decrease in density and natural gamma counts suggest a stony till layer is present above the bedrock which incorporates some of the underlying shale into the matrix. The lower contact between the till and the esker is best defined by a small decrease in density and more subtly by gradual upward decrease in gamma counts. It is not apparent from the logs that a distinct gravel unit is present in the esker core. The characteristic log responses in the esker units are relatively elevated and variable magnetic susceptibilities suggesting layering of the sands, which likely contain finer grained material in some intervals.

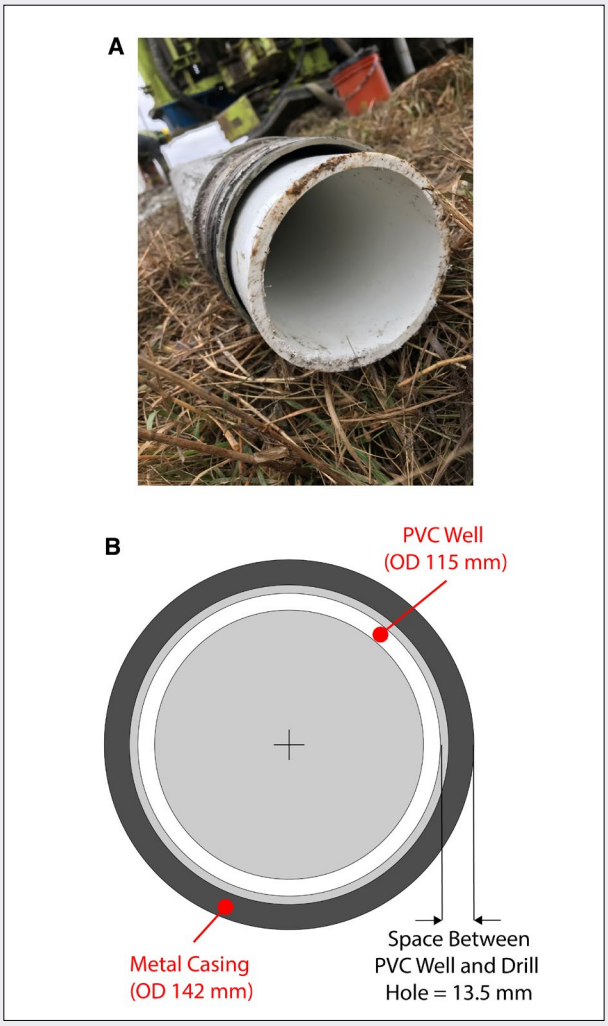


Figure 4. (A) Picture of the PVC well inserted into the metal casing used for well installation. (B) Drawing showing the dimensions of the PVC well relative to the drilling hole. The space between the well and the drilling hole was kept as thin as possible to ensure the collapse of the sediments on the well screen.

All logs indicate an abrupt contact with the top of the esker in boreholes 01, 02, and 04. The muds are defined by relatively low magnetic susceptibilities and densities, and relatively elevated bulk conductivities. Sand beds in the upper 12 m could be identified from small increases in magnetic susceptibility. In the off-esker borehole (GSC-SN2-17-03), the bulk conductivity near the base of the muds reaches levels approximately three times higher than in the thinner muds above the esker, reflecting more conductive pore waters from an earlier time in the history of the Champlain Sea.

Fluid properties were also measured using downhole instruments. Groundwater temperatures within the esker ranged from 8.3 to 8.8°C, and were typically 8.5 ± 0.1°C

within the esker core. The NMR responses identified changes in how groundwater was contained within the sediments, from clay-bound in muds to largely mobile water in the esker. NMR logs reveal elevated porosities up to 76% in the muds, in close agreement with lab-measured values from samples recovered in adjacent boreholes (GSC-BH-07-02). Esker porosities were closer to 40%, but the elevated and variable magnetic susceptibilities in the sands may have the effect of lowering NMR porosities — a topic of ongoing study within this project.

The density and NMR logs also provided information on borehole conditions. Stable density responses in the esker indicated sediments had collapsed relatively uniformly around the casing forming a seal with the screen. In the muds, intervals of abrupt density decreases coupled with free water contents in the NMR responses indicated water-filled voids behind the casing. This well completion information supported the interpretation of other logs in the suite, and guided the selection of hydraulic test intervals.

4.4 Resistivity surveys

Electrical resistivity (*R*) and time-domain induced polarization (*P*) data were acquired for the Vars-Winchester Esker using both surface, well, and well-to-surface surveys. Surface surveys were conducted along Route 200, Route 300, and St. Pierre using 5 m electrode spacing and mixed multi-gradient and dipole-dipole arrays on a 64-electrode layout, deployed in an overlapping fashion over 635 m, 955 m, and 555 m respectively. Surveys were conducted down each of the four observation wells using circulating dipole-dipole surveys with in-hole electrodes at 1 m spacing below the water table. Well electrodes were combined with 32 surface electrodes at 1 m spacing on both sides of the well, or in orthogonal directions to acquire well-to-surface data using mixed multi-gradient and dipole-dipole arrays.

Resistivity and IP data will be inverted in 2-D for surface surveys and 3-D for well-to-surface surveys, resulting in distributions of bulk *R* and chargeability. At the boreholes, in-hole and surface-to-well measurements will allow for high-resolution comparison to *K* measurements, and for assessment of resolution limitations of the larger-spacing surface data. The surface-based *R* models will provide additional means of assisting facies distribution and discrimination away from the observation wells.

4.5 Vertical interference slug tests

Hydraulic property values used to establish relations with geophysical data were obtained by vertical interference slug tests carried out in the four fully screened wells. A vertical interference slug test involves the use of packers to isolate a stressed and an observation interval along a well to conduct a slug test (Paradis and Lefebvre 2013). This test allows estimating horizontal and vertical hydraulic conductivities (K_h and K_v, respectively) as well as specific storage of sediments. Slug tests were performed at 1-m intervals using a pneumatic method to induce large displacements of water level. Interval lengths were selected to have similar vertical resolution as the geophysical measurements. A total of 100 intervals were tested and hydraulic responses were analyzed using numerical inversion method.

5. Hydrogeophysical data integration

The application of the workflow for data acquisition (Figure 1) led to the collection of a training dataset representative of the hydrogeophysical conditions in the study area. This training dataset will provide colocated hydraulic parameters K_h, K_v and n (derived from NMR) and geophysical parameters natural gamma, bulk conductivity, magnetic susceptibility, gamma-gamma density, V_p, V_s, P and R. The next sub-sections describe the different data integration approaches that will be applied and compared to define site-specific hydrogeophysical relations. These relations will form the basis for the conversion of the geophysical data into hydraulic properties.

5.1 Theoretical petrophysical expressions

A correlation exists between *R* and *K* of unconsolidated sediments due to a mutual dependence on connected porosity. However, this correlation is complicated by a competing influence of surface conduction (e.g., Slater 2007). Furthermore, although *R* estimates may provide a proxy, additional information on grain size or surface area is required to develop a predictive relationship.

Recent laboratory results (e.g., Weller et al. 2015) will be used to investigate the potential for utilizing the chargeability obtained from *P* measurements to provide field scale information on interface conduction and hydraulic length scales required for estimates of *K*.

5.2 Statistical relations

The statistical methods used in this study will be primarily based on the training of a learning machine as applied by Paradis et al. (2015). The definition of relations with this approach involves first the recognition of hydrofacies (or groups with similar hydrogeophysical responses), and then the establishment of specific hydrogeophysical relations for each of these hydrofacies. This is carried out through the application of various supervised and unsupervised classification and regression algorithms.

Different kind of relations will be investigated and verified for their accuracy in predicting hydraulic properties. For example, borehole geophysics parameters alone will be used with hydraulic parameters to define relations when only borehole logs are available. This will allow for estimation of high-resolution hydraulic conductivity profiles along wells without having to complete extensive hydraulic testing.

Also, seismic and resistivity surveys parameters will be used independently or in combination to estimates hydraulic properties along geophysical cross-sections. This will help to provide a better coverage of hydraulic properties and identify heterogeneity structures and trends in hydraulic property values within these structures.

6. Project status

This paper proposes an integrated hydrogeophysical approach to estimate hydraulic properties from geophysical data. Important preliminary observations resulting from this effort include the following:

- The seismic wave reflections generated by the newly developed MicroVibe provides very high-resolution data of the architecture of the esker system (aquifer and aquitard units). Vertical resolution of approximately 1 m for shear-wave and 3 m for compressional-wave were achieved. The use of a landstreamer that allows fast acquisition of high-quality reflection data (~1 km per day) also permits mapping of the large esker structures.
- Preliminary *R* models indicate a resistive esker feature thickest at the center and thinning on the flanks, in agreement with seismic reflection sections. Resolution of the bedrock/esker contact is limited, but heterogeneity is apparent within the esker, and the confining mud sequences.
- Porosity values derived from NMR logs are in close agreement with lab-measured values from mud and sand samples recovered in adjacent boreholes, despite variable magnetic susceptibilities in the sands that may impact NMR porosity estimates.
- Preliminary hydraulic test analysis suggests that hydraulic short-circuiting along well screens completed in the muds is present, as also revealed by NMR logs, which may impact hydraulic properties estimations in these sediments. Short-circuits may be the result of incomplete collapse of sediments along the well screens or liquefaction of the muds due to drilling operations. K_h values can nevertheless be estimated using existing analytical equations, but simultaneous estimates of K_h, K_v/K_h and S_s will require further numerical developments.

Ongoing research is addressing the integration of the different hydraulic and geophysical datasets in order to be able to translate seismic, resistivity and borehole geophysics surveys to well correlated estimates of hydraulic property values. The development of a hydrogeophysical approach will provide a more successful way to characterise hydrogeological heterogeneities than either traditional hydrogeological or geophysical approaches taken independently.

7. Acknowledgements

The authors would like to acknowledge the important technical field support provided by X. Malet, K. Brewer, T. Cartwright, B. Dietiker, and M. Griffiths. An internal review at the GSC was completed by N. Benoit. A special thank also to A. Brisson, R. Bordeau and the South Nation Conservation Authority who provided access to their land for field surveys. This study was supported by the Geological Survey of Canada under the Groundwater Geoscience Program. This work is a contribution of the GSC–OGS Southern Ontario project on groundwater 2014–2019.

8. References

American Society for Testing and Materials-ASTM 2004. D6724: Standard guide for installation of direct push ground water monitoring wells. ASTM International, 9 pp.

Binley, A., Slater, L.D., Fukes, M., and Cassiani, G. 2005. Relationship between spectral induced polarization and hydraulic properties of saturated and unsaturated sandstone. Water Resources Research, 41(12), W12417.

Bradford, J.H., and Babcock, E. 2013 The need to adapt the exploration model from the oil patch to contaminated-site characterization: A case from Hill AFB, Utah, USA, The Leading Edge, 32: 7, 750-756.

Butler, Jr.J.J. 2005. Hydrogeological methods for estimation of hydraulic conductivity. In Rubin,Y. and Hubbard, S. Eds. Hydrogeophysics, 23-58, Springer, New York.

Chen, J., Hubbard, S., and Rubin, Y. 2001. Estimating Hydraulic Conductivity at the South Oyster Site from Geophysical Tomographic Data using Bayesian Techniques based on the Normal Linear Regression Model. Water Resources Research, 37: 6, 1603-1613.

Crow, H.L., Pugin, A. J.-M., Dietiker, B., Paradis, D., Brewer, K., Cartwright, T., Griffiths, M., and Russell, H.A.J. 2020. Lithological and hydrogeological properties from a downhole geophysical dataset in the Vars-Winchester esker, Ontario. In Russell, H.A.J. and Kjarsgaard, B.A. Eds. Southern Ontario groundwater project 2014–2019: summary report. Geological Survey of Canada, Open File 8536, 147-157 https://doi.org/10.4095/321100

Cummings, D.I. and Russell, H.A.J., 2007. The Vars-Winchester esker aquifer, South Nation River watershed, Ontario: CANQUA Fieldtrip Guidebook, Geological Survey of Canada, Open File 5624. https://doi.org/10.4095/224424

Cummings, D.I., Gorrell, G., Guilbault, J.-P., Hunter, J.A., Logan, C., Ponomarenko, D., Pugin, J.-M., Pullan, S.E., Russell, H.A.J., and Sharpe, D.R. 2011. Sequence stratigraphy of a glaciated basin fill with a focus on esker sedimentation. GSA Bulletin, 123: 7-8, 1478-1496. https://doi.org/10.1130/B30273.1

Dafflon B., J. Irving and Holliger, K. 2009. Simulated annealing-based conditional simulation using high-resolution geophysical data for the local-scale characterization of heterogeneous aquifer. Journal of applied geophysics, 68: 60-70, https://doi.org/10.1016/j.jappgeo.2008.09.010

Dubreuil-Boisclair C., Gloaguen, E., Marcotte, D., and Giroux, B. 2011. Heterogeneous aquifer characterization from Ground-penetrating radar tomography and borehole hydrogeophysical data using nonlinear bayesian simulations. Geophysics, 76: J13-J25. https://doi.org/10.1190/1.3571273

Oldenborger, G.A., Logan, C.E., Hinton, M.J., Sapia, V., Pugin, A.J.-M., Sharpe, D.R., Calderhead A.I., and Russell, H.A.J. 2014. 3D hydrogeological model building using airborne electromagnetic data. European Meeting of Environmental and Engineering Geophysics, Tu-PA1-07.

Oldenborger, G.A., Logan, C.E., Hinton, M.J., Pugin, A.J.-M., Sapia, V., Sharpe, D.R., and Russell, H.A.J. 2016. Bedrock mapping of buried valley networks using seismic reflection and airborne electromagnetic data. Journal of Applied Geophysics, 128: 191–201. https://doi.org/10.1016/j.jappgeo.2016.03.006

Paasche H., Tronicke, J., Holliger, K., Green, A.G., and Maurer, H. 2006. Integration of diverse physical-property models: Subsurface zonation and petrophysical parameter estimation based on fuzzy c-means cluster analyses. Geophysics, 71: H33-H44. https://doi.org/10.1190/1.2192927

Paradis, D., Tremblay, L., Lefebvre, R., Gloaguen, E. Rivera, A., Parent, M., Ballard, J.-M., Michaud Y., and Brunet, P. 2014. Field characterization and data integration to define the hydraulic heterogeneity of a shallow granular aquifer at a sub-watershed scale. Environmental Earth Sciences, 72: 5, 1325-1348. https://doi.org/10.1007/s12665-014-3318-2

Paradis, D. and Lefebvre, R. .2013. Single-well interference slug tests to assess vertical hydraulic conductivity. Journal of Hydrology, 478: 102-118. doi: 10.1016/j.jhydrol.2012.11.047

Paradis, D., Lefebvre, R., Gloaguen, E., and Rivera, A. 2015 Predicting hydrofacies and hydraulic conductivity from direct-push data using a data-driven relevance vector machine approach: motivations, algorithms and application. Water Resources Research, 51: 481-505. https://doi.org/10.1002/2014WR015452

Pugin, A.J.-M., Pullan, S.E., Hunter, J.A., and Oldenborger, G.A. 2009a. Hydrogeological prospecting using P- and S-wave landstreamer seismic reflection methods. Near Surface Geophysics, 7: 315–327. https://doi.org/10.3997/1873-0604.2009033

Pugin, A.J.-M., Pullan, S.E., and Hunter, J.A. 2009b. Multicomponent high-resolution seismic reflection profiling. The Leading Edge, 28: 10, 1182-1265.

Pugin, A.J.M., Brewer, K., Cartwright, T., Pullan, S.E., Perret, D., Crow, H., and Hunter, J.A. 2013. Near surface S-wave seismic reflection profiling — New approaches and insights: First Break, 31: 49–60. https://doi.org/10.1190/1.3249782

Pugin, A. J.-M., Crow, H.L., Brewer, K., Cartwright, T., Dietiker, B., Griffiths, M., and Paradis, D. 2020. High-resolution seismic reflection profiles for groundwater studies of the Vars-Winchester esker, southeastern Ontario. In Russell, H.A.J. and Kjarsgaard, B.A. Eds. Southern Ontario groundwater project 2014–2019: summary report. Geological Survey of Canada, Open File 8536, 139-146. https://doi.org/10.4095/321099

Rubin, Y. and Hubbard, S. 2005. Hydrogeophysics. Springer, Netherlands, Water and Science Technology Library, v. 50, 523 p.

Ruggeri, P., Irving, J., Gloaguen, E., and Holliger, K. 2013 Regional-scale integration of multiresolution hydrological and geophysical data using a two-step Bayesian sequential simulation approach. Geophysical Journal International, 194:1, 289-303. https://doi.org/10.1093/gji/ggt067

Slater, L. 2007. Near surface electrical characterization of hydraulic conductivity: From petrophysical properties to aquifer geometries—A review. Surveys in Geophysics, 28: 169–197. https://doi.org/10.1007/s10712-007-9022-y

Weller, A., Slater, L., Binley, A., Nordsiek, S., and Xu, S. 2015. Permeability prediction based on induced polarization: Insights from measurements on sandstone and unconsolidated samples spanning a wide permeability range. Geophysics, 80: D161–D173. https://doi.org/10.1190/geo2014-0368.1

High-resolution seismic reflection profiles for groundwater studies of the Vars-Winchester esker, southeastern Ontario

André J.-M. Pugin[1]*, Heather L. Crow[1], Kevin Brewer[1], Tim Cartwright[1], Barbara Dietiker[1], Matthew Griffiths[2], and Daniel Paradis[3]

Abstract: As part of a hydrogeophyscial study of the Vars-Winchester esker three seismic profiles have been acquired using a novel in-house two component (horizontal and vertical) Microvibe seismic source with a 48-channel, three component landstreamer. This new hardware has allowed for the acquisition and processing of very high-resolution 2-D images of the esker for groundwater exploration. Following the acquisition of the profiles, four boreholes have been drilled to bedrock. The lithologies of the esker system such as marine mud (silt and clay), sand, gravel, and diamicton, are well characterised by the seismic facies and shear-wave velocities.

1. Introduction

As part of a hydrogeophysical study multiple datasets (reflection seismic, electrical resistivity imaging, and downhole geophysics) were collected in South Nation River watershed near Embrun, Ontario, during 2017 and 2018 (Paradis et al. 2020, this vol.). The geophysical data will be integrated with hydraulic data as part of a study on how to provide improved continuous hydraulic information for a sparsely sampled esker system. This study supplements geophysical data collected as part of the collaborative Geological Survey of Canada (GSC) and South Nation Conservation Authority study completed between 2007 and 2009 to map the Winchester-Vars esker (Pullan et al. 2007; Logan et al. 2009; Pugin et al. 2009, Cummings et al. 2011; Yilmaz 2015).

Eskers are ridges of sand and gravel that can be 10s–100s of kilometres long, deposited in meltwater conduits that form at the base of glaciers. In eastern Ontario, groundwater from esker aquifers is the primary municipal drinking water source for a number of towns and villages. In the Ottawa River Valley, few details of esker geometry (lateral extent), their internal stratigraphy, or spatial variability are available because they are buried along much of their length by fine-grained Champlain Sea sediments (Cummings et al. 2011). These overlying muds were deposited when the Atlantic Ocean (Champlain Sea) inundated the area with retreat of the Laurentide Ice Sheet approximately 12,000 years ago (Parent and Occhietti 1988). Lack of data on the esker, and as a consequence, associated uncertainties regarding esker properties, severely limit the accuracy of any assessment, or aquifer protection, plan for this groundwater resource.

High-resolution multi-component reflection seismic data were acquired along 5 km of public roads (Figure 1) using a Microvibe, a new seismic source developed at the GSC (Pugin et al. 2013). The work was performed using a vertical and horizontal vibrating source (Microvibe) with a towed "landstreamer" (Pugin et al. 2009a). Seismic sections were processed and converted into depth aided by information gained by surficial mapping and sediment drilling programs. The seismic method permits measurement of the thicknesses of aquitards and aquifers at a resolution of approximately 1 m for shear-wave (S-wave) and 3 m for compressional-wave (P-wave) reflection data. The location of four boreholes were selected based on the preliminary reflection seismic results. Downhole geophysical logging was undertaken in boreholes drilled in late 2018. The holes were logged using natural gamma, apparent conductivity, magnetic susceptibility, gamma-gamma density, fluid temperature and seismic P- and S-wave velocity (Crow et al. 2020, this vol.).

The objective of this paper is to document how a novel S-wave reflection seismic technique can be used for regional mapping of aquifers through the spatial characterization of seismic units. The importance of utilizing high-quality geophysical data in choosing borehole locations that target

[1] Geology Survey of Canada, Natural Resources Canada, 601 Booth Street, Ottawa, ON K1A 0E8
[2] Department of Earth Sciences, Carleton University, 1125 Colonel By Drive, Ottawa, ON K1S 5B6
[3] Geological Survey of Canada, 490 rue de la Couronne, Quebec City, QC G1K 9A9
*corresponding author: andre.pugin@canada.ca

Recommended citation: Pugin, A. J.-M., Crow, H.L., Brewer, K., Cartwright, T., Dietiker, B., Griffiths M., and Paradis D. 2020. High-resolution seismic reflection profiles for groundwater studies of the Vars-Winchester esker, southeastern Ontario. In Russell, H.A.J. and Kjarsgaard, B.A. Eds. Southern Ontario groundwater project 2014–2019: summary report. Geological Survey of Canada, Open File 8536, 139-146. https://doi.org/10.4095/321099

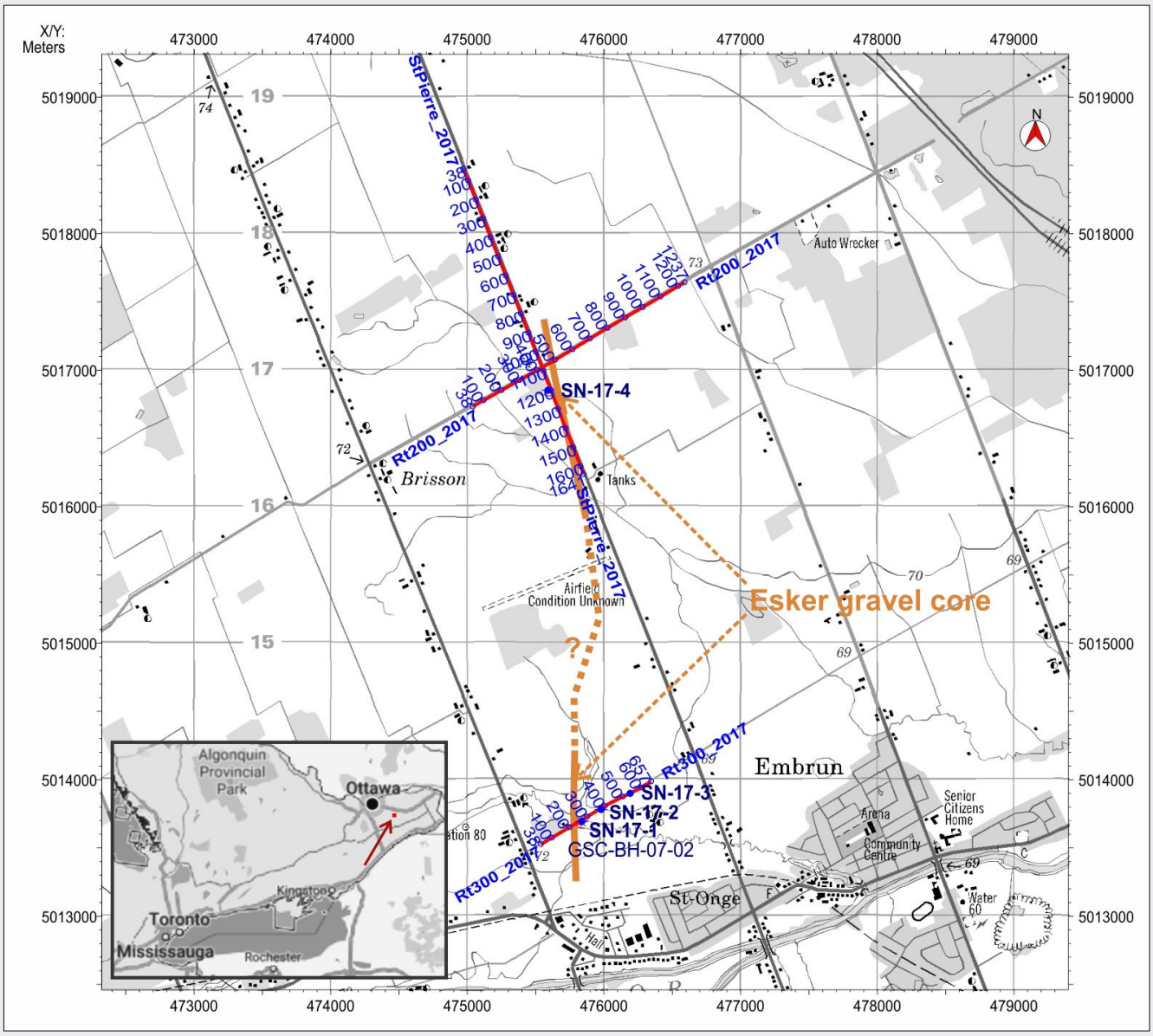


Figure 1. Locations of the seismic profiles collected as part of this study. The five boreholes used for seismic interpretation are labelled starting with GSC-BH and SN.

a viable aquifer (i.e. a porous lithology, such as a gravel layer) is described. The discussion considers future research linking hydrologic parameters with seismic reflection data.

2. Methods and data acquisition

The seismic method permits measurement of aquitard and aquifer thicknesses to a S-wave vertical high-resolution of approximately 1 m. The GSC-developed seismic system used in this survey (Figure 2) couples an array of 48 geophones (a landstreamer) towed behind a seismic vibrator source (the Microvibe) (Pugin et al. 2013). The source is battery-powered with up to 2,000 watts, and uses transducer units to vibrate a ~8 kg mass in either vertical or horizontal modes. The operator can program a sweep through a frequency range of 20 to 800 Hz. For this study, the Microvibe generated a 9 second linear sweep from 20–450 Hz in vertical (V) vibrating mode, and 20 to 350 Hz in transverse horizontal mode (H2) with a listening time of 1.5 seconds.

The GSC's landstreamer is designed for use along paved or gravel roads, with the number of receivers and spacing being varied depending on near-surface velocities and the targeted depths of investigation. In this study, the landstreamer array consisted of 48 3-kg metal sleds, spaced 0.75 m apart, connected by a polyester cargo strap. Each sled was equipped with a



Figure 2. Microvibe/landstreamer data acquisition system in operation in the South Nation River watershed, eastern Ontario.

3-component (3-C) geophone block constructed in-house with 30 Hz omni-directional geophone elements oriented in three orthogonal directions: one vertical (V) and two horizontal, in-line (H1) and cross-line (H2). For each shot point, spaced 2.25 m apart, six-component data were recorded using six 24-channel Geometrics Geode engineering seismographs. The data consisted of two source vibration directions V and H2 multiplied by the three receiver directions (V, H1, H2).

For this shallow application, a high-precision distance-measuring odometer was linked to a small readout screen mounted in the towing vehicle, allowing the operator to move quickly and accurately between shot points. Using the Microvibe/landstreamer system in the configuration described (Figure 2), ~1 line-km of data was typically collected per day. A sample field record (144 channels) is shown in Figure 3. Channels 1–48 are the vertical (V) geophones; 49–95 are the in-line horizontal (H1) geophones and channels 97–144 are the cross-line or transverse horizontal (H2) geophones.

Uncorrelated records were collected in the field to allow for post-collection processing of the data. As presented in Pugin and Yilmaz (2019), the highest quality P-wave reflection data is processed when using the vertical source and the vertical receivers (V,V). For brevity, only the highest resolution S-wave sections are presented in this paper, but P-wave sections will be used in the full hydrogeophysics characterization. S-wave sections were processed using 1 sec records with both the Microvibe and receivers oriented in a transverse horizontal direction (H2,H2).

The processing sequence is presented in Table 1. Careful choice of the correlating function was the first step in the data

Table 1. Processing flows for S-wave seismic data reported in this document.

Initial processing (all data)
Format conversion, SEG2 to KGS SEG-Y Pilot trace based cross-correlation, 1 sec listening time Separation of V, H1, H2 components Editing of the geometry / Sort, based on GPS data CMP binning to 1.125 m
S-wave (H2,H2) component data
Frequency filter (Low Cut 20–45 Hz) Scaling (trace normalization) Top mute (P-wave, surface waves, distorted far offset reflections removal) Velocity analysis (CMP super gathers: 1.125 m bins) NMO Corrections (~80–350 m/s) Stack, nominal fold: 24 Correction for ground surface topography using 250 m/s Migration Conversion to depth (using Boreholes and NMO velocities)

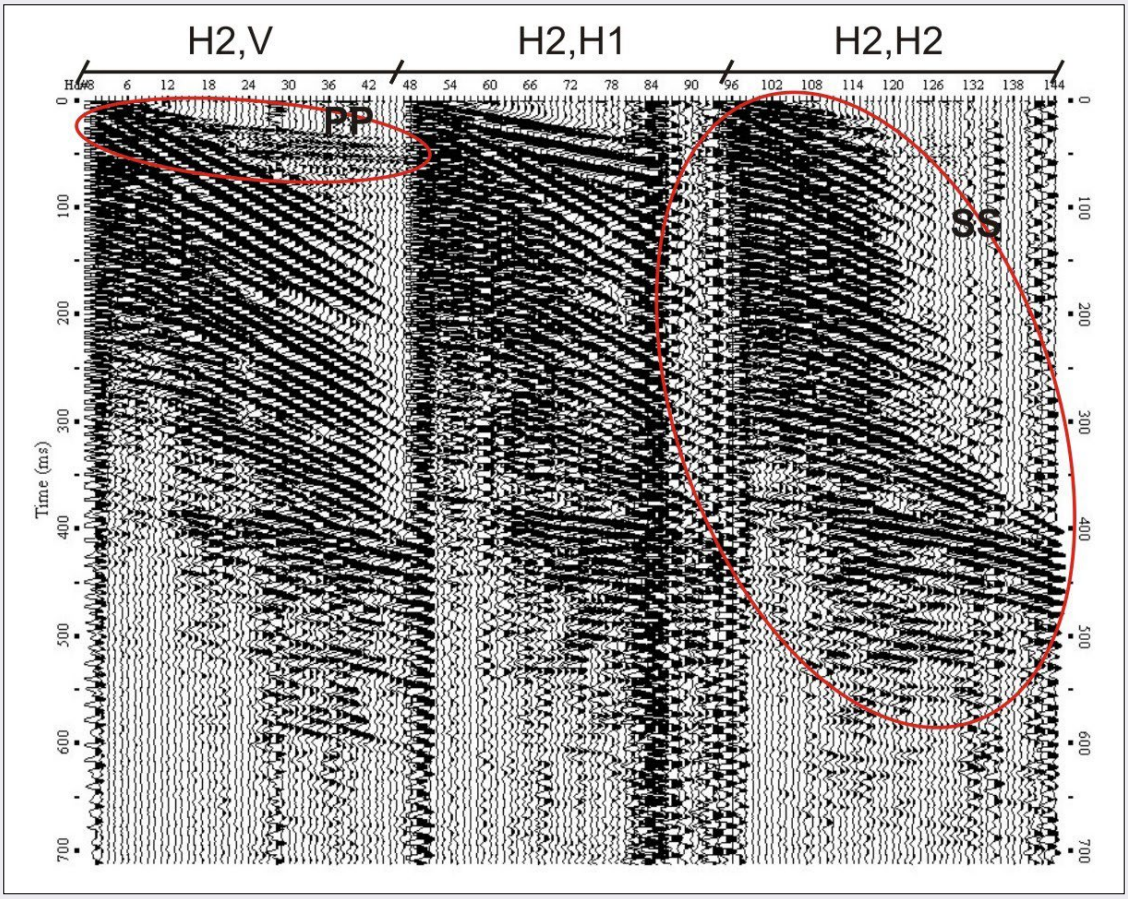


Figure 3. Correlated 3-C seismic record from the survey. The source was vibrated in the H2, cross-line horizontal direction. S-wave (SS) is best recorded in the horizontal H2,H2 component and P-wave (PP) can also be seen on the H2,V component.

processing sequence. The velocity information was derived from a picked semblance analysis. Semblance velocities are used to determine the normal move-out correction to apply to the common mid-point (CMP) records before the final stack operation is applied. This information was cross-checked with lithological depths from boreholes, and with downhole P- and S-wave measurements (Figure 4). An illustrative section is documented in Figure 5.

3. Results

3.1 Downhole geophysical logs

Downhole geophysical logging was undertaken in boreholes drilled in late 2017 (Crow et al. 2020, this vol.). Downhole P- and S-wave velocities were acquired as part of the log suite to verify the depth conversion of travel time to depth sections. Lithologies can be characterized by S-wave velocities: the fine-grained, post-glacial muds range from 70 m/s to 200 m/s, the sand from 250 m/s to 400 m/s, and the gravel and diamicton from 400 m/s to >1,000 m/s.

3.2 Seismic sections

Due to better quality equipment and processing, the Route 300 seismic section (Figure 5) has a remarkably higher resolution than sections acquired in 2007 (Pullan et al. 2007; Pugin et al. 2009b; Yilmaz 2015). The section is only slightly oblique to the orientation of the esker. The post-glacial mud velocities vary from less than 100 m/s up to 200 m/s, sand from 200 m/s up to 350 m/s and gravel or till above 450 m/s (Figure 5). The time section (Figure 5a) displays pull-up structures at the bedrock surface below the esker due to higher velocity of the sands and gravel. In the depth section (Figure 5d), this interface has been corrected and matches the borehole data. The chaotic seismic facies at the base of the esker is associated with gravel and is approximately 300 m wide. The overlying discontinuous reflections and complex reflection patterns are associated with sand and sandy silt. The continuous reflections are associated with reflecting horizons within the muds. A major reflection in this mud sequence is associated with a continuous ~5 cm-thick sand layer (see Figure 3 in Crow et al. 2020, this vol.).

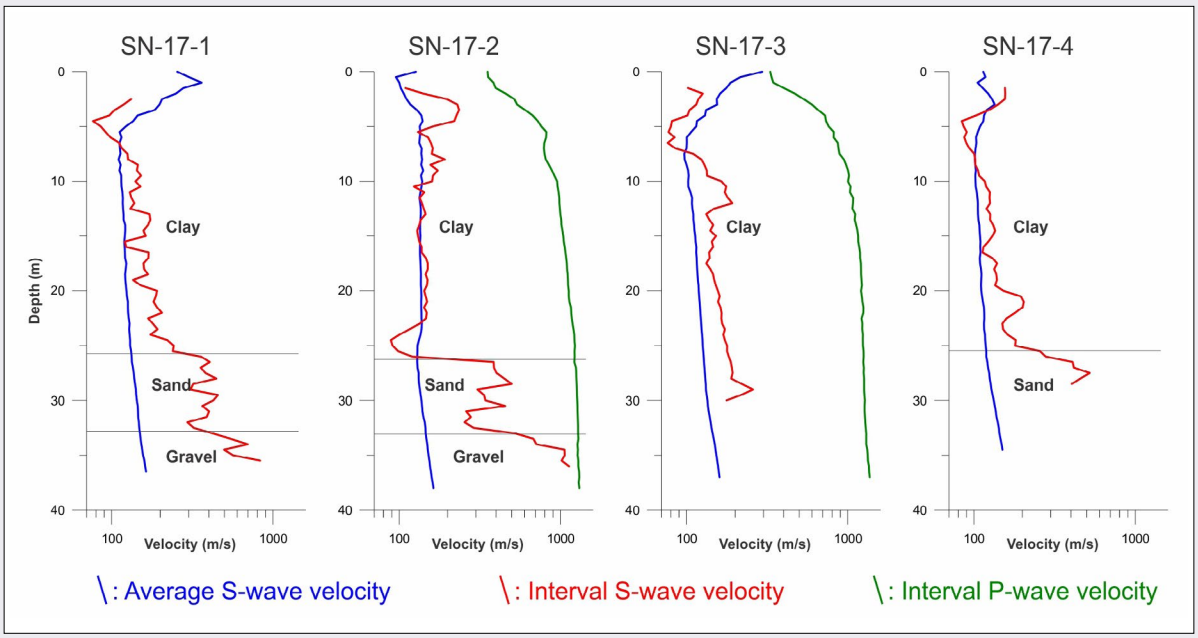


Figure 4. Velocity logs acquired in the SN-series boreholes.

Four seismic facies can be described using continuity and amplitudes of reflections. 1) A diamicton facies that is similar to the gravel facies, but with a strong and continuous top reflection; 2) complex or chaotic reflections with discontinuous top reflections characterize the gravel due to great heterogeneity; 3) discontinuous light reflections are related to the esker sand to; and 4) strong, continuous, and more-or-less parallel reflections characterize the post-esker mud deposits of the Champlain Sea.

A remarkable feature not observed in the 2007 sections along route 300 is a 15 m deep and 60 m wide concave erosional feature centered at the coordinate ~270 m of the section (Figure 5). This depression underlined by diffractions is associated with a feature that can be interpreted as a kettle hole (Maries et al., 2017), in-filled with Quaternary sedimentary deposits, above the bedrock.

The Route 200 seismic section (Figure 6) crosses the esker (obliquely) with a NE-SW orientation and has a gravelly esker core with a width of ~150 m that is narrower than along Rte 300 with a width of ~200 m (Figure 5). Dome-shaped seismic reflections overlying bedrock have been intercepted by boreholes which have confirmed the presence of diamicton. Based on the seismic facies, the gravelly esker core is likely situated in a 10 m deep trough associated with two collapse features also observed at coordinate 620 m to 670 m along the section. The sandy cap is fully mapped in this section with a width of about 1,300 m.

The Route St Pierre seismic section-oriented NNW-SSE (Figure 7) crosses the esker at an approximately 20 degree angle and thus provides an exaggerated oblique esker cross-section, similar to the Route 200 section. The borehole SN-17-4 has confirmed the presence of gravel associated with the esker. An interesting 15 m thick gravel facies is indicated in this section, but located away from the borehole.

4. Discussion and conclusions

Shear-wave (S-wave) seismic reflection profiles generated by the Microvibe provides very high-resolution subsurface images. With a production of more than 1 km of 6 components data per day, the use of a landstreamer allows for fast acquisition of high-quality reflection data to map subsurface interfaces characterized by impedance contrasts. The processed reflections are presented as 2-D sections through the esker with a resolution constrained by the frequency of the subsurface materials; the fact that the gravel core directions of the esker does not line up between the northern sections and the southern sections implies that it may be sinuous or even discontinuous, other geophysical techniques would be required to determine the path of it across the fields. The reflection data resolution corresponds theoretically to a quarter wavelength. S-wave resolution decreases with depth depending upon the geology, as high-frequency energy is quickly absorbed.

This geophysical data set will be one contribution among other geophysical and hydrological data sets such as surface and downhole electrical resistivity profiling, downhole geophysical logging, and borehole hydraulic tests (Paradis et al. 2020, this vol.). Spatial hydrogeophysical mapping will be realized using lithological and geophysical facies using statistical tools. Further analysis of seismic data would enhance the current seismic

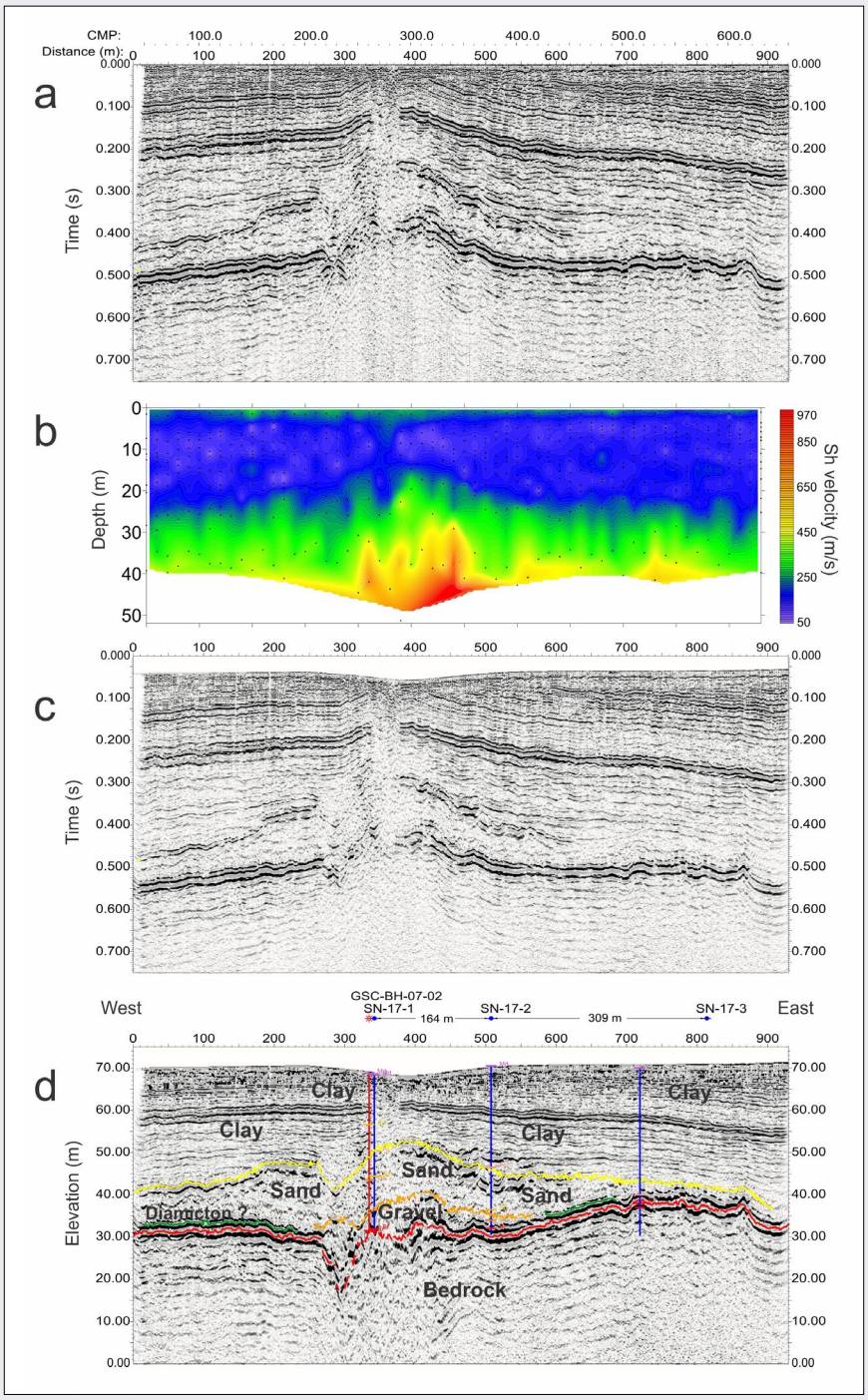


Figure 5. Route 300 seismic section oriented NW-SE, north of Embrun, ON. **a:** time s-wave seismic section; **b:** velocity seismic section; **c:** migrated and topographic time seismic section; **d:** seismic section with depth correction, borehole location and major seismic sediment units indicated.

facies characterization. An analysis of the Hilbert transform is planned to extract seismic wave attributes in instantaneous amplitude, instantaneous phase and instantaneous frequency (Luo et al. 2003). Future tests may investigate Amplitude Versus Offset (AVO) information to characterize groundwater reservoirs. This method has been applied effectively for oil and gas reservoir characterization (Yilmaz 2001).

This data set displays complex features with steep slopes and diffractions as kettle holes for example that can only

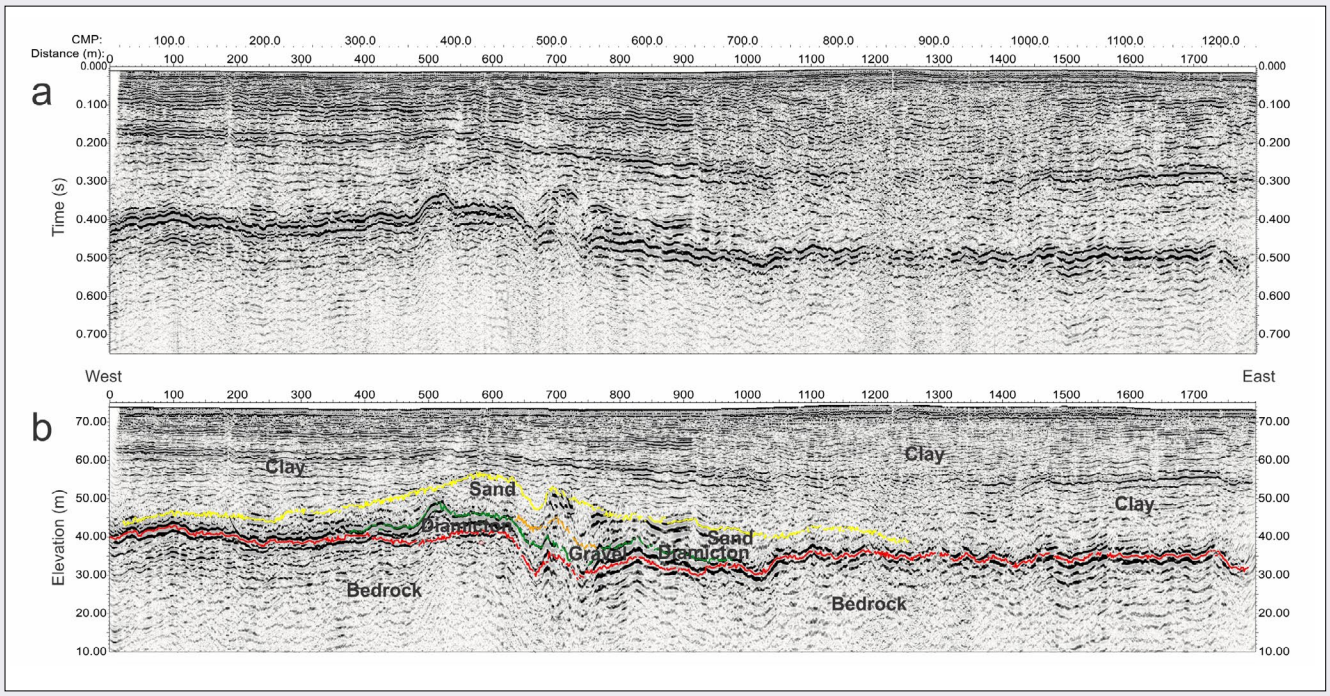


Figure 6. Route 200 seismic section oriented NE–SW, north of Embrun, ON. **a:** time migrated seismic section; **b:** seismic depth section with seismic unit interpretations. Note gravel core and wide carapace of sand.

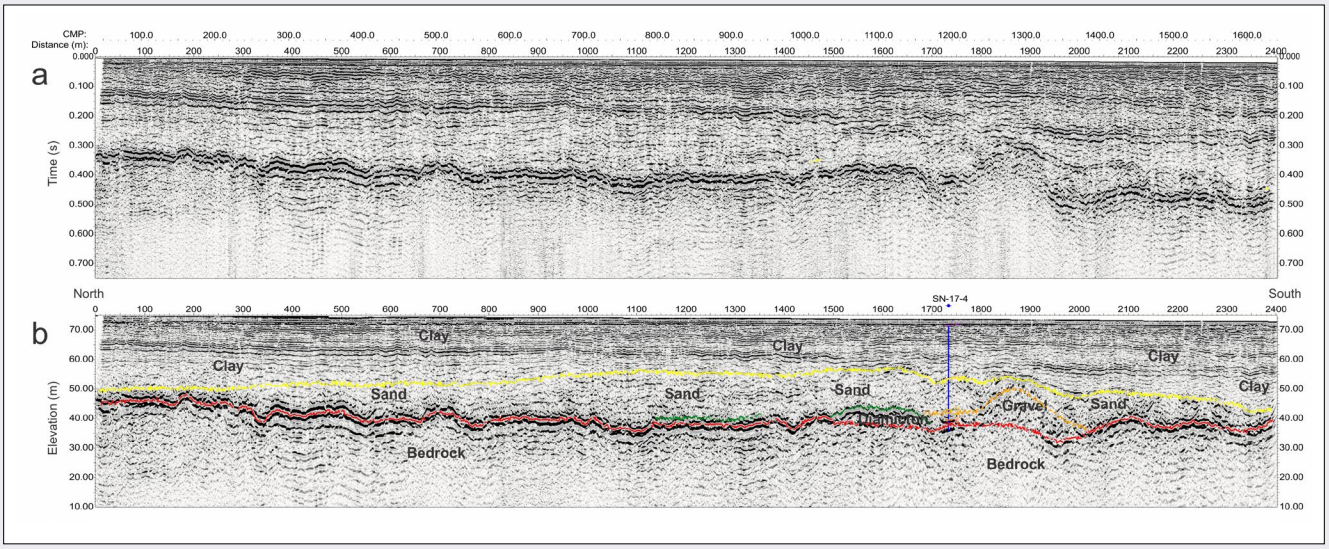


Figure 7. Route St Pierre seismic section oriented NNW–SSE, north of Embrun, ON. **a:** time migrated seismic section; **b:** seismic depth section with interpretations.

be revealed by a migration operation. Borehole data and velocity log calibrations are essential for an accurate time to depth conversion of the sections. These high-resolution sections provide insight into the complexity and details of this subsurface aquifer system. S-wave velocities provide information on lithologies related to grain size. Phases and amplitudes provide information on the texture (grain-size), sedimentary structures, and bed thickness within this portion of the Vars-Winchester esker.

5. Acknowledgements

An internal review at the GSC was completed by Hazen Russell and Bruce Kjarsgaard. The work was funded by the Groundwater Geoscience Program of the Geological Survey of Canada. This work is a contribution to the GSC–OGS southern Ontario project on groundwater 2014–2019.

6. References

Crow, H.L., Pugin, A.J.-M., Dietiker, B., Paradis, D., Brewer, K., Cartwright, T., Griffiths, M. and Russell, H.A.J. 2020. Lithological and hydrogeological properties from a downhole geophysical dataset in the Vars-Winchester esker, Ontario. In Russell, H.A.J. and Kjarsgaard, B.A. Eds. Southern Ontario groundwater project 2014–2019: summary report. Geological Survey of Canada, Open File 8536, https://doi.org/10.4095/321100

Cummings, D.I., Gorrell, G., Guilbault, J.-P., Hunter, J.A., Logan, C., Ponomarenko, D., André J.-M. Pugin, A. J.-M., Pullan, S.E., Russell H.A.J. and Sharpe, D.R. 2011. Sequence stratigraphy of a glaciated basin fill with a focus on esker sedimentation. GSA Bulletin, 123: 1288-1316.

Logan, C., Cummings, D.I, Pullan, S.E., Pugin, A.J.-M., Russell, H.A.J, and Sharpe, D.R. 2009. Hydrostratigraphic model of the South Nation watershed region, south-eastern Ontario. Geological Survey of Canada, Open File 6206, 17 pages 1 DVD.

Luo,Y., Al-Dossary, S., Marhoon, M. and Alfaraj, M. 2003. Generalized Hilbert transform and its applications in geophysics. The Leading Edge, 22: 3, 198-202.

Maries, G., Ahokangas, E., Mäkinen, J., Pasanen, A., and Malehmir, A. 2017. Interlobate esker architecture and related hydrogeological features derived from a combination of high-resolution reflection seismics and refraction tomography, Virttaankangas, southwest Finland. Hydrogeology Journal, 25: 829–845. https://doi.org/10.1007/s10040-016-1513-9

Paradis, D., Pugin, A.J.-M., Crow, H.L., Oldenborger, G., Russell, H.A.J. and Melaney, M. 2020. Hydrogeophysics data acquisition for the characterization of hydraulic properties of the Vars-Winchester esker, southeastern Ontario. In Russell, H.A.J. and Kjarsgaard, B.A. Eds. Southern Ontario groundwater project 2014–2019: summary report. Geological Survey of Canada, Open File 8536, 131-138. https://doi.org/10.4095/321098

Parent M. and Occhietti S. 1988. Late Wisconsinan deglaciation and Champlain Sea invasion in the St. Lawrence Valley, Quebec. Geographie Physique et Quaternaire, 42: 215–246.

Pugin, A.J.-M., Pullan, S.E., and Hunter, J.A. 2009a, Multicomponent high-resolution seismic reflection profiling. The Leading Edge, 28: 10, 1182-1265.

Pugin, A.J.-M., Pullan, S.E., Hunter, J.A., and Oldenborger, G.A. 2009b: Hydrogeological prospecting using P- and S-wave landstreamer seismic reflection methods. Near Surface Geophysics, 315-327.

Pugin, A.J.-M., Brewer, K., Cartwright, T., Pullan, S.E., Perret, D., Crow, H., and Hunter, J.A. 2013a. Near surface S-wave seismic reflection profiling — New approaches and insights. First Break, 31: 49–60.

Pugin, A. and Yilmaz, O. 2019, Optimum source-receiver orientations to capture PP, PS, SP, and SS reflected wave modes. The Leading Edge, 38:1, 45-52.

Pullan, S.E., Pugin, A.J.-M., and Hunter, J.A. 2007. Shallow seismic reflection methods for the delineation of hydrogeological characterization of buried eskers in Eastern Ontario. In Proceedings, SAGEEP 07 (Symposium on the Application of Geophysics to Engineering and Environmental Problems), Denver, CO, April 1-5, 2007, 10 p.

Richards, P.G. and Frasier, C.W. 1976. Scattering of elastic wave from depth-dependent inhomogeneities: Geophysics, 41: 441–458.

Yilmaz, Ö. 2001. Seismic data analysis. Society of Exploration Geophysicists, Reservoir Geophysics. Seismic Data Analysis, 2: 11, 1793-2028.

Yilmaz, Ö. 2015. Engineering Seismology with Applications to Geotechnical Engineering. Investigations in Geophysics Series No. 17. Society of Exploration Geophysicists, Tulsa Oklahoma, 954 p.

Lithological and hydrogeological properties from a downhole geophysical dataset in the Vars-Winchester esker, Ontario

Heather L. Crow[1]*, André J.-M. Pugin[1], Barbara Dietiker[1], Daniel Paradis[2], Kevin Brewer[1], Tim Cartwright[1], Matthew Griffiths[1], and Hazen A.J. Russell[1]

Abstract: A study examining the relationship between hydraulic and geophysical properties is underway in the South Nation Conservation Area, southeast of Ottawa, Ontario. Groundwater resources for the local community are drawn from a sand and gravel esker, which is capped by a thick sequence of post-glacial massive to laminated mud sediment. Surface geophysical techniques (high-resolution seismic and electrical resistivity) identified the depth, shape, and general stratigraphy of the esker within the 2-km study area. Four boreholes were then drilled into the center and flanks of the esker to install fully screened PVC casings to conduct hydraulic packer testing and downhole geophysical logging.

The geophysical log suite provided a number of insights into the esker stratigraphy and overlying Champlain Sea mud. Gamma, conductivity, magnetic susceptibility, and density logs refined the depths of lithological boundaries and the nature of these contacts (abrupt vs transitional). Bulk conductivity profiles revealed differences in pore water conductivities in the mud sediments overlying and lateral to the esker. Magnetic susceptibility logs revealed the presence of stratigraphic layering within the esker, which nuclear magnetic resonance (NMR) logs identified as having variable porosity.

1. Introduction

A project is underway south-east of Ottawa, ON, to characterize hydraulic properties of the Vars-Winchester esker (Figure 1), an unconsolidated sandy aquifer, using geophysical datasets. The esker supplies groundwater to the rural community of Embrun, ON. Capping this esker are post-glacial muds (silts and clays) and thus it does not have a visible surface expression in the study area. Surface geophysical methods have been used to identify the location of the esker (Pugin et al. 2009; Pugin et al. 2020), allowing accurate placement of four fully screened boreholes that intersect the core and flanks of the esker. By extending hydrogeophysical methodologies previously developed by the Geological Survey of Canada (GSC) (Pugin et al. 2009; Oldenborger et al. 2014, 2016; Paradis et al. 2014, 2015), the goal of this study is to estimate the hydraulic properties of the esker and surrounding sediments from geophysical data, and to compare these results with localized hydrogeological studies at the boreholes (Paradis et al. 2020).

To support this study, a suite of downhole geophysical logs was acquired in all four boreholes to develop a better understanding of the in situ lithological and hydrogeological properties of the sediments. Natural gamma, induction (bulk apparent conductivity and magnetic susceptibility), and gamma-gamma density logs were acquired to refine depths of lithological contacts, and measure the physical and chemical properties of the main sedimentary units. Downhole seismic logs (compression (Vp), and shear (Vs)) provided material velocities for lithological interpretation and verified the conversion of seismic reflection time sections into depth sections. High-resolution temperature and conductivity logs were recorded within the borehole fluids to capture variation in groundwater properties within the esker. Slim-hole nuclear magnetic resonance (NMR) tools were deployed experimentally for the first time in this geological setting to measure sediment porosity and estimate hydraulic conductivities (K) in these unconsolidated surficial sediments. The log suites described in this article support the interpretation of the hydraulic tests performed in the wells, and the surface geophysical datasets with distance away from the boreholes.

[1] Geology Survey of Canada, Natural Resources Canada, 601 Booth Street, Ottawa, ON K1A 0E8
[2] Geological Survey of Canada, 490 rue de la Couronne, Quebec City, QC G1K 9A9

*corresponding author: heather.crow@canada.ca

Recommended citation: Crow, H.L., Pugin, A.J.-M., Dietiker, B., Paradis, D., Brewer, K., Cartwright, T., Griffiths, M., and Russell, H.A.J. 2020. Lithological and hydrogeological properties from a downhole geophysical dataset in the Vars-Winchester esker, Ontario. In Russell, H.A.J. and Kjarsgaard, B.A. Eds. Southern Ontario groundwater project 2014–2019: summary report. Geological Survey of Canada, Open File 8536, 147-157. https://doi.org/10.4095/321100



Figure 1. General location of the study area between Ottawa, ON and Montreal, QC, and the Vars-Winchester esker (after Cummings et al. 2011). (b) Study area showing locations of the 2017 boreholes (in blue), 2007 boreholes (in brown), and surface geophysical survey alignments followed in this study.

2. Geological setting

The study area is located 35 km south-east of Ottawa near the town of Embrun, ON and has a footprint of approximately 3 km × 3 km (Figure 1). Knowledge of bedrock and surficial sediment properties in the study area is provided by drilling and continuous core collection by the GSC in 2007–08 (GSC-BH-07 series; Cummings et al. 2011), and in 2017 drilling cuttings recovery (GSC-17-SN2 series; Paradis et al. 2020).

Bedrock as encountered in boreholes drilled throughout the region in 2007–08 is generally carbonate mudstone, whereas in the study area the bedrock is a black shale (Cummings 2011). A dense, competent diamicton (glacial till) was intersected throughout the region above bedrock. The diamicton has a predominantly silty-sandy rich matrix and contains some gravel-sized clasts consisting of local carbonaceous mudstone and subordinate igneous rock types. It is described as being 1–3 m thick, grey in colour, and massive in texture (Cummings et al. 2011). Overlying diamicton or bedrock in the study area is the Vars-Winchester esker which has a north-south orientation and extends approximately 80 km from the Ottawa River in the north, to Chesterville in the south. Regionally the esker is a few hundred metres across and consists of a narrow gravelly central ridge (or core) and a broad sandy carapace. The ridge is interpreted to have been deposited in a meltwater conduit at the base of the glacier. Clasts within the gravel core are typically similar to the underlying diamicton: carbonate and mudstone with some igneous and sandstone clasts, with medium to coarse sand typically filling pore spaces. Sandy fan deposits, containing variable amounts of pebbles, overlie the gravelly core. Drillcore data suggest the distal parts of this sandy fan carapace commonly overlie diamicton. In outcrop, observed north of the study area, the carapace is composed of multiple units ("lobes") that are stacked atop one another in upward fining, upward coarsening, and ungraded sequences. These lobes may contain abrupt bases which are often gravelly (Cummings et al. 2011).

The sequence of the Laurentide Ice Sheet retreat and the incursion of the Atlantic Ocean into the Ottawa and St Lawrence River valleys forming the Champlain Sea left a record of post-glacial marine sedimentation in the region. The esker is covered by muds (silts and clays), which were deposited in the western Champlain Sea basin. Gadd (1986) first identified three units in this mud package that are all observed in the study area: grey rhythmites, containing mud and sand; massive bioturbated mud, and; red-and-grey rhythmites, which can contain sand seams. Drillcores from 2007–08 have a 2-m thick, sharp-based upward fining grey rhythmite unit of alternating thin (<1 cm) layers of light grey silt or very fine sand, with dark grey mud, which typically reacts strongly with HCl. This unit transitions upward into, massive bioturbated dark grey mud, and typically reacts strongly to HCl, but less so than the unit below. Pore water salinities are low to moderate. Finally, a red and grey stratified mud overlies (and intercalates with) the massive muds. Couplet thicknesses typically increase upward from <1 cm at the base to tens of cm near the top. These beds react less strongly to HCl than the underlying massive muds and beds also become increasingly sandier upward (Cummings et al. 2011).

Mineralogy of this till–esker–mud sediment sequence has an important influence on the geophysical log response. At the base of the sequence, diamicton and esker gravel clasts are predominantly carbonate mudstone (>90%). The content of Shield-derived sediments increases upward through the sequence from diamicton, to esker, to red and grey stratified mud. A study of Champlain Sea sediments to the north in nearby Breckenridge, QC, indicates the silt- and clay-sized

particles, and fine sand found in seams, are dominated by a mineral assemblage reflecting a Shield provenance. In descending order, these minerals are plagioclase feldspar and quartz, with subordinate biotite mica, potassium feldspar, and amphibole. Although the clay-size fraction (often termed "rock flour") can exceed 60%, clay minerals such as chlorite and illite are present in only trace amounts (<7% by weight of silt and clay sized grains). Also present in trace amounts are iron oxides, verified under the scanning electron microscope (Crow et al. 2017). Analyses of the red and grey rhythmites in the upper mud unit from cores recovered approximately 40 km north-east of the study area indicate the presence of hematite in the red bands and trace amounts of magnetite in the grey bands (Percival et al. 2001).

The silt and clay-sized particles flocculated within the Champlain Sea to produce a sediment with a loose framework and elevated porosities, reaching 69% in cores recovered from the Embrun study area. Although porosities are often high, scanning electron microscope work in Champlain Sea sediments close to Montreal has shown the clay-sized fraction consists of aggregated grains, separated by a porous network of small pores approximately 0.5–1 microns (Delage 1982).

3. Geophysical logging methods and applications

Four boreholes were drilled in December 2017; one into the esker core (GSC-SN2-17-01), two into the esker flanks (GSC-SN2-17-02, and -04) and one off-esker location (GSC-SN2-17-03) (Figure 1). The PVC casings are solid in the upper 4 to 6.5 m and screened to the base of each well. Geophysical logging was completed between May and July 2018. Logging techniques are discussed below in the context of the lithological units encountered in the study area and the properties of fluids within the sediments.

3.1 Lithological logs

Logs used together to interpret changes in sediment properties are herein termed 'lithological logs'. In this study, nuclear logs (natural gamma, gamma-gamma density), induction logs (apparent conductivity and magnetic susceptibility) and velocity logs were acquired to refine depths of lithological contacts and measure the physical and chemical properties of the sedimentary units. The nuclear and induction logs were acquired using a Mount Sopris logging system with a Matrix console and interchangeable downhole probes. A laptop computer recorded the data using Matrix Logger Software. Details of the instruments, logging system, calibrations, and tool parameters can be found in Crow et al. (2015).

Natural (or passive) gamma logs record gamma radiation emitted from surrounding sediments. The most significant, naturally-occurring radioisotopes are potassium (K), uranium (U), and thorium (Th). Clay minerals are typically K-rich and will have more elevated gamma responses than a unit that contains clay-sized grains, but few clay minerals (e.g. 'rock flour' from the Precambrian Shield). Where pore waters are fresh, the apparent conductivity response mirrors the trends of the natural gamma log, where fine grained materials tend to be more conductive than coarse grained materials. In the presence of conductive pore fluids (e.g. remnant saline pore water from the Champlain Sea), the apparent conductivity response to the sediment matrix is overwhelmed by that of the ionic pore fluids. In the study area, magnetic susceptibility is more positively influenced by the presence of sand-sized particles. A Shield-derived sand, with a greater percentage of ferromagnetic iron oxides (e.g. magnetite), will have a higher magnetic susceptibility response than a carbonate bedrock-derived (i.e. magnetite-poor) sand or gravel. Therefore, log response to any particular sediment is strongly influenced by the mineralogy of the source material, the pore water conductivity, the depositional setting, and the distribution of the grain sizes within the unit.

The gamma-gamma density logs contribute to the lithological interpretation through the measurement of bulk sediment density, which varies, often abruptly, between the main lithological units. Runs are presented uncorrected for the effect of the 0.64-cm thick PVC pipe wall, which has a lower density (1.4 g/cm^3) than the surrounding sediments and bedrock (range of 1.6–2.6 g/cm^3). Lab calibrations with a 0.55-cm thick PVC pipe suggest the pipe wall effect could range from overestimates of true densities by up to 0.03 g/cm^3 in the muds, to underestimates of true densities of up to 0.04 g/cm^3 in the esker sands and gravels. These small deviations are less than the variation observed at lithological contacts (typically >0.1 g/cm^3), so a correction has not been applied to the data presented herein. An important aspect of the density logging was also qualitative, identifying intervals in the muds where the log response would drop abruptly. In this way, the log was extremely useful in identifying the locations of water-filled voids behind the casing where sensitive sediments became disturbed during drilling and did not fully collapse against the casing wall. At least two density runs were collected in each well to look for any non-uniform sediment gaps around the borehole.

Velocity logging was carried out using a clamped, 3-component downhole receiver with 15 Hz omni-directional geophones manufactured by Geostuff Ltd. The receiver was lowered by hand to the bottom of the hole, and pulled up-hole at half metre spacings where stationary shots were recorded. A hammer striking a GSC-designed metal plate was used as a source. The plate, set 1.1 to 1.5 m away from the borehole collar, was coupled with the ground by driving a vehicle over it. The plate was struck vertically to generate P-waves, and on an angle to generate S-waves. A Geometrics 24-channel Geode seismograph was used and data were recorded on a laptop computer after reviewing each record on screen. Velocity log results are presented in Pugin et al. (2020).

3.2 Fluid logs

Fluid logs were used to interpret the presence, distribution, and properties of fluids found within the sediments. Changes in fluid conductivity and temperature inside the screened PVC casing were measured using a Mount Sopris fluid temperature/conductivity probe, modified in-house with an additional exposed thermistor for fast thermal response and high-resolution (0.001°C) fluid temperature logging. The probe was run on a Mount Sopris logging system, and was the first tool deployed in each well in the undisturbed fluid on a slow downward run (1 m/min). All fluid conductivities reported are corrected to 25°C. The probe is calibrated in the lab and rechecked in the field after each run using handheld calibration meters.

Nuclear magnetic resonance (NMR) slim-hole tools were deployed experimentally in the three boreholes intersecting the core and flank of the esker. Although NMR logging tools have been in use by the oil industry since the early 1990s, only in recent years have they been adapted for slim-hole logging applications. Until recently, measuring parameters related to fluids within sediments and rock (water content, porosity, and pore size distribution) could not be directly measured with logging tools. NMR technology provides an in situ technique, which has sensitivity spatially beyond the borehole to quantify the amount and mobility of water in sediment and rock directly. However, the Quaternary sediments of the Ottawa Valley were expected to challenge NMR technology due to small pores, high water contents, and magnetic mineral content. This aspect of the downhole study was, therefore, to evaluate the performance of NMR technology in this environment for aquifer/aquitard characterization.

NMR measurements use magnets in a downhole tool to polarize hydrogen in the groundwater, transmitting a complex sequence of radio-frequency pulses by an antenna in the tool, and recording the returning signal (e.g., Allen et al. 1997; Coates et al. 1999; Allen et al. 2000). In a calibrated tool, the amplitude of the signal indicates the total amount of groundwater in the formation surrounding the borehole. The rate of signal decay is influenced by the distribution of pore sizes in the sediment. Bound water in small pores (e.g. clays and silts) decays very quickly, whereas mobile water in larger pores (e.g. clean sands, gravels) decays more slowly. This provides information on fluid mobility (i.e. whether water is formation-bound or able to flow), which can be used to compute hydraulic conductivity (K). Ideally, a full suite of geophysical logs is plotted together to display complementary information about the lithology, and presence of any voids or sediment disturbance around the casing impacting log interpretation (i.e. borehole completion conditions).

Two Vista Clara NMR downhole tools were deployed in this study: the Dart and the JP238 Javelin models. The Dart was manually lowered downhole on a logging cable and powered by a light-weight surface console with internal batteries. The tool operates at two frequencies (475, 425 kHz), providing two shells (or cylinders) of investigation of 14.0 and 16.5 cm diameters, respectively, around the tool. The JP238 is a larger tool which was deployed on a motorized IFG logging winch connected to a surface console powered by a 240 V generator. The tool operates at four frequencies (415, 360, 300, 250 kHz) allowing for four shells of investigation around the tool (23, 25.5, 28, 30.5 cm diameters, respectively). The data were collected in both stationary and slow-moving (20–30 m/hour) continuous modes. For both probes, a laptop computer was used to set acquisition parameters and record data, allowing for real-time QA/QC in the field. Data were processed using Vista Clara's JavelinProcess (v4.5) and JavelinInterpret (v.1.8) software. The software estimates hydraulic conductivity (K) from interpreted pore distributions, using pre-established settings for unconsolidated sands and gravels.

4. Results and discussion

Log data and casing completion details were imported into WellCAD software (v5.1) to interpret as a data suite. Log responses are discussed in the context of lithology, fluid properties, and completion conditions around the casings (Figures 2, 3, 4, 5).

4.1 Geophysical properties of the lithological units

Bedrock in the study area is described in core and cuttings as a black shale. The top of the bedrock is most strongly defined in the logs by an abrupt rise in natural gamma counts, indicating an increase in clay mineral content relative to all overlying units. An increase in density, and a drop in magnetic susceptibility also defined the contact (Figure 2).

Texturally, the diamicton encountered in cores around the region differs from the overlying sands and gravels, but mineralogically, seems to represent a transition between the underlying bedrock and the overlying esker. The geophysical logs in all four wells indicate a distinct unit exists above the bedrock, ranging in thickness from 0.7 to 3.8 m. It is defined at the lower contact by an abrupt decrease in gamma counts above the bedrock surface, and a second decrease at the top of the unit, which is abrupt in GSC-SN2-17-01 and more transitional in GSC-SN2-17-02 and -04. This indicates that the diamicton has a greater clay content than the overlying esker. A small but abrupt decrease in density at the bedrock contact is coupled with a second abrupt decrease at the upper contact (base of the esker), which indicates that the till has an elevated density and is compacted relative to the overlying materials. The magnetic susceptibilities and NMR porosities are more elevated in the diamicton than in the underlying bedrock, but significantly lower than in the overlying sand-rich part of the esker. Fluctuations in the magnetic susceptibility in the till suggest the presence of igneous clasts (e.g., GSC-SN2-17-01, 34 m, Figure 2). These responses could indicate an interval of weathered bedrock into which esker materials

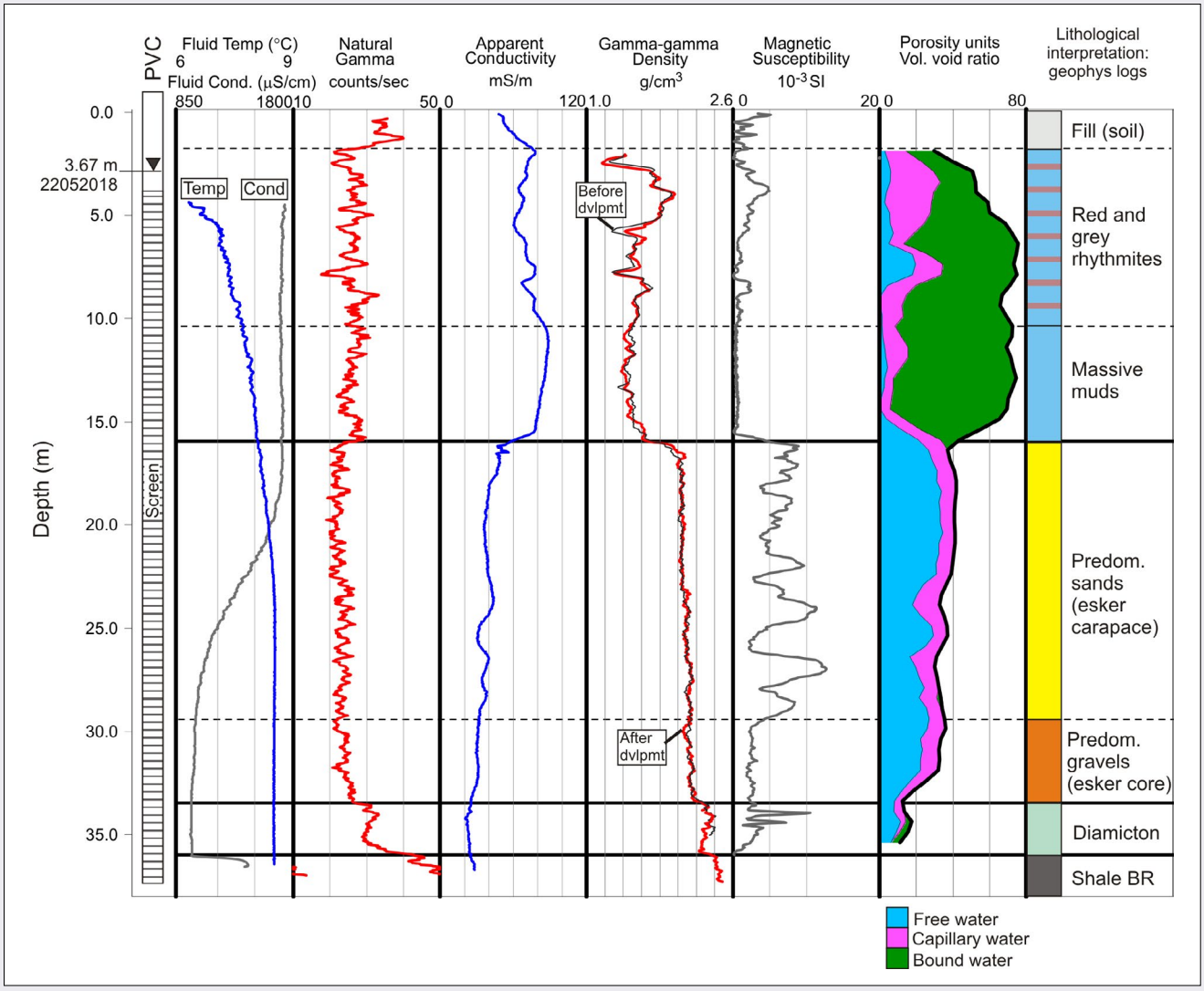


Figure 2. Log suite from GSC-SN2-17-01 with lithological interpretation based on geophysical log response. dvlpm = development

are mixed. However, cores from a borehole drilled in 2007 adjacent to well GSC-SN2-17-02 indicate a diamicton is present beneath the esker (Cummings et al. 2011), in agreement with observations from the geophysical logs.

The gravelly central ridge of the esker is described in core as having clast lithologies similar to the underlying diamicton with predominant carbonate mudstone and minor granite, sandstone, and shale clasts (Cummings et al. 2011). In GSC-SN2-17-01 (Figure 2), an interval of relatively low and stable magnetic susceptibility is consistent with a carbonate-dominated gravel being present. Other factors supporting a gravel interpretation include an increase in NMR free water content from underlying materials, coupled with low and stable natural gamma and conductivity responses. This indicates the material has little fine-grained (i.e. clay minerals and clay-sized) content; cuttings reveal medium to coarse sands can be present in gravel pore spaces. In GSC-SN2-17-04 (Figure 5), conversely, magnetic susceptibilities are elevated in the lower part of the esker, which suggests that if gravels are present, they are mixed with Shield-derived sands.

The distinguishing feature contrasting the esker sand from the esker gravel is relatively elevated and variable magnetic susceptibility, indicating the presence of ferromagnetic iron oxides (e.g., magnetite). These log patterns are different in each of the wells, which suggest variations in layering within the esker, consistent with the model of multiple stacked lobes. Lab analyses of six samples of sand cuttings recovered from GSC-SN2-17-01, -02, and -04 indicate grain size varies from very fine to very coarse sand. Magnetic susceptibility levels recorded on each of these samples with a handheld

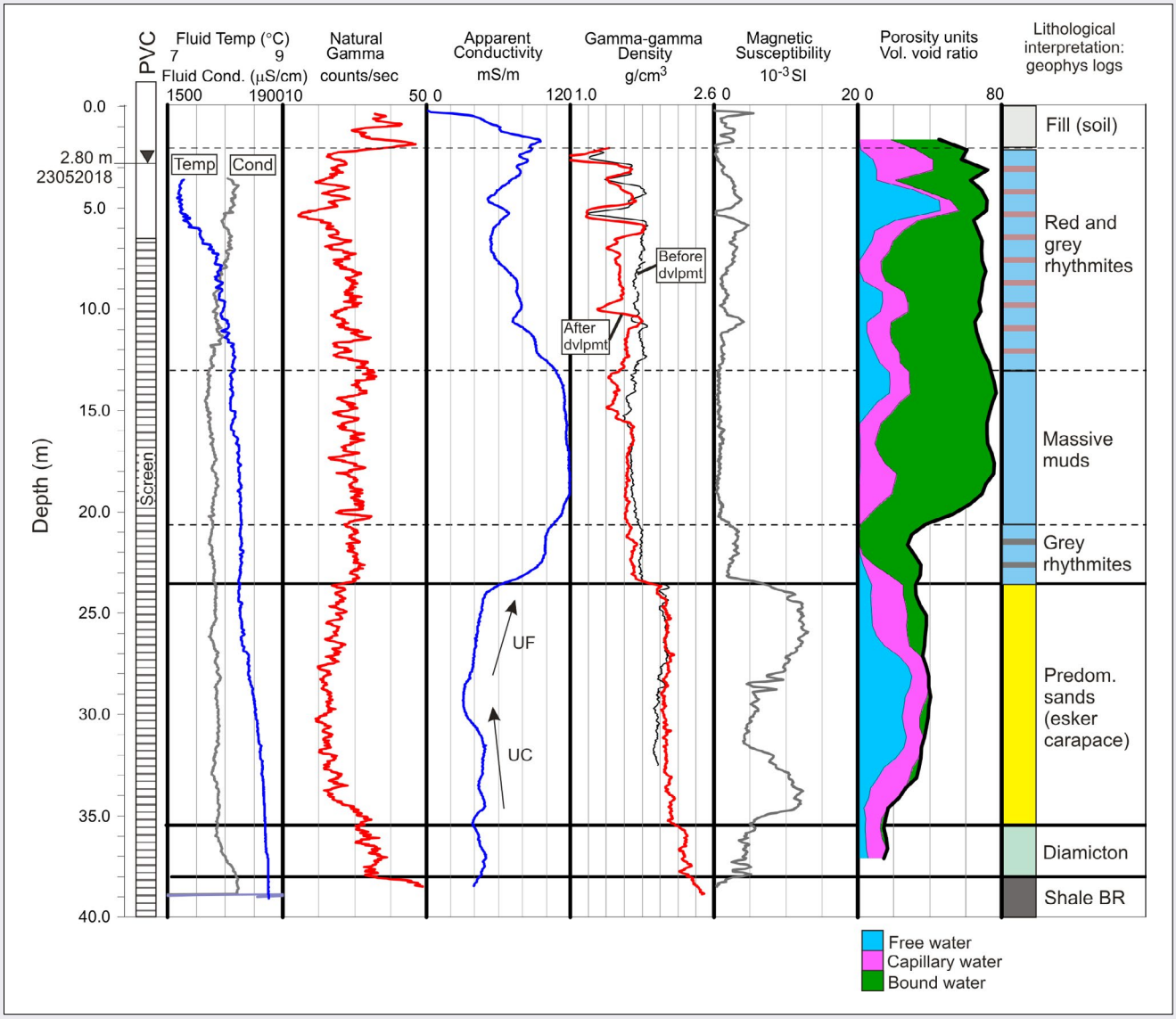


Figure 3. Log suite from GSC-SN2-17-02 with lithological interpretation based on geophysical log response. UF = upward fining, UC = upward coarsening.

susceptibility meter measures the most elevated responses in samples with finer grain sizes (Table 1). This suggests that elevated magnetic susceptibility response in the downhole logs indicates relatively finer sand. Conductivity log response provides complementary information about mud content in the esker. In GSC-SN2-17-01 and -02, apparent conductivity response is relatively low (30–50 mS/m) with some variability (up to ±20 mS/m), suggesting increases in mud (in particular, clay) content, where conductivity increases. An upward trend of increasing conductivity in GSC-SN2-17-01 suggests an increase of clay content in mud upward through the unit, an observation supported by the grain size analyses (Table 1). In contrast, GSC-SN2-17-04 has a stable and low response across the entire unit, and although mud content is relatively elevated in the sample from 25 m, lab analyses show most of this is silt. Within the esker, the variability of grain sizes (gravel to fine sand) and structure is best interpreted from the magnetic susceptibility response as the main lithological indicator log. The gradual upward decrease of the density log does not convey that a distinct boundary is present between the core and the carapace, indicative of a more transitional contact between gravels and sands, a feature also noted by Cummings et al. (2011) at this site. In borehole GSC-SN2-17-03 (Figure 4), an interval of elevated magnetic susceptibility and density, with reduced apparent conductivity relative to the overlying muds suggests the esker was intersected between 30.2 and 31.8 m. As it is distal from the esker core, it may be a more compacted silt with sandy layers, but presents a density

Table 1. Grain size analyses and magnetic susceptibility measurements from esker sand samples. The more elevated magnetic susceptibility responses (highlighted orange) come from the finer sand fraction. Blue highlighted boxes represent at least 75% of the predominant size fractions in each sample. *Depths are approximate as they are recovered from cuttings. ** Measured using a JH-8 handheld magnetic susceptibility (electromagnetic induction) meter.

				Size Fraction (% volume)					
Well	Sample depth (m)*	Esker Unit	Mag Susc** $\times 10^{-4}$ SI	very coarse sand	coarse sand	medium sand	fine sand	v. fine sand	Silt / clay
				2.00 - 1.00 mm	0.99 - 0.50 mm	0.49 - 0.25 mm	0.24 - 0.125 mm	0.125 - 0.063 mm	<0.0625/<0.002 mm
01	18	sand	35	0.07	7.21	54.13	23.06	6.02	6.65 / 2.86
	23	sand	28	0.17	3.96	51.60	35.06	5.01	2.98 / 1.20
	30–34	gravel	7.5	31.74	47.81	12.81	3.33	1.12	2.27 / 0.91
02	29	sand	25	0.09	11.68	54.80	21.65	7.11	3.65 / 1.03
04	20–22	sand	10	1.96	36.79	39.16	11.19	6.13	3.59 / 1.19
	25	sand	50	0.17	0.42	1.44	31.24	44.41	20.01 / 2.32

contrast with the overlying mud-rich sediments detectable in the density log and the seismic profiling (see Pugin et al. 2020). In all boreholes, the top of the esker is marked by an abrupt decrease in density and magnetic susceptibility, with an increase in apparent conductivity, natural gamma, and NMR porosity responses.

The fine-grained deposits of the Champlain Sea have been identified as consisting of three main mud units with minor amounts of sand near the top and bottom of the sequence (Cummings et al. 2011). The conductivity and magnetic susceptibility logs in boreholes GSC-SN2-17-02 and -03 define the transition between all of these units (Figures 3, 4). At the lower contact with the esker, the conductivity increases upward, and magnetic susceptibility indicates the presence of minor sand. This unit appears to be absent in the boreholes drilled through the center (top) of the esker (GSC-SN2-17-01, -04) i.e. not draped over a topographic high. Within the massive mud unit, apparent conductivities are relatively elevated, reflecting preserved remnant pore water salinity from the Champlain Sea. Magnetic susceptibility drops to its lowest levels, which indicates magnetite-bearing sand is nearly absent from this unit. The uppermost unit is a stratified mud with sand layers. The base of this unit is best defined by a subtle increase in magnetic susceptibility that increases further upward throughout the unit, indicative of a transitional contact. Apparent conductivity through this interval generally decreases upward and magnetic susceptibility increases. Sand-rich beds, indicated by higher magnetic susceptibility and density log signals, can be correlated with high-amplitude seismic reflections at the (near) top and base of the massive mud unit, creating marker horizons which can be traced with distance away from the boreholes (Figure 4).

Based on these analyses of geophysical log responses, the contact depths between the lithological units are provided in Table 2.

4.2 Fluid properties & hydrogeological parameters of the sediments

From a regional perspective, Hinton et al. (2011) discuss the hydrostratigraphy of the sediments and bedrock in the study area. As geophysical logs were limited to only a few meters of penetration into bedrock, discussion here is limited to observations from within the unconsolidated surficial sediments. Downhole fluid temperature and conductivity measurements provide information on groundwater conditions in open borehole fluid, whereas NMR logs provide information on the distribution and volume of this fluid within the sediments surrounding the borehole, which allow for estimations of K.

Fluid logs were recorded in the screened portions of the three wells that intersect the esker. Fluid temperatures in the muds ranged from 6.3–8.8°C, temperatures in the esker ranged from 8.3–8.8°C, and within the esker core in GSC-SN2-17-01 and -04, fluid temperatures ranged from 8.5–8.6°C.

Fluid conductivity profiles in all three boreholes were different. Relatively elevated fluid conductivities were measured in the mud intervals, likely influenced to different degrees by fine-grained particles suspended in the water column, and more elevated pore water conductivities present in the muds. A week prior to logging, the boreholes were developed to remove accumulated sediments at the base of the wells, and to unclog the screens and surrounding formations that may have become blocked by sediment during drilling operations. In borehole GSC-SN2-17-04, which had the longest post-

Table 2. Depth to top of unit contacts based on geophysical log interpretation. N/A indicates unit not observed or undefined by geophysical logs. *Contact depth assigned with some uncertainty.

Top of Unit	Borehole			
	SN2-17-01	SN2-17-02	SN2-17-03	SN2-17-04
	(m)	(m)	(m)	(m)
Mud - red and grey rhythmites	1.70	2.07	1.90	2.18
Mud - massive	10.35	13.03	15.05	11.67
Mud - grey rhythmites	N/A	20.65	24.09	N/A
Sand	15.95	23.55	30.21	16.48
Gravel	29.40	N/A	N/A	N/A
Diamicton	33.46	35.37	31.77	31.45
Bedrock	35.98	38.01	35.56*	32.31

pumping settlement period (10 days), fluid conductivity decreased downward, reaching 770 µs/cm in the esker core – the lowest observed in all three wells. Conductivity measured one day earlier in a nearby stream with a calibrated handheld conductivity meter was 740 µS/cm. In the other wells, pumping had occurred closer to the logging dates. In GSC-SN2-17-01, fluid conductivities decreased downward to 990 µs/cm in the esker core, while conductivities in GSC-SN2-17-02 remained relatively elevated (1625–1675 µs/cm) and did not decrease downward into the esker. While this could be reflective of variable water chemistry in the esker, the timing of the pumping had an unknown influence on the resulting borehole fluid conductivities and hence more study is needed to assess a relationship between fluid conductivity and esker properties.

In the muds, qualitative NMR results indicate the log responses correctly identified formation fluid as predominantly bound water, due to the micron-sized pores present in the clay and silt-sized grains. Hydraulic conductivities have not yet been estimated from these data and are a topic of ongoing study. In the esker, qualitative results indicate NMR responses are correctly identifying predominantly free water in the coarser grain sizes. Where magnetic susceptibilities are relatively low (identified from cuttings as coarser sands), free water contents increase relative to capillary-bound water. Conversely, where susceptibilities are elevated (identified from cuttings as finer sands), capillary-bound water increases relative to free water (see Figure 5). This suggests some variability in permeability at the metre scale may be expected across the sandy carapace. Capillary-bound water was detected in the esker in all three wells, indicating fine-grained material (clay, silt, fine sands) are present in variable amounts, which is consistent with grain size analyses from cuttings samples (Table 1). The NMR log did not reveal a significant increase in porosity or free water content within the interpreted gravel unit of GSC-SN2-17-01, which suggests the unit also contains finer grain sizes (see Table 1). The NMR porosity decreases at the base of the gravel unit as the natural gamma increases, an effect visible in the base of the esker in all three boreholes, suggesting the base of the esker contains some shale. The decrease of NMR porosities below the esker supports the interpretation of a compact, low-permeability diamicton above bedrock. Quantitative results (porosities, hydraulic conductivities) in the sands and gravels are a topic of current study due to the unknown effect of the elevated magnetic susceptibilities. Preliminary lab NMR tests on esker sands revealed shortened relaxation times, an effect also observed in downhole NMR responses where magnetic susceptibilities were relatively elevated. Preliminary results suggest NMR-estimated K values reach 10^{-3} m/s in the gravels of GSC-SN2-17-01, while esker sands typically range between 10^{-6} m/s (finer/siltier) to 10^{-4} m/s (medium to coarse). Ongoing research will compare the NMR-K profiles to K values calculated from packer tests in the esker to provide a more quantitative indication of magnetite influence on NMR measurements.

5. Summary

The suite of natural gamma, bulk density, apparent conductivity, magnetic susceptibility, and NMR porosities together identified depths of the various lithological unit contacts. Elevated natural gamma counts provide a clear geophysical marker for the top of shale bedrock underlying the sediments. Within the sediment sequence, an increase in gamma counts (clay content), alongside an increase in the density log (stiffness), and a drop in NMR porosity relative to overlying units, suggest the presence of a till layer (0.7–3.8 m in thickness), distinct from the overlying esker unit. The presence of a distinct esker core (ridge) described in cores as predominantly carbonate-rich gravels was only observed in one borehole (GSC-SN2-17-01). Density logs do not reveal that a sharp boundary exists between the gravel core and sand carapace in GSC-SN2-17-01 suggesting that the boundary is transitional. The sandy carapace was best defined by relatively

elevated and variable magnetic susceptibility responses, often revealing fining upward and coarsening upward sequences, which may represent multiple lobes similar to those identified in outcrop (e.g., Cummings et al. 2011). The contact with the top of the esker was abrupt and well defined by all the logs. Transitions within the muds were identified by changes in relatively elevated bulk conductivities related to changes in pore water salinity, and by small variations in magnetic susceptibilities related to changes in (magnetite-bearing) sand content. Density variation caused by increased sand content within the muds forms marker horizons at the top and bottom of the massive mud unit, which can be traced in the seismic profiles for hundreds of metres away from the boreholes.

Fluid logs indicate water temperature in the esker ranges between 8.3 and 8.6°C. Fluid conductivities in the esker intersected in boreholes GSC-SN2-17-01 and -04 were closer to that of surface water measured in a nearby stream, while fluid conductivities were elevated along the entire length of the borehole screen in GSC-SN2-17-02.

Borehole nuclear magnetic resonance (NMR) technology was applied experimentally in boreholes GSC-SN2-17-01, -02, and -04 to estimate porosity in the muds and the esker, and hydraulic conductivity (K) within the sands and gravels of the esker. Qualitatively, it correctly identified how water was contained in sediments, widely ranging from clay-bound in micron-sized pores, to free water in the sandy-gravelly esker core. Within the esker, results show increasing pore size (free water) correlates with decreased magnetic susceptibility trends (gravel plus coarser sand grain sizes). In parallel, decreasing pore size (capillary-bound water) correlates with increased

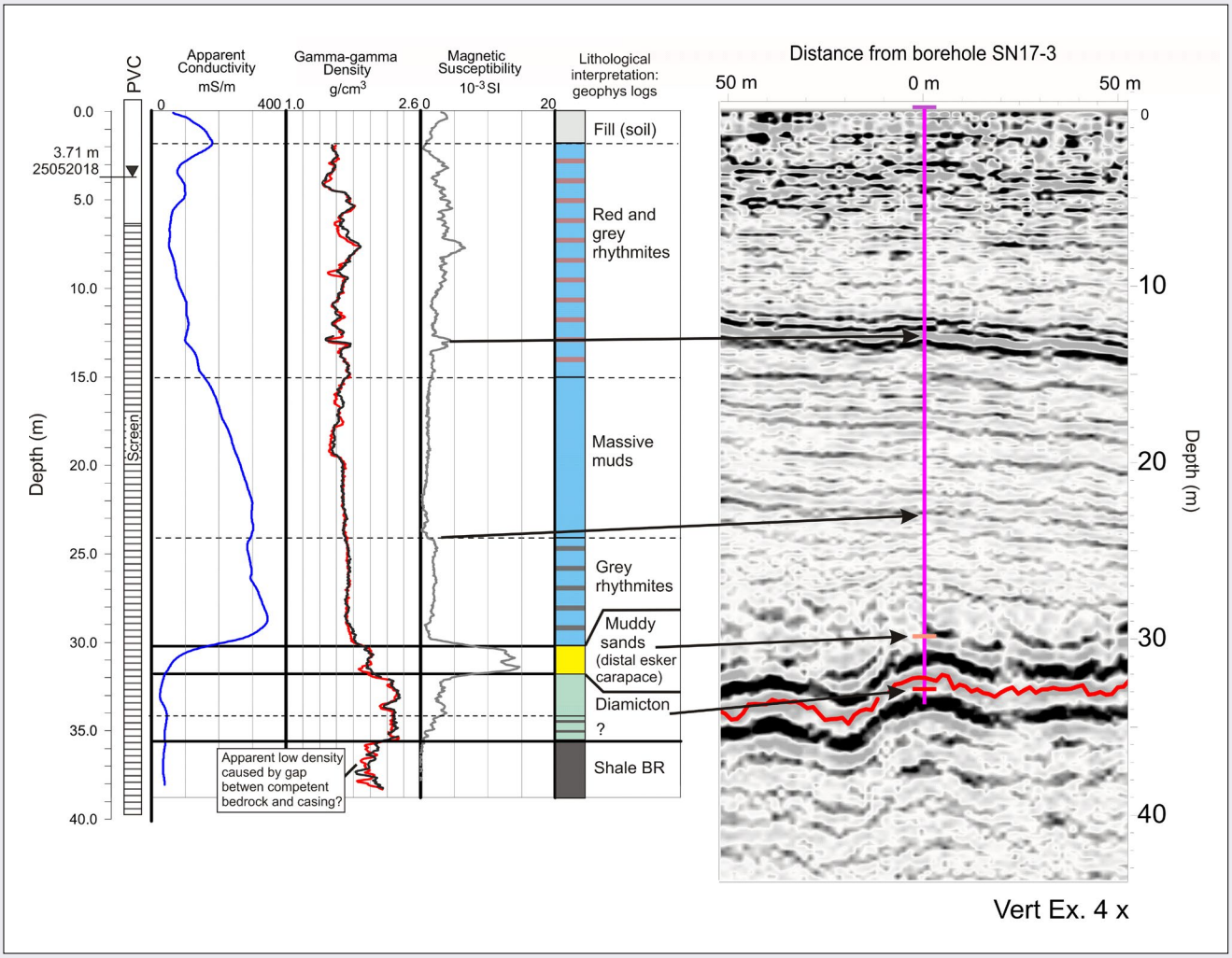


Figure 4. Log suite from GSC-SN2-17-03 with lithological interpretation based on geophysical log response. 100 m of seismic profile around the borehole, set 10 m off line, shows the relationship between stratigraphic features and seismic response, and the continuity of reflectors in the muds away from the borehole. Seismic profile from Pugin et al. 2020.

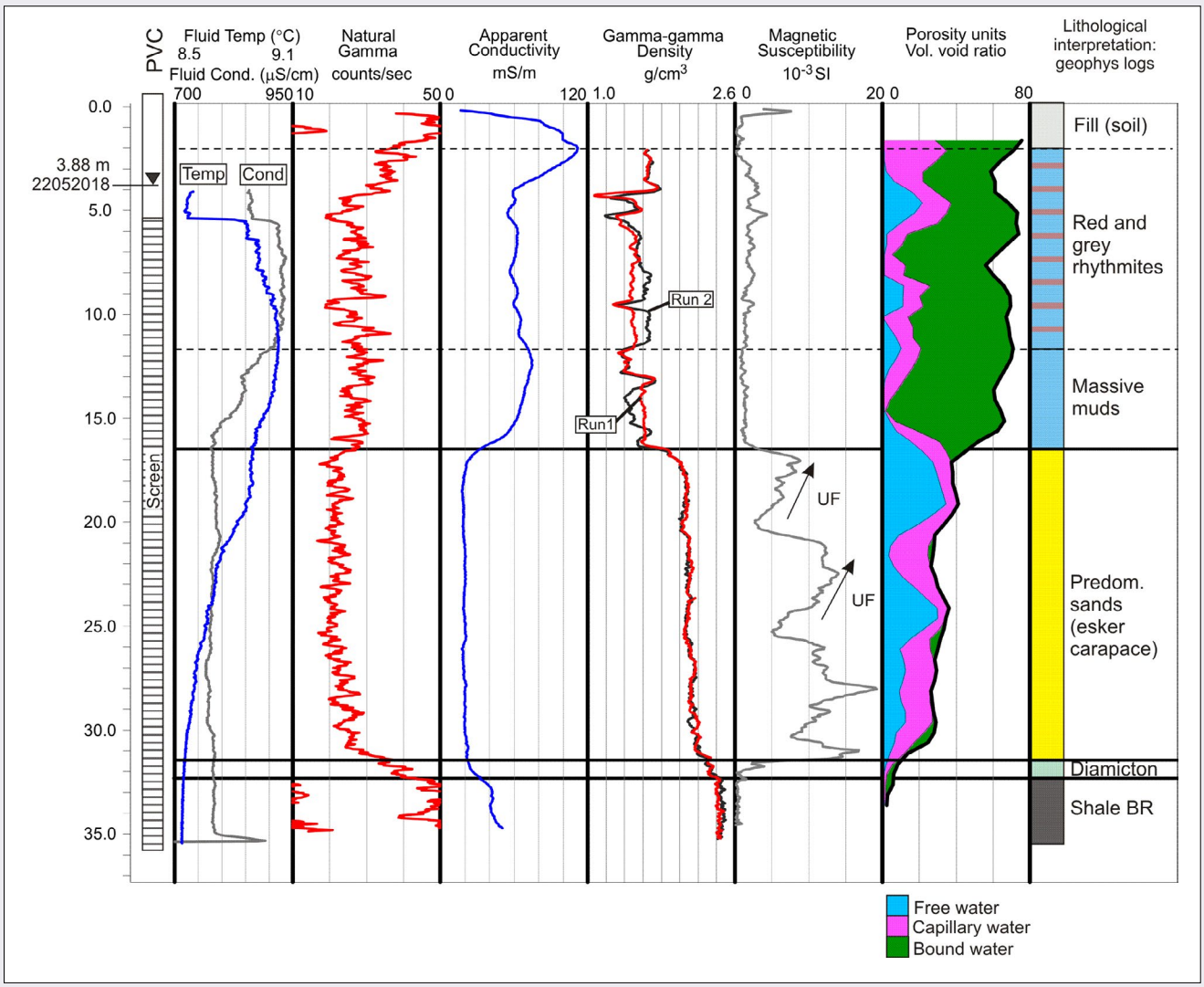


Figure 5. Log suite from GSC-SN2-17-04 with lithological interpretation based on geophysical log response. Free water detected by the NMR response in the muds, collocated with abrupt decreases in the density logs from two separate runs, indicates intervals where sediments have unevenly or not fully collapsed around the PVC casing. UF = upward fining.

magnetic susceptibility trends (finer sand grain sizes), which suggests some variation in permeability within the esker may be expected at the metre scale. Within the esker, where hydrogeological calibration datasets are still being analysed, preliminary NMR porosities reached 40%. Estimates of K from NMR porosities reached 10^{-3} m/s in the gravelly core, and ranged from 10^{-6} to 10^{-4} m/s in the sandy carapace. However, the influence of relatively elevated and variable magnetic susceptibilities on the quantitative results in the sands is a topic of ongoing research.

Geophysical logs created a dataset of physical and chemical parameters which aided in the interpretation of lithological and hydraulic conditions around the wells, and which can be extrapolated beyond the boreholes using surface geophysical data. Ongoing research will continue examining the quantitative comparison between calibration datasets and NMR survey data.

6. Acknowledgements

The authors gratefully acknowledge a peer review of this contribution by M. Hinton, S. Alpay, and B. Kjarsgaard. A special thank you to the South Nation Conservation Authority for providing land access for this field study. This study was supported by the Geological Survey of Canada under the Groundwater Geoscience Program. This work is a contribution of the GSC–OGS Southern Ontario project on groundwater 2014–2019.

7. References

Allen, D., Crary, S, Freedman, B., Andreani, M., Klopf, W., Badry, R., Flaum, C., Kenyon, B., Kleinberg, R., Gossenberg, P., Horkowitz, J., Logan, D., Singer, J., and White, J. 1997. How to Use Borehole Nuclear Magnetic Resonance, Oilfield Review, 9: 2, 34-57.

Allen, D., Flaum, C., Ramakrishnan, T.S., Bedford, J., Castelijin, K., Fairhurst, D, Gubelin, G., Heaton, N., Minh, C.C., Norville, M.A., Seim, M.R., and Pritchard, T. 2000. Trends in NMR Logging, Oilfield Review. 12: 3, 2-19.

American Society for Testing and Materials-ASTM, 2004. D6724: Standard guide for installation of direct push ground water monitoring wells. ASTM International, 9 pp.

Coates, G.R., Xiao, L., and Prammer, M.G. 1999. NMR Logging Principles and Applications. Halliburton Energy Services, Houston, Publication H02308.

Crow, H.L., Alpay, S., Hinton, M.J., Knight, R.D., Oldenborger, G.A., Percival, J.B., Pugin, A J –M., and Pelchat, P. 2017. Geophysical, geotechnical, geochemical, and mineralogical data sets collected in Champlain Sea sediments in the Municipality of Pontiac, Québec. Geological Survey of Canada, Open File 7881, 51 p. https://doi.org/10.4095/301664

Crow, H.L., Good, R.L., Hunter, J.A., Burns, R.A., Reman, A., and Russell, H.A.J. 2015. Borehole geophysical logs in unconsolidated sediments across Canada. Geological Survey of Canada, Open File 7591, 39 p. https://doi.org/10.4095/295753

Cummings, D.I., Gorrell, G., Guilbault, J.-P., Hunter, J.A., Logan, C., Ponomarenko, D., Pugin, A.J.-M., Pullan, S.E., Russell, H.A.J., and Sharpe, D.R. 2011. Sequence stratigraphy of a glaciated basin fill, with a focus on esker sedimentation. Geological Society America Bulletin, 123: 1478–1496. https://doi.org/10.1130/B30273.1

Delage,P., Tesier, D., and Marcel-Audiguier, M. 1982. Use of Cryoscan apparatus for observation of freeze-fractured planes of a sensitive Quebec clay in scanning electron microscopy. Canadian Geotechnical Journal, 19: 111-114. https://doi.org/10.1139/t82-011

Gadd, N.R. 1986. Lithofacies of Leda Clay in the Ottawa Basin of the Champlain Sea. Geological Survey of Canada, Paper 85-21, 44p. https://doi.org/10.4095/120619

Hinton, M.J., Alpay, S., and Logan, C. 2011. Stop 1.2B. Hydrogeology. In: Deglacial history of the Champlain Sea basin and implications for urbanization. In Russell, H.A.J., Brooks, G.R. and Cummings, D.I. Eds. Joint annual meeting GAC-MAC-SEG-SGA, Ottawa, Ontario, May 25-27, 2011, Field Guide Book, 30-35. Geological Survey of Canada, Open File 6947. https://doi.org/10.4095/289555

Oldenborger, G.A., Logan, C.E., Hinton, M.J., Sapia, V., Pugin, A.J.-M., Sharpe, D.R., Calderhead A.I., and Russell, H.A.J. 2014. 3D hydrogeological model building using airborne electromagnetic data. European Meeting of Environmental and Engineering Geophysics, Tu-PA1-07.

Oldenborger, G.A., Logan, C.E., Hinton, M.J., Pugin, A.J.-M., Sapia, V., Sharpe, D.R., and Russell, H.A.J. 2016. Bedrock mapping of buried valley networks using seismic reflection and airborne electromagnetic data. Journal of Applied Geophysics, 128: 191-201. https://doi.org/10.1016/j.jappgeo.2016.03.006

Paradis. D., Lefebvre, R., Morin, R.H., Gloaguen, E. 2011. Permeability profiles in granular aquifers from flowmeter in direct push wells. Ground Water, 49: 4, 534-47. https://doi.org/10.1111/j.1745-6584.2010.00761.x

Paradis, D., Tremblay, L., Lefebvre, R., Gloaguen, E., Rivera, A., Parent, M., Ballard, J.-M., Michaud, Y., and Brunet, P. 2014. Field characterization and data integration to define the hydraulic heterogeneity of a shallow granular aquifer at a sub-watershed scale. Environmental Earth Sciences, 72: 5, 1325-1348. https://doi.org/10.1007/s12665-014-3318-2

Paradis, D., Lefebvre, R., Gloaguen E., and Rivera, A. 2015.Predicting hydrofacies and hydraulic conductivity from direct-push data using a data-driven relevance vector machine approach: motivations, algorithms and application. Water Resources Research, 51: 481-505. https://doi.org/10.1002/2014WR015452

Paradis, D., Pugin, A.J.-M., Crow, H.L., Oldenborger, G., Russell, H.A.J., and Melaney, M. 2020. Hydrogeophysics data acquisition for the characterization of hydraulic properties of the Vars-Winchester esker, southeastern Ontario. In Russell, H.A.J. and Kjarsgaard, B.A. Eds. Southern Ontario groundwater project 2014–2019: summary report. Geological Survey of Canada, Open File 8536, 131-138. https://doi.org/10.4095/321098

Percival J.B., Aylsworth A.M., and Fritz A. 2001. Analysis of colour rhythmites in sensitive marine clays (Leda Clay) from eastern Canada. In Dominguez, E.A. Mas, G.R., and Cravero, F. Eds. 2001 A Clay Odyssey; Proceedings of the 12th International Clay Conference, Bahia Blanca, Argentina, Elsevier, 147-154.

Pugin, A.J.-M., Pullan, S.E., Hunter, J.A., and Oldenborger, G.A. 2009. Hydrogeological prospecting using P- and S-wave landstreamer seismic reflection methods. Near Surface Geophysics, 7, 315–327. https://doi.org/10.3997/1873-0604.2009033

Pugin, A.J.-M., Crow, H.L., Brewer, K., Cartwright, T., Dietiker, B., Griffiths M. and Paradis, D. 2020. High-resolution seismic reflection profiles for groundwater studies of the Vars-Winchester esker, southeastern Ontario. In Russell, H.A.J. and Kjarsgaard, B.A. Eds. Southern Ontario groundwater project 2014–2019: summary report. Geological Survey of Canada, Open File 8536, 139-146. https://doi.org/10.4095/321099

Improved analysis of Horizontal-to-Vertical Spectral Ratio measurements for groundwater investigations

Barbara Dietiker, Jim A. Hunter, and André J.-M. Pugin

Abstract: Ambient seismic noise, and specifically the Horizontal-to-Vertical Spectral Ratio (HVSR), is routinely used for seismic microzonation, assessment of earthquake site characteristics and bedrock depth information for hydrogeological studies. These measurements not only provide peak frequency or period of a seismic resonator, but the shape of the spectral ratio can also give insight into the architecture of subsurface structure. For example a dipping resonator decreases the peak amplitude and increases the peak frequency of the spectrum. Effects of two-dimensional (2-D) subsurface structure (non-horizontal layering) have been successfully modelled and can be observed on the orthogonal Horizontal-to-Vertical Spectral Ratios, where N-S/V and E-W/V have different peak frequencies and peak amplitudes. By analysis of both horizontal spectral ratios the practitioner is able to determine whether one-dimensional (1-D) subsurface layering is present and hence 1-D assumptions are appropriate, e.g. inverting shear-wave velocities (Vs), calculating average Vs and depth to the resonator. HVSR measurements collected along seismic reflection profiles with known resonator topography, e.g. over steeply dipping bedrock resonators, are used to investigate both orthogonal horizontal components separately. Differences between the orthogonal H/V components are able to identify 2-D subsurface structure. Results demonstrate that extending analysis beyond the peak frequency to include orthogonal Horizontal-to-Vertical Spectral Ratios adds important information related to dipping surfaces and their orientations. Due to the ease and rapidity of HVSR data collection, the technique is ideally suited for reconnaissance scale survey work but also for infill where other data is sparse.

1. Introduction

Southern Ontario is covered by extensive thick surficial sediment with depth to bedrock of up to 200 m. Groundwater sources and flow paths are controlled by the texture and geometry of the glacial sediments with a key boundary at the bedrock interface. Often the depth to bedrock is poorly known. Borehole surveys are the most widely used method for groundwater investigations of the surficial sediment in southern Ontario (e.g., Mulligan 2017). They provide highly detailed, but very localized information that is expensive to obtain. Shear-wave reflection 2-D profiles (e.g., Pugin et al. 2018) provide high-resolution detail on local to regional scales assessing lateral heterogeneity accurately, but at a relatively high cost. The Horizontal-to-Vertical Spectral Ratio (HVSR) method is routinely used for seismic site characterizations (Lermo and Chavez-Garcia 1994; Konno and Ohmachi 1998; SESAME 2004) and for groundwater studies to obtain bedrock depth estimates (e.g. Chandler and Lively 2014, Chandler and Lively 2016, Ibs-von Seht and Wohlenberg 1999; Sorensen and Asten 2007; Lane et al. 2008). HVSR measurements have been used to invert for shear-wave velocity (Vs) through H/V amplitudes and depth to resonator or bedrock through the fundamental frequency under the assumption of flat layering in the subsurface, where only Vs is changing in depth (one-dimensional subsurface, 1-D geometry; e.g., Herak 2008). This assumption is not always valid (Cornou et. al. 2007; Liu et. al. 2007); the assumption of a 1-D geometry can be incorrect and negatively impact the estimation of resonator depth. With additional processing HVSR measurements have the potential to provide information on lateral variation of the subsurface (two-dimensional, 2-D, where Vs changes in depth and in one lateral direction) and on three-dimensional variation (3-D; Vs changes in depth, and two orthogonal direction; e.g., Grippa et al. 2011) of the surficial sediment as well as bedrock. There is an abundance of information in southern Ontario (Figure 1) to ground truth HVSR data and to verify the HVSR signal against other datasets that can substantiate the interpretation of subsurface geometry. This complementary data provides a context for an assessment of HVSR signal character of 1-D,

Geology Survey of Canada, Natural Resources Canada, 601 Booth Street, Ottawa, ON K1A 0E8

*corresponding author: barbara.dietiker@canada.ca

Recommended citation: Dietiker, B., Hunter, J.A., and Pugin, A.J.-M. 2020. Improved analysis of Horizontal-to-Vertical Spectral Ratio measurements for groundwater investigations. In Russell, H.A.J. and Kjarsgaard, B.A. Eds. Southern Ontario groundwater project 2014–2019: summary report. Geological Survey of Canada, Open File 8536, 159-170. https://doi.org/10.4095/321101

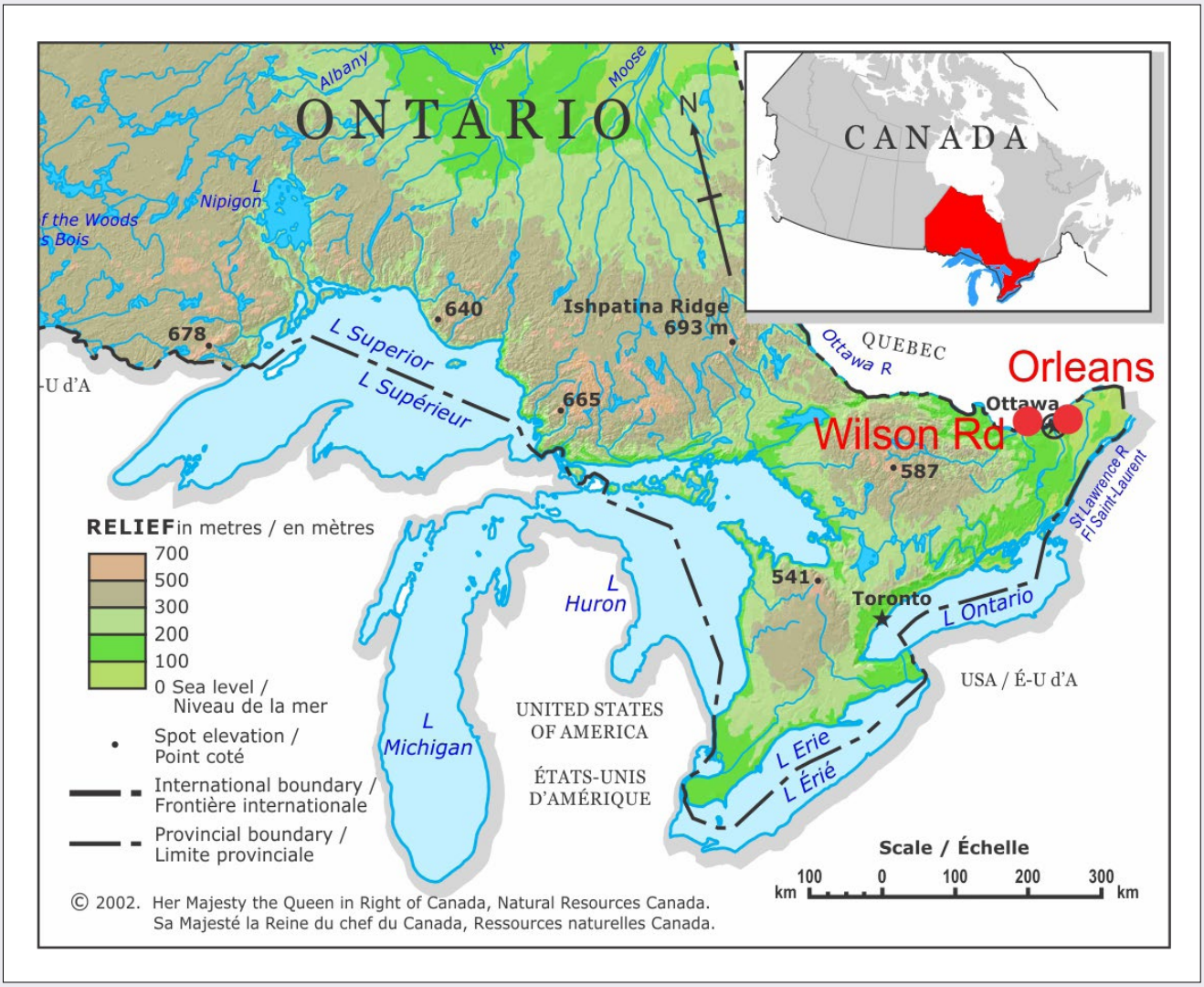


Figure 1. Relief map of Southern Ontario showing the study areas of Orleans and Wilson Road.

2-D and 3-D geometries in the area of HVSR stations.

Detailed information about the subsurface structure (depth to bedrock and/or shear wave velocities) is needed to calibrate the HVSR results (Ibs-von Seht and Wohlenberg 1999); a-priori information is crucial (Chandler and Lively 2016). A wide variety of depths should optimally be sampled and flat layers should locally be present at these calibration sites (Ibs-von Seht and Wohlenberg 1999). Calibration and subsequent depth estimation of bedrock is only accurate in flat-layered areas (Dobry et al. 1976) with no overlying resonators (e.g. gravel or diamicton). Where a survey objective is identification of the bedrock surface supporting evidence is needed that the resonance stems from bedrock. Sedimentary units such as diamicton or gravel overlying bedrock can have similar impedance contrast as the bedrock and thus create similar resonance. Depth to bedrock is underestimated when diamicton or gravel is present, when Vs is locally higher than average, and when local 2-D structures are present (Roten et al. 2006). These effects are cumulative and in complex cases cannot be resolved.

The study objective is to demonstrate how additional processing using the difference between orthogonal H/V spectral signals can be used to provide information to reduce uncertainty in the analysis. Using co-located seismic reflection data and HVSR it is demonstrated that in a simple case the effect of a 2-D structure can be detected in the HVSR signal. It is also demonstrated that using the shape of H/V amplitudes and analysis of the orthogonal H/V amplitudes improves the determination of depth to bedrock.

Data from two study sites (Figure 1) are used to demonstrate changes in HVSR signal with increasing levels of complexity of subsurface geometry (from flat layering, one-dimensional (1-D) to complex (3-D) as well as stratigraphic composition

(from glaciomarine sediments over bedrock, to a complex glacial sequence over bedrock).

2. Instrumentation and data collection

Three-component seismographs (Tromino®) were used to record 30 min of ambient seismic noise at each station. The Tromino® measures ground velocity and acceleration in 3 directions (one vertical and two perpendicular horizontal components) from 0.1 to 500 Hz (Castellaro et. al. 2005). The recorded data is split into windows of 30 seconds duration for which frequency spectra are calculated (Figure 2). Averaged horizontal-to-vertical ratios are calculated, and spectral ratios for both orthogonal horizontal components (north-south and east-west) are calculated and averaged over all windows.

Seismic reflection data were acquired in 2007 and 2014 with a landstreamer developed by the Geological Survey of Canada (GSC) consisting of 24 and 48 (3 kg) sleds. Each sled has 3 geophones (8 or 30 Hz, depending on survey), oriented in three orthogonal directions: vertical, parallel and perpendicular to the survey direction. An IVI (Industrial Vehicles International, Inc) "Minivib 1" source was used to create a perpendicularly oriented vibrating sweep, which depending upon survey parameters ranges from 20 up to 320 Hz. More information on acquisition and processing is detailed in Pugin et al. (2007).

2.1 Study area

The two HVSR study areas are the Orleans and Wilson Road sites, in the Ottawa River valley in eastern Ontario (Figure 1). The subsurface structure is known and the surficial sediments are well characterized through interpreted shear-wave reflection surveys and boreholes (Pugin et al. 2007). In

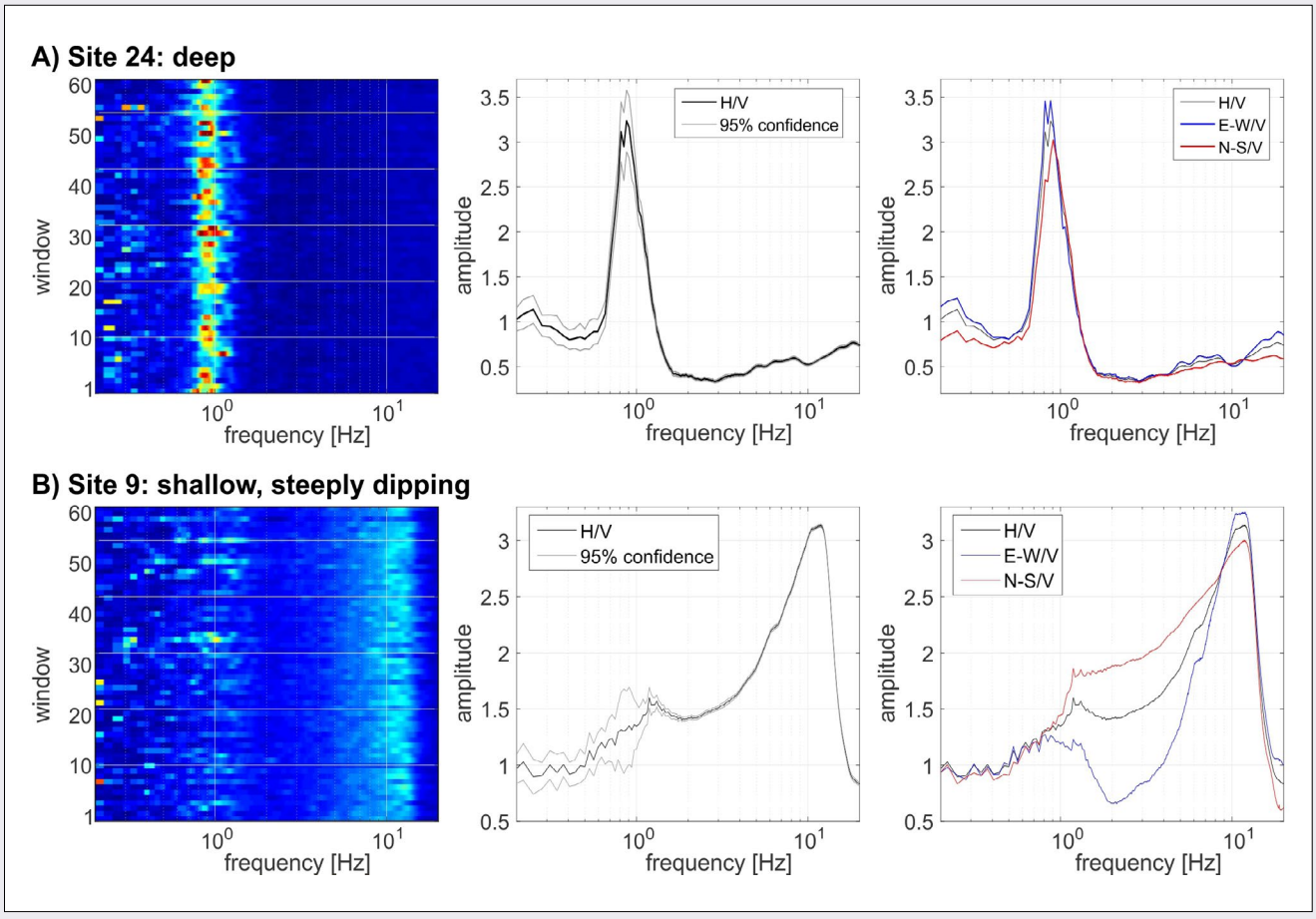


Figure 2. Illustrative Horizontal-to-Vertical Spectral Ratio data from 2 Orleans sites. A) Site 24 has a fundamental frequency of 0.91 Hz visible as orange band across the 60 windows showing H/V amplitudes (left). Center: HVSR amplitudes as a function of frequency after averaging 60 windows. Left: Averaged H/V spectral ratio amplitudes (black) compared with the orthogonal spectral ratios (blue = E-W/V and red = N-S/V). B) Site 9 has a fundamental frequency of 11.9 Hz and a broad H/V amplitude peak (center). The orthogonal H/V spectral amplitudes are very different (right). The amplitude of the N-S/V component (red) is up to 2.5 times higher than E-W/V (blue).

the Ottawa River valley, shear-wave velocities are very low at the surface (marine sediments) and steadily increase with depth (positive Vs gradient), providing an ideal environment for ambient noise microtremor spectral measurements.

The study areas have unique datasets with the combination of the passive source mictrotremor surveys and the active source seismic reflection profiles. Subsurface variation in depth and distance can be assessed using velocities obtained during processing of the seismic reflection profiles, and can support and validate observations and analyses of microtremor data.

The two profiles were chosen to exemplify scenarios of increasing Quaternary sediment complexity (Table 1). The first section from Orleans is a simple two-layer case with one sediment layer covering bedrock; the deep and the shallow bedrock are mostly subhorizontal, fitting a 1-D scenario where only Vs changes with depth (Figure 3A). The transition between deep and shallow bedrock fits the 2-D scenario where Vs and bedrock depth change laterally (Figure 3B). The Wilson Road study area is a 2-D case with the added complexity of at least two distinct sedimentary layers.

2.1.1 Study area 1: Orleans

The Orleans study area is located in an eastern suburb of Ottawa, Ontario (Figure 1). Along the 500 m of the Orleans profile, 26 HVSR stations were recorded at irregularly spaced (~10–30 m) intervals (red lines represent HVSR data in Figure 4A). Shear-wave seismic data confirm the depth to Paleozoic bedrock surface varies from 2 m to 70 m and is mostly subhorizontal with a <100 m long steeply dipping section (Figure 4A, Pugin et al. 2007). Seven stations (O8 to O14) are located across the steeply dipping buried cliff where bedrock descends from 3.5 m to 57 m depth with local slopes of 14 to 48°. Surficial sediments consist of Champlain Sea silts and clays, which in this setting form a simple two-layer case with a strong impedance contrast between sediments and bedrock that creates a distinct resonance peak (Mallozzi 2019).

2.1.2 Study area 2: Wilson Road

The Wilson Road study area is situated ~40 km NW of Ottawa (Figure 1) at the northern edge of the Quaternary Champlain Sea where the Paleozoic bedrock overlies Precambrian Grenville Province bedrock of the Canadian Shield. The Eardley Escarpment rises steeply just 150 m north of the profile and is the northern normal-fault boundary of the Ottawa Graben. The seismic reflection profile is 2 km long, orientated S-N, perpendicular to the escarpment, and 19 HVSR stations were recorded at 100 m intervals along its length. The shear-wave seismic data confirmed the depth to the bedrock (Figure 5A), and that it is comprised of steeply dipping Precambrian rocks (maximum slope of 31° at station W3, Figure 5A) overlain by gently dipping (maximal 8.5°) to horizontal Paleozoic rocks south of station W5. Bedrock reflections (red horizon in Figure 5A) can be poorly defined due to a high-velocity layer overlying bedrock (green horizon), which decreases the impedance contrast between sediments and bedrock (Figure 5A).

At the Wilson Road site the overlying surficial stratigraphy consists of two distinct sediment types, 1) fine silts/muds with

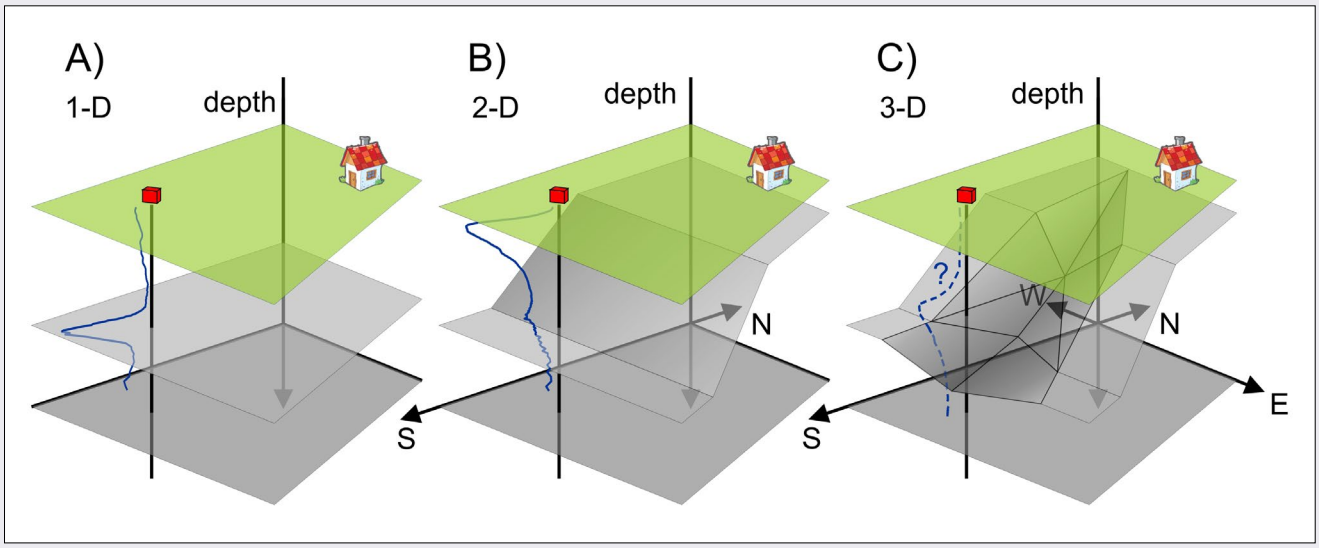


Figure 3. Sketches explaining dimensionality of the suburface. A) One-dimensional (1-D) case with change in depth or the vertical direction shown by the top of the resonating layer (light gray) with HVSR results (blue trace) displayed from a similar environment. B) Two-dimensional (2-D) subsurface structure with changes in depth and an incline in N-S direction. HVSR results (blue trace) from a similar feature are shown. C) Three-dimensional (3-D) structure with changes in depth, N-S and E-W directions exemplified as an erosional feature with a hypothetical HVSR trace.

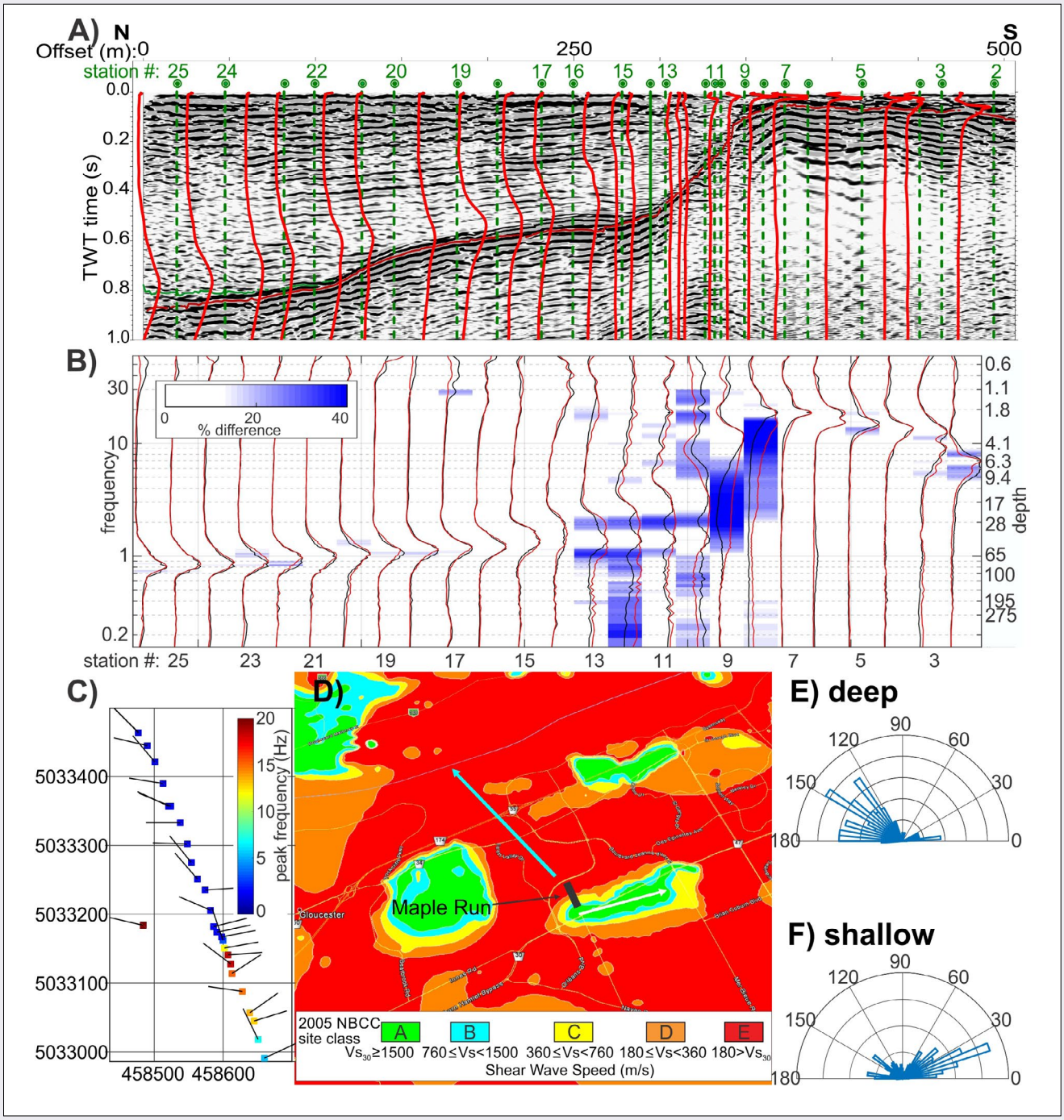


Figure 4. Orleans study area. A) Seismic shear-wave reflection profile with bedrock (red) and diamicton (green) reflections indicated and HVSR converted to time. B) Difference of both orthogonal H/V (blue patches) with N-S/V (red) and E-W/V (black). C) Site locations with peak frequency in colour and associated preferred orientation. D) Vs_{30} map (Hunter et al. 2010) as a proxi for bedrock topography with main vectors (white , light-blue arrows). Seismic profile (Maple Run) is indicated as a black line. Preferred orientations in rose diagrams for deep (E) and shallow (F) resonators.

a slow shear-wave velocity (blue) and continuous, narrowly spaced, parallel reflections, and 2) higher shear-wave velocity silt/sand (green with continuous, parallel reflections) and sand and gravel (yellow-orange), with discontinuous and chaotic reflections, (orange horizons). The very top 1.5 to 2.5 m of the muds form a crusty layer with increased Vs of ~200 m/s

Table 1. Comparison of study areas.

Study area	Length	Number stations	Spacing (m)	Depth bedrock (m)	Stratigraphy units	Bedrock dimensions	Maximum slope
Orleans	0.5 km	26	10–30	2–70	1 layer over bedrock	1-D and 2-D	48°
Wilson Road	2.0 km	19	100	36–106	2 layers over bedrock	1-D and 2-D	31°

leading to a velocity inversion (negative Vs gradient). Within the surficial sediments, dipping reflections with a slope of 6° are visible at the northern end of the seismic profile. This case provides an example of a complex case with a 2-D subsurface structure, and a layer of high shear-wave velocities from surficial sediment overlying the bedrock.

3. Horizontal-to-Vertical Spectral Ratio method

3.1 Basic Horizontal-to-Vertical Spectral Ratio (HVSR)

The Horizontal-to-Vertical Spectral Ratio (HVSR) method uses ambient seismic noise generated by natural (e.g. wind, ocean waves) and anthropogenic sources (e.g., traffic). It measures the orthogonal horizontal components and the vertical component. Results are expressed as averaged horizontal/vertical amplitude ratios for frequencies generally between 0.2 and 20 Hz that reflect the instrument sensitivity and the local geology. Frequency and depth have an inverse relationship with the low-frequency HVSR signal created at depth and high-frequency signal from the shallow subsurface. A high H/V ratio at low frequency is linked to a deep impedance contrast acting as main resonator. A high H/V ratio at high frequency is created by an impedance contrast close to the ground surface. For example, in muddy Champlain Sea sediments with Vs of ~ 120 m/s, a measured 15 Hz peak is linked to an impedance contrast at a depth of 2 m.

To calculate the average horizontal-to-vertical ratio the signal is sampled for 60 discrete windows of 30 seconds length (Figure 2, left). Windows with high-amplitude transient noise are discarded before the average over all windows is calculated and displayed with a 95% confidence interval (Figure 2 center). Spectral ratios for the orthogonal H/V components (north-south and east-west) are calculated and averaged over all windows (Figure 2 right).

Using station O24 as an example, the fundamental frequency is 0.91 Hz, with a narrow peak, and an amplitude of 3.2 (Figure 2A). This is the frequency of the seismic resonance of this particular site. When an earthquake excites this site, it will resonate at this fundamental frequency (resonance frequency or peak frequency). The orthogonal horizontal component ratios (N-S/V and E-W/V) will be similar in both directions for an ideal 1-D site. For station O24 there is only a slight difference (Figure 2A right); the amplitude of N-S/V is generally lower and the peak frequency is a little higher at 0.91 Hz compared to 0.87 Hz for E-W/V.

A site with a two-dimensional subsurface will have large differences between the two orthogonal H/V components. For example, station O9 has a slope of 14°. The fundamental frequency is 11.9 Hz (Figure 2B) and the amplitude is 3.1. The peak is much broader than for station O24 and asymmetrical in shape with a steep slope at high frequencies and a gentler slope towards low frequencies. The amplitudes of the orthogonal H/V components have major differences, especially in the frequency range between 1 and 12.5 Hz.

3.2 Fundamental frequency and depth to horizontal resonator

The relation between fundamental frequency and resonator depth (= H) is given as:

$$H=Vs_{av}/(4F_0) \qquad \text{eq. 1}$$

In eq. 1 Vs_{av} is the average shear-wave velocity and F_0 is the fundamental frequency (or frequency at the maximum H/V amplitude). As Dobry et al. (1976) have shown, this is the analytical solution to the equation of motion of shear waves in uniform (constant density and velocity), horizontal layers. They also suggested that velocity gradients within the sediment layer possibly alter the computed resonator depth significantly. Hunter et al. (2010) observed and documented this case within post-glacial sediments in the Ottawa area.

Ibs-von Seht and Wohlenberg (1999) have demonstrated that with sufficient confirmed resonator depths (e.g. drilling or seismic reflection) and observations of F_0, the empirical factors a and b can be obtained from nonlinear regression fits in the form of

$$H=a\,F_0^{\,b} \qquad \text{eq. 2}$$

For the Ottawa area these factors were calculated by Hunter et al. (2010) and used for both case studies (depth scale in Figures 4 and 5). Equation 2 does not incorporate local inhomogeneity and provides only an averaging of vertical properties. Therefore calculated depths provide only estimates of the real resonator depths.

3.2.1 Observations and analysis

Good depth estimates are obtained from the Orleans study area (Figure 4A) at stations O26 to O16. Deep bedrock is

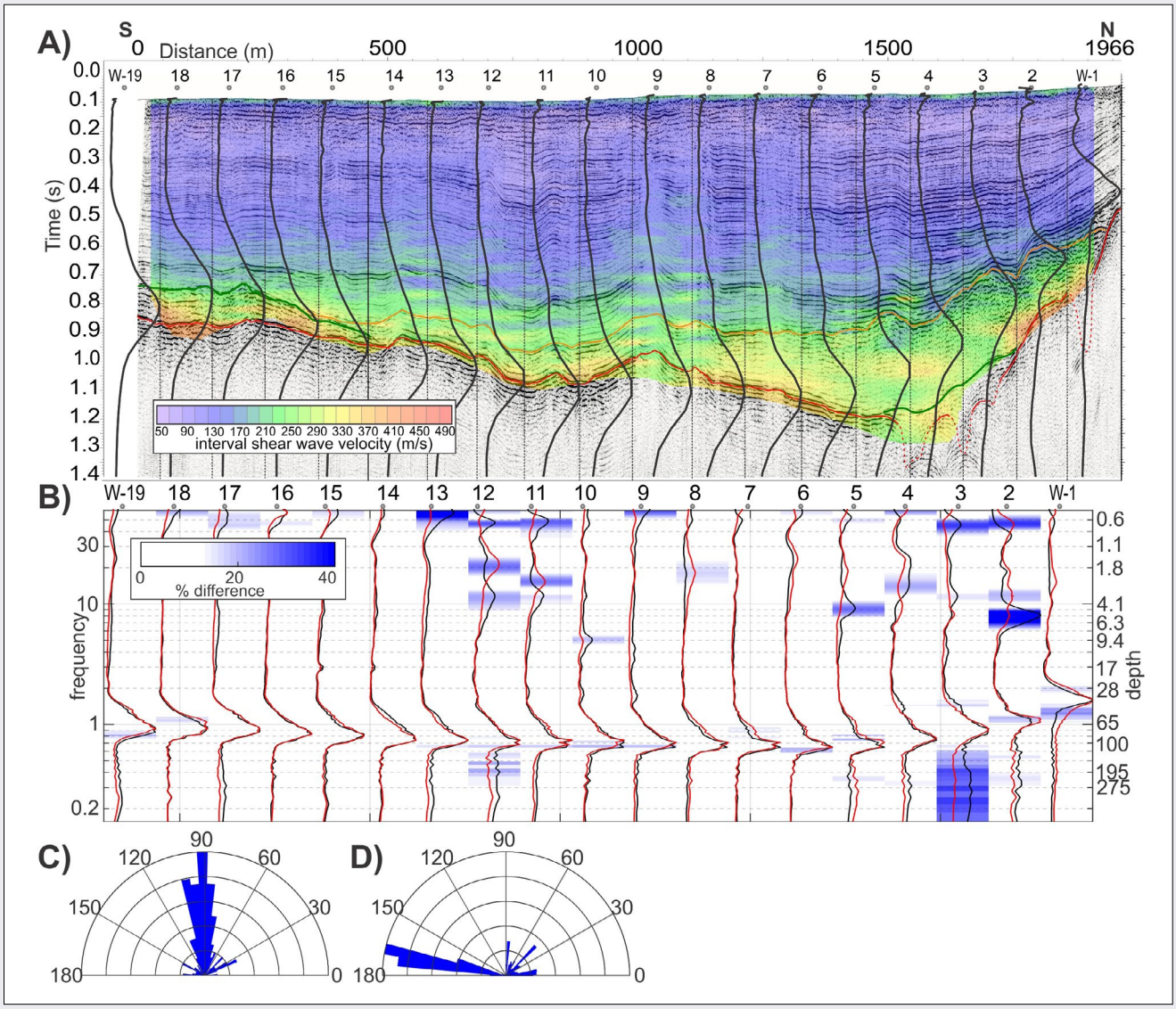


Figure 5. Wilson Road study area. A) Seismic shear-wave reflection profile along Wilson Rd overlain with HVSR converted to time (black) and shear-wave velocities. B) Differences (blue patches) between N-S/V (red) and E-W/V (black). C) Orientations of deep resonance (F <2.3 Hz) and E) shallow resonance (F >2.3 Hz) where H/V >2.

the resonating layer and HVSR peak amplitudes match the bedrock reflection very well. Peak frequencies range from 0.84 to 1.41 Hz. Station O24 (Figure 2) is part of these deep stations at a relatively deep (~70 m) depth. Likewise, peak HVSR amplitudes between 5.3 and 18.8 Hz match bedrock reflections very well at stations with shallow bedrock (O7 to O2). However, stations O8 to O14 are located over steeply dipping bedrock which will be discussed in the following section.

The Orleans study area has the simplest geological setting with a basic two-unit geology (mud over bedrock) and mostly horizontal bedrock with a steep dipping surface restricted to a <100 m section. The principal resonator is the bedrock surface and estimates of the depth of this surface correlated well with the associated seismic reflection profile where the surface is subhorizontal.

At Wilson Road the HVSR amplitudes (black traces in Figure 5A) resolve bedrock as the resonating surface at stations W7 to W15 with peak frequencies in range of 0.69 to 0.81 Hz. These peaks approximately match the bedrock seismic reflection in depths of 83 to 100 m. At stations W16 to W19 the HVSR peak amplitudes between 0.88 and 0.97 Hz are shallower than the bedrock reflection because the resonance is created by a gravel/diamicton layer (~ 0.75 s TWT – green horizon; Figure 5) above bedrock. At stations W1 to W6, there are two factors to consider. Firstly, there is a gravel/diamicton

layer above the deepest bedrock (W3 to W5, green horizon; Figure 5) creating the resonance layer. The second factor is the dipping bedrock, which is discussed below.

The Wilson Road study area has a three-layer case with two sediment units and a mostly positive Vs gradient, where the principal resonator is not always bedrock. Depth to bedrock is underestimated where a layer of gravel/diamicton is present.

3.3 HVSR from dipping resonators (2-D effect)

Dipping resonators form 2-D scenarios in the subsurface that are common components of buried bedrock slopes, the flanks of eskers, drumlins, etc. In the case of bedrocks slopes which are part of a buried valleys, seismic waves may create a 2-D resonance pattern (Roten et al. 2006). Matsushima et al. (2014) have shown that over a bedrock valley (2-D case) peak H/V amplitude decreases, fundamental frequency increases, and orthogonal H/V ratios are different as compared to a 1-D scenario with the same seismic parameters. Dietiker et al. (2018) also observed that over a bedrock cliff the peak shape was modified, that the peak decreased and broadened.

At all sites of 2-D cases the fundamental frequencies and H/V amplitudes differ from expected frequency and amplitude according to a 1-D resonator depth. This means that depth inversions using 1-D assumptions will underestimate the resonator depth.

Matsushima et al. (2014) also observed that spectral ratios from both orthogonal horizontal components (N–S/V and E–W/V) have different peak amplitudes, peak frequencies, and peak widths. This suggests that the scaled difference (= Dif) of both ratios (eq. 3) might be a good indicator of a 2-D subsurface structure.

$$\text{Dif} = \text{abs}\left(\frac{\text{EW}}{\max(\text{EW})} - \frac{\text{NS}}{\max(\text{NS})}\right) \qquad \text{eq. 3}$$

In eq. 3 abs is the absolute value, EW (east–west) is the E–W/V spectral ratio, NS (north–south) is the N–S/V spectral ratio, and max is the maximum amplitude of each component's spectral ratio.

The comparison of 1-D and 2-D sites reveals very different shapes of H/V spectral ratios: a narrow, symmetrical peak with little difference between the orthogonal H/V components stemming from a horizontally layered subsurface structure in the 1-D case (station O24 in Figure 2 and Figure 3A) and a broad, asymmetrical peak with a large difference between the orthogonal H/V components (station O9, Figure 2) stemming from a steeply dipping 2-D subsurface structure (Figure 3B).

3.3.1 Observations and analysis

Spectral ratios of the 26 Orleans stations are used to illustrate differences between 1-D and 2-D responses (Figure 4B; black: E–W/V and red: N–S/V). Seven station signals (O14 to O8) have irregularly shaped amplitudes (broad peaks) and large differences between the orthogonal H/V spectral ratios. These differences are indicators of the 2-D layering in the subsurface: six out of seven cliff stations (O8 to O13) have a large (>30%, dark blue) difference calculated with equation 3, where the bedrock is steeply inclined (slopes of 14 to 48°). Differences <15% are omitted, whereas those ~20% (light blue) are considered to have low (gentle) slopes.

At the stations O8 to O14, located over steeply dipping bedrock, the peak amplitudes occur at much shallower depth than bedrock depth determined by seismic reflection data. This underestimation is in accordance with the observations from Matsushima et al. (2014).

In a simple two-layer case such as Orleans horizontal component analysis with differences of >30% between orthogonal H/V ratios indicate a steeply dipping resonator structure. In this simple case it can confidently be estimated that a slope of more than 14° creates a 2-D effect which leads to observable orthogonal differences. If these fundamental frequencies were used to calculate the resonator depth, it would be underestimated because the depth is calculated for a 1-D scenario and steeply dipping bedrock requires a 2-D solution. This means, these sites should be discarded for the estimation of the empirical fundamental frequency to depth relation (equation 2).

At the Wilson Road study area bedrock is dipping at an average 13° in the northern part of the profile (W5 to W1) with local slopes of 17 to 31°. The maximum slope is reached at W3. Slopes in the southern part of the profile range up to 8.5°. All slopes look steeper on the seismic reflection profile because of the vertical exaggeration. Based on bedrock slopes the largest differences between orthogonal H/V components are expected in the northern part. At site W3 (Figure 5B) a large difference exists below the peak frequency where the dipping structure reaches its maximum slope of 31°. Other northern sites (e.g. W1, W2, W5) have small differences (15–20%) at the peak frequency. Many of the southern sites (W6, W9–W12, W18, W19) have small differences that correlate well with local slopes of 3.5° at the resonating interface. Large differences (>30%) are mainly present in the high frequencies (>8 Hz, less than 5 m deep (eq. 1) or ~0.06s). They might be associated with the velocity inversion at very shallow depth (green to blue colours in Figure 5A).

The resonating layer may be created by a gravel/diamicton unit which leads to the underestimation of bedrock depth. Furthermore, the extent of the dipping surface means the northern stations are recording data with a 2-D signature and differences between orthogonal horizontal-to-vertical spectral ratios are visible. This 2-D effect leads to increased fundamental frequencies which results in an underestimation of the resonator depth. Along the undulating surface of the main resonating layer (bedrock and gravel/diamicton) in the southern part orthogonal H/V differences are notable but not as strong as expected; likely because the slope in the range of 3.5° to 8.5° is low. In these cases there is no 2-D effect, and calculated depths match seismic depths. In common with

the simple Orleans case, in this more complex case slopes smaller than 18.5° do not create a 2-D effect. It is necessary to have slopes ≥ 11° to observe orthogonal differences and an increased F_0 which leads to an underestimation of resonator depth.

3.4 Orientation of the resonating layer and geometry of the subsurface structure

The measurement of N-S and E-W components of ground velocities and accelerations by the Tromino seismometer allows for the calculation of orientations. The theory behind this calculation is based on projecting one coordinate system (measured N-S and E-W motions labelled X and Y) onto a second rotated system (X′ and Y′) such that the vector of interest (in this case H/V) is maximized. The rotation angle α between X and X′ is varied between 0 and 180°, and for each α H_α/V is calculated. The maximum polarization / preferred orientation is calculated for the whole range of frequencies of interest (usually 0.2–20 Hz). This is quite computationally intense, depending on the frequency and angular steps, or the desired resolution.

The maximum polarization / preferred orientation of the fundamental frequency might provide insight regarding the orientation of the subsurface structure. Due the small number of samples (one peak frequency per site), there might be considerable variation. To improve the sample count and decrease variation, preferred orientations are calculated for amplitudes larger than 2 (criterion for a relevant peak, SESAME 2004), and H/V amplitudes can be used to provide a quality factor for the preferred orientations.

In general, the preferred orientation is defined as a counter-clockwise rotation from east, e.g. north-south is expressed as 90°; east-west is 0° and 180°.

3.4.1 Observations and analysis

In Orleans the preferred orientation at the fundamental frequency (vectors in Figure 4C) reveals that for shallow resonating sites (southern stations with peak frequencies of 6 Hz and higher) the preferred orientation is to ENE, whereas stations located above deep bedrock (blue squares) have preferred orientations to the NW. There is considerable variation. Rose diagrams (Figure 4E and F) are presented for preferred orientations with H/V >2 for deep (F_0 <2Hz) and shallow stations (F_0 >2Hz). This distinction between stations with low-peak frequencies (Figure 4E: stations O15–O26, deep bedrock) and stations with high frequencies (Figure 4F: stations O1–O7, shallow bedrock) summarizes and enforces the observation of two distinct directions. The preferred orientation of the shallow HVSR stations is perpendicular to the bedrock dip and parallel to the long axis of the bedrock buried upland structure (white arrow in Figure 4D; after Hunter et al. 2010; high Vs_{30}, shear-wave velocities to 30 m depth, green >1500 m/s implies shallow bedrock). The preferred orientation of the deep HVSR stations (O15–O26) indicates the direction of the maximum elongation of this deep structure (light-blue arrow in Figure 4D). Whether this observation can be applied in other locations needs to be tested. A further test with more stations across this structure to observe 3-D effects would be very beneficial.

Peak frequency orientations for nine of 19 stations along Wilson Road (site W3, W9–W11, W13–W15, W17, W19) cluster around north; this is perpendicular to the Eardley Escarpment. At other stations, preferred orientations align NW and NE, but there is no correlation with peak frequency. For H/V with amplitudes >2, preferred orientations align generally with 2 orientations. Low frequencies <2.3 Hz, which are correlated with the bedrock resonance frequency, orientate north (90–110°, Figure 5C). The high frequency (F0 >2.3 Hz) orientations from the surficial sediments cluster roughly at E-W (170–180°, Figure 5D), parallel to the Eardley Escarpment.

4. Recommendations for groundwater applications

In Canada most groundwater is extracted from surficial sediments and the bedrock surface may form a distinct hydraulic divide. Bedrock is also an important surface as it delineates two distinct geological terrains, especially in glaciated terrain. HVSR studies have gained considerable attention and interest for regional groundwater studies due to the speed and cost effectiveness of the method (e.g., Lane et al. 2008). The method can be applied for reconnaissance studies or for infill surveys to improve resolution. Existing depth to bedrock data is needed for calibration. Analysis of HVSR data commonly relies on an implicit 1-D geological model for the subsurface with a positive Vs gradient, a good impedance contrast between surficial deposits and bedrock, and subhorizontal bedrock beneath the stations. This is commonly not the case and divergence from each of these assumptions will introduce errors and uncertainty into the analysis (Chandler and Lively 2016). Several stations at each of the study sites provide information on how these factors impact the signal analysis and interpretation.

Bedrock topography was identified with varying degrees of accuracy for Study Area 1 (Orleans) and partially for Study Area 2 (Wilson Road). It is very important to have some means of verification (borehole or seismic reflection) such that resonance peaks are not falsely attributed to bedrock. Incorrect interpretations can occur when overlying units of diamicton and sand/gravel have large Vs contrasts (Wilson Road), or large Vs contrasts exist within the surficial sediment. Since the resonating layer is created by gravel/diamicton at Study Area 2, fundamental H/V peaks might indicate aquifer top surfaces.

SESAME (2004) recommends that at least 3 closely spaced measurements are collected where spacing is relative to the scale of investigation and the survey objectives. For a

regional profile of 1 km or longer, 100 m spacing is adequate to obtain a sense of the subsurface and its diversity; spacing should be decreased iteratively to 50 m or less when a 2-D subsurface geometry is suspected. For a local profile in the range of hundreds of meters spacing should be less than 25 m when the survey goal is to delineate areas of dipping resonators. For a single site investigation the distance should be less than 10 m. The nesting of measurements can provide the advantage of identifying the presence of either 1-D, 2-D or 3-D geometries.

Based on the observations from the two study areas the following recommendations can be made:

(1) A preliminary impression of subsurface changes can be obtained by investigating the frequency of the peak amplitudes; a change in the subsurface structure is expressed by changing peak frequencies. In this case, depth should be estimated using a simplified average Vs in eq. 1 or if established eq. 2. In any area with a slope of more than 8.5° further investigations are needed. The calculated depth is likely underestimated.

(2) Subsurface changes are also indicated by changing amplitudes. H/V amplitude changes stem from changes in Vs contrasts but also from 2-D effects. Clear signatures of 2-D effects are broadening peaks with decreasing amplitudes. A very strong indication of a 2-D subsurface is expressed through the combination of amplitude and frequency change. Over a steeply dipping resonator the peak flattens and broadens (e.g., the Orleans study area, Matsushima et al. 2014). SESAME (2004) states that a peak with an amplitude below 2 should be discarded. However, several flat and broad peaks indicate a steeply dipping resonator.

(3) It is suspected that 2-D subsurface structure might also be responsible for other non-standard peak shape (e.g., asymmetrical peaks, and double peaks). A steeply dipping resonator surface can be inferred through a non-standard peak shape. Commonly this type of shape is created by differing orthogonal H/V components where one component has a peak at a different frequency than the other (e.g., cliff in Orleans profile, Figure 4B stations O8 to O13). However, non-standard peak shapes could also be caused by a velocity inversion (negative Vs gradient; documented by Castellaro and Mulargia 2009).

(4) An estimate of the dip of a slope might be gained through the difference between E-W and N-S components of spectral ratios. Small dips of ~8.5° were observed to create a difference of spectral ratios of more than 20%. Differences of more than 30% indicate strong subsurface changes and slopes of 14° and more. These differences indicate an environment where 1-D subsurface assumptions are no longer valid and should not be used for depth calculations or velocity and depth inversions.

(5) Strike directions of geological structures can possibly be found in preferred orientations / main polarizations around peak H/V (amplitudes are larger than 2). Orientations from deep resonance are mostly parallel with the longest elongation of the structure. This was also observed by Chandler and Lively (2016). Orientations of shallow resonance are parallel with the shallow structure and perpendicular to its dip. Usually, there is considerably more scatter associated with orientations at peak frequency. It is therefore recommended to investigate orientations for amplitudes larger than 2 or 3 (or higher depending on the case) to remove background noise while maintaining a good sample size.

(6) It is important to remember that the bedrock surface might not be the resonance layer. Resonance occurs when the shear-wave velocity increases considerably. Especially within a Quaternary glacial sediment sequence the resonance can occur at any depth where a strong velocity increase is encountered, e.g. a gravel or diamicton unit. Borehole or seismic reflection control is always crucial; but with sparse additional information miss-interpretation is still a possibility.

5. Summary and conclusions

HVSR data were collected and interpreted along two profiles in the Ottawa River valley in eastern Ontario. Both profiles are co-located with seismic reflection profiles, which provide validation and calibration. The two case study sites illustrate how additional H/V signal processing and improved analysis can help resolve some of the challenges and lead toward higher confidence in the results. Some HVSR signals were deemed not useful because of their abnormal peak shape, but they can actually provide interesting information. In several locations these observed signals were directly linked to steeply dipping resonating layers e.g. a bedrock cliff; a bedrock trough. In accordance with current research and accepted theoretical explanations these sites are underestimating the actual bedrock depth. Calculating differences between orthogonal horizontal-to-vertical spectral ratios seems a promising approach to delineating areas where the resonator has a significant slope. Slopes of resonating layers (2-D or 3-D structures) of more than 11° could be identified by the difference of orthogonal H/V. More than 30% difference between E W/V and N-S/V indicates a slope steeper than 14°.

Preferred orientations / main polarizations of HVSR signals seem to infer a directional trend of the subsurface. Along both profiles, shallow and deep resonating layers can be distinguished and have different orientations. For shallow resonators, preferred orientations where H/V amplitudes are larger than 2 orientate along the long axis of the subsurface structure. Deep resonators also have orientations parallel to the long axis of the subsurface structure in one case and perpendicular in the other case. Likely because there are more complex local structures present. Further investigations using areal HVSR studies might be helpful to clarify the reasons of these observations.

Practitioners of ambient noise/microtremor analysis are encouraged to investigate both orthogonal Horizontal-to-Vertical Spectral Ratios and their differences, to assess the

possibility of two-dimensional subsurface structures. Calculation, simulation and inversion strategies for depth and/or velocity estimation can then be adjusted accordingly.

6. Acknowledgements

The support and dedication of the Near Surface Geophysics Group of K. Brewer, T. Cartwright, and H. Crow is greatly appreciated in collecting and processing seismic reflection, microtremor and geophysical borehole data. A huge thanks to Gilles Bellefleur and Hazen Russell for their work completing an internal GSC review of this report which led to considerable improvements. The work was funded by the Geological Survey of Canada through the Public Safety Geoscience Program and the Groundwater Geoscience Program, and the Ontario Geological Survey (OGS). This work is a contribution of the GSC–OGS Southern Ontario project on groundwater 2014–2019.

7. References

Bignardi, S., Yezzi, A. J., Fiussello, S., and Comelli A. 2018. OpenHVSR-Processing toolkit: Enhanced HVSR processing of distributed microtremor measurements and spatial variation of their informative content. Computers & Geosciences, 120: 10-20. https://doi.org/10.1016/j.cageo.2018.07.006

Bignardi, S., Mantovani, A., and Abu Zeid, N. 2016. OpenHVSR: imaging the subsurface 2D/3D elastic properties through multiple HVSR modeling and inversion. Computers & Geosciences, 93: 103-113. https://doi.org/10.1016/j.cageo.2016.05.009

Castellaro, S., Mulargia, F., and Bianconi, L. 2005. Passive Seismic Stratigraphy: A new efficient, fast and economic technique Stratigrafia sismica passiva: una nuova tecnica accurata, veloce ed economica. J. Geotech. Environ. Geol. 3: 51–77.

Castellaro, S. and Mulargia, F. 2009. The Effect of Velocity Inversions on H/V. Pure applied geophysics, 166: 567–592. https://doi.org/10.1007/s00024-009-0474-5

Chandler, V.W. and Lively, R.S. 2014. Evaluation of the horizontal-to-vertical spectral ratio (HVSR) passive seismic method for estimating the thickness of Quaternary deposits in Minnesota and adjacent parts of Wisconsin. Minnesota Geological Survey Open File Report 14-01, 52 p. http://www.mngs.umn.edu/

Chandler, V.W. and Lively, R.S. 2016. Utility of the horizontal-to-vertical spectral ratio passive seismic method for estimating thickness of Quaternary sediments in Minnesota and adjacent parts of Wisconsin. Interpretation 4 (3): SH71–SH90. https://doi.org/10.1190/INT-2015-0212.1

Cornou, C., Guillier, B., Boussoura, K., Selmi, K., and Renalier, F. 2007. Limite de la technique H/V comme outil d'exploration géophysique pour les structures 2D et 3D. 7ème colloque de l'Association Francaise de Génie Parasismique, Paris (France), juillet 2007.

Dietiker, B., Hunter, J., Pugin, A.J.-M., Crow, H., Mallozzi, S., Brewer, K., and Cartwright, T. 2018. HVSR measurements in complex sedimentary environment and highly structured resonator topography – comparisons with seismic reflection profiles and geophysical borehole logs. In Proceedings, SAGEEP 2018 (Symposium on the Application of Geophysics to Engineering and Environmental Problems), Nashville, TN, March 25-29, 2018, 7p. https://www.eegs.org/sageep-2018-seismic-methods-i

Dobry, R., Oweis, I., and Urzua, A. 1976. Simplified procedures for estimating the fundamental period of a soil profile. Bulletin of the Seismological Society of America, 66: 4, 1293–1321.

Grippa, A., Bianca, M., Tropeano, M., Cilumbriello, A., Gallipoli, M.R., Mucciarelli, M., and Sabato, L. 2011. Use of the HVSR method to detect buried paleomorphologies (filled incised-valleys) below a coastal plain: the case of the Metaponto plain (Basilicata, southern Italy). Bollettino di Geofisica Teorica ed Applicata, 52: 2. https://doi.org/10.4430/bgta0011

Herak, M. 2008. ModelHVSR – A Matlab tool to model horizontal-to-vertical spectral ratio ambient noise. Computers & Geosciences, 34: 1514–1526. https://doi.org/10.1016/j.cageo.2007.07.009

Hunter, J.A., Crow, H.L., Brooks, G.R., Pyne, M., Motazedian, D., Lamontagne, M., Pugin, A.J.-M., Pullan, S.E., Cartwright,T., Douma, M., Burns, R.A., Good, R.L., Kaheshi-Banab, K., Caron, R., Kolaj, M., Folahan, I., Dixon, L., Dion, K., Duxbury, A., Landriault, A., Ter-Emmanuil, V., Jones, A., Plastow, G., and Muir, D. 2010. Seismic Site Classification and Site Period Mapping in the Ottawa Area Using Geophysical Methods, Geological Survey of Canada, Open File 6273, 1 DVD. 2010, Seismic Site Classification and Site Period Mapping in the Ottawa Area using geophysical Methods, Geological Survey of Canada, Open File 6273, 80 p.

Ibs-von Seht, M. and Wohlenberg J. 1999. Microtremor measurements used to map thickness of soft sediments. Bull. Seismol. Soc. America, 89: 250-259.

Konno, K. and Ohmachi, T. 1998. Ground-motion characteristics estimated from spectral ratio between horizontal and vertical components of microtremor. Bulletin of the Seismological Society of America, 88: 228–241.

Lane, J.W., Jr., White, E.A., Steele, G.V., and Cannia, J.C. 2008. Estimation of bedrock depth using the horizontal-to-vertical (H/V) ambient-noise seismic method, in Symposium on the Application of Geophysics to Engineering and Environmental Problems, April 6-10, 2008, Philadelphia, Pennsylvania, Proceedings: Denver, Colorado, Environmental and Engineering Geophysical Society, 13 p.

Lermo, J. and Chavez-Garcia, F.J. 1994. Are microtremors useful in site response evaluation? Bulletin of the Seismological Society of America, 84: 1350–1364.

Liu, L., Zhu, L., and Lane, J.W., Jr. 2007. Analysis of the two-dimensional effect in the H/V spectral ratio method for bedrock depth estimation on bedrock depth estimation by the H/V seismic method [abs]: EOS Transactions, American Geophysical Union, v. 88, no. 52, Fall Meeting Supplement, Abstract H21A-0187.

Mallozzi, S. 2017. Testing the horizontal to vertical spectral ratio of seismic microtremors as a subsurface mapping method in Orleans, ON. BSc. Thesis, Department of Earth Science, Carleton University, Ottawa ON.

Matsushima, S., Hirokawa, T., De Martin, F., Kawase, H., and Sánchez-Sesma F. 2014. The Effect of Lateral Heterogeneity on Horizontal- to-Vertical Spectral Ratio of Microtremors Inferred from Observation and Synthetics. Bulletin of the Seismological Society of America; 104: 1, 381–393. https://doi.org/10.1785/0120120321

Mulligan, R.P.M. 2017. An update on three-dimensional sediment mapping in the central part of the County of Simcoe, southern Ontario; in Summary of Field Work and Other Activities, 2017, Ontario Geological Survey, Open File report 6333, p.25-1 to 25-10.

Pugin, A.J.-M., Dietiker, B., Mulligan, R.P.M., Crow, H.L., Brewer, K., Cartwright, T., Rainsford, D.R.B., Bajc, A.F., Sharpe, D.R., and Russell, H.A.J. 2018. High-resolution seismic-reflection profiles for groundwater studies in Simcoe County, southern Ontario. Geological Survey of Canada, Open File 8383, 1 .zip file. https://doi.org/10.4095/308388

Pugin, A. J.-M., Hunter, J.A., Motazedian, D., Brooks, G., and Khaheshi-Banad, K. 2007. An application of shear-wave reflection landstreamer technology to soil response evaluation of earthquake shaking in an urban area, Ottawa, Ontario. In Proceedings, SAGEEP' 07 (Symposium on the Application of Geophysics to Engineering and Environmental Problems), Denver, CO, April 1-5, 2007, 11p.

Roten, D., Fäh, D., Cornou, C., and Giardini, D. 2006. Two-dimensional resonances in Alpine valleys identified from ambient vibration wavefields. Geophysical Journal International, 165: 3, 889-905.

SESAME 2004. Guidelines for the implementation of the H/V spectral ratio technique on ambient vibrations-Measurements, processing and interpretation. SESAME European research project, Deliverable D23. 12., Project No. EVG1-CT-2000-00026 SESAME, 62 pp.

Sorensen, C. and Asten, M. 2007. Microtremor methods applied to groundwater studies. Exploration Geophysics, 38: 2, 125-131. https://doi.org/10.1071/EG07016

Downscaling SMAP soil moisture using radarsat constellation mission (RCM) compact polarimetric SAR data: A case study in southern Ontario

Junhua Li[1]*, Shusen Wang[1], and Hazen A.J. Russell[2]

Abstract: This paper presents an improved algorithm for downscaling SMAP soil moisture using C-band SAR data. It is developed using multi-temporal C-band Radarsat Constellation Mission (RCM) compact polarimetric (CP) SAR data. In this improved algorithm, the effect of vegetation on soil moisture retrieval from SAR data is minimized by using a normalized scattering based empirical model, in which vegetation contribution is quantified using the volume scattering derived from RCM CP decomposition. The influence of soil surface roughness is eliminated by using multi-temporal data. The multi-temporal SMAP soil moisture and RCM CP data (simulated from Radarsat-2 QuadPol data) are the only inputs of this downscaling model. The model is tested in southern Ontario, Canada to downscale 36 km resolution SMAP soil moisture to 1 km. The downscaled results have good agreement with the in-situ soil moisture collected in June of 2017 with an unbiased root-mean-square-error (RMSE) of 0.047 m^3/m^3 and a coefficient of determination (R^2) of 0.43. The results suggest that the improved algorithm can be applied for C-band RCM CP data to provide continuous soil moisture mapping over large area at higher resolutions because of RCM's high-revisit frequency and large areal coverage characteristics.

Keywords: soil moisture, downscaling, RCM, SMAP, compact polarimetry

1. Introduction

Soil moisture has a key role in the water cycle. Soil moisture data over large areas is difficult to obtain from in situ networks due to high temporal and spatial variations in soil moisture. Current soil moisture products derived from passive microwave satellites, such as Soil Moisture Active Passive (SMAP) and Soil Moisture Ocean Salinity (SMOS), can provide global coverage on a 2–3 day cycle. Their very coarse resolutions (~40 km^2); however, limits the soil moisture products in applications where 1 km to 10 km resolution is needed, e.g. localized drought monitoring, crop management, and fine-scale water budget assessment and ecological modelling (Hanesiak 2011; Wang et al. 2014).

Attempts have been made to downscale the coarse resolution of passive microwave soil moisture products through the use of high resolution Synthetic Aperture Radar (SAR) imagery (Piles et al. 2009; Das et al. 2011; Li et al. 2018). The most obvious advantages of SAR data, compared to optical data, are the high sensitivity to soil moisture with a large contrast of the microwave relative permittivity between dry soil (ε=2~3) and water (ε=80) (Ulaby et al. 1986; Prakash et al. 2012), and the ability of SAR signals to penetrate cloud, haze, and smoke, and hence observe the earth's surface in all weather conditions, day and night. Among various active-passive combined methods, the most often-used is the change detection algorithm (Njoku et al. 2001; Piles et al. 2009; Das et al. 2011). Das et al. (2011) modified the algorithm by introducing scale-invariant parameters for describing spatial heterogeneity, which was employed as a baseline algorithm for the SMAP 9-km combined active/passive soil moisture product.

Most of these change detection algorithms were developed for L-band SAR data since the low frequency penetrates further through vegetation/soil than C-band and X-band, and can minimize the effect of vegetation canopy and surface roughness. However, the L-band SAR that was deployed in SMAP stopped transmitting in July 2015. Currently, ALOS-2/PALSAR is the only long wavelength (L-band) SAR sensor in orbit. Since its data is less frequently acquired especially for regions outside Japan, the use of ALOS-2/PALSAR is considerably hampered for operational soil moisture retrieval. Sentinel-1A/1B, and Radarsat-2, which are C-band SAR satellites currently in orbit

[1] Canada Centre for Mapping and Earth Observation, Natural Resources Canada, 560 Rochester Street, Ottawa, ON K1A 0E4
[2] Geology Survey of Canada, Natural Resources Canada, 601 Booth Street, Ottawa, ON K1A 0E8

*corresponding author: junhua.li@canada.ca

Recommended citation: Li, J., Wang, S., and Russell, H.A.J. 2020. Downscaling SMAP soil moisture using Radarsat Constellation Mission (RCM) compact polarimetric SAR data: A case study in southern Ontario. In Russell, H.A.J. and Kjarsgaard, B.A. Eds. Southern Ontario groundwater project 2014–2019: summary report. Geological Survey of Canada, Open File 8536, 171-178. https://doi.org/10.4095/321102

with revisit time of 12 days and 24 days respectively, can provide routine observations of Earth's surface over large areas. With the launch of Canada's Radarsat Constellation Mission (RCM) in 2019, the RCM will further enhance soil moisture monitoring capability with its rapid revisit (<4 days) and compact polarimetric (CP) configuration. Improved soil moisture retrieval using Quad-polarized (QP) SAR data was reported even under dense vegetation canopy conditions (Barrett et al. 2009; Hajnsek et al. 2009) but the narrow swath limits its application in soil moisture retrieval over large areas. The RCM CP is considered as a possible alternative of the QP system but with a wider image swath. Therefore the use of CP data in the downscaling model could achieve a better result over a large area even under a dense vegetation canopy.

C-band has a short wavelength (~5.6 cm wavelength) that exhibits backscatter signal interaction from both the vegetation canopy and soil. Soil moisture retrieval using C-band needs accurate characterization of vegetation and surface roughness. Therefore, the existing change detection algorithms may be problematic when C-band SAR is used, especially considering these algorithms assume vegetation is unchanged between acquisitions. This may invalidate change detection algorithms (even with L-band SAR data) for cropland regions where the land surface vegetation varies rapidly over periods as short as several days (i.e. during the growing season).

The objective of this study is to produce enhanced resolution soil moisture by downscaling coarse-resolution SMAP soil moisture using high-resolution C-band RCM CP SAR data. In this study, we improve the SMAP soil moisture baseline algorithm by including a normalized scattering based empirical model, developed by Prakash et al. (2012), for minimizing the influence of vegetation on soil moisture retrieval for C-band SAR data. The improved algorithm addresses the aforementioned problems of existing downscaling algorithms, including that they are: 1) not applicable to C-band SAR with respect to soil moisture retrieval, and 2) not suitable for crop lands where vegetation changes rapidly.

2. Methodology

2.1 SAR backscatter model

A normalized scattering based empirical model, developed by Parkash et al. (2012), is used in this study. The model is based on the concept that for a specific antenna configuration the ratio of the soil surface scattering σ°_{soil} (in power) over the total scattering σ°_{tot} (in power) is primarily influenced by vegetation (Josef et al. 2010). The ratio $\Delta\sigma^\circ_{pp}$, hereafter referred to as the normalized scattering coefficient, for a given polarization (pp) is expressed as (Parkash et al. 2012):

$$\Delta\sigma^\circ{}_{pp} = \frac{\sigma^\circ{}_{tot,pp}}{\sigma^\circ{}_{soil,pp}} = f(V) \quad (1)$$

Where the V represents vegetation parameter (e.g., NDVI, LAI), the pp represents the polarization (e.g., HH, VV), which is considered for the development of the soil moisture retrieval. Parkash et al. (2012) developed an empirical relationship between $\Delta\sigma^\circ_{pp}$ in decibel (dB) and NDVI. In general, the empirical relationship is formulated as:

$$\Delta\sigma^\circ{}_{pp} = P_1 \times V^2 + P_2 \times V + P_3 \quad (2)$$

Where P_1, P_2, *and* P_3 are the empirical coefficients and they will differ for the different polarizations (Parkash et al. 2012). When $\Delta\sigma^\circ_{pp}$ is in dB, the scattering coefficient of soil is given in Eq. (3):

$$\sigma^\circ{}_{soil,pp} = \sigma^\circ{}_{tot,pp} - \Delta\sigma^\circ{}_{pp} \quad (3)$$

Where $\sigma^\circ_{soil,pp}$, $\sigma^\circ_{tot,pp}$, and $\Delta\sigma^\circ_{pp}$ are in dB.

The bare soil scattering $\sigma^\circ_{soil,pp}$ (in dB) is represented by the function *f(R, θ)* of surface roughness (*R*) and soil moisture (*θ*). For an agriculture field during the crop growing time period, *R* is considered constant for a short period and its effect can be minimized by using multi-temporal data over the same field. In such a case, the temporal change in bare soil scattering only reflects the change of soil moisture with time for a site, and the σ°_{soil} (in dB) has a linear relationship with θ, which can be expressed as:

$$\sigma^\circ{}_{soil,pp} = a\theta + b \quad (4)$$

where a can be considered as the sensitivity of SAR to soil moisture and b indicates the backscatter due to surface roughness. Combining Equations (2) – (4), the soil moisture θ can be retrieved through the equation:

$$\theta = K_1\sigma^\circ{}_{tot,pp} + K_2V^2 + K_3V + K_4 \quad (5)$$

Where K_1 = 1/a, K_2 = -P_1/a, K_3 = -P_2/a, and K_4 = -(P_3-b)/a. The V is often parameterized using in-situ measured or remotely sensed vegetation descriptors, such as Leaf Area Index (LAI), Vegetation Water Content (VWC), and NDVI. Recently, some advances have been made toward developing SAR parameters for characterizing vegetation canopies. For example, Kumar et al. (2013) showed that the radar vegetation index (RVI) provides an improvement compared to NDVI for monitoring soybean and cotton. The HV backscattering coefficients were found to be very sensitive to the vegetation biomass (Kasischke et al. 2011; Rao et al. 2013) and correlated with LAI (Paloscia 1998). Li and Wang (2018) showed that the backscatter of SAR HV polarization and RVI can replace optical image derived vegetation parameters in the Water Cloud Model (WCM) and further improve soil moisture retrieval. In addition, the volume scattering derived from the polarimetric decomposition could be another option for the vegetation descriptor. Studies have shown that HV (or VH) is associated with volume scattering and volume scattering is a strong indicator of crop growth development (Cloude and Pottier 1996). Jiao et al. (2011) also reported a strong relationship

between volume scattering and the LAI for both corn and soybeans (increase with increasing LAI).

2.2 SMAP Soil moisture downscaling algorithm

The key components of the algorithm for downscaling SMOS/SMAP soil moisture products using C-band SAR images include: (1) the influence of vegetation on soil moisture retrieval being minimized by the normalized scattering based empirical model, in which the conditions of vegetation are characterized by a vegetation descriptor (V) derived from SAR data itself; (2) the spatial heterogeneity between scales is taken into account through a special parameter derived from the SAR data; and (3) time series data used to eliminate the effect of surface roughness. The downscaling algorithm is summarized in Figure 1 with further details explained as follows.

2.2.1 SAR image aggregation

The time series of C-band SAR backscatter images at fine resolution (F) are spatially aggregated to the target medium resolution (M), which the downscaling process will achieve, and the coarse resolution (C), which is the same as the current SMAP soil moisture. The aggregation of SAR images is implemented by averaging the original pixels that coincide with a pixel at the medium (or coarse) resolution. Time series of medium and coarse resolution SAR images are generated at this step.

2.2.2 SAR backscatter models at the coarse resolution

The normalized scattering based empirical model at coarse resolution (C) is:

$$\theta_C = K_{1,C}\sigma^{\circ}{}_{tot,pp,C} + K_{2,C}{V_C}^2 + K_{3,C}V_C + K_{4,C} \quad (6)$$

Where $\sigma^{\circ}{}_{tot,pp,C}$ is the aggregated backscatter coefficient (in dB) at coarse resolution (C), θ_C is the SMAP soil moisture. The model is built for each pixel by using the time series aggregated SAR backscatter and SMAP soil moisture at the coarse resolution, in which the unknown model parameters $K_{1,C}$, $K_{2,C}$, $K_{3,C}$, and $K_{4,C}$ can be calculated.

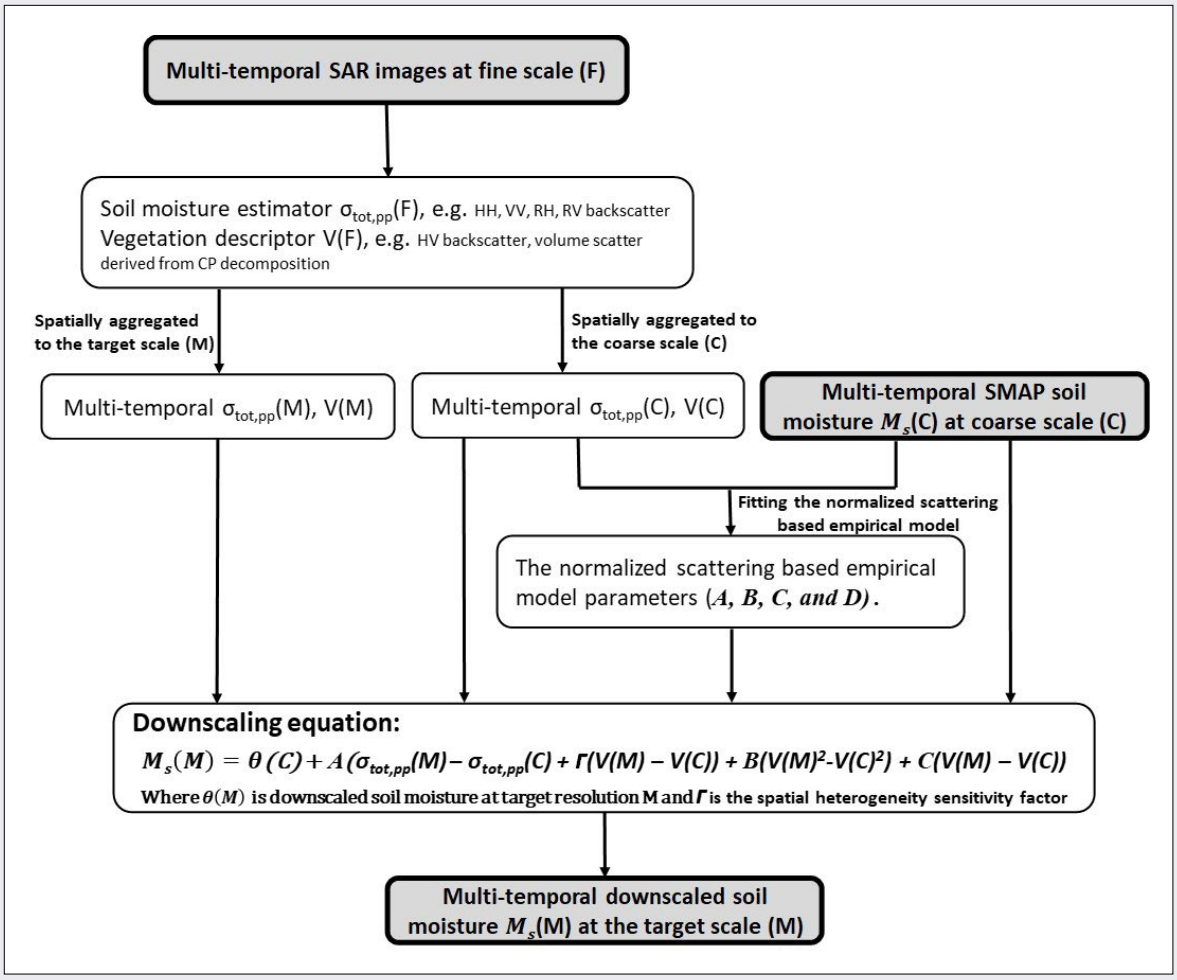


Figure 1. Flowchart of the SMAP soil moisture downscaling algorithm.

2.2.3 Formulation of the downscaling algorithm

To develop the downscaling algorithm, Eq. (5) can also be evaluated at medium resolution M within the SMAP footprint C as follows:

$$\theta_M = K_{1,M}\sigma^\circ{}_{tot,pp,M} + K_{2,M}{V_M}^2 + K_{3,M}V_M + K_{4,M} \quad (7)$$

Where $\sigma^\circ{}_{tot,pp,M}$ is the aggregated backscatter coefficient (in dB) at medium resolution M. θ_M is the target of the downscaling algorithm and it is referred as the downscaled soil moisture thereafter. We cannot directly estimate the model parameters $K_{1,M}$, $K_{2,M}$, $K_{3,M}$, and $K_{4,M}$ in the manner that was followed at resolution C since θ_M is unknown. Subtracting Eq. (7) from Eq. (6), we have:

$$\begin{aligned}\theta_M - \theta_c = {} & (K_{1,M}\sigma^\circ{}_{tot,pp,M} - K_{1,C}\sigma^\circ{}_{tot,pp,C}) + \\ & (K_{2,M}{V_M}^2 - K_{2,C}{V_C}^2) + \\ & (K_{3,M}V_M - K_{3,C}V_C) + (K_{4,M} - K_{4,C})\end{aligned} \quad (8)$$

Eq. (8) can be further algebraically rewritten as:

$$\theta_M = \theta_c + \quad \text{RHS I}$$

$$\{K_{1,C}\left(\sigma^\circ{}_{tot,pp,M} - \sigma^\circ{}_{tot,pp,C}\right) + K_{2,C}\left({V_M}^2 - {V_C}^2\right) + K_{3,C}(V_M - V_C)\}+ \quad \text{RHS II}$$

$$\{(K_{1,M} - K_{1,C})\sigma^\circ{}_{tot,pp,M} + (K_{2,M} - K_{2,C}){V_M}^2 + (K_{3,M} - K_{3,C})\,V_M + (K_{4,M} - K_{4,C})\} \quad \text{RHS III} \quad (9)$$

The left-hand-side (LHS) of Eq. (9) is the downscaled soil moisture at resolution M. The first term on the right-hand-side (RHS Term I), θ_C is the SMAP soil moisture at 36 km or resolution C. The calculations for the variables in RHS Term II have already been discussed. The RHS Term III represents the spatial heterogeneity in vegetation and surface roughness due to the resolution's change. It accounts for the deviations of the model parameters K_1, K_2, K_3, and K_4 within the grid cell at the resolution C. The RHS Term III can be substituted by $K_{1,C}\Gamma(\sigma^\circ{}_{tot,pq,C} - \sigma^\circ{}_{tot,pq,M})$ (Entekhabi et al. 2014; Wu et al. 2013), in which $\sigma^\circ{}_{tot,pq,M}$ and $\sigma^\circ{}_{tot,pq,C}$ are the cross-polarization backscatter at resolutions M and C, respectively. Γ is the sensitivity parameter and can be estimated by using co-polarization and cross-polarization backscatter data within resolution C through statistical regression. More detail about Γ can be found in Entekhabi et al. (2014). Through the substitution of the RHS Term III, the downscaling algorithm is formulated as:

$$\begin{aligned}\theta_M = {} & \theta_c + \\ & K_{1,C}\left[\left(\sigma^\circ{}_{tot,pp,M} - \sigma^\circ{}_{tot,pp,C}\right) + \right. \\ & \left.\Gamma\left(\sigma^\circ{}_{tot,pq,C} - \sigma^\circ{}_{tot,pq,M}\right)\right] + \\ & K_{2,C}\left({V_M}^2 - {V_C}^2\right) + \\ & K_{3,C}(V_M - V_C)\end{aligned} \quad (10)$$

2.3 Validation method

The downscaling results for soil moisture are compared to in-situ measurements using the coefficient of determination (R^2), the mean error (or bias) and the unbiased root mean square error ($RMSE$). The formula for the $RMSE$ is given in Eq. 8 (Entekhabi et al. 2014).

$$RMSE = \sqrt{\frac{\sum_{i=1}^{n}(\theta o_i - \theta p_i)^2}{n} - \left(\frac{\sum_{i=1}^{n}(\theta o_i - \theta p_i)}{n}\right)^2} \quad (11)$$

where ϑo_i and ϑp_i are the downscaled and in-situ soil moisture at measurement i separately. n is the number of soil moisture measurements. The unbiased $RMSE$ can remove the bias by characterizing random error and thus provide a better reliable estimation of root mean square error.

3. Study region

The study is located within one SMAP pixel in southern Ontario, Canada (Figure 2). It is the southernmost region in Canada and is a densely populated region with intense agriculture. The climate is among the mildest in Canada with annual precipitation ranging from 750 to 1000 mm and an annual mean temperature of 10 °C, with hot, humid summers and a longer growing season than most of Canada (Sharpe et al. 2014). Combined with fertile surficial sediment, it is a prosperous agricultural region with established field crop, livestock (including pasture/forages) and horticulture production systems. The study area is just north of Lake Erie and west of London, Ontario. The region is mostly flat plain with gently rolling hills. The dominant land cover classes are agricultural crops interlaced with some permanent grassland, wetlands, mixed forest cover and built-up regions. According to the 2017 crop inventory map of Canada (http://open.canada.ca), the major crop types (areal extent >5% of whole area) include corn, soybean, wheat (winter wheat), and pasture/forages. The soil types mapped across the study area, in decreasing order of clay contents, are: silty clay loam, silty loam, loam, and sand (Figure 2; Soil Landscapes of Canada Working Group 2010). The silty clay loam has the largest areal extent and occupies most of the south part of the study area. Loam soils occur in the north portion of the study area. Sand soil has the least areal extent and only appears in the south-east corner the study area. Therefore, generally, the southern region has more clay than the northern region. A query of the Soil Landscapes of Canada version 3.2 database returns three major soil types for the area with coverages >5%, those are: silty clay loam, silty loam, and loam.

4. Data collection and processing

4.1 Satellite data

The satellite datasets used in this study include Radarsat-2 (RS-2) QP (HH, HV, VH, and VV) wide-fine mode acquisitions, and SMAP soil moisture products. There were a total of 20

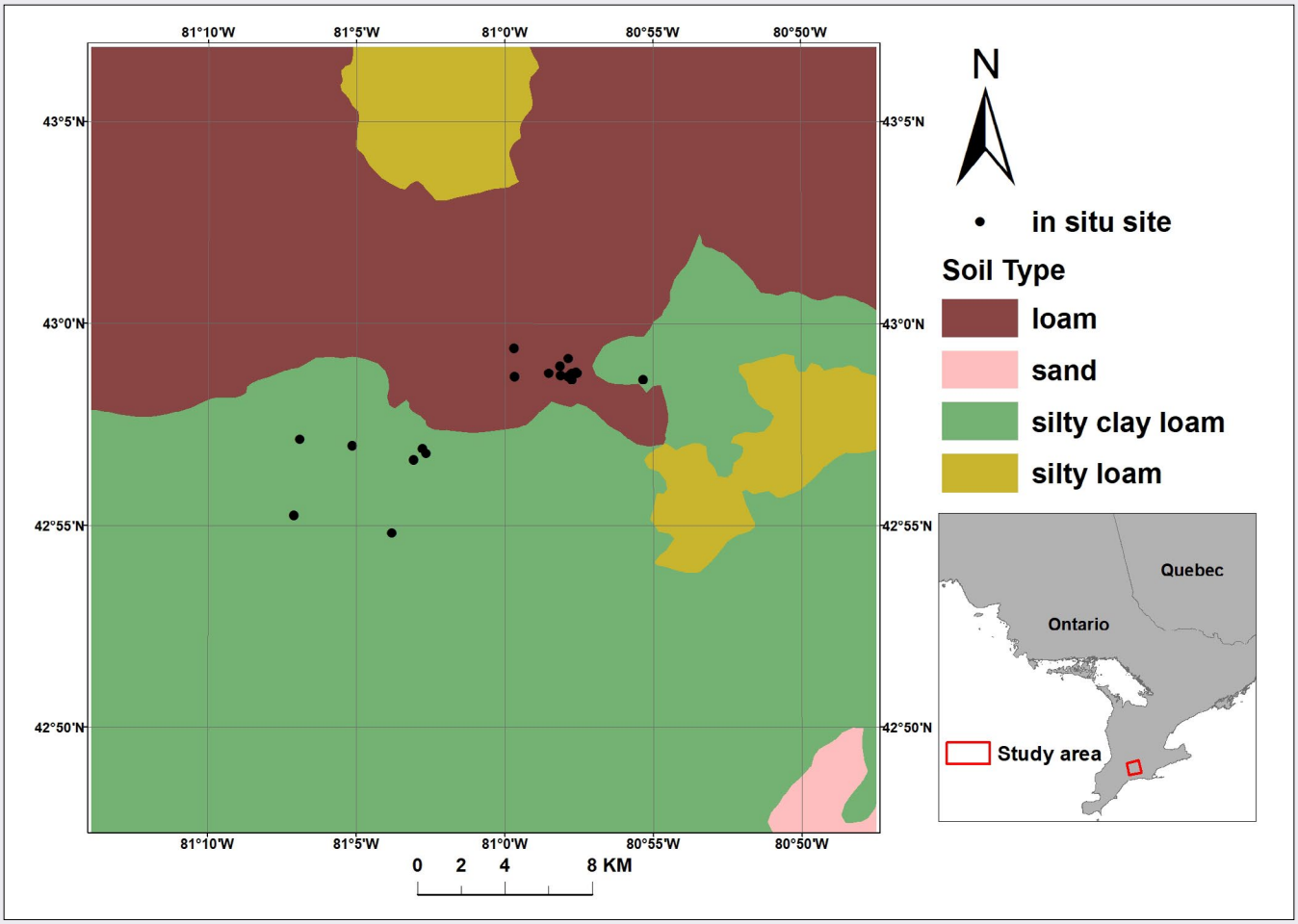


Figure 2. Soil type map and location of the study area.

RS-2 scenes (in single look complex format) and 10 SMAP Level 2 soil moisture data acquired during the time period of May 9th, 2017 to July 10th, 2017. All the SMAP soil moisture data was re-projected to UTM projection with 36 km resolution and then subset to match the study area. Table 1 lists the acquisition parameters of the Radarsat-2 scenes. For each acquisition date, two scenes were acquired to cover the study area. In this study, the RCM CP mode data was simulated from the RS-2 QP data. The CP mode in RCM synthesizes a right circular transmitter with linear horizontal and linear vertical receivers, RH and RV. Like QP mode data, CP mode data can be decomposed to different polarimetry parameters such as volume scattering and double bounce scattering. The RCM RH and RV backscatter coefficients, and their decomposition parameter – volume scattering were generated by using PCI Geomatica software. RS-2 and the simulated RCM data were then orthorectified in UTM projection with 20 m resolution by using the SRTM DEM data. While orthorectifying the images, the incidence angle for each pixel was computed scene by scene. A 5x5 enhanced Lee filter was applied to reduce speckle noise. All the processes were completed in the PCI Geomatica software. We denote HH, HV, RH and RV backscattering coefficients and volume scattering as $\mathring{\sigma}_{HH}$, $\mathring{\sigma}_{HV}$, $\mathring{\sigma}_{RH}$, $\mathring{\sigma}_{RV}$, and $\mathring{\sigma}_{vol}$, respectively.

Given a short time period, the number of repeat-pass RS-2 images may not be sufficient for fitting the normalized scattering based empirical model due to their low temporal resolutions. As a solution, all available RS-2 images during the study period were used to produce a time series dataset. Without correction, these images may not be radiometrically comparable because they could be captured at different incidence angles (Table 1). For more accurate quantitative analysis of radar backscatter, we normalized the observed backscatter to a reference of 30° based on the theoretical model of Lambert's law,

$$\sigma^{\circ}(\theta_{ref}) = \frac{cos^{n}(\theta_{ref})}{cos^{n}(\theta_{i})}\sigma^{\circ}(\theta_{i}) \quad (12)$$

where n is the power index characterizing surface roughness and is normally set to 2, $\sigma^{\circ}(\theta_{i})$ is the incidence angular

Table 1. Information for the Radarsat-2 images used in the study.

Date	Direction	Acquisition Mode	Incidence angle (near range – far range)
2017-05-09	Ascending	FQ3W	20.0°–23.6°
2017-06-02	Ascending	FQ3W	20.0°–23.6°
2017-06-06	Descending	FQ17W	35.7°–38.6°
2017-06-12	Ascending	FQ13W	31.7°–34.7°
2017-06-23	Descending	FQ12W	30.6°–33.7°
2017-06-26	Ascending	FQ3W	20.0°–23.6°
2017-06-30	Descending	FQ17W	35.7°–38.6°
2017-07-03	Descending	FQ2W	19.0°–22.7°
2017-07-06	Ascending	FQ13W	31.7°–34.7°
2017-07-10	Descending	FQ7W	24.9°–28.3°

dependent radar backscatter, θ_i and θ_{ref} represent the local incidence angle and the reference incidence angle respectively, and $\sigma^o(\theta_{ref})$ is the normalized radar backscatter to a reference incidence angle θ_{ref}. The effect of topography on Radarsat-2 backscatter is not a factor due to relatively flat terrain in most of the study area.

4.2 In-situ measurements

In-situ soil moisture was measured at 19 sites (black dots in Figure 2) to a depth of 5 cm (Figure 2), during satellite overpass on June 12 of 2017 (±1 day) using a Delta-T soil Moisture Meter (Type HH2) and Thetaprobe sensor model ML2x. The Thetaprobe probe measures soil moisture to a depth of 5 cm. A total of more than forty soil moisture samples were acquired for each field site, where the sampling design was to acquire soil moisture samples at 10 meter interval along the north-south and the east-west cardinal directions. Due to limited field accessibility and acquisition times, in-situ sampling only occur in 3 different soils: silty clay loam, silty loam, and loam and 4 different crop types: forage, corn, soybean, and wheat.

5. Results and discussion

Multi-temporal soil moisture maps at 1 km resolution are generated by applying the proposed SMAP soil moisture downscaling algorithm to the multi-temporal SMOS soil moisture data, and C-band RCM CP data as detailed in Section 3, where σ^o_{RH} and σ^o_{vol} are used as the soil moisture retrieval $\sigma^o_{tot,pp}$ and the vegetation descriptor *V*, respectively. Figure 3 shows the multi-temporal soil moisture maps at 1 km resolution. The temporal variability of soil moisture could be influenced by precipitation events, soil texture, and water usage due to crop phenology. There is a tendency (especially on dry dates) in the downscaled soil moisture maps for the southern region, which has a silty clay loam soil type, to be wetter than the northern region, which has a loam soil type. This indicates that the spatial pattern of the downscaled soil moisture has a relationship with soil types. In addition, crop types may also affect soil moisture due to their different phenology (Li et al. 2018).

To evaluate the performance of the downscaling model, the downscaled soil moisture is compared to the in-situ soil moisture measured in June of 2017. The correlation coefficient (R^2), *bias*, and unbiased root mean square error ($RMSE$), were calculated to compare the downscaled results with the in-situ measurements. The relationship between the downscaled soil moisture and the in-situ soil moisture measured in June of 2017 give R^2, $RMSE$, and *bias* of 0.43, 0.047 m^3/m^3, and 0.017 m^3/m^3. Figure 4 and positive bias both indicate that the downscaled soil moisture is overestimated. This is not considered to be caused by an error in the downscaling algorithm. It is likely due to the difference between the depth of the soil layer contributing to the SAR backscatter signal (~2 cm) and the soil depth of the in-situ measurements (~5 cm). The $RMSE$ between the downscaled and in situ soil moisture is of similar magnitude to those obtained from the validation studies for SMOS soil moisture (e.g. 0.044 m^3/m^3 for the REMEDHUS network in Spain (Sanchez et al. 2012) and 0.043 m^3/m^3 for the in situ soil moisture networks located in the U.S. (Jackson et al. 2012). They are also close to SMAP target accuracy of 0.04 m^3/m^3.

The performance of the downscaling model can be affected by the density of vegetation and the wavelength of SAR data. The downscaling model could be more robust in sparse vegetated areas than dense vegetated areas when C-band SAR data is used due to its relatively short wavelength and limited penetration under a dense vegetation canopy compared to

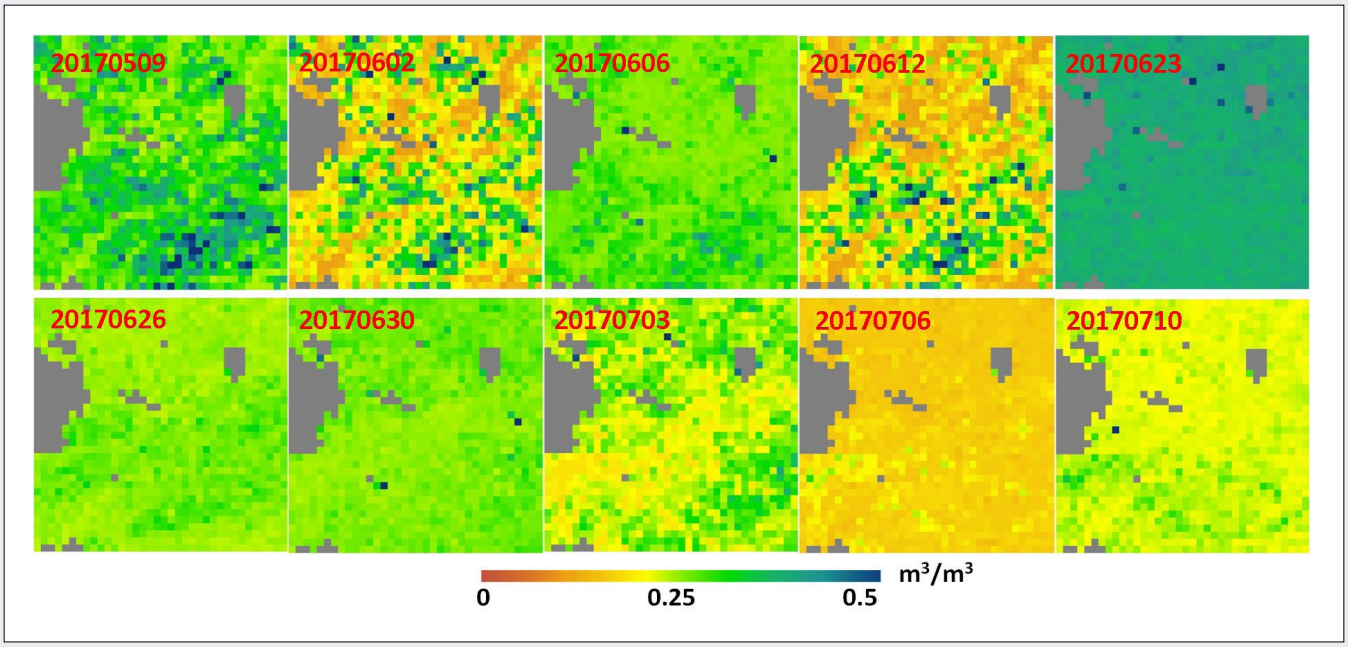


Figure 3. Multi-temporal downscaled soil moisture at 1 km resolution.

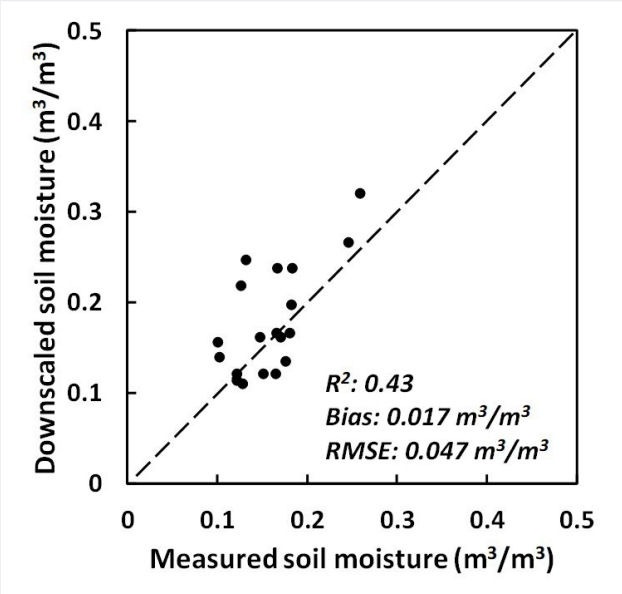


Figure 4. Plots of the in-situ soil moisture and the downscaled soil moisture.

L-band SAR with longer wavelengths (Li et al. 2018). Therefore, the use of L-band SAR data in this downscaling model may reduce errors of estimation especially in areas with dense vegetation cover.

To reduce the effect of SAR incidence angle, we normalized all RS2 and simulated RCM CP images to a reference angle theoretical model of Lambert's law. However, it should be noted that the theoretical approach may not be the most appropriate one and could introduce errors (Lievens and Verhoest 2011). The assessments of errors and different approaches are beyond the scope of this paper. Once the RCM is operational, the incidence angle normalization is not needed because RCM has a 4-day revisit time, which makes it possible to acquire sufficient repeat pass SAR images in a short period. Although the downscaling model is tested to be applicable to SMAP soil moisture and C-band RCM CP data in this study, this method is not limited to this data combination. It can be applied to other passive microwave (e.g. SMOS) soil moisture products.

6. Conclusion

The SMAP soil moisture downscaling algorithm presented in this paper is an additional contribution to the SMAP soil moisture downscaling algorithms. The improved algorithm addresses limitations, which initially stated that they were not suitable for regions where vegetation changes rapidly, and consequently C-band SAR data would not be appropriate. The two key points of the model include: 1) use of a normalized scattering based empirical model to remove effect of vegetation on soil moisture retrieval from C-band SAR, in which the conditions of vegetation are characterized by the volume scattering derived from the RCM CP decomposition; 2) use of time series data to minimize the influence of soil surface roughness by assuming the surface roughness doesn't change over a short period. The improved algorithm is tested with C-band RCM CP images simulated from RS2 QuadPol images, and the SMAP soil

moisture observed for an agricultural crop region in southern Ontario, Canada. Downscaled soil moisture was retrieved at 1 km resolution. The results are in good agreement with the in-situ measurements collected in June of 2017, with $RMSE$ (R^2) of 0.047 m^3/ m^3. With the upcoming operational deployment in 2019 of RCM with a compact polarimetric configurations and a revisit time of less than 4 days, this algorithm provides the potential for fusing RCM CP data with SMAP/SMOS soil moisture to permit continuous mapping of soil moisture at higher resolutions over large areas. The technique presented provides a methodological multi-sensor alternative to the failed active radar that was integrated on SMAP with the passive sensor. It provides an ability to estimate soil moisture at an order of magnitude greater resolution than the passive SMAP and SMOS satellites.

7. Acknowledgements

An internal review by F. Canisus is much appreciated. This work was supported by the Groundwater Geoscience Program and Remote Sensing Program of Natural Resources Canada. This work is a contribution of the GSC–OGS Southern Ontario project on groundwater 2014–2019.

8. References

Cloude, S.R. and Pottier, E. 1996. A review of target decomposition theorems in radar polarimetry. IEEE Transactions on Geoscience and Remote Sensing, 34: 2, 498-518. doi:10.1109/36.485127

Das, N.N., Entekhabi, D., and Njoku, E.G. 2011. An algorithm for merging SMAP radiometer and radar data for high-resolution soil-moisture retrieval. IEEE Transactions on Geoscience and Remote Sensing, 49: 5, 1504-1512. doi:10.1109/TGRS.2010.2089526

Entekhabi, D., Yueh, S., O'Neill, P.E., Kellogg, K.H., Allen, A., Bindlish, R., Brown, M., Chan, S., Colliander, A., and Crow, W.T. 2014. SMAP Handbook-Soil Moisture Active Passive: Mapping soil moisture and freeze/thaw from space. Jet Propulsion Laboratory: Pasadena, CA, USA.

Hanesiak, J.M., Stewart, R.E., Bonsal, B.R., Harder, P., Lawford, R., Aider, R., Amiro, B.D., Atallah, E., Barr, A.G., Black, T.A., Bullock, P., Brimelow, J.C., Brown, R., Carmichael, H., Derksen, C., Flanagan, L.B., Gachon, P., Greene, H., Gyakum, J., Henson, W., Hogg, E.H., Kochtubajda, B., Leighton, H., Lin, C., Luo, Y., McCaughey, J.H., Meinert, A., Shabbar, A., Snelgrove, K., Szeto, K., Trishchenko, A., van der Kamp, G., Wang, S., Wen, L., Wheaton, E., Wielki, C., Yang, Y., Yirdaw, S., and Zha, T. 2011. Characterization and summary of the 1999-2005 Canadian prairie drought. Atmosphere-ocean, 49: 4, 421-452. https://doi.org/10.1080/07055900.2011.626757

Jackson, T.J., Bindlish, R., Cosh, M.H., Zhao, T., Starks, P.J., Bosch, D.D., Seyfried, M, Moran, M.S., Goodrich, D.C., Kerr, Y.H., and Leroux, D. 2012. Validation of soil moisture and ocean salinity (SMOS) soil moisture over watershed networks in the U.S. IEEE Transactions on Geoscience and Remote Sensing, 50: 5, 1530 – 1543. doi:10.1109/TGRS.2011.2168533

Jiao, X., McNairn, H., Shang, J., Pattery, E., Liu, J., and Champagne, C. 2011. The sensitivity of Radarsat-2 polarimetric SAR data to corn and soybean leaf area index. Canadian Journal of Remote Sensing, 37: 1, 69-81. https://doi.org/10.5589/m11-023

Joseph, A.T., van der Velde, R., O'Neil, P.E., Land, R., and Gisg, T. 2010. Effects of Corn on C- and L-band radar backscatter: A correction method for soil moisture retrieval. Remote Sensing of Environment, 114: 2417-2430. https://doi.org/10.1016/j.rse.2010.05.017

Kasischke, E.S., Tanase, M.A., Bourgeau-Chavez, L.L., and Borr, M. 2011. Soil moisture limitations on monitoring boreal forest regrowth using spaceborne L-band SAR data. Remote Sensing of Environment, 115: 1, 227-232. https://doi.org/10.1016/j.rse.2010.08.022

Li, J. and Wang, S. 2018. Using SAR-derived vegetation descriptors in a Water Cloud Model to improve soil moisture retrieval. Remote Sensing, 10: 1370. https://doi.org/10.3390/rs10091370

Li, J, Wang, S., Gunn, G., Joosse, P., and Russell, H.A.J. 2018. A model for downscaling SMOS soil moisture using Sentinel-1 SAR data. International Journal of Applied Earth Observation and Geoinformation, 72: 109-121. https://doi.org/10.1016/j.jag.2018.07.012

Lievens, H. and Verhoest, E.C. 2011. On the retrieval of soil moisture in wheat fields from L-band SAR based on water cloud modelling, the IEM, and effective roughness parameters. IEEE Geoscience and Remote Sensing Letters, 8: 4, 740 – 744. https://doi.org/10.1109/LGRS.2011.2106109

Njoku, E. G., Wilson, W. J., Yueh, S.H., Dinardo, S.J., Jackson, T.J., Lakshmi, V., and Bolten, J. 2002. Observations of soil moisture using a passive and active low frequency microwave airborne sensor during SGP99. IEEE Transactions on Geosciences and Remote Sensing, 40: 12, 2659 – 2673. https://doi.org/10.1109/TGRS.2002.807008

Paloscia, S. 1998. An Empirical Approach to Estimating Leaf Area Index from Multifrequency SAR Data. International Journal of Remote Sensing, 19: 2, 359–364. https://doi.org/10.1080/014311698216323

Piles, M., Entekhabi, D., and Camps, A. 2009. A change detection algorithm for retrieving high-resolution soil moisture from SMAP radar and radiometer observations. IEEE Transactions on Geoscience and Remote Sensing, 47: 4125–4131. https://doi.org/10.1109/TGRS.2009.2022088

Prakash, R., Singh, D., and Pathak, N.P. 2012. A fusion approach to retrieve soil moisture with SAR and optical data. IEEE Journal of Selected Topics in Applied Earth Observations and Remote Sensing, 5: 10, 196-206. https://doi.org/10.1109/JSTARS.2011.2169236

Rao S.S., Kumar, S.D., Das, S.N., Nagaraju, M.S.S., Venugopal, M.V., Rajankar, O., Laghate, P., Reddy, M.S., Joshi, A.K., and Sharma, J.R. 2013. Modified Dubois model for estimating soil moisture with dual polarized SAR data. Journal of Indian Society of Remote Sensing, 41: 4, 865-872. https://doi.org/10.1007/s12524-013-0274-3

Sanchez, N., Martinez-Fernandez, J., Scaini, A., and Perez-Gutierrez, C. 2012. Validation of the SMOS L2 soil moisture data in the REMEDHUS network (Spain). IEEE Transaction on Geoscience and Remote Sensing, 50: 1602-1611. doi: 10.1109/TGRS.2012.2186971

Sharpe, D.R., Piggott, A., Carter, T., Gerber, R.E., MacRitchie, S.M., de Loë, R.C., Strynatka, S., and Zwiers, G. 2014. Southern Ontario hydrogeological region. In: Rivera, A. (Ed.), Canada's Groundwater Resources. Fitzhenry & Whiteside, pp. 443–499. https://doi.org/10.4095/296947

Soil Landscapes of Canada Working Group, 2010. Soil Landscapes of Canada version 3.2. Agriculture and Agri-Food Canada. (digital map and database at 1:1 million scale).

Ulaby, F.T., Moore, R.K., and Fung, A.K. 1986. Microwave Remote Sensing: Active and Passive. Vol. III. Dedham, Mass., Artech House.

Wang, S., McKenney, D.W., Shang, J., and Li, J. 2014. A national-scale assessment of long-term water budget closures for Canada's watersheds. J. Geophys. Res., 119: 8712–8725, https://doi.org/10.1002/2014JD021951

Zribi, M., Baghdadi, N., Holah, N., and Fafin, O. 2005. New methodology for soil surface moisture estimation and its application to ENVISAT-ASAR multi incidence data inversion. Remote Sensing of Environment, 96: 485–496. https://doi.org/10.1016/j.rse.2005.04.005

Progressing toward an understanding of groundwater geochemistry of Innisfil Creek watershed, southern Ontario

Francis Proteau-Bedard[1], Nicolas Benoit[2]*, Paul Baudron[1,3], Ryan Post[4], and Angela Mills[4]

Abstract: Groundwater represents an important source of water for agriculture in the Innisfil Creek watershed, southern Ontario, where water vulnerability issues were evident through recent drought conditions. Uncertainties remain regarding the groundwater flow pattern of the multi-layer aquifer system and further understanding is required to plan for sustainable groundwater use. A hydrogeological study based on geochemistry and isotopes ($\delta^{2}H$, $\delta^{18}O$, $\delta^{13}C$, ^{14}C-DIC, and ^{226}Ra) is being developed to better characterize and quantify recharge, regional flow patterns, and potential inter-aquifer flow. In this paper, we present on work completed in 2018. The study objectives were to gather existing hydrogeological and geochemical data into a comprehensive database, to analyse the data in order to support targeted additional water sampling, and to develop preliminary interpretations. The ongoing project is now set for the development of an initial conceptual model based on the geochemical and isotopic interpretations combined with statistical analyses and physical hydrogeology processes observed in the region.

1. Introduction

The Innisfil Creek watershed in the South Simcoe area of southern Ontario has a watershed area of 490 km^2 and is a tributary to the Nottawasaga River (Figure 1). It has intensive agriculture, making groundwater use an important component of the region's economic activities (Matrix Solutions Inc. and Blumetric Environmental Inc. 2017). The occurrence of droughts in the past decade (e.g., 2002; NVCA 2006) has highlighted the vulnerability of both surface water and groundwater (Post et al. 2018) to changes in seasonal precipitation regimes.

The geology of the area is dominantly surficial sediment with bedrock limited to areas near the Niagara Escarpment. The geology of the area has been assigned to 17 distinct hydrostratigraphic units, including multiple aquifers (Mulligan et al. 2018) that form a complex hydrogeological system. In such a context, comprehensive knowledge of groundwater flow within this multi-layer aquifer system is a key task for a sustainable management of the resource. It requires a characterization and quantification of major processes such as recharge and inter-aquifer groundwater flow. Physical hydrogeology characterization is useful; however, it is insufficient to understand these processes. Insights from chemical hydrogeology can increase and help constrain the understanding of complex aquifer systems (e.g., Cloutier et al. 2006).

The main objective of this project is to characterize groundwater flow dynamics using geochemical and isotopic tracers within the Innisfil Creek watershed. More precisely, it seeks to increase knowledge regarding the characterization and quantification of processes such as recharge, hydrologic connection between hydrostratigraphic units, and natural chemical evolution of the groundwater resource. The approach builds upon existing studies in the area (Marchildon et al. 2016; Matrix Solutions Inc. and Blumetric Environmental Inc. 2017; Oni et al. 2014; Post et al. 2018). This paper presents a short review of the state of the work completed in 2018. After describing existing hydrogeochemical data collection and interpretation, the new sampling survey is described. Preliminary results and interpretation are then presented with a few perspectives on the next steps of the study.

2. Hydrostratigraphic units

The geology of the area consists of Paleozoic bedrock which subcrops beneath a thick cover of Quaternary sediments.

[1] Polytechnique Montréal, Département des génies civil, géologique et des mines, 2500 Chemin de Polytechnique, Montréal, QC H3T 1J4
[2] Geological Survey of Canada, Natural Resources Canada, 490 rue de la Couronne, Quebec City, QC G1K 9A9
[3] GEOTOP Research Centre, 201 Avenue Président-Kennedy, Montréal, QC H2X 3Y7
[4] Nottawasaga Valley Conservation Authority, 8195 8th Line of Essa, Utopia, ON L0M 1T0
*corresponding author: nicolas.benoit@canada.ca

Recommended citation: Proteau-Bedard, F., Benoit, N., Baudron, P., Post, R., and Mills, A. 2020. Progressing toward an understanding of groundwater geochemistry of Innisfil Creek watershed, southern Ontario. In Russell, H.A.J. and Kjarsgaard, B.A. Eds. Southern Ontario groundwater project 2014–2019: summary report. Geological Survey of Canada, Open File 8536, 179-189. https://doi.org/10.4095/321104

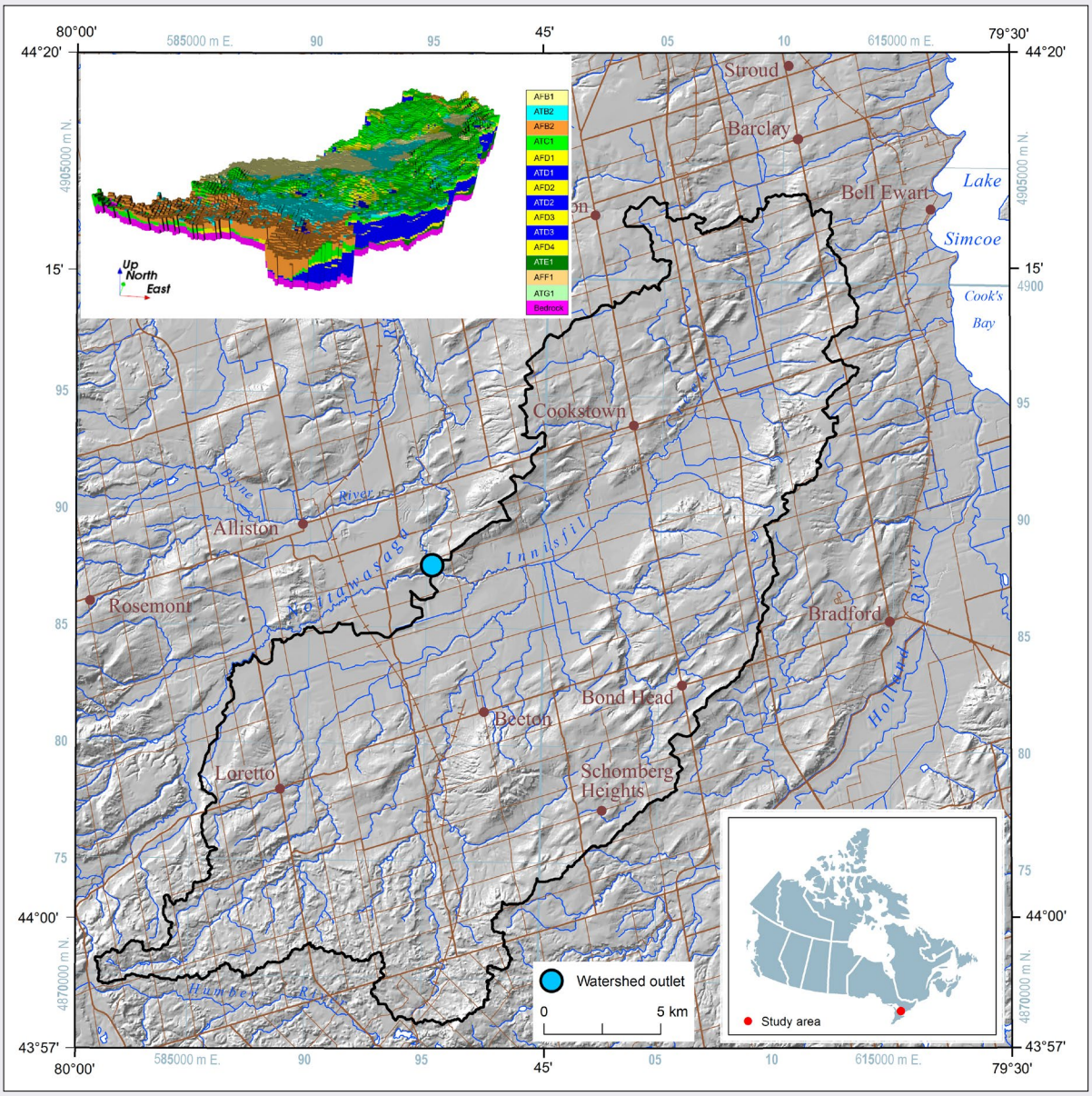


Figure 1. Study area with outline of Innisfil Creek watershed draped on a digital elevation model (DEM; hillshade)

Bedrock consists of four distinct Paleozoic lithostratigraphic units, including the Queenston shale, Georgian Bay muddy limestone, and Blue Mountain and Lindsay limestone formations (Bajc et al. 2015). The surficial stratigraphy is similar to the regional stratigraphy of the Laurentian trough (e.g., Eyles et al. 1984; Mulligan and Bajc 2018; Mulligan et al. 2018; Sharpe et al. 2018). Based on field investigations and modelling of Bajc et al. (2015) 17 units were consolidated into 11 hydrostratigraphic units (HSU) by Benoit et al. (2018)

The surficial geology of the watershed is the product of different deposition events which results in deposits of different characteristics (till, gravel, sand, mud). The 16 surficial geological units in increasing stratigraphic age are: recent, Lake Algonquin, and Oak Ridges Moraine deposits (AFA1, ATB1, AFB1, ATB2, AFB2), Newmarket Till (ATC1), Thorncliffe Formation (AFD1, ATD1, AFD2, ATD2, AFD3, ATD3, AFD4) and older glacial formations (ATE1, AFF1, ATG1). For the purpose of this preliminary study, bedrock forms a 17th unit considered to be an aquifer without a distinction between the lithologies (Figure 2). The absence of evidences of a karstic system in the carbonates (Hamilton 2018) and the undefined fracture level of the rock did not highlight a need for further grouping. The 16 surficial units were reduced to 10 hydrostratigraphic units (HSU) based on their hydrogeological properties. An

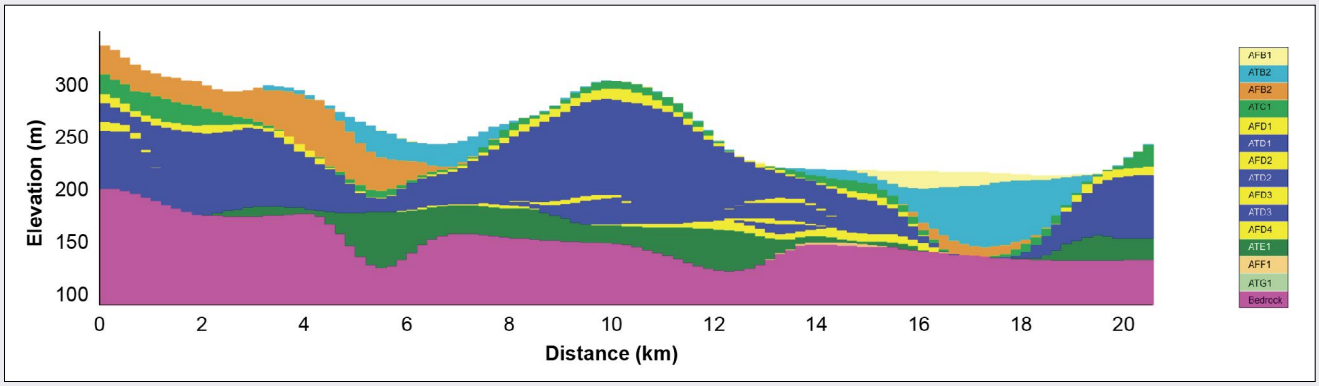


Figure 2. Geological section of the watershed highlighting distribution and continuity of respective hydrostratigraphic Units (HSU). HSU AFA1 and ATB1 are not present in the cross-section, and hence the legend.

HSU represents either an aquifer or an aquitard unit. The HSU code applied by the OGS (Bajc et al. 2015) is composed of four characters to identify the type of permeability and the geological formation of the HSU. The two first letters of the HSU code refer to the type of permeability: AF means "aquifer" and AT means "aquitard". The third letter refers to the formation (e.g., Thorncliffe) position of the unit (A to G, from top to bottom). The last character is a number related to its position in the formation, 1 represents the top and the number increases to the bottom of the unit.

Of the seventeen HSU, eight are considered to be aquifer units. Of those eight, six main aquifer units have more than one sample: AFB2, AFD1, AFD2, AFD4, AFF1 and a bedrock aquifer group made of Queenston, Lindsay, Georgian Bay formations. AFB2 is a gravely sand glaciofluvial unit forming a high permeability aquifer of the Oak Ridges Moraine. In the southern part of the watershed, this HSU is unconfined, can directly overlie bedrock, and be over 40 m thick. In the central and northern part of the watershed, this HSU is confined, occurs at a depth of 50 m, and is usually less extensive than in the southern part of the study area (Bajc et al. 2015). Units AFD1, ATD1, AFD2, ATD2, AFD3, ATD3 and AFD4 belong to the Thorncliffe Formation and consist of interbed aquifers and aquitards of finer-grained deposits with sand layers. AFD1, AFD2 and AFD4 are overlaid by aquitards for most of the watershed but are unconfined in small areas of the lowlands (central part of the watershed). Even where Thorncliffe Formation has a thickness >50 m, the aquifer components are usually <15 m thick. The Thorncliffe Formation is highly heterogeneous, with most of it considered as an aquitard with aquifers distributed within it. Nevertheless, it is an important HSU group in the study area. Connectivity with other HSU in the model has not been identified, however, there could be hydraulic connectivity between the Thorncliffe aquifers and surrounding aquifers through zones identified as aquitards. AFF1 consists of confined sand and gravel lenses in older glacial sediments. The permeable sand and gravel units are intercepted in a limited number of boreholes and form discontinuous lenses with small aerial extend surrounded by aquitard material. Due to the scarcity of sampling the individual occurrences have been combined in AFF1. Most HSUs have discontinuities due to erosional events and their thickness is variable, forming a complex structural arrangement.

3. Hydrogeochemical and isotopic data

3.1 On the use of hydrogeochemical and isotopic data

This study uses a hydrogeochemical and isotopic approach to understand the dynamics of the regional groundwater flow system. Hydrogeochemistry of the major ions (Ca, Na, Fe, Mg, NO_3, SO_4, HCO_3 and Cl) is an indicator of the chemical processes throughout the infiltration zone to the sampling location. Hydrogeochemistry is therefore used as an indicator for the water evolution in the system.

The stable isotopes used in the study were hydrogen δ^2H, oxygen $\delta^{18}O$, carbon $\delta^{13}C$ (dissolved organic carbon) and ^{14}C-DIC (dissolved inorganic carbon) and ^{226}Ra isotope of dissolved radium. δ^2H, $\delta^{18}O$ are used to understand the meteoritic conditions at the time of infiltration. Differences from the actual meteoritic signals would be signs of a colder or warmer meteoritic condition at the infiltration time. $\delta^{13}C$ and ^{14}C-DIC isotopes will be used for age dating to estimate the time since water infiltration at the surface. ^{226}Ra is used as an indicator of rock-water interactions, as a semi-quantitative time tracer to be compared with radiocarbon data and as a tool to identify anthropogenic contamination of the samples (Lagace et al. 2018).

3.2 Compilation of existing data

An initial database was compiled using data collected by the Geological Survey of Canada in 2016 and from the Oak Ridges Moraine Groundwater Program (Steve Holysh, personal communication 2018) provided by the Conservation Authorities Moraine Coalition (Figure 3). The compiled initial

database included a total of 66 wells with their corresponding depth, elevation, major ion concentration, pH and specific conductivity. Of these, sixteen wells had analysis of $\delta^{2}H$, $\delta^{18}O$ of water and $\delta^{13}C$, ^{14}C isotopes of DIC. This legacy data did not include any ^{226}Ra analysis.

A quality assurance and quality control (QA/QC) process was performed on the database to identify the wells with a consistent geochemical dataset, locate them, and assess the time period of sampling. The information was then analysed and interpreted to identify areas with a need for additional information for understanding of groundwater flow evolution.

The interpretation of compiled data revealed:

- areas with low geochemical information density,
- variable density and spatial distribution of samples by hydrostratigraphic and aquifer units,
- limited water geochemistry dataset regarding major ions, or isotopes, limiting the possibilities of interpretation.

Based on this information a groundwater sampling survey was planned in order to complement and complete the hydrogeochemical and isotope dataset. The outcome of the survey should help answer science questions raised by the preliminary data interpretation.

3.3 Survey in June 2018

A groundwater sampling survey was conducted in the 2018 field season in the Nottawasaga Valley Conservation Authority (NVCA) jurisdiction (Figure 3). Locations from the initial database and permits to take water reported in the Oak Ridges Moraine Groundwater Program database were identified. Some wells had been decommissioned or were not accessible, so alternative wells were used.

A total of twenty-four additional well sites were sampled. The PGMN well sampling protocol (McPhie and Post 2016) was used for the provincial wells. This protocol requires well construction information so that a volume estimation can be completed. At least three well volumes were purged before sampling. For the other wells, where the well volume was unknow, the CEAEQ protocol (CEAEQ 2012) was used, using physical parameters stabilisation as an indicator of adequate purging. For more details, please refer to the cited sampling protocols.

The sampled wells belong to one of three types: i) Provincial Groundwater Monitoring Network (PGMN), ii) municipal wells, and iii) domestic wells. The NVCA operates wells for the PGMN in this area and have conducted testing for geochemical parameters in these wells, but no sampling for isotopic analyses had been performed. The second type of well corresponds to municipal wells. Seven municipalities agreed to provide access for sampling and to provide historical data such as geochemical analyses and well infrastructure information. The third type was privately operated domestic wells. Unfortunately, for these wells no precise information on the screen depth could be obtained.

3.4 Definition of a reliability index for the interpretation of geochemical data

Due to different sampling conditions, varying sources, and differing availability of data, the database analysis was complicated. For most of the samples the HSU was not known and needed to be assigned to permit data integration and interpretation. The geochemical parameters were obtained from different laboratories, time periods and geochemical surveys. There was therefore a need for a critical assessment of the reliability of each sample.

A reliability index was created as a tool for more effective interpretation of geochemical data (Table 1). A three digits system was developed to describe every data entry. It is

Table 1. Reliability index code and definitions.

Factor	Code	Definition
Source	P	Polytechnique – geochemical survey
	C	Geological Survey of Canada – geochemical survey
	H	Oak Ridges Moraine Groundwater Program – geochemistry database
Screen position's quality	A	The screen is located within a unique aquifer
	B	The screen is located in one aquifer and partially in an aquitard
	C	The screen is located within in an aquitard, but close to an aquifer (+/- 5 m)
	D	The screen is surrounded by metres of aquitard
Geochemistry	1	Geochemistry contains every major ion & ionic balance error <15%
	2	Geochemistry does not contain every major ion & ionic balance error <15%
	3	Geochemistry contains every major ion & ionic balance error >15%
	4	Geochemistry does not contain every major ion & ionic balance error >15%

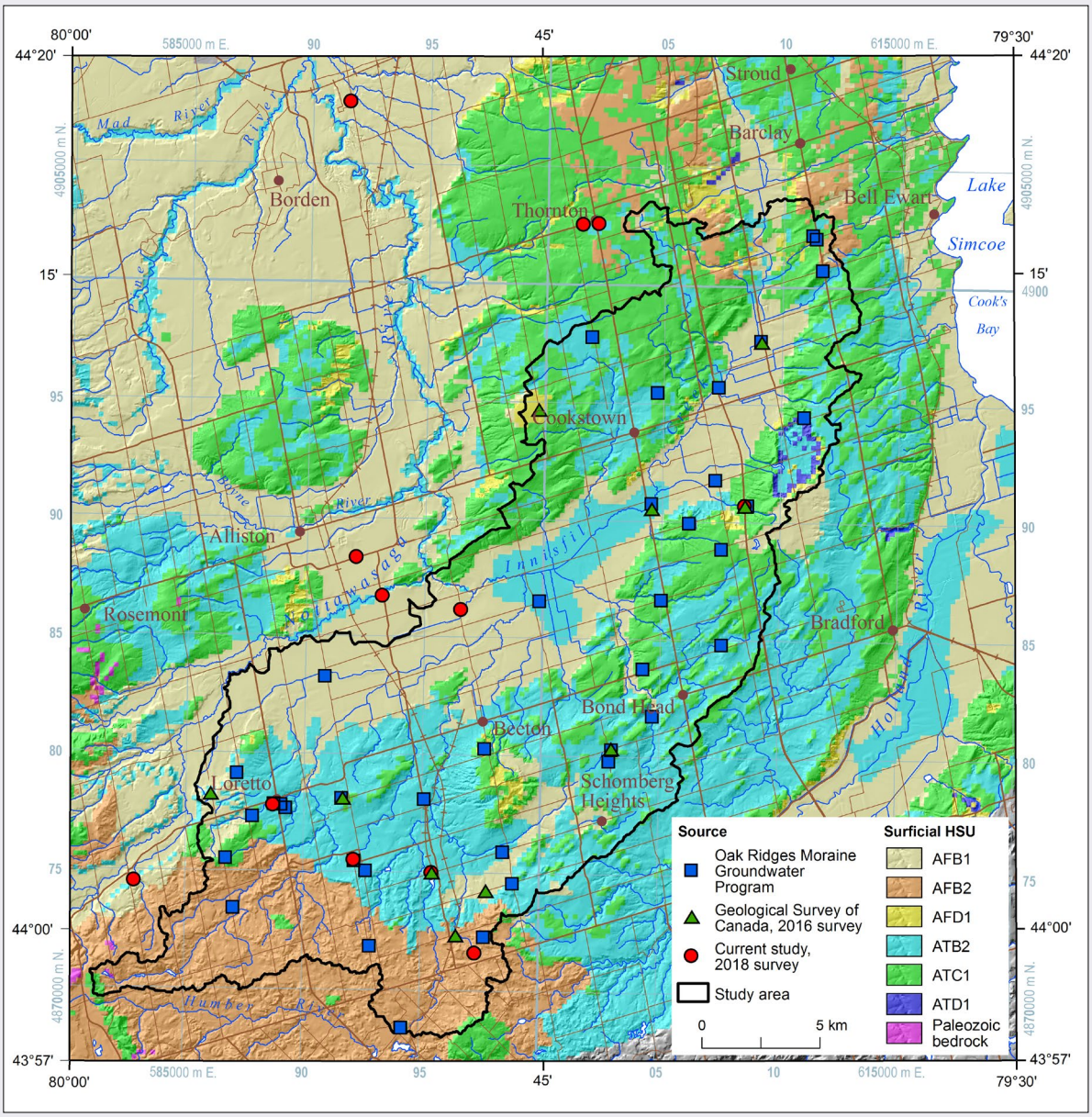


Figure 3. Location of hydrogeochemical data sites overlain on the surficial hydrostratigraphic units (HSU) draped on the regional DEM.

composed of three factors, as detailed in the next sub-sections: i) source of the data, ii) reliability of screen's position within an aquifer, and iii) quality of the geochemical analysis obtained.

3.4.1 Reliability factor 1: Source of the data

The first reliability factor aims at identifying the origin of the sample. There are three listed sources: Oak Ridges Moraine Groundwater Program, Geological Survey of Canada 2016 survey, and Polytechnique 2018 survey. Data from recent surveys by Polytechnique Montreal and Geological Survey of Canada are comprehensively documented with comments and boring logs compiled during the surveys at owner/operator offices. These samples are also linked to a known sampling protocol, laboratory and conservation procedure, so it is relatively straightforward to evaluate the data reliability.

3.4.2 Reliability factor 2: Screen position

One of the challenges of the study was to accurately identify the hydrostratigraphic interval intercepted by well screens in the database. The preliminary 3-D hydrostratigraphic model of the region developed by the Ontario Geological Survey (Bajc et al. 2015) provided the necessary framework (Benoit

et al. 2018). Knowing the location and depth of the well, the screen length was linked to intercepted units within the 3-D geology model. The number of intercepted hydrostratigraphic units can vary from 1 to 3 (depending upon the length of the screen), and may include different aquifers and aquitards. The assigned screen – HSU intersection were sometimes inconsistent, as when the screen was located within an aquitard by the model. In such cases, water volumes extracted during the sampling provided confirmation of the validity of the an HSU assignment, e.g., where the permeability of the aquitard(s) would not have provided the volume of water extracted. To resolve such inconsistencies, it was decided that the sampled aquifer should be validated for every well from the database before further analysis.

Every well screen was located within the 3-D model or compared to borehole logs to identify its corresponding hydrostratigraphic unit (Figure 4). This step revealed significant differences in the validity of some of the pre-existing data. The majority of screens were related to a single aquifer (97%). The remaining 3% of the screens were either (1) located in an aquitard, but close to an aquifer (+/- 5 m), or (2) more than 10 metres from an aquifer. It was determined that these wells had only minor inconsistencies between their depth and the model information. For screens >10 metres from an aquifer

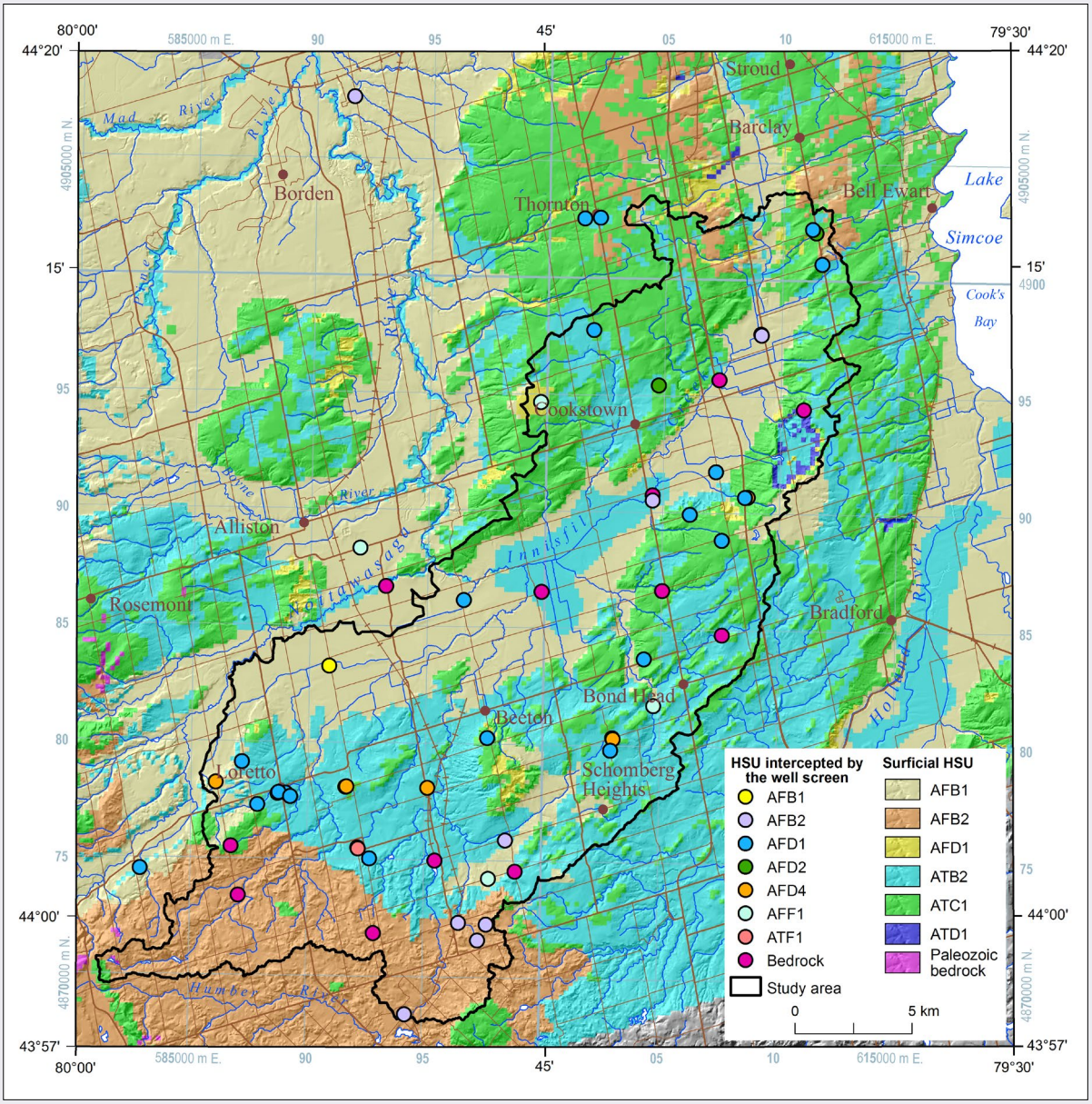


Figure 4. Hydrostratigraphic units associated with borehole screen depth plotted on a background surficial hydrostratigraphic units (HSU) draped on the regional DEM.

the HSU was assigned with the surrounding sediments. Facing these different levels of uncertainty within the dataset, the reliability factor for the screen position appeared to be a useful tool. Locations with greater uncertainties were identified and could be omitted from the modelling exercise if their uncertainties were influencing the interpretation.

The database has an uneven distribution of samples between various hydrostratigraphic units, which reflects the availability of wells available for sampling (Figure 4). The HSU with the lowest sample density are AFB1 (1 sample), AFD2 (8 samples) and AFF1 (6 samples). In contrast, AFB2 (25 samples), AFD1 (29 samples), AFD4 (13 samples) and bedrock (19 samples, 1 in Queenston formation, 8 in Georgian Bay formation and 10 in Lindsay formation) have larger datasets.

3.4.3 Reliability factor 3: Geochemical data

The reliability of existing geochemical analyses was identified as a challenge for the study. Uncertainties in some of the measured ion values would affect the interpretation. An approach to reveal the existence of incorrect determinations is to calculate the ion balance error (e.g., Clark 2015) of a sample: as electronegativity is always achieved in any water samples, positive (cations) and negative (anions) ions are necessarily equilibrated. Ion balance errors (IBE) were therefore calculated. A reliability factor for the quality of geochemical data was created by considering an IBE tolerance of ±15% as a maximum threshold for acceptable samples. This value is higher than in small-scale studies, but often considered reasonable in regional contexts (e.g., Beaudry et al. 2018). With 15% tolerance, 91% of the database samples were retained. With 10% tolerance, only 76% would have been retained.

4. Preliminary results and discussion

4.1 Survey wells selection

Aquifers with few or no sampling sites in the database were identified as a primary objective of the current study. Limited information on the study zone could be compared to a neighbouring watershed, as long as the same hydrostratigraphic unit (HSU) was sampled. Adding more sampling locations in poorly sampled aquifers, including outside the surface watershed boundaries, allowed for a more regional view on the aquifer dynamics and recharge. A secondary objective of this survey was to add new information to the isotope database to assist with the geochemical interpretation. $\delta^{2}H$, $\delta^{18}O$, $\delta^{13}C$ have been sampled at every well. ^{14}C-DIC was sampled on strategic wells. Wells in a confined context, with low activities of $\delta^{2}H$, $\delta^{18}O$ from previous studies and where a vertical comparison with a nearby well could be done were identified as the main needs for a ^{14}C-DIC survey.

Despite a concerted effort to sample the maximum number of wells during a three weeks field survey, several information gaps remain. Some areas do not have wells, or it was not possible to coordinate sampling with the well owner. Another gap is water quality information in the deeper hydrostratigraphic units, due to a lack of deep wells. In the study area, it is unusual for people to withdraw water from deep aquifers when water is recoverable from shallow aquifers. The complete database includes 84 wells (Figure 3).

4.2 Reliability index

The entire dataset was classified according to the screen and geochemical reliability factors and to the resulting reliability index (tables 2 and 3). Data with less reliability could then be easily identified and excluded from the analysis and modelling. As illustrated in Table 2 and 3, 69% of the samples come from wells with screens (Table 2 and 3), 92% of the samples feature the main data on geochemistry and ionic balance error lower than the absolute tolerance of 15% (Table 2 and 3). Finally, 61% combine the well screen with acceptable geochemical data (B or 2 as the lowest reliability index). Samples from the GSC and current surveys were grouped in tables 3 because field notes are available for these samples, allowing further verification of sampling procedures.

4.3 Ionic balance

Despite the presence of all major ions and using a +/- 15% threshold for the ionic balance some data, mostly archival information, did not meet acceptable ionic balances to reliably include them in the analysis, High ionic balance errors for a number of samples could not be explained, since the description of the sampling methods, sample preservation, and laboratory analysis procedures were not sufficiently detailed. For some

Table 2. Oak Ridges Moraine Groundwater Program combined reliability index (n = 76)

	1	2	3	4	Total
A	41	3	2	3	49
B	1	0	0	0	1
C	7	1	0	0	8
D	14	2	0	2	18
Total	63	6	2	5	76

Table 3. Geological Survey of Canada and current surveys combined reliability index (n = 38)

	1	2	3	4	Total
A	26	0	2	0	28
B	3	0	0	0	3
C	2	0	0	0	2
D	5	0	0	0	5
Total	36	0	2	0	38

other samples, the imbalance could be explained by inadequate values for dissolved carbonates. In most cases, this parameter was later measured in the laboratory rather than by titration in the field. Dissolved carbonates (HCO_3) are likely to vary significantly when groundwater is exposed to the atmosphere, since CO_2 degassing can affect the balance and speciation of dissolved carbonates. If the sample was not properly sealed or if the sample contained air, the sample can equilibrate with air and the HCO_3 value would be underestimated.

4.4 Piper diagram

4.4.1 General Piper diagram

A Piper Diagram of the complete dataset (Figure 5) illustrates variable water types from the different aquifers. Every HSU except AFD2 present a distribution of the water type throughout the Ca-HCO_3 and Na-Cl poles. There is no specific water type for any aquifer. Many factors such as geographic position, proximity to a recharge zone, screen depth, and other parameters could explain the variations in water types. The observed trends need further and specific investigation that will be provided by the ongoing project. The high variability of the geochemistry and the low association between geochemistry and HSU (Figure 5) confirms the relevance of our hydrogeochemical and isotopic approach to provide complementary insights to understand the hydrogeochemical evolution of groundwater and the conditions at the infiltration time.

Many parameters interact together to explain the hydrogeochemical results from the samples. Combining all the wells, with different depths, confinement, associated geological unit and other geochemical drivers in a single figure makes a complex figure for interpretation. The geochemistry itself

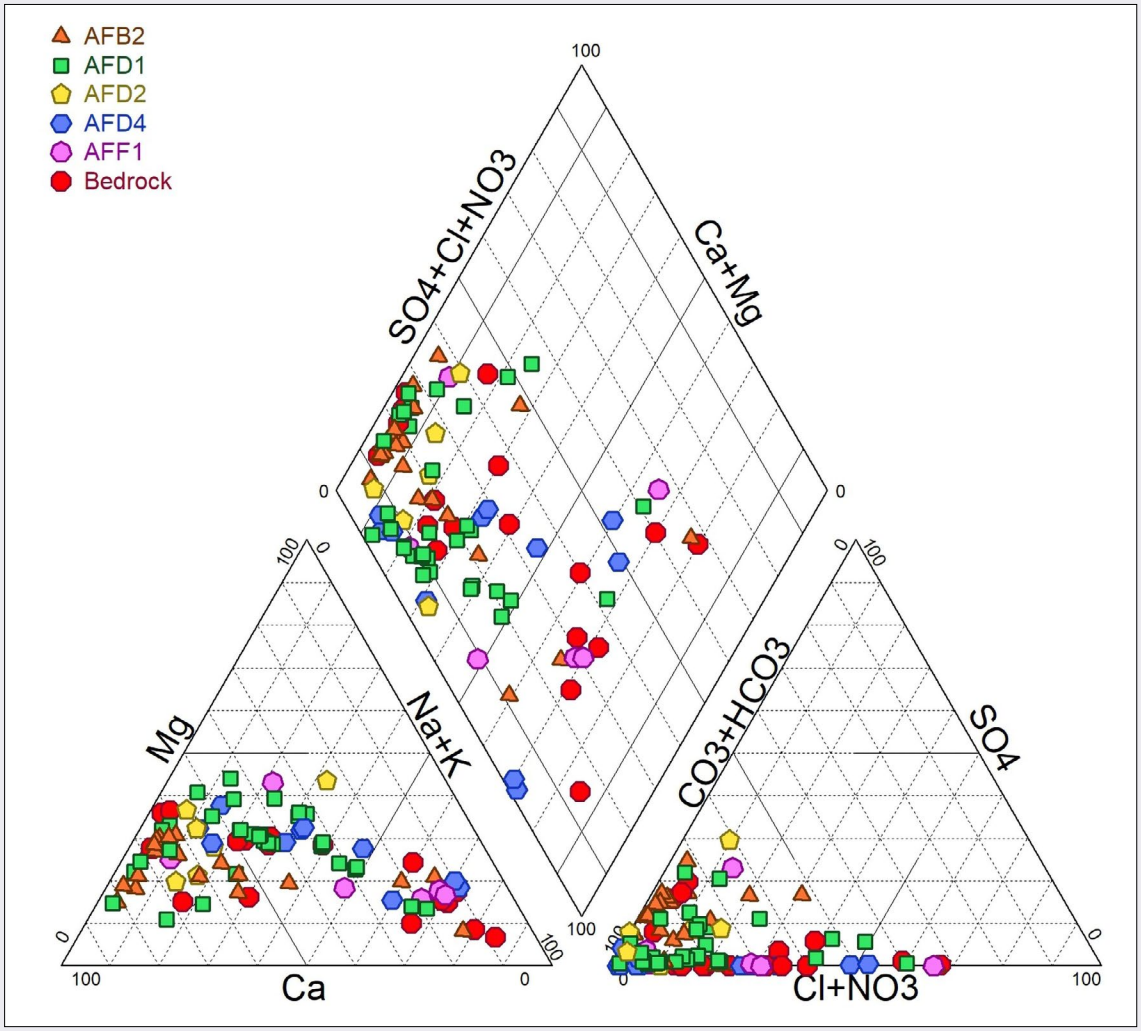


Figure 5. Piper plot (top) and location of the AFB2 aquifer samples with hydrostratigraphic units (HSU) in background (bottom).

could be more easily explained if parameters with a possible influence on the hydrogeochemistry could be separated.

As described previously, the glaciofluvial unit AFB2 is of interest due to its high aquifer potential and its complex 3-D spatial distribution. In the lowlands, the unit is confined below thick low permeability deposits and shows a low vulnerability to direct surface contamination. However, in the southern part of the study area, AFB2 is unconfined and is in a preferential recharge area, with higher vulnerability. The evolution of the groundwater within AFB2 from the recharge area to deep buried valley in the lowland is of important interest for resource characterization. A case study of AFB2 is presented below.

4.4.2 AFB2 Piper diagram and preliminary interpretation

This section presents preliminary results using a Piper diagram corresponding to aquifer AFB2 (Figure 6 and table 4). Water types were separated into distinct geochemical groups (Ca-HCO_3, Na-HCO_3 and Na-Cl). Only screen reliability index values from A to C and geochemical reliability index values from 1 and 2 were used, thus ensuring that low-quality data (categories D, 3 and 4) would not influence the interpretations (Table 4). A total of 24 analyses from 12 wells were considered.

The southern part of the region, next to Beeton, has a calcium-bicarbonate (Ca-HCO_3) type of water (Figure 6) and is found in five locations, one of which was sampled thirteen times. In the upper central part of the area, southeast of Cookstown, the aquifer has a mixed sodium-bicarbonate Na-CO_3 water type, while northeast of Cookstown, samples have a sodium-chloride (Na-Cl) water type. These results suggest different processes affecting groundwater water types in this shallow aquifer unit. The Ca-HCO_3 water type is generally characteristic of recent recharge. The corresponding samples are located in a higher elevation area (southern part of the watershed) where AFB2 unit is outcropping. On the other side of the area, the three samples from this aquifer are confined by an aquitard (ATB2) and show a geochemical signature usually describing older groundwater. This process could include mixing water from different units and ionic exchange. Further work is ongoing to investigate this preliminary interpretation using isotopic data. When integrated with other hydrogeologic information, such preliminary interpretations can support the development of a conceptual model of groundwater flow of the Innisfil Creek watershed.

5. Future work

In addition to the current results, further geochemical interpretation will be undertaken, including multivariate analysis to strengthen the definition of geochemical end-members and the description of geochemical evolution.

Isotopes analysis have been recently completed in the laboratory and the interpretation is ongoing. The addition also of stable δ^2H and $\delta^{18}O$ isotopes of water to the interpretation will help improve understanding of water origin, mixing between groundwater masses, and recharge dynamics. Evaporation signals and isotope ratios will be used to compare zones

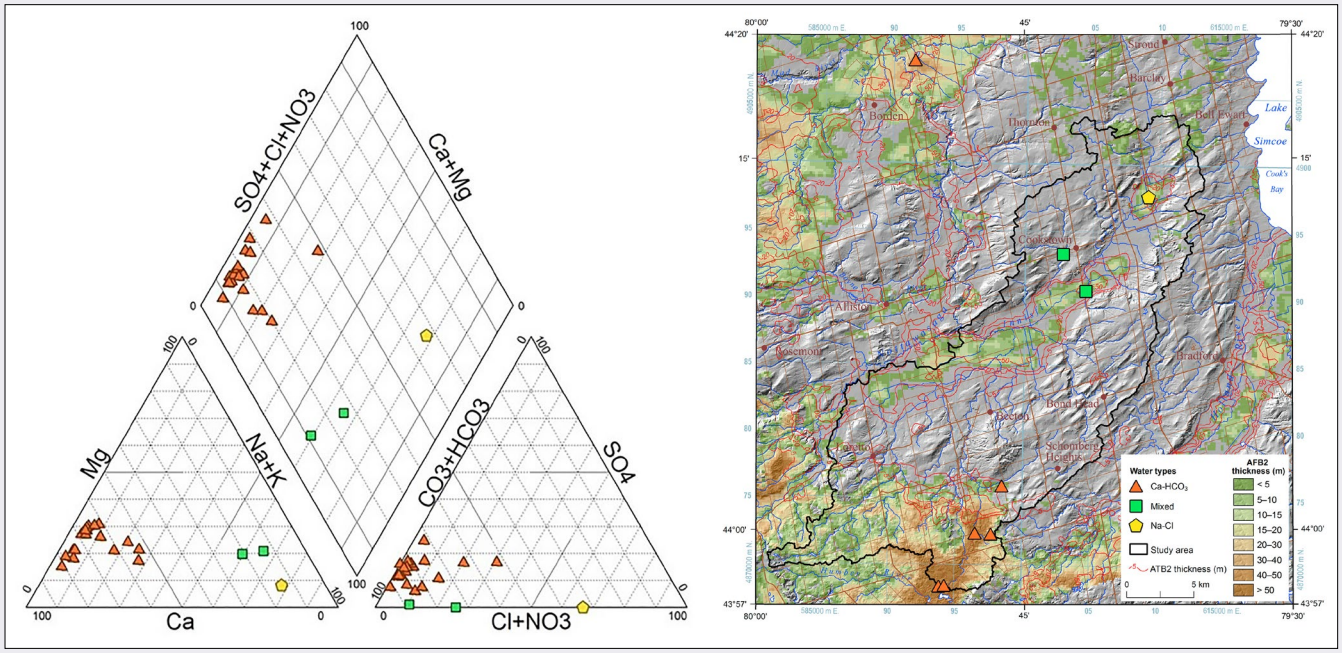


Figure 6. Left: Piper plot for AFB2 samples. Right: Location of the main water types of AFB2 samples and thicknesses of ATB2 and AFB2.

Table 4: AFB2 geochemical dataset.

Project ID	Reliability factors	Ca(meq/L)	Na(meq/L)	Fe(meq/L)	Mg(meq/L)	SO_4(meq/L)	HCO_3(meq/L)	Cl(meq/L)
IC-10	PA1	3.57	0.22	0.03	1.40	0.97	4.23	0.40
IC-13	PB1	3.56	0.21	0.02	1.01	0.70	4.43	0.17
IC-20	PA1	2.81	0.81	0.01	0.96	0.23	3.30	0.32
IC-24	PA1	4.46	0.36	0.00	1.07	0.55	3.89	0.45
IC-28	CA1	0.78	3.78	0.01	1.20	0.00	3.48	1.21
IC-31	CA1	0.95	5.22	0.01	0.54	0.00	1.98	3.95
IC-33	CA1	3.34	0.14	0.00	0.80	0.79	2.31	0.11
IC-34	CA1	5.30	0.36	0.04	1.51	0.92	3.52	1.13
IC-40	HA1	5.30	0.26	0.01	0.99	0.52	5.38	0.34
IC-41	HC1	4.50	2.22	0.00	1.40	1.08	3.43	1.78
IC-42	HA1	2.90	0.23	0.01	1.23	0.52	3.69	0.09
IC-43	HA1	3.09	0.26	0.01	1.23	0.26	3.26	0.04
IC-44	HA1	2.10	0.78	0.00	0.91	0.29	3.21	0.42
IC-45	HA1	2.00	0.96	0.00	0.80	0.56	2.98	0.17
IC-46	HA2	3.11	0.23	0.01	1.32	0.58	4.08	0.00
IC-47	HA1	3.04	0.22	0.01	1.29	0.55	4.21	0.07
IC-48	HA1	3.29	0.23	0.01	1.43	0.55	4.16	0.08
IC-49	HA1	2.69	0.21	0.01	1.25	0.61	3.07	0.08
IC-50	HA1	2.30	0.30	0.02	1.15	0.62	3.13	0.13
IC-51	HA1	2.82	0.20	0.02	1.26	0.60	2.85	0.07
IC-52	HA1	2.40	0.26	0.02	1.15	0.62	3.44	0.11
IC-53	HA1	2.87	0.49	0.00	1.18	0.52	2.98	0.07
IC-54	HA1	3.04	0.22	0.01	1.28	0.55	4.08	0.08
IC-83	HA1	1.30	3.70	0.03	1.23	0.06	5.38	0.62

with apparent water evolution. In addition, ongoing ^{14}C-DIC dating will be used to calculate groundwater mean residence time of the samples. Links between mean residence time and sources of water will therefore be considered. Dating will also be a powerful asset to estimate the mixtures between different hydrostratigraphic units with the help of Lumped Parameters Models (e.g., Jurgens et al. 2012). ^{226}Ra would be a good indicator of the anthropogenic influence on the water chemistry. It will also help to improve overall understanding of the data used in the study.

To synthetize all interpretations of the groundwater dynamics and evolution within the Innisfil Creek watershed, the last step will be the creation of a conceptual model of groundwater flow. The model will show hydrostratigraphic flow interaction, flow lines, and geochemical evolution and mixing. Preferential recharge zones will be suggested, and impact of confinement will be discussed. Finally, some insight regarding climatic and anthropogenic impacts will be suggested.

6. Summary

This paper presents the progress of a groundwater hydrogeochemistry and stable isotope study of the Innisfil Creek watershed. Diverse data sets, from three main sources

were utilized. The preliminary database was validated and interpreted to plan and undertake a new survey that could fill the main identified data gaps. A complete database was built, and a reliability index was created to ensure better control of data quality and to provide more robust interpretations. Preliminary results presented have generated scientific questions to be addressed in the next phase of the study. Future work will include stable isotopic data analyses and further geochemical analyses to permit the development of a conceptual hydrogeochemical model of the Innisfil Creek watershed.

7. Acknowledgements

An internal review at the Geological Survey of Canada (GSC) was completed by M. Hinton. This contribution is part of a MSc study by the first author at the École Polytechnique de Montréal. This work was funded by the GSC and Polytechnique Montreal. This is a contribution of the GSC–OGS Southern Ontario project on groundwater 2014–2019.

8. References

Bajc, A.F., Mulligan, R.P.M., Rainsford, D.R.B., and Webb, J.L. 2015. Results of 2011–13 overburden drilling programs in the southern part of the County of Simcoe, south-central Ontario. Ontario Geological Survey, Miscellaneous Release—Data 324.

Beaudry, C., Lefebvre, R., Rivard, C., and Cloutier, V. 2018. Conceptual model of regional groundwater flow based on hydrogeochemistry (Montérégie Est, Québec, Canada). Canadian Water Resources Journal, 43(2): 152-172. https://doi.org/10.1080/07011784.2018.1461579

Benoit, N., Marcotte, D., Boucher, A., D'Or, D., Bajc, A., and Rezaee, H. 2018. Directional hydrostratigraphic units simulation using MCP algorithm. Stochastic Environmental Research and Risk Assessment, 32: 5, 1435-1455. https://doi.org/10.1007/s00477-017-1506-9

CEAEQ. 2012. Guide d'échantillonnage à des fins d'analyses environnementales. Chap 3 : Échantillonnage des eaux souterraines. Centre d'expertise en analyse environnementale du Québec. Québec http://www.ceaeq.gouv.qc.ca/documents/publications/echantillonnage/eaux_soutC3.pdf

Clark, I. 2015. Groundwater geochemistry and isotopes. Boca Raton, Florida, CRC press. 456 pp.

Cloutier, V., Lefebvre, R., Savard, M.M., Bourque, É., and Therrien, R. 2006. Hydrogeochemistry and groundwater origin of the Basses-Laurentides sedimentary rock aquifer system, St. Lawrence Lowlands, Québec, Canada. Hydrogeology Journal, 14: 4, 573-590. https://doi.org/10.1007/s10040-005-0002-3

Crossman, J., Futter, M.N., Oni, S.K., Whitehead, P.G., Jin, L., Butterfield, D., and Dillon, P.J. 2013. Impacts of climate change on hydrology and water quality: future proofing management strategies in the Lake Simcoe watershed, Canada. Journal of Great Lakes Research, 39: 1, 19-32. https://doi.org/10.1016/j.jglr.2012.11.003

Eyles, N., Clark, B.M., Kaye, B.G., Howard, K.W.F., and Eyles, C. 1985. The application of basin analysis techniques to glaciated terrains: an example from the Lake Ontario basin, Canada. Geoscience Canada 12: 22–32.

Hamilton, S. 2018. The use of wide-spectrum groundwater geochemistry in regional groundwater mapping in Ontario, In Regional-scale groundwater geoscience in southern Ontario : an Ontario Geological Survey, Geological Survey of Canada, and Conservation Ontario geoscientists open house. Geological Survey of Canada, Open File 8363, 45 p. https://doi.org/10.4095/306472

Holysh, S. 2018. Personal communication. Oak Ridges Moraine Groundwater Program, March 13, 2018. Regional Municipalities of York, Peel, and Durham, and the City of Toronto and Conservation Authorities Moraine Coalition, https://oakridgeswater.ca

Jurgens, B.C., Böhlke, J.K., and Eberts, S.M. 2012. TracerLPM (Version 1): An Excel® workbook for interpreting groundwater age distributions from environmental tracer data. U.S. Geological Survey Techniques and Methods Report 4-F3, 60 p.

Lagace, F., Foucher, D., Surette, C., and Clarisse, O. 2018. Radium geochemical monitoring in well waters at regional and local scales: an environmental impact indicator-base approach. Chemosphere, 205, 627-634. http://dx.doi.org/ 10.1016/j.chemosphere.2018.04.098

Marchildon, M., Thompson, P.J., Cuddy, S., Wexler, E.J., Howson, K., and Kassenaar, J.D.C. 2016. A methodology for identifying ecologically significant groundwater recharge areas. Canadian Water Resources Journal, 41: 4, 515-527. http://dx.doi.org/10.1080/07011784.2015.1080125

Matrix Solutions Inc and Blumetric Environmental Inc. 2017. Innisfil Creek drought management plant pilot summary report Report 16568-528, BluMetric Environmental and Matrix Solution Inc, Kitchener 35pp https://www.nvca.on.ca/Shared%20Documents/Innisfil_Creek_Drought_Management_Pilot_Summary.pdf

McPhie, S. and Post, R. 2016. Annual Groundwater Monitoring Report - 2015. Nottawasaga Valley Conservation Authority, Utopia https://www.nvca.on.ca/Shared%20Documents/NVCA_Annual_Groundwater_Monitoring_Report_2015_web.pdf

Mulligan, R.P.M. and Bajc, A.F. 2018. The pre-Late Wisconsin stratigraphy of southern Simcoe County, Ontario: implications for ice sheet buildup, decay, and Great Lakes drainage evolution. Canadian Journal of Earth Sciences, 55: 7, 709–729. https://doi.org/10.1139/cjes-2016-0160

Mulligan, R.P., Eyles, C.H., and Bajc, A.F. 2018. Stratigraphic analysis of Late Wisconsin and Holocene glaciolacustrine deposits exposed along the Nottawasaga River, southern Ontario, Canada. Canadian Journal of Earth Sciences, 55: 7, 863–885. https://doi.org/10.1139/cjes-2017-0081

Nottawasaga Valley Conservation Authority. 2006. Innisfil Creek Subwatershed Plan. http://www.nvca.on.ca/Shared%20Documents/Innisfil%20Creek%20Subwatershed%20Plan.pdf

Oni, S. K., Futter, M. N., Molot, L. A., Dillon, P. J., and Crossman, J. 2014. Uncertainty assessments and hydrological implications of climate change in two adjacent agricultural catchments of a rapidly urbanizing watershed. Science of the Total Environment, 473: 326-337. https://doi.org/10.1016/j.scitotenv.2013.12.032

Post, R. and Mills, A. 2018. Hydrologic Function: Framework Considerations and Approach to Subwatershed Baseline Characterization. Nottawasaga Valley Conservation Authority, Utopia https://www.nvca.on.ca/Shared%20Documents/NVCA_Hydrologic_Function_Report_2018.pdf

Sharpe, D.R., Pugin, A.J.-M., and Russell, H.A.J. 2018. Geological framework of the Laurentian Trough aquifer system, southern Ontario. Canadian Journal of Earth Sciences, 55: 7, 677–708. https://doi.org/10.1139/cjes-2017-0113

Assessment of nearshore groundwater discharge to Lake Simcoe, Ontario and identification of regional hydrogeological controls

Hayley Wallace[1] and Clare E. Robinson[1]*

Abstract: Groundwater discharge may be an important pathway for delivering pollutants to large lakes, but this pathway is not well understood. The objective of this study was to quantify the spatial variability and volume of direct nearshore groundwater discharge to Lake Simcoe, Ontario, and evaluate linkages between the observed spatial distribution of groundwater discharge and regional hydrogeological features. Direct nearshore groundwater discharge was quantified using the naturally occurring radon isotope tracer, ^{222}Rn. Boat surveys were conducted along 80% of the Lake Simcoe shoreline using portable radon detection equipment. Shoreline areas with high direct groundwater discharge were identified and the total direct nearshore groundwater discharge to Lake Simcoe was estimated to be 11.3 ± 2% of the total tributary inputs. Shoreline areas with high groundwater discharge were related to the presence of permeable nearshore surficial sediments and tunnel channel deposits. These features are thought to provide connectivity between the regional aquifer system and the lake. The study findings can be broadly applied in other studies evaluating direct groundwater inputs into large lakes of glacial origin.

1. Introduction

The influence of direct groundwater discharge on the water quality in large lakes is often poorly understood despite recent studies showing that groundwater-derived pollutants can impact lake water quality and ecosystem health (Lewandowski et al. 2015; Meinikmann et al. 2015; Naranjo et al. 2019). The magnitude of groundwater discharge is often a small component of the water budget for large lakes: however, concentrations of pollutants can be elevated in groundwater compared to surface waters leading to high groundwater-derived pollutant loads to a lake (Lewandowski et al. 2015; Naranjo et al. 2019). For instance, shallow urban groundwater adjacent to Lake Simcoe, a large inland lake in southern Ontario (Figure 1) and the focus of this study, has been shown to have high concentrations of pollutants including nitrate, ammonium, phosphorus, and chlorinated solvents (Roy & Malenica 2013). Evaluating the magnitude of groundwater discharge to large lakes and its potential impact on lake water quality is challenging as groundwater discharge is generally characterized by low specific fluxes as well as high spatial variability (Dimova et al. 2013; Kornelsen and Coulibaly 2014; Rosenberry et al. 2015).

Local- and regional-scale field methods for quantifying groundwater discharge into lakes are available. Methods include seepage meters, hydraulic gradient/piezometer measurements, numerical groundwater models, electrical resistivity tomography (ERT) imaging, thermal imaging, and geochemical/isotope tracer methods (e.g., Dimova et al. 2013; Karan et al. 2014; Kazmierczak et al. 2016; Meinikmann et al. 2015; Sebok et al. 2013). A tracer that has been applied to estimate groundwater discharge in lake, marine, and riverine environments is the naturally occurring radioactive isotope, radon-222 (^{222}Rn) (e.g., Burnett and Dulaiova 2003; Cable et al. 1996; Dimova et al. 2013). Tracers such as ^{222}Rn are generally more suitable for regional scale groundwater discharge investigations, as opposed to seepage meters and hydraulic gradient measurements, which are local scale measurement techniques (Burnett et al. 2006; Ji et al. 2017).

Groundwater discharge to lakes is often highly spatially variable. Understanding this variability is challenging, but identifying areas with high groundwater discharge is needed to determine areas where groundwater is more likely to impact lake water quality. Groundwater can enter a lake indirectly, through tributaries that are groundwater fed and flow into the lake, or directly through discharge from (often multiple) aquifers. This study focuses specifically on direct nearshore groundwater discharge. Many factors control the spatial variability of direct groundwater discharge. These include regional aquifer sediment type (i.e., hydraulic conductivity,

[1] Civil and Environmental Engineering, Western University, London, ON N6A 5B9

*corresponding author: crobinson@eng.uwo.ca

Recommended citation: Wallace, H. and Robinson, C.E. 2020. Assessment of nearshore groundwater discharge to Lake Simcoe, Ontario and identification of regional hydrogeological controls. In Russell, H.A.J. and Kjarsgaard, B.A. Eds. Southern Ontario groundwater project 2014–2019: summary report. Geological Survey of Canada, Open File 8536, 191-201. https://doi.org/10.4095/321105

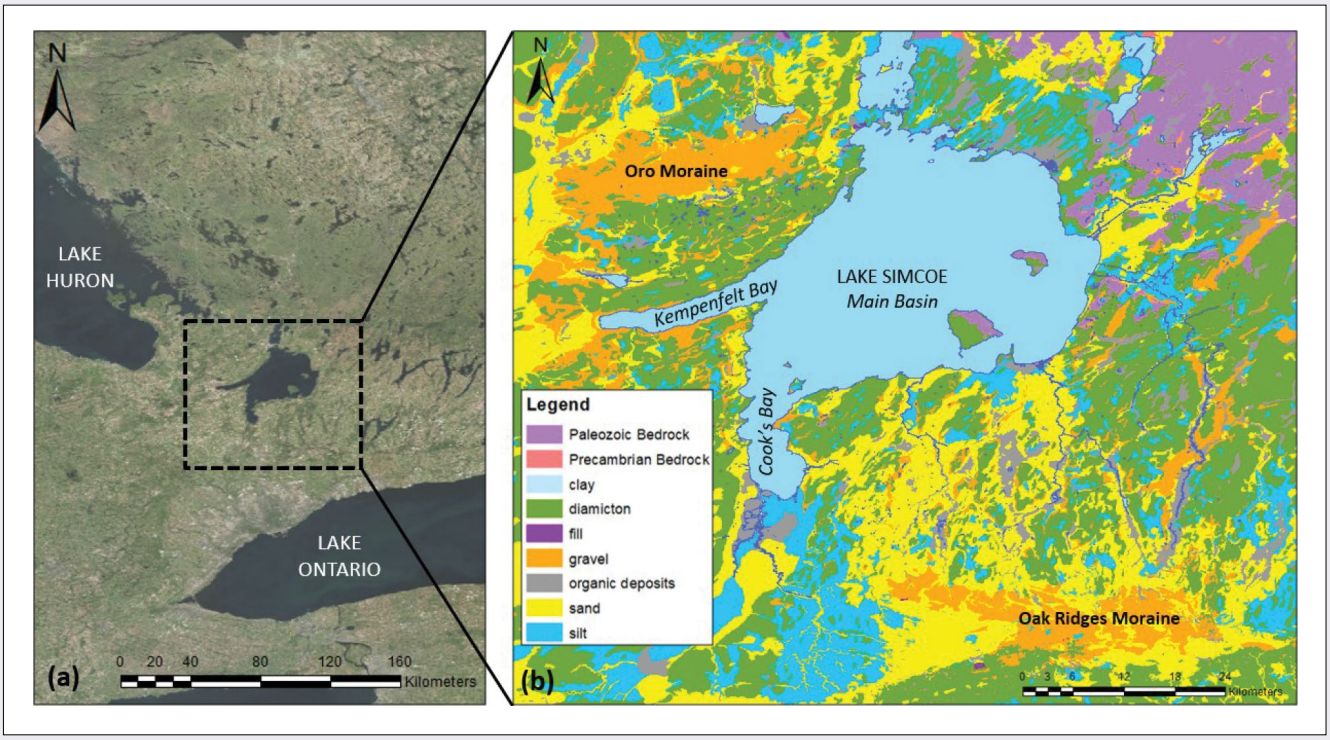


Figure 1. (a) Location of Lake Simcoe in southern Ontario, Canada, and (b) surficial geology around Lake Simcoe modified from (Ontario Ministry of Northern Development and Mines 2016).

preferential flow paths), the hydraulic gradient between the groundwater piezometric levels and the lake, shoreline configuration, nearshore topography, and anthropogenic modifications to the shoreline (e.g., manmade canals and erosion control structures) (Cherkauer and Hensel 1986; Cherkauer and McKereghan 1991; Kornelsen and Coulibaly 2014; Schneider et al. 2005; Tecklenburg and Blume 2017). In general, direct groundwater discharge into a lake from a shallow unconfined aquifer is highest close to the shoreline and decreases further offshore but this depends on the homogeneity of the adjacent aquifer system (Kazmierczak et al. 2016; Lee 1977; Pfannkuch and Winter 1984; Tecklenburg and Blume 2017). In some lakes, complex hydrogeological conditions including aquifer heterogeneity and the presence of deeper confined layers that intersect the lake bed can lead to high groundwater discharge offshore (Fukuo and Kaihotsu 1988; Schneider et al. 2005; Woessner and Sullivan 1984).

Although ^{222}Rn has been previously used to quantify regional scale direct groundwater discharge into large lakes, prior studies (e.g., Burnett et al. 2017; Corbett et al. 1997; Dimova and Burnett 2011; Dimova et al. 2013; Schmidt et al. 2010) provide limited insight into the factors controlling the observed spatially variability, particularly the hydrogeological controls. Regional scale assessment of groundwater discharge is resource intensive so there is a need to develop transferrable knowledge that can be applied to more easily identify areas of high groundwater discharge to large lakes of glacial origin. Schneider et al. (2005) investigated groundwater discharge into a glacial lake, Oneida Lake, NY, using seepage meter measurements and found that the deeper bedrock geology and regional precipitation patterns had a larger influence on the spatial distribution of groundwater discharge than the local surficial sediment type. More recently, Ji et al. (2017) conducted ^{222}Rn and electrical resistivity measurements in Nottawasaga Bay, Lake Huron and demonstrated that a zone of high direct groundwater discharge occurred where a large tunnel channel aquifer feature intersected the lake shoreline. These findings vary from other studies conducted in more homogeneous geological settings, which indicate the importance of surficial sediment type and topography (e.g., Tecklenburg and Blume 2017).

Lake Simcoe, a large lake of glacial origin in Southern Ontario (Figure 1), represents an ideal setting for evaluating the influence of the hydrogeology on spatial variability in groundwater discharge due to the diverse geological conditions around the lake. Over the past several decades rapid population growth combined with intensification of agriculture in the Lake Simcoe watershed has led to the deterioration of the ecological health of the lake (North et al. 2013; Young et al. 2011). Increased nutrient loading to the lake, particularly phosphorus, has stimulated algal growth, reduced dissolved oxygen levels, and in turn impaired cold-water fish habitats (Eimers et al. 2005; North et al. 2013; Winter et al. 2007). Lake water quality management actions have largely focused

on point source and tributary inputs in an effort to reduce nutrient (and other pollutant) loads, while little attention has been given to quantifying direct groundwater inputs (Winter et al. 2007). Seismic surveys revealed the presence of large submarine hollows at the bottom of Kempenfelt Bay (Lewis et al. 2007). These are thought to be zones of groundwater discharge causing local differences in oxygen concentrations and affecting the local habitat for cold-water fish (North et al. 2013). Aside from this work, there has been no attempt to quantify direct groundwater discharge into Lake Simcoe.

The study objectives are to (i) characterize the spatial distribution of direct nearshore groundwater discharge to Lake Simcoe, (ii) compare the total direct nearshore groundwater discharge to Lake Simcoe to tributary inputs, and (iii) evaluate potential links between spatial variability in groundwater discharge and hydrogeological features. To our knowledge, no prior studies have used ^{222}Rn to quantify the total nearshore direct groundwater discharge to a lake as large as Lake Simcoe (722 km^2), and assessed factors controlling the spatial variability in groundwater discharge to a large glacial lake. The study findings are needed to improve understanding and quantification of the contribution of direct groundwater discharge to the lake water and chemical budgets.

2. Field site

Lake Simcoe is the largest lake in Ontario, aside from the Laurentian Great Lakes, with a surface area of 722 km^2, shoreline of 240 km, and contributing watershed area of 3,400 km^2 (Eimers et al. 2005). The lake consists of three main areas: Kempenfelt Bay, Cook's Bay, and the main basin (Figure 1b). The geological conditions across the Lake Simcoe watershed are diverse with varying surficial sediment, aquifer systems, topography, and depositional/ erosional features. The surficial geology around the Lake Simcoe shoreline is dominated by areas of continuous sand, gravel, and diamicton (glacial till) in the south and east, and thin sediment and exposed Paleozoic bedrock in the north (Figure 1b). Large moraine features within the watershed, most notably the Oro Moraine near the northwest shoreline (405 masl) and the Oak Ridges Moraine near the southern shoreline (340 masl), represent topographic high points and regional recharge features (AquaResource 2013; Genivar 2013). Large erosional channels in the regionally extensive Newmarket Till aquitard layer are also important hydrogeological features, particularly along the lake's southern shoreline (Russell et al. 2003). These channels are characterized by a fining upward sequence of sediment that often have hydraulic conductivities an order of magnitude higher than adjacent sediments. Both Kempenfelt Bay, which is situated within a narrow and deep sand-gravel corridor, and Cook's Bay, which is found within a shallow and wide silt-organics area, are large tunnel valley features (Russell et al. 2003).

3. Methods

3.1 Field ^{222}Rn measurements

Boat surveys during which ^{222}Rn was continuously measured were conducted between June 2015 and July 2018 to quantify direct nearshore groundwater discharge to Lake Simcoe. Surveys were performed along 80% (190 km) of the lake's shoreline (Figure 2).^{222}Rn is produced from the radioactive decay of radium (^{226}Ra) and is naturally occurring in almost all aquifer materials including glacial sediment (Je and Eyles 1998; Schmidt et al. 2010). ^{222}Rn is a suitable tracer for evaluating groundwater discharge because it (i) is a chemically inert gas,

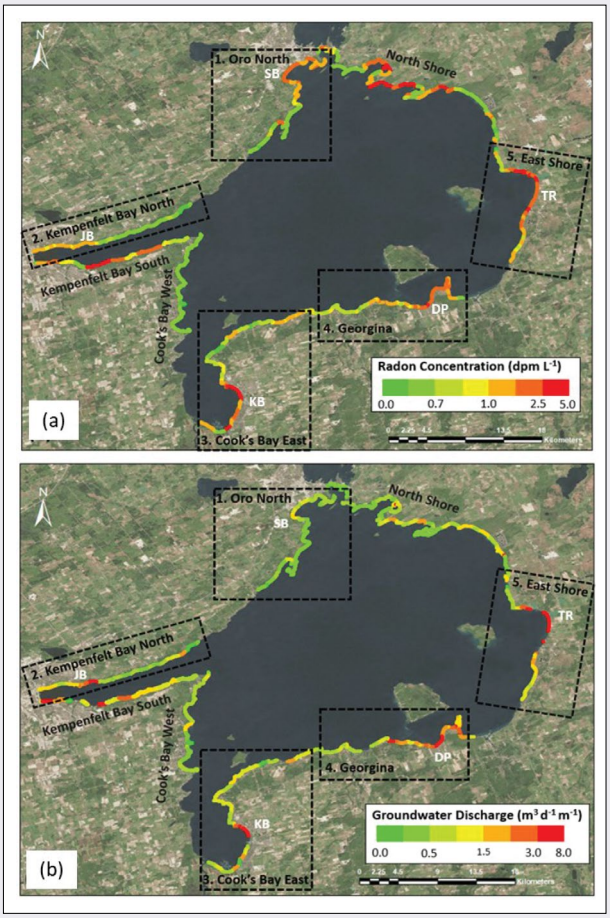


Figure 2. Average (a) measured in-lake ^{222}Rn concentrations and (b) calculated nearshore direct groundwater discharge (m^3 d^{-1} m^{-1}) along the Lake Simcoe shoreline. The black dash boxes indicate shoreline areas that were surveyed multiple times. Locations where high ^{222}Rn concentrations were identified during repeat surveys are labelled with white letters; Shingle Bay (SB), Johnson's Beach (JB), Keswick Beach (KB), Duclos Point (DP), and Talbot River (TR). ^{222}Rn concentrations and calculated direct groundwater discharge along the shoreline in the Kempenfelt Bay South, Cook's Bay West, and North Shore area are shown, but the results in these areas are considered preliminary as repeat surveys were not conducted.

(ii) is often present in groundwater in concentrations that are 3–4 orders of magnitude higher than receiving surface waters, and (iii) has a short half-life of 3.82 days (Burnett and Dulaiova 2003; Cable et al. 1996).

The field methods used are briefly described here with additional details provided in Wallace (2018). Surveys were conducted by continuously sampling ^{222}Rn in lake water from a boat travelling between 3–5 km h^{-1} along the shoreline at an offshore distance of 10–50 m. A submersible pump was used to pump lake water continuously from 0.5–1 m below the lake water surface to an air-water exchanger (RAD AQUA; Durridge). ^{222}Rn concentrations were then measured by RAD7 portable electronic radon detectors (Durridge). Multiple RAD7 units were used in parallel to decrease the initial equilibration time, improve sensitivity to changes in concentrations, and reduce the overall measurement errors (Dulaiova et al. 2005; Wallace 2018). The reported error provided for each ^{222}Rn measurement is the one sigma standard deviation (σ) following Poisson statistics (Taylor 1982). Measurements were taken over a 15 minute integration cycle as the boat travelled along the shoreline. Electrical conductivity (EC) measurements were also taken alongside ^{222}Rn measurements, but no clear relationship between ^{222}Rn and EC was observed as in-lake EC spatial trends were found to be overwhelmed by urban sources. The in-lake ^{222}Rn concentrations were found to vary temporally in response to changing weather conditions (primarily wind, precipitation, waves), and so potential areas with high direct groundwater discharge (Figure 2) were surveyed multiple times to ensure the repeatability of results. All ^{222}Rn surveys were conducted during the summer months (May – September) and therefore the results represent summer groundwater discharge conditions.

To calculate the magnitude of nearshore direct groundwater discharge using in-lake ^{222}Rn concentrations, ^{222}Rn was also measured in nearshore shallow groundwater around Lake Simcoe. Following recommendations by prior studies (e.g., Chanyotha et al. 2014; Dimova et al. 2013), groundwater ^{222}Rn concentrations were measured using two methods: shallow groundwater samples and sediment equilibration experiments. Groundwater samples were collected using temporary, shallow, nearshore wells installed at 20 beaches around Lake Simcoe. Dissolved ^{222}Rn decays and re-equilibrates with radium in the aquifer sediments as groundwater travels towards the lake. As the ^{222}Rn half-life is relatively short (3.82 d), groundwater samples were taken within 5–10 m of the shoreline so that the samples would reflect the ^{222}Rn concentrations in groundwater that is discharging to the lake. Generally, three wells were installed approximately 5–10 m apart in an along-shore transect to capture the spatial variability in groundwater ^{222}Rn concentrations at each site. Samples were analyzed using the RAD H2O (Durridge) system with a RAD7 detector (Durridge). Groundwater ^{222}Rn concentrations were also calculated using a sediment equilibration method (Chanyotha et al. 2014). For this method, nearshore lakebed sediment was collected in 250 mL airtight bottles and left to equilibrate with ambient lake water in the closed bottle for at least 20 d (or 5 x ^{222}Rn half-life). Following equilibration, the samples were analyzed using the RAD H2O (Durridge) system and RAD7 detector (Durridge). Groundwater ^{222}Rn concentrations were calculated using the equilibrium concentration of ^{222}Rn in the water after the 20 d period and the sediment porosity and bulk density. Lake bed sediment samples for the sediment equilibration method were collected from 13 nearshore sites around the lake.

3.2 ^{222}Rn mass balance

Direct nearshore groundwater discharge rates along the shoreline were estimated by applying a steady state mass balance model that considers the measured in-lake ^{222}Rn concentrations and groundwater ^{222}Rn concentrations (e.g., Corbett et al. 1997; Dulaiova et al. 2010). Details of the mass balance model are provided in Wallace (2018). The model considers the various sources and sinks of ^{222}Rn for a well-mixed surface water volume. ^{222}Rn sources considered include (1) ^{222}Rn input from groundwater discharge (J_{gw}, dpm m^{-2} d^{-1}), (2) diffusion of ^{222}Rn from lake bed sediment (J_{diff}, dpm m^{-2} d^{-1}), and (3) production of ^{222}Rn from ^{226}Ra decay (J_{prod}, dpm m^{-2} d^{-1}). In lake environments, J_{prod} is negligible as ^{226}Ra concentrations are low in freshwater and therefore this source can be neglected (Dimova et al. 2013). In addition, J_{diff} is negligible where there is advective flux of groundwater across the lake bed (Dimova et al. 2013; Ji et al. 2017). Losses considered in the model include (1) evasion of ^{222}Rn to the atmosphere (J_{atm}, dpm m^{-2} d^{-1}), (2) decay of ^{222}Rn (J_{decay}, dpm m^{-2} d^{-1}), and (3) offshore mixing with low ^{222}Rn surface waters (J_{mix}, dpm m^{-2} d^{-1}). Although J_{mix} is often neglected for non-tidal lake environments (e.g., Corbett et al. 1997; Santos et al. 2008), J_{mix} was considered in our mass balance model given the large size of Lake Simcoe and therefore potential importance of coastal processes driving offshore mixing. Based on these assumptions, the steady state mass balance model is given as:

$$J_{gw} = J_{atm} + J_{decay} + J_{mix} \quad (1)$$

The groundwater discharge rate (Q, m^3 d^{-1}) along the shoreline is calculated as:

$$Q = \frac{J_{gw} A}{C_{gw}} \quad (2)$$

where C_{gw} (dpm m^{-3}) is the groundwater ^{222}Rn concentration, and A (m^2) is the lakebed area for the volume over which the mass balance was applied. A was calculated as the length of shoreline travelled during each 15-minute ^{222}Rn measurement cycle and the average distance offshore during this cycle. As ^{222}Rn concentrations in groundwater often exhibit high spatial variability, analysis was conducted to determine a representative value for C_{gw} (see Section 4.1.2).

The ^{222}Rn loss fluxes in equation (1) were calculated as follows:

1. Evasion of ^{222}Rn to the atmosphere (J_{atm}, dpm m^{-2}d^{-1}) was calculated using (Dimova et al. 2013; MacIntyre et al. 1995):

$$J_{atm} = k(C_{sw} - \alpha C_{air}) \quad (3)$$

where C_{air} (dpm m^{-3}) is the measured ambient air ^{222}Rn concentration and α (dimensionless) is the Ostwald's solubility coefficient. k is the ^{222}Rn gas transfer coefficient which is a function of wind speed for which data was taken from the nearest Environment Climate Change Canada weather station (located 5–28 km away from a survey site). Additional details on calculation of k and α are provided in Wallace (2018).

2. Decay of ^{222}Rn in the lake water volume (J_{decay}, dpm m^{-2}d^{-1}) was calculated by:

$$J_{decay} = z\lambda_{Rn}C_{sw} \quad (4)$$

where λ_{Rn} (d^{-1}) is the decay rate of ^{222}Rn which is 0.181 d^{-1}, and z is the lake depth (m) which was determined from 50 m resolution bathymetric data (Ontario Ministry of Natural Resources and Forestry 2015).

3. The horizontal offshore mixing loss, J_{mix}, (dpm m^{-2}d^{-1}) was estimated using an iterative method described in Santos et al. (2008). Shore-perpendicular ^{222}Rn and EC transect data were collected in three different locations in Lake Simcoe (Kempenfelt Bay, Cook's Bay, and the main basin) to calculate the offshore concentration gradients at each location. Measured ^{222}Rn (non-conservative tracer) and EC (conservative tracer) offshore gradients were used in the steady state advection diffusion equation to estimate the horizontal eddy diffusion coefficient K_h (m^2 d^{-1}):

$$K_h\frac{\partial^2 C}{\partial x^2} - \omega\frac{\partial C}{\partial x} - \lambda C = 0 \quad (5)$$

where ω (m d^{-1}) is the horizontal surface advection, C is the concentration of the tracer (^{222}Rn and EC in this case), and λ is the ^{222}Rn decay constant. When using the equation for the offshore EC transect, the decay term was removed. To calculate K_h, the measured offshore ^{222}Rn concentrations must be corrected for J_{decay} and J_{atm} over the time taken for ^{222}Rn to travel to the measurement location. As such an iterative approach was used whereby the ^{222}Rn concentrations are corrected for J_{decay} and J_{atm} and then used in (5) to estimate a new K_h and ω. Iterations were continued until convergence was reached. The final K_h value was then used to calculate J_{mix} using (Santos et al. 2008):

$$J_{mix} = -K_h\left(\frac{C_{S+1} - C_{S-1}}{2\Delta x}\right) \times \frac{A_{CS}}{A} \quad (6)$$

where $\frac{C_{S+1} - C_{S-1}}{2\Delta x}$ (dpm m^{-3} m^{-1}) is the measured offshore ^{222}Rn gradient, and A_{CS} is the average along-shore cross sectional area (A_{CS}, m^2) for the lake water volume represented by the 15-minute measurement cycle.

Groundwater discharge values (Q) were calculated for each 15-minute measurement cycle and the values were divided by the shoreline length travelled during the respective cycle to obtain the groundwater discharge rate per unit of shoreline (m^3 d^{-1} m^{-1}). Reported uncertainties for each groundwater discharge value represent the propagation of uncertainties associated with the ^{222}Rn concentrations used to calculate each source and sink term. As tributary inputs (and associated in-direct groundwater discharge) were not included in the ^{222}Rn mass balance model, calculations were not performed for shoreline areas within 500 m of a tributary. While field validation of the ^{222}Rn survey method was not performed in this study, ^{222}Rn survey results have previously been compared with direct groundwater discharge rates determined from piezometers and vertical temperature gradient measurements in Nottawasaga Bay, Lake Huron (Ji et al. 2017). Direct groundwater discharge results determined in this current study were compared with model output from two regional-scale groundwater-surface water models developed for subwatersheds along the north and south of Lake Simcoe. Details of this comparison are provided in Wallace (2018).

4. Results and discussion

4.1 ^{222}Rn field measurement results

4.1.1 In-lake ^{222}Rn concentrations

In-lake ^{222}Rn concentrations were highly variable along the shoreline with values ranging from 0.0 ± 0.2 to 5.1 ± 2.1 dpm L^{-1} (Figure 2a). Concentrations shown in Figure 2a are the average concentration values for all surveys with multiple surveys conducted along shoreline areas indicated by the black dashed boxes. To aid the discussion of the results, the lake is divided into eight main areas: Oro North, Kempenfelt Bay North, Kempenfelt Bay South, Cook's Bay West, Cook's Bay East, Georgina, East Shore, and North Shore (Figure 2a; Table 1). Five shoreline areas were consistently identified during repeat surveys to have elevated in-lake ^{222}Rn concentrations. These areas are near Shingle Bay (SB), Johnson's Beach (JB), Keswick Beach (KB), Duclos Point (DP), and Talbot River (TR; Figure 2a). The average ^{222}Rn concentrations in these areas were 20–40% higher than in-lake ^{222}Rn concentrations measured along the adjacent shorelines. Elevated in-lake ^{222}Rn concentrations were also observed in the Kempenfelt Bay South (max = 3.3 ± 0.4 dpm L^{-1}) and North Shore areas (max = 4.9 ± 0.7 dpm L^{-1}), however repeat surveys were not conducted along these shoreline areas. The following discussion of the ^{222}Rn results focuses on areas that were identified in repeat surveys to have elevated ^{222}Rn concentrations. Areas with high ^{222}Rn concentrations were observed in sheltered bay areas (e.g., SB, DP) as well as along more exposed shoreline areas (e.g., JB, KB) where there was higher potential for ^{222}Rn losses due to stronger wind and currents (i.e., higher offshore mixing). Areas with high ^{222}Rn concentrations were also observed in both shallow and deep nearshore waters (e.g., 2–4 m depth

Table 1. Maximum, minimum and total direct nearshore groundwater discharge along the shoreline for each area of the lake (shoreline areas shown in Figure 2).

Shoreline Area	Shoreline Length (m)	Maximum ($m^3 d^{-1} m^{-1}$)	Minimum ($m^3 d^{-1} m^{-1}$)	Total Groundwater Discharge (m^3 d^{-1})
Oro North	24,800	1.6 ± 0.3	0.03 ± 0.03	12,200 ± 4,000
Kempenfelt Bay North	24,800	3.8 ± 0.9	0.07 ± 0.07	18,700 ± 5,600
Kempenfelt Bay South	16,500	3.3 ± 0.9	0.75 ± 0.07	20,100 ± 2,700
Cook's Bay West	16,300	2.0 ± 0.2	0.16 ± 0.12	11,700 ± 2,800
Cook's Bay East	19,400	4.3 ± 0.6	0.57 ± 0.06	26,400 ± 4,100
Georgina	28,200	4.6 ± 0.5	0.70 ± 0.17	44,400 ± 8,600
East Shore	17,800	8.1 ± 0.6	0.29 ± 0.09	31,300 ± 3,100
North Shore	42,300	3.3 ± 0.2	0.08 ± 0.01	32,400 ± 6,900
Total	**190,100**			**197,200 ± 14,500**

near SB, and 6–20 m depth near JB) (Ontario Ministry of Natural Resources and Forestry 2015).

4.1.2 Groundwater ^{222}Rn concentrations

^{222}Rn concentrations in groundwater samples ranged from 50 ± 5 dpm L^{-1} to 463 ± 44 dpm L^{-1}, with a mean concentration of 178 ± 17 dpm L^{-1}. ^{222}Rn concentrations derived from sediment equilibration experiments were slightly higher ranging from 133 ± 6 dpm L^{-1} to 479 ± 10 dpm L^{-1} with a mean value of 322 ± 9 dpm L^{-1}. For the nine sites where both groundwater and sediment samples were collected, the mean groundwater sample concentration was 244 ± 18 dpm L^{-1}, while sediment sample ^{222}Rn results had a mean concentration of 343 ± 9 dpm L^{-1}. The higher concentrations from sediment samples is consistent with other studies (Burnett and Dulaiova 2006).

The correlation between both the groundwater sample and sediment equilibration sample ^{222}Rn concentrations, and the in-lake ^{222}Rn concentrations measured near each groundwater/sediment sampling location is poor (Figure 3). While various factors affect the in-lake ^{222}Rn concentrations, the poor correlation in Figure 3 indicates that the observed variability in the in-lake ^{222}Rn concentrations is not controlled by variability in the concentrations of ^{222}Rn in the groundwater. The measured groundwater concentrations (groundwater and sediment samples) were grouped based on the surficial geology type (gravel, sand, diamicton, and silt; surficial geology shown in Figure 1b) and the surficial permeability (high and low permeability) (Ontario Ministry of Northern Development and Mines 2016) at each of the groundwater and sediment sampling sites. No relationships were found between the ^{222}Rn groundwater concentrations and the surficial geology or permeability (Figure 3). Importantly, however, areas with low permeability sediments generally have low in-lake ^{222}Rn concentrations regardless of the groundwater ^{222}Rn concentration (Figure 3c,d). Based on the poor correlation between the ^{222}Rn concentrations in the lake and groundwater, together with the lack of relationship between the groundwater concentrations and the surficial geology and permeability, a mean groundwater ^{222}Rn concentration (C_{gw}) of 235 ± 14 dpm L^{-1} was used for the mass balance calculations (Equation 2). This value represents the average ^{222}Rn concentration for all sampled sites, including both groundwater sample and sediment equilibrium sample results.

4.1.3 ^{222}Rn-derived groundwater discharge results

Groundwater discharge per meter of shoreline calculated using the in-lake ^{222}Rn concentrations and mass balance model ranged from 0.01 ± 0.06 m^3 d^{-1} m^{-1} to 12.8 ± 0.9 m^3 d^{-1} m^{-1} (Figure 2b). Areas of high groundwater discharge occur near Shingle Bay (SB; average= 1.6 ± 0.3 m^3 d^{-1} m^{-1}), Johnson's Beach (JB; average= 3.8 ± 0.9 m^3 d^{-1} m^{-1}), Keswick Beach (KB; average= 4.3 ± 0.6 m^3 d^{-1} m^{-1}), Duclos Point (DP; average= 4.6 ± 0.5 m^3 d^{-1} m^{-1}), and Talbot River (TR; average= 8.1 ± 0.6 m^3 d^{-1} m^{-1}). Groundwater discharge results generally show a similar pattern to the in-lake ^{222}Rn concentration data (Figure 2), where the same locations (i.e. SB, JB, KB, DP, TR; Figures 4, 5) were identified as having groundwater discharge values 25–80% higher than adjacent shoreline areas. However, the relative magnitudes of the groundwater discharge compared with the ^{222}Rn concentrations are adjusted based on the survey conditions (i.e., lake depth, distance covered during survey cycle, atmospheric losses due to wind speed on survey day).

The total nearshore groundwater discharge calculated based on ^{222}Rn surveys conducted along 190 km of the lake's shoreline

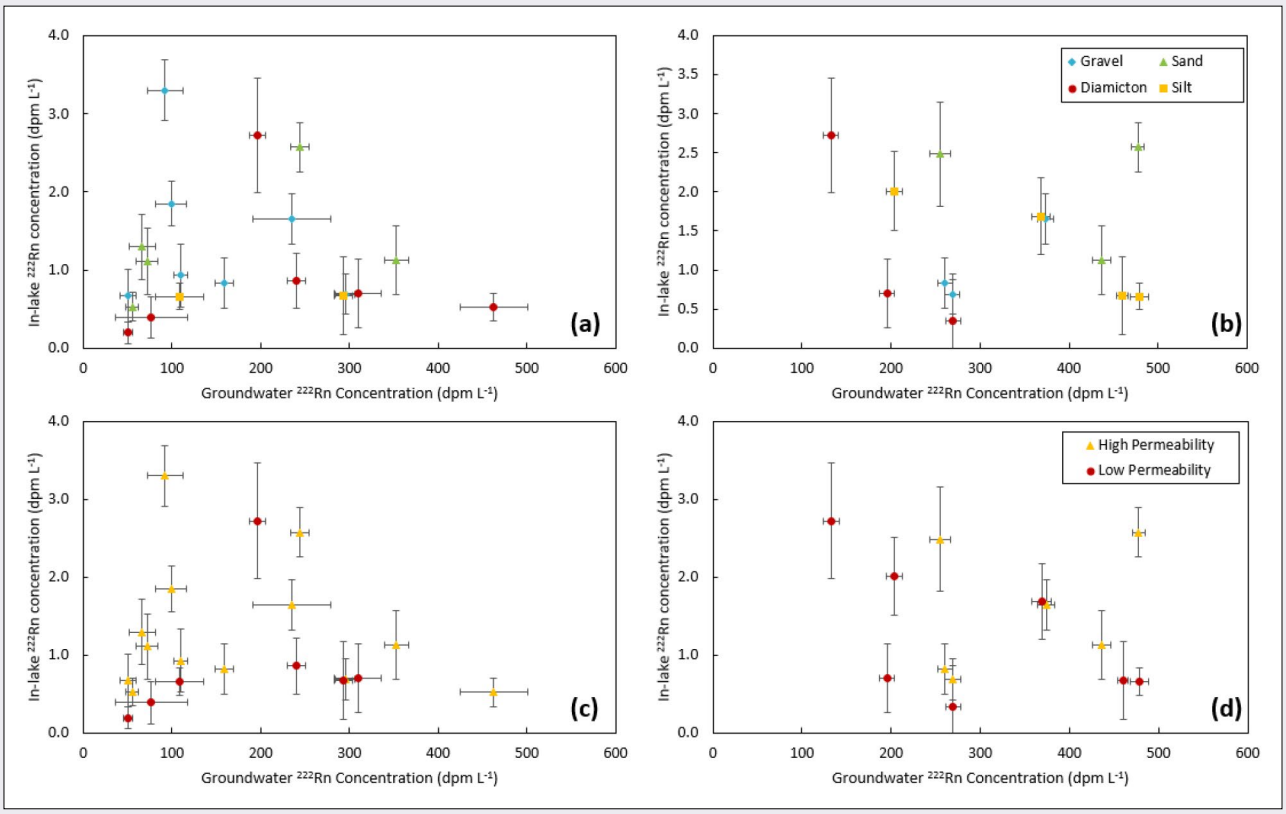


Figure 3. Average in-lake ^{222}Rn concentrations measured during boat surveys plotted against measured (a, c) groundwater sample and (b, d) sediment equilibrium sample ^{222}Rn concentrations. Data have been classified using (a, b) surficial geology type, and (c, d) surficial sediment permeability (Ontario Ministry of Northern Development and Mines 2016).

is 197,200 ± 14,500 m^3 d^{-1} (Table 1). Comparing this to the total volume of tributary inputs to Lake Simcoe for the 2011 summer season (1,731,500 m^3 d^{-1}) (O'Connor et al. 2017), the total groundwater discharge is approximately 11.3 ± 2% of the total volume of tributary inputs during this season. Sensitivity analysis where the upper and lower quartile groundwater ^{222}Rn concentrations (346 ± 25 dpm L^{-1} and 165 ± 17 dpm L^{-1}, respectively) were used to calculate the total groundwater discharge show that the total groundwater discharge may range from 7 ± 1% and 16 ± 2%, respectively, of the total volume of tributary inputs during the summer season. It is important to note that while nearshore groundwater discharge may represent only 7–16% of the total tributary input into the lake, in some areas pollutant concentrations in groundwater may be higher than in tributaries, and therefore it is possible that in these areas groundwater discharge could account for a higher percentage of the pollutant loading to the lake. Further, while groundwater discharge may not be a major component of the lake-wide water budget, groundwater discharge may be an important component in shoreline areas where there is high groundwater discharge and negligible tributary inputs. Finally, quantifying groundwater discharge using ^{222}Rn boat surveys only accounts for the nearshore direct groundwater discharge and does not include offshore groundwater discharge which may also be important in Lake Simoce given the complexity of the geological environment.

4.2 Controls on direct groundwater discharge

It is resource intensive to conduct a detailed regional scale assessment of direct groundwater inputs into a large lake, as was done in this study. To focus available resources in other glacial lake environments, identifying hydrogeological features that may contribute to the direct groundwater discharge patterns is needed to better target groundwater discharge investigations. Factors generally known to influence spatial variability in direct groundwater discharge include regional aquifer sediment type and hydraulic conductivity, recharge to aquifers connected to the lake, hydraulic gradient between the groundwater and surface water, and nearshore topography (Cherkauer and Hensel 1986; Kazmierczak et al. 2016; Schneider et al. 2005; Tecklenburg and Blume 2017). In addition, direct groundwater discharge can be lower in areas where there are tributaries as the tributaries may intercept shallow groundwater travelling towards the lake (Conant et al. 2019; Sawyer et al. 2016). Consistent with these factors, the main hydrogeological features found to be associated with

areas identified to have high direct nearshore groundwater discharge to Lake Simcoe were: permeable nearshore surficial sediments, proximity and connectivity to regional recharge features, and presence of aquifer tunnel channel deposits. Areas identified to have high groundwater discharge were found to be under the influence of one, or a combination of, these features as described below. Shoreline configuration also may have influenced the spatial variability in direct groundwater discharge with higher groundwater discharge observed in sheltered embayments (e.g., SB, DP) where there may be a convergence of groundwater flow paths (Cherkauer and McKereghan 1991). Overall, the identified high groundwater discharge areas are attributed to local scale hydrogeological features rather than the regional scale hydrogeological conditions which makes *a priori* prediction of areas with high groundwater discharge challenging.

The areas of high direct groundwater discharge identified at Johnson's Beach (JB), Keswick Beach (KB), and Talbot River (TR) correspond to areas with surficial sand and gravel deposits along the shoreline (Figure 4). The high direct groundwater discharge in these areas may be due to the more permeable nearshore deposits facilitating connectivity between the regional aquifer system and the lake. For example, Johnson's Beach is located within a continuous sand and gravel corridor associated with the shallow aquifer units in the Kempenfelt Bay valley. Direct groundwater discharge is highest where these shallow aquifer units intersect the lakebed in the nearshore area (AquaResource 2013). The potential importance of the permeable surficial sediment near Johnson's Beach, Keswick Beach, and Talbot River is in spite of different geological conditions. For example, the subwatershed area where Talbot River is located is characterized by flat topography and thin soil covering karst limestone, while the north Kempenfelt Bay area where Johnson's Beach is located is characterized by steep topography and a large valley feature infilled by a series of four glaciofluvial sand and gravel aquifer units (AquaResource Inc. 2013; Earthfx Inc. 2014a).

There are two large glacial moraines in the Lake Simcoe watershed that are topographic high points and regional recharge features: the Oro Moraine and the Oak Ridges Moraine (Figure 1b). The observed high groundwater discharge near Shingle Bay is thought to be influenced by its proximity and hydraulic connection to the Oro Moraine. The steep topography between the moraine and shoreline, and high recharge to the shallow aquifer layers adjacent to the lake may also contribute to the observed high groundwater discharge (Figure 5a). This is supported by regional scale integrated surface-water–groundwater modelling that was conducted for the Oro-North area to support assessment of ecologically significant recharge areas (Earthfx 2013; Wallace 2018). The Oak Ridges Moraine is not as close to the Lake Simcoe shoreline as the Oro Moraine and regional hydraulic gradients and topography suggest that the high groundwater discharge areas along the lake's southern shoreline may not be due to groundwater flow from the Oak Ridges Moraine (Figure 5b). However, high groundwater discharge observed near Keswick Beach and Duclos Point coincide with the locations of tunnel channel deposits along the southern shoreline (Figure 6). These channels affect the groundwater flow systems with channel infill sediments often having hydraulic conductivities an order of magnitude higher than the surrounding till material which otherwise acts as a barrier between shallow and deep aquifer layers in the region (Russell et al. 2003). It is possible that the tunnel channel deposits may recharge the shallow aquifer layers that are in direct contact with the lake, thus explaining the high groundwater discharge near Keswick Beach and Duclos Point. It is important to note that high direct groundwater discharge does not occur in all shoreline areas where the tunnel channel aquifers are inferred to extend towards the lake (Figure 6). This is because rivers/streams occupy some of the tunnel channel features and for these

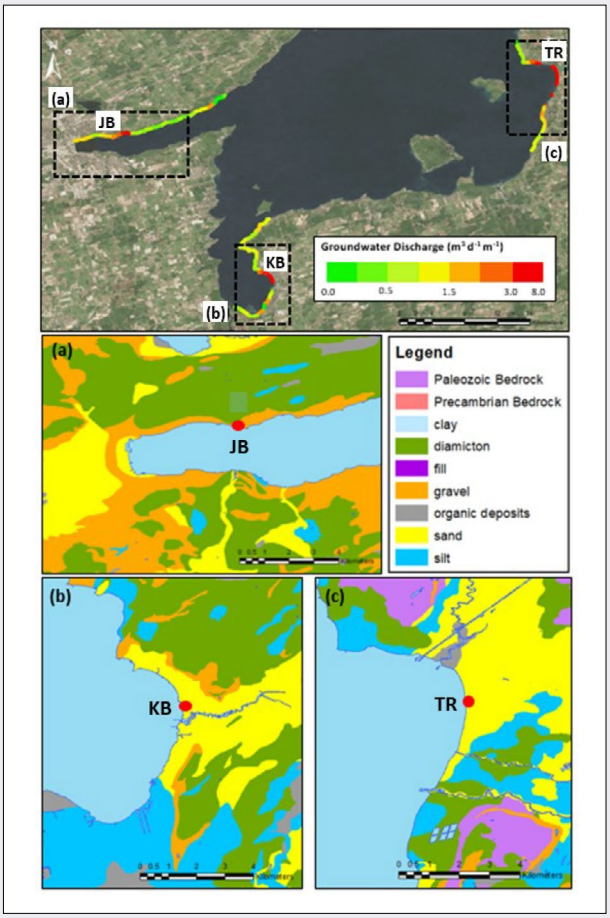


Figure 4. Average groundwater discharge ($m^3\ d^{-1}\ m^{-1}$) along the shoreline near Johnson's Beach (JB), Keswick Beach (KB), and Talbot River (TR) areas. Surficial geology is shown for (a) Johnson's Beach (JB), (b) Keswick Beach (KB), and (c) Talbot River (TR) with maps modified from Ontario Ministry of Northern Development and Mines (2016). The black dashed boxes in (a) represent the areas shown in (b)-(d).

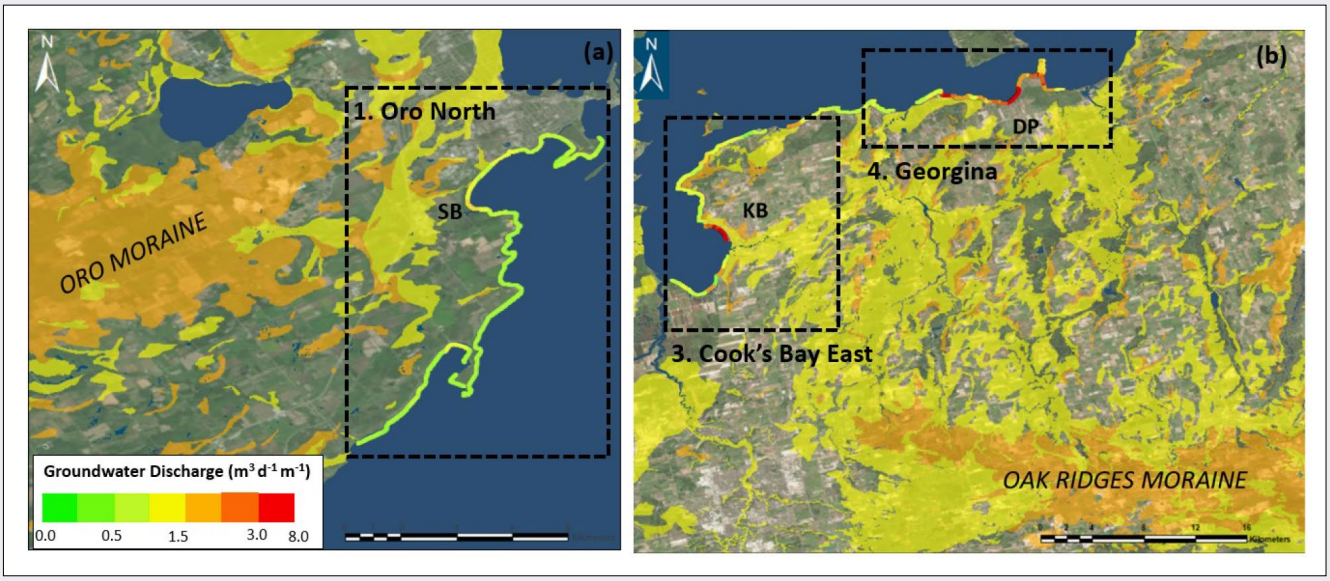


Figure 5. Average groundwater discharge ($m^3 d^{-1} m^{-1}$) along the shoreline near (a) Shingle Bay (SB) in the Oro North area, and (b) the Keswick Beach (KB) and Duclos Point (DP) in the Cook's Bay East and Georgina areas. Surficial sand (yellow) and gravel (orange) sediment associated with the Oro Moraine and Oak Ridges Moraine in these areas is also shown in (a) and (b) respectively (modified from Ontario Ministry of Northern Development and Mines (2016)). The black dashed boxes in (a) and (b) represent the shoreline areas where repeat boat surveys were conducted.

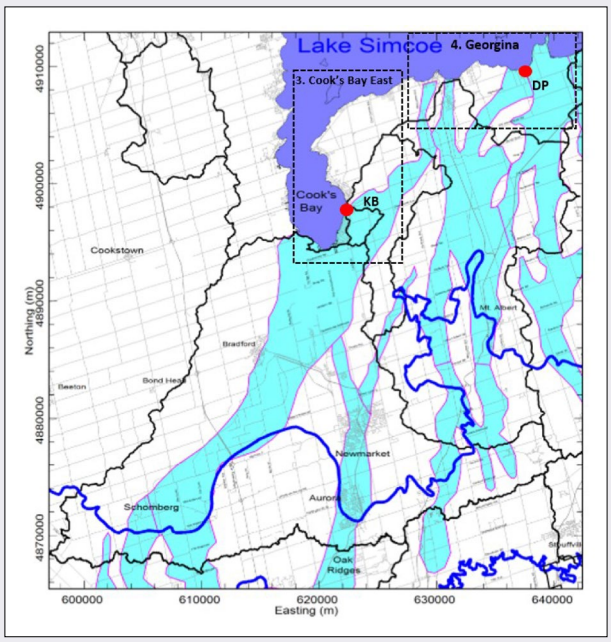


Figure 6. Interpreted tunnel channel locations along the southern shoreline of Lake Simcoe (modified from Earthfx Inc. and Gerber Geosciences 2008). Areas with high direct groundwater near Keswick Beach (KB) and Duclos Point (DP) are marked (red dots). The black dashed boxes represent the shoreline areas where repeat boat surveys were conducted.

cases groundwater would tend to discharge to the river/stream rather than flow to Lake Simcoe.

5. Conclusions

Nearshore direct groundwater discharge to Lake Simcoe varies considerably along the shoreline with ^{222}Rn boat survey data revealing five main areas with high groundwater discharge. Areas with high groundwater discharge were identified in sheltered bays as well as exposed shoreline areas, and in areas with both shallow and deep nearshore waters. Poor correlation between measured in-lake ^{222}Rn concentrations and shallow nearshore groundwater ^{222}Rn concentrations suggests that the spatial variability in the in-lake ^{222}Rn concentrations is not due to spatial variability in the ^{222}Rn groundwater concentrations. The total direct groundwater discharge to Lake Simcoe was estimated during the summer season to be 197,200 ± 14,500 $m^3 d^{-1}$, which represents approximately 11.3 ± 2.0% of the total estimated volume of tributary inputs. Shoreline areas with high groundwater discharge were related to the presence of one or more of the following features: permeable nearshore surficial sediments, tunnel channel deposits, and proximity and connectivity to regional recharge features (moraines). The permeable surficial sediments and tunnel channel deposits are thought to provide connectivity between the regional-scale aquifer system and lake. Evaluating linkages between shoreline areas of high groundwater discharge and hydrogeological features is important to better target future field campaigns investigating groundwater discharge to glacial lakes. The findings of this study can be broadly applied in other studies evaluating direct groundwater inputs in glacial lake environments.

6. References

AquaResource. 2013. Barrie Tier Three Water Budget and Local Area Risk Assessment, Appendix A: Conceptual Understanding Memorandum. Prepared for Lake Simcoe Region Conservation Authority, Breslau, Ontario.

Burnett, W.C., Aggarwal, P.K., Aureli, A., Bokuniewicz, H., Cable, J.E., Charette, M.A., Kontar, E., Krupa, S., Kulkarni, K.M., Loveless, A., Moore, W.S., Oberdorfer, J.A., Oliveira, J., Ozyurt, N., Povinec, P., Privitera, A.M.G., Rajar, R., Ramessur, R.T., Scholten, J., Stieglitz, T., Taniguchi, M., and Turner, J.V. 2006. Quantifying submarine groundwater discharge in the coastal zone via multiple methods. Sci. Total. Environ., 367: 2–3, 498-543. https://doi.org/10.1016/j.scitotenv.2006.05.009

Burnett, W.C. a ndDulaiova, H. 2003. Estimating the dynamics of groundwater input into the coastal zone via continuous radon-222 measurements. J. Environ. Radioact., 69: 1-2, 21-35. https://doi.org/10.1016/s0265-931x(03)00084-5

Burnett, W.C. and Dulaiova, H. 2006. Radon as a tracer of submarine groundwater discharge into a boat basin in Donnalucata, Sicily. Cont. Shelf Res., 26: 7, 862-873. https://doi.org/10.1016/j.csr.2005.12.003

Burnett, W.C., Wattayakorn, G., Supcharoen, R., Sioudom, K., Kum, V., Chanyotha, S., and Kritsananuwat, R. 2017. Groundwater discharge and phosphorus dynamics in a flood-pulse system: Tonle Sap Lake, Cambodia. J. Hydrol., 549: 79-91. https://doi.org/10.1016/j.jhydrol.2017.03.049

Cable, J.E., Bugna, G.C., Burnett, W., and Chanton, J.P. 1996. Application of ^{222}Rn and CH4 for assessment of groundwater discharge to the coastal ocean. Limnol. Oceanogr., 41: 6, 1347-1353. https://doi.org/10.4319/lo.1996.41.6.134.

Chanyotha, S., Kranrod, C., and Burnett, W.C. 2014. Assessing diffusive fluxes and pore water radon activities via a single automated experiment. J. Radioanalytic. Nuclear Chem., 301: 2, 581-588. https://doi.org/10.1007/s10967-014-3157-3

Cherkauer, D.S. and Hensel, B.R. 1986. Groundwater flow into Lake Michigan from Wisconsin. J. Hydrol., 84: 3, 261-271. https://doi.org/10.1016/0022-1694(86)90126-5

Cherkauer, D.S. and McKereghan, P.F. 1991. Ground-water discharge to lakes: Focusing in embayments. Ground Water, 29: 1, 72-80. https://doi.org/10.1111/j.1745-6584.1991.tb00499.x

Conant, B., Robinson, C.E., Hinton, M.J., and Russell, H.A.J. 2019. A framework for conceptualizing groundwater-surface water interactions and identifying potential impacts on water quality, water quantity, and ecosystems. J. Hydrol., 574: 609-627. https://doi.org/10.1016/j.jhydrol.2019.04.050

Corbett, D.R., Burnett, W.C., Cable, P.H., and Clark, S.B. 1997. Radon tracing of groundwater input into Par Pond, Savannah River site. J. Hydrol., 203: 1, 209-227.

Dimova, N.T. and Burnett, W.C. 2011. Evaluation of groundwater discharge into small lakes based on the temporal distribution of radon-222. Limnol. Oceanogr., 56: 2, 486-494. https://doi.org/10.4319/lo.2011.56.2.0486

Dimova, N.T., Burnett, W.C., Chanton, J.P., and Corbett, J.E. 2013. Application of radon-222 to investigate groundwater discharge into small shallow lakes. J. Hydrol., 486: 112-122. https://doi.org/10.1016/j.jhydrol.2013.01.043

Dulaiova, H., Camilli, R., Henderson, P.B., and Charette, M.A. 2010. Coupled radon, methane and nitrate sensors for large-scale assessment of groundwater discharge and non-point source pollution to coastal waters. J. Environ. Radioact. 101: 7, 553-63. https://doi.org/10.1016/j.jenvrad.2009.12.004

Dulaiova, H., Peterson, R., Burnett, W., and Lane-Smith, D. 2005. A multi-detector continuous monitor for assessment of ^{222}Rn in the coastal ocean. J. Radioanalytic. Nuclear Chem., 263: 2, 361-363. https://doi.org/10.1007/s10967-005-0595-y

Earthfx. 2013. Tier 2 Water Budget Analysis and Water Quantity Stress Assessment for the Oro North, Oro South, and Hawkestone Creeks Subwatersheds, Prepared for Lake Simcoe Region Conservation Authority, Toronto, Ontario.

Earthfx Inc. and Gerber Geosciences. 2008. Holland River, Maskinonge River and Black River Watersheds Water Budget Study. Prepared for Lake Simcoe Region Convervation Authority.

Eimers, M.C., Winter, J.G., Scheider, W.A., Watmough, S.A., and Nicholls, K.H. 2005. Recent changes and patterns in the water chemistry of Lake Simcoe. J. Great Lakes Res., 31: 3, 322-332. https://doi.org/10.1016/S0380-1330(05)70263-X

Fukuo, Y. and Kaihotsu, I. 1988. A theoretical analysis of seepage flow of the confined groundwater into the lake bottom with a gentle slope. Water Resour. Res., 24: 1949-1953. https://doi.org/10.1029/WR024i011p01949

Genivar. 2013. Tier 2 Water Budget and Ecologically Significant Groundwater Recharge Area Assessment for the Black River and Georgina Creeks Subwatersheds. Prepared for Lake Simcoe Region Conservation Authority.

Je, I. and Eyles, N. 1998. Bedrock structure control on soil-gas Radon-222 anomalies in the Toronto Area, Ontario, Canada. Environ. Eng. Geosci., 4: 445-454. https://doi.org/10.2113/gseegeosci.IV.4.445

Ji, T., Peterson, R.N., Befus, K.M., Peterson, L.E., and Robinson, C.E. 2017. Characterization of groundwater discharge to Nottawasaga Bay, Lake Huron with hydraulic and ^{222}Rn measurements. J. Great Lakes Res., 43: 5, 920-929. https://doi.org/10.1016/j.jglr.2017.07.003

Karan, S., Kidmose, J., Engesgaard, P., Nilsson, B., Frandsen, M., Ommen, D.A.O., Flindt, M.R., Andersen, F.Ø., and Pedersen, O. 2014. Role of a groundwater–lake interface in controlling seepage of water and nitrate. J. Hydrol., 517: 791-802. https://doi.org/10.1016/j.jhydrol.2014.06.011

Kazmierczak, J., Müller, S., Nilsson, B., Postma, D., Czekaj, J., Sebok, E., Jessen, S., Karan, S., Stenvig Jensen, C., Edelvang, K., and Engesgaard, P. 2016. Groundwater flow and heterogeneous discharge into a seepage lake: Combined use of physical methods and hydrochemical tracers. Water Resour. Res., 52: 11, 9109-9130. https://doi.org/10.1002/2016WR019326

Kornelsen, K.C. and Coulibaly, P. 2014. Synthesis review on groundwater discharge to surface water in the Great Lakes Basin. J. Great Lakes Res., 40: 2, 247-256. https://doi.org/10.1016/j.jglr.2014.03.006

Lee, D.R. 1977. A device for measuring seepage flux in lakes. Limnol. Oceanogr., 22: 1, 140-147. https://doi.org/10.4319/lo.1977.22.1.0140.

Lewandowski, J., Meinikmann, K., Nützmann, G., and Rosenberry, D.O. 2015. Groundwater – the disregarded component in lake water and nutrient budgets. Part 2: effects of groundwater on nutrients. Hydrolog. Proc., 29: 13, 2922-2955. https://doi.org/10.1002/hyp.10384.

Lewis, C.F.M., Todd, B.J., King, J.W., Goodyear, D.R., and Slattery, S.R. 2007. Hydrogeology of the Lake Simcoe basin: a geophysical view of stratigraphy beneath the lake, 60th Canadian Geotechnical Conference and 8th Joint CGS/IAH,CNC Specialty Groundwater Conference. Diamond Jubliee Proceedings, Ottawa, Ontario.

MacIntyre, S., Wanninkhof, R., and Chanton, J. 1995. Trace gas exchange across the air-water interface in freshwater and coastal marine environments. In Matson, P.A. and Hariss, R.C. Eds. Biogenic trace gases: Measuring emissions from soil and water. Wiley-Blackwell Science, New York.

Meinikmann, K., Hupfer, M., and Lewandowski, J. 2015. Phosphorus in groundwater discharge – A potential source for lake eutrophication. J. Hydrol., 524: 214-226. https://doi.org/10.1016/j.jhydrol.2015.02.031

Naranjo, R.C., Niswonger, R.G., Smith, D., Rosenberry, D., and Chandra, S. 2019. Linkages between hydrology and seasonal variations of nutrients and periphyton in a large oligotrophic subalpine lake. J. Hydrol., 568: 877-890. https://doi.org/10.1016/j.jhydrol.2018.11.033

North, R.L. et al. 2013. The state of Lake Simcoe (Ontario, Canada): the effects of multiple stressors on phosphorus and oxygen dynamics. Inland Waters, 3: 1, 51-74. https://doi.org/10.5268/iw-3.1.529

O'Connor, E.M., Aspden, L.P., Lembcke, D., Young, J., Lucchese, M., Stainsby, E.A., and Winter, J.G. 2017. Annual Water Balances and Total Phosphorus Loads to Lake Simcoe (2010–2011), Lake Simcoe Region Conservation Authority.

Ontario Ministry of Natural Resources and Forestry. 2015. Lake Simcoe bathymetry layer (50m resolution), Source data: Canadian Hydrographic Services Field Sheet 2790.

Ontario Ministry of Northern Development and Mines. 2016. Surficial geology of Southern Ontario, Dataset, Availiable at: http://www.mndm.gov.on.ca/en/mines-and-minerals/applications/ogsearth/surficial-geology.

Pfannkuch, H.O. and Winter, T.C. 1984. Effect of anisotropy and groundwater system geometry on seepage through lakebeds: 1. Analog and dimensional analysis. J. Hydrol., 75: 1, 213-237. https://doi.org/10.1016/0022-1694(84)90051-9

Rosenberry, D.O., Lewandowski, J., Meinikmann, K., and Nützmann, G. 2015. Groundwater - the disregarded component in lake water and nutrient budgets. Part 1: effects of groundwater on hydrology. Hydrolog. Proc., 29: 13, 2895-2921. https://doi.org/10.1002/hyp.10403

Russell, H.A.J., Sharpe, D., Brennand, T.A., Barnett, P.J., and Logan, C. 2003. Tunnel channels of the Greater Toronto and Oak Ridges Moraine areas, southern Ontario Geological Survey of Canada, Open File 4485. https://doi.org/10.4095/214777

Santos, I.R., Niencheski, F., Burnett, W., Peterson, R., Chanton, J., Andrade, C.F.F., Milani, I.B., Schmidt, A., and Knoeller, K. 2008. Tracing anthropogenically driven groundwater discharge into a coastal lagoon from southern Brazil. J. Hydrol., 353: 3, 275-293. https://doi.org/10.1016/j.jhydrol.2008.02.010.

Sawyer, A.H., David, C.H., and Famiglietti, J.S. 2016. Continental patterns of submarine groundwater discharge reveal coastal vulnerabilities. Science, 353: 6300, 705-707. https://doi.org/10.1126/science.aag1058

Schmidt, A., Gibson, J.J., Santos, I.R., Schubert, M., Tattrie, K., and Weiss, H. 2010. The contribution of groundwater discharge to the overall water budget of two typical Boreal lakes in Alberta/Canada estimated from a radon mass balance. Hydrol. Earth Syst. Sci., 14: 1, 79-89. https://doi.org/10.5194/hess-14-79-2010

Schneider, R.L., Negley, T.L., and Wafer, C. 2005. Factors influencing groundwater seepage in a large, mesotrophic lake in New York. J. Hydrol., 310: 1, 1-16. https://doi.org/10.1016/j.jhydrol.2004.09.020

Sebok, E., Duque, C., Kazmierczak, J., Engesgaard, P., Nilsson, B., Karan, S., and Frandsen, M. 2013. High-resolution distributed temperature sensing to detect seasonal groundwater discharge into Lake Væng, Denmark. Water Resour. Res., 49: 9, 5355-5368. https://doi.org/10.1002/wrcr.20436

Taylor, J. 1982. An Introduction to Error Analysis. University Science Books, Mill Valley, California.

Tecklenburg, C. and Blume, T. 2017. Identifying, characterizing and predicting spatial patterns of lacustrine groundwater discharge. Hydrol. Earth Syst. Sci., 21: 10, 5043-5063. https://doi.org/10.5194/hess-21-5043-2017

Wallace, H.A. 2018. Use of regional scale field and modelling methods to evaluate nearshore groundwater discharge to a large glacial lake, Masters of Engineering Science Thesis, University of Western Ontario. https://ir.lib.uwo.ca/etd/5873/

Winter, J.G., Eimers, M.C., Dillon, P.J., Scott, L.D., Scheider, W.A., and Willox, C.C. 2007. Phosphorus inputs to Lake Simcoe from 1990 to 2003: declines in tributary loads and observations on lake water quality. J. Great Lakes Res., 33: 2, 381-396. https://doi.org/10.3394/0380-1330(2007)33[381:PITLSF]2.0.CO;2

Woessner, W.W. and Sullivan, K.E. 1984. Results of seepage meter and mini-piezometer study, Lake Mead, Nevada. Groundwater, 22; 5, 561-568. https://doi.org/10.1111/j.1745-6584.1984.tb01425.x

Young, J.D., Winter, J.G., and Molot, L. 2011. A re-evaluation of the empirical relationships connecting dissolved oxygen and phosphorus loading after dreissenid mussel invasion in Lake Simcoe. J. Great Lakes Res., 37: 7-14. https://doi.org/10.1016/j.jglr.2010.12.008

Constraining groundwater flow in Champlain Sea muds

Marc J. Hinton[1]* and Sam Alpay[1]

Abstract: One-dimensional groundwater transport modelling replicates the distribution of chloride ion concentrations measured in pore water from Champlain Sea muds, 2.8 km southeast of Kinburn, Ontario. The best fitting model simulations produce quantitative estimates of upward vertical specific discharge (q) between 0.84 and 0.97 mm/annum (mm/a) for the boundary conditions used. The average measured porosity of n = 0.55 allows calculation of a well-constrained range of average linear groundwater velocities, v = 1.5 to 1.8 mm/a. The ~100-m thickness of Champlain Sea muds at the Kinburn site is large relative to the solute transport distance. Consequently, up to 98% of the modelled initial Champlain Sea water signature in pore water was preserved at the measured peak concentration. Chloride concentrations decrease to fresh water values both above and below the position of the maximum concentration. This study demonstrates that transport modelling of such a complete concentration profile effectively constrains the range of groundwater flow rates in Champlain Sea muds.

1. Introduction

Aquitards constitute key hydrostratigraphic components of groundwater flow systems. They confine aquifers, limit groundwater recharge and flow, protect aquifers from chemical and microbial contamination, and serve for long-term storage of domestic, industrial, and radioactive waste (Cherry et al. 2006). During the retreat of the Laurentide ice sheet at the end of the last glaciation, the Champlain Sea inundated lowlands within the St. Lawrence and Ottawa valleys from approximately 12k to 10k ^{14}C years before present (BP; radiocarbon dating; Fulton and Richard 1987; Parent and Occhietti 1988; Figure 1). Clay- and silt-sized deposits (i.e., mud) from the Champlain Sea, known locally as Leda clay (Crawford, 1968), form a low-permeability, regionally extensive aquitard. The properties of Champlain Sea muds influence ground settlement, development of sensitivity (ratio of undisturbed to remoulded compressive strength), landslide risk, earthquake hazard (amplification of ground motion) and building code provisions (Crawford 1968; Penner and Burn 1978; Carson 1981; Crow et al. 2011; Quinn et al. 2011; Banab et al. 2012; Crow et al. 2014).

Groundwater transport processes modify pore water concentrations in Champlain Sea sediments post-deposition. Transport processes considered in this study include advection, dispersion, and diffusion (Fetter 1992). Advective groundwater flow is the physical movement of groundwater through the subsurface by gravity and pressure. Advection is expressed quantitatively as the specific discharge (q), also known as the Darcy flux, which is the volumetric groundwater flow per unit cross-sectional area. Solute transport by the bulk motion of groundwater flow is by advection. Dispersion is the process of solute transport at a rate different from the average linear groundwater velocity, which results in spreading of the solute, either perpendicularly or in the same direction as the flow path. Diffusion is a dispersion process of solutes on the ionic or molecular scales, driven by a concentration gradient. Diffusive transport becomes more significant in conditions of low groundwater flow (e.g., Freeze and Cherry 1979).

Modelling groundwater transport in Champlain Sea muds quantifies the relative influences of flow velocity, dispersion, and diffusion. Despite non-zero measurements of vertical hydraulic gradients, Quigley et al. (1983) and Desaulniers and Cherry (1989) assumed that advection was negligible as a transport process in their modelling of pore water data and that diffusion, alone, controlled the mobility of major ions in Champlain Sea sediments. The specific aim of this study is to model the processes that generated the observed chloride ion concentrations in pore water, which will constrain vertical groundwater flow estimates within a thick succession of Champlain Sea muds near Kinburn, Ontario. In so doing, this study constitutes a first attempt to model 1-D groundwater transport at the Kinburn site.

Geology Survey of Canada, Natural Resources Canada, 601 Booth Street, Ottawa, ON K1A 0E8

*corresponding author: marc.hinton@canada.ca

Recommended citation: Hinton M.J. and Alpay, S. 2020. Constraining groundwater flow in Champlain Sea muds. In Russell, H.A.J. and Kjarsgaard, B.A. Eds. Southern Ontario groundwater project 2014–2019: summary report. Geological Survey of Canada, Open File 8536, 203-215. https://doi.org/10.4095/321106

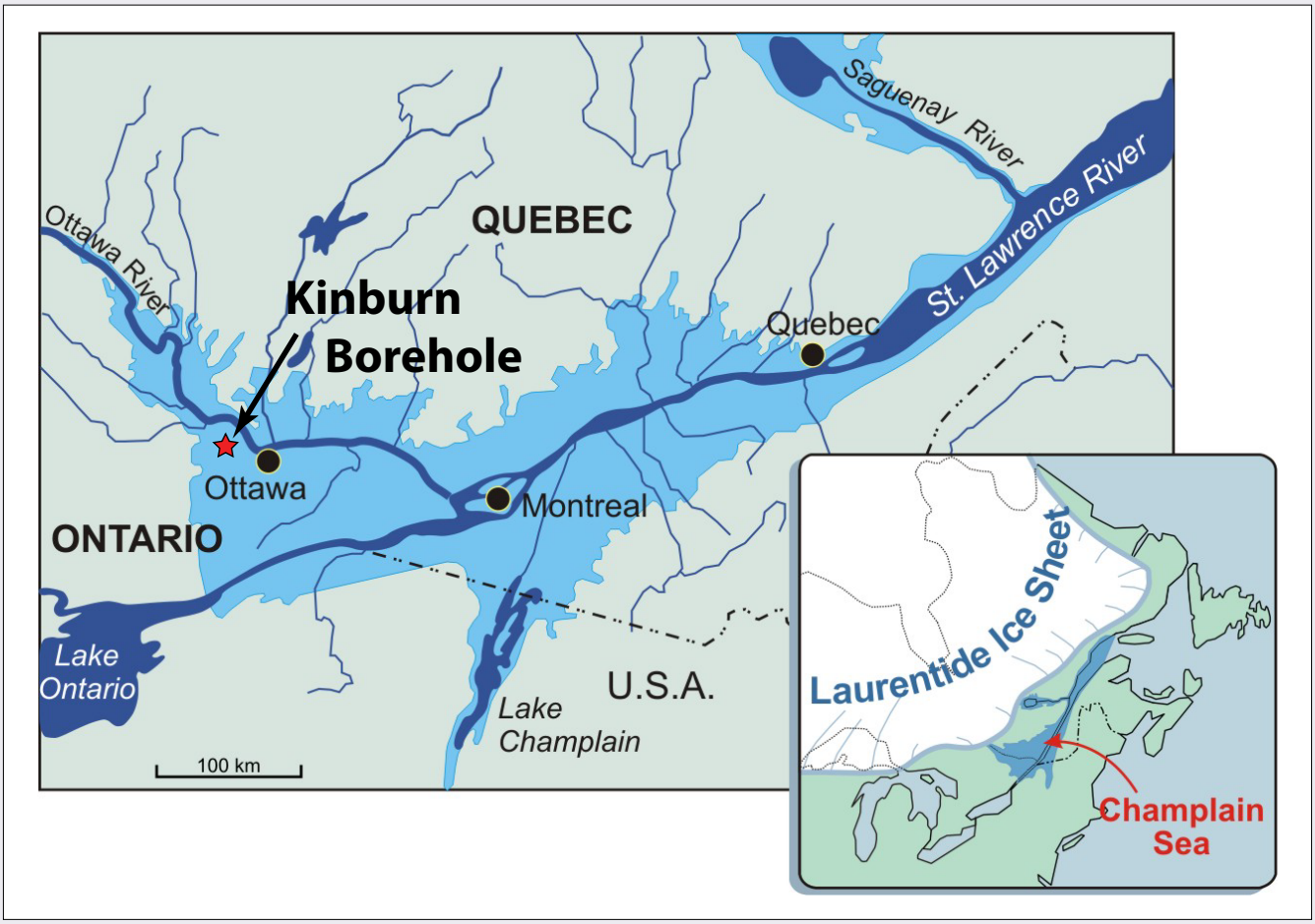


Figure 1. Location of the Kinburn borehole in the western Champlain Sea basin (after Aylsworth 2012).

2. Study site

The Kinburn borehole, drilled to a depth of 96.7 m, is located 2.8 km southeast of the town of Kinburn, Ontario. Sediment samples from the borehole chronicle one of the thickest successions of muds recorded within the western Champlain Sea basin (~101 m; Medioli et al. 2012; Figure 1). Artesian conditions in the piezometer installed at the base of the borehole, as well as artesian flow reported by residents with neighbouring water wells, indicate upward groundwater flow. Pore water chemistry and the downhole geophysical log of apparent conductivity demonstrate that the Kinburn site has a high proportion of relic marine salinity preserved within Champlain Sea muds (Medioli et al. 2012), one of only a few examples documented in the western Champlain Sea basin (e.g., Torrance 1979, 1988; Crow et al. 2017).

Seven stratigraphic facies represent distinct depositional environments and salinity conditions (Table 1; Medioli et al. 2012). Five stratigraphic facies (A to E) are observed in borehole geophysical logs and drill core. The lowermost two facies (Z and Y) are located between the base of the borehole and the bedrock surface; their depths and descriptions are interpretated from seismic reflections (Figure 2; Medioli et al. 2012) and local water well record descriptions, which report units of "sand silt", "sand", "clay gravel sand" and "gravel sand" above bedrock (GIN 2018).

3. Methods

3.1 Field and laboratory methods

Mud rotary coring allowed nearly continuous recovery (93%) of a thick sequence of Champlain Sea muds until drilling intercepted artesian conditions (Medioli et al. 2012). Centrifuging sediment samples from core segments yielded 57 pore water samples for chemical analyses (Medioli et al. 2012). Chloride concentrations, [Cl^-], were analysed by inductively coupled plasma optical emission spectrometry (described by Crow et al. 2017).

3.2 Modelling approach

One-dimensional finite-element modelling was conducted using FEFLOW (version 7.1.4) software to replicate chloride

Table 1. Facies boundaries and salinity conditions for hydrogeological modelling.

Facies, description[a]	**Depth range** (m)	**Facies thickness** (m)	**Salinity conditions** assumed at initial deposition, during CS (Champlain Sea) and post-CS
E, upper clayey silt	0 to 8.5	8.5	Fresh water, transitioning to brackish by upward transport post-CS
D, upper red and grey rhythmites	8.5 to 19	10.5	Transition from high salinity marine to freshwater
C, massive marine clay	19 to 62	43	High salinity marine
B, grey rhythmites	62 to 91.5	29.5	High salinity marine
A, interstratified silty clay and sand	91.5 to 96.7[b]	5.2	Fresh water or transition from freshwater to high salinity marine, possibly displaced by seawater during CS, displaced by fresh water post-CS
Z, sand with silt (lithology unconfirmed)	96.7[b] to 101.1[c]	4.4	
Y, gravel with sand, esker (lithology unconfirmed)	101.1[c] to 120.6[c]	19.5	Fresh water initially, likely displaced by seawater during CS, displaced by fresh water post-CS

[a] based on Medioli et al., 2012. [b] base of borehole, near facies boundary, according to seismic section (Figure 2).
[c] interpreted from seismic section (Figure 2).

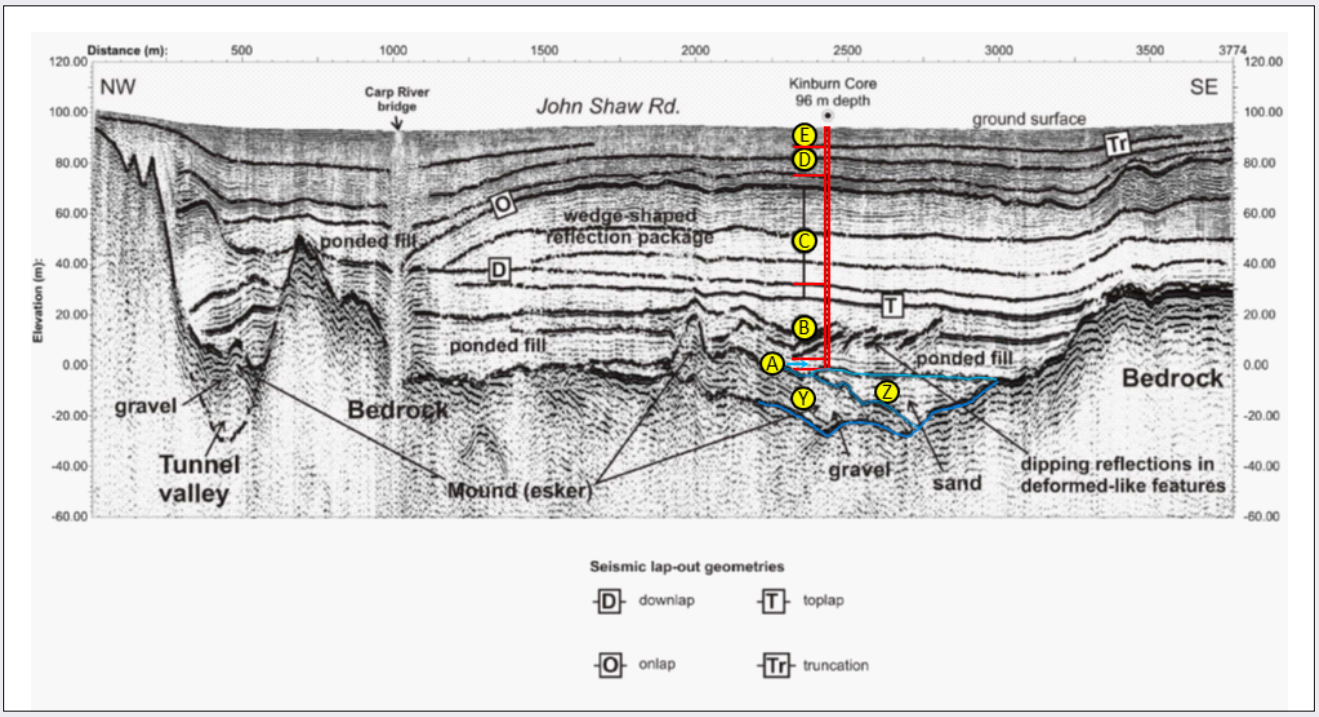


Figure 2. Interpreted seismic section, including the Kinburn borehole, inferred structures and lithologies (after Medioli et al., 2012). Facies A-E and Y-Z are described in Table 1.

concentrations measured in pore water. The vertical, saturated, and confined 2-D hydrogeological model simulates steady state flow and transient transport conditions. There is only one column of quadrilateral elements. Holding parameters constant in the x-direction allows modelling of 1-D vertical flow and transport. The quadrilateral mesh is 1 × 12,278 elements with an approximate vertical element thickness of 1 cm.

The main strategies of the modelling are to constrain vertical groundwater flow and to optimize parameters to match the observed chloride concentrations in pore water using realistic assumptions. Model runs simulate [Cl^-] distributions in pore water with three different positions of the lower freshwater boundary (Table 2), which in turn, provide low, high and intermediate estimates of vertical groundwater flow velocity.

Table 2. Model parameters, boundary (BC), and initial (IC) conditions.

	Depth range (m)	Simulation 1 Low q	Simulation 2 High q, shallow freshwater IC	Simulation 3 High q, deeper freshwater IC
Flow parameters				
$K_{surface}$ (m/s)	0.0 – 2.0	1.0E-08	1.0E-08	1.0E-08
$K_{CS\ sediments}$ (m/s)	2.0 – 96.7	4.97E-10[a]	1.07E-09[a]	1.07E-09[a]
$K_{sand/silt}$ (m/s)	96.7 – 101.1	1.0E-07	1.07E-09[a]	1.07E-09[a]
K_{gravel} (m/s)	101.1 – 120.6	1.0E-07	1.0E-07	1.0E-07
Flow BC				
$h_{surface}$ (m)	0.0 – 2.0	-2.0	-2.0	-2.0
h_{base} (m)	variable depth	3.093 (@96.7 m)	3.341 (@120.6 m)	3.341 (@120.6 m)
Mass transport parameters				
n_{mud}	0.0 – 96.7	measured	measured	measured
$n_{sand/silt}$	96.7 – 101.1	0.51	0.51	0.51
n_{gravel}	101.1 – 120.6	0.30	0.30	0.30
D_0 (m^2/s)	0.0 – 120.6	2.03E-09	2.03E-09	2.03E-09
D^* (m^2/s)	0.0 – 120.6	calculated Eq. 3	calculated Eq. 3	calculated Eq. 3
α_L (m)	0.0 – 120.6	2.14[a]	1.52[a]	1.52[a]
Mass transport BC				
$C_{surface}$ (t) (ppm)	0.0 – 2.0	10	10	10
C_{base} (t) (ppm)	variable depth	1000 (@96.7 m)	1000 (@120.6 m)	1000 (@120.6 m)
Mass transport IC				
$C_{Facies\ E}$ (0) (ppm)	0 – 8.5	10	10	10
$C_{Facies\ D}$ (0) (ppm)	8.5 – 19	10000	10	10[b]
$C_{Facies\ C\ and\ B}$ (0) (ppm)	19 – 91.5	17600	17600	17600[c]
$C_{Facies\ A}$ (0) (ppm)	91.5 – 96.7	10000	17600	17600
$C_{sand/silt}$ (0) (ppm)	96.7 – 101.1	1000	17600	17600
C_{gravel} (0) (ppm)	101.1 – 120.6	1000	17600	17600
Duration of simulation (years)		10460	10460	10460

K = hydraulic conductivity.
h = hydraulic head.
n = porosity.
D_0 = Free diffusion coefficient (25°C).
D* = Effective diffusion coefficient (corrected to 8°C).
α_L = longitudinal dispersivity.
C (t) = concentration at time t.
C (0) = initial concentration.

[a] parameters (K, αL) adjusted for optimized fit to [Cl^-] profile.
[b] applied IC from 8.5 – 36.0 m depth.
[c] applied IC from 36.0 – 91.5 m depth.

Table 2. (continued). Model parameters, boundary (BC) and initial (IC) conditions.

	Depth range (m)	Simulation 4 Intermediate q, Med reservoir effect	Simulation 5 Intermediate q, Min reservoir effect	Simulation 6 Intermediate q, Max reservoir effect
Flow parameters				
$K_{surface}$ (m/s)	0.0 – 2.0	1.0E-08	1.0E-08	1.0E-08
$K_{CS\ sediments}$ (m/s)	2.0 – 96.7	5.73E-10 [a]	5.38E-10 [a]	6.10E-10 [a]
$K_{sand/silt}$ (m/s)	96.7 – 101.1	5.73E-10 [a]	5.38E-10 [a]	6.10E-10 [a]
K_{gravel} (m/s)	101.1 – 120.6	1.0E-07	1.0E-07	1.0E-07
Flow BC				
$h_{surface}$ (m)	0.0 – 2.0	-2.0	-2.0	-2.0
h_{base} (m)	variable depth	3.329 (@101.1 m)	3.329 (@101.1 m)	3.329 (@101.1 m)
Mass transport parameters				
n_{mud}	0.0 – 96.7	measured	measured	measured
$n_{sand/silt}$	96.7 – 101.1	0.51	0.51	0.51
n_{gravel}	101.1 – 120.6	0.30	0.30	0.30
D_0 (m^2/s)	0.0 – 120.6	2.03E-09	2.03E-09	2.03E-09
D^* (m^2/s)	0.0 – 120.6	calculated Eq. 3	calculated Eq. 3	calculated Eq. 3
α_L (m)	0.0 – 120.6	1.97[a]	1.52[a]	2.41[a]
Mass transport BC				
$C_{surface}$ (t) (ppm)	0.0 – 2.0	10	10	10
C_{base} (t) (ppm)	variable depth	1000(@101.1 m)	1000(@101.1 m)	1000(@101.1 m)
Mass transport IC				
$C_{Facies\ E}$ (0) (ppm)	0 – 8.5	10	10	10
$C_{Facies\ D}$ (0) (ppm)	8.5 – 19	5000	5000	5000
$C_{Facies\ C\ and\ B}$ (0) (ppm)	19 – 91.5	17600	17600	17600
$C_{Facies\ A}$ (0) (ppm)	91.5 – 96.7	10000	10000	10000
$C_{sand/silt}$ (0) (ppm)	96.7 – 101.1	10000	10000	10000
C_{gravel} (0) (ppm)	101.1 – 120.6	1000	1000	1000
Duration of simulation (years)		10460	11210	9760

K = hydraulic conductivity.
h = hydraulic head.
n = porosity.
D_0 = Free diffusion coefficient (25°C).
D* = Effective diffusion coefficient (corrected to 8°C).
α_L = longitudinal dispersivity.
C (t) = concentration at time t.
C (0) = initial concentration.

[a] parameters (K, αL) adjusted for optimized fit to [Cl^-] profile.
[b] applied IC from 8.5 – 36.0 m depth.
[c] applied IC from 36.0 – 91.5 m depth.

3.2.1 Variables

Three model variables are adjusted to match measured [Cl^-] in pore water: vertical specific discharge (Darcy flux; q); the longitudinal hydrodynamic dispersion coefficient (D_L); and the initial chloride concentration ($[Cl^-]_0$) when the Champlain Sea withdrew from the site. Using Darcy's Law (Freeze and Cherry 1979),

$$q = K \cdot i = v \cdot n \qquad (1)$$

q is directly controlled by varying the hydraulic conductivity (K) because the hydraulic gradient (i) is held constant in the model. In a one-dimensional flow model, the vertical q is constant over the length of the sediment column, however, the average groundwater velocity, v, varies slightly and inversely with porosity, n. Sixty-four measurements of n, sampled at drill core intervals of approximately 1.5 m (Medioli et al. 2012), are interpolated for each model element and, thereby, are incorporated directly into the model.

D_L is calculated in terms of two components (Fetter 1992),

$$D_L = \alpha_L \cdot v + D^* \qquad (2)$$

where α_L is the longitudinal dispersivity and D^* is the effective diffusion coefficient. Desaulniers and Cherry (1989) and Benabdallah (2010) assumed that α_L has a negligible effect on D_L because of low groundwater flow velocities in Champlain Sea muds. In this study, however, α_L is considered to have a measurable effect on D_L . D^* is calculated as a function of the free-water diffusion coefficient (D_0) and n,

$$D^* = D_0 \cdot n^m \qquad (3)$$

where m is an empirical constant (m = 2.3 for Cl^-; Harrington et al. 2013) and D_0 = 2.032E-09 m^2/s for Cl^- at 25°C (Chemical Rubber Company 2010). As diffusion varies with temperature, the approach of Harrington et al. (2013, their Equation 9) is used to calculate a temperature correction factor of 0.614 (from 25°C to 8°C). Using Equation 3 and the temperature correction factor causes D^* to vary along the vertical profile and to be scaled according to the measured porosities. As D^* is constant for a fixed value of porosity (3.12E-10 m^2/s for Cl^- at 8°C for the average n = 0.55), only α_L is adjusted in the model to vary D_L to match the shape and slope of the pore water [Cl^-] profile.

Allowing $[Cl^-]_0$ values to vary with depth or with facies affects the total initial mass of Cl^- in the sediment profile. It also influences the shape of the final [Cl^-] profile and requires adjustment to replicate measured data. In this study, $[Cl^-]_0$ values are held constant for each facies (Table 2). The one exception is Simulation 3, where it is necessary to extend the fresh water zone initial condition into Facies C to a depth 36 m to match the final concentration profile. After manually adjusting variables to fit the [Cl^-] profiles, FePEST (version 7.1.4; parameter estimation software) is used to optimize the values of K and α_L for fixed values of $[Cl^-]_0$.

3.2.2 Boundary conditions and assumptions

Drilling encountered artesian conditions at the base of the borehole, an observation supported by upward groundwater flow recorded in the borehole piezometer (Medioli et al. 2012). Accordingly, this modelling exercise assumes upward 1-D groundwater flow from the bottom boundary condition to the surface boundary. Near ground surface, a hydraulic head 2 m below ground surface (mbgs) is assumed for all nodes between 0 and 2 m depth, consistent with water levels in the adjacent stream. Any vertical infiltration into the ground surface is assumed to flow laterally within the upper 2 m and not to affect 1-D upward groundwater flow. At the base of the model, the depth of the specified head is different for each simulation (Table 2), adjusted to obtain the measured hydraulic head of 2.9 m above ground surface (mags) at the mid-screen depth of the piezometer (93.12 mbgs) and to maintain a constant hydraulic gradient.

The [Cl^-] at the upper boundary is assumed constant at 10 ppm for a depth of 0–2 m, which is comparable to that of the uppermost pore water sample at a depth of 0.72 m ([Cl^-] = 13.3 ppm). The position of the lower boundary condition (BC) for [Cl^-] is chosen to coincide with the depth of the hydraulic head BC. Its value is set at an assumed concentration of 1,000 ppm to provide a reasonable fit with the [Cl^-] data.

Certain assumptions allow more straightforward model development as a first approximation. For example, the model activates immediately after the marine waters of the Champlain Sea recede. Thus, it represents the salinity profile at the end of Champlain Sea deposition and does not account for advection, dispersion and diffusion during the Champlain Sea episode or for post-depositional changes from compaction or diagenesis. The best estimate for the timing of Champlain Sea withdrawal from the western basin is 10k ^{14}C years BP or 11.5k calendar years BP (Fulton and Richard 1987; Parent and Occhietti 1988). Incorporating dead carbon with marine fossils used for radiocarbon dating causes overestimation of age dates (Ascough et al. 2005). This reservoir effect is typically 400 calendar years for global oceans (Ascough et al. 2005) and ranges between 350 and 1800 calendar years in the Champlain Sea (Cronin et al. 2008). A reservoir effect of 1,100 calendar years, the mid-point of published ranges, is selected in Simulations 1–4 for an estimated 10,460 calendar years from the Champlain Sea regression to the time of sampling (approximately 60 years after 1950, the reference year for ^{14}C measurements). The full range of the estimated reservoir effect, between 350 and 1,800 calendar years, is used for Simulations 5 and 6 (11,210 and 9,760 years, respectively, Table 2).

Additional simplifying assumptions are inherent in the model. As previously noted, the initial chloride concentration at the start of the simulations is assumed constant across each facies thickness except where indicated for Simulation 3. Freshwater displaces marine water from the basal aquifer immediately after withdrawal of the Champlain Sea. A further simplification is

that the vertical groundwater flux (*q*) is spatially and temporally constant (i.e., steady state and uniform along the profile) and starts uniformly once the Champlain Sea retrogresses.

4. Results

Three sets of model simulations assume different boundary conditions (Table 2). The different groundwater transport distances generate a range of Darcy fluxes.

4.1 Simulation 1, low q

Modelling results for Simulation 1 (low *q*; Figure 3, Table 3) estimate a lower limit of specific discharge (q) by defining boundary conditions that set a shorter vertical distance for lower salinity fresh water ([Cl^-] = 1,000 ppm) to displace marine water in the pore water profile. Simulation 1 assumes that the lower two facies, Z and Y, identified in the seismic section (Figure 2), are permeable and that they are flushed rapidly by horizontal flow of fresh water below a depth of 96.7 m (Table 2). The $[Cl^-]_0$ in Facies B and C is modelled to be 17,600 ppm, whereas those in Facies A and D are transitional between marine and fresh water (Table 2). A longitudinal dispersivity (α_L) of 2.14 m and a Darcy flux (*q*) of 0.84 mm/a reproduce the concentration profile optimally. This lower estimate of *q* is equivalent to an average groundwater velocity of 1.54 mm/a (Table 3).

4.2 Simulations 2 and 3, high q

Results from Simulations 2 and 3 (high *q*) rely on the assumption that fresh water occurs only in the bedrock at the base of the gravel unit and that its transit through the silty sand and gravel units is by vertical transport. These simulations estimate the upper limit of specific discharge by setting boundary conditions that allow fresh water a longer vertical distance of travel to displace seawater in the lower portion of sediment profile (Figure 4). However, the resulting higher specific discharge would also displace high [Cl^-] pore water into the shallow sediment horizons, which is inconsistent with

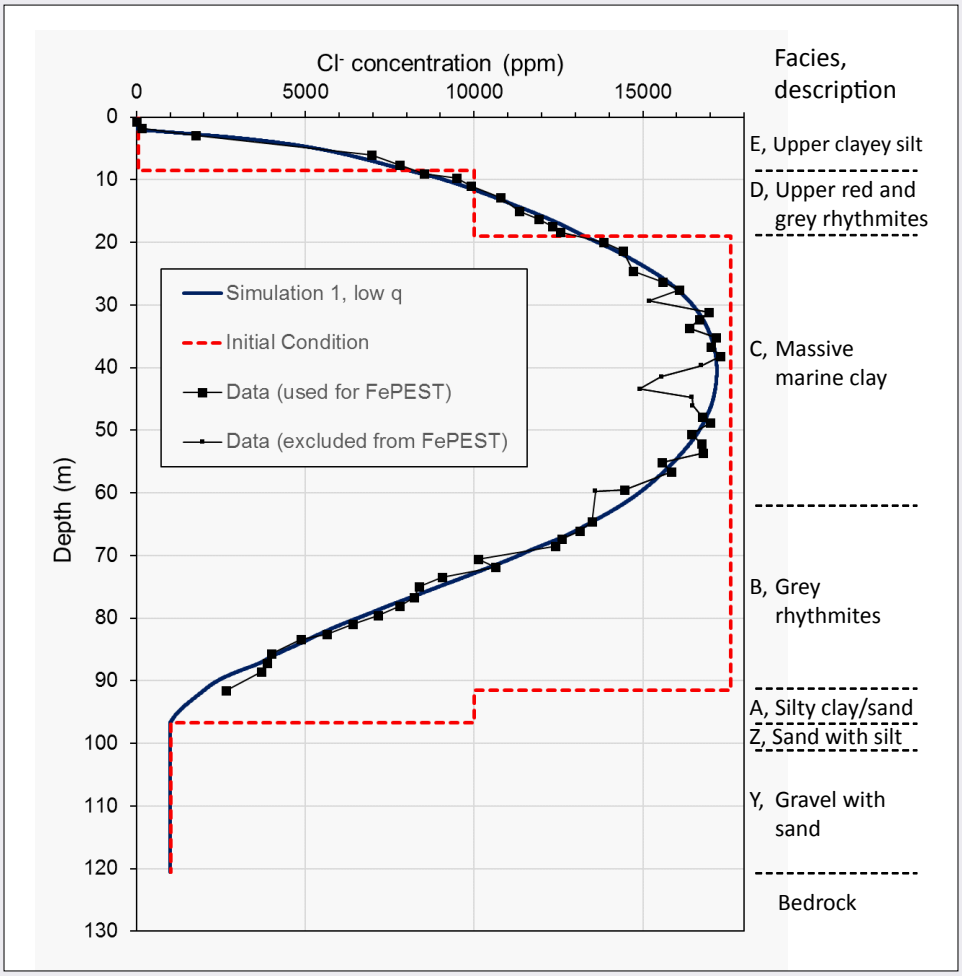


Figure 3. Model results for Simulation 1 (low q).

Table 3. Model results.

	Specific discharge, q		Velocity, v[a]		Hydraulic conductivity, K
	(m/s)	(mm/a)	(m/s)	(mm/a)	(m/s)
Simulation 1 – low q (t = 10460 a)	2.67E-11	0.84	4.88E-11	1.54	5.0E-10
Simulations 2 and 3 – high q (t = 10460 a)	5.77E-11	1.82	1.06E-10	3.33	1.1E-09
Simulation 4 – intermediate q (t = 10460 a)	3.08E-11	0.97	5.63E-11	1.78	5.7E-10
Simulation 5 – intermediate q (t = 11210 a)	2.89E-11	0.91	5.29E-11	1.67	5.4E-10
Simulation 6 – intermediate q (t = 9760 a)	3.28E-11	1.03	6.00E-11	1.89	6.1E-10

[a] Assuming average porosity of 0.55 (from Medioli et al., 2012) using Equation 1.

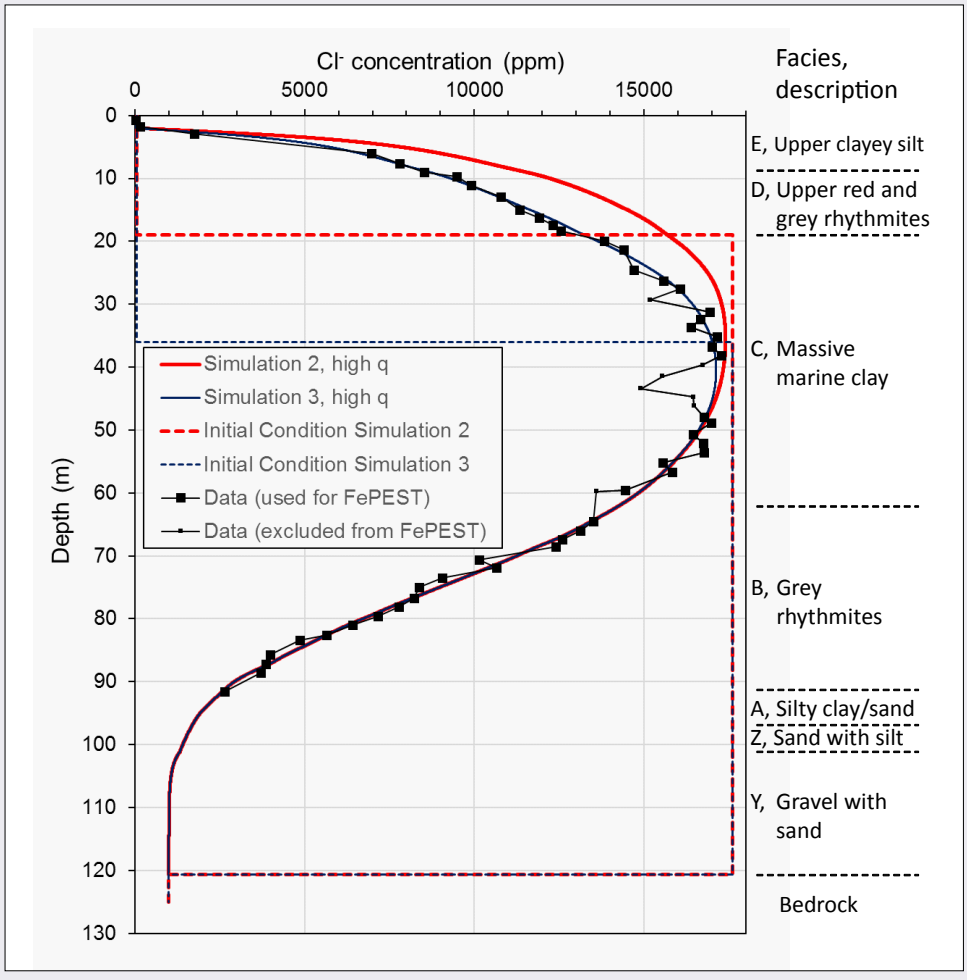


Figure 4. Model results for Simulations 2 and 3 (high *q*; two initial conditions).

the measured [Cl^-] profile (Simulation 2, Figure 4). Therefore, the $[Cl^-]_0$ in the upper 36 m is set to 10 ppm in Simulation 3 to provide a more robust fit to the observed upper [Cl^-] profile (Figure 4). For Simulations 2 and 3, the upper estimate of q is 1.82 mm/a, which is equivalent to an average linear velocity of 3.33 mm/a (Table 3).

4.3 Simulations 4, 5 and 6, intermediate q

In the final three simulations (intermediate q; Figure 5), it is assumed that the underlying gravel unit is flushed with fresh water by horizontal flow and that transport through Facies Z is vertical. Facies Z is assigned the K of the Champlain Sea sediments and the $[Cl^-]_0$ of Facies A. Simulation 4 yields an estimate of q = 0.97 mm/a, which is equivalent to an average velocity, v, of 1.78 mm/a (Table 3). Simulations 5 and 6 serve to compare the effects of simulation time in the model runs with reference to Simulation 4 (Figure 5). Simulated durations of 11,210 and 9,760 years, respectively, represent the full range of estimated reservoir effects for the Champlain Sea (Cronin et al. 2008). Modelled [Cl^-] profiles for Simulations 5 and 6 are nearly identical to Simulation 4, but the q changes by ±6% to produce similar net transport for different model durations (Table 3).

5. Discussion

Simulations of chloride ion concentrations in pore water from Champlain Sea muds provide quantitative estimates of upward, 1-D groundwater flow (specific discharge), with q ranging from 0.84 to 1.82 mm/a. However, model solutions are not unique. Various combinations of boundary condition positions, q, D_L and $[Cl^-]_0$ can be adjusted in the model to

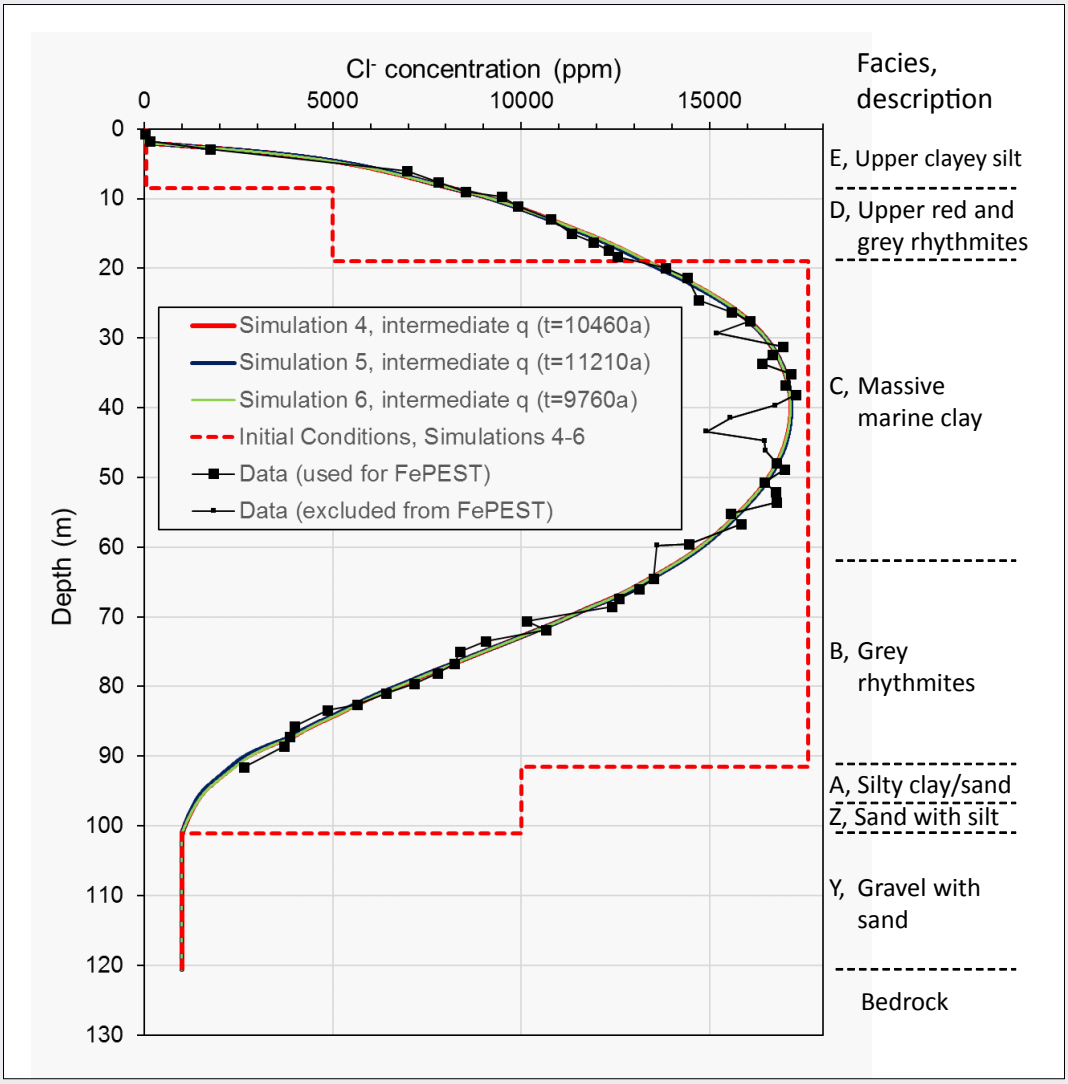


Figure 5. Model results for Simulations 4, 5, and 6 (intermediate q) over three different model run durations of 9760, 10460 and 11210 years, respectively.

approximate the observed [Cl^-] profile in pore water. The validity of each simulation depends on how accurately it characterizes true groundwater conditions. For example, the initial condition for Simulation 3 is unrealistic because it requires an initial fresh water condition to a depth of 36 m (all of Facies D and a portion of Facies C). Such a condition is not viable because geotechnical sensitivities exceeding 20 were observed at a depth of 10 m, which would have likely required rapid flocculation in marine or brackish water with a minimum salinity of 2–3 ‰ (Torrance 1979) or $[Cl^-]_0$ of approximately 1,100–1,700 ppm. In contrast, the initial chloride concentrations for Facies D in Simulations 1 and 4–6 are more realistic. Consequently, advective flow is likely at the lower end of the range, with q = 0.84 to 0.97 mm/a.

The measured pore water [Cl^-] profile in thick Champlain Sea deposits characterizes low salinity near the base, an increase to peak salinity within the muds, and an upward decrease towards fresh water near the ground surface. The nearly complete pore water [Cl^-] profile at the Kinburn site enables better constraints on 1-D groundwater flow estimates and initial conditions because transport modelling results must fit both the increase and decrease in concentrations with depth for a common q. Although all simulations reproduce the lower part of the concentration profile by modifying q according to the initial position of the fresh water boundary, simultaneously matching the upper part of the profile requires significant modification of $[Cl^-]_0$ in the upper profile. Increasing the upward q requires a decrease in $[Cl^-]_0$ of Facies D to match the measured [Cl^-] data. However, there is a threshold at which imposing both an increase in q and a decrease in $[Cl^-]_0$ becomes unrealistic as demonstrated in Simulation 3. Matching measured concentration data requires a balance between q and the initial distribution of mass, hence, a linkage between the initial conditions and the modelled q.

For a given position of the lower boundary condition, the range of q is well constrained to obtain good correlation between model results and measured [Cl^-]. Therefore, the challenge is to identify the correct lower boundary location and $[Cl^-]_0$ conditions. The positions of the lower fresh water boundary differ substantially in Simulations 1 and 3 (depths of 96.7 and 120.6 m, respectively). The resulting difference in q is 1.02 mm/a (116% of the low flow estimate), which is a small value with respect to the magnitude of water cycle fluxes, but a large relative difference in Darcy flow. Comparing the more realistic Simulations 1 and 4 indicates a 4.4-m difference in the depth of the fresh water boundary, which results in a 15% difference in q (0.13 mm/a). Consequently, the estimate of q (0.84–0.97 mm/a) appears to be well constrained, despite the uncertainty in the position of the lower fresh water boundary.

The groundwater velocity estimates in this study (Table 3) compare well with those of Desaulniers and Cherry (1989), using measured K, i and n (Equation 1) in a Champlain Sea sequence at Varennes, 35 km northeast of Montreal. They found v ranges between 0.3 and 1.7 mm/a (q from 0.2 to 1.1 mm/a) with an average value of 1.3 mm/a (q = 0.83 mm/a). Flow estimates from this study are also comparable to those from Benabdallah's (2010) 2-D model along an incised cross-section of Champlain Sea muds. His model indicates vertical velocities of v = 0.5–2.8 mm/a (q = 0.3–1.7 mm/a) at four sites distal from the Rivière-des-Mille-Îles to 23 mm/a (q = 14 mm/a) at a site adjacent to the river, where the hydraulic gradient was highest (i = 0.24) and, therefore, not comparable to the gradients at the Kinburn site.

The average vertical K of the muds for Simulations 1 and 4 are 5.0E-10 and 5.7E-10 m/s, respectively (Table 3). Given the narrow range of estimated q, it follows from Equation 1 that the range in the average vertical K is also relatively small. However, the additional uncertainty in vertical hydraulic gradient must be taken into account. The hydraulic gradient across the muds for all simulations is held constant at 0.054 to ensure that q is a function of only one variable, K. The hydraulic gradient at this site could vary from approximately 0.03 to 0.07, using the range in hydraulic heads estimated at the upper boundary and measured in the lower piezometer. Therefore, the potential value of average vertical K could vary by about a factor of 3 from 3.8E-10 to 1.0E-09 m/s. Estimates of K are consistent with measured values at other sites within the Champlain Sea basin (Table 4). Note that there is no distinction made between vertical and horizontal hydraulic conductivity as Tavenas et al. (1983a) found anisotropy of permeability in Champlain Sea muds to be negligible.

Preservation of a marine signature is evident from pore water ion concentrations, their distributions and previous parallel results (e.g., downhole geophysical log of apparent conductivity and pore water conductivity; Medioli et al. 2012). The modelled $[Cl^-]_0$ of 17,600 ppm (Table 2) is slightly higher than the maximum measured concentration of 17,290 ppm and corresponds to a salinity of approximately 31.8 or 90% of the seawater [Cl^-] during the Champlain Sea episode (Figure 8 in Adkins and Schrag 2003). Although it is possible to use initial concentrations as high as that of seawater during the Champlain Sea phase for Facies B and C, the effect on q is negligible (<0.4%), but the model fit is inferior.

The effect of varying simulation time on q is minimal (6%; Figure 5, Table 3). However, realistically fresh water cannot displace marine waters at the lower boundary instantaneously after the Champlain Sea recedes. The additional time for fresh water to displace marine water from basal aquifers would require a slightly higher q. For example, a displacement time of 2,000 years would increase q to 1.08 mm/a (11% increase). However, there is a limit to optimizing fit to measured data. Increasing the time delay for fresh water input and Darcy flux eventually necessitates decreasing $[Cl^-]_0$ in Facies D, which would be close to the lower limit of salinity for this unit, as in Simulation 3.

A variety of approaches could achieve better constraints on estimates for groundwater advection through Champlain Sea muds. Deeper drilling to bedrock would allow for confirmation

Table 4. Hydraulic conductivity estimates of unweathered Champlain Sea muds.

Source	Mean K (m/s)	Minimum K (m/s)	Maximum K (m/s)	Method
This study	5.7E-10[a]	3.8E-10[b]	1.0E-09[b]	Modelling [Cl^-] profile
Benabdallah (2010)	1.8E-09	7.7E-10	3.7E-09	Triaxial cell
Benabdallah (2010)	9.8E-10	4.6E-10	3.4E-09	Slug/bail tests
GSI Environnement (2001, as reported in Benabdallah, 2010)	2.3E-09	6.7E-10	8.8E-09	Triaxial cell and oedometer
Desaulniers and Cherry (1989)	3.4E-10	7.5E-11	4.9E-10	Bail tests
Tavenas et al. (1983b)	–	5.5E-11	8.3E-10	Oedometer
Tavenas et al. (1983a)	–	5.2E-10	5.0E-09	Triaxial cell
Sauriol (2016)	–	2.0E-06[c]	7.0E-06[c]	Modelling of hydraulic response

[a] Simulation 4.

[b] Using Equation 1 with q from Simulations 1 and 4 and i from 0.03 – 0.07.

[c] Overlying an esker.

of the stratigraphy at the Kinburn site and determination of pore water [Cl^-] in the lower sand/silt and gravel units (Facies Y and Z). Measurements of groundwater [Cl^-] in the underlying aquifer from nearby domestic wells could be a more cost-effective approach to aid estimation of pore water [Cl^-] for the lower boundary condition. Additionally, 1-D modelling of multiple chemical tracers (ionic, isotopic) may provide further constraints on boundary conditions and flow estimates. Regional 2- or 3-D groundwater transport modelling could simulate the [Cl^-] over time at the lower boundary. Although the 1-D model adequately reproduces the [Cl^-] profile, there is some evidence of minor 2-D or 3-D flow. For example, small decreases in [Cl^-] within the vertical pore water profile could indicate minor components of horizontal flow (i.e., the data points excluded for parameter estimation using FePEST, Figures 3–5), particularly in facies with observed fine laminations or partings of sand/silt within the muds. The most notable excursion in the pore water [Cl^-] profile occurs at a depth of 44.4 m (Figures 3, 4, 5) and is corroborated by a coincident decrease in apparent conductivity from geophysical borehole logging (Medioli et al. 2012), as a possible indication of a horizontal groundwater flow component. Additionally, measurements of hydraulic head along the profile and, particularly for the upper boundary condition, would help constrain vertical hydraulic gradients and estimates of hydraulic conductivity within the different facies.

At the Kinburn site, both advection and dispersion (including diffusion) contribute to the transport of chloride. This finding contrasts with modelling results of Quigley et al. (1983) and Desaulniers and Cherry (1989), who concluded that invoking diffusion as the only transport mechanism was sufficient to explain ion concentration profiles and that advection was negligible. However, non-zero hydraulic gradients were measured in their piezometer nests, indicating the presence of vertical advection. In the current study, *q* is nearly identical to that estimated from the piezometric data of Desaulniers and Cherry (1989). However, the greater thickness of unweathered mud at the Kinburn site (>95 m), compared to the Varennes site (25–27 m, Desaulniers and Cherry 1989), ensures better preservation of the [Cl^-] profile, thereby allowing more precise constraints on the modelled parameter estimates. The estimated values of *v* (Table 3) at Kinburn correspond to a total advective groundwater transport distance of approximately 16.1 and 18.6 m (in Simulations 1 and 4, respectively) for the 10.4 k-year simulations. Transport distances of these magnitudes would displace a significant proportion of the initial chloride mass from the Varennes profile. At the estimated velocities, plug flow (without diffusion and dispersion) would take between approximately 54k and 63k years to displace the initial seawater from the aquitard at Kinburn.

6. Conclusions

One-dimensional groundwater transport modelling simulates chloride ion concentrations in pore water of Champlain Sea muds at the Kinburn site. Simulations produce quantitative estimates of upward, vertical specific discharge with q ranging from 0.84 to 0.97 mm/a in the two most realistic groundwater scenarios. Using the average measured porosity of n = 0.55 for these muds, results are equivalent to an average linear groundwater velocity of v = 1.5 to 1.8 mm/a. These estimates are particularly well constrained because of the thickness of Champlain Sea deposits at the Kinburn site and preservation of up to 98% (fraction of current peak [Cl^-] to [$Cl^-]_0$) of the modelled initial Champlain Sea water signature in pore water. Simulations demonstrate the utility of transport modelling to estimate groundwater flow rates at sites with thick Champlain Sea muds, using results from drill core and pore water samples. Subsequent investigations can include

other pore water analyses (ionic, isotopic) at the Kinburn site and another site (Breckenridge, Crow et al. 2017), where thick Champlain Sea sediments were cored. Although the focus of this study is modelling pore water [Cl^-] to constrain estimates of groundwater flow, a similar approach could be used to establish constraints on the $[Cl^-]_0$ of the Champlain Sea and to simulate temporal variations in pore water salinity in Champlain Sea sediments.

This study addresses a missing element of aquitard characterization from Cherry et al.'s (2006) review of aquitards and their properties, namely typical hydrogeological data from an aquitard of glaciomarine origin. Understanding advection-dispersion processes in Champlain Sea muds provides greater insights on: hydrogeological issues (e.g., contaminant transport, aquitard integrity); geotechnical concerns (e.g., risk of sensitivity development and landslides); and the history of the Champlain Sea itself.

7. Acknowledgments

Scientific peer review of this contribution by H.L. Crow, H.A.J. Russell, and B.A. Kjarsgaard is gratefully acknowledged. J.M. Aylsworth graciously provided Figure 1 graphics and B.E. Medioli Figure 2. It is on the foundation of Champlain Sea research of numerous colleagues, including those at the Geological Survey of Canada (GSC), past and present, that this investigation was achievable. The Groundwater Geoscience Program, Natural Resources Canada, provided research funding for this study. This work is a contribution to the GSC–OGS southern Ontario project on groundwater 2014–2019.

8. References

Adkins, J.F. and Schrag, D.P. 2003. Reconstructing Last Glacial Maximum bottom water salinities from deep-sea sediment pore fluid profiles. Earth Planet. Sci. Lett., 216: 1-2, 109-123. https://doi.org/10.1016/S0012-821X(03)00502-8

Ascough, P., Cook, G., and Dugmore, A. 2005. Methodological approaches to determining the marine radiocarbon reservoir effect. Prog. Phys. Geog., 29: 4, 532-547. https://doi.org/10.1191/0309133305pp461ra

Aylsworth, J.M. 2012. New Canadian Teaching Resources from Natural Resources Canada for Earthquakes, Landslides and Tsunamis (lesson plans, maps and event timelines) (Jaunary 2012). Geological Survey of Canada, Open File 7073, 7 p. + 48 PDF files, 317 p. https://doi.org/10.4095/289872

Banab, K.K., Kolaj, M., Motazedian, D., Sivathayalan, S., Hunter, J.A., Crow, H.L., Pugin, A.J.M., Brooks, G.R., and Pyne, M. 2012. Seismic site response analysis for Ottawa, Canada: A comprehensive study using measurements and numerical simulations. Bull. Seismol. Soc. Am., 102: 5, 1976-1993. https://doi.org/10.1785/0120110248

Benabdallah, E.M. 2010. Mouvement des eaux souterraines et des ions majeurs dans une argile Champlain depuis sa formation, École polytechnique de Montréal, Montréal, Québec, 400 p.

Carson, M.A. 1981. Influence of porefluid salinity on instability of sensitive marine clays: A new approach to an old problem. Earth Surf. Processes Landforms, 6: 6, 499-515. https://doi.org/10.1002/esp.3290060602

Chemical Rubber Company, 2010. CRC handbook of chemistry and physics, 91st edition 2010-11. CRC Press (Taylor and Francis Group), Boca Raton, FL.

Cherry, J.A., Parker, B.L., Bradbury, K.R., Eaton, T.T., Gotkowitz, M.B., Hart, D.J., and Borchardt, M.A. 2006. Contaminant transport through aquitards: A state-of-the-science review. Dever, CO, 126 p.

Crawford, C.B. 1968. Quick clays of eastern Canada. Eng. Geol., 2: 4, 239-265. https://doi.org/10.1016/0013-7952(68)90002-1.

Cronin, T.M., Manley, P.L., Brachfeld, S., Manley, T.O., Willard, D.A., Guilbault, J.P., Rayburn, J.A., Thunell, R., and Berke, M. 2008. Impacts of post-glacial lake drainage events and revised chronology of the Champlain Sea episode 13-9 ka. Palaeogeography, Palaeoclimatology, Palaeoecology, 262: 1-2, 46-60. https://doi.org/10.1016/j.palaeo.2008.02.001

Crow, H., Alpay, S., Hinton, M.J., Knight, R.D., Oldenborger, G.A., Percival, J.B., Pugin, A.J.-M., and Pelchat, P. 2017. Geophysical, geotechnical, geochemical, and mineralogical data sets collected in Champlain Sea sediments in the Municipality of Pontiac, Quebec. Geological Survey of Canada, Open File 7881. https://doi.org/10.4095/301664.

Crow, H., Hunter, J.A., and Motazedian, D. 2011. Monofrequency in situ damping measurements in Ottawa area soft soils. Soil Dynam. Earthquake Eng., 31: 12, 1669-1677. https://doi.org/10.1016/j.soildyn.2011.07.002

Crow, H.L., Hunter, J.A., Pugin, A.J.-M., Pullan, S.E., Alpay, S., and Hinton, M.J. 2014. Empirical geophysical/geotechnical relationships in the Champlain Sea sediments of Eastern Ontario. In L'Heureux, J.-S. Ed. Landslides in Sensitive Clays: From Geosciences to Risk Management, Chapter 20. Advances in Natural and Technological Hazards Research 36. Springer Science+Business Media, Dordrecht, 253-263.

Desaulniers, D.E. and Cherry, J.A. 1989. Origin and movement of groundwater and major ions in a thick deposit of Champlain Sea clay near Montreal. Can. Geotech. J., 26: 1, 80-89. https://doi.org/10.1139/t89-009

Fetter, C.W. 1992. Contaminant hydrogeology, 2nd ed. Macmillan Publishing Company, New York, NY, 458 p.

Freeze, R.A. and Cherry, J.A. 1979. Groundwater. Prentice-Hall, Englewood Cliffs, New Jersey, 604 p.

Fulton, R.J. and Richard, S.H., 1987. Chronology of late Quaternary events in the Ottawa region. In R.J. Fulton (Editor), Quaternary geology of the Ottawa region, Ontario and Quebec. Geological Survey of Canada, GSC Paper 86-23, Ottawa, Ontario, 24-30. https://doi.org/10.4095/122374

Gadd, N.R. 1986. Lithofacies of Leda clay in the Ottawa basin of the Champlain Sea. Geological Survey of Canada, Paper 85-21, Ottawa, Ontario, 44 p. https://doi.org/10.4095/120619

GIN, 2018. Groundwater Information Network. http://gin.gw-info.net/service/api_ngwds:gin2/en/gin.html. Accessed: 20 November 2018.

GSI Environnement, 2001. Étude hydrogéologique-Agrandissement du secteur Nord, lots parties 77 à 87, 90, 93, 94, 99 et 100-BFI usine de triage Lachenaie Ltée, N/D : 293-2549-150. 62 p.

Harrington, G.A., Gardner, W.P., Smerdon, B.D., and Hendry, M.J. 2013. Palaeohydrogeological insights from natural tracer profiles in aquitard porewater, Great Artesian Basin, Australia. Water Resour. Res., 49: 7, 4054-4070. https://doi.org/10.1002/wrcr.20327

Medioli, B.E., Alpay, S., Crow, H.L., Cummings, D.I., Hinton, M.J., Knight, R.D., Logan, C., Pugin, A.J.-M., Russell, H.A.J., and Sharpe, D.R. 2012. Integrated data sets from a buried valley borehole, Champlain Sea basin, Kinburn, Ontario. Geological Survey of Canada, Current Research 2012-13: 16. https://doi.org/10.4095/289597

NRCan, 2016. Canadian Digital Elevation Model, Edition 1.1. https://open.canada.ca/data/en/dataset/7f245e4d-76c2-4caa-951a-45d1d2051333. Accessed: 30 October 2018.

Parent, M. and Occhietti, S. 1988. Late Wisconsinan Deglaciation and Champlain Sea Invasion in the St. Lawrence Valley, Québec. Géog. Phys. Quat., 42: 3, 215-246. https://doi.org/10.7202/032734ar

Penner, E. and Burn, K.N. 1978. Review of engineering behaviour of marine clays in eastern Canada. Can. Geotech. J., 15: 2, 269-282. https://doi.org/10.1139/t78-024

Quigley, R.M., Gwyn, Q.H.J., White, O.L., Rowe, R.K., Haynes, J.E., and Bohdanowicz, A. 1983. Leda clay from deep boreholes at Hawkesbury, Ontario. Part 1: Geology and geotechnique. Can. Geotech. J., 20: 2, 288-298. https://doi.org/10.1139/t83-032

Quinn, P.E., Hutchinson, D.J., Diederichs, M.S. and Rowe, R.K. 2011. Characteristics of large landslides in sensitive clay in relation to susceptibility, hazard, and risk. Can. Geotech. J., 48: 8, 1212-1232. https://doi.org/10.1139/t11-039

Sauriol, J. 2016. Provenance of buried esker groundwater: the case of Vars-Winchester esker aquifer, Eastern Ontario, Canada. Hydrogeol. J. 24: 123. https://doi.org/10.1007/s10040-015-1327-1

Tavenas, F., Jean, P., Leblond, P., and Leroueil, S. 1983a. The permeability of natural soft clays. Part II: permeability characteristics. Can. Geotech. J., 20: 4, 645-660. https://doi.org/10.1139/t83-073.

Tavenas, F., Leblond, P., Jean, P., and Leroueil, S. 1983b. The permeability of natural soft clays. Part I: methods of laboratory measurement. Can. Geotech. J., 20: 4, 629-644. https://doi.org/10.1139/t83-072

Torrance, J.K. 1979. Post-depositional changes in the pore-water chemistry of the sensitive marine clays of the Ottawa area, eastern Canada. Eng. Geol., 14: 2-3, 135-147. https://doi.org/10.1016/0013-7952(79)90081-4

Torrance, J.K. 1988. Mineralogy, pore-water chemistry and geotechnical behaviour of Champlain Sea and related sediments. In Gadd, N.R. Ed. The Late Quaternary development of the Champlain Sea basin. Geological Association of Canada Special Paper 35, St. John's, Nfld., 259-280.

Stochastic hydrogeological modelling workflow in a glacial sedimentary basin, southern Ontario

Nicolas Benoit[1-2]*, Denis Marcotte[2], John W. Molson[3], Andy F. Bajc[4], and Hazen A.J. Russell[5]

Abstract: The focus of this study is to explore and assess the uncertainty related to geological heterogeneity in regional groundwater flow models. A stochastic approach is adopted in which the hydrostratigraphic architecture and respective hydrofacies variability directly controls the three-dimensional hydraulic conductivity (K) field. The following procedural steps were applied to develop the stochastic flow model: 1) generation of multiple equivalent hydrostratigraphic models honouring observed hydrostratigraphic units and stratigraphic transitions; 2) determination of the statistical scalar K distribution for each hydrostratigraphic unit along with the respective spatial correlation at the local-scale; 3) upscaling of the scalar K field (quasi-point) to its full 3-D tensor at the regional scale (block); 4) determination of the K-tensor structures and simulation of the K-tensor for hydrogeological models; 5) calibration of the models by numerical inversion of the K-tensor and preserving their component correlations including the recharge rate; and 6) quantification of the uncertainties in the groundwater flow model. The capability and performance of the suggested workflow is illustrated using a case study in southern Ontario. Results highlight the efficiency of the method in assessing model uncertainties and their impact on regional groundwater flow models.

1. Introduction

Geological heterogeneity related to hydrostratigraphic architecture and hydrofacies distribution within hydrostratigraphic units (HSU) can have a major impact on the behaviour of groundwater flow and mass transport (Jakeman et al. 2016; Molson and Frind 2012; Refsgaard et al. 2012). Heterogeneity is represented in most hydrogeological models based on expert knowledge to support a geological framework to guide development of a 3-D deterministic model. Deterministic models, however, usually fail to convey the intrinsic uncertainties regarding the geometry, connectivity, and relative proportions of the hydrostratigraphic units and the internal hydrofacies. Quantifying uncertainty related to hydrostratigraphic and hydrofacies heterogeneity on numerical groundwater flow models is important for the assessment of probable flow transport patterns and for risk assessment in hydrogeology.

This paper presents a workflow for stochastic hydrogeological modelling to permit quantification of hydrogeological uncertainty. To demonstrate the capability and versatility of the proposed approach, the workflow is applied to the Innisfil Creek sub-watershed, part of the Nottawasaga watershed in southern Ontario, Canada. This paper is a synthesis of individual workflow elements described in Benoit et al. (2017a, 2017b, 2017c, 2018a, 2018b).

2. Stochastic hydrogeological modelling workflow

The proposed workflow is divided into four primary tasks (Figure 1): (i) data compilation and preparation (Section 2.1), (ii) hydrostratigraphic modelling (Section 2.2), (iii) assessment of hydraulic conductivities (Sections 2.3), and (iv) groundwater flow modelling (Section 2.4).

2.1 Data compilation and preparation

The data process consists of compiling existing data, conducting field work for acquiring information in areas where data are lacking, and data validation (i.e. preparation for modelling). Although data selection is usually limited to the study area

[1] Geological Survey of Canada, 490 rue de la Couronne, Quebec City, QC G1K 9A9
[2] École Polytechnique de Montréal, Montréal, QC
[3] Université Laval, Québec, QC
[4] Ontario Geological Survey, Ministry of Energy, Northern Development and Mines, 933 Ramsey Lake Road, Sudbury, ON P3E 6B5
[5] Geology Survey of Canada, Natural Resources Canada, 601 Booth Street, Ottawa, ON K1A 0E8
*corresponding author: nicolas.benoit@canada.ca

Recommended citation: Benoit, N., Marcotte, D., Molson, J.W., Bajc, A.F., and Russell, H.A.J. 2020. Stochastic hydrogeological modelling workflow in a glacial sedimentary basin, southern Ontario. In Russell, H.A.J. and Kjarsgaard, B.A. Eds. Southern Ontario groundwater project 2014–2019: summary report. Geological Survey of Canada, Open File 8536, 217-229. https://doi.org/10.4095/321107

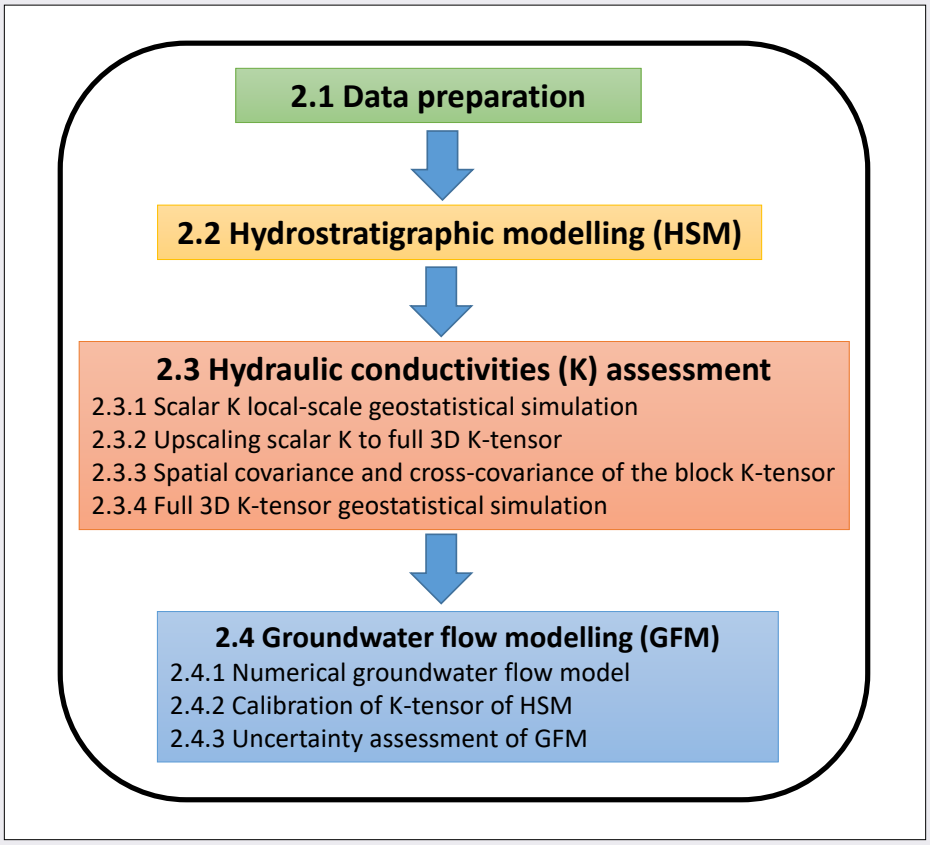


Figure 1. Stochastic hydrogeological modelling workflow.

reflecting the local hydrostratigraphic context and hydraulic conditions, certain key data (e.g., hydraulic conductivity) can also be imported from nearby study areas with similar geological units. The compiled dataset should include:

- a digital elevation model;
- hydrostratigraphic observations from boreholes or surficial mapping;
- assessment of local-scale hydraulic conductivities;
- observations of hydraulic heads;
- estimation of groundwater recharge;
- spatial distribution of surface water (streams, rivers, lakes, wetlands, etc.).

These data provide the information needed for the development of conceptual hydrostratigraphic models and subsequent hydrogeological models (Anderson et al. 2015).

2.2 Stochastic hydrostratigraphic modelling

This section describes the generation of equivalent realizations of the hydrostratigraphic model of the groundwater flow domain. This is achieved through stochastic simulation of discrete HSU categories at the scale of flow model grid. The assignment of hydraulic conductivities of the simulated architecture of the HSU assemblage will be described in the next section.

Geostatistical simulation methods offer efficient algorithms for assessing HSU uncertainty. To include geological knowledge in the simulation, a training image (TI) of the hydrostratigraphic settings can be used. The TI can be represented by a deterministic or a conceptual model.

From a regional numerical hydrostratigraphic modelling perspective, a 3-D numerical hydrostratigraphic model is critical in that it reveals an important aspect for regional models, the directional ordering of hydrostratigraphic units. Benoit et al. (2017a, 2017b, 2017c), for example, illustrate the ability of the Markov-type categorical prediction (MCP) to simulate distinct vertically-ordered units which are generally present in regional hydrostratigraphic models.

The MCP is a geostatistical simulation method introduced by Allard et al. (2011) as an efficient substitute for the more computationally intensive Bayesian maximum entropy method (Bogaert 2002; Bogaert and D'Or 2002, 2003). In the MCP approach using categorical variables, the parameters of the joint discrete distributions are estimated to simultaneously match the bivariate probabilities involving the estimation point and each observed data point, while ignoring bivariate probabilities between pairs of data points. The joint category

distributions at locations x_i, $i=1…n$ are considered independent once the category at estimation location x_0 is known. The bivariate probability functions are calculated directly with the training image using a fast Fourier transform (Marcotte 1996). In the MCP method, the conditional independence hypothesis is assumed. Hence, the conditional probability to observe category i_0 at location x_0 given the categories $i_1,…i_n$ observed at locations $x_1,…x_n$ is by definition:

$$p^{MCP}_{i_0|i_1,\ldots,i_n} = \frac{p_{i_0}\prod_{k=1}^{n} p_{i_k|i_0}}{\sum_{i_0=1}^{I} p_{i_0}\prod_{k=1}^{n} p_{i_k|i_0}} = \frac{p_{i_0}^{1-n}\prod_{k=1}^{n} p_{i_k,i_0}}{\sum_{i_0=1}^{I} p_{i_0}^{1-n}\prod_{k=1}^{n} p_{i_k,i_0}}$$

where, I is the number of categories, p_{i_0} is the marginal probability of category i_0, p_{i_k,i_0} is the bivariate probability and $p_{i_k|i_0}$ is the conditional probability (or transition probability) of observing category i_k at point x_k given category i_0 is present at point x_0.

Only the bivariate distributions (p_{i_k,i_0}) involving the estimated point x_0 are required in the MCP approach. Another interesting feature of MCP, referred to as the zero-forcing property, is the proper integration of 0/1 probabilities. With this property, MCP is capable of forcing or forbidding a unit. MCP reproduces observed HSU transition probabilities between all pairs of categories and in all directions. Directional sequences of categories can therefore be easily reproduced by MCP, which makes the method particularly attractive to simulate stratigraphic models with naturally ordered units. In the MCP approach, observations from boreholes and surficial mapping are used to constrain the simulation.

Further details regarding the MCP simulation methodology are presented by Benoit et al. (2017c). The authors present the simulation algorithm, the methodology to assess the quality of the realizations, as well as an illustration of the properties and sensitivity of the simulation parameters on a synthetic Gaussian case and a real case study (see Section 3.1 of this paper).

The MCP simulation generates *n* realizations of alternative models of the TI where each realization is an input to a flow simulator from which a response to a specified stimulus is computed. For each hydrostratigraphic unit, the spatial distribution of the hydraulic conductivity (K) needs to be assessed.

2.3 Hydraulic conductivity (K) assessment

All simulated hydrostratigraphic models need to be assigned appropriate hydraulic conductivity fields at a block scale suitable for flow simulation (block K-tensor). K data are local-scale scalar values. A multi-step method is proposed herein to upscale the spatial distribution of K from local-scale values (quasi-point) to a full 3-D hydraulic block conductivity tensor. The approach comprises four main steps: (i) local-scale simulation of the scalar K field for each HSU; (ii) upscaling of local (quasi-point) realizations into full 3-D block K-tensors using a block-by-block finite element flow simulator; (iii) definition of the spatial covariance and cross-covariance of the block K-tensors; and (iv) direct geostatistical simulation of the block K-tensors at the regional-scale.

2.3.1 Scalar K local-scale geostatistical simulation

The scalar local-scale hydraulic conductivity data are K field measurements or laboratory data. The K data can be estimated from grain size analyses, laboratory tests on borehole samples, specific capacity tests or pumping tests. For geostatistical processing, it is important to use consistent data, preferably from the same type of tests (similar support) to avoid scale issues and to ensure similar levels of measurement error and spatial uncertainty.

A HSU can comprise one or many hydrofacies. The point-K values can span several orders of magnitude. The spatial structure of point K-conductivity is therefore important to assess for block upscaling. K values within a given HSU are spatially structured according to depositional processes, where the individual structures are characterized by the spatial covariance function used in the geostatistical simulations of the local-scale K fields. For each HSU, K fields are simulated over a fine grid using a non-conditional turning band simulation algorithm (Marcotte 2016). Non-conditional simulation is used as the objective is to determine block covariance K-tensor functions. The simulations are constrained to the pre-defined quasi-point K statistical distribution of each unit (but not by individual quasi-point K values).

2.3.2 Upscaling scalar K to full 3-D K-tensor

For regional-scale 3-D numerical modelling, the K field is discretized as blocks. The quasi-point K simulation must therefore be upscaled to equivalent block conductivity tensors accounting for the structural connectivity of hydrofacies (Gomez-Hernandez and Journel 1990) within each block.

Equivalent K values have to be defined for each block discretizing a given HSU. The major challenge under such conditions is to determine the spatial distribution of the block's full 3-D K-tensor considering the effect of local-scale variability in K. To this end, the Zhou et al. (2010) method for upscaling the full non-local 3-D hydraulic conductivity tensor was revisited (Figure 2). We use the block size of the MCP simulation. Each individual block was upscaled with a block skin on each side. Thus, nine blocks were needed with the flow simulator to calculate the K-tensor of the centre block. The method was used with different sets of prescribed head conditions (three for flow between opposing faces, three for flow between opposing corners and two for flow between opposing edges). The Saltflow simulator was used to obtain the 3-D velocity and head fields (Molson and Frind 2017). Mean 3-D components of the flux (qx, qy, qz) and respective gradients (dhx, dhy, dhz) were calculated and used in combination with Darcy's law to solve the full 3-D K-tensor.

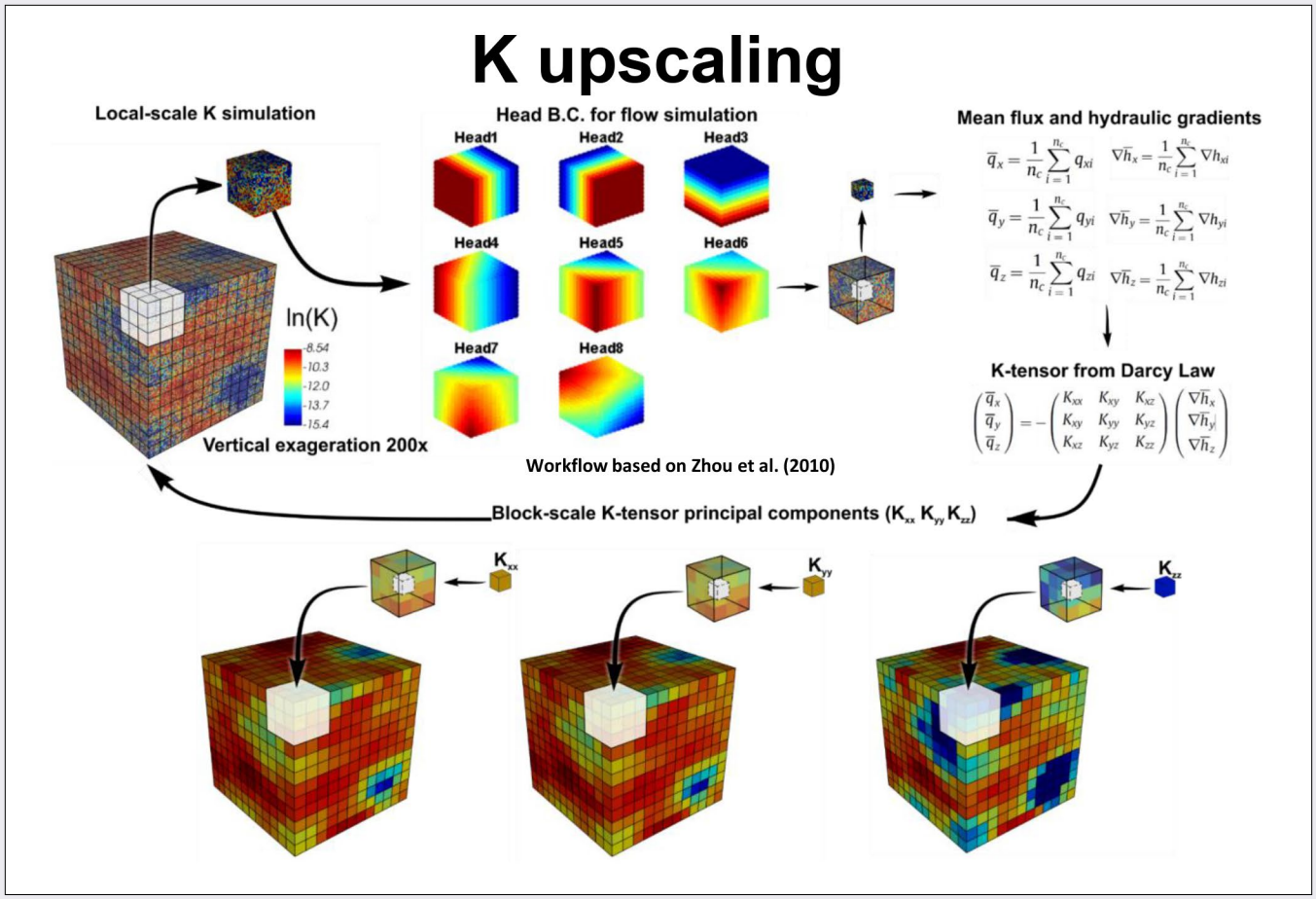


Figure 2. Upscaling scalar hydraulic conductivity with the full 3-D tensor approach.

2.3.3 Spatial covariance and cross-covariance of the block K-tensor

The spatial covariance and cross-covariance of the block K-tensor components are computed and modelled by a linear model of co-regionalisation. To simplify the modelling, components of relatively negligible amplitude can be discarded. Components uncorrelated to the others can be treated separately. The off-diagonal tensor components were considered negligible with respect to diagonal terms. Among the diagonal terms, K_{xx} appeared highly correlated to K_{yy}. So finally the covariance for two variables $K_{horizontal}$ and $K_{vertical}$ was modelled by a linear co-regionalisation model.

2.3.4 Full 3-D K-tensor geostatistical simulation

The last step consists of simulating the full 3-D K-tensor for each of the equivalent hydrostratigraphic models. The turning band method using a linear model of co-regionalisation is used, which works on Gaussian-transformed tensor components. We use non-conditional simulations as no data are available at the block-scale.

2.4 Groundwater flow modelling

The fourth major step of the proposed workflow is groundwater flow modelling of all HSU models parametrized with *n* K-tensor fields. This step usually includes the construction of the numerical groundwater flow model, model calibration and assessment of model uncertainty.

2.4.1 Numerical groundwater flow model

Development of the numerical groundwater flow model includes discretizing the 3-D domain, and defining hydrostratigraphic layers, hydraulic conductivities and boundary conditions. For this component of the workflow, it is more efficient to build a model based on deformable 3-D isoparametric elements that match the stochastic hydrostratigraphic models. This allows for direct correspondence of respective grids between the groundwater flow model, the HSU model and the simulated K-tensor. Note that there is no limitation to refinement within each element. The boundary conditions (constant head and boundary fluxes) are defined and fixed by calibrating the HSU deterministic model with a single mean K-tensor value for each unit. During the stochastic modelling, all parameters

are kept invariant, except for the hydrostratigraphy, K-tensor values and surface recharge.

2.4.2 Calibration of K-tensor of hydrostratigraphic modelling

In the previous publications (Benoit 2018a, 2018b) the PEST algorithm was used for inverse model calibration (Doherty 2005). Usually, for calibration of the deterministic model, PEST is run once for each homogeneous K value of the HSUs. For the heterogeneous model, PEST needs to be run as many times as the number of finite elements in the model. To avoid the large number of forward runs, which would be a major drawback, the inversion was first performed once on the deterministic model with a homogeneous K per HSU. This inversion provides a global correction factor for each of the units. Next, the global factor was applied to the stochastic fields, simultaneously preserving the covariance structure. An example is presented in Section 3.3.

2.4.3 Uncertainty assessment of groundwater flow modelling

The uncertainty assessment is performed considering the entire set of calibrated hydrostratigraphic models. Simple examples are presented in Section 3.3 based on simulation of the groundwater age and delineation of capture zones of streams.

3. Case study – Innisfil Creek Watershed

This section summarizes the results of applying the proposed workflow described in Section 2. The workflow was tested and validated on the Innisfil Creek Watershed, Ontario, Canada (Figure 3, top). The study area contains 14 HSUs of unconsolidated glacial sediments, as illustrated by the hydrostratigraphic model (Figure 3, bottom left) provided by the Ontario Geological Survey (Bajc, pers. comm.). The first two letters of the HSU labels refer to sand and gravel aquifers (AF) or silty and clayey aquitards (AT).

The hydrostratigraphic units are comprised of (from the base up): Ordovician bedrock, mainly limestone (Lindsay Formation), shale with various proportions of limestone (Blue Mountain, Georgian Bay and Queenston formations), Illinoian or older aquitard (ATG1), aquifer (AFF1) and aquitard ATE1. The overlying Don-Scarborough-Thorncliffe formation equivalents consist of interbedded aquifers (AFD4, AFD3, AFD2, AFD1) and aquitards (ATD3, ATD2, ATD1). Stratified deposits of AFD4 unconformably overlie ATE1 which, in this area, consists of a fine-textured diamicton. Newmarket Till (ATC1) caps the sedimentary sequence and acts as a regional aquitard. The till is eroded locally and has been traced down into broad valleys (Mulligan et al. 2018) interpreted as tunnel valleys (Russell et al. 2003). Glaciofluvial sand and gravel aquifer (AFB2) occurs at the base of the tunnel channels and is roughly equivalent in age to early Oak Ridges Moraine deposits. AFB2 includes gravelly and sandy sediment at the base and is capped by a sequence of glaciolacustrine silt and clay with subordinate sand (aquitard ATB2). Overlying deposits of sand and gravel (AFB1) complete the stratigraphic sequence.

The HSU thickness is highly variable. Although each HSU is composed of one or more successive stratigraphic sub-units (hydrofacies) with similar hydrogeologic properties, the model statistical parameters and ensuing simulations are defined on a HSU basis, not hydrofacies. The hydrofacies will indirectly influence the spatial structure of quasi-point K. The HSU numerical model was discretized in uniform HSU blocks of 200 x 200 x 1 meters. Each block is assumed to be part of only one HSU

3.1 Simulation of hydrostratigraphic units

To demonstrate the ability of the MCP method to simulate hydrostratigraphic units, a small portion of the deterministic model of the watershed was used as a training image (TI) (Figure 3). This TI (cross-section S1) was selected for its complex hydrostratigraphic trends with strong vertical ordering, thickness variability and variation of the unit proportions. The bivariate probabilities between pairs of HSU, required for MCP, were obtained by direct computation on the TI (Figure 3, bottom right).

One hundred MCP realizations were simulated using 2 boreholes and 176 picks as data (Figure 4). A pick corresponds to the top of a certain HSU interpreted by the geologist from low-quality borehole logs from a public domain database (WWIS, 2018). The results are presented for the middle of the cross-section S1 (y = 3) for two realizations. A dissimilarity map (Figure 4c) is computed to assess the difference between the model used as the TI and the different realizations (a value of 0 represents no difference and 100 indicates that all realizations are different). Finally, a boxplot of HSU proportions is shown together with the HSU proportions of the TI and data.

The results reflect the strong effects of the conditioning data on MCP realizations. Data help reproduce the main TI structures. Uncertainty is greater close to the HSU contacts (Figure 4c). We note that many HSUs have mean proportions in the realizations different from the TI. For the three most abundant HSUs (ATB2, ATD1 and bedrock), the mean proportions are less in the realizations than in the TI. Tests considering only the picks (i.e., excluding borehole data), resulted in proportions for ATB2, ATD1 and bedrock HSU that were also less abundant than in the TI. Hence, in the initial steps of MCP, a simulated location which is far from the boreholes will find fewer ATB2, ATD1 and bedrock data in its neighbourhood than present in the TI. This could explain the observed disparity between the MCP and TI HSU proportions.

Despite the trends present in the deterministic model, MCP proved robust to datasets over-representing some HSUs. Despite the relative over-representation of some HSUs in the datasets, the simulated unit proportions still reproduced

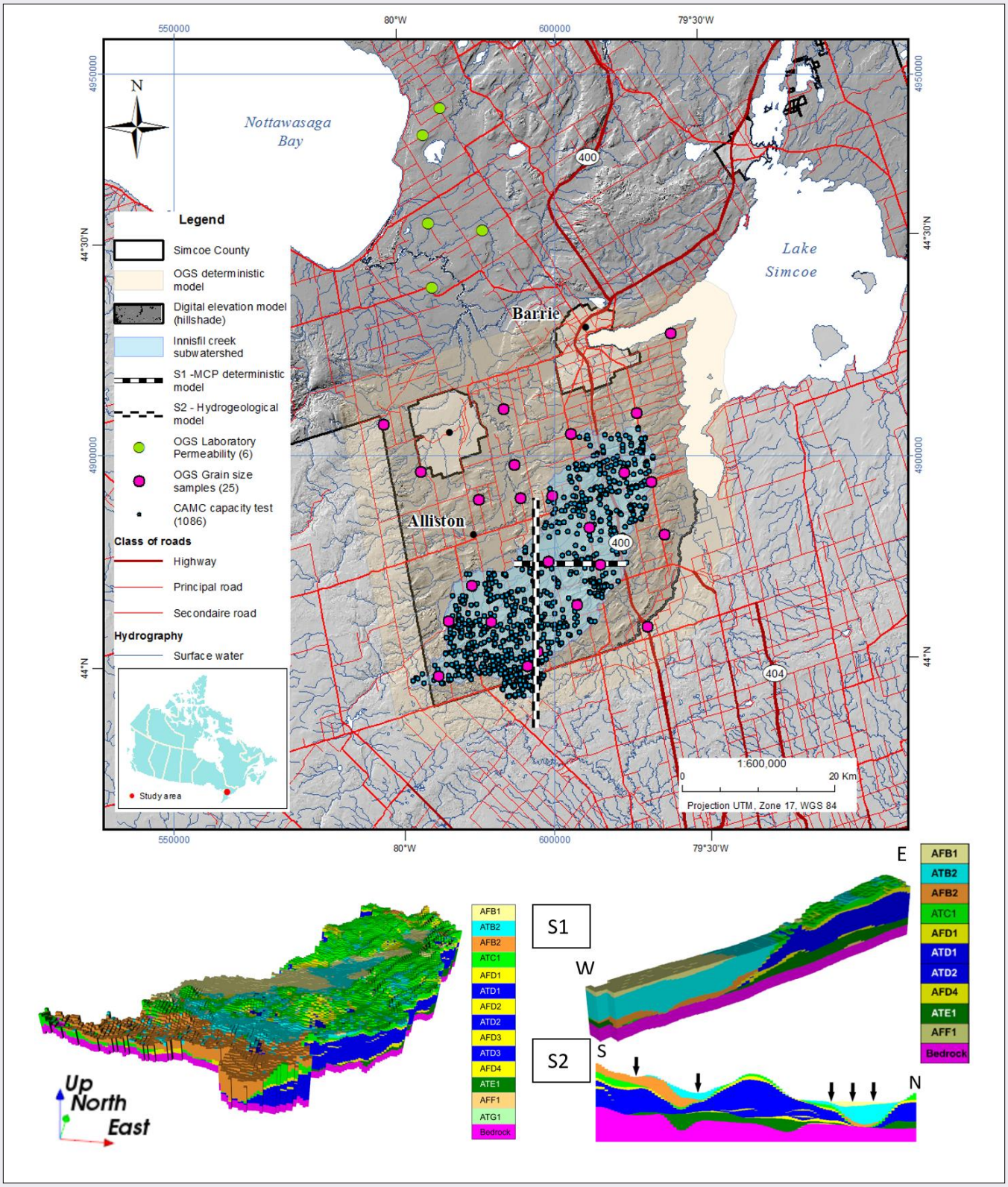


Figure 3. Study area of the Innisfil Creek watershed with cross-sections and location of field observations (top); 3-D deterministic hydrostratigraphic model (bottom left); Cross-section S1 (west – east) used as a training image (TI) and cross-section S2 (south – north) used for hydrogeological modelling (vertical exaggeration 15x – bottom right) (adapted from Benoit et al. 2017c, 2018a).

the target proportions. The inter-realization variability closely follows the amount and quality of data provided. Results with different conditioning datasets show that MCP replicates the directional arrangement of the units. Vertical ordering of each HSU is respected without any unit inversion (see HSU legend on the right of Figure 4a). The method is unbiased in the non-conditional case (Benoit et al. 2017c). In this case, with preferential sampling, the bias between TI proportions and simulated proportions is relatively small. MCP is demonstrated to be an efficient method for generating stochastic models in a 3-D hydrostratigraphic context.

3.2 Full 3-D hydraulic conductivity tensor

Regional hydrostratigraphic systems generally encompass numerous hydrostratigraphic units (HSUs), where an individual

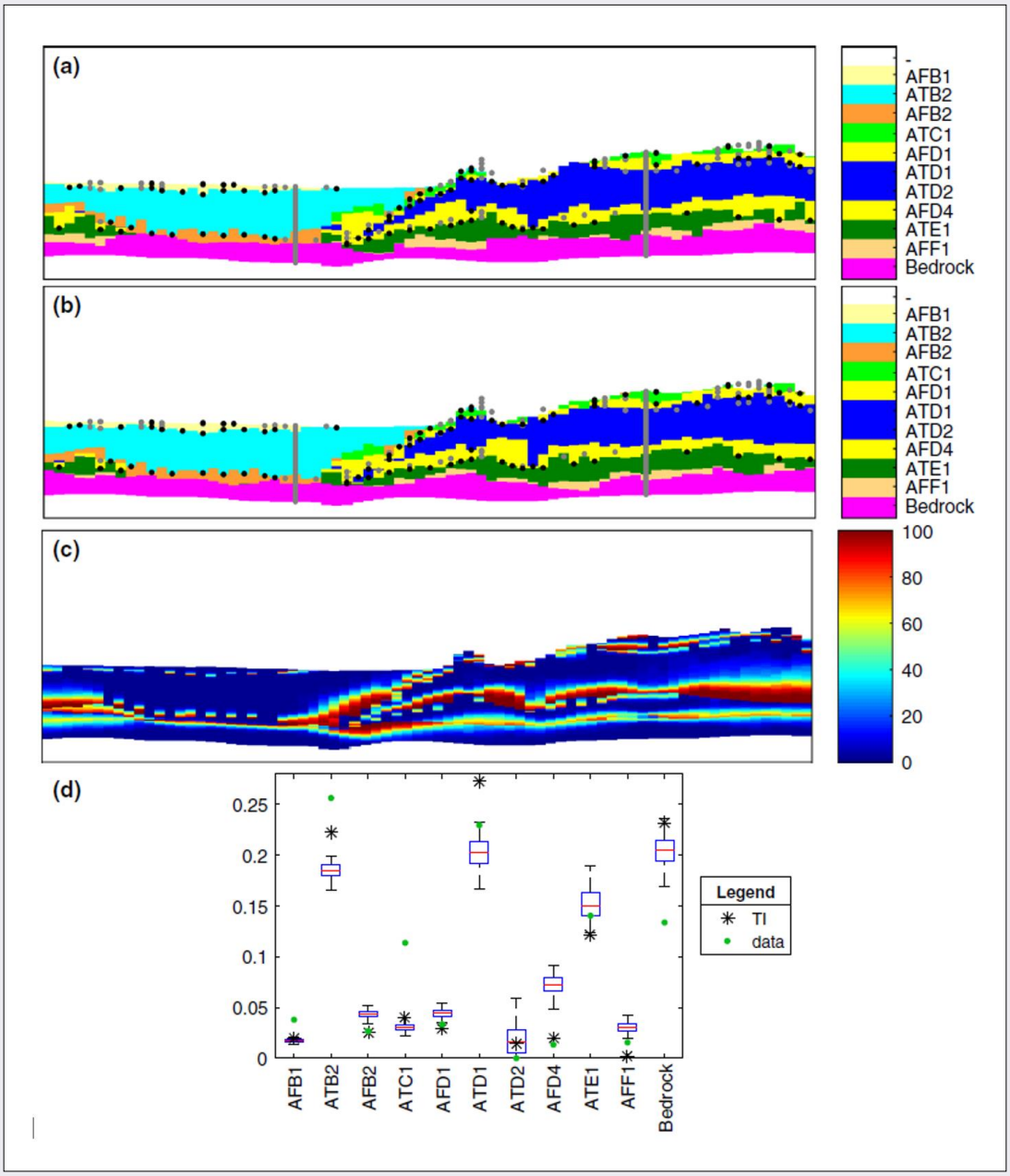


Figure 4. MCP simulation based on 2 boreholes and 176 HSU picks for cross-section S1 (view from the middle or y = 3) of two realizations (a) and (b). The dissimilarity is shown in (c) where 0 represents no difference with TI and 100 indicates that all realizations are different. Boxplots of HSU proportions, for 100 realizations shown in (d), reproduced from Benoit et al. (2017c). Aquifers are represented by AF, aquitards are AT.

HSU may include different hydrofacies described by a specific distribution of local K values spanning several orders of magnitude. This section summarizes previous results obtained by Benoit et al. (2018a, 2018b) on determination of the spatial distribution of the full 3-D hydraulic conductivity tensor blocks in the Innisfil Creek watershed.

The K database was built using 1,086 transmissivity measurements from wells included in a public database (YPDT-CAMC 2016). Data are sourced from two unconsolidated surficial sediment datasets, thirty-two (32) samples from six boreholes, and analysed in the laboratory with constant and falling head permeability tests (Pasquier et al. 2016), as well as from 1,694 grain size analysis in 15 boreholes (Bajc et al. 2015).

Among the available data, the grain-size samples present the only sufficiently dense and high-quality information of scalar K values across and within the HSUs (Table 1). These values, estimated using the Sauerbrei method (Vukovic and Soro 1992), are in good agreement with laboratory permeability measurements (Benoit et al. 2018a). Of note, however, K values estimated from specific capacity tests (Bradbury and Rothschild 1985) are biased toward the higher permeability values, and the agreement with laboratory permeability tests is less than that observed for K values from grain size analyses. Grain size analysis data were used for local scalar assessments of K, which produced a highly variable K distribution. Among the 14 HSUs, six are aquitards, six are considered aquifers, whereas two HSUs appear transitional from aquifer to aquitard conditions.

These data have a high-resolution in the vertical direction allowing vertical variograms of ln(K) to be modelled separately for each of the 14 HSUs. These variograms were modelled either with spherical or exponential structures with a nugget effect representing 0–49% of the total variance. The practical vertical ranges vary between 1.1 and 19.5 m (Benoit et al. 2018a). Due to the large distances between boreholes, the horizontal variograms could not be defined based on the grain size analyses alone. Instead, a global horizontal range of about 1,800 m was estimated from K values based on specific capacity tests with relatively dense spatial coverage, which represents a horizontal/vertical anisotropy ratio of about 300. This ratio was applied to each HSU, with the anisotropy ratio of 300 being comparable to the horizontal/vertical block length ratio in the model.

Scalar K fields were simulated using a non-conditional turning band simulation (TBS) algorithm (Emery and Lantuéjoul 2006) over a grid of 120 x 120 x 120 points on a mesh of size 2 m x 2 m x 0.01 m. This simulation grid was divided into 12 x 12 x 12 blocks. 3-D hydraulic conductivity tensors for each block were obtained by upscaling the local-scale simulation to the block-scale (Figure 2).

An illustrative example of an upscaled block K_{xx} component of the scalar field for HSU AFB1 is presented in Figure 5. Analysis of the upscaled K-tensor components revealed a clear dominance of diagonal components over off-diagonal elements. Off-diagonal tensor components were negligible for all HSUs. The K-tensors of the different HSUs have correlation ranges of a few to several blocks with no nugget effect. The variogram behaviour at the origin appears parabolic due to the large change of support from quasi-point to block-scale. Simple correlations (at h=0) between $\ln(K_{xx})$ and $\ln(K_{yy})$ components vary between $0.75<r<0.99$. Correlations between horizontal components and $\ln(K_{zz})$ were also strong (10 HSUs

Table 1. Scalar K estimates from grain size analyses for each hydrostratigraphic unit (HSU).

HSU	n	$\overline{lnK}$	$\sigma^2_{ln_K}$	$\overline{K(m/s)}$	$\overline{K+2\sigma(m/s)}$	$\overline{K-2\sigma(m/s)}$
AFB1	104	-11.98	11.51	6.27e-06	5.55e-03	7.10e-09
ATB2	268	-19.50	1.15	3.41e-09	2.92e-08	3.98e-10
AFB2	198	-10.78	6.50	2.07e-05	3.40e-03	1.27e-07
ATC1	178	-14.90	10.30	3.39e-07	2.08e-04	5.54e-10
AFD1	86	-11.40	12.04	1.12e-05	1.16e-02	1.09e-08
ATD1	194	-19.40	1.48	3.74e-09	4.27e-08	3.28e-10
AFD2	44	-10.99	9.82	1.69e-05	8.89e-03	3.19e-08
ATD2	77	-19.69	0.80	2.80e-09	1.67e-08	4.69e-10
AFD3	46	-10.23	5.97	3.59e-05	4.75e-03	2.71e-07
ATD3	28	-18.88	1.24	6.32e-09	5.87e-08	6.81e-10
AFD4	32	-13.71	23.54	1.11e-06	1.81e-02	6.77e-11
ATE1	301	-19.29	1.05	4.21e-09	3.25e-08	5.44e-10
AFF1	32	-10.40	6.00	3.05e-05	4.09e-03	2.27e-07
ATG1	101	-18.38	3.36	1.05e-08	4.10e-07	2.67e-10

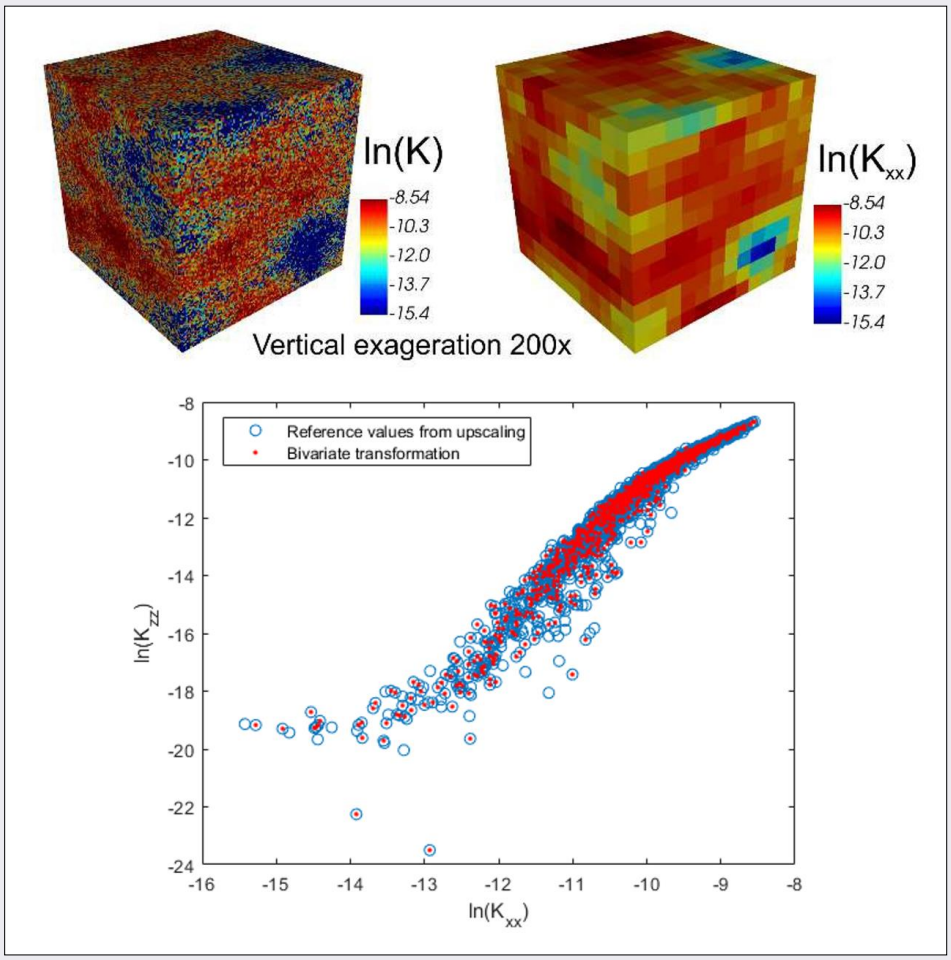


Figure 5. Local-scale scalar K fields (K in m/s) of unit AFB1 obtained from a non-conditional TBS (top – left); the corresponding upscaled K_{xx} tensorial component (top – right); and bivariate transformation of the K_{zz} component from a realization generated with LMC TBS (bottom) (reproduced from Benoit et al. 2018b).

showed r>0.91). A linear model of coregionalisation (LMC) adequately describes the variograms and cross-variograms of $\ln(K_{xx})$, $\ln(K_{yy})$ and $\ln(K_{zz})$ in each HSU. Based on the upscaling results, two constraints were imposed: $\ln(K_{yy}) = \ln(K_{xx})$ and $\ln(K_{zz}) \leq \ln(K_{xx})$. The latter constraint was applied a posteriori using the transformation of the $\ln(K_{zz})$ realisation to the reference bivariate distribution ($\ln(K_{xx})$, $\ln(K_{zz})$) of the upscaled results (Figure 5, bottom).

3.3 Hydrogeological models

The developed block K tensor coregionalisation models were used to assess all HSUs of the regional 3-D groundwater model of the Innisfil Creek watershed. For the application example, we present results based on cross-section S2 (Figure 3), representing a large 2-D vertical groundwater flow model extracted from the watershed, and chosen parallel to the flow direction based on the kriged head field. This regional cross-section includes five streams and cuts through the three main physiographic features in the watershed (Figure 6): lowlands (north), uplands (south-central) and the highly permeable Oak Ridges Moraine (south). Although the model is based on real data, the assumption that the cross-section is aligned with the regional flow direction represents a potential limitation of the model. The study can thus be seen as a partially conceptual exercise. The objective was to isolate only the effect of K-tensor variability within the HSUs. The combination of MCP simulations including the full 3-D tensor of the watershed will be considered in another publication.

Groundwater flow was simulated using both homogeneous (deterministic) and stochastic K_{xx} and K_{zz} fields. The model boundary conditions were: no-flow conditions for the lateral boundaries corresponding to the watershed divide, a no-flow condition at the model base, seepage conditions to simulate streams, and imposed flux (recharge) conditions at the surface of the model. Initial K_{xx} and K_{zz} values were assigned according to the upscaled geometric mean. First, the calibration was

conducted on the deterministic model by adjusting K_{xx} per HSU using the kriged regional zero-pressure surface as a calibration target. The K_{xx} parameter was adjusted by applying numerical inversion with the PEST algorithm. The K_{zz} values were derived from this updated K_{xx} field using the K_{xx} and K_{zz} ratio from the initial values. Next, stochastic modelling was conducted varying the K_{xx} and K_{zz} fields and keeping the other settings unchanged. No further calibration was conducted in this modelling. However, for each realization, the K_{xx} field was modified based on the HSU ratio obtained for the calibration of the deterministic model (K_{xx}_PEST/ K_{xx}_initial). Bedrock was not included in the upscaling process. A constant K value of 10^{-5} m/s was assigned at the bedrock surface, decreasing log-linearly with depth to 10^{-10} m/s.

Stochastic realizations with variable K-tensors generated the water table elevations comparable to that of the calibrated deterministic model (Figure 6, middle right). The impact of the K-tensor uncertainty on a typical flow simulation was assessed and proved non-negligible as supported by the simulations of the mean groundwater age (Cornaton 2012). The stochastic simulations show that the mean age variation is indeed affected by the K-tensors' variation within the HSUs.

The stochastic models were also used to calculate the capture zones of the simulated streams and their uncertainty using the backward-in-time transport equation (Cornaton and Perrochet 2006). The capture zones of the lowland are well defined with the current information (Figure 6, bottom). Note that the current assessment probably underestimates uncertainty as the same deterministic HSU model was used for all realizations. Nevertheless, the alternative K-tensor fields define different capture zones. By combining capture zones with mean groundwater age or its mean life expectancy, one can assess the vulnerability of each stream to a land contamination event and therefore determine possible land use restrictions.

4. Discussion

To our knowledge, the MCP method has never been tested on a complex model based on real geological data such as the hydrostratigraphic system of Innisfil Creek watershed. In this case the different HSUs have quite different proportions and a clear directional control. The 0/1 forcing property of MCP can deal with transitional cases as present in this case study. As an example, from Figure 3, HSU ATB2 can be overlain only by AFB1 (or nothing). The bivariate probability measured upward from ATB2 will therefore be 0 for all facies except AFB1. Accordingly MCP will prevent simulation of all facies other than AFB1 and ATB2 over an ATB2 point.

Segmentation of the studied field into homogeneous subdomains is not necessary as MCP can handle the simulated field globally, which greatly facilitates the analysis. The definition of the data neighborhood is the most practical and influential aspect in the application of MCP.

Despite the significant expertise involved in the design of the deterministic model, it nevertheless remains a quite idealized and smoothed interpretation of the real field conditions. If the stratigraphy and global proportions of each HSU are well represented in the deterministic model, the HSUs vertical thicknesses are likely much more variable than those assumed in the model. Likewise, the lateral continuity of HSUs are probably exaggerated in the deterministic model. As these thicknesses and lateral variations might significantly influence the response of the flow model, it is important to consider alternate models to the deterministic one to enable an assessment of flow uncertainty.

An efficient method was developed for regional characterisation of HSUs using 3-D K-tensors which was tested with 2-D cross-sectional deterministic and stochastic groundwater flow simulations. It was found that within each HSU, the K-tensor variability has only a moderate effect on groundwater ages computed by the flow simulator but has a relatively stronger effect on the definition of the stream capture zones. The results emphasize the different effects of homogeneous and heterogeneous HSU K-tensors under the same hydrogeologic settings and boundary conditions. These effects were quantified by simulating the groundwater age distribution and the capture zones of streams. The proposed methodology appears well suited for determining the uncertainty of groundwater flow and transport models. Using alternative models will provide confidence intervals on simulation scenarios for better decision-making related to aquifer vulnerability.

The proposed workflow is still in development and refinement. Current efforts are focussed on model calibration using a geostatistical approach and metrics for uncertainty analyses. Once the full workflow is completed, it will be reapplied to modelling groundwater flow in the watershed.

4.1 Calibration using gradual deformation

For more efficient calibration, an updated inversion methodology is currently under development. The current challenge is to develop algorithms for automatic calibration of the K-tensor and recharge for each HSU realization. The objective is to adjust simultaneously the K values for each element and recharge rates, while preserving their covariance structure. The gradual deformation method (GDM; Hu 2000) appears promising as spatial structures of the parameters as well as their respective statistical distribution are preserved with this approach. To facilitate convergence, calibration of the recharge rates will also be done simultaneously with the calibration of the K values. Moreover, while the flow models are currently calibrated against head observations, the next version will also consider calibration against the baseflow estimates.

4.2 Uncertainty analysis

Based on *n* realizations of the fully calibrated hydrostratigraphic realizations, the following target responses of the groundwater

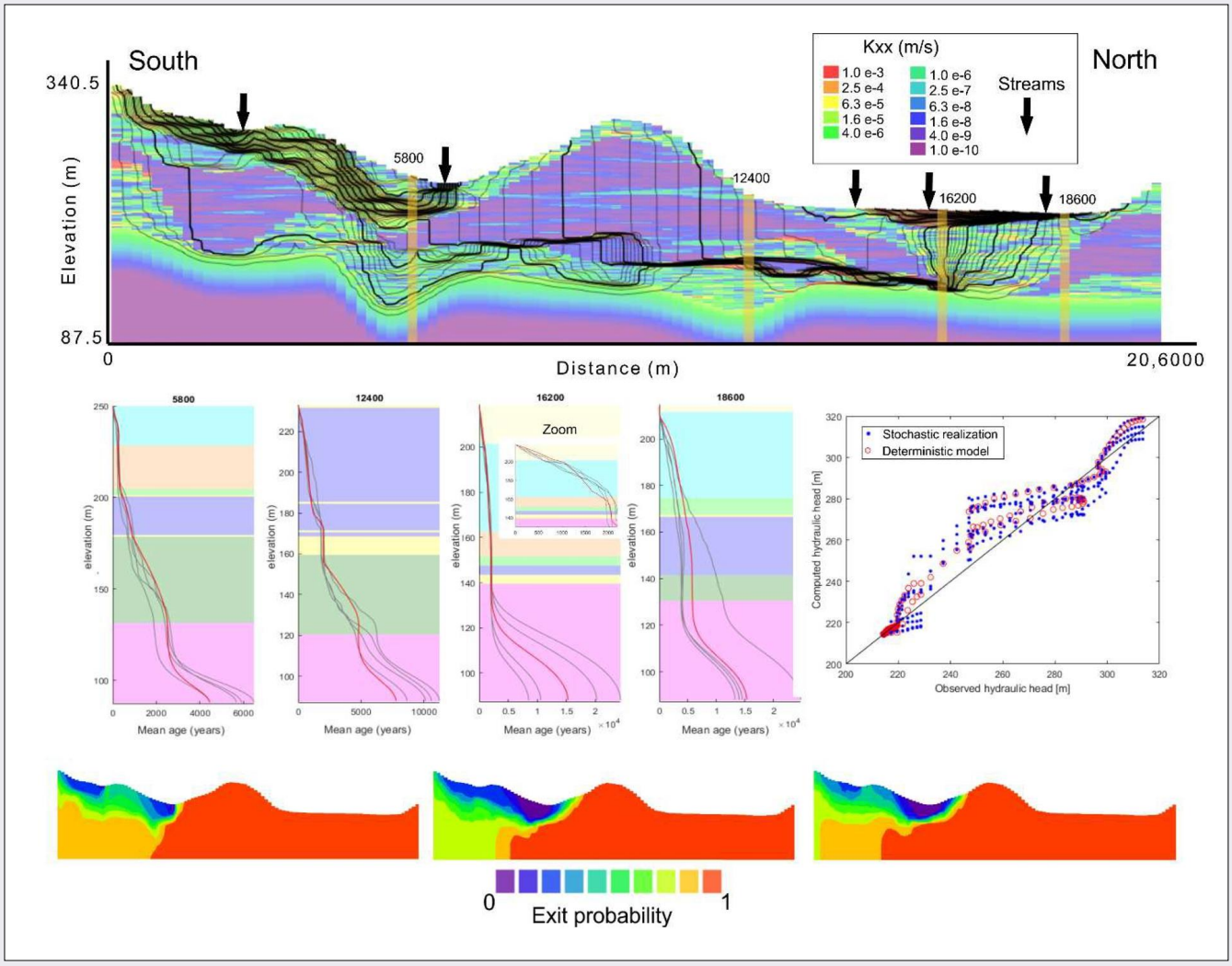


Figure 6. Top: cross-section S2 showing simulated Kxx with stream function isolines via a vorticity equation; Middle: HSU units and computed mean groundwater age for four realizations (left) along cut lines (yellow lines in top row) and computed vs observed hydraulic heads (right) for four realization and the deterministic model; Bottom: Capture zones of the streams located in lowland area (north) for the deterministic model (left) and two realizations (centre and right). The capture zones were defined by the exit probability (0.1 colour intervals) of the random walk particle paths toward the lowland streams (reproduced from Benoit et al. 2018b).

flow simulation are considered: the capture zones of the pumping wells and streams, and the mean groundwater age along the flow path from surface recharge. The eventual objective is to propose indicators that can be used to quantify the prediction uncertainties for these responses.

This comprehensive study will produce a set of hydrostratigraphic models with equivalent 3-D K-tensor parameters, which will be used to assess the impact of uncertainties in the K tensor and HSU on the resulting simulated groundwater flow system. This work will help quantify the effect of uncertainty in the hydrostratigraphic architecture and its inner hydrofacies variability.

5. Conclusion

This study focused on stochastic simulations of groundwater flow, offering an efficient workflow from data acquisition to model forecasting. The complete stochastic groundwater simulation workflow was applied to the Innisfil Creek watershed.

The Markov-type categorical prediction – MCP simulation method was applied to a complex stratigraphic succession within the glacial sedimentary basin. The MCP simulation method was successful in simulating this complex depositional system containing numerous units with a clear directional trend inducing strong asymmetry of transitional probabilities between units. An efficient method was developed for regional characterization of the HSUs with derived values of

the full 3-D K-tensor. The groundwater flow simulations using heterogeneous K-tensors have significant impacts on the head distribution and flow velocity fields. This stochastic realisation is only one of the possible results, which illustrates the impact of K tensor variability on groundwater flow.

The proposed methodology appears well suited for determining the uncertainty of groundwater flow and transport models including those used for aquifer vulnerability assessment and delineation of wellhead protection areas. Evaluation of alternative models is essential for assessing uncertainty on groundwater flow and transport problems. The use of MCP for regional modelling is a new and useful approach for conceptual hydrostratigraphic modelling with stratigraphically ordered units. One of the largest remaining challenges is the computational time required for processing very large models (with millions of elements). A future step will be to complete a full workflow implementation on a computer cluster.

The remaining development regarding the calibration using gradual deformation and the uncertainty analysis will complete the workflow for 3-D stochastic simulation. Based on *n* realizations of the fully calibrated hydrostratigraphic model, the main features of groundwater flow will be characterized. It will be possible to outline the probable capture zones of the streams and pumping wells and the mean groundwater age along the flow path from main recharge. An objective is to propose metrics to quantify prediction uncertainties and to assess aquifer vulnerability. This work will help to better quantify effects of uncertainty with respect to the hydrostratigraphic architecture and its inner hydrofacies variability.

6. Acknowledgements

An internal review by A. Desbarats is much appreciated. This work is a contribution of the GSC–OGS Southern Ontario project on groundwater 2014–2019.

7. References

Allard D., D'Or D., and Froidevaux R. 2011. An efficient maximum entropy approach for categorical variable prediction. Eur. J. Soil Sci., 62: 381–393. https://doi.org/10.1111/j.1365-2389.2011.01362.x

Anderson, M.P., Woessner, W.W., and Hunt, R.J. 2015. Applied Groundwater Modeling: Simulation of Flow and Advective Transport. Academic Press.

Bajc, A.F., Mulligan, R.P.M., Rainsford, D.R.B., and Webb, J.L. 2015. Results of 2011–13 overburden drilling programs in the southern part of the County of Simcoe, south-central Ontario. Ontario Geological Survey Miscellaneous Release —Data 324.

Benoit, N., Marcotte, D., Boucher, A., and Bajc, A.F. 2017a. Directional geostatistical simulation for regional hydrostratigraphic units uncertainty characterization of the Innisfil Creek sub-watershed, Ontario. In, Regional-scale groundwater geoscience in southern Ontario: an Ontario Geological Survey, Geological Survey of Canada, and Conservation Ontario open house; Geological Survey of Canada, Open File 8212, p. 2. https://doi.org/10.4095/299758

Benoit, N., Marcotte, D., Boucher, A., D'Or, D. and Bajc, A. 2017b. Regional Hydrostratigraphic Unit Modelling Using Directional MCP Simulation, Regional Hydrostratigraphic Unit Modelling Using Directional MCP Simulation. Presented at the 2017 NGWA Summit, 2017 NGWA Summit, Nashville, Tennessee, USA, December 4th 2017.

Benoit, N., Marcotte, D., Boucher, A., D'Or, D., Bajc, A., and Rezaee, H. 2018. Directional hydrostratigraphic units simulation using MCP algorithm. Stochastic Environmental Research and Risk Assessment, 32: 5, 1435–1455. https://doi.org/10.1007/s00477-017-1506-9

Benoit, N., Marcotte, D., Molson, J.W., Pasquier, P., and Mulligan, R. 2018a. Characterization of full 3D hydraulic conductivity tensors of hydrostratigraphic units applied to Innisfil Creek watershed, Ontario. In: Regional-scale groundwater geoscience in southern Ontario: an Ontario Geological Survey, Geological Survey of Canada, and Conservation Ontario geoscientists open house Geological Survey of Canada, Open File, 8363, 2–2. https://doi.org/10.4095/306485

Benoit, N., Marcotte, D., Molson, J.W., and Pasquier, P. 2018b. Geostatistical simulations of the full 3D block hydraulic conductivity tensor considering inner local-scale variability. In: 12th Conference on Geostatistics for Environmental Applications. Presented at the geoENV 2018, Belfast, p. 6.

Bogaert, P. 2002. Spatial prediction of categorical variables: the Bayesian maximum entropy approach. Stochastic Environmental Research and Risk Assessment, 16: 6, 425–448. https://doi.org/10.1007/s00477-002-0114-4

Bogaert, P. and D'Or, D. 2002. Estimating soil properties from thematic soil maps: the Bayesian Maximum Entropy approach. Soil Sci. Soc. Am. J., 66: 5, 1492–1500. https://doi.org/10.2136/sssaj2002.1492

Bradbury, K.R. and Rothschild, E.R. 1985. A Computerized Technique for Estimating the Hydraulic Conductivity of Aquifers from Specific Capacity Data. Ground Water 23: 240–246. https://doi.org/10.1111/j.1745-6584.1985.tb02798.x

Cornaton F. 2012. Transient water age distributions in environmental flow systems: The time-marching Laplace transform solution technique. Water Resources Research, 48: W03524. https://doi.org/10.1029/2011WR010606

Cornaton, F. and Perrochet, P. 2006. Groundwater age, life expectancy and transit time distributions in advective–dispersive systems: 1. Generalized reservoir theory. Advances in Water Resources, 29: 1267–1291. https://doi.org/10.1016/j.advwatres.2005.10.009

D'Or, D. 2003. Spatial prediction of soil properties, the Bayesian Maximum Entropy approach. Ph.D. thesis, Universite´ catholique de Louvain.

Doherty, J. 2005. PEST: Model Independent Parameter Estimation. User Manual. fifth ed. Watermark Numerical Computing, Brisbane, Australia.

Emery, X. and Lantuéjoul, C. 2006. TBSIM: A computer program for conditional simulation of three-dimensional Gaussian random fields via the turning bands method. Computers & Geosciences. 32: 1615–1628. doi:10.1016/j.cageo.2006.03.001

Gomez-Hernandez, J. and Journel, A.G. 1990. Stochastic Characterization of Grid-Block Permeabilities: from Point Values to Block Tensors. https://doi.org/10.3997/2214- 4609.201411102

Hu, L.Y. 2000. Gradual Deformation and Iterative Calibration of Gaussian-Related Stochastic Models. Mathematical Geology 32: 87–108. https://doi.org/10.1023/A:1007506918588

Jakeman, A., Barreteau, O., Hunt, R., Rinaudo, J.D. and Ross, A. 2016. Integrated groundwater management—concepts, approaches and challenges, vol 1. Springer, Berlin.

Marcotte, D. 1996. Fast variogram computation with FFT. Computers & Geosciences, 22: 10, 1175–1186. https://doi.org/10.1016/S0098-3004(96)00026-X

Marcotte, D. 2016. Spatial turning bands simulation of anisotropic non-linear models of coregionalization with symmetric cross-covariances. Computers & Geosciences, 89: 232-238. https://doi.org/10.1016/j.cageo.2016.01.004

Molson, J.W. and Frind, E.O. 2012. On the use of mean groundwater age, life expectancy and capture probability for defining aquifer vulnerability and time-of-travel zones for source water protection. J Contam Hydrol 127: 1–4, 76–87. https://doi.org/10.1016/j.jconhyd.2011.06.001

Molson, J.W. and Frind, E.O. 2017. SALTFLOW, User Guide, Density-dependent flow and mass transport model in three dimensions, Version 4.0, Université Laval and University of Waterloo.

Mulligan, R.P.M., Bajc, A.F., and Eyles, C. 2018. Drumlinized tunnel valleys in south-central Ontario. Quaternary Science Reviews, 97: 49-74. https://doi.org/10.1016/j.quascirev.2018.07.026

Pasquier, P., Benoit, N., Delahaye, Y., Gagnon, L., and Mulligan, R. 2016. Hydraulic Conductivity Database, Simcoe County, Southern Ontario. Geological Survey of Canada, Open File 8105, 68 p. https://doi.org/10.4095/299048

Refsgaard J.C., Christensen S., Sonnenborg T.O., Seifert D., Højberg A.L., and Troldborg L. 2012. Review of strategies for handling geological uncertainty in groundwater flow and transport modeling. Advances Water Resources, 36: 36–50. https://doi.org/10.1016/j.advwatres.2011.04.006

Russell, H.A.J., Arnott, R.W.C., and Sharpe, D.R. 2003. Evidence for rapid sedimentation in a tunnel channel, Oak Ridges Moraine, southern Ontario, Canada. Sedimentary Geology, 160: 33–55. https://doi.org/10.1016/S0037-0738(02)00335-4

Russell, H.A.J., Priebe, E.H., and Parker, J.R. 2015. Workshop summary and gap analysis report: unifying groundwater science in southern Ontario. Ontario Geological Survey, Open File Report 6310, 1–80.

Vuković, M. and Soro, A. 1992. Determination of hydraulic conductivity of porous media from grain-size composition. Littleton, Colorado. Water Resources Publications. 83 p.

Water Well Information System (WWIS), 2018. Ontario Ministry of Environment (OME). computer file, https://www.ontario.ca/data/well-records

YPDT-CAMC. 2016. Comprehensive York Peel Durham Toronto - Conservation Authorities Moraine Coalition (YPDT-CAMC), 2016. Water Management SQL Database. Oak Ridges Moraine Groundwater Program, 2002 - 2018. Presently referred to as Oak Ridges Groundwater Program (ORMGP). Data provided in 2016. URL https://oakridgeswater.ca/

Zhou, H., Li, L., and Gómez-Hernández, J. 2010. Three-dimensional hydraulic conductivity upscaling in groundwater modeling. Computers & Geosciences, 36: 1224–1235. https://doi.org/10.1016/j.cageo.2010.03.008

A fully integrated groundwater–surface-water model for southern Ontario

Steven K. Frey[1]*, Omar Khader[1], Amanda Taylor[1], Andre R. Erler[1], David R. Lapen[2], Edward A. Sudicky[1], Steven J. Berg[1], and Hazen A.J. Russell[3]

Abstract: A prototype groundwater–surface-water model for southern Ontario has been developed with HydroGeoSphere (HGS), which provides a three-dimensional (3-D), physics-based simulation of fully integrated groundwater–surface-water flow. To-date, the model has been tested for its ability to reproduce average monthly surface-water flow rates and groundwater levels, and its sensitivity to spatial and temporal resolution. Model utility has been demonstrated through an assessment of groundwater extraction influences on regional groundwater levels, which demonstrates how it could be used to address water resources and hydrologic questions.

The model domain encompasses 109,565 km^2, with approximately 79,000 km^2 being land area and the remainder being area within the Great Lakes. To assess sensitivity to spatial resolution, low- and high- resolution model versions have been constructed, with surface water features resolved to Strahler order 4 and Strahler order 3, respectively. The hydrostratigraphy is based on 3-D Paleozoic and Quaternary geological models, along with mapping of depth to the base of high-sulphur content groundwater. The low- and high- resolution models consist of 21 and 16 layers, and 874,398 and 2,127,760 3-D finite element mesh nodes. Both models incorporate spatially distributed soil, landcover, and spatially and temporally distributed evapotranspiration.

To assess model performance, 321 wells from the Provincial Groundwater Water Monitoring Network and 29 hydrometric stations from the Water Survey of Canada were incorporated as validation targets. Simulation results show that both the low- and high- resolution versions of the model were able to capture the magnitude and seasonal variation in both groundwater levels and surface water flow rates. As the model was subjected to minimal calibration, this is a meaningful validation of its performance. Differences in performance between the low- and high- resolution model versions were minimal for both the surface-water flow rates and groundwater level results.

Results demonstrate the utility of a regional scale, fully integrated hydrologic model for investigating water resources issues of southern Ontario. The model could evolve into a multi-objective groundwater/surface-water simulation tool for southern Ontario, wherein seasonal water balances and general trends in groundwater and surface water availability under climate change and anthropogenic influences within the Great Lakes Region can be assessed.

1. Introduction

Water resources within southern Ontario are a focal point for a wide range of concerns by stakeholders who are faced with addressing climate change impacts and resiliency, surface water and groundwater sustainability, and Great Lakes water quality (GLWQA, 2012). Because of the complexity of these challenges, modern science-based decision support tools are required. As exemplified by water resources management projects underway in the Canadian Prairies and Europe, fully-integrated groundwater–surface-water (GW–SW) models are increasingly being used as multi-stakeholder decision support tools for complex hydrologic problems (Frey et al. 2016).

The multi-stakeholder functionality of this next generation of water resource simulation tools is primarily possible because fully integrated GW–SW models seamlessly couple

[1] Aquanty Inc. 564 Weber Street North, Unit 2 Waterloo, ON N2L 5C6
[2] Agriculture and Agri-Food Canada, Ottawa Research and Development Centre, 960 Carling Ave, Ottawa, ON K1A 0C6
[3] Geology Survey of Canada, Natural Resources Canada, 601 Booth Street, Ottawa, ON K1A 0E8

*corresponding author: sfrey@aquanty.com

Recommended citation: Frey, S.K., Khader, O., Taylor, A., Erler, A.R., Lapen, D.R., Sudicky, E.A., Berg, S.J., and Russell, H.A.J. 2020. A fully integrated groundwater–surface-water model for southern Ontario. In Russell, H.A.J. and Kjarsgaard, B.A. Eds. Southern Ontario groundwater project 2014–2019: summary report. Geological Survey of Canada, Open File 8536, 231-245. https://doi.org/10.4095/321108

surface water (SW) and groundwater (GW) flow systems, including the unsaturated zone, and are driven by spatially and temporally varying climate or weather patterns derived from either observational/reanalysis data or climate system projections. As such, traditional groundwater-only and surface-water only models can now be replaced by a single simulation platform that employs holistic physics-based approaches for emulating the entire terrestrial water cycle, with full accounting of water balances within and between the various hydrological compartments. Furthermore, fully integrated physics-based modelling provides additional benefit when simulating hydrologically complex settings such as the Great Lakes Basin (GLB) (Figure 1), because crucial GW–SW interaction processes are inherently captured, and hence difficult-to-derive boundary conditions designed to explicitly represent processes like recharge and discharge in GW only models are not required.

Fully-integrated models have been commonly employed on local-scale problems (10's to 100's of km^2) for well over a decade; however, their application towards resolving high-resolution three-dimensional (3-D) water resources questions at scales approaching 100,000 km^2 or more has only been recently demonstrated, such as in the work of Hwang et al. (2018) that studied the 160,000 km^2 Athabasca River Basin in Western Canada. This increase in model scale, as well as complexity and spatial resolution, has evolved because of a number of factors, including the mainstream accessibility to high-performance computing resources, improved numerical techniques, and the increasing availability of the large spatially-distributed datasets required to construct these models. With regard to data availability, one limiting factor tends to be the sparsity of detailed 3-D hydrostratigraphic information, as land surface characteristics such as soil, land cover, topography, and surface water features, are in

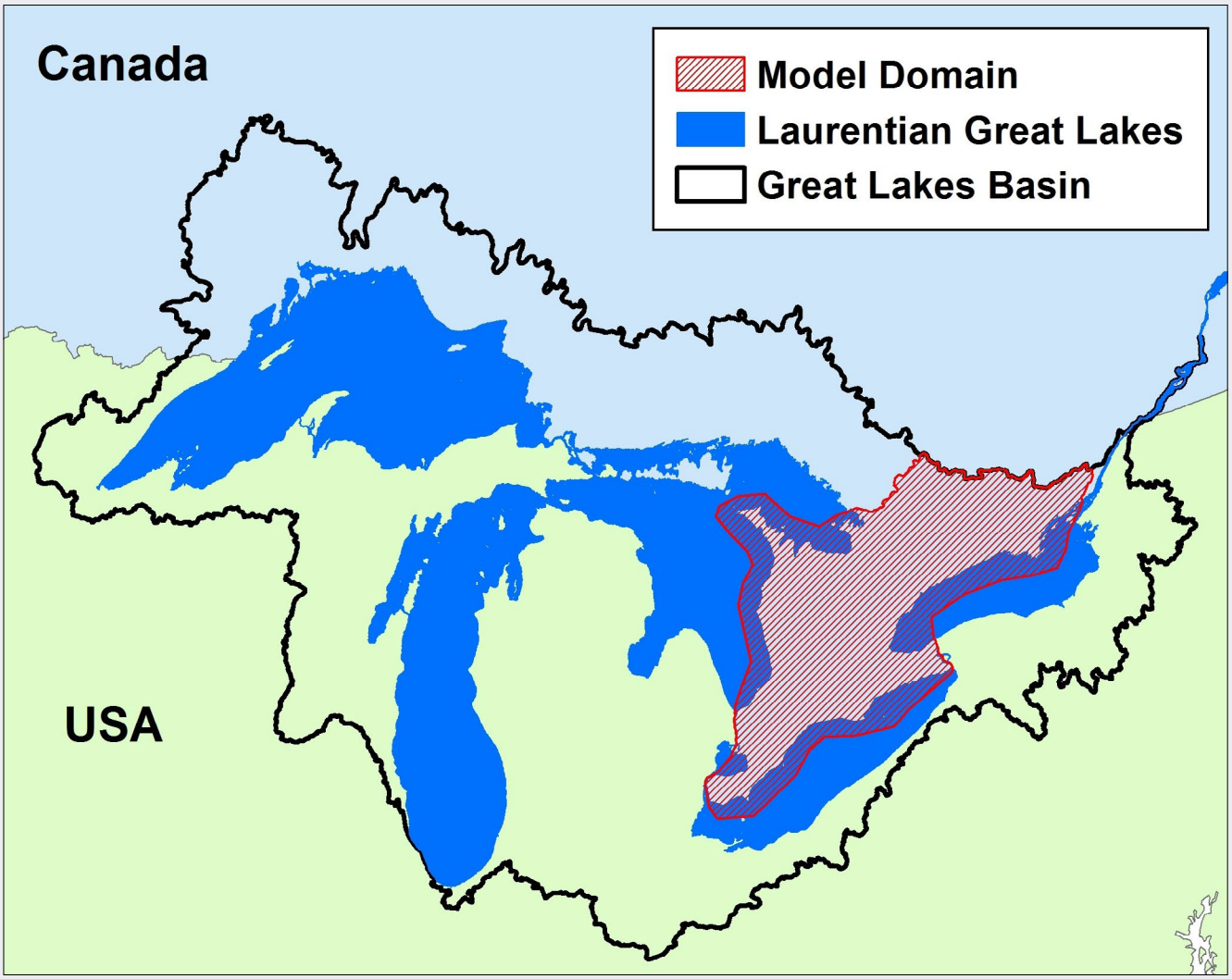


Figure 1. Geographical depiction of the Southern Ontario regional model domain within the Laurentian Great Lakes basin.

comparison relatively well defined.

In southern Ontario, the geoscience community has recently benefited from the OGS-GSC southern Ontario Geoscience initiative, wherein 3-D geological models have been assembled for both the Paleozoic basin sedimentary sequence (Carter et al. 2019, 2020) and the overlying Quaternary sediments (Logan et al. 2020). These new geologic models, combined with the existing data describing topography, surface water, land cover, and soils, provides the requisite information required to construct a regional-scale fully integrated GW–SW model with unprecedented subsurface resolution. Now, with the need for such a model apparent and the requisite data available, questions regarding the feasibility and utility of a high-resolution fully-integrated GW-SW model for southern Ontario can be addressed.

Accordingly, the work herein focuses on the construction and demonstration of a HydroGeoSphere (Aquanty 2019) model for southern Ontario (Figure 1), as well as a series of sensitivity tests that characterize the influence of model spatial resolution and groundwater extraction on simulated hydrologic conditions. Although framed as a proof-of-concept study, the resulting model has the potential to help address a wide range of questions pertaining to southern Ontario's GW and SW resources under historic, current, and future conditions.

2. Model construction

A description of the data sources and data processing used for model construction is provided in Frey et al. (2019), whereas the information provided here is meant to provide a general understanding of the overall model construction process. The design of the HydroGeoSphere (HGS) model followed from the development of a conceptual model that incorporates key components of the southern Ontario surface water and groundwater flow system, including the South-West structural dip of the Paleozoic units along with lithologic heterogeneities, the emplacement of high total dissolved solids (TDS) basin brines, land surface topography, and regional gradients imposed by variation in water levels between the Great Lakes that border the model domain (Figure 2). From the conceptual model, it was also determined

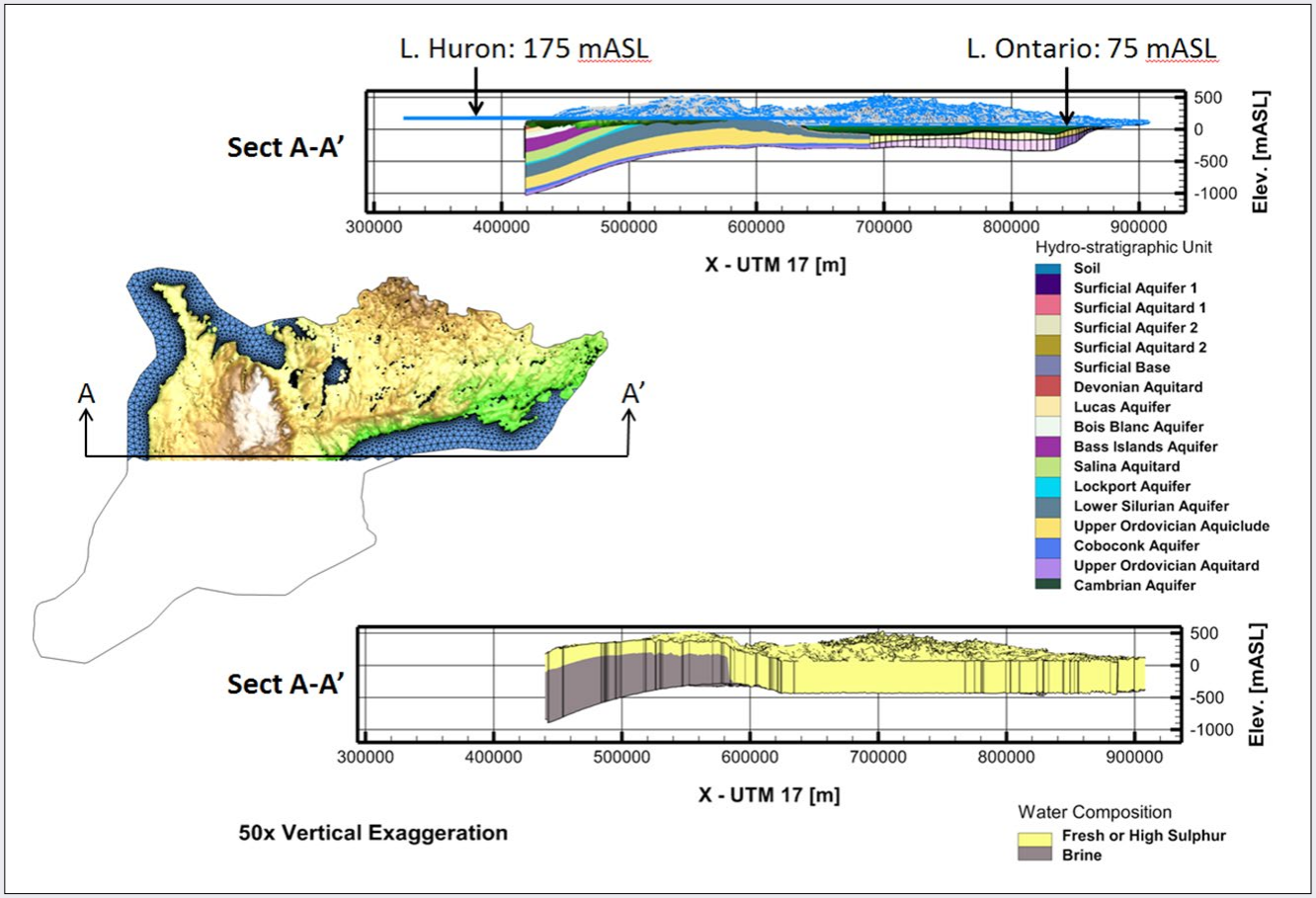


Figure 2. Conceptual depiction of regional hydrostratigraphy (top panel) in relation to L. Huron and L. Ontario water levels, as depicted through an east-west cross section (middle inset). Bottom panel shows the approximate location of high TDS brines within the Paleozoic hydrostratigraphy south-west of the Niagara Escarpment.

that the northern periphery of the model domain would extend into the Precambrian shield in order to capture the full surface water catchment area for watersheds draining south into the Paleozoic sedimentary basin. In total, the model domain encompasses 13 watershed management areas in southern Ontario (Figure 3), 78,687 km^2 of land area and 30,878 km^2 of surface water area within the Great Lakes, for a total model area of 109,565 km^2.

The foundation of the HGS model is a three-dimensional finite element mesh (FEM). In order to evaluate the influence of mesh resolution on the accuracy of hydrologic simulations, low- and high- resolution FEMs were constructed for the study area (Figure 3). The low-resolution version of the model resolves Strahler order 4 (and greater) streams, contains 41,638 nodes per mesh sheet, and extends vertically through a 21 layer sequence composed of a land surface layer, three soil layers, five surficial hydrostratigraphic layers (Table 1), and 11 Paleozoic bedrock hydrostratigraphic layers, with the base layer of the model being Precambrian bedrock. The high-resolution version resolves Strahler order 3 (and greater) streams, contains 132,985 nodes per sheet, and extends vertically through a 16 layer sequence composed of a land surface layer, 3 soil layers, 5 surficial geology layers, and 7 bedrock layers, with the base of the model being the top of the high TDS brine surface to the west of the Niagara Escarpment, and Precambrian bedrock to the east of the escarpment. In total, the high-resolution FEM contains 2,127,760 subsurface nodes, while the low-resolution FEM contains 874,398 subsurface nodes.

Both the land topography and the river network are derived from the Ontario Integrated Hydrology Dataset (MNRF 2015), with the river network having undergone simplification so that vector segments were resolved at 1,000 m and 500 m lengths for the respective low- and high- resolution versions of the model. In order to create a complete hydrologically correct top surface for the model, land topography was stitched to lake bathymetry (NOAA 2017), and a hydrologic correction was applied in order to enforce downgradient flow along the simplified river networks. The channel elevation along surface water channels between the individual Great Lakes

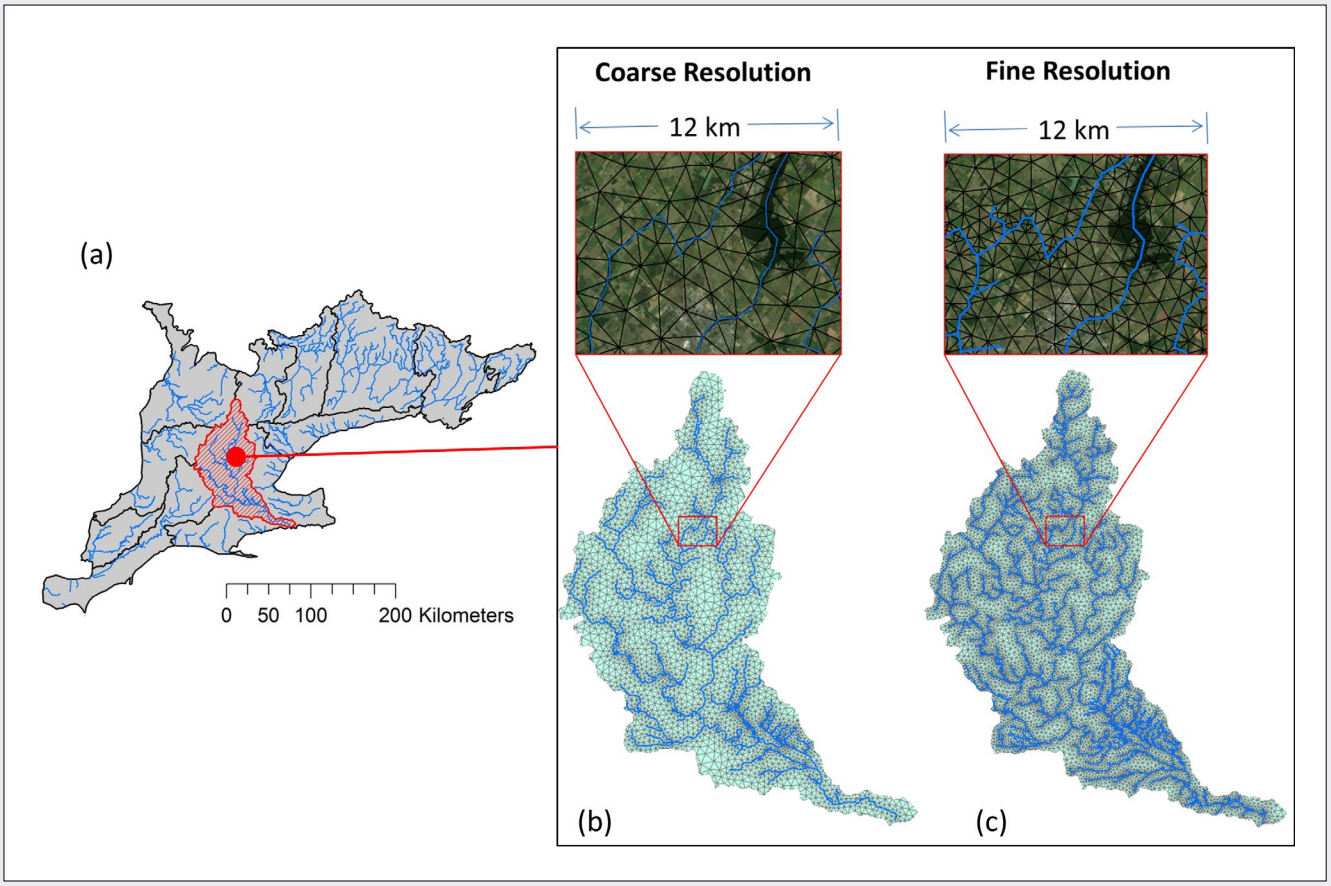


Figure 3. (a) Relative location of the Grand River watershed (GRW, one of 13 watershed management areas encompassed by the regional model), and using the GRW as an example, spatial resolution of the finite element mesh for the low resolution (b), and high resolution (c) versions of the model, along with their respective Strahler order 4 and Strahler order 3 stream networks.

Table 1. Bedrock hydrostratigraphic sequence, and summary statistics for the hydraulic conductivities of each bedrock layer. The top table shows values for non-karst areas of the unit. The bottom table shows values for karst areas of the unit. For insight on how municipal wells were used as a data source, readers are referred to Russell et al. (2017a,b).

Hydrostratigraphic Layer Unit (Model base is 01)		Data Source and Representative K Values (m s^{-1})								Model K and Anisotropy Values		
		OGSRL (2018)	Golder (2003)	Intera (1988)	Intera (2011)	[a]Municipal Wells	Novakowski et al. (1988, 2000)	Priebe et al. (2017)	Raven et al. (1992)	Kh Geomean	Kv:Kh Ratio	Kv
Non Karst	(12) Devonian Aquitard	5.18E-07		4.73E-09	1.77E-09				2.28E-10	5.61E-09	0.119	6.70E-10
	(11) Lucas Aquifer	1.17E-05		1.47E-07	1.00E-06				2.83E-08	4.70E-07	0.036	1.70E-08
	(10) Bois Blanc Aquifer	1.72E-05	6.71E-08	1.33E-08	2.15E-07				5.03E-10	2.40E-07	0.116	2.79E-08
	(09) Bass Islands Aquifer	3.00E-06		3.16E-07	5.50E-05					3.74E-06	0.046	1.71E-07
	(08) Salina Aquitard	7.29E-07			2.42E-12					1.33E-09	0.039	5.24E-11
	(07) Lockport Aquifer	2.58E-05			4.93E-11	5.51E-05	6.21E-08	2.32E-05	2.52E-08	3.70E-07	0.010	3.70E-09
	(06) Lower Silurian Aquitard	1.13E-06			6.89E-13		2.41E-09		1.16E-10	6.84E-10	0.010	6.84E-12
	(05) Upper Ordovician Aquiclude	5.41E-07	3.85E-11	2.31E-10	1.62E-14		3.16E-10		1.81E-12	5.96E-11	0.010	5.96E-13
	(04) Coboconk	5.33E-06			2.00E-11					1.03E-08	0.010	1.03E-10
	(03) Upper Ordovician Aquitard	3.34E-07	1.58E-09		4.47E-11				9.43E-13	3.86E-10	0.010	3.86E-12
	(02) Cambrian Aquifer	1.62E-05			3.00E-06					6.97E-06	1.000	6.97E-06
	(01) Precambrian Aquitard	1.12E-06			1.00E-11					3.35E-09	1.000	3.35E-09
Karst	(11) Lucas Aquifer	4.95E-04		1.00E-06					3.20E-07	5.41E-06	0.01	5.41E-08
	(10) Bois Blanc Aquifer	1.37E-03	9.00E-05	1.00E-06					7.90E-09	4.98E-05	0.01	4.98E-07
	(09) Bass Islands Aquifer	1.05E-03		1.00E-06						3.24E-05	0.01	3.24E-07
	(07) Lockport Aquifer	9.15E-04			3.00E-08	7.00E-04	3.75E-04	9.09E-04	6.30E-05	8.63E-05	0.01	8.63E-07
	(04) Coboconk	7.06E-05								7.06E-05	0.01	7.06E-07

[a] Derived from the work of Russell et al. (2017a,b).

was manually adjusted to minimize the difference between simulated and observed lake depth.

The land surface representation in the model governs surface water movement both over the land surface and in the river channels, as well as evapotranspiration. To characterize the land surface, the 250 m resolution North American Land Change Monitoring System (NALCMS) 2010 land cover data was used (Latifovic et al. 2016); however, prior to implementation, the original 19 land classes were simplified into six categories (water, developed, wetland, grassland, cropland, and forest) deemed most relevant for southern Ontario. As evapotranspiration is heavily controlled by the plant canopy, spatially and temporally varying leaf area index values were extracted from MODIS remote sensing data (Myneni et al. 2015) that were averaged on a monthly basis over the 2002 to 2018 interval for each of the six land surface classes.

The model subsurface can be effectively divided into 3 components that represent soil, surficial hydrostratigraphy and bedrock hydrostratigraphy, with configuration of the soil and surficial hydrostratigraphy common to both the low- and high- resolution versions of the model. Soil composes the top 1 m of the model subsurface, with discrete layers at the 0.25, 0.5, and 1 m depths. The spatial distribution of soil hydraulic properties is derived from the AAFC Soil Landscapes of Canada v3.2 (SLC) dataset (Soil Landscapes of Canada Working Group 2010), which defines 245 unique soil polygons across the model domain. The soil hydraulic property parameterization was based on permeability, porosity, and residual saturation information directly from the SLC database, while the α and n coefficients for the van Genuchten soil moisture retention parameterization were derived from the Rosetta pedotransfer function model (Schaap et al. 2001) based on soil textural class.

Surficial hydrostratigraphy was derived from an eight layer surficial geology model (Logan et al. 2020) that was modified at the top and bottom in order to conform to the respective topographic surface and the top of bedrock surface. Further simplification reduced the surficial model to five layers that can be broadly characterized from top to bottom as surface sediment/aquifer, upper aquitard, upper aquifer, mid aquitard, and lower deposits. Hydraulic properties for the surficial hydrostratigraphy were derived from textural information associated with the borehole data used to construct the

surficial geology model, such that each hydrostratigraphic layer is unique. Textural information was converted to hydraulic properties using the Rosetta pedotransfer model (Schaap et al. 2001), and the hydraulic properties were interpolated across each layer using inverse distance weighting in order to produce spatially varying K maps.

For the low-resolution model, the bedrock hydrostratigraphy extended to the Precambrian, which was classified as an aquitard in regions overlain by Paleozoic deposits. In the Northern region of the model domain (where Paleozoic deposits are absent), the Precambrian was represented by a two-layer sequence consisting of higher permeability bedrock (in order to represent fractures) near surface, underlain by intact aquitard bedrock. The Paleozoic hydrostratigraphic sequence was derived from a 58 layer geological model (Carter et al. 2019), which was simplified to 12 layers (Table 1) for the low-resolution version of the model. Bedrock hydrostratigraphy in the high-resolution version extends to the base of high-sulphur groundwater (Carter and Clark 2018) west of the Niagara Escarpment, and to the Precambrian in the region east of the Escarpment. In order to minimize total node count in the high-resolution version, the number of bedrock layers was reduced from 12 to 7. This was facilitated by merging hydrostratigraphic contact surfaces at the Niagara Escarpment (e.g., the Devonian Aquitard west of the Escarpment and the Upper Ordovician Aquiclude east of the Escarpment were both represented in the same model layer), such that east of the Escarpment there is little difference in hydrostratigraphy between the low- and high-resolution models. In both the low- and high-resolution models, the minimum layer thickness within the 3-D FEM is one meter, and where individual hydrostratigraphic units are not present or pinch out, hydraulic properties from the underlying hydrostratigraphic unit (model layer) were mapped onto the overlying layer in order to avoid regions of missing data in the model layer framework. For hydraulic property assignment, the bedrock hydrostratigraphy in the high-resolution version of the model was divided in 18 zones, defined by intact and fractured Precambrian zones, and the 11 Paleozoic units, of which 5 units were further subdivided into karst–non-karst (Table 1). The karst–non-karst subdivision occurred at the fresh-water–high-sulphur water interface, with karst representing the up-dip region of each unit. Bedrock zonation in the high-resolution version of the model was reduced in order to reflect hydrostratigraphy that only exists above the high TDS brine surface (Figure 2).

Recognizing that extensive heterogeneity can exist within each zone, existing literature was reviewed for information regarding bedrock hydraulic properties and associated spatial variability (Table 1). For zones with sufficient data (i.e. Lockport Karst, Lockport Aquifer, Bass Islands Aquifer, Bois Blanc Aquifer, and Lucas Aquifer), spatially varying K maps were produced via interpolation. For zones with limited data, geometric mean K values were calculated. Vertical vs. horizontal K anisotropy was incorporated into zones for which such information was available (Intera 1988, 2011), or for lithology that can be reasonably expected to exhibit directional variation in K, such as the karst units, for which an estimated Kv:Kh ratio of 0.01 was applied (Table 1). For the fractured Precambrian zone, a bulk K value was derived through manual calibration against surface water flow rates (primarily baseflow) at observation points local to the exposed Precambrian region of the model.

The surface-water flow-rates and groundwater levels computed by the model were assessed at the respective location of 29 Water Survey of Canada hydrometric stations (Table 2) and 321 Provincial Groundwater Monitoring Network (PGMN) wells (Figure 4). The surface water gauges are located

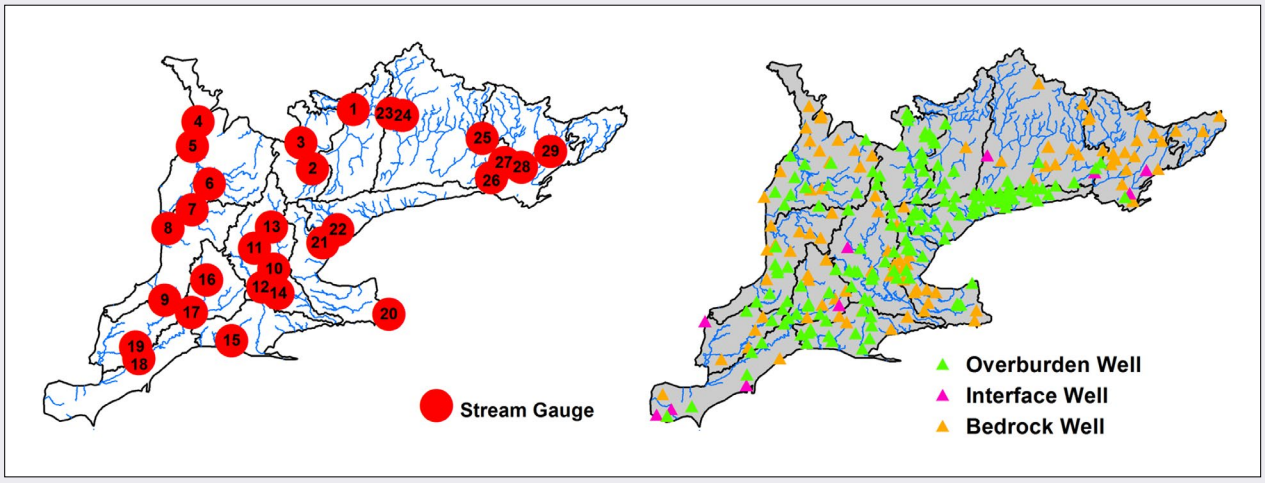


Figure 4. Relative location of the 29 WSC hydrometric stations (note that numbers correspond with Table 2), and the 321 PGMN Wells, that were used to assess model performance.

on Strahler 4+ order streams so that they would be present in both the low- and high- resolution versions of the model, and with a reasonable spatial distribution in order to provide a spatial perspective on surface water flow performance. Of the PGMN wells, there are 191, 13, and 117 located in the surficial hydrostratigraphy, surficial-bedrock interface aquifer, and Paleozoic hydrostratigraphy, respectively. Well location in the FEM involved positioning the well at the node closest to the actual geographic coordinate of the PGMN well. Due to considerable uncertainty in colocation of individual PGMN wells with the correct hydrostratigraphic layer, the monitoring wells in the model were characterized as either surficial or bedrock, and aggregated across all layers in the respective hydrostratigraphic sequence.

In order to assess the model's ability to characterize the impact of groundwater extraction on regional groundwater levels, a prototype high-resolution version was developed with operating extraction wells. In total, 196 extraction wells (a small subset of the total number of wells in southern Ontario) were built into the model, with representation from the following sectors: agriculture, commercial, dewatering, industrial, remediation, and water supply. The extraction

Table 2. Station No. for the stream flow gauges configured in the model, along with corresponding Water Survey of Canada station code and name, location, and catchment (drainage) area.

Station No.	Station Code	Station Name	Latitude	Longitude	Drainage Area (km^2)
1	02EC002	BLACK RIVER NEAR WASHAGO	44.714	-79.282	1510
2	02ED003	NOTTAWASAGA RIVER NEAR BAXTER	44.250	-79.821	1231
3	02ED027	NOTTAWASAGA RIVER NEAR EDENVALE	44.485	-79.966	2686
4	02FA001	SAUBLE RIVER AT SAUBLE FALLS	44.678	-81.256	913
5	02FC001	SAUGEEN RIVER NEAR PORT ELGIN	44.456	-81.326	3954
6	02FC002	SAUGEEN RIVER NEAR WALKERTON	44.120	-81.115	2136
7	02FE002	MAITLAND RIVER BELOW WINGHAM	43.887	-81.326	1644
8	02FE015	MAITLAND RIVER AT BENMILLER	43.718	-81.626	2545
9	02FF002	AUSABLE RIVER NEAR SPRINGBANK	43.072	-81.660	865
10	02GA003	GRAND RIVER AT GALT	43.353	-80.316	3515
11	02GA006	CONESTOGO RIVER AT ST. JACOBS	43.541	-80.553	790
12	02GA010	NITH RIVER NEAR CANNING	43.190	-80.455	1034
13	02GA016	GRAND RIVER BELOW SHAND DAM	43.731	-80.341	785
14	02GB001	GRAND RIVER AT BRANTFORD	43.133	-80.267	5201
15	02GC026	BIG OTTER CREEK NEAR CALTON	42.711	-80.841	665
16	02GD005	NORTH THAMES RIVER AT ST. MARYS	43.256	-81.146	1080
17	02GE002	THAMES RIVER AT BYRON	42.963	-81.332	3083
18	02GE003	THAMES RIVER AT THAMESVILLE	42.545	-81.967	4370
19	02GG003	SYDENHAM RIVER AT FLORENCE	42.651	-82.008	1149
20	02HA013	NIAGARA RIVER AT FORT ERIE	42.930	-78.914	682980
21	02HB029	CREDIT RIVER AT STREETSVILLE	43.582	-79.709	774
22	02HC003	HUMBER RIVER AT WESTON	43.699	-79.520	802
23	02HF002	GULL RIVER AT NORLAND	44.732	-78.818	1281
24	02HF003	BURNT RIVER NEAR BURNT RIVER	44.710	-78.678	1252
25	02HK003	CROWE RIVER AT MARMORA	44.482	-77.685	1935
26	02HK010	TRENT RIVER AT TRENTON	44.124	-77.592	12400
27	02HL001	MOIRA RIVER NEAR FOXBORO	44.254	-77.419	2595
28	02HM003	SALMON RIVER NEAR SHANNONVILLE	44.207	-77.209	907
29	02HM007	NAPANEE RIVER AT CAMDEN EAST	44.335	-76.839	700

rates associated with each well were derived from reported water taking information that allowed a use-ratio (i.e. ratio of reported water taken to permitted-maximum-extraction) for each sector to be calculated, such that the sector-use-ratio multiplied by permitted-maximum-extraction provided the simulated actual extraction rate for each well. For all wells combined, the total simulated extraction rate was 112,320 $m^3\ d^{-1}$. The simulated extraction amounts to approximately 0.04% of the total precipitation and can be considered a very small proportion of total consumptive groundwater use in southern Ontario.

3. Climatology

The HGS simulations are forced with 1970–2000 monthly normal climatology, providing an average seasonal cycle based on 30 year average monthly conditions as the atmospheric boundary condition in the HGS model. HGS simulations repeat the same average year until there is minimal change in year-to-year simulated hydrologic behavior, which indicates a quasi-steady state condition has been reached. The monthly normal forcing data for the study was assembled from the NRCan dataset described in McKenney et al. (2011), and carries a spatial resolution of approximately 10 km across the model domain. The HGS model requires total liquid water influx which is the sum of liquid precipitation and snowmelt, where snowmelt was estimated from changes in snow accumulation, as determined from the McKenney et al. (2011) dataset. In order to estimate changes in snow accumulation, snow depth was first converted to Snow Water Equivalent (SWE) using monthly snow density climatology (Sturm et al. 1995), then monthly changes in SWE were computed by differencing the SWE values at the end of each month and adding the water-equivalent snowfall over the same period. The resulting values were used as the snowmelt component of total liquid water influx. Apart from total liquid water influx, HGS also requires potential evapotranspiration, which was taken directly from the McKenney et al. (2011) dataset.

For a detailed discussion of how the climatic boundary conditions were prescribed, as well as advantages and disadvantages of this approach, see Erler et al. (2019a).

4. Model performance

A statistical comparison between simulated and observed surface water flow rates based on the Nash Sutcliffe Efficiency Coefficient (NSE) is shown in Figure 5, where values larger than 0.5 can be considered satisfactory performance (Moriasi et al. 2007). Additionally, a visual comparison of simulated vs. observed monthly normal streamflow rates is presented in Figure 6, which shows a subset of the data from all 29 WSC stations provided in Frey et al. (2019). The NSE was calculated for hydrometric stations with a data record that extended over the bulk of the 30 year climate interval (18 in total), with 14 of the 18 stations demonstrating acceptable performance for reproduction of the monthly normal flow conditions; only one of the 18 stations (station 9) showed a NSE value approaching 0 (for the high-resolution version)

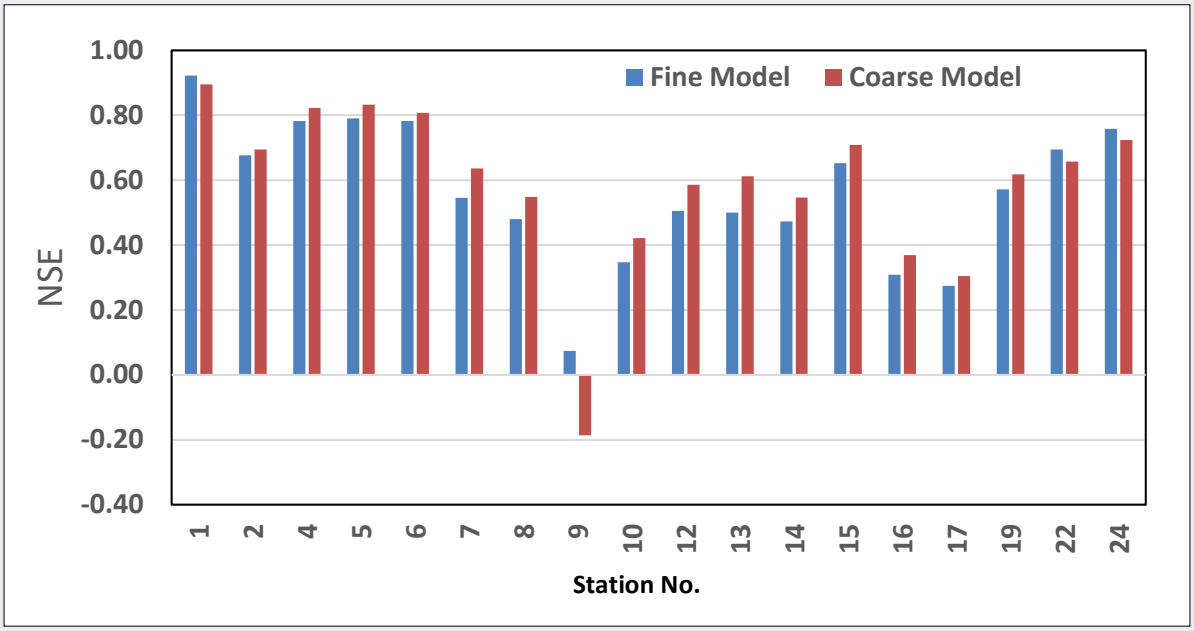


Figure 5. Nash Suttcliffe Efficiency (NSE) coefficient values for simulated stream flow rates at 18 of the WSC hydrometric station locations (note that numbering corresponds to Figure 4 and Table 2).

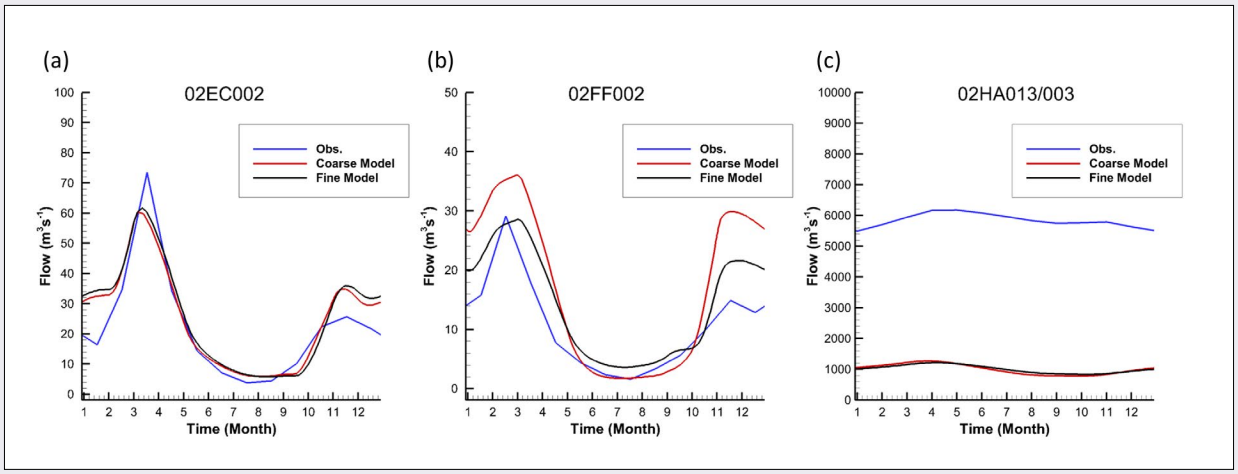


Figure 6. Simulated vs. observed monthly normal stream flow rates at (a) WSC station 02EC002 (best performing – corresponding to location 1 in Figure 5), (b) 02FF002 (worst performing – corresponding to location 9 in Figure 5), and (c) 02HA013/003, located on the Niagara River. Note that the large difference between simulated and observed flows at 02HA013/003 is due to the model only capturing flow contribution from Southern Ontario while the gauge station captures flow from the entire upstream Great Lakes Basin.

or a negative value (for the low-resolution version), which respectively indicate that model performance is no better, or worse, than predictions based on the mean of the observed data. As Figure 6 shows, the visual difference between the best (station 1) and worst (station 9) performing stations is minimal with respect to seasonal cycle and the magnitude of summer baseflow. However, station 9 depicts a clear positive bias in simulated flow and a lag in the timing of the simulated spring freshet. Conversely, station 1 captures the timing of the spring freshet closely but underestimates its magnitude. It is important to note that simulation results from both station 1 and 9, as well as the majority of other stations (Frey et al. 2019) over-estimate winter flow rates, and that this phenomenon has been observed in other higher resolution watershed scale modelling work within the southern Ontario domain (Erler et al. 2019a). This can in part be attributed to uncertainties in snow accumulation and melting in the climate forcing data. It can also be expected that the averaging associated with the monthly normal climate forcing data, and the observation data, will introduce additional uncertainty that will translate through to the assessment of model performance.

A further noteworthy point regarding the simulated surface water behavior relates to the difference between simulated and observed flow rates at WSC station 02HA013/003 (Figure 6c). The seemingly large under prediction of flows is attributed to the station being located on the Niagara River, which has a catchment area that encompasses approximately 683,000 km^2 of the Great Lakes Basin (Figure 1). However, the simulated flows at this location only reflect the contribution of water from the southern Ontario model domain upstream from the Niagara River, and hence the simulation results indicate that approximately 18% of the flow observed in the Niagara River originates from southern Ontario.

The groundwater performance of the model is presented in Figure 7, with linear correlation tests between simulated and observed water levels specific to the surficial, interface, and bedrock aquifers. It should be noted that the results presented in Figure 7 reflect simulations with no consideration of the groundwater extraction wells. As evidenced by the correlation coefficients, the ability of the model to reproduce the observed depth to groundwater progressively diminishes between the surficial and bedrock aquifers. It is also apparent that the model tends to overestimate water levels in the surficial aquifers, whereas in the interface and bedrock aquifers there is not such an obvious bias. The positive bias in simulated water levels in the surficial aquifers can possibly be attributed to three factors, with one being the fact that the model tends to be too wet near surface, which is supported by the consistent overestimation of surface water flow rates during fall and winter; the second being the spatial resolution of the FEM, and the fact that much of the sub-mesh-scale topography that forms the actual land surface (and the measurement plane from which water level measurements are made) will not be resolved; and the third being the absence of groundwater extraction, which is addressed in a subsequent section. Accordingly, improvements to the climate forcing data, and higher FEM resolution (also discussed below) may offer improvements to the match between simulated and observed water levels in the surficial aquifers. Furthermore, if the well locations had been used as control points during FEM generation, it is possible that the impact of sub-mesh topography would have been reduced through reduction of

elevation mismatch due to the geographic offset. However, for the purpose of this study it was only the surface water network that was used to control mesh geometry. Although not all that useful from a model diagnostics perspective, when sea level was used as the vertical datum for groundwater level comparison between modelled and observed conditions, the R^2 for simulated vs. observed groundwater levels was 0.98 and 0.99, for the respective low- and high-resolution versions of the model.

Additional uncertainty that cannot be overlooked pertains to the PGMN monitoring well data, and the challenge associated with matching the hydrostratigraphy in the simplified hydrostratigraphic model with the proper screened interval in the monitoring well. While there is reasonable confidence with the wells being classified as either surficial or bedrock, in some cases there is considerable guesswork associated with the hydrostratigraphic unit assignment.

5. Spatial resolution influence

Simulation results for surface water and groundwater are provided for both the low- and high-resolution versions of the model. As observed in Figure 5, the difference in NSE-based surface water performance between the low- and high- resolution versions is in most cases quite small, and in fact at 14 of the 18 surface water gauging locations, there is slightly better performance from the low-resolution version. Interestingly, the largest difference in simulation performance between the low- and high- resolution versions occurs at station 9 (worst performing station), where the high-resolution model provides a notably better visual match with observed conditions (Figure 6b) even though neither version produces an acceptable NSE value.

Differences in groundwater simulation performance between the low- and high- resolution versions are also small, with Figure 7 demonstrating subtly better R^2 values for the high-resolution version in the surficial (R^2 of 0.48 vs. 0.43) and bedrock (R^2 of 0.19 vs. 0.16) aquifers, while the low-resolution version demonstrates somewhat better performance for the interface aquifer (R^2 of 0.33 vs. 0.15). It should be

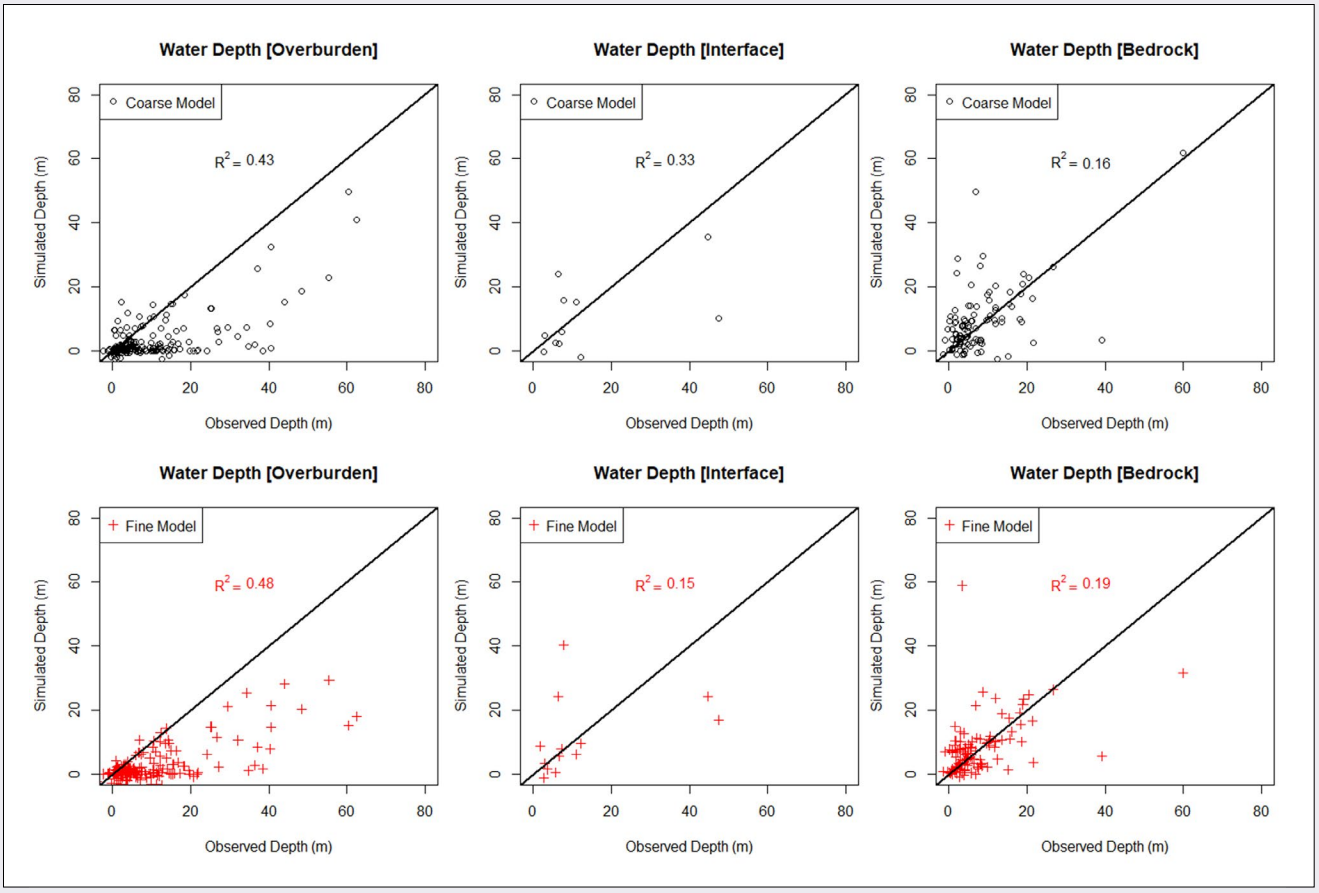


Figure 7. Groundwater simulation performance (water depth from surface) for the low-resolution (Coarse Model – top row), and high-resolution (Fine Model – bottom row) versions of the model, for wells in the overburden, interface, and bedrock aquifers.

noted, however, that the number of samples available for the interface aquifer correlation test was quite small (n = 13). The differences in simulated vs. observed water depth between the low- and high- resolution versions, particularly as it pertains to scatter amongst the outlier points, indicates that model resolution and the location of FEM nodes relative to topography is likely to be influencing results. As the differences between measured well elevation and model well elevation show (Table 3), even the high-resolution version can have ground elevations that have a notable difference from the surveyed elevation at the actual observation well. In terms of uncertainty with the elevation data, it should also be noted that the model uses a hydrologically corrected DEM as the land surface, and it would be expected that some difference between the DEM and well survey data will exist.

6. Extraction well influence

Simulated vs. observed groundwater depth is depicted in Figure 7 without any consideration for operating groundwater extraction wells. It can be expected that the inclusion of groundwater extraction would reduce the positive bias (i.e. produce lower groundwater levels) witnessed in the simulated surficial aquifer water levels, and also increase the physical realism associated with simulated groundwater flow within the surficial, interface, and bedrock aquifers. As demonstrated in Figure 8, groundwater extraction, even with the reduced volumes associated with only 196 of the operating permits to take water, does have an impact, with groundwater levels declining by an average of 1.7 m at the 8 wells that were randomly selected for analysis. The spatial extent of groundwater level decline is also widespread across the model domain, with results presented in Table 3 demonstrating that an observation well (W0000258-1) almost 50 km from the nearest extraction well saw a 6.7 m decline in bedrock aquifer water levels; however, this may be in part due to short circuiting of water across aquitards via the simulated boreholes. The impact of short circuiting is perhaps most obvious in the case of observation well W0000297.1, where the addition of extraction wells caused a seemingly non-intuitive response, in that simulated water levels (during June-July-August) are actually higher than levels from the model that does not include extraction wells. This rise in water levels is attributed to the hydraulic connection that the extraction well makes across aquifer units that are otherwise separated by aquitards, which in turn limits well drawdown during relatively dry summer months. In regards to seasonal variability and sensitivity to groundwater extraction, half of the wells depicted in Figure 8 exhibit an exaggerated response, which suggests that transmissivity may be underestimated for key aquifer units that are effectively represented in the model. In terms of overall groundwater simulation performance, inclusion of extraction wells in the high-resolution version of the model made only a small positive improvement, with R^2 values increasing from 0.48 to 0.50 and 0.15 to 0.17 for the respective surficial and interface aquifers; while the R^2 for bedrock aquifer performance saw no change. In this

Table 3. Monitoring well information pertaining to the eight PGMN wells selected for the groundwater extraction focused sensitivity analysis (per Figure 8); along with corresponding observation (Obs.) well information from the high resolution version of the model, distance to nearest simulated extraction well and its associated extraction rate.

Well Name	Ground Elev. Obs. (m A.S.L.)	Ground Elev. Model (m A.S.L.)	Water Depth (WD) Obs. (m)	WD: Model with Extraction (m)	WD: Model no Extraction (m)	Formation	Obs. To Nearest Extraction Well (Km)	Extraction Rate ($m^3\ s^{-1}$)
W0000068-1	188.13	168.5	6.01	8.17	6.03	Surficial	3.8	0.0007
W0000218-4	368.9	363.5	1.75	2.24	1.06	Surficial	11.6	0.0595
W0000258-1	204.74	203.6	7.98	11.36	4.62	Bedrock	48.9	0.0013
W0000276-3	439.65	419.7	5.14	5.8	5.17	Bedrock	8.2	0.0091
W0000291-1	186.2	186.6	1.22	0.46	0.31	Surficial	12.2	0.011
W0000297-1	268.07	262.2	0.44	-0.49	-0.14	Surficial	2.1	0.0015
W0000315-1	188.54	188.1	4.72	5.33	2.82	Bedrock	20.3	0.004
W0000342-1	257.67	255.9	9.81	2.55	2.31	Bedrock	4.6	0.0093

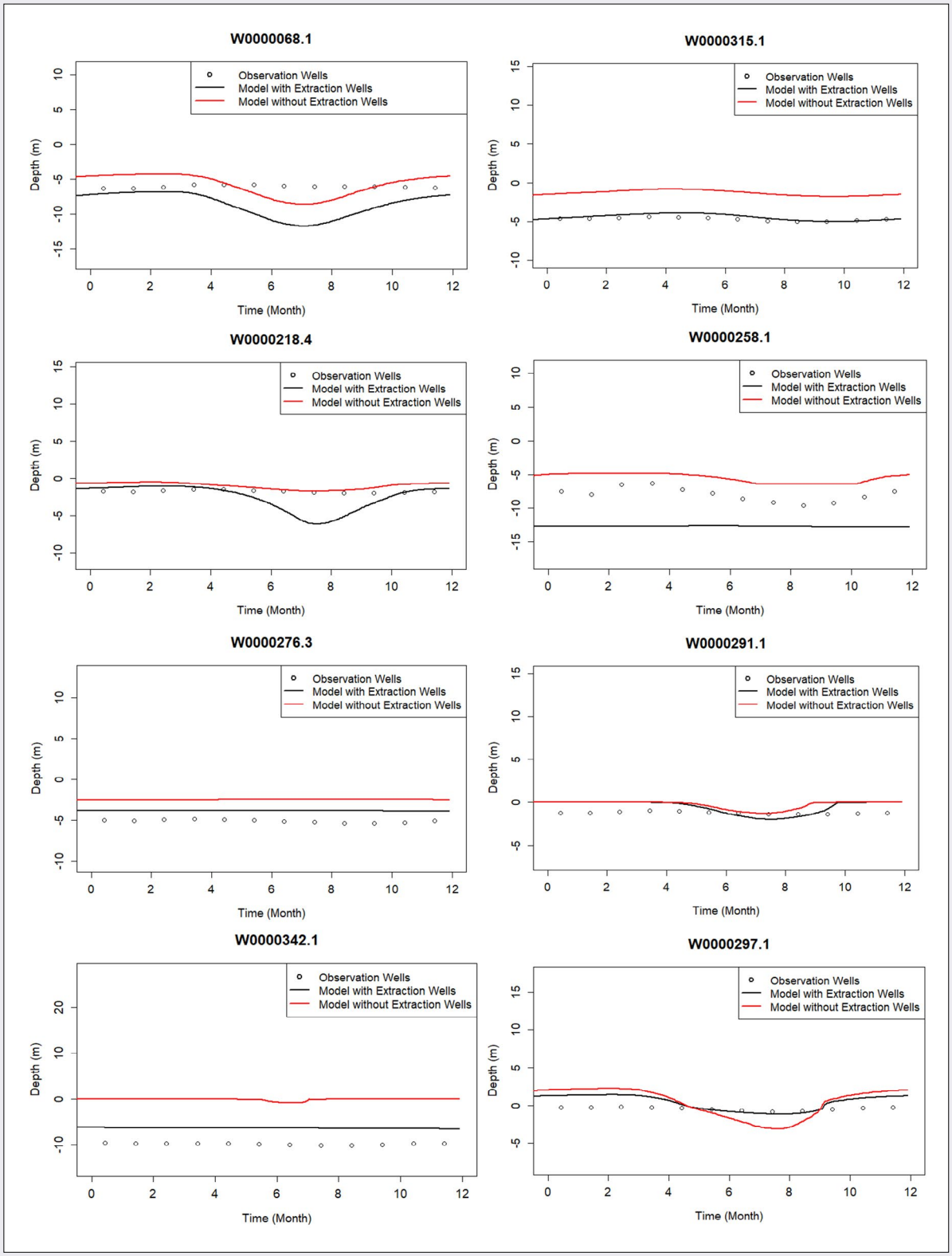


Figure 8. Influence of large-scale groundwater extraction on regional water levels, as depicted by eight randomly selected PGMN monitoring wells embedded into the regional model. Note that well numbers (panel titles) correspond to Table 3.

regard, it should be noted again that the extraction wells included in this sensitivity test make up a small proportion of total groundwater extraction across southern Ontario. It should also be noted that including a large number of extraction wells into a regional scale model is a challenging task from both a data management and model construction perspective. Accordingly, while this proof-of-concept attempt lays out the framework and demonstrates the sensitivities associated with simulating groundwater extraction at the regional scale, considerable work would be required to fully operationalize a southern Ontario model that incorporates all the extraction wells. In addition to characterizing how uncertainties associated with extraction well data and abstracted hydrostratigraphy invariably influence modelled vs. real world behavior, research that addresses spatial/topographic resolution issues and the potential applicability of effective K approaches (Bierkens, 1996; Sanchez-Vila et al. 2006) towards aquifer and aquitard parameterization in regional scale models, will help advance these models as tools to assess anthropogenic impacts on GW.

7. Conclusions

Results from this work demonstrate that high-resolution large-scale regional modeling with the fully integrated HydroGeoSphere simulation platform is feasible, even for complex hydrological terrains such as in southern Ontario. Considering that neither the low- or high- resolution models were subject to systematic calibration, the magnitude and seasonality of the simulated surface water flow rates matched well with observed conditions. Likewise, groundwater levels are also reproduced quite well; although, based on a linear correlation analysis, the model does demonstrate stronger groundwater simulation performance for the surficial monitoring wells as compared to those for the bedrock.

Perhaps surprisingly, there was not a dramatic difference in the simulated surface water and groundwater behavior between the low- and high- resolution version of the model; however, it needs to be recognized that the high-resolution model carries additional detail in the surface water network that would be useful for applications that involve detailed assessment of surface water flow or GW–SW interactions. Conversely, it should be noted that the low-resolution model, with its faster run times, would be quite amenable to performing large ensemble simulations, which would prove useful in climate change scenario analysis, where uncertainty associated with forcing data is likely to greatly exceed the additional structural uncertainty introduced into the model through the degradation of spatial resolution. It is also important to note that the model did show sensitivity to large-scale groundwater extraction. Although there was only a very small improvement in groundwater simulation performance when groundwater extraction was introduced, the simulated drawdown in regional GW levels was commensurate with the magnitude of differences between simulated and observed conditions. Overall, the groundwater extraction testing highlights the need for additional work on data conditioning and implementation methods, especially as it pertains to the potential incorporation of 1000's of extraction wells into a regional scale model.

The model in its current form could readily serve as a common platform to study adaptation and mitigation strategies for water resources related risks, including those from climate change, for which methodology to couple HydroGeoSphere with climate projection scenarios has recently been demonstrated for the Grand River Watershed (Erler et al. 2019a; Erler et al.2019b). It also provides a ready-built simulation tool to generate hydrologic scenarios from which extreme weather events such as floods and droughts can be assessed for their regional- or basin- scale impacts. From a practical hydrologic modelling perspective, the models can be used to generate external boundary condition information for smaller scale watershed or sub-watershed models developed to serve local water resources investigations. This boundary condition information can be in the form of regional gradients or fluxes that would impart a regional flow field onto a local scale model, or in the form of spatially and temporally varying GW recharge and discharge information that can be used to inform a top-surface boundary condition in GW-only models.

The model also has applications towards policy focussed water resources management endpoints; in particular, the Great Lakes Water Quality Agreement (GLWQA), where it can provide state-of-the-art science-based insight towards:

- Annex 4 – Nutrients: by evaluating loading characteristics and cumulative impacts on water quality.
- Annex 8 – Groundwater: by providing a large-scale platform to assess information gaps and science needs, as well as to investigate climate change impacts on groundwater.
- Annex 9 – Climate change: by providing a hydrologic modelling platform to test the impact of different regional climate projections on surface and groundwater resources at different spatial and temporal scales.
- Annex 10 – Science: by serving as a standardized platform to assess emerging environmental concerns, help identify science priorities, and foster collaboration on science efforts.

8. Acknowledgements

Input provided by T. Carter from Carter Geologic, and F. Brunton from the Ontario Geological Survey helped clarify aspects of the hydrostratigraphy during model construction. Internal reviews at the GSC by D. Paradis and M. Bunn are much appreciated. This work was funded under contract 3000652127 to Aquanty by the GSC Groundwater Geoscience

Program and Agriculture and Agrifoods Canada (AAFC). This work is a contribution of the GSC–OGS southern Ontario project on groundwater 2014–2019.

9. References

Aquanty. 2019. HydroGeoSphere: A three-dimensional numerical model describing fully-integrated subsurface and surface flow and solute transport, Waterloo, ON. https://www.aquanty.com/hgs-download

Carter, T.R., Brunton, F.R., Clark, J.K., Fortner, L., Freckelton, C., Logan, C.E., Russell, H.A.J., Somers, M., Sutherland, L., and Yeung, K.H., 2019. A three-dimensional geological model of the Paleozoic bedrock of southern Ontario; Geological Survey of Canada, Open File 8618; Ontario Geological Survey, Groundwater Resources Study 19, 1 .zip file. https://doi.org/10.4095/315045

Carter, T.R., Brunton, F.R., Clark, J.K., Fortner, L., Logan, C.E., Russell, H.A.J., Somers, M., Sutherland, L., and Yeung, K.H. 2020. Three-dimensional geological modelling of the Paleozoic bedrock of southern Ontario: Status update. In Russell H.A.J. and Kjarsgaard, B.A. Eds. Southern Ontario groundwater project 2014–2019 summary. Geological Survey of Canada, Open File 8536, 7-21. https://doi.org/10.4095/321080

Carter, T.R. and Clark, J. 2018. Base of fresh groundwater, inferred bedrock karst, and the contact aquifer in southern Ontario, as interpreted from water well records; Ontario Oil, Gas and Salt Resources Library, Open File Data Release 2018-1, 16 p.

Bierkens, M.F.P. 1996. Modeling Hydraulic Conductivity of a Complex Confining Layer at Various Spatial Scales, Water Resources. Research, 32: 8, 2369– 2382, doi:10.1029/96WR01465.

Erler, A. R., Frey, S. K., Khader, O., d'Orgeville, M., Park, Y.-J., Hwang, H.-T., Lapen, D.R., Peltier, W.R. and Sudicky, E.A. 2019a. Simulating climate change impacts on surface water resources within a lake-affected region using regional climate projections. Water Resources Research, 55: 130-155. https://doi.org/10.1029/2018WR024381

Erler, A. R., Frey, S. K., Khader, O., d'Orgeville, M., Park, Y.-J., Hwang, H.-T., Lapen, D.R., Peltier, W.R. and Sudicky, E.A. 2019b. Evaluating Climate Change Impacts on Soil Moisture and Groundwater Resources within a Lake-Affected Region. Water Resources Research, 55: 8142–8163. https://doi.org/10.1029/2018WR023822

Frey, S.K., Berg, S.J., and Sudicky, E.A. 2016. A Feasibility Study of Merits and Development Strategies for a Regional Water Resources Modelling Platform for Southern Ontario – Great Lakes Basin. Geological Survey of Canada, Open File 8021 46. https://doi.org/10.4095/298816

Frey, S.K., Khader, O., Taylor, A., Erler, A.R., Lapen, D.R., Sudicky, E.A., Berg, S.J., and Russell, H.A.J. 2019. Fully integrated groundwater – surface-water model for southern Ontario: proof of concept and data release. Geological Survey of Canada, Open File 8639, 1 .zip file. https://doi.org/10.4095/321042

GLWQA. 2012. Canada - US Great Lakes Water Quality Agreement, https://www.canada.ca/en/environment-climate-change/services/great-lakes-protection/canada-united-states-water-quality-agreement.html

Golder Associates Ltd. 2003. LLW geotechnical feasibility study, Western Waste Management Facility, Bruce Site, Tiverton, Ontario. Golder Associates, report to Municipality of Kincardine and Ontario Power Generation, Technical Report 021-1570.

Hwang, H.-T., Park, Y.-J., Sudicky, E.A., Berg, S.J, McLaughlin, R., and Jones, J.P. 2018. Understanding the water balance paradox in the Athabasca River Basin, Canada. Hydrological Processes. 32: 729– 746. https://doi.org/10.1002/hyp.11449

Intera Engineering Ltd. 1988. Inventory and assessment of hydrogeological condition of underground openings in sedimentary rocks. Report to Ontario Hydro, H87-040.

Intera Engineering Ltd. 2011. Descriptive geosphere site model. Nuclear Waste Management Organization, Report NWMO DGR-2011-24, 425 pp.

Latifovic, R., Homer,C., Ressl, R., Pouliot, D., Nazmul Hossain, S., Colditz, R.R., Olthof, I., Giri C., and Victoria, A. 2016. North American Land Change Monitoring System. In Giri, C. Ed. Remote sensing of land use and land cover: principles and applications, pp 303-324, Taylor & Francis Group, ISBN 978-1-4200-7074-3.

Logan, C.E., Russell, H.A.J., Mulligan, R.P.M., Burt, A., Bajc, A.F., and Sharpe, D.R. 2020. A three-dimensional surficial geology model of southern Ontario: Progress report. In Russell H.A.J. and Kjarsgaard, B.A. Eds. Southern Ontario groundwater project 2014–2019 summary. Geological Survey of Canada, Open File 8536, 49-64. https://doi.org/10.4095/321084

McKenney, D.W., Hutchinson, M.F., Papadopol, P., Lawrence, K., Pedlar, J., Campbell, K., Milewska, E., Hopkinson, R., Price, D., and Owen T. 2011. Customized spatial climate models for North America. Bulletin of the American Meteorological Society, 92: 12, 1611-1622. https://doi.org/10.1175/2011BAMS3132.1

MNRF (2015). Ontario Integrated Hydrology Data. Spatial Data Infrastructure, Mapping and Information Resources Branch, Corporate Management and Information Division, Ministry of Natural Resources and Forestry. https://www.javacoeapp.lrc.gov.on.ca/geonetwork/srv/en/main.home?uuid=5383ed26-4a12-4026-b624-65c2e431c861

Moriasi, D.N., Arnold, J.G., Van Liew, M.W., Bingner, R.L., Harmel, R.D., and Veith T.L.2007. Model evaluation guidelines for systematic quantification of accuracy in watershed simulations. Trans. Asabe, 50: 3, 885-900. https://doi.org/10.13031/2013.23153

Myneni, R., Knyazikhin, Y., and Park, T. 2015. MCD15A3H MODIS/Terra+Aqua Leaf Area Index/FPAR 4-day L4 Global 500m SIN Grid V006. NASA EOSDIS Land Processes DAAC. http://doi.org/10.5067/MODIS/MCD15A3H.006

NOAA. 2017. Great Lakes Bathymetry. National Oceanic and Atmospheric Administration https://www.ngdc.noaa.gov/mgg/greatlakes/greatlakes.html

Novakowski, K., and Lapcevic, P. (1988) Regional hydrogeology of the Silurian and Ordovician sedimentary rocks underlying Niagara Falls, Ontario Canada. Journal of Hydrogeology 104: 211-236. https://doi.org/10.1016/0022-1694(88)90166-7

Nowakowski, K., Lapcevic, P., Bickerton, G., Voralek, J., Zanini, L., and Talbot, C. 2000. The development of a conceptual model for contamination transport in the dolostone underlying Smithville, Ontario. Smithville Phase IV Bedrock Remediation Program.

OGSRL. 2018. Core analysis calculations from OGSR library. Spreadsheet provided by Terry Carter.

Priebe, E. H., Neville, C. J., and Brunton, F. R. 2017. Discrete, High-Quality Hydraulic Conductivity Estimates for the Early Silurian Carbonates of the Guelph Region. Ontario Geological Survey: Groundwater Resources Study 16.

Raven, K., Novakowski, K., Yager, R., and Heysteee, R. 1992. Supernormal fluid pressure in sedimentary rocks of southern Ontario – western New York state. Canadian Geotechnical Journal 29: 80-93. https://doi.org/10.1139/t92-009

Russell, H.A.J., Baranova, N., Hinton, M.J., and Sharpe, D.R. 2017a. Consolidating the Value of Ontario Drinking Water Source Protection: Data Mining for Well and Aquifer Information, in: 70th Canadian Geotechnical Conference and the 12th Joint CGS/IAH-CNC Groundwater Conference, GeoOttawa 2017, Ottawa, Ontario, Canada.

Russell, H.A.J., Baranova, N., Crow, H.L., Cummings, D.I., Logan, C.E., McBride, A., Pugin, A.J-M. and Sharpe, D.R. 2017b. Building a geological framework to support regional groundwater management: Data capture, consolidation and reclassification in southern Ontario; in Summary of Field Work and Other Activities, 2017, Ontario Geological Survey, Open File Report 6333, p.29-1 to 29-9

Sanchez-Vila, X., Guadagnini, A. and Carrera, J. 2006. Representative hydraulic conductivities in saturated groundwater flow. Reviews of Geophysics, 44: RG3002. https://doi.org/10.1029/2005RG000169

Schaap, M.G., Leij, F.J., Van Genuchten, M.T., 2001. Rosetta: A computer program for estimating soil hydraulic parameters with hierarchical pedotransfer functions. Journal of hydrology, 251: 3-4, 163-176. https://doi.org/10.1016/S0022-1694(01)00466-8

Soil Landscapes of Canada Working Group. 2010. Soil Landscapes of Canada V.3.2. Agriculture and Agri-Food Canada; Science and Technology Branch. https://open.canada.ca/data/en/dataset/5ad5e20c-f2bb-497d-a2a2-440eec6e10cd

Sturm, M., Holmgren, J., and Liston, G. E. 1995. A seasonal snow cover classification system for local to global applications. Journal of Climate, 8: 5, 1261-1283. https://doi.org/10.1175/1520-0442(1995)008<1261:ASSCCS>2.0.CO;2